PETROGENESIS OF BATUR CALDERA, BALI, AND THE GEOCHEMISTRY OF SUNDA-BANDA ARC BASALTS

by

Graeme Eric Wheller B.Sc.(Hons) ANU

submitted in fulfilment of the requirements
for the degree of

Doctor of Philosophy

University of Tasmania

Hobart
April 1986

This thesis reports the major results of my research at the University of Tasmania from February 1982 to March 1986. It contains no material which has been accepted for the award of any other degree or diploma in any university and, to the best of my knowledge and belief, contains no copy or paraphrase of material previously published or written by another person, except where due reference is made in the text.

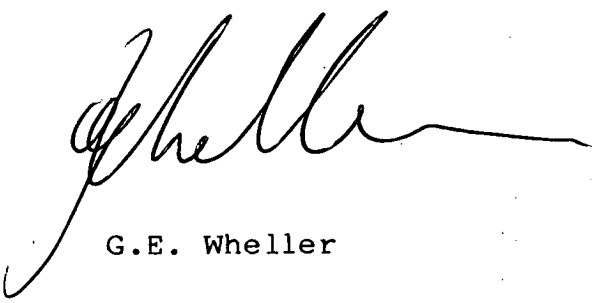

G.E. Wheller

To my

parents, sisters and brother

ABSTRACT

The active Batur volcano on the island of Bali in the eastern Sunda arc, Indonesia, has produced a wide variety of basaltic to dacitic volcanic rock types during its evolution and now possesses a large, well-formed, double caldera. A new basaltic stratovolcano is forming centrally within the caldera.

The evolution of Batur can be divided into precaldera, caldera and postcaldera stages from the volcanic stratigraphy. Beginning more than 500,000 years ago, the precaldera stage produced basaltic to andesitic lava flows and pyroclastics, forming a stratovolcano possibly 2500-3000 m high above sea-level. The subsequent caldera stage produced widely distributed deposits of dacitic pyroclastics and less abundant lava flows, which contrast markedly in lithology, mineralogy and composition with the precaldera products.

Following the formation of the first Batur caldera by collapse about 100,000 years ago, and its subsequent partial filling by a thick sequence of near-vent pyroclastics and lavas during continued explosive dacitic activity, the caldera stage culminated about 23,670 years ago with the generation of the Bali ignimbrite, which covers at least 450 km^2 of southern Bali. This eruption led to formation of the second, inner Batur caldera. Basaltic and basaltic andesite material, including nine lava flows since 1849, has been erupted from within the caldera during the postcaldera stage which may have begun about 20,000 years ago.

Although separated by a 6 wt % SiO_2 gap, the caldera stage dacitic rocks are more closely related geochemically to the postcaldera mafic rocks than to the basaltic andesite and andesitic volcanics that preceded them. Combined major and trace element modelling indicates that the dacites and postcaldera lavas could be genetically related by closed-system fractional crystallization involving the observed phenocryst assemblages. Sr, Nd, O, Be and U-Th isotopic evidence suggests that crustal material was not substantially involved in production of any of the Batur volcanics.

This temporal and geochemical relationship is consistent with an evolutionary model involving early production of dacitic liquids in a thin boundary layer at the sides of a new basaltic magma chamber, leading to formation and subsequent eruption of a dacitic cap. Comparison of the unusual Batur dacite phenocryst assemblage, which includes Fe-rich olivine, with published experimental results indicates that the dacites began to crystallize at < 1.5 km depth, 1070-930 ^{o}C, and contained from < 1 to 2 wt % H_2O. In this model, the post-caldera lavas are derived from the relatively unmodified basaltic magma forming the core of the chamber which, from mafic liquidus phase relationships, probably lies within the crust at depths much less than about 15 km.

In addition, some of the precaldera mafic volcanics show unusual enrichments of incompatible elements, and may have been produced by open-system magmatic processes. These processes may also have led to substantial volatile-enrichment, which could explain the occurrence of many of these rocks in deposits apparently formed by pyroclastic flow.

From the geochemical characteristics of its basaltic to dacitic products, including those of Bali, the Sunda-Banda arc east of Sumatra can be divided into four geochemical arc sectors with boundaries that correlate with major changes in regional tectonic setting and geological history of the arc. Correlations between geochemistry and Sr isotope values in these sectors indicate involvement in the subarc mantle of three distinct components. The dominant component is probably peridotitic mantle. The second component appears to be crustal material, and the degree to which it was involved in production of the arc rocks varies with regional tectonic setting.

However, K-variation in the mafic arc volcanics is primarily due to the third component, which is rich in K and other incompatible elements. The isotopic characteristics of this component indicate that it is unlikely to be crustal material and, instead, suggest a close association with the sources of some southern hemisphere intraplate basalts.

There is also a close geochemical similarity between the

arc basalts and continental ultrapotassic volcanics that are temporally and geographically isolated from orogenic tectonic processes, and it is speculated that K-enrichment of the mantle beneath island arcs accompanies decreasing regional heat flow during the evolutionary transition from island arc to continent.

TABLE OF CONTENTS

PART 2

A Review of the Geological, Geochemical and Isotopic Characteristics of Quaternary Volcanism in the Sunda-Banda Arc: The Role of Subcontinental Mantle Enrichment in Arc Basalt Genesis

LIST OF FIGURES

LIST OF TABLES

LIST OF PLATES

ACKNOWLEDGEMENTS

I have benefitted immeasurably during the last four years from the involvement in various ways of many people. I am particularly grateful to my supervisor, Dr Rick Varne, for his constant and enthusiastic stimulation, support, encouragement and criticism. Although youthful rebellion has caused me to deliberately develop them in a new direction, the ideas expressed in Part 2 of this thesis are largely based on conclusions reached from his own research of Indonesian volcanism.

I am also grateful to the Indonesian Institute of Sciences, the University of Gadja Mada and the Provincial Governments of Bali and Nusa Tenggara Timor for allowing me to twice visit Indonesia to do the fieldwork, and to the villagers and local authorities on Bali, Flores, Adonara and Lembata whose friendly help made working in their country even more enjoyable than I had expected. Rick steered me through the bureaucratic maze associated with a research project based in another country, and Dr Mal Abbott from Flinders University provided support and good cheer during our excursion to Nusa Tenggara Timor. QANTAS brought my samples safely back to Australia for a generously discounted price.

The students and staff of the Department of Geology have provided a varied and scientifically stimulating environment in which to work. I am grateful to Prof. David H. Green in his role as Head of Department for maintaining that environment, and also for his active support of my activities. My graduate student colleagues, Malcolm Wallace, Margaret Wallace, Wayne Taylor, Ewan Reid, Nic Odling, Klaus Nickel, Winfried Naschwitz, Scott Kuehner, David Huston, Jocelyne Hughes, Jafar Hajitaheri, Steve Foley, Trevor Falloon, Steve Eggins and John Adam have all provided friendship and enjoyable discussions of innumerable aspects of rocks, life and the universe. Steve Foley and Trevor Falloon also generously provided access to their substantial compilations of rock analyses.

The XRF and electron microprobe which I used to obtain most of my data were maintained and calibrated by Phil Robinson

and Wislaw Jablonski respectively, and Dr David C. Green taught me how to use the silicate oxygen extraction line and the VG 602D mass spectrometer. Prof. Tom O'Donnell and his students at the University of Melbourne showed me how chemists handle volatile fluorides and provided many ideas on how to reconstruct our silicate line. Dr John Foden from the University of Adelaide generously provided his analyses of Indonesian volcanics, and June Pongratz and Gabrielle Mengel drafted several of the figures in this thesis.

I am particularly grateful to Dr Ian McDougall from the Australian National University for allowing me to obtain K-Ar ages of some Balinese volcanics in his laboratory and for discussion of the results, and to Terry Davies (Ar extraction), Robyn Maier (K analyses), Richard Rudowski (mineral separation) and Maurie Cowan (rock crushing) for technical help and tuition during that work. I am similarly grateful to Dr Bruce Chappell from the Australian National University for generously analysing 28 rock samples from Bali by neutron activation, and to Liz Webber and Ross Freeman for their help in processing those samples. I acknowledge receipt of a Commonwealth Postgraduate Research Award from 1982 to 1986.

INTRODUCTION

Scope of Study

This thesis consists of two parts which address two aspects of the Cainozoic volcanism of the Sunda-Banda arc in Indonesia. The first part consists of a stratigraphic, geochemical and mineralogical study of Batur volcano on the island of Bali in the eastern Sunda arc. Batur is typical of many large island arc volcanoes and has erupted a wide variety of volcanic rock types ranging in composition from basaltic to dacitic. It now possesses a large caldera within which a recently active central cone has produced many basaltic lava flows.

A study of the evolution of Batur is important because large volcanoes in oceanic island arc settings are poorly represented among the major modern studies of evolving volcanoes, particularly of those volcanoes which have produced substantial calderas. Batur caldera was described by van Bemmelen (1949) as "one of the largest and finest calderas in the world". In this part of the thesis, the petrogenesis of Batur is investigated, particularly the nature of the chemical and physical fractionation processes that led to production of the dacitic magmas and the formation of Batur caldera.

The second part of the thesis encompasses a compilation of modern geochemical and isotopic analyses of volcanic rocks erupted from Cainozoic volcanoes lying along most of the length of the Sunda-Banda arc. This part also provides the regional chemical and tectonic context in which the explosive volcanism of Batur occurred. In the second part, regular compositional variations among the volcanic rocks are identified in conjunction with summaries of the geological, structural and tectonic settings of the arc.

From this treatment, regular and marked variations in the compositions of the basaltic rocks along the arc are observed. These variations appear to be related to the inferred positions of previous island arcs that occurred during the geological history of the Indonesian archipelago. A large-scale, partly

speculative, interpretation of the causes of compositional variation among the Sunda-Banda arc basaltic rocks is proposed, involving an evaluation of the relative importance of crust- and mantle-derived metasomatic components in the source regions of the basalt magmas.

Overall, this thesis includes new major and trace element analyses of 315 volcanic rocks in a compilation of 679 wholerock analyses from 56 volcanoes. In addition to the samples from Bali which are used in Part 1 of the thesis, new samples were collected from Quaternary volcanoes on the islands of Flores, Adonara, Lembata and Batu Tara. The new data from the latter islands are discussed in Part 2 and help fill a large gap in our knowledge of the geochemical variation along the Sunda-Banda arc.

Previous Studies of Indonesian Volcanism

The Indonesian archipelago, from Sumatra eastwards through Java and Bali to the line of small island-volcanoes lying east of Wetar, is one of the world's longest and most complex active island arc systems. Comprising the Sunda arc in the west from Sumatra to Wetar, and the Banda arc eastwards from Romang (Fig. 1.1), it has been the subject of several important early studies which related the distribution and composition of island arc volcanism to plate tectonic theory (e.g. van Bemmelen 1949; Rittman 1953; Hatherton & Dickinson 1969).

The most comprehensive summary of the geology and volcanism of the Sunda-Banda arc, and the Indonesian region in general, is that of van Bemmelen (1949). More recently, Hamilton (1979) also summarized the geology of Indonesia but concentrated more on the tectonic setting of the region than on the nature of the volcanism.

Van Bemmelen (1949, p. 214-215) cited several early studies of the chemical compositions and petrology of Indonesian volcanic rocks, of which the compilation by Willems (1940) of 1220 wet chemical major element analyses is the most substantial. Subsequently, Neumann van Padang (1951) made the first compilation of modern Indonesian volcanic activity, which

included a large number of chemical analyses obtained by wet chemical methods by earlier geologists, particularly Brouwer (1940). Hutchison (1982) has recently summarized the compositional characteristics of Indonesian Cainozoic volcanic rocks.

Following the observations by Brouwer (1940) of increasing alkalinity of the volcanic rocks of Adonara and Lembata across the arc, Rittman (1953), using Neumann van Padang's (1951) compilation of analyses, showed that an apparently regular and general relationship existed between the K contents of the volcanic rocks and the distance away from the arc trench. The relationship between K contents of island arc volcanic rocks and the depth to the Benioff zone was determined in part by a study of Sunda arc volcanism and seismicity by Hatherton and Dickinson (1969), and later by Whitford and Nicholls (1976) using new analytical data. Hutchison (1976) extended this relationship to include the trace elements Sr and Rb using data obtained by Whitford (1975a).

Whitford (1975a) was the first to apply modern analytical techniques to the study of the origins of Indonesian volcanic rocks. His work essentially comprised a reconnaisance study of 23 Quaternary volcanoes, some of them extinct, on Java and Bali involving from 2 to 15 samples from each volcano, except for leucite-bearing Muriah volcano in central Java from which 27 samples were obtained.

Whitford produced a large amount of geochemical and isotopic data which he used to investigate the nature and causes of compositional variation among the basaltic rocks in Java and Bali. The results of this work have been published in a number of papers, particularly Whitford (1975b), Whitford and Nicholls (1976), Whitford and Jezek (1979,1982), Whitford et al. (1979, 1981) and Nicholls and Whitford (1976,1983).

The second recent geochemical study of Indonesian volcanoes was that of Foden (1979) who studied five Quaternary volcanoes on Lombok and Sumbawa, including Tambora which had a major caldera-forming eruption in 1815, using similar petrological, geochemical and isotopic methods to those of

Whitford. This work has also led to publication of a number of papers, particularly Foden and Varne (1980,1981), Foden (1983,1986), Varne and Foden (1986) and Varne (1985).

Morrice et al. (1983) and Morris et al. (1983) studied the lavas of other young Indonesian volcanoes in the Sangihe and Halmahera arcs respectively, using similar methods and with similar aims to those of Whitford and Foden. These two island arcs, situated in northern Indonesia near the Philippines, are unusual in that they face each other across narrow straits and strike northwards, normal to the general strike of the Sunda-Banda arc.

Each of these modern studies was based mainly on 'grab' samples obtained from around the flanks of the volcanoes. In Indonesia, the geochemical and stratigraphic patterns of few large volcanoes have been comprehensively studied. Most of the published studies of the most famous Indonesian volcano, Krakatau, concern the effects of the major 1883 eruption on surrounding populations and world weather, and the volcanology and petrology of the 1883 and subsequent eruptions. These studies include Judd (1888), Verbeek (1884), Escher (1919, 1948: cited in van Bemmelen 1949, p. 201), Stehn (1929) and de Neve (1981). The centenary of the eruption in 1983 was marked by publication of several modern studies, including Francis and Self (1983), Camus and Vincent (1983) and Simkin and Fiske (1983).

Recently, Foden (1983,1986) studied in detail the geochemistry and genesis of volcanic rocks from Rindjani and Tambora volcanoes on the islands of Lombok and Sumbawa respectively. However, the stratigraphic evolution of these two volcanoes prior to caldera formation, and of Krakatau, is still largely unknown.

Previous Studies of Batur Volcano

Many early Dutch geologists described various aspects of Batur volcano, with the studies of Kemmerling (1918) and Stehn (1928) being the most substantial. These two studies essentially describe the eruptions of Batur in 1917 and in 1926

respectively but both also provide information about the type and distribution of some of the older postcaldera lava flows and pyroclastic deposits lying within the caldera. Stehn (1928) also produced the first major map of the caldera, showing the outline of the caldera and the distribution of cones, craters and postcaldera lava flows.

Marinelli and Tazieff (1968) were the first to record the existence of the Bali ignimbrite and to relate its production to the formation of Batur caldera. The Bali ignimbrite is an extensive pyroclastic flow deposit which is widely quarried and carved to produce the distinctive Balinese statues.

The eruptions of Batur since 1963 have been recorded in unpublished reports of the Indonesian Volcanological Survey, mainly by K. Kusumadinata. A compilation of previous reports concerning Batur, and other Indonesian volcanoes generally, is given by Kusumadinata (1979).

Fieldwork in Indonesia

Fieldwork in Indonesia was undertaken during a two month period from October to December, 1982, followed by a second two month period from March to May, 1984. Permission to do fieldwork in Indonesia was granted by the Indonesian Institute of Sciences (LIPI) following applications submitted up to 12 months prior to the fieldwork periods. Research permits and travel documents were collected in person from LIPI in Jakarta. During each fieldwork period visits were made to collaborators and sponsors at the University of Gadja Mada in Yogyakarta and at the Indonesian Geological Survey in Bandung.

The fieldwork mainly consisted of mapping and sampling in and around Batur caldera, and reconnaisance sampling of other volcanoes in eastern Bali and on the islands of Flores, Adonara, Lembata and Batu Tara in the eastern Sunda arc. Many of these volcanoes had not been previously sampled. On Bali, hired motorcycles were used for transport. Local buses and chartered vehicles were used on the other islands. Inter-island ferries and chartered boats used to reach the remote islands.

Good rock outcrop occurs in the lower part of the Batur caldera walls and across the caldera floor, but the near-vertical caldera walls are largely inaccessible. Outcrop on Bali outside Batur caldera is generally poor because of the fragmental nature of the volcanic rocks, the high rates of vegetation growth and soil development in this tropical region. Also, the young pyroclastic products of Batur, particularly the Bali ignimbrite and younger pumice, lie over a wide area of central and southern Bali and essentially cover all of the products of the other volcanoes.

Outcrops in eastern Bali are therefore generally restricted to river beds, rare cuttings along tracks and roads, or coastal exposures. Outside Batur caldera, the useful outcrops discovered so far are not sufficiently closely-spaced for detailed correlations except on broad lithological criteria. In addition, the Balinese volcanoes generally are youthful and few are sufficiently incised by erosion to allow satisfactory study of their older products. Only a few outcrops of volcanic rocks produced during the early stages of the evolution of Batur, in particular, were located during this study.

PART 1

PETROGENESIS OF BASALT-ANDESITE-DACITE VOLCANISM AT THE ACTIVE BATUR VOLCANO, BALI, EASTERN SUNDA ARC: IMPLICATIONS FOR THE ORIGINS OF STRATOVOLCANO CALDERAS AND THE EFFECTS OF MAGMA DYNAMICS ON ERUPTIVE MECHANISMS

1. TECTONIC AND GEOLOGICAL SETTING OF BALI

The Sunda-Banda volcanic island arc extends for 4700 km from the northern tip of Sumatra in the west to the small island of Nila in the east, after which it curves tightly for 600 km to the north (Fig. 1.1). In Sumatra and western Java, volcanism may have been occurring since Triassic times but in the eastern part of the arc it seems to have begun only in the Middle to Late Miocene (Hamilton 1979). The basement on which the modern volcanism occurs changes progressively from continental crust 20-30 km thick in Sumatra and Java, through intermediate-type crust near Bali and Lombok, to crust with oceanic thickness near Wetar and the Banda Islands (Curray et al. 1977; Purdy & Detrick 1978).

The crust beneath Bali is about 18 km thick and has seismic velocities similar to those of oceanic crust. Curray et al. (1977) suggest this crust is old, trapped oceanic crust that may have been thickened by reverse or thrust faulting caused by horizontal compression but Hamilton (1979) considers it to be the edge of a continental shelf that underlies eastern Java and the Java Sea and which was built largely of subduction melange during the Cretaceous and Early Tertiary.

The oceanic part of the Indian-Australian plate is converging in a north-northeasterly direction towards the Sunda arc at 7.0 to 7.5 cm/yr (Moore & Karig 1980). The seismic zone of earthquake foci beneath the arc reaches approximately 650 km depth between Java and Flores, with a gap in seismicity between 300 and 500 km depth (Fitch & Molnar, 1970; Cardwell & Isacks, 1978). Beneath 100 km depth the seismic plane dips at about 65^{o}. Batur volcano lies approximately 160 km above the middle of the seismic zone (=Benioff Zone).

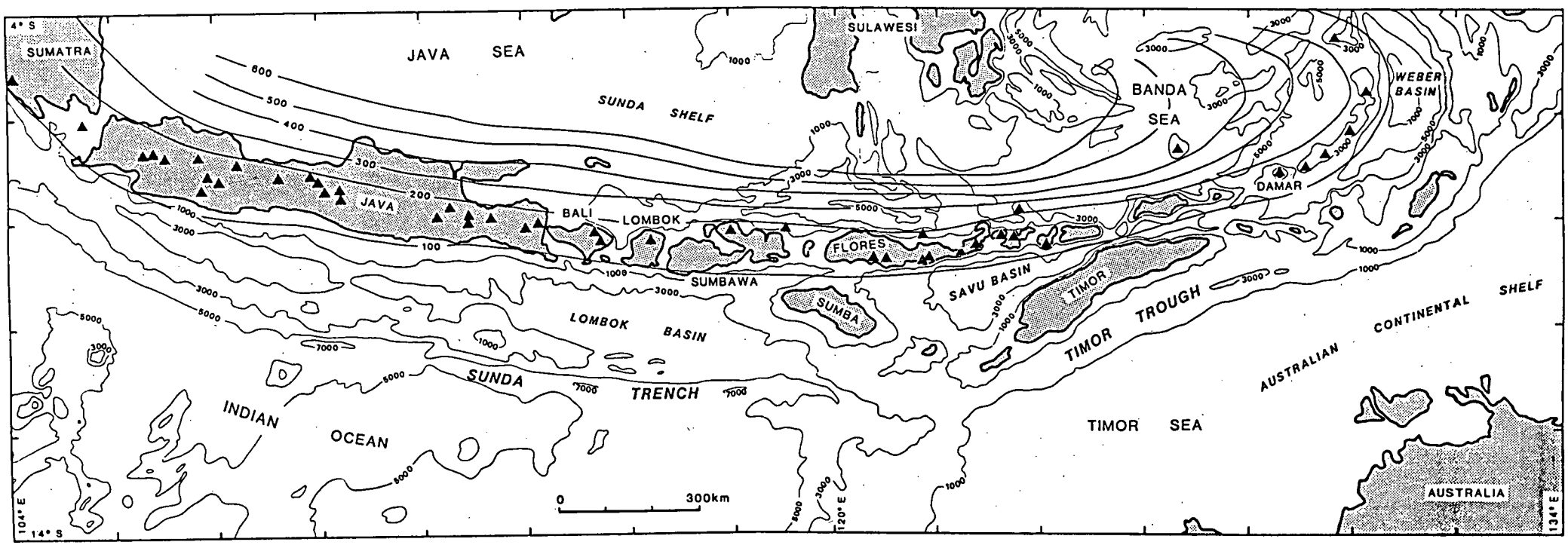

Figure 1.1 Location map of the Sunda-Banda arc showing volcanoes known to have erupted within the last 10,000 years (solid triangles; Simkin et al. 1981), together with contours indicating depths (in kilometres) to the Benioff zone (Hamilton 1979); oceanic bathymetry contours in metres.

Most of Bali consists of young volcanic rocks, with older calcareous sandstones and limestones being exposed mainly around the western and southern margins of the island (Fig. 1.2). In places in southeastern and central Bali, the sedimentary rocks contain foraminifera of Late Miocene age (Kadar 1972), and recently uplifted coral reefs forming the southern peninsula and the small island of Nusa Penida are younger in age than Pliocene-Pleistocene (Kadar 1977). The older marine sequences, particularly the Ulakan Formation, also contain substantial amounts of volcanic material, and pillow basalts and tuffs are exposed in hills and at sea-level over an area of approximately 200 km^2 in southeastern Bali.

The younger, subaerial volcanic rocks have been erupted from several volcanoes, which can be conveniently subdivided into eastern, central and western groups. The eastern group comprises the two active volcanoes Batur and Agung, and the substantially eroded remnants of the extinct Seraja volcano. The latter forms the easternmost tip of Bali and its highest peak is now only 1058 m above sea-level. The summit of Agung volcano occurs at 3140 m above sea level and lies 18 km southeast of the new Batur volcano.

The most recent major eruption of a Balinese volcano was that of Agung in 1963. The eruptions began on 18 February, led to the deaths of 1000-2000 people (Zen & Hadikusomo 1964; Surjo 1965) and provided the first well-documented evidence that large volcanic eruptions contribute substantially to the stratospheric sulphate aerosol layer which lies about 20 km above the earth's surface (Castleman & Keesee 1981). The first major eruptive phase began with earth tremors and shocks which were followed by vulcanian explosions. On 24 February, accompanied by numerous nuees ardentes, a lava flow spilled from the summit crater over the northern flank, reaching 7.5 km in length by early May.

A major explosion occurred on 17 March, producing an ash column that is estimated to have reached heights of about 20 km (Rampino & Self 1982). Nuees ardentes flowed down the southern and southeastern flanks for up to 14 km from the summit,

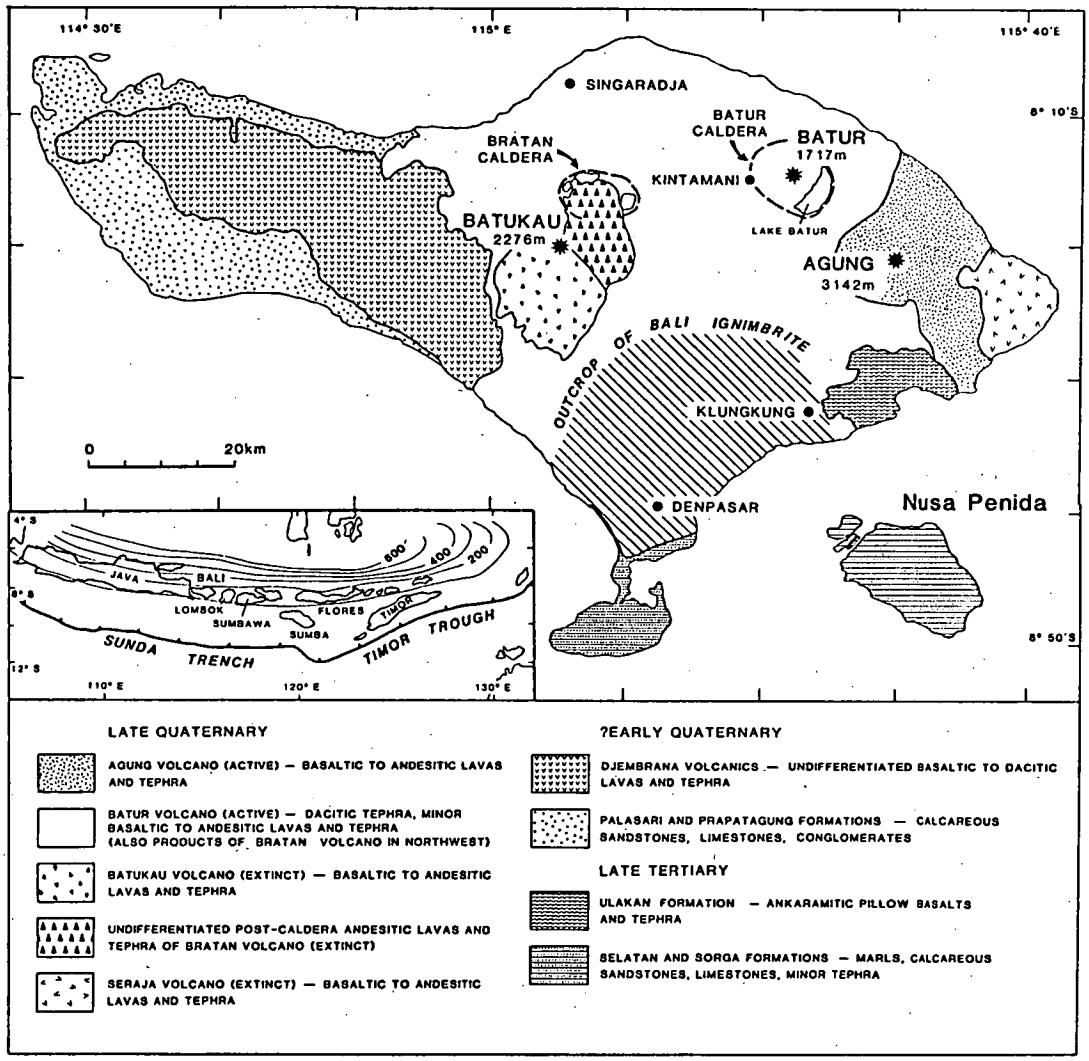

Figure 1.2 Geological sketch map of Bali (after Purbo-Hadiwidjojo 1971).

generally following river valleys. Substantial amounts of ash were deposited over Bali and Java as far west as Jakarta, 988 km west of Agung. After this phase of the eruption torrential rain led to the formation of lahars.

A second major explosion occurred during the late afternoon of 16 May. This was preceded by rumbling noises and weak earthquakes and, like the first, was accompanied by numerous nuees ardentes. The ash column reached a height of about 22 km (Meinel & Meinel 1964) and ash was deposited across western Bali and eastern Java. Substantial activity, including explosions, rumblings, ash columns and nuees ardentes, continued to occur for several days after 16 May, decreasing in intensity with time until ceasing in January 1964.

Each of the volcanoes comprising the central group appears to be extinct, although some appear from their morphology and reconnaisance stratigraphic evidence to be of very young age. The oldest and largest of these volcanoes, Bratan, lies 28 km west of Batur and possesses a large elliptical caldera, 10.8 km by 6.2 km, with 3 intracaldera lakes. Its rim lies between 2098 m (G. Bratan) and 1300 m above sea-level. This caldera was first described by Marinelli and Tazieff (1968).

Unlike that of Batur, the Bratan caldera is partly filled by the products of several small, postcaldera, stratovolcanoes which straddle its southern margin. The summit of the largest of the Bratan postcaldera cones, Batukau, lies 10 km southwest of Bratan caldera and 2276 m above sea-level. Some of these cones are well-formed and possess deep summit craters. However, their thick vegetation and soil cover suggest that they have been inactive for a substantial period of time, perhaps hundreds or thousands of years.

In addition, pumice deposits that were probably erupted from Batur, and which are a few metres thick inside Bratan caldera at the southern edge of D. Bratan, were not observed on the flanks of two of the postcaldera cones, Tapak and Lesong. This suggests that these two cones are younger in age than the most recent eruptions of dacitic pumice from Batur.

The western group of Balinese volcanoes form a deeply dissected mountain range, with several peaks lying between 1000 and 1400 m above sea-level, which is much less densely populated than the other parts of Bali. The substantial degree of erosion of these volcanoes suggest they are at least as old as Seraja. Little is known of the rocks in this region, except for brief petrographic descriptions by Marinelli and Tazieff (1968) of rocks collected from river beds near the northern coast of Bali. The products of the western volcanoes have not been sampled for this thesis.

2. K-Ar DATING AND THE AGE OF VOLCANISM IN EASTERN BALI

K-Ar ages were obtained at the Research School of Earth Sciences at the Australian National University from samples of lavas from Batur (4 samples), Bratan (2) and Seraja (4) volcanoes, and from the Ulakan Formation (2). Samples for K-Ar dating were chosen for their fresh appearance and well-developed crystallinity. The pillow basalts from the Ulakan Formation contain small amounts of groundmass clays, chlorite and zeolites, and two lavas from Batur (University of Tasmania Geology Department sample numbers 67334 and 67340) contain moderate amounts of brown groundmass glass but show no evidence of alteration.

After removal of weathered surfaces, the rocks were crushed and sieved to between 0.59 and 0.25 mm grainsize (30 to 60 mesh). Because all of the samples are likely to be of young age, phenocrysts of olivine, pyroxene and plagioclase were removed from each sample by heavy liquid and magnetic separation methods. This technique minimizes the effect of any pre-existing excess radiogenic Ar (McDougall et al. 1969). An aliquot of the seived material was then crushed to a fine powder in a tungsten carbide swing mill and analysed for K by flame photometry.

Ar was extracted from about 15 g, precisely weighed, of the coarser seived material for all of the rocks except the K-rich Ulakan samples, for which about 8 g of material was used. The concentration of radiogenic ^{40}Ar was determined by isotope dilution, after addition of a ^{38}Ar spike, using a

substantially modified AEI MS10 mass spectrometer with on-line data reduction. In some cases, separate isotopic measurements were done on two aliquots of the extracted Ar, and two separate extractions were done for some samples. All results are listed in Table 1.1.

The ages obtained from these samples indicate that volcanic activity has been occurring in eastern Bali for nearly 3 Ma, since the Late Pliocene. Although the results for the Ulakan rocks should be regarded only as good minimum ages, because of the possibility of Ar loss during alteration, their location in stratigraphically low parts of the Ulakan Formation, suggests a younger age for the volcanic sequence in southeastern Bali than the Late Miocene age suggested previously by Kadar (1972) using its association with foraminifera-bearing sediments. The K-Ar ages of the Ulakan Formation volcanics are actually more consistent with the Pliocene-Pleistocene ages determined for limestone sequences in southern Bali (Kadar 1977), given that these two groups of rocks at present lie at or below sea-level.

One of the samples from Seraja volcano was obtained from a lava flow on its northern flank, while three other samples occurred as float on its western flank. The uppermost stratigraphic position of these rocks, particularly the lava flow on the northern flank, suggests that their ages, which are effectively identical at about 0.76 Ma, record approximately the age of extinction of Seraja volcano. This old age compared to those obtained from the Bratan and Batur rocks is consistent with the high degree of erosion shown by Seraja.

The ages of samples from both Bratan and Batur volcanoes span wide ranges. For Bratan, because sample 67410 is of a lava flow lying within the caldera, formation of the caldera must have occurred more than 0.10 Ma ago. For Batur, samples 67334 and 67333 essentially possess little or no radiogenic Ar, which indicates they are of very young age, certainly less than 0.1 Ma. These results indicate that the Bratan caldera is substantially older than that of Batur. Given that the products of the active Agung volcano are basaltic and andesitic in composition, it is likely that the uppermost, siliceous

UT#	ANU#	rock type	K (wt %)	radiogenic ^{40}Ar (10^{-12} mol/g)	% rad. ^{40}Ar	calculated age +- s.d.	remarks
Batur volcano							
67334	84-76	olivine basalt	1.219	-0.24986	-0.57	-0.12 +- -0.065	flow near base of caldera wall,
			1.223	-0.33927	-0.77	-0.16 +- -0.065	1 km southwest of Kedisan
67333	84-75	olivine basalt	1.059	0.02344	0.13	0.013 +- 0.035	flow near base of caldera wall,
			1.057	-0.05053	-0.28	-0.028 +- 0.027	1 km southwest of Kedisan
67340	84-77	olivine basalt	0.8613	0.49864	2.75	0.335 +- 0.047	flow near base of T. Meja valley,
			0.8559	0.46552	2.57	0.313 +- 0.033	12.2 km northwest of Batur
67341	84-78	olivine basalt	0.5324	0.46643	11.63	0.501 +- 0.017	flow near base of T. Meja valley,
			0.5421	0.47493	11.84	0.510 +- 0.016	12.2 km northwest of batur
Bratan volcano							
67410	83-221	olivine basalt	0.7293	0.13588	3.84	0.108 +- 0.007	flow, south side of D. Bratan
			0.7275	0.10869	3.06	0.086 +- 0.009	near Hotel Bedugal
67405	83-220	olivine basalt	0.7891	0.58786	7.03	0.429 +- 0.015	creek boulder, 10 km west of
			0.7896	0.57319	7.01	0.419 +- 0.014	Bratan caldera rim at Globleg

Table 1.1

continued over ..

UT#	ANU#	rock type	K (wt %)	radiogenic ^{40}Ar (10^{-12} mol/g)	% rad. ^{40}Ar	calculated age +- s.d.	remarks
Seraja volcano							
67386	83-219	basaltic andesite	1.612 1.606	2.1585	36.10	0.774 +- 0.010	creek boulder, west flank
67382	83-217	basaltic andesite	1.348 1.352	1.7621	25.08	0.752 +- 0.011	creek boulder, west flank
67383	83-218	basaltic andesite	1.319 1.322	1.7295 1.7266 1.7670	18.28 18.28 18.53	0.755 +- 0.012 0.754 +- 0.013 0.771 +- 0.012	creek boulder, west flank
67396	84-79	basaltic andesite	1.638 1.648	2.1377 2.1382	36.6 36.6	0.750 +- 0.009 0.750 +- 0.009	flow near sea-level, 1.5 km east of Amed, north flank
Ualakan Formation							
67412	83-222	ankaramite	1.718 1.718	7.3863	40.80	2.48 +- 0.03	massive flow, 600 m north of Padangbai intersection
67421	84-80	ankaramite	2.128 2.127	10.541 10.503	38.2 38.2	2.854 +- 0.035 2.844 +- 0.034	creek boulder, T. Bete, Antiga

Table 1.1 K-Ar ages of volcanic rocks from central and eastern Bali. Decay constants and natural abundance of ^{40}K given in Steiger and Jager (1977).

pyroclastic deposits in central and eastern Bali were produced from Batur volcano.

The remaining samples from Bratan and Batur indicate that both volcanoes existed for at least 0.3 and 0.4 Ma respectively before caldera-formation occurred.

3. GEOLOGY OF BATUR VOLCANO

The following description of the products of Batur volcanism is based on observations made in the eastern half of Bali. Exposure is generally poor due to the nature of the deposits and to the vegetation cover but, in southern Bali, some sequences up to nearly 20 m thick have been found at places along the coast and in the deep gorges formed by the generally south-flowing rivers. The localities examined so far are widely spaced and provide information only on the large-scale stratigraphic variations of Batur volcanism.

3.1 Morphology

Batur volcano now comprises a stratovolcano lying centrally within two concentric caldera scarps (Fig. 1.3; Plates 1-3). The summit of the new stratovolcano has reached approximately 700 m above the caldera floor, and 1700 m above sea level. The southern flanks of the Batur dip gently for 60 km to the south coast of Bali but its northern flanks dip steeply to reach sea level within 6 km. The rim of the outer caldera margin is elliptical in shape, 13 km by 10 km, and lies between 300 and 700 m above the level of an intra-caldera lake, Lake Batur, which covers about one third of the caldera floor.

The inner caldera margin is marked by a prominent, mostly vertical, scarp up to 300 m high in places inside the northern half of the outer caldera. This semi-circular scarp is about 7.5 km in diameter. It is not certain whether the southern margin of the inner caldera lies beneath Lake Batur, or whether it coincided with the southern part of the outer caldera margin. Stehn (1928) thought that the depression now filled by Lake Batur may have marked the site of an asymmetric third caldera which straddled the southern margin of the older second

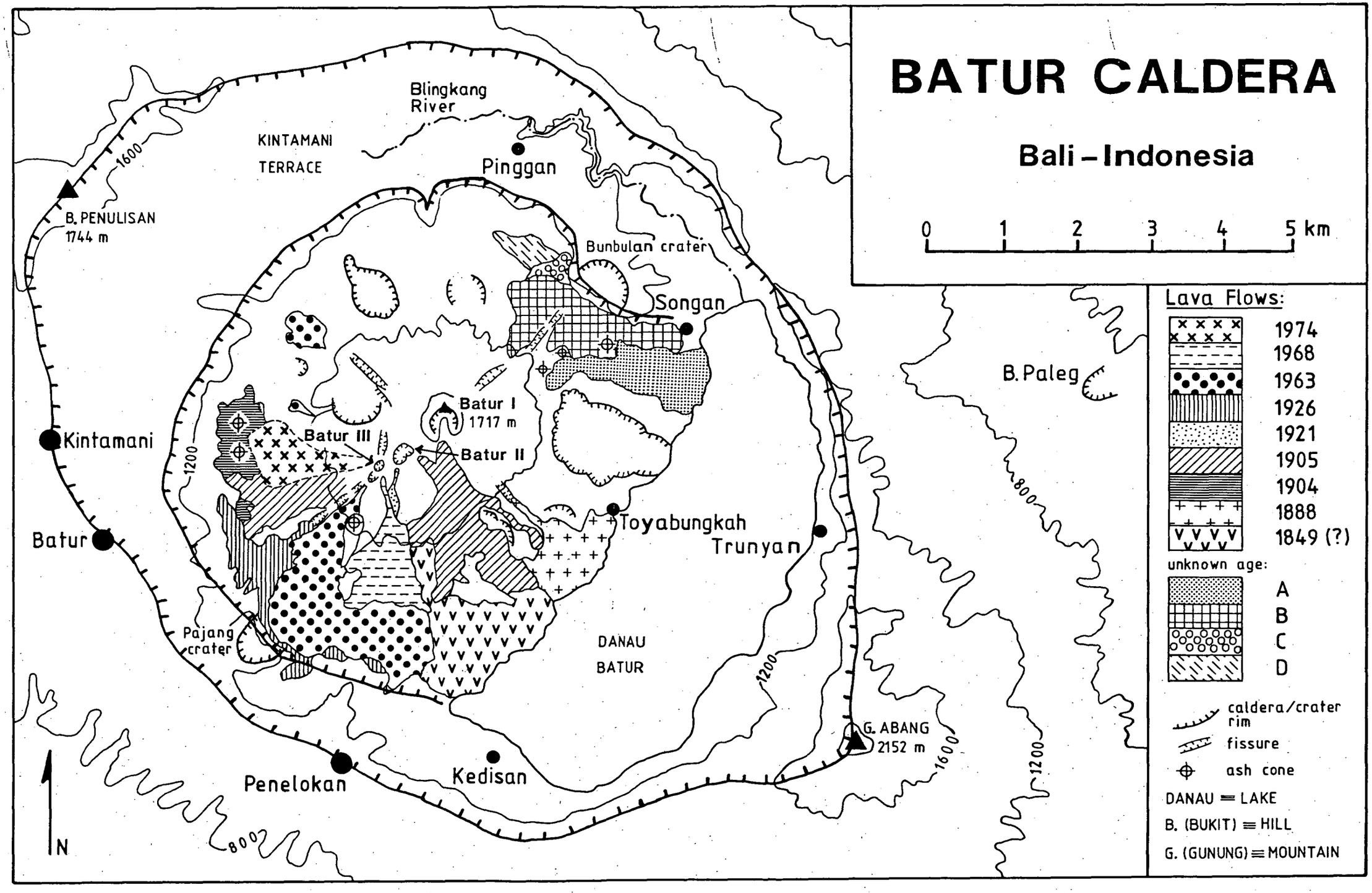

Figure 1.3 Geological sketch map of Batur caldera. Ages of pre-1963 lava flows from Stehn (1928).

Plate 1. Western side of intracaldera Batur volcano (viewed from western caldera margin) showing Batur I, II, III cones, postcaldera lava flows (1963 and 1968 are dark-coloured) and eastern caldera rim (horizon).

Plate 2. Eastern side of intracaldera Batur volcano (viewed from eastern caldera rim) showing Batur I cone, prehistoric fissure (flank) and lava flows (foreground), and western caldera rim (horizon).

Plate 3. Photomosiac showing Batur I cone (left), Bunbulan crater rim (below Batur I), Kintamani terrace (foreground and right of Bunbulan crater), Blinkang river valley (below left) and outer caldera rim (horizon). Viewed from eastern side of outer caldera rim.

caldera. However, at this stage, there is no strong evidence for the existence of this third caldera and, as will be shown, it is possible to explain the existence of a depression in the southern half of the outer caldera satisfactorily if only two caldera-formation eruptions occurred.

Inside the northwestern half of Batur caldera a near-horizontal terrace, referred to as the Kintamani terrace by Stehn (1928) and van Bemmelen (1949), lies between the outer and inner caldera scarps (Plate 3). The eastern part of this terrace is deeply dissected by the seasonal Blinkang River which flows eastwards into Lake Batur near the village of Songan.

3.2 Stratigraphy

The stratigraphic evolution of Batur volcano can be subdivided broadly into precaldera, caldera and postcaldera stages. The precaldera stage encompassed the growth of the first Batur stratovolcano by eruption of mainly basaltic to andesitic material, including unusual pumiceous andesitic clasts found up to 50 km from Batur. As discussed, results of K-Ar age measurements indicate that this is the most long-lived stage in the evolution of Batur.

During the subsequent caldera stage most of the dacitic pyroclastic rocks of Batur were erupted. This stage is marked by at least two episodes of caldera-formation. As will be shown, the caldera stage possibly occurred over a period of only several tens of thousands of years. The postcaldera stage of the evolution of Batur probably began soon after the second caldera-forming episode and is distinguished by the eruption of basaltic and basaltic andesite lava flows and the growth of the new intra-caldera Batur volcano. The general relationships of these three main stages in the evolution of Batur to the present outline of Batur volcano are shown in Fig. 1.4.

3.2.1 Postcaldera Stage

The new Batur stratovolcano has erupted many basaltic lava flows across the caldera floor (Fig. 1.3; Plate 1). These are

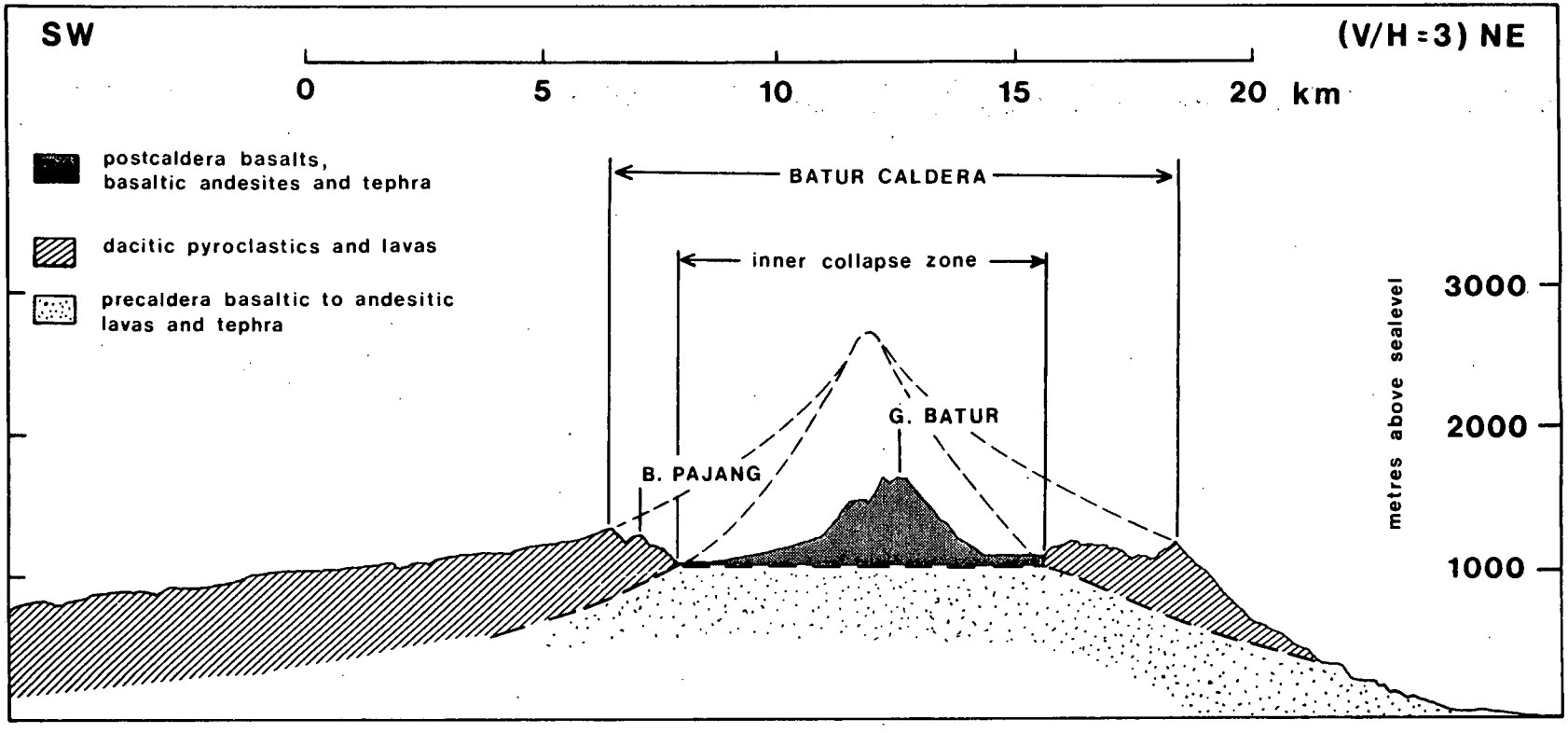

Figure 1.4 Northeast-southwest cross-section of Batur caldera.

relatively small-volume, vesicular flows which contain olivine, clinopyroxene, plagioclase and Ti-magnetite as phenocrysts. Nine flows have been erupted since 1849 over the western and southern parts of the caldera floor (Stehn 1928; Neumann van Padang 1951; Simkin et al. 1981) and several older flows occur in the northeastern part. The total area covered by these lava flows is 17.4 km^2 which is approximately 37 % of the area of the floor of the inner caldera. Outcrops of flows that are largely buried also occur in places.

The new stratovolcano is mainly composed of basaltic ash, scoria, bombs and blocks, and comprises three aligned coalesced cones, referred to as Batur I, II and III respectively by Stehn (1928) (Fig. 1.3; Plate 1). Explosive eruptions from the new Batur stratovolcano have been recorded since 1804. In November 1983 and April-May 1984, the volcanic activity consisted only of occasional thin columns of steam from craters on Batur II and hot springs at lake level at Toyabungkah.

The most recent lava was erupted during March and early April 1974 and flowed to the west from a vent near the summit of Batur III. This flow is about 2 km long. More voluminous flows were produced in 1968 and in 1963 when neighbouring Agung volcano also erupted, but more explosively (Zen & Hadikusumo 1964; Rampino & Self 1982). These two lavas flowed from vents located on the western side of Batur III, with the 1963 vent lying near the foot of Batur III and the 1968 vent lying near the summit. At present, Batur III is essentially free of vegetation and consists mainly of basaltic ash and blocks.

Although the 1963 eruption of Batur, which is the largest eruption of Batur to have occurred in recent time, was preceded and overshadowed by the much more explosive and socially damaging eruption of Agung, its effects were recorded by Kusumadinata in unpublished reports of the Indonesian Direktorat Geologi (Kusumadinata 1963, 1964). The eruption began at 9.45 a.m. on 5 September but was preceded by frequent, short-duration tremors that were felt at Kintamani, at the western outer caldera rim, beginning at about 6 a.m. Initially, loud rumblings were heard. These were followed soon after by thick columns of 'smoke' which rose vertically from a fissure

at the southwestern foot of the Batur cone, in a similar position to that formed during the 1926 eruption. Lava flowed from the fissure towards the south and west, accompanied by lava fountains which reached heights of approximately 200 m.

At 2 p.m. lava also began to flow from two sources at the northwestern foot of Batur. However, much less lava was erupted from these than from the southwestern fissure (Fig. 1.3). During this time, and for two days after, 'lapilli rain' and, eventually, a 'fine sand shower' fell at Kintamani and at other places along the western caldera rim. The distribution of the pyroclastic deposits formed a wide lobe lying west of the summit of Batur, with the thickest part forming an elongate lobe that trended due west from the fissure (Kusumadinata 1964). Most of the western caldera rim was covered by 0.2 to 10 cm of ash, with a small section centred on Kintamani receiving up to 20 cm of ash. The thickest deposits, up to 75 cm, formed almost entirely within the inner caldera.

Lava stopped flowing from the fissure on 26 September but visible activity continued until 10 May 1964. Kusumadinata (1964) estimated that approximately 41×10^6 m^3 of lava was erupted, covering an area of approximately 5.88×10^6 m^2, together with at least 0.51×10^6 m^3 of ash which was distributed over approximately 7.48×10^6 m^2. No increase in temperature of the Toyabungkah hot springs was recorded and no activity was seen to occur at the summit craters.

The 1926 lava also flowed from near the foor of Batur III. The eruption was extensively described by Stehn (1928). It began during the night of 2-3 August, preceded by earthquakes. Lava flowed from a long, radial fissure at the southwestern foot of the Batur III and eventually reached the western part of the inner caldera wall where it was diverted to the north and south. The southern part of the flow eventually engulfed the old village of Batur, destroying one of the most important Hindu temples on Bali on 27 August. The 1905 lava flow had also threatened the temple but stopped at the entrance.

Stehn (1928) estimated that approximately 21×10^6 m^3 of lava and at least 1.75×10^6 m^3 of scoria were erupted.

Visible volcanic activity ended on 21 September. The temperature of hot springs on the northern shore of D. Batur at Toyabungkah rose 16.5°C during the eruption but, like the 1963 eruption, no activity was observed in the central craters near the summits of Batur I and II.

Batur II formed on the southwest flank of Batur I and its summit area contains many overlapping, moderate-sized (20-50 m across), steep-sided craters. The small volume, and now completely covered, 1921 lava flowed from a summit crater of Batur II.

The largest cone, Batur I, lies at the centre of the caldera and its highest part of Batur I is higher than most of the outer rim of the caldera, lying about 700 m above the caldera floor and the surface of Lake Batur. Batur I contains the largest of the summit craters. This crater is about 300 m in diameter and about 120 m deep, possesses steep inner walls and is open to the south. The 1905 lava flowed from this crater through the southern opening to the caldera floor as well as from summit craters on Batur II. The 1888 lava flowed from an elongate vent at the southern foot of Batur I and reached as far as the western shore of Lake Batur. Several older, prehistoric postcaldera lavas lying on the northeast part of the caldera floor were erupted from fissures and vents lying on the northeastern flank of Batur I.

As pointed out by Stehn (1928) the sites of recent volcanic activity within Batur caldera have shifted markedly. The source of the 1849 lava is not known but the location of the flow south of Batur I indicates that it was accompanied, or preceded, by a major change in the subvolcanic 'plumbing' system following production of the older, prehistoric lava flows in the northeast. The subsequent 1888 lava flowed from a vent near the southeastern foot of Batur I, but the 1904 activity, however, appears to have been accompanied by another substantial change as it occurred in a small area located close to the inner caldera wall to the west of Batur II (Fig. 1.3). Two large ash cones lie over the 1904 lava. The 1905 lava flowed from summit craters on both Batur I and Batur II, indicating another substantial change in the location of the

activity. The absence of ash on the 1905 lava flow indicates that the two ash cones overlying the 1904 lava formed during the 1904 activity.

Several large explosion craters and depressions punctuate the Batur caldera floor, providing more evidence that the surface location of postcaldera Batur volcanism has shifted markedly with time. Most of these were first recognized by Stehn (1928) by ground reconnaissance. However, the largest depression, located east of Batur between Toyabungkah and Songan (Fig. 1.3), was identified by interpretation of aerial photographs. This depression is irregular in shape, although generally elliptical, and is approximately 1.7 km long and 1.1 km wide. It is marked on three sides by steep, scalloped walls that are up to 100 m high but is open at its eastern end where it is truncated by the western shore of D. Batur. Three other craters, or depressions, 0.5 to 1 km in diameter, occur in the northwestern part of the caldera floor, and two arcuate ridges, which may represent craters older than the 1888 lava flow, lie in the southeastern part.

The focus of the postcaldera volcanic activity appears to be controlled by regional crustal structure, although no evidence of faulting, other than the inferred caldera ring faults, has yet been found around Batur caldera. However, the crustal control on the location of volcanism can be identified from regular patterns in the positions of craters and fissures within the caldera (Fig. 1.3). In particular, a series of small ash cones define a fissure 1.8 km long on the northeastern flank of Batur I which trends towards the Bunbulan crater at the inner caldera margin, and from which at least the youngest of the northeastern postcaldera lavas flowed. Two vegetation-covered ash cones lie on the eastern side of this fissure. A new fissure formed during the 1926 eruption on the southwest flank of Batur III trends towards the Pajang vent on the southwest inner caldera margin. Together with the northeastern fissure on the flank of Batur I, this fissure forms a northeast-trending fissure system that extends across the floor of Batur caldera from Pajang vent in the west to Bunbulan crater in the east.

In addition, a second fissure/crater system trends across the caldera floor orthogonally to the Pajang-Bunbulan system. From northwest to southeast it consists of the vent formed during the 1963 eruptions northwest of Batur I, the elongate ash cone, or fissure, of G. Butus on the northwestern shoulder of Batur I, the summit craters of Batur I and the elongate vent of the 1888 lava flow. The Batur postcaldera stratovolcano therefore lies at the intersection of the two fissure systems. It is interesting to note that these two fissure/crater systems are also oriented parallel to the minor and major axes respectively of the ellipse formed by the outer caldera rim.

These geometrical relationships suggests that the location of Batur volcano was controlled by the intersection of regional-scale faults. The positions of G. Penulisan, G. Abang and Agung volcano on regional extensions of the northwest-trending fissure system support this interpretation. Also, the intersections of the northeast-trending fissure with the inner caldera wall may have controlled the positions of Pajang and Bunbulan craters.

3.2.2 Caldera Stage

The Batur caldera walls expose a thick volcanic sequence which consists almost entirely of dacitic pyroclastic deposits and lava flows. Other pyroclastic sequences which possess essentially identical chemical and mineralogical characteristics to those exposed in the caldera walls also crop out outside Batur caldera in many areas in eastern Bali.

The thickness and volume of the dacite sequence, given its exposure in the caldera walls and extent outside the caldera, and the general rarity of basaltic lavas or pyroclastics lying within it, suggest that the production of dacitic magma was a major but relatively short-lived stage in the evolution of Batur. Because it encompasses the formation of the Batur caldera this stage is referred to here as the caldera stage.

To simplify the following discussion of its stratigraphic relationships the caldera stage is further divided into three phases, relative to the Bali ignimbrite which is the most

voluminous of the pyroclastic sequences outside Batur caldera. These phases are:

(i) the post-Bali ignimbrite phase during which widespread but thin dacitic pumice deposits were produced from a vent at the margin of the inner Batur caldera,

(ii) the Bali ignimbrite phase, which marks the production of the Bali ignimbrite and, by inference, the formation of the second Batur caldera, and

(iii) the pre-Bali ignimbrite phase, during which most of the caldera wall material was produced and which culminated in formation of the first Batur caldera.

a) Post Bali-ignimbrite phase

The Bali ignimbrite is overlain west and north of Batur by several plinian pumice deposits and, possibly, by at least one thick pyroclastic flow deposit south of Batur. The plinian pumice deposits, some of which contain abundant glassy lithic clasts, are locally up to 1.5 m thick in places along the western part of the outer caldera rim between Penelokan and Penulisan. Moreover, they can be observed to drape erosional gullies inside Batur caldera adjacent to the Penelokan-Kedisan road, which indicates that they were produced a substantial period of time after the caldera was formed. The thickest pumice deposits, which also contain the largest pumice clasts, occur on B. Pajang which suggests, together with its crater-like form, that it is the vent from which the post Bali ignimbrite deposits were erupted. Some of the large pumice clasts in these deposits are prominently colour-banded, which will be discussed further in a later section.

Using the work of Kemmerling (1918) and Stehn (1928), van Bemmelen (1949) suggested that the pumice that covers the western part of the outer caldera rim and the northern terrace area was related to a plinian eruption that caused the collapse of the inner Batur caldera. However, these pyroclastic deposits and those which overlie the Bali ignimbrite elsewhere in eastern Bali are relatively thin and have restricted

distributions so they are unlikely to have been related to an eruption of the large magnitude required to produce either or both of the inner and outer parts of Batur caldera.

Several hills lying northeast of Gianyar are capped by deposits at least 10 m thick of pumice-rich breccia which is, in turn, overlain by 1-2 m of laminated, very fine-grained tuff. Although the bases of the breccia deposits have not been observed, the high topographic position of these deposits suggests that they overlie the Bali ignimbrite. The breccia typically consists of leucocratic, finely-vesicular pumice clasts up to 3-4 cm in size supported by a sandy matrix of fine-grained pumice and dark lithics. Larger and darker pumice clasts are present in some places. The breccia shows diffuse subhorizontal lineations, which possibly are due to compaction rather than to sedimentation. The thickness, poor sorting and lack of definite sedimentary structures suggest this deposit is an ignimbrite.

The overlying tuff sequence consists of alternating light- and dark-coloured beds 5-10 cm thick which, in places, show irregular layering caused, possibly, by hydroplastic deformation, suggesting an origin involving water. This interpretation is supported by the presence of load casts in places at the contacts between fine-grained, light-coloured tuff and overlying dark sandy material. Also, an outline of a small fish has been found in the light-coloured tuff. This sequence may have been deposited in water, perhaps in a shallow lake lying on the ignimbrite surface, and been subsequently disturbed.

b) Bali-ignimbrite phase

The Bali ignimbrite was first recognized as a pyroclastic rock by Marinelli and Tazieff (1968) who correlated its production with the formation of the Batur caldera. Virtually all of the basal deposits of the caldera stage sequence identified so far from outside Batur caldera consist of grey, fine-grained, incipiently-welded ignimbrite, or pumice that can be inferred to have been deposited during the same eruption that produced the overlying ignimbrite. The overall character

of these ignimbrite deposits suggest that they are all parts of the Bali ignimbrite. No dacitic deposits that are definitely older than the Bali ignimbrite have yet been found outside Batur caldera.

The main part of the Bali ignimbrite is locally up to 16 m thick and is exposed over approximately 450 km^2 south of Batur, extending almost to the southern coast (Fig. 1.3). It forms the gently south-sloping plains in southern Bali which are intensively cultivated.

Two facies of the Bali ignimbrite are distinguished here. The 'core facies' is composed almost entirely of crystal-poor pumiceous sillar, forming a grey (when dry), homogeneous, fine-grained rock which is widely quarried and carved into the distinctive Balinese statues. Thick deposits of this rock have been observed in deep river valleys near the villages of Kengatan (T. Wos), Pliatan (T. Petanu), Tegalaling, Mengwi (T. Penet), Marga and Pandakgede (T. Jehsung) (Fig. 1.5; Plate 4). In some places (for example, Kengatan), the 'core facies' shows moderately well-developed columnar jointing.

The 'marginal facies' contains abundant, large, dark pumice clasts and generally occurs at the top and distal margins of the Bali ignimbrite. Many of the clasts are rounded but none are flattened. At Kengatan and near Mengwi (where the Denpasar-Tabanan main road crosses T. Penet), the core facies grades upwards into the pumice-rich marginal facies. Enrichment of pumice clasts towards the tops of ignimbrites, often accompanied by reverse grading of the clasts, is thought to be a widespread characteristic of this type of deposit (Sparks et al. 1973; Sparks 1976). Sparks (1976) shows that marginal enrichment and reverse grading of pumice clasts occurs by flotation upwards and outwards of pumice clasts having relatively lower density than the matrix of the pyroclastic flow.

The base of the Bali ignimbrite is best exposed at Marga, where it rests on reddened and gypsum-bearing soil. There, a thick section of the core facies, containing scattered charcoal clasts 10-15 cm in size at its base, is immediately underlain

Plate 4. Bali ignimbrite exposed in the Wos River near Kengatan, central southern Bali. Cliff sequence is about 16 m thick and is being quarried.

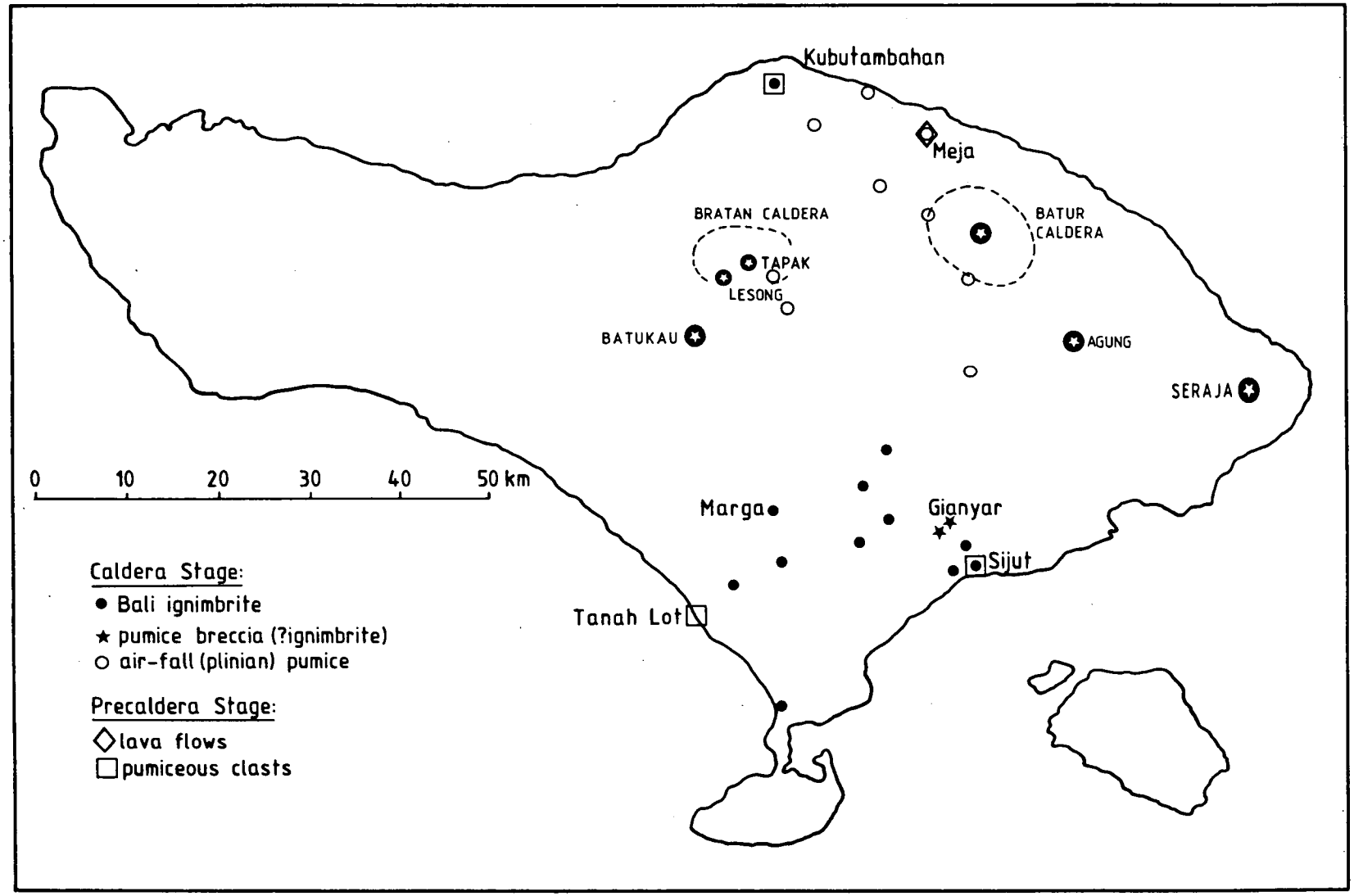

Figure 1.5 Locations of known outcrops of precaldera and caldera stage Batur volcanics outside Batur caldera.

by a 2-3 cm thick deposit of leucocratic, coarse sand-sized pumice which may be part of a co-eruptive, pre-ignimbrite airfall deposit. The thinness of this deposit may suggest that it is a distal part of a deposit which is thicker elsewhere, but not generally exposed.

New ^{14}C ages (analyses by M. Barbetti, The N.W.G. MacIntosh Centre for Quaternary Dating, University of Sydney) of two charcoal clasts from the base of the ignimbrite at Marga are in excellent agreement and give a pooled age of 23,670 +- 210 yrs b.p. for the ignimbrite (Table 1.2), in good agreement with an earlier ^{14}C age of 22,000 +-1500 yrs b.p. from charcoal collected about 20 km east near T. Melangit by Marinelli and Tazieff (1968).

sample	conventional radiocarbon age
SUA2230	23,570 +- 300
SUA2231	23,770 +- 300
pooled age:	23,670 +- 210 years before 1950

Table 1.2 Radiocarbon ages of charcoal clasts from the Bali ignimbrite.

The production of the Bali ignimbrite can be related to formation of Batur caldera rather than Bratan caldera from temporal and also, as will be shown in later discussion, chemical and mineralogical evidence. In particular, as discussed previously, a basaltic lava flow lying over the floor of Bratan caldera is about 100,000 years old, indicating that Bratan caldera formed more then 100,000 years ago. However, the age of the Bali ignimbrite is only about 23,670 years. Therefore, given that its uppermost stratigraphic position, mode of origin, large volume and wide distribution imply that it was produced during a recent, major, highly explosive eruption, the Bali ignimbrite appears most likely to be associated with the formation of the inner, or second, Batur

caldera. Later discussion will show that the chemical and mineralogical characteristics of the Bali ignimbrite are identical to those of dacitic lavas and pyroclastic material exposed in the Batur caldera walls.

a) Pre Bali-ignimbrite phase

The Batur caldera walls expose many types of welded and non-welded airfall and pyroclastic flow deposits which must have been erupted prior to material produced during either of the two caldera-forming eruptions. This sequence is approximately 700 m thick at some localities around the caldera.

Figure 1.6a shows a sketch of the northwestern half of the caldera wall and indicates the main units of the stratigraphy. The steepness of the caldera sides made access to outcrops difficult so most observations were made along their base and in the deep gully in the northernmost part of the caldera wall. Most of the southeastern part of the caldera wall can be reached only by boat and deposits there are less well-exposed than those in the north. Except for a small area in the south near Kedisan, the south-eastern caldera wall was not visited.

In general, as will be discussed, the northern half of the caldera wall consists mainly of breccias and tuffs in the north, together with a thick lava dome, and thick sequences of pyroclastic rocks in the west. In the northern half of the caldera, the Kintamani terrace lies between the inner caldera wall and the outer caldera rim (Fig. 1.3).

Two large explosion craters, Pajang and Bunbulan, occur at opposite sides of the inner caldera, to the southwest and northeast respectively (Fig. 1.3). Pajang straddles the inner caldera wall at the western side of Batur caldera and, as discussed previously, is thought to have been active after formation of the Bali ignimbrite. A strongly-welded, lithic-rich, fiamme-bearing ignimbrite about 7-10 m thick is exposed in the inner caldera wall immediately below and to the south of Pajang.

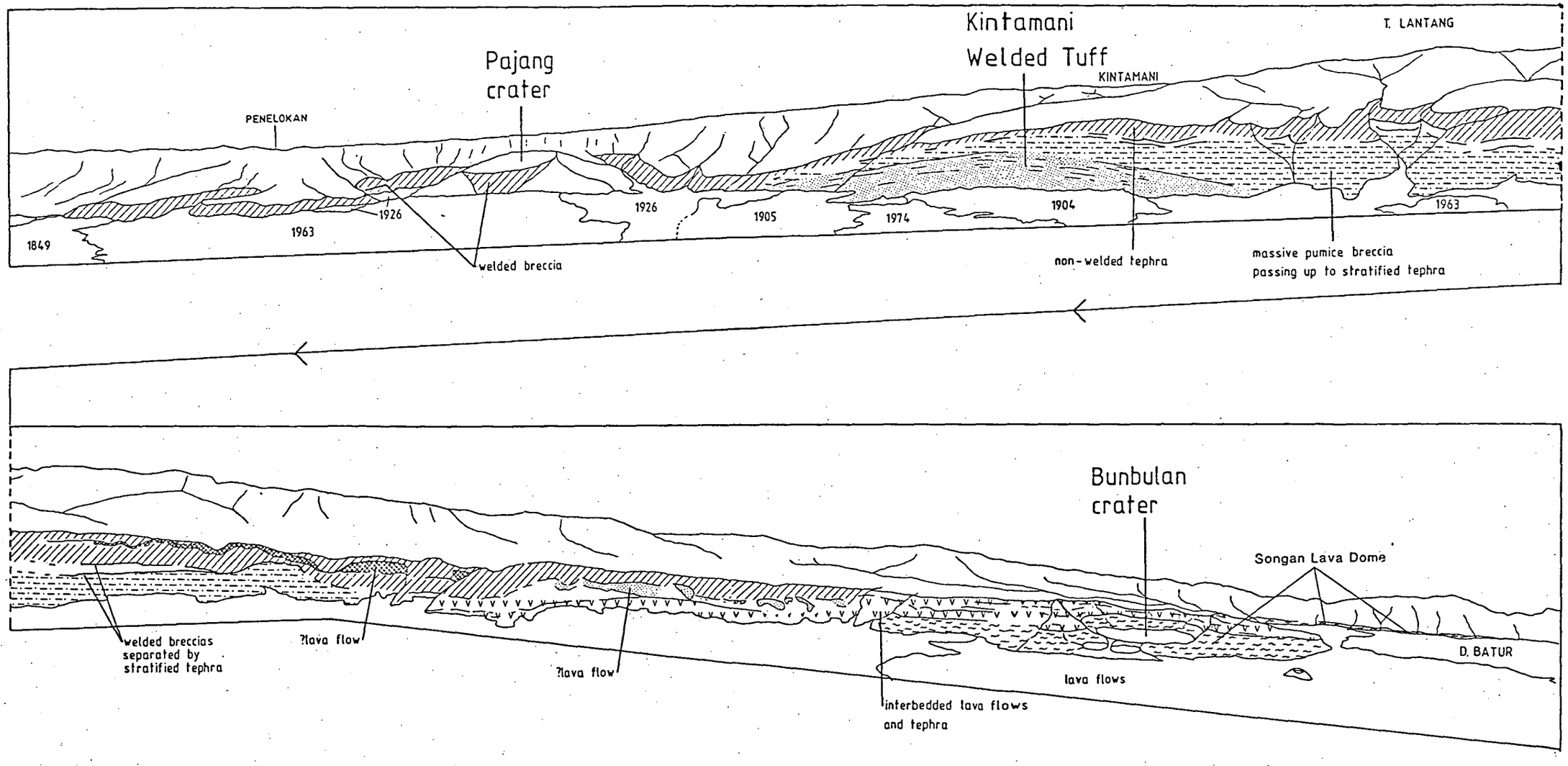

Figure 1.6a General stratigraphy of the northern part of the Batur caldera wall, from a photomosaic taken from the summit of Batur I (Scale: 3 cm is about 1 km).

Bunbulan crater possess a well-formed conical shape when viewed from the northeast and its surface is continuous with the Kintamani terrace (Plate 3). However, the crater is truncated by the inner caldera wall and open towards the centre of the caldera. This suggests that it formed prior to formation of the inner caldera. Several smaller craters lie on the southwestern side of Bunbulan crater and straddle the inferred inner caldera ring fault, suggesting that some localized activity may have occurred close to Bunbulan soon after the inner caldera formed.

A thick, massive dacite lava is exposed in the caldera walls around Bunbulan crater and forms prominent vertical cliffs up to about 100 m high in the lower part of the inner caldera wall near the village of Songan. The sequence is thickest close to Bunbulan crater, where its base is not exposed. It thins laterally for up to 1.7 km northeastwards towards the outer caldera wall.

The top of the lava appears to be slightly convex upwards and its uppermost surface consists of highly fractured black dacitic glass several metres thick. The glass becomes grey, micro-crystalline, and more phenocryst-rich downwards into the main part of the unit. In several places close to the outer caldera wall and along the lower course of the Blinkang River the lava varies markedly in thickness from about 20 m down to 1-2 m within short distances, fills valleys in underlying pumice deposits and directly abuts the outer caldera wall (Plates 5-8).

The form of the lava, particularly the marked decrease in its thickness away from around Bunbulan crater towards the outer caldera wall, suggests that it formed as a large lava dome erupted from a vent located in approximately the same position as the present Bunbulan crater. For convenience, it is named here the Songan Lava Dome.

Prominent red discolouration of adjacent, typically horizontal or inward-dipping, truncated, pumice deposits occurs wherever the sides and base of the lava dome are exposed (Plates 5 and 6). The intensity of the discolouration decreases

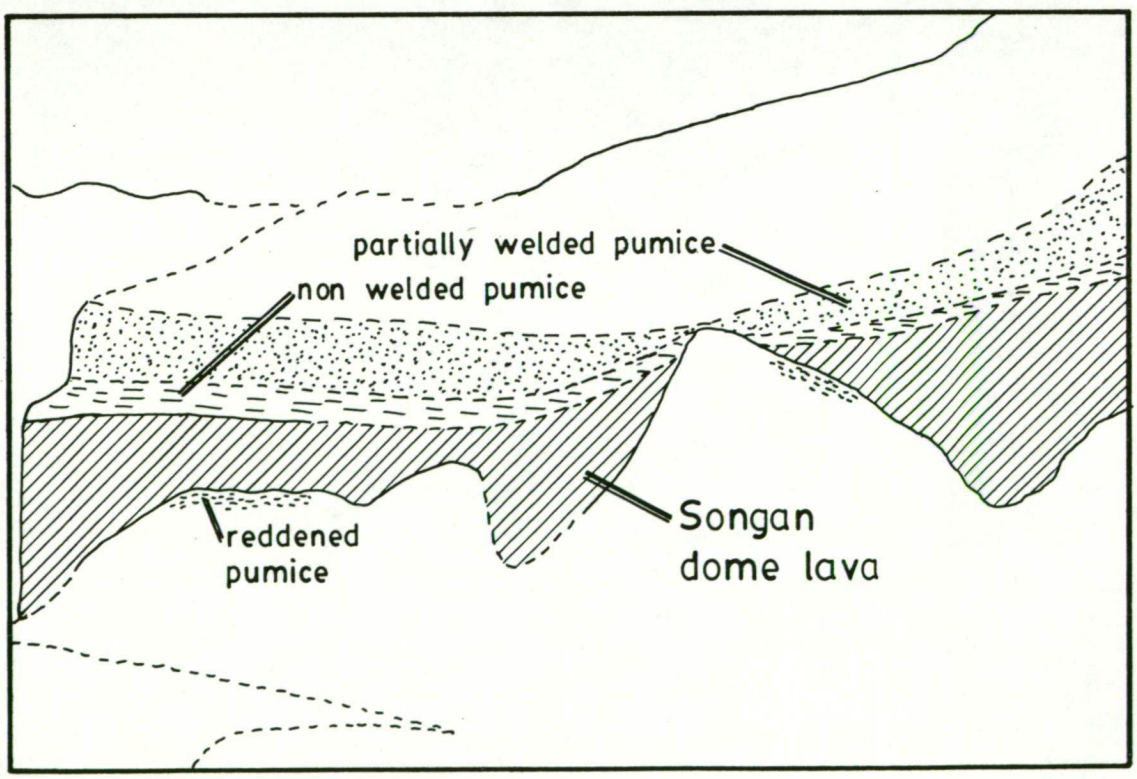

Plate 5. Songan lava dome and conformable pyroclastic sequence unconformably overlying non-welded pyroclastic deposits northeast of Bunbulan crater in Blinkang river valley.

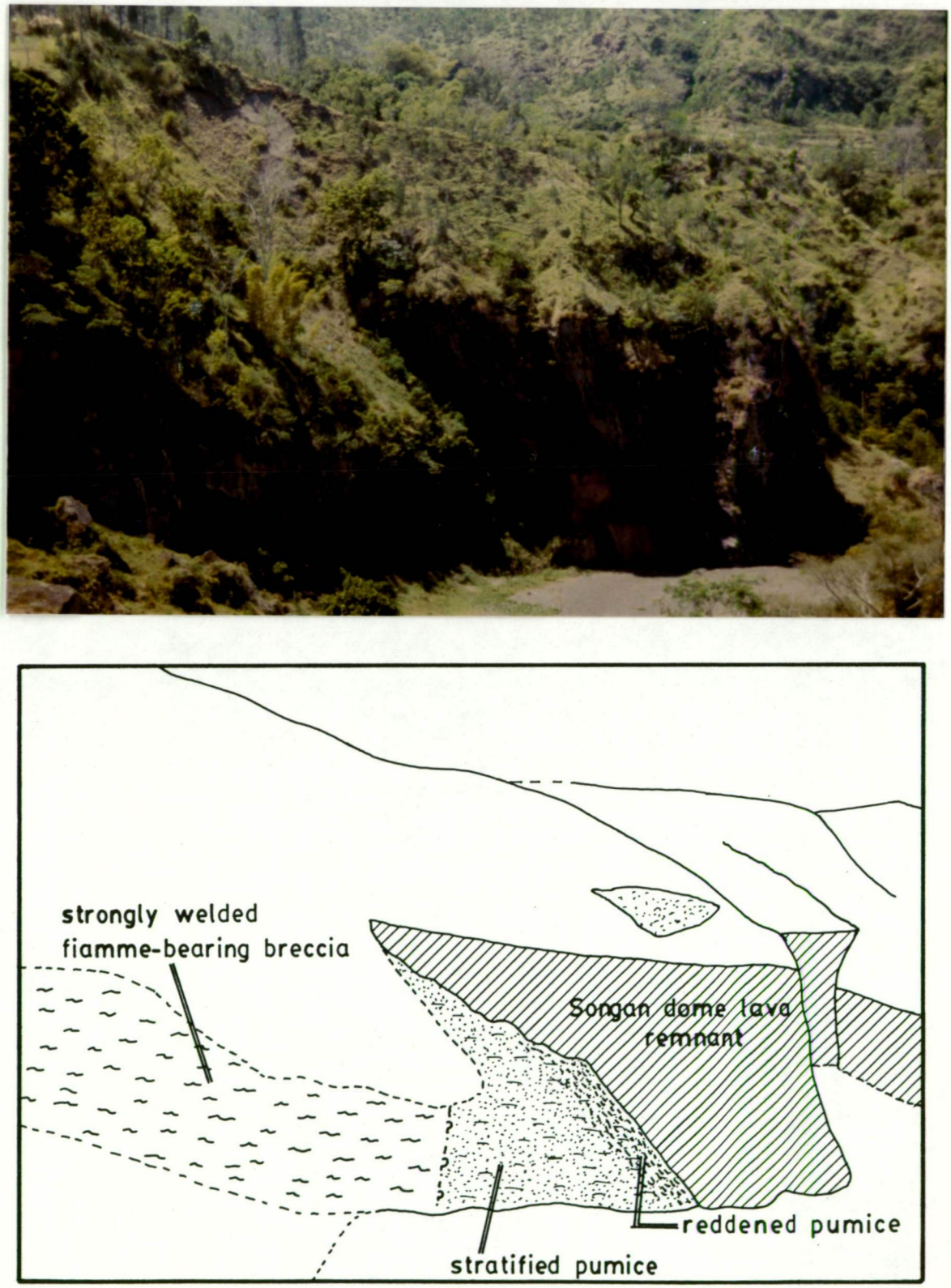

Plate 6. High-angle unconformable contact between the Songan lava dome and underlying pyroclastic deposits exposed in the wall of the Blinkang river valley.

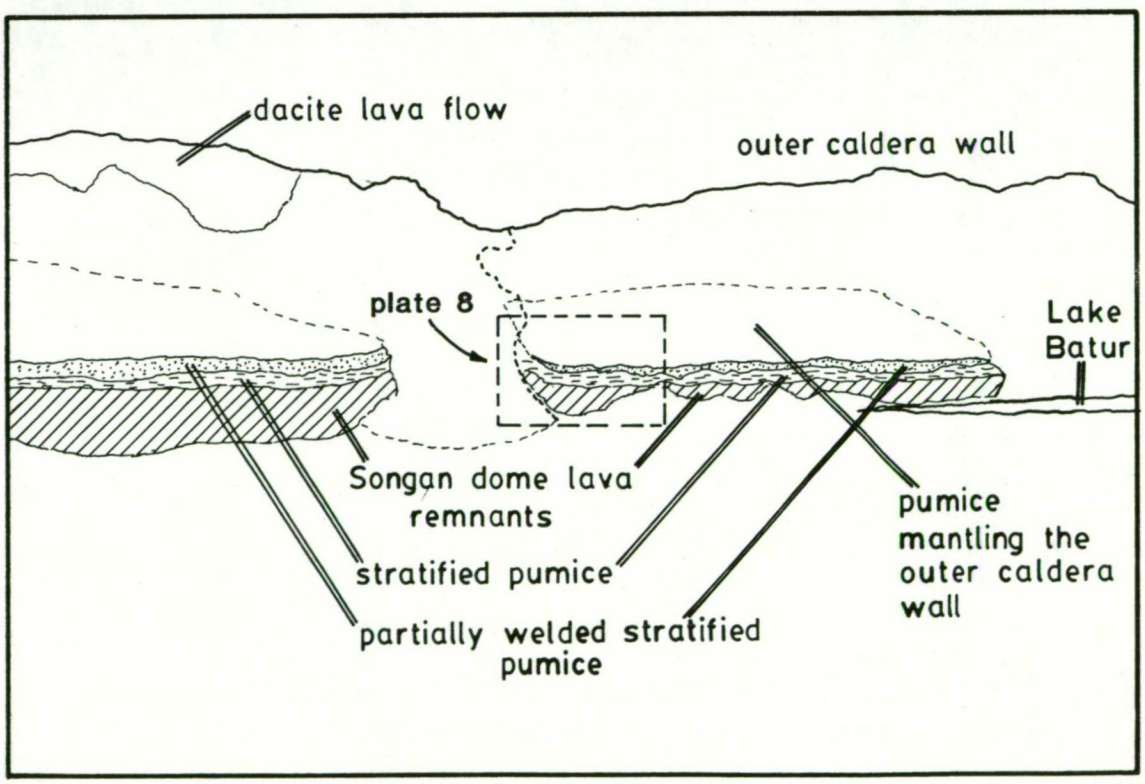

Plate 7. Remnants of the Songan lava dome and conformably overlying pyroclastic sequence lining the base of the eastern part of the caldera wall at the northern end of Lake Batur, east of Songan.

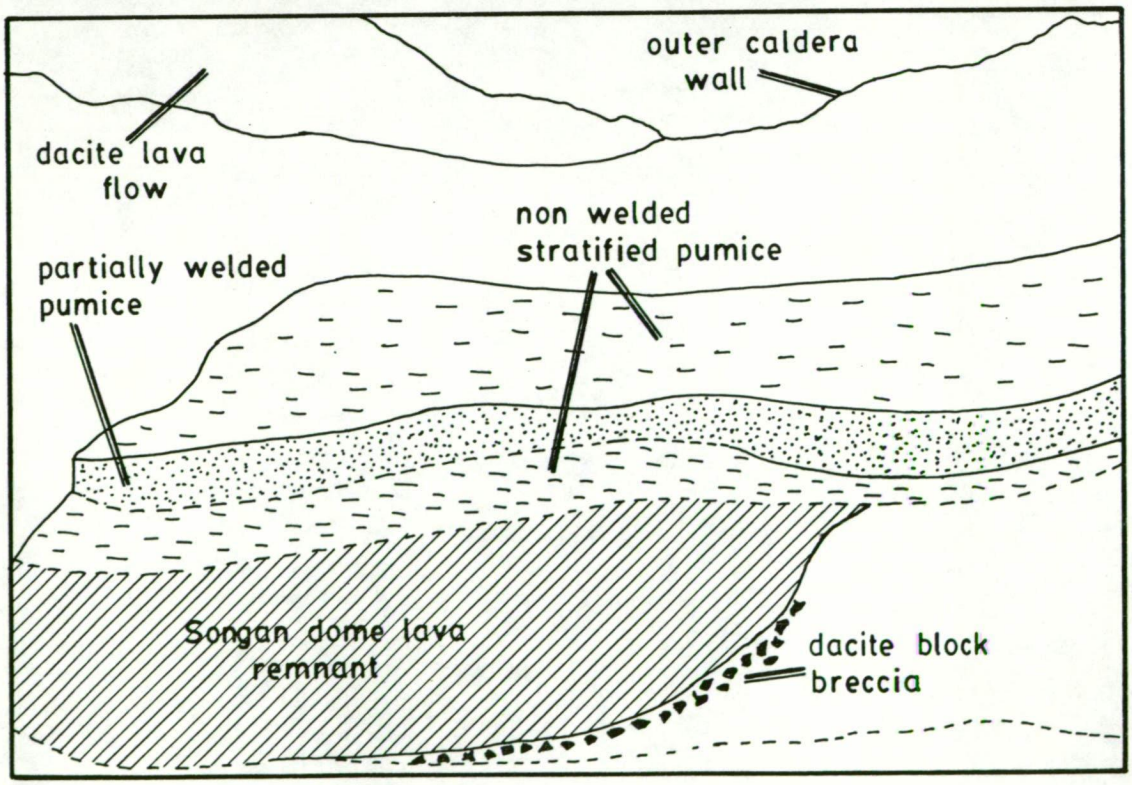

Plate 8. Remnant of the Songan lava dome and conformably overlying pyroclastic sequence in the eastern caldera wall showing high-angle unconformble contact with underlying pyroclastic deposits (see Plate 7 for location).

markedly away from the contact zones which, in some places, are also marked by breccia zones about 1 m thick consisting of black glassy dacite blocks up to about 1 m in size (Plate 8). No evidence that these contacts represent intrusion of the dacite into the pyroclastic sequence, such as occurrences of veining of the dacite lava into the pyroclastic sequence or of sharp chilled margins to the dacite, were found.

Near the northernmost shore of Lake Batur large remnants of the lava dome line the base of the outer caldera wall (Plates 7 and 8), abutting colluvium or truncated pyroclastic pumice deposits. The latter generally consist of bedded, well-sorted, airfall pumice and possess both horizontal and inward-dipping bedding. The remnants are everywhere conformably overlain by a sequence 3-5 m thick of pumice and clastic airfall deposits and, uppermost, a 5-10 m thick, bedded, incipiently to strongly welded, airfall pyroclastic deposit. Individual beds within this unit are up to 10 cm thick.

Although these overlying pyroclastic deposits show apparent horizontal layering when viewed from the west (Plate 7) they actually dip and face into the caldera, mantling both the mid parts of the outer caldera wall and the abutting Songan lava dome. This pyroclastic sequence thins upwards and outwards from the caldera, terminating beneath the outer caldera rim where the slope is probably too steep for the material to have accumulated. The sequence also outcrops almost continuously over the lava dome in the Blinkang river valley walls but cannot be reliably identified elsewhere in the caldera wall sequence.

The relationship of the Songan lava dome to older dacitic rocks is particularly important for identifying the structural evolution of Batur. The presence of the high-angle, non-intrusive, contact zones between the lava dome and essentially horizontally bedded dacitic pumice deposits in the base of the outer caldera wall indicates that the lava dome formed after the outer caldera was produced, and prior to formation of the inner caldera.

Also, the western and southern parts of the Songan lava

dome probably now lie beneath the inner caldera floor, with the inner caldera ring fault having passed through near the centre of the dome. If those parts were as extensive as the north-eastern part then the overall diameter of the unit was perhaps 3-4 km. The lava remnants lining the base of the outer caldera wall east of Songan were probably produced as the inner ring fault passed close to the site of the outer caldera wall.

In turn, therefore, because it largely overlies the Songan lava dome west of Bunbulan crater, the thick dacite sequence exposed in the inner caldera wall, and underlying the Kintamani Terrace, must also have been produced in the period between the formation of the outer caldera and the formation of the inner caldera. The stratified pumice deposits which overlie the lava dome and which mantle the outer caldera wall also suggest this relationship.

Another prominent deposit in the Batur caldera walls is a thick, parallel-bedded, strongly welded pyroclastic breccia which forms a broad, apparently anticlinal sequence in the inner caldera wall beneath the village of Kintamani. The sequence is about 100 m thick and is unlike the equally strongly welded ignimbrite, described previously, lying beneath Pajang vent which possesses no internal sedimentary structures.

Individual beds in this unit vary in thickness from 5-10 cm to approximately 1 m and, in many places, display prominent black, glassy fiamme and small, angular lithic clasts in a pinkish-red matrix. In other places, the fiamme are grey to purple in colour and lie in a dark grey matrix. The fiamme vary generally from 1 to 10 cm in length and appear to be flattened pumice. The black fiamme are generally smaller and may represent flattened black, glassy bombs and clasts which are moderately abundant in many of the caldera stage pyroclastic deposits.

This strongly welded sequence is possibly that occurring beneath Kintamani which Marinelli and Tazieff (1968) describe as a 'very compact, red with black fiamme' ignimbrite and which they correlated with the Bali ignimbrite. However, its

anticlinal form suggests that it is mantling pre-existing topography, and the parallel-bedding indicates that it was produced by airfall processes, rather than by pyroclastic flow. These characteristics suggest that the unit is a welded airfall tuff. For convenience, it is named here the 'Kintamani Welded Tuff' (KWT).

Strongly-welded airfall tuffs have been recognized at Santorini (Greece) and Askja (Iceland) volcanoes (Sparks & Wright 1979) and at Pantelleria volcano (Italy) (Wright 1980). This type of pyroclastic deposit is thought to be produced close to vent as a result of high rates of discharge and accumulation of pyroclastic material (Sparks & Wright 1979). The KWT of Batur is much thicker than any known deposit of this type, although a sequence 70 m thick of Ordovician age has been indentified in Norway (Suthren & Furnes 1980).

The KWT is overlain by a thick sequence of non-welded pumice which is thickest where the northwestern wall is incised by T. Lantang and which appears to thin substantially towards the west. The lower part of this sequence, which is exposed at the base of the T. Lantang valley walls, consists of an approximately 70 m thick, massive deposit of mainly leucocratic pumice and scattered black, glassy clasts and blocks. The material is generally poorly sorted, with the larger clasts, mainly of pumice, being supported in a matrix of finer material. The largest pumice clasts are typically approximately 10 cm across, and the glassy blocks range up to approximately 30 cm in size. Crystalline, plagioclase-phyric lithic clasts are also present but are typically of small size. A persistent layer of large glassy blocks occurs in this deposit 1-2 m above the valley floor. The upper part of the sequence consists of stratified deposits of fine-grained ash and pumice.

The general characteristics of this deposit, including its variable thickness (apparently valley-filling), poor sorting and lack of internal sedimentary structures, suggest it was produced by pyroclastic flow. The occurrence of a concentration of large glassy blocks near the base of the deposit is consistent with this interpretation. Similar lithic concentrations in pyroclastic flow deposits elsewhere are

thought to be the result of the relatively high densities of the blocks, which cause them to sink during fluidized flow (Sparks et al. 1973; Sheridan 1979). If this interpretation is correct then, according to the column collapse model for the production of high-volume pyroclastic flows (Sparks & Wilson 1976; Sparks et al. 1978), it is possible that the strongly-welded KWT and the overlying non-welded pyroclastic flow, or ignimbrite, were produced during the same eruption.

The upper part of the northern caldera wall sequence in the T. Lantang valley consists of a series of approximately 1 m thick units which consist of massive, poorly-sorted pumice underlain by finer pumice showing low-angle crossbedding. These are interpreted to be small pyroclastic flows with ground surges. Stratified airfall pumice deposits also occur in this sequence.

Two dark, welded breccias, each 3-4 m thick and separated by stratified pumice deposits, are also prominent in the northwestern caldera wall. The breccias contain abundant, angular lithic blocks supported in a glassy matrix and display wavy, sub-horizontal lineations. The two units are unlike the KWT, because they do not show internal sedimentary structures, and are probably ignimbrites. A similar welded breccia, approximately 10 m thick and displaying prominent black fiamme, occurs at the base of the western part of the caldera wall near B. Pajang. This deposit is underlain by non-welded pumice and is much thicker than either of the welded breccias lying above the KWT. However, if each of the welded deposits are ignimbrites then it is possible that the thick breccia near B. Pajang represents a valley-filling equivalent of at least one of the two welded breccias farther north.

Black, glassy material is a ubiquitous component of the caldera-stage pyroclastic deposits. Although it typically occurs as angular clasts and blocks, breadcrust and fusiform bombs have also been found. Many samples show prominent, irregular, lenticular colour-banding, with individual bands ranging generally in thickness from a few to about 50 millimetres. The light-coloured bands are much duller than the dark-coloured bands, which show vitreous lustre.

3.2.3 Precaldera Stage

There is no direct evidence available to indicate the size and form of Batur volcano during its precaldera stage but it presumably was similar to other large island arc basaltic to andesitic stratovolcanoes, such as Agung. Based on its present area and the slopes of its flanks, Batur volcano may have grown to 2500-3000 m above sea level before its caldera was formed (Fig. 1.4).

Inside the caldera, mafic volcanics which were erupted before Batur caldera formed have been found in only one locality, at the base of the outer caldera wall near Kedisan. There, a sequence of eight thin basalt lava flows, separated from each other by breccias, is exposed. This sequence is interpreted as marking the top of the precaldera stage volcanic sequence (Fig. 1.4).

Rocks erupted from Batur volcano prior to eruption of the dacitic sequence during the caldera stage crop out rarely outside Batur caldera because of the widespread cover of younger tephra and the absence of substantial erosion of the flanks of the volcano. However, an outcrop consisting of several basaltic lavas was found in a deep river valley formed in the northern flank of Batur volcano. In addition, thinly-bedded, mafic pyroclastic sequences, which are lithologically, mineralogically and chemically unlike those in the caldera stage sequence, crop out in several localities near the northern and southern coastlines of Bali. In all localities these rocks underlie the Bali ignimbrite.

At Tanah Lot, at the south coast of Bali and about 50 km southwest of Batur (Fig. 1.5a), a 5-6 m thick sequence consisting of generally well-sorted, parallel-bedded, gravel-sized pumice and scoria occurs. The sequence extends beneath sea level and is capped by an approximately 1.5 m thick soil deposit that contains short, light-coloured streaks that may represent decomposed roots or twigs. Some pyroclastic beds contain rounded, black, pumiceous andesite clasts up to 10-15 cm in size and a few show reverse grading. Metre-scale scours and high angle cross-bedding are present in places. These

appear to have been produced by post-eruption fluvial reworking processes.

The pumice clasts in these deposits are usually denser, darker and less vesicular than the pumice that was erupted during the caldera stage. As will be shown in a later section, they are also more mafic in composition.

Similar pyroclastic material occurs in deposits located 37 km south of Batur in southeastern Bali, in the T. Mengit valley near Sijut. Deposits consisting mainly of large, black pumice clasts occur at the base of the sequence, forming the floor of the valley. These pass upwards into a series of about ten 20-30 cm thick deposits of generally poorly-sorted, thinly-stratified deposits of black ash and pumice, many of which show low-angle, 'wavy' cross-stratification at their bases. Some massive beds are also present. This sequence is interpreted to be a series of thin ignimbrites, some of which possess ground surge deposits. It is overlain by approximately 3 m thick deposit of moderately sorted, probably airfall, pumice which is, in turn, overlain by approximately 4 m of incipiently welded, pumice-rich breccia.

The topmost unit at the Sijut locality is lithologically very similar to occurrences elsewhere of the Bali ignimbrite, which forms a major part of the caldera stage deposits. If it is part of the Bali ignimbrite, or is a similar but separate pyroclastic flow, then, according to the column collapse mechanism for the production of pyroclastic flows (Sparks et al. 1973; Sheridan 1979), the underlying pumice deposit may have been its airfall precursor. Both of these deposits, therefore, probably form part of the caldera stage sequence.

The basal deposits of large pumice clasts, and the material forming the thin ignimbrites, are lithologically very similar to the pyroclastic material at Tanah Lot and, therefore, form part of the precaldera stage deposits. Similar pyroclastic material, together with large palaeosoil boulders, also occurs in the bed of T. Mengit 2.3 km north of the Sijut locality (Fig. 1.5), where the main road between Gianyar and Klunkung crosses the river.

A thick, poorly-sorted breccia containing abundant black pumice clasts up to 10 cm in size occurs at the base of a river valley near Kubutambahan in northern Bali, 29 km northwest of Batur. The pumice clasts are like those at Tanah Lot and at Sijut. This deposit is at least 5 m thick and extends laterally for at least 1 km. It is overlain generally by a 2-3 m thick, grey, massive breccia consisting of large, highly vesicular, undeformed pumice clasts supported in a compact, ashy matrix. Like the topmost deposit at Sijut, this rock is similar to the Bali ignimbrite.

The sequences at these three widely-spaced localities are generally very similar, and two of them contain the stratigraphic boundary between the precaldera and caldera stages. The top of the precaldera stage is marked by thick deposits of mainly dark, dense pumice and ash and their wide distribution indicates that Batur volcanism was affecting nearly all of eastern Bali at the time they were produced.

Because of their large size, relatively high density and substantial distance from Batur volcano, many of the pumice clasts contained in the precaldera pyroclastic deposits are unlikely to have reached their present positions ballistically. The most likely transport mechanism, which is indicated also by the characteristics of some of the deposits, seems to be pyroclastic flow, although eruptions of this type are rarely associated with such mafic compositions. However, a substantial pyroclastic flow of basaltic material is known to have occurred during the 1970 eruptions of Ulawan volcano in Papua New Guinea (Johnson et al. 1972). The 1886 Tarawera eruption in New Zealand, which produced a plinian eruption column thought to be about 28 km high, was also of basaltic composition (Walker et al. 1984). Pyroclastic eruptions of the St-Vincent type also involve basaltic andesite material but are typically associated with the formation of domes and contain lithic rather than pumiceous clasts (Roobol & Smith 1976).

The precaldera stage lava flows exposed in the northern flank of Batur volcano generally contain abundant plagioclase together with olivine, rare clinopyroxene and Ti-magnetite

phenocrysts, and have glassy groundmasses. A weathered lava lying at the top of the northern flank of Batur possesses abundant, particularly large (4-8 mm) plagioclase phenocrysts.

Another lava, that is exposed along the coast north of Batur, in places shows well-developed, large-scale spheroidal jointing, forming slate-like rock fragments which are quarried as local building material. It is overlain generally by less than 2 m of dacitic tephra and soil, which includes a thin plinian pumice deposit that may correlate with stratigraphically high outcrops of similar material in northern and central Bali, indicating that it was erupted late in the precaldera stage or, more likely, during the subsequent caldera stage. It is important to note that thick sequences of dacitic pyroclastics, similar to those that occur generally south of Batur, are not present in the north.

3.3 Evolution of Batur Volcano

Because of its association with relatively small volumes of siliceous pyroclastic deposits (compared to the large rhyolitic calderas in, for example, Japan, New Zealand and North and South America) and with basaltic lava flows, Batur caldera falls into the 'Krakatoan' (Williams & McBirney 1979), or 'stratocone' (Wood 1984), class of calderas. These calderas are thought to form by collapse of the upper parts of large stratovolcanoes following explosive evacuation of shallow, underlying magma chambers (Williams & McBirney 1979). The 'Katmai' type is similar but drainage of the magma chamber occurs via new volcanoes or fissures that lie outside the base of the stratovolcano (Williams & McBirney 1979).

Williams and McBirney (1979) compared Batur caldera (they referred to it as a cauldron) with the 'Masaya' class of calderas, which they consider to form by subsidence of the central parts of broad basaltic shields in the absence of explosive eruptions. This comparison is inappropriate because of the evidence from the dacitic pyroclastics of highly explosive volcanism during the evolution of Batur volcano.

However, the near-coeval eruptions of Batur and Agung

volcanoes in 1963 and the short distance between them (18 km) suggests that their respective plumbing systems may be interconnected. This possibility, together with presence of the B. Paleg vent to the northeast of Batur, outside the caldera, suggests that some Katmai-type activity may have occurred during formation of Batur caldera but there is no evidence that it was substantial. The concentration of pyroclastic material in the Batur caldera walls suggests that eruptions from a central vent comprised the primary pattern of activity.

In summary, the evolution of Batur volcano has been divided into three main stages based on the stratigraphy of its products. The structural evolution of Batur is shown diagrammatically in Fig. 1.6b.

The oldest-known volcanic products of Batur are those found in the valley of the Meja river on the outer northern flanks of Batur caldera. K-Ar age determinations of two of these basaltic and basaltic andesite rocks indicate that some of these rocks are more than 0.5 Ma old.

These flows and associated mafic breccias and ashes pass upwards into unusual deposits of dark, pumiceous, andesitic material located on both the northern and southern coasts of eastern Bali up to 50 km from Batur. Parts of these deposits show evidence of having been affected by secondary, fluvial reworking processes but other characteristics such as the presence of poorly-sorted massive beds with thin underlying deposits showing wavy cross-stratification, suggest that they were erupted as pyroclastic flows. These two groups of early volcanic material from Batur were erupted during the precaldera stage.

The subsequent caldera stage is characterized mainly by the explosive eruption of dacitic material, forming thick sequences of pyroclastic deposits of many types exposed in the walls of Batur caldera and elsewhere in eastern Bali, and at least one large lava dome inside Batur caldera. The age of the start of the caldera stage is unknown but, from the presence of about eight basaltic lava flows interbedded with dacitic material at the base of the Batur caldera wall which contain no

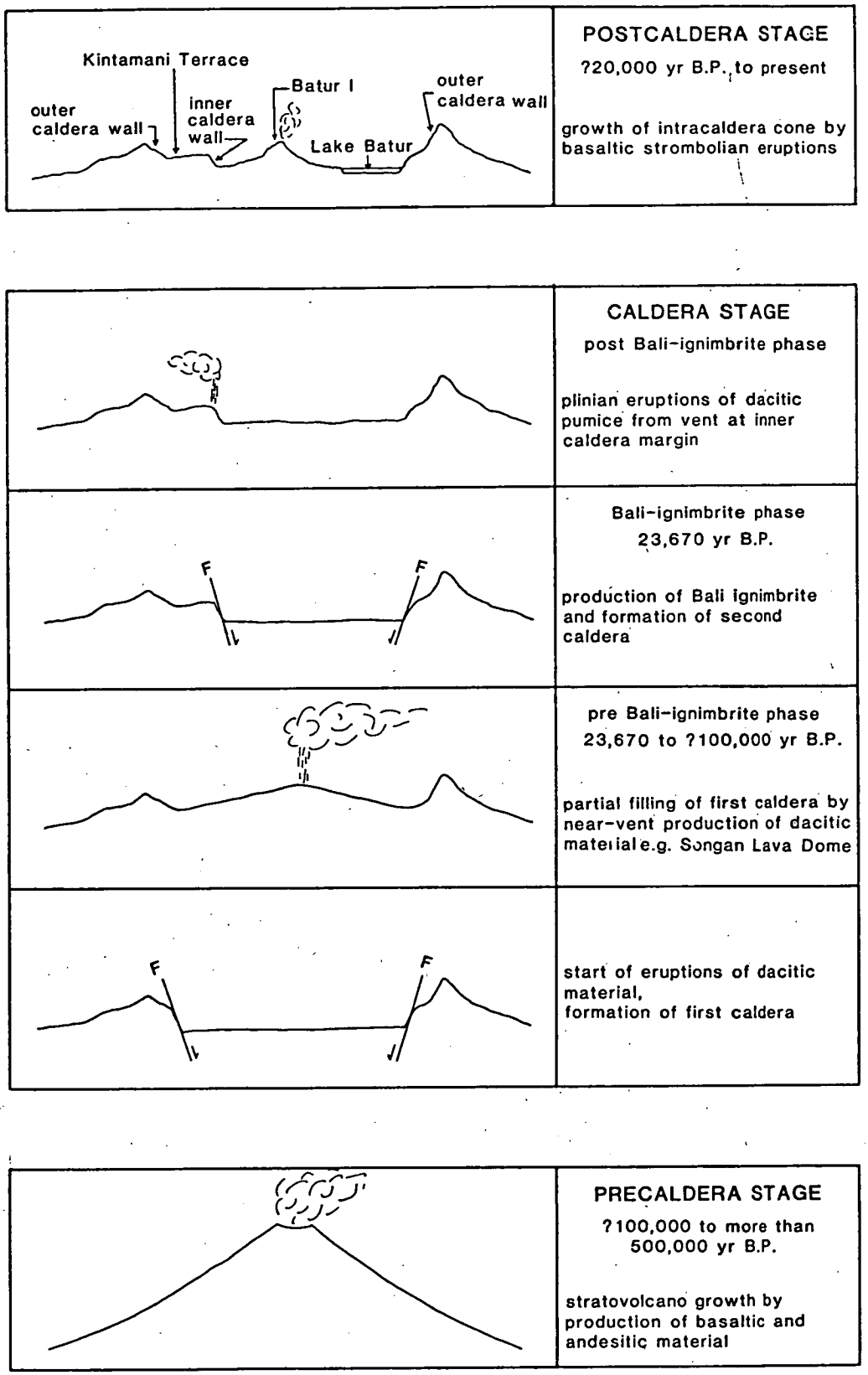

Figure 1.6b Major stages in the evolution of Batur volcano.

radiogenic Ar, it probably began much less than 100,000 years ago.

Batur caldera now possesses two prominent, concentric scarps, separated in the northern half of the caldera by the Kintamani terrace. Stehn (1928), van Bemmelen (1949), Marinelli and Tazieff (1968) and Williams and McBirney (1979) deduced that Batur caldera was formed by at least two caldera-forming eruptions. It is not clear whether these authors considered the Kintamani terrace to be either a fault block bounded by the concentric caldera ring faults, or a caldera-filling sequence bounded on one side by an angular unconformity against the outer caldera margin and truncated on the other by the inner caldera ring fault.

The volcanic stratigraphy exposed in the eastern part of the caldera walls around Songan indicates that the terrace originates from partial filling of a pre-existing caldera. In particular, the Songan Lava Dome clearly abuts truncated pyroclastic deposits in the lower part of the outer caldera wall east of Songan and is overlain by a thick, partially welded, stratified airfall pumice deposits which form the floor of the terrace and in places mantles the middle and upper parts of the outer caldera wall.

The apparent accumulation of dacitic, near-vent, filling material in the northern part of the outer caldera compared to the southern part, which is now occupied by Lake Batur, may suggest that the source of the filling material lay in an eccentric position relative to the outer caldera margin, that is, north of the centre of the outer caldera. Alternatively, the northern and southern halves of the inner caldera ring fault may not have been continuous, with the southern half being displaced towards the southeast and essentially coincident with the southern part of the outer caldera ring fault.

The second, inner caldera therefore formed as a result of the partial collapse of the filling material into a magma chamber that was largely emptied by another major eruption of dacitic material. Material ejected from the chamber during this

eruption now forms the voluminous and widespread Bali ignimbrite. This caldera-forming event occurred about 23,670 years B.P. as deduced from ^{14}C ages of charcoal clasts in the base of the Bali ignimbrite.

These stratigraphic and isotopic age relationships imply that the first Batur caldera formed a substantial period of time before the second Batur caldera but less than 100,000 years ago. During that period, the Songan Lava Dome was produced, possibly soon after formation of the first caldera, together with the Kintamani Welded Tuff and the overlying welded and non-welded airfall pumice deposits, pumiceous surges and rare dacite lava flows exposed in the inner caldera walls.

At present, no ignimbrite or other pyroclastic deposits which could be associated with formation of the first Batur caldera are known from either inside or outside the caldera. Similarly, no pyroclastic deposits produced during formation of Bratan caldera, located 28 km west of Batur, have been identified. These deposits presumably exist, given that the formation of virtually all large stratovolcano calderas is also marked by eruption of voluminous pyroclastic material, but they are now covered by the widespread Bali ignimbrite and younger pyroclastic deposits.

Following formation of the inner caldera dacitic material continued to be erupted from the Pajang vent at the western margin of the inner caldera. This peak possesses conical form, as well as a crater that is open towards the centre of Batur caldera. It is also draped by a thick deposit of dacitic pumice which includes the largest pumice clasts found around Batur caldera. Several pumice deposits, up to about 3 m thick, drape the western rim and inner wall of the caldera, and others, less thick, occur up to west and north of the caldera. The ages of these deposits are unknown, although they overlie the Bali ignimbrite outside Batur caldera and therefore must have been erupted less than about 23,000 years ago.

The dacitic material erupted from the Pajang vent represents the terminal stage of dacitic activity of Batur volcano, and presumably ceased when all of the dacitic magma

had been erupted or had crystallized at depth. Since then the composition of the material erupted from Batur has changed markedly to basaltic, with the growth of the new Batur stratovolcano during the lastest, and continuing, postcaldera stage of the evolution of Batur. The character of the volcanic activity of Batur consequently changed to the much less explosive strombolian style which characterizes the historical eruptions.

4. PETROGRAPHY AND MINERALOGY

4.1 Petrography

4.1.1 Mafic Volcanics

The basaltic and basaltic andesite lava flows from the pre- and postcaldera stages are generally similar petrographically, consisting mainly of 20 to 30 % olivine, clinopyroxene and abundant plagioclase phenocrysts in hypocrystalline groundmasses. Ti-magnetite occurs abundantly in some rocks but orthopyroxene has been found in only one sample. Basaltic andesites and andesites of the precaldera stage are petrographically distinct from the more mafic volcanics, being much poorer in crystals. Point-counted modes of 13 postcaldera basaltic lavas are listed in Table 1.3.

Plagioclase phenocrysts in the basalts are typically tabular, up to 2 mm in size, and multiply twinned, with most showing large skeletal or mottled, unzoned cores and thin, oscillatory-zoned rims. Glass forms most of the inclusions in these crystals, with clinopyroxene and olivine inclusions less abundant. Another type of plagioclase phenocryst also shows tabular habit and twinning but contains few, if any, melt or mineral inclusions. The cores of many of these phenocrysts are surrounded by narrow mottled regions which, in turn, are surrounded by clear, oscillatory-zoned crystal rims. These 'clear' phenocrysts are the dominant type in some lavas, particularly the postcaldera 1888 (67257) and 1904 (67250) lavas, and a precaldera lava (67339) which contains abundant, euhedral crystals up to 8 mm in size.

sample	year of eruption	OLV	CPX	PLAG	MAG	GMASS
67238	1974	1.3	0.4	17.5	0	80.8
67240	1963	0.5	0.3	19.1	0	80.1
67247	1905	2.2	0.1	15.7	0.2	81.8
67250	1904	1.6	0.4	21.6	0.1	76.3
67257	1888	2.2	0.5	20.5	0.1	76.7
67259	1849	0.6	0.4	25.2	0	73.8
67272		0.1	0.2	23.3	0.4	76.0
67271		1.0	0.8	19.7	0.6	77.9
67266		0.2	0.2	21.5	0	78.1
67264		1.7	2.7	20.6	0.2	74.8
67263		0	1.3	10.9	0.6	87.2
67262		1.5	5.6	19.9	0.5	72.6
67261		2.0	3.3	17.5	0.2	77.0

Table 1.3 Point-counted, vesicle-free modes of selected postcaldera basaltic lava flows from Batur volcano. Modes determined by counting a grid of 2604 points over a photomicrograph showing approximately 2 x 1.5 cm of a thin section. (OLV=olivine,CPX=clinopyroxene,PLAG=plagioclase, MAG=Ti-magnetite,GMASS=groundmass)

Similar crystals, together with olivine crystals, form scattered clusters 2 to 3 cm across in a postcaldera lava flow (67265) exposed at the northern foot of the present Batur cone. Both types of plagioclase phenocryst occur in the 1905 (67247) lavas as well as in many of the prehistoric, postcaldera lavas. The 'skeletal' type is dominant in the historical lavas erupted since 1926.

Clinopyroxene phenocrysts occur in all mafic rocks, although in very low abundance in some rocks. They typically occur as subhedral crystals up to 0.5 mm in size which generally contain inclusions of, or lie in contact with, Ti-magnetite crystals. Olivine occurs in slightly higher abundance than clinopyroxene (Table 1.3), generally as subhedral crystals up to 0.5 mm in size, although embayed and rounded crystals are prominent in some rocks and euhedral crystals in others. A few olivine crystals contain very small inclusions of Cr-spinel and glass. Large olivine crystals, possessing well-formed crystal faces but typically with skeletal morphology, occur in the precaldera stage andesite flow (67342). The abundance of Ti-magnetite phenocrysts, which occur as small euhedral crystals, seems to correlate positively

with clinopyroxene abundance (Table 1.3), although they are absent from many of the basaltic lavas.

The groundmasses of the basaltic lavas varies widely in texture. In the recently erupted historical lavas the groundmass typically consists of black glass and scattered, small plagioclase laths and clinopyroxene grains. In some of the older lavas the glass is brown in colour. However, most of the lavas contain more crystalline and, in some rocks, fluidal groundmasses, which consist of abundant plagioclase laths and microgranular clinopyroxene and Ti-magnetite.

4.1.2 Dacitic volcanics

The dacitic rocks contain a larger assemblage of phenocrysts than the basaltic lavas, which consists of plagioclase, clino- and orthopyroxene, olivine, apatite, Ti-magnetite and, in one sample, ilmenite. Pigeonite occurs in the groundmasses of some of the rocks. However, the dacites contain much fewer phenocrysts than the basalts and are characterized by their glassy, or very fine-grained, appearance and the presence in some glassy blocks and larger pumice clasts of prominent, fluidal colour banding.

In contrast to the skeletal phenocrysts in the basaltic rocks, plagioclase phenocrysts in the dacites contain only scattered inclusions of clinopyroxene, apatite and glass. The phenocryst are typically tabular in shape and range in size up to about 2 mm in size. They are usually optically irregularly zoned, with only some larger crystals showing strong oscillatory zoning. Thin crystal rims are typically absent. Many plagioclase phenocrysts lying within the light-coloured bands are rounded and embayed compared with those in the darker bands.

Clinopyroxene, orthopyroxene and olivine occur as subhedral crystals up to 1 mm in size, some of which contain apatite laths as inclusions. Like those in the basaltic rocks, pyroxene crystals typically are associated closely with Ti-magnetite crystals. A few clinopyroxene crystals in some rocks are surrounded by thin rims of pigeonite. Several rocks

contain ophitic glomerocrysts consisting of plagioclase crystals enclosed by clinopyroxene.

Ti-magnetite phenocrysts are abundant in all of the dacites, occurring as small euhedral crystals. Ilmenite has been found in only one rock (67277). Apatite typically occurs as small laths that form inclusions in other minerals. However, larger laths up to 0.5 mm long occur as discrete phenocrysts in some rocks.

The groundmasses of the dacitic blocks and lavas vary widely in crystallinity and appearance, with the lavas typically containing the more crystalline groundmasses. The banding shown by many of the glassy blocks is very striking in thin sections and in many places wraps around large phenocrysts. The dark-coloured bands consist mainly of black glass, while the light-coloured bands have an variolitic, cryptocrystalline appearance, showing sperulitic birefringence and, in some rocks, intermeshed and radiating ?plagioclase microlites. The dacitic lava flows show a pilotaxitic texture with groundmasses consisting of plagioclase laths, granular Ti-magnetite, interstitial glass and, in some rocks, small prisms of pigeonite.

The dacitic pyroclastic rocks, including the Kintamani Welded Tuff and other welded deposits, pumice clasts and the Bali ignimbrite, are markedly more heterogeneous in texture than the glassy blocks and lavas. The welded pyroclastics typically contain abundant, small lithic and pumice clasts which are supported in a glassy, phenocryst-bearing matrix. The matrix material contains the same phenocryst assemblage as the dacitic blocks and lavas. The lithic clasts usually show sharp, angular boundaries with the matrix and mostly resemble the dacitic lavas in phenocrysts and texture. Clasts of basaltic material, showing olivine, clinopyroxene, Ti-magnetite and skeletal and complex plagioclase phenocrysts in a black, glassy groundmass, are rare. The pumice clasts are generally lenticular in shape, poor in phenocrysts and show diffuse boundaries with the matrix.

The core facies of the Bali ignimbrite, and pumice clasts

from non-welded deposits and the marginal facies of the Bali ignimbrite, generally contain very few phenocrysts. Where they are found, their mineral assemblage is like that of the dacitic blocks and lavas. Mostly, however, these rocks consist of highly vesicular pale brown glass, together with very rare lithic and other pumice clasts. Vesicles in the Bali ignimbrite have been slightly flattened.

4.2 Mineral Chemistry

The chemical compositions of minerals in the Batur volcanic rocks were determined using an energy dispersive analytical system attached to a JEOL JXA-50A scanning electron microprobe. The beam current used was 7×10^{-10} amps at 15 kV. Spectra between 0 and 20 keV were counted for 60 seconds and data reduction was done on-line by a computer program TAS-SUEDS (Griffin 1979).

A list of all mineral analyses obtained from the Batur volcanic rocks is given in Appendix 3. Representative analyses of phenocrysts in a basalt, basaltic andesite, dacite and rhyodacite are given in Table 1.4.

4.2.1 Olivine

The compositions of olivine phenocryst cores and rims, and of groundmass olivine crystals, are summarized in Figure 1.7. The 100Mg/(Mg+Fe) values of olivine phenocryst cores in the basaltic lavas generally lie in a restricted range from 71 to 66, while those of the dacites show a wider range of between 56 and 32. Overall, assuming that Fe^{2+}/(total Fe) in the rocks equals 0.9, the phenocryst cores generally lie along the line defined by a bulk $(Fe/Mg)_{ol}/(Fe/Mg)_{rock}$ distribution coefficient (K_D) value of 0.4 (there is no substantial change to this observation if the value of Fe^{2+}/(total Fe) is varied between 1 and 0.85, values which are generally applied to basaltic lavas). This (K_D) value was obtained experimentally by Nicholls (1974) for olivine-liquid equilibrium involving water-saturated, Q-normative basaltic to andesitic liquids, and is higher than the value of about 0.3 obtained by Roeder and Emslie (1970) using water-undersaturated

	basalt 67244			basaltic andesite 67272				dacite 67331					rhyodacite 67277				
	OLV	PLG	MAG	OLV	CPX	PLG	MAG	OLV	OPX	CPX	MAG	PLG	OLV	CPX	PLG	MAG	ILM
SiO_2	36.90	53.28		36.69	51.77	50.06		34.27	52.31	50.70		57.20	32.43	51.19	60.89		
TiO_2			10.98		0.45		11.15			0.59	18.15			0.28		21.49	49.64
Al_2O_3		29.16	4.07		1.64	31.52	4.30		0.77	2.46	1.86	27.05		0.89	24.74	2.10	0.26
Cr_2O_3			1.73														
Fe_2O_3			1.73		1.57		43.51		2.35	1.55	32.42			0.54		25.77	6.92
FeO	27.31	0.70	36.36	27.91	10.87	0.58	38.69	38.71	19.77	10.44	45.40	0.29	49.86	15.79		48.24	39.89
MnO	0.43		0.26	0.57	0.53		0.28	1.37	0.83	0.58	0.94		2.30	0.97		1.06	1.47
MgO	35.18	0.25	3.48	34.68	16.78		2.07	25.68	22.43	13.93	1.23		15.24	11.58		1.35	1.83
CaO	0.19	12.53		0.14	16.39	15.27			1.53	19.75		9.49	0.16	18.77	6.72		
Na_2O		3.85				2.44						5.69			7.19		
K_2O		0.23				0.14						0.28			0.45		
Si	0.986	2.417		0.985	1.929	2.287		0.977	1.950	1.907		2.566	0.987	1.964	2.706		
Ti			0.300		0.012		0.307			0.017	0.506			0.008		0.596	0.931
Al		1.559	0.174		0.072	1.697	0.186		0.034	0.109	0.081	1.430		0.040	1.296	0.091	0.008
Cr			0.050														
Fe3+			1.177		0.044		1.200		0.066	0.044	0.906			0.016		0.716	0.130
Fe2+	0.610	0.027	1.103	0.626	0.339	0.022	1.186	0.923	0.616	0.328	1.409	0.011	1.269	0.507		1.489	0.832
Mn	0.010		0.008	0.013	0.017		0.009	0.033	0.026	0.018	0.030		0.059	0.032		0.033	0.031
Mg	1.420	0.017	0.188	1.387	0.932		0.113	1.090	1.246	0.781	0.068		0.692	0.662		0.074	0.068
Ca	0.005	0.609		0.004	0.654	0.747			0.061	0.796		0.456	0.005	0.772	0.320		
Na		0.339				0.216						0.494			0.619		
K		0.013				0.008						0.016			0.026		
total	3.031	4.981	3.000	3.015	3.999	4.977	3.001	3.023	3.999	4.000	3.000	4.973	3.013	4.001	4.967	2.999	2.000
oxygens	4	8	4	4	6	8	4	4	6	6	4	8	4	6	8	4	3
Mg#	0.697			0.689	0.733			0.541	0.669	0.704			0.353	0.567			
Ca#		0.643				0.776						0.480			0.341		

Table 1.4 Representative microprobe analyses of phenocrysts in selected Batur volcanic rocks. All oxide compositions normalized to total 100 %. Fe^{3+} calculated from stoichiometry.

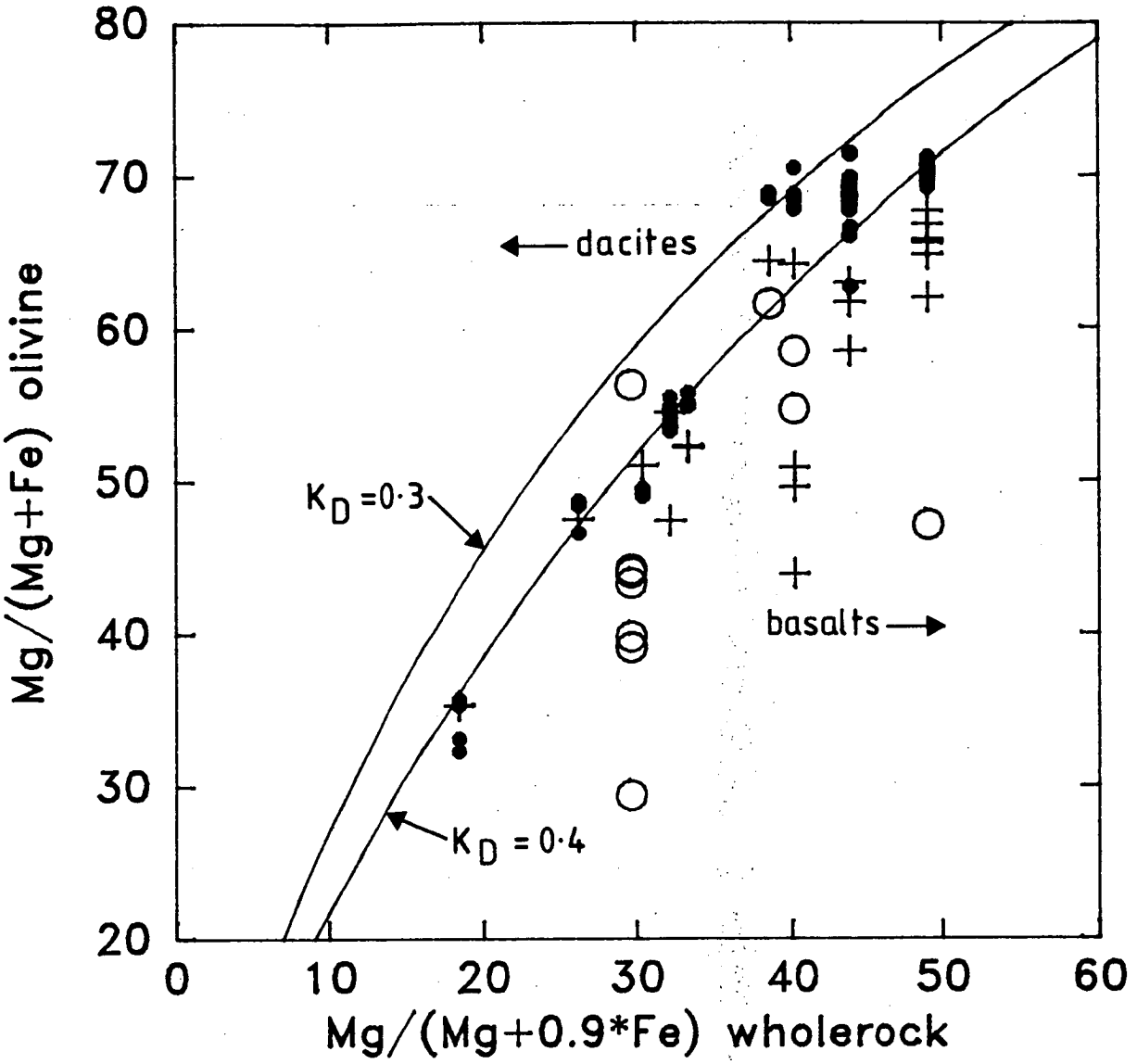

Figure 1.7 Olivine Mg/(Mg+Fe) against wholerock Mg/(Mg+Fe) of selected Batur volcanic rocks (all Fe as FeO; dots = cores; crosses = rims; open circles = groundmass).

basaltic compositions at 1 atm.

Rim compositions are typically more Fe-rich than those of the cores in the basaltic rocks, indicating substantial normal zoning, but those of the dacite olivines are generally similar to their corresponding core compositions, indicating little zoning.

CaO contents range irregularly from 0 to 0.30 wt %, with no systematic differences in distribution between phenocryst and rim and groundmass compositions. MnO ranges in abundance from 0.30 to 2.4 wt %. It is notable that the caldera stage dacites and the pre- and postcaldera stage basaltic rocks show different trends on a plot of Mn versus Fe (Fig. 1.8), with the dacites showing distinctly higher Mn/Fe^{2+} values than the basaltic rocks. This feature is probably due to the presence in the dacites of a higher proportion of Ti-magnetite phenocrysts, which have high Fe^{2+}/Mn values, than in the basalts.

The Batur dacitic volcanic rocks are unusual in containing olivine phenocrysts with intermediate 100Mg/(Mg+Fe) values, which are more typically found in intermediate-SiO_2 alkaline rocks. In subalkaline dacites, pyroxenes and, particularly in dacites from island arcs, hornblende generally comprise the ferro- magnesian mineral assemblage (Ewart 1979,1982). The significance of the evolved olivine compositions in the Batur dacites will be discussed in the next section in conjunction with the pyroxene data.

4.2.2 Pyroxenes

The compositions of phenocryst and groundmass pyroxene in the pre- and postcaldera rocks are shown in Figure 1.9. Generally, the clinopyroxene phenocryst cores show little variation in composition and are similar to those observed in other island arc basaltic lavas (Gill 1981). Scattered clinopyroxene microphenocrysts in the andesite flow 67342 possess more Fe-rich compositions. The groundmass crystals and several phenocryst cores are relatively Ca-poor, with some possessing subcalcic augite compositions.

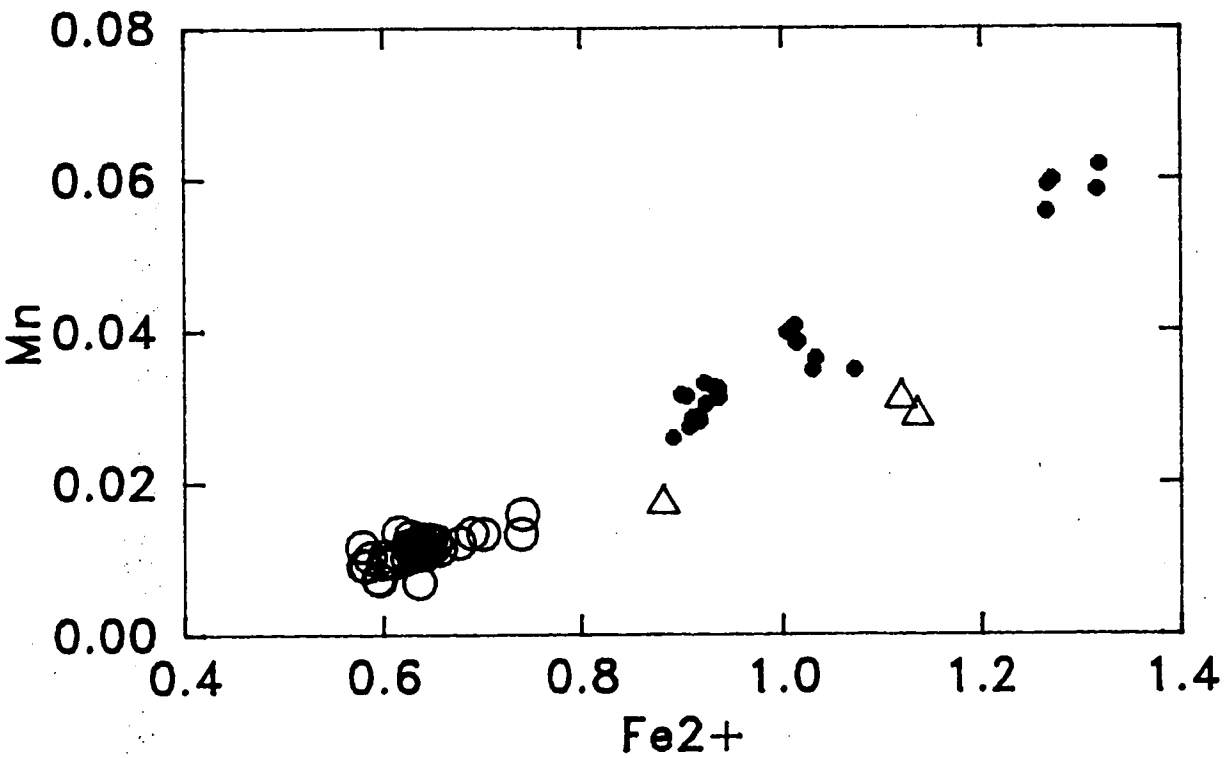

Figure 1.8 Mn against Fe^{2+} in olivine phenocryst cores from selected Batur volcanic rocks (dots = dacites; open circles = basalts; open triangles = quench-textured 'phenocrysts' in andesite lava 67342).

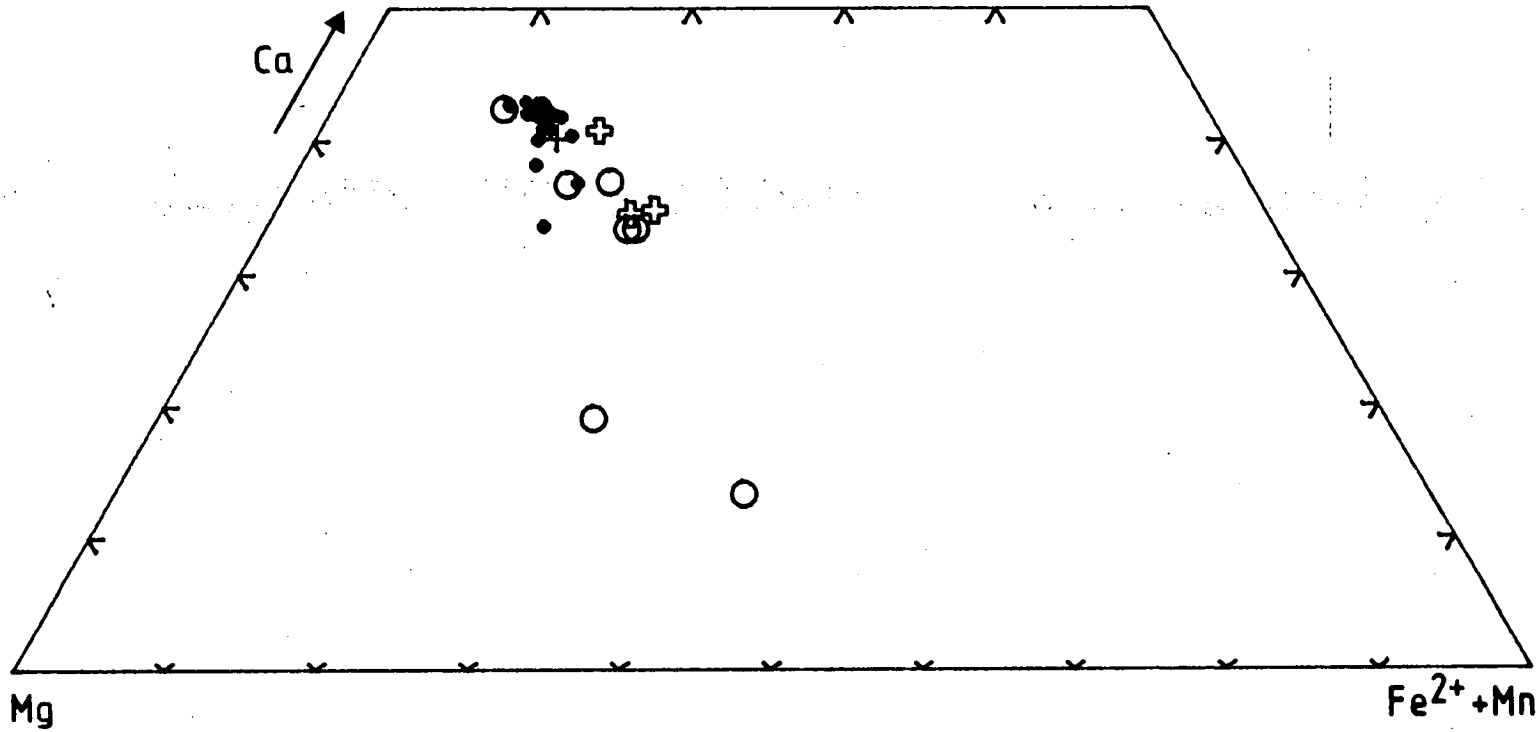

Figure 1.9 Compositions of pyroxenes in Batur pre- and postcaldera stage basaltic volcanics (dots = cores; crosses = rims; open circles = groundmass).

Dacite pyroxene compositions, and tielines between coexisting pryoxenes and olivine, are shown in Figure 1.10. The Batur dacite pyroxenes show a wide range in Fe and Mg proportions but, apart from a slight decrease in the most Mg-rich clinopyroxenes, little variation in the proportion of Ca. Phenocryst rim compositions fall within the range shown by the cores and all of the groundmass crystals possess pigeonite compositions.

In addition, as pointed out by Kuno (1969) in reference to coexisting Fe-rich pyroxene and olivine phenocrysts in dacitic dykes occurring in the Asio and Sidara districts in Japan, the distribution of Fe and Mg between orthopyroxene and coexisting olivine varies substantially with increasing Fe content, with the value of the distribution coefficient $(Fe/Mg)^{olv}/(Fe/Mg)^{opx}$ varying progressively from 1.4 to 1.8 in the Batur dacites. This behaviour contrasts markedly with that of coexisting Mg-rich olivines and orthopyroxene in basaltic rocks in which the value of this coefficient is typically about 0.9.

Figure 1.11 shows the Batur dacite pyroxenes compared to those in other subalkaline, dacitic suites, including some anorogenic, tholeiitic types. The Batur phenocryst cores are most similar compositionally to pyroxenes from Tongan dacites. Like the Batur suite, many rocks in these suites contain groundmass or phenocryst pigeonite. It is notable that pyroxenes from the orogenic dacites (Mt Shasta, Rabaul, Talasea, Tonga, and Batur) lie on differentiation trends similar to those of anorogenic icelandites from Thingmuli volcano and from Western Scotland.

The Asio and Sidara dykes from Japan are the only other subalkaline dacitic rocks known to contain coexisting Fe-rich orthopyroxene and olivine as phenocrysts. However, these minerals also occur as coexisting groundmass microlites in some dykes and lavas on St Lucia island in the Antilles arc (Le Guen de Kerneizon et al. 1982) and coexisting pigeonite and Fe-rich olivine phenocrysts occur in icelandites from Thingmuli volcano (Carmichael 1967). The most SiO_2-rich, rhyolitic, rocks in each of these suites contain ferroaugite and fayalite phenocrysts, with orthopyroxene absent. The Batur dacites also

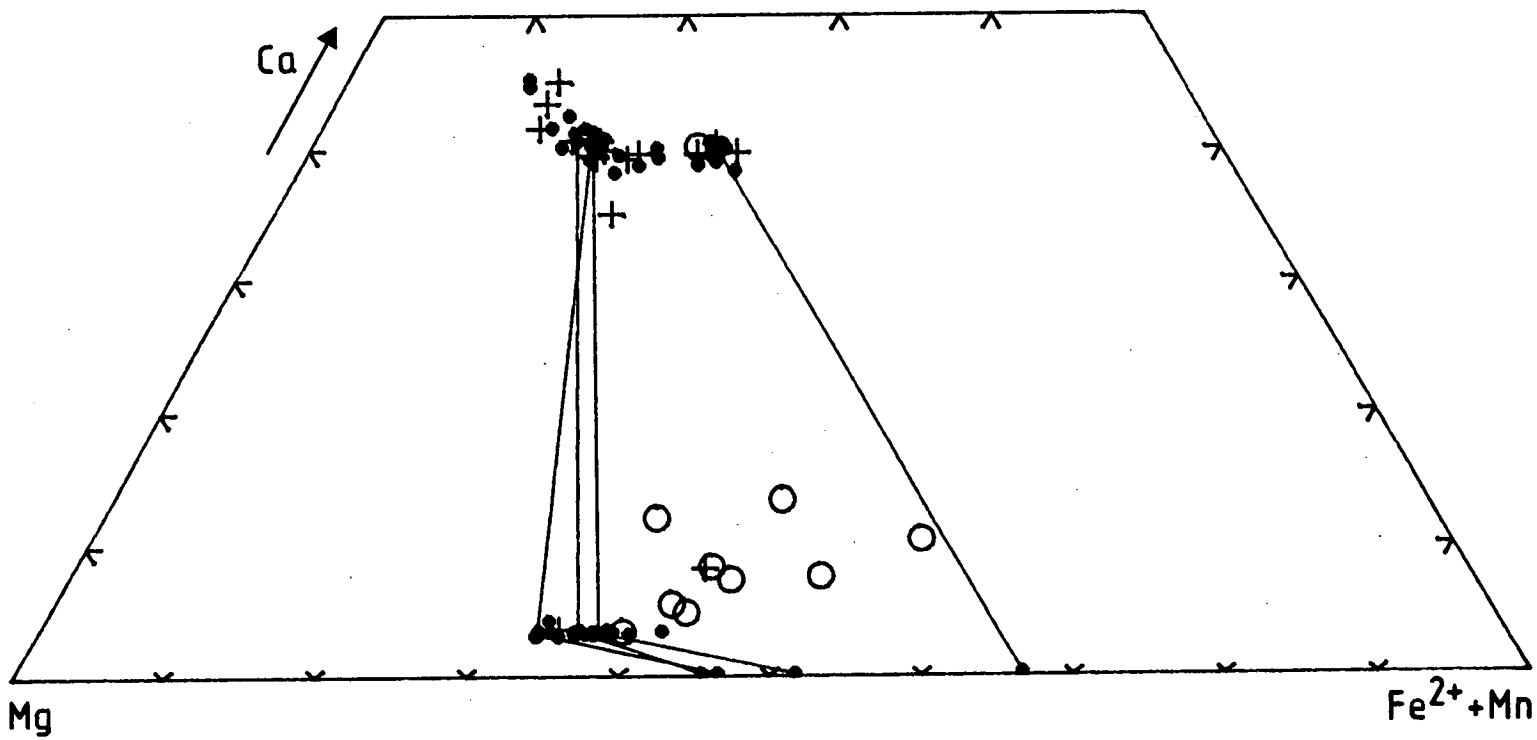

Figure 1.10 Compositions of pyroxenes in Batur caldera stage dacitic volcanics (dots = cores; crosses = rims; open circles = groundmass). Tielines join averages of coexisting pyroxene and olivine phenocryst cores.

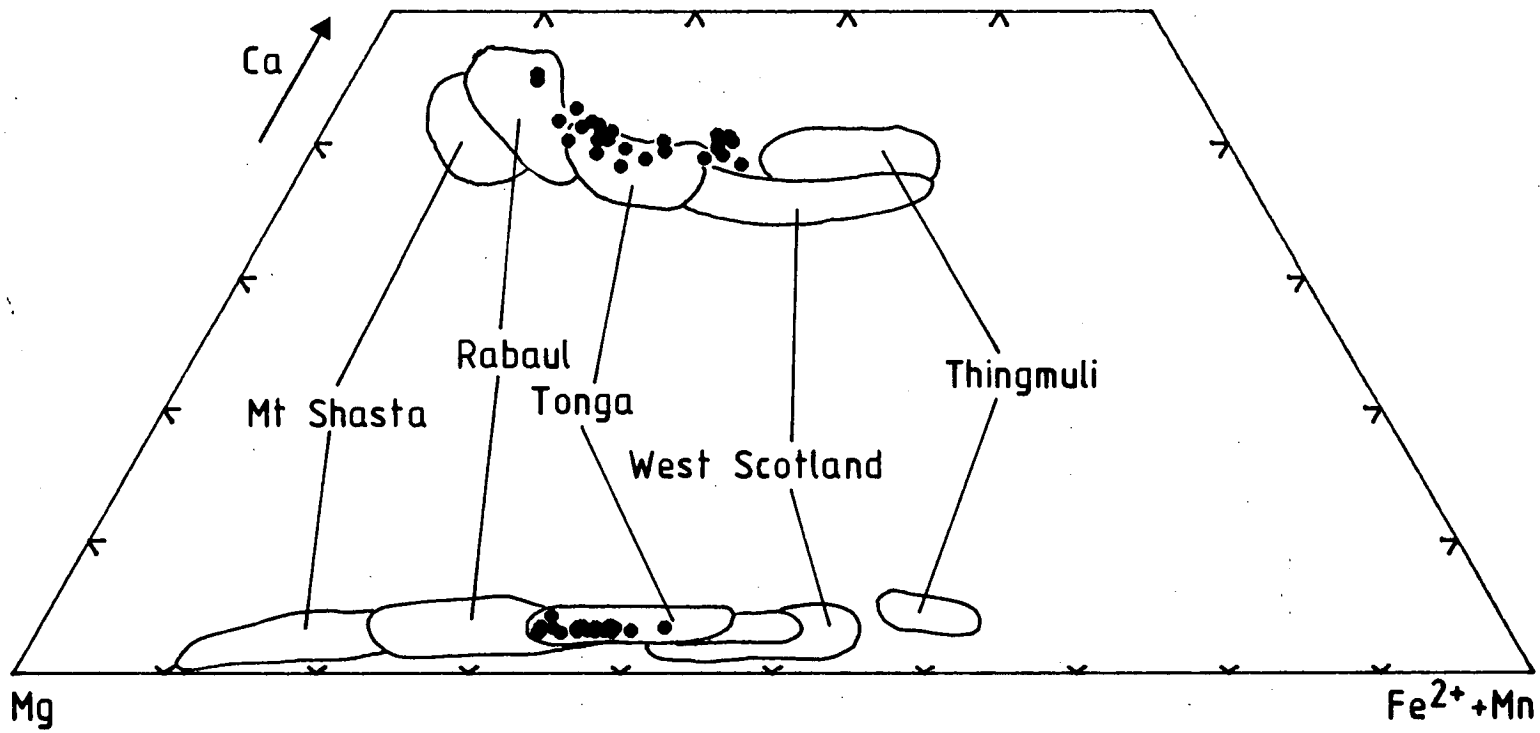

Figure 1.11 Compositions of pyroxene phenocryst cores in selected Batur caldera stage dacites compared to other subalkaline dacitic to rhyodacitic volcanic rocks using the compilation of Ewart (1979).

follow this pattern. Generally, the modal abundance of orthopyroxene decreases and that of olivine increases with increasing SiO_2 contents of the dacites. Orthopyroxene is absent in the most SiO_2-rich Batur dacites.

The Fe^{2+} and Mn contents of clinopyroxene phenocryst cores of the basalts (including 67342) and dacites show similar contrasting behaviour as those of the olivine phenocrysts from the two groups, with the dacite clinopyroxene cores showing higher Mn relative to Fe^{2+} than those in the basalts (Fig. 1.12). The dacites crystals also contain lower abundances of Fe^{3+} and Al. These features are generally consistent with the substantial amounts of Ti-magnetite in the dacites preferentially incorporating Fe^{2+} relative to Mn, togther with Fe^{3+}.

The crystallization temperatures of coexisting clino- and orthopyroxene phenocrysts in three Batur dacites are shown in Figure 1.13, using Lindsley and Anderson's (1983) graphical pyroxene thermometer and projection scheme. Temperatures range approximately from 1070 ^{o}C to 1000 ^{o}C with increasing SiO_2 contents of the rocks.

Temperatures calculated using the solution models of Wells (1979) and Kretz (1982) for coexisting pyroxenes are close to those indicated by Figure 1.13 (Table 1.5), with temperatures decreasing progressively with increasing SiO_2 contents and decreasing Mg/(Mg+Fe) of the rocks, but those obtained by Wood and Banno's (1973) method are approximately one hundred degrees cooler.

4.2.3 Plagioclase

The cores of plagioclase phenocrysts in the Batur volcanics cover a wide range in compositions. Those from the basaltic rocks, including the precaldera andesite 67342, vary between An_{95} and An_{57} while those from the dacites lie between An_{60} and An_{32} (Fig. 1.14). K_2O contents increase with decreasing CaO abundance. MgO occurs in some crystals in the most mafic basaltic rocks, with abundances typically of 0.2-0.3 %, while FeO occurs in most Batur plagioclase crystals,

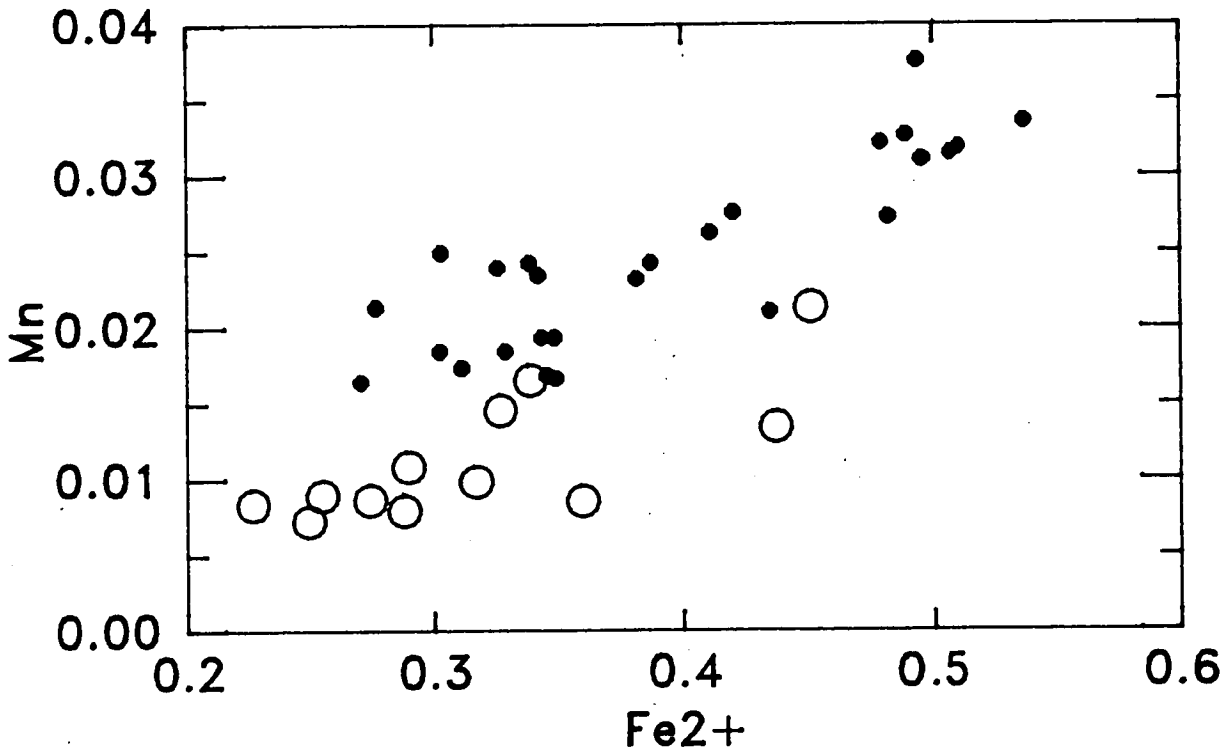

Figure 1.12 Mn against Fe^{2+} in clinopyroxene phenocryst cores from selected Batur volcanic rocks (dots = dacites; open circles = basalts and andesites).

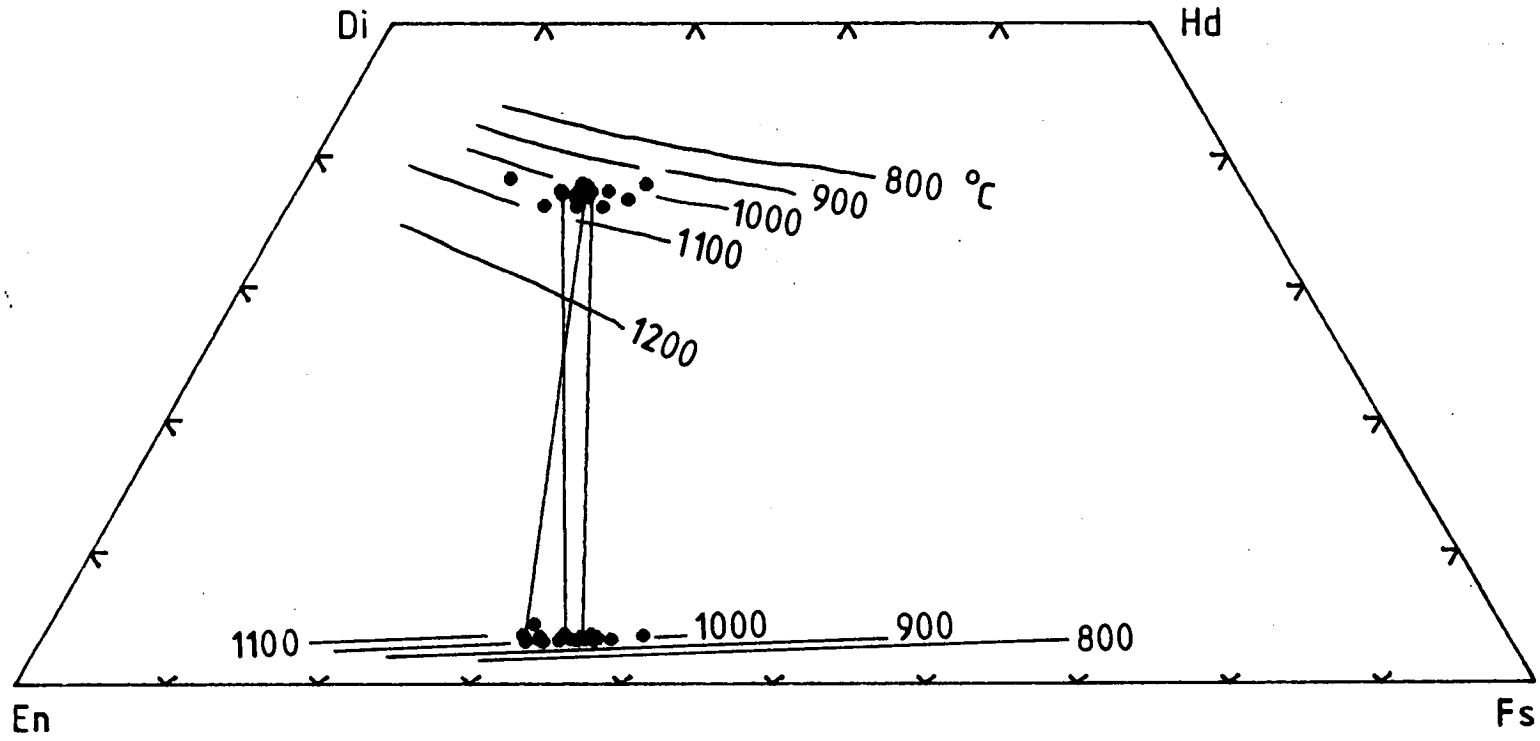

Figure 1.13 Graphical pyroxene thermometer (Lindsley & Anderson 1983) showing crystallization temperatures of coexisting pyroxene phenocryst cores in Batur dacites. Tielines join averages of coexisting phenocryst assemblages.

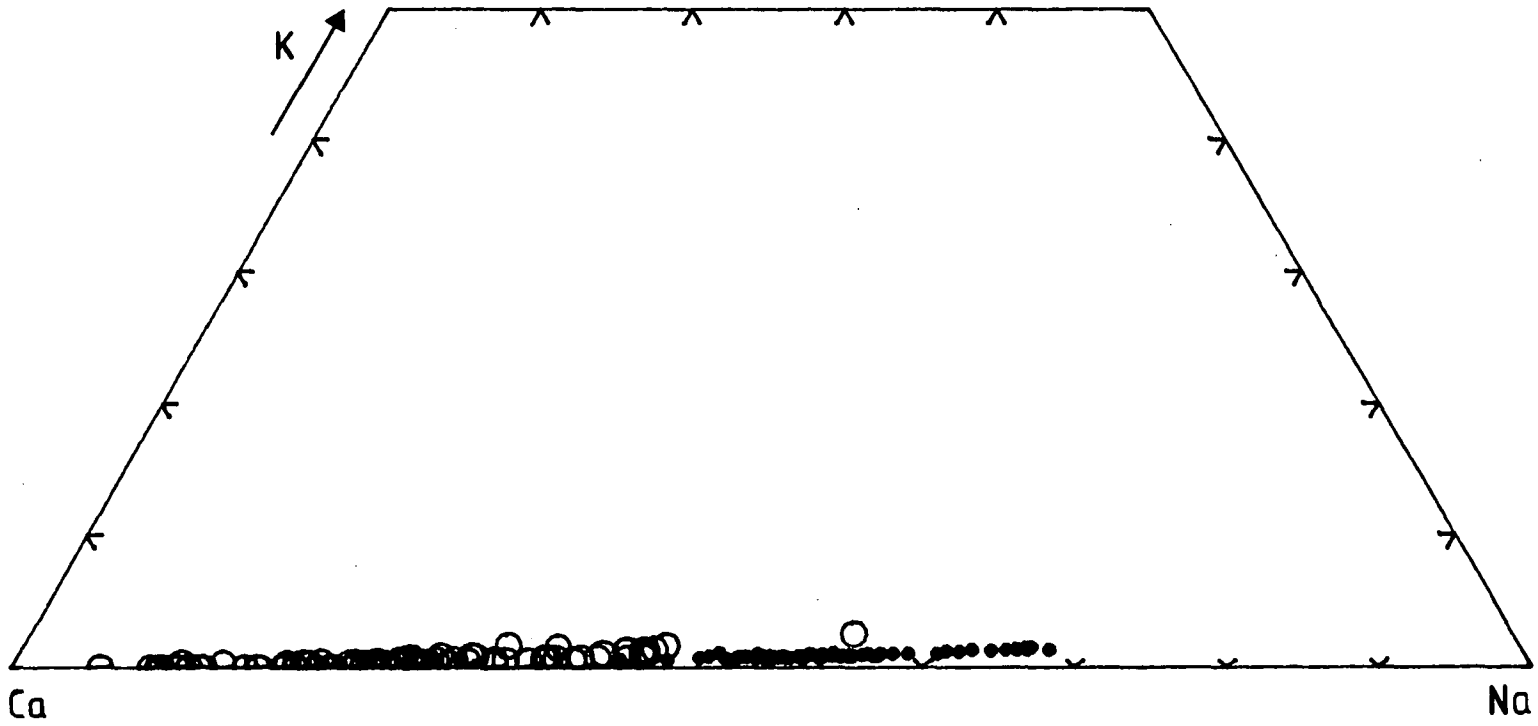

Figure 1.14 Compositions of plagioclase phenocryst cores from selected Batur volcanic rocks (dots = dacites; open circles = basalts and andesites).

	67275	67331	67273
Wood & Banno (1977)	971	970	934
Wells (1979)	1053	1023	1006
Kretz (1982) (Ca-distribution)	1067	1061	1004
rock 100Mg/(Mg+Fe)	31.1	29.9	28.3
rock SiO_2	62.2	62.9	65.4

Table 1.5 Estimates of crystallization temperatures (^0C) of average coexisting ortho- and clinopyroxene phenocryst pairs in Batur dacites.

ranging from 0.6 to 1.0 % in those from the basalts and from 0 to 0.4 % in crystals from the dacitic rocks. The most Ca-rich plagioclase crystals, An_{94}, form glomerocrysts with Fo_{77} olivine crystals in the postcaldera basalt 67339.

The zoning characteristics of the Batur plagioclase phenocrysts are shown by the compositions of core-rim pairs in Figure 1.15. Rim analyses were obtained from as near to the crystal edges as possible. The compositions of the phenocryst rims vary widely from those of the cores in the basaltic rocks, mostly towards normal zoning, while the plagioclase phenocrysts in the dacitic rocks show less scatter and are distributed evenly on both sides of the equiline.

Although the bias of the basalt plagioclase crystals towards low-An rim compositions is probabaly due to quenching on eruption, the occurrence of reversely-zoned, and inclusion-rich, plagioclase phenocrysts in many of the basalts suggests that some degree of magma mixing has occurred.

Sakuyama (1981), in a comprehensive study, found that bimodal compositional frequency distributions of plagioclase phenocrysts from basaltic lavas of two Japanese volcanoes correlated with the presence of reversely-zoned olivine and pyroxene phenocrysts, indicating that mixing of magmas containing phenocrysts of contrasting compositions had occurred. The frequency distributions of plagioclase groundmass and phenocryst core and rim compositions of representative

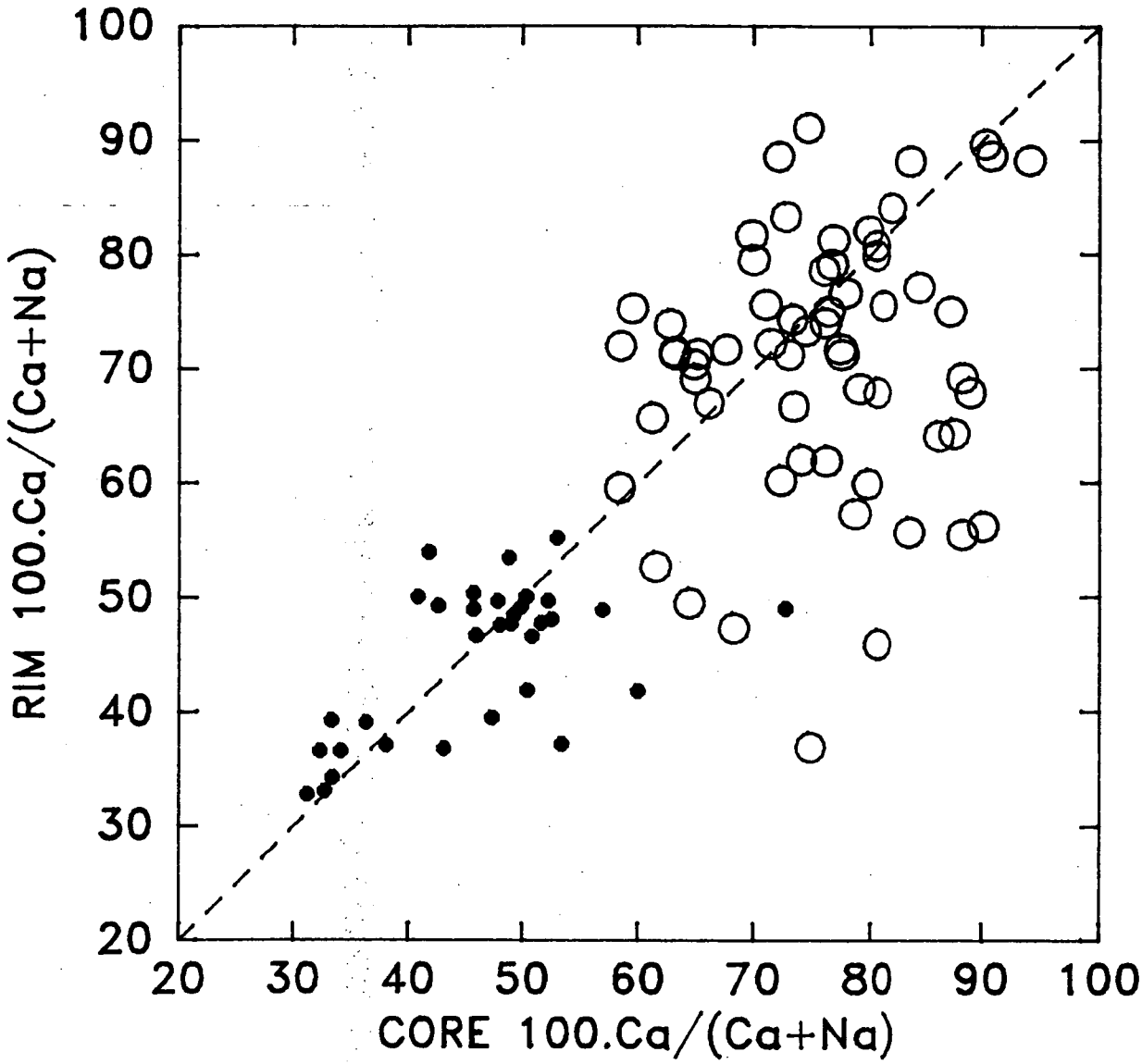

Figure 1.15 Anorthite contents of core-rim pairs in plagioclase phenocrysts from selected Batur volcanic rocks (dots = dacites; open circles = basalts and andesites).

basaltic and dacitic lavas are shown in Figure 1.16.

The basalt shows a wide range of plagioclase core and rim compositions compared to the dacite but it is not clear that it contains a bimodal distribution of core compositions. This suggests that the variation is not due to substantial mixing of discrete crystal populations although, given the range of variation, more data are required to be certain. It is possible that mixing between slightly different, but still basaltic, magmas has occurred.

Alternatively, if magma mixing was not a major factor, plagioclase compositional variation in the basalts could conceivably have been promoted by vigorous convection of relatively low viscosity magma through varying pressure, temperature and volatile gradients within the magma chamber, given that because plagioclase will tend to float in basaltic magma because of its generally similar density. Once plagioclase crystals have become entrained in the magma, possibly as a result of having been scavenged from the chamber walls or by crystallization from the liquid, convection will further inhibit plagioclase-liquid separation, leading to the production of increasingly compositionally complex crystals with time.

The dacite, however, shows a clear unimodal distribution of core compositions, together with similarly regular variation of rim and groundmass compositions. The lower An contents of the groundmass plagioclase crystals relative to the phenocryst cores are consistent with their production during quench solidification of the magma. The phenocryst rim compositions are mostly similar to those of the cores, with a few which correspond to groundmass compositions. The similar, and restricted, ranges of the cores and rims precludes the possibility of mixing of rhyolitic and basaltic magmas having being involved in the genesis of the dacitic rocks (cf Eichelberger 1975).

Zoning profiles of three, optically-zoned, euhedral plagioclase phenocrysts from two of the dacitic rocks (Fig. 1.17), obtained from a series of equidistant microprobe

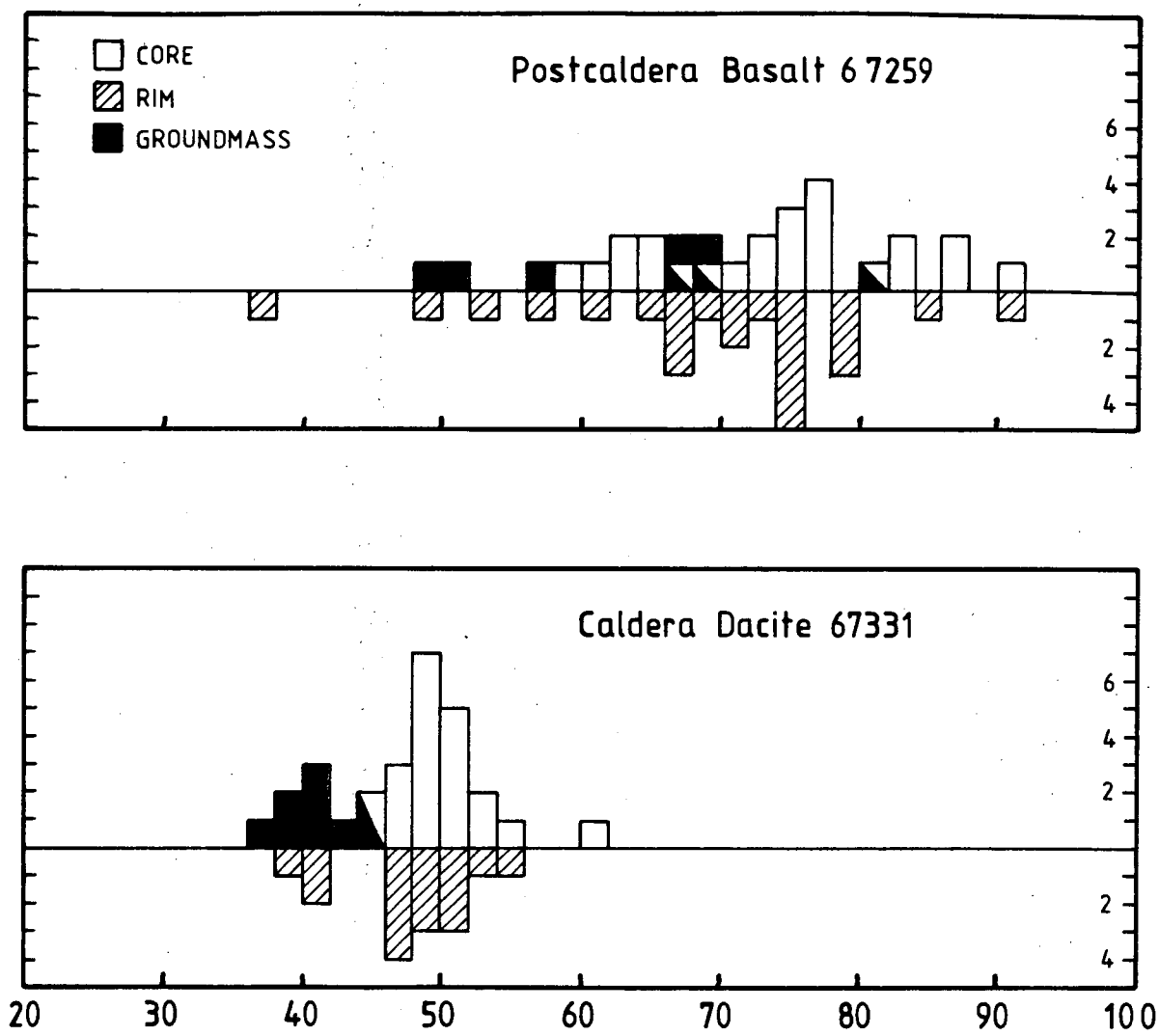

Figure 1.16 Frequency distributions of plagioclase compositions in representative basaltic and dacitic rocks. See text for explanation.

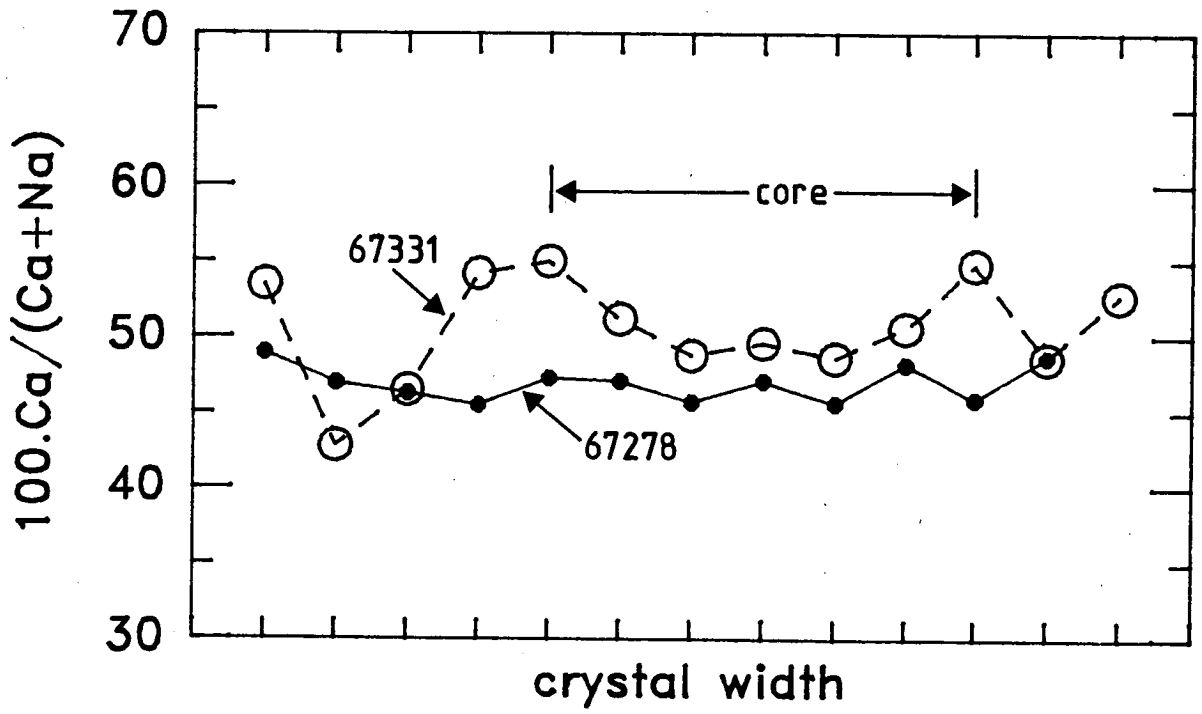

Figure 1.17 Zoning profiles of two selected plagioclase phenocrysts in Batur dacitic rocks.

analyses across the crystals, indicate crystallization histories more complex than those suggested by simple core-rim relationships. One crystal from a glassy dacite block (67278) shows a generally flat profile with slight increases of An content towards the margins. This type of pattern is different from those which would be expected in crystals grown under ideal fractional crystallization conditions. Those crystals would show wide, unzoned core regions that pass into margins showing logarithmic decreases in An contents (Klusman 1972; Lofgren 1980; Loomis 1982; Smith & Lofgren 1983). The slight marginal increase in An contents shown by the 67278 crystal is therefore a substantial departure from the ideal normally-zoned profile.

The other profile, from a crystal in a dacite lava flow (67331) shows a more complex profile, with a U-shaped core and V-shaped marginal profiles. The core pattern resembles the profile inferred for the 67278 crystal. The marginal pattern, however, resembles the discontinuous, reversely-zoned profiles produced experimentally by Lofgren (1972) and Smith and Lofgren (1983) by rapid temperature decreases followed by re-equilibration between the crystals and host liquids.

In those experiments, marked decreases in An contents accompanied supercooling, or supersaturation, imposed by rapid temperature changes, while the reverse zoning was produced subsequently as isothermal crystal growth reduced the degree of supersaturation until equilibrium at the new temperature was reached (Loomis 1982; Smith & Lofgren 1983). In the magmatic environment, rapid supersaturation is more likely to be produced by rapid transfer of the magma into low pressure environments than by sharp temperature variation (Smith & Lofgren 1983). This could occur, for example, by intrusion of the magma into a shallow, intermediate chamber prior to eruption.

The U-shaped core profile shown by the 67331 crystal and inferred for the 67278 crystal implies progressive reverse zoning virtually since the time of nucleation. This could conceivably be produced by an analogous process to that explained above, in that nucleation of the crystal may have

occurred as a result of a substantial 'supersaturation event', with subsequent reversely-zoned crystal growth during re-equilibration. The 'event' could have occurred by transfer of essentially plagioclase-free dacitic liquid from deep to shallow chambers, or parts of the same chamber.

This mechanism implies that the liquid was produced before the observed phenocrysts and that, therefore, if the dacitic liquids were produced by crystal-liquid fractionation processes, the observed phenocrysts do not necessarily represent those which fractionated to form the dacitic magma. This interpretation of the causes of the zoning profiles shown by some plagioclase phenocrysts in two of the dacites has particularly important implications for identification of the process which produced the Batur dacitic rocks, as will be outlined in a later section.

4.2.4 Fe-Ti Oxides

The core compositions of Fe-Ti oxide phenocrysts in the basaltic and dacitic rocks are shown in Figure 1.18. Ti-magnetite crystals in the dacite are clearly characterized by their higher ulvospinel contents compared to those from the basalts. These crystals typically show few compositional differences between cores and rims.

Coexisting ilmenite and Ti-magnetite phenocrysts have been found only in the most SiO_2-rich dacite block (67277). These give estimates of about 930 ^{o}C and $10^{-12.6}$ for the temperature and oxygen fugacity respectively of the high-SiO_2 dacitic magma, using the temperature-composition-oxygen fugacity diagram of Spencer and Lindsley (1981) and recalculation algorithm of Stormer (1983).

This point lies on the FMQ buffer curve and suggests correlation of the Batur dacitic magma to those of anorogenic bimodal associations in Iceland, California, Papua New Guinea and Queensland (Ewart 1979). Ewart (1979) attributes the relatively high temperature and reduced magmatic environment of these rocks, compared with orogenic suites from the western U.S.A., the southwestern Pacific and Japan which show

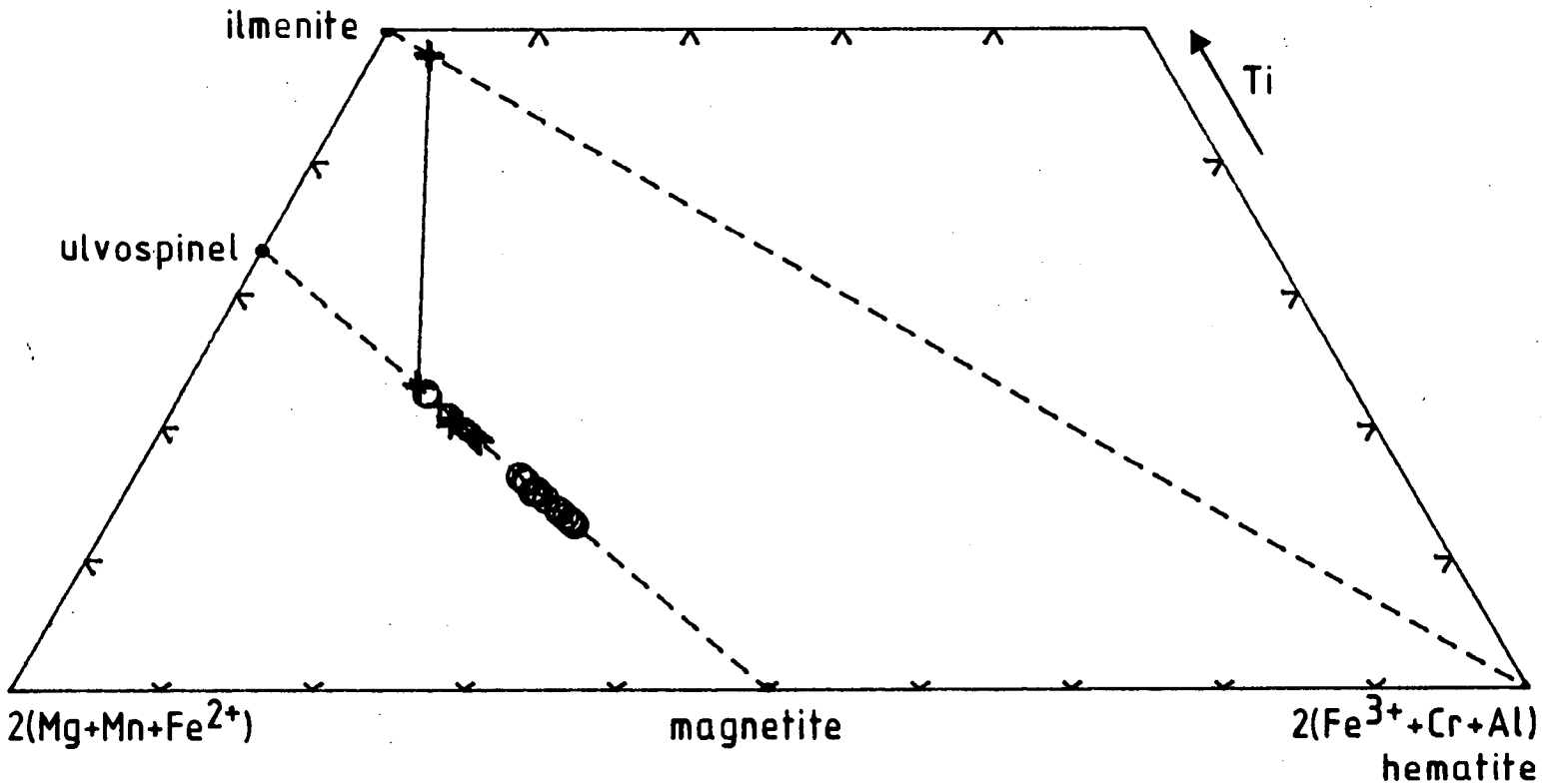

Figure 1.18 Compositions of Fe-Ti oxide phenocrysts from selected Batur volcanics (crosses = dacites; open circles = basalts and andesites). Full tieline joins average coexisting Ti-magnetite and ilmenite phenocrysts in dacite 67277.

relatively high oxygen fugacities and low temperatures, largely to low magmatic H_2O contents. The Batur dacites also share the characteristics of low phenocryst contents and Fe-enriched phenocryst assemblages which Ewart (1979) observed in the anorogenic rocks.

The temperature indicated by the Batur dacite, 930 ^{o}C, is substantially lower than the temperatures indicated by coexisting pyroxenes in the less SiO_2-rich dacites, but is consistent with the trend shown by those temperatures to decrease with increasing SiO_2 contents. This temperature range, 1070-930 ^{o}C, is slightly higher than the range, 1035-835 ^{o}C, determined from coexisting Fe-Ti oxides for dacitic pyroclastics from Rabaul caldera by Heming and Carmichael (1973).

4.2.5 Cr-Spinels

The aluminous Cr-spinel crystals from the olivine+ plagioclase glomerocrysts in 67339 show a restricted range of compositions that fall within the field formed by spinels from subalkaline basalts from Grenada (Fig. 1.19). Other Cr-spinels known from Sunda-Banda arc volcanics, from Rindjani basalts (Foden 1979), Ulakan ankaramites and a single analysis from a Batu Tara olivine leucitite (new data), are shown for comparison. Most of these show high Cr contents that are similar to those of 'arc picrites' from New Georgia and Aoba (Ramsay et al. 1984), and the Type III Alpine-type peridotites, Alaskan-type ultramafic intrusions and arc-related mafic volcanics discussed by Dick and Bullen (1984).

The Batur spinels possess lower $100Cr/(Cr+Al)$, $100Mg/(Mg+Fe)$ and higher $100Fe^{3+}/(Fe^{3+}+Cr+Al)$ values than the more MgO-rich basaltic rocks in the Sunda arc, suggesting that they crystallized from basaltic magma that had been affected by an earlier fractional crystallization process (Dick & Bullen 1984).

4.2.6 Glass Inclusions

A few phenocrysts in some of the Batur volcanics contain

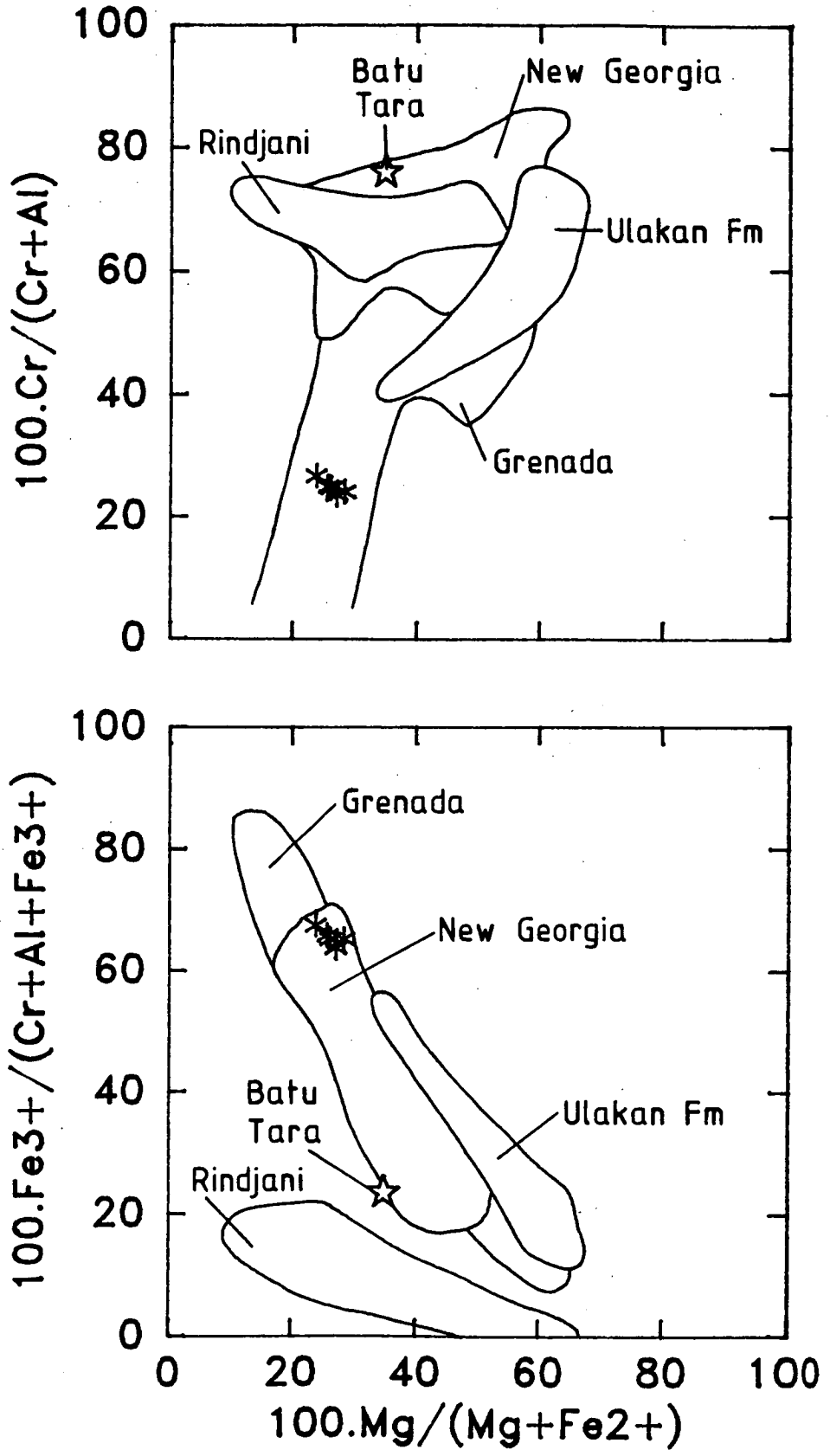

Figure 1.19 Compositions of Cr-spinel inclusions in olivine xenocrysts from Batur basalt 67339 compared to those from other orogenic basaltic lavas. Other data from Foden (1979), Arculus (1978) and Ramsay et al. (1984).

glass inclusions, which are generally thought to be samples of the liquid from which the phenocryst crystallized. Inclusions in olivine and pyroxene typically have ovoid shapes while those in plagioclase crystals are usually irregular in shape.

Generally, the compositions of the inclusions in phenocrysts from both the basalts and dacites are very similar to those of glass in the groundmasses of the rocks, where it is present (Table 1.6). No evidence was found from glass inclusions to indicate the presence of mixed magmas. Rather, the close similarities between the compositions of the groundmass glass and those of the the phenocryst inclusions suggest either that the phenocrysts crystallized after the dacitic liquid was formed, because glass trapped by crystallizing phenocrysts would be expected to have mafic compositions compared to the groundmass glass, or that the melt inclusions continued to crystallize after being trapped (cf Anderson 1974).

	67275		67273			67277	
	gmass	opx	gmass	opx	cpx	gmass	olv
SiO_2	69.7	69.6	68.4	70.8	69.7	69.0	69.9
TiO_2	0.4	0.3	0.5	0.5	0.4	0.4	0.3
Al_2O_3	16.4	16.4	15.8	16.4	16.4	15.6	15.8
FeO	2.3	3.2	4.0	2.2	2.8	4.3	3.4
MgO	nd	0.1	0.6	0.5	0.8	0.4	0.2
CaO	2.3	2.0	2.2	2.0	2.9	2.0	1.5
Na_2O	5.6	5.3	5.3	4.6	3.8	4.8	5.0
K_2O	3.1	2.7	3.1	2.9	3.1	3.5	4.1
P_2O_5	nd	0.2	nd	nd	0.1	nd	nd

Table 1.6 Average compositions of glass inclusions in phenocrysts and in the groundmasses of selected Batur dacitic volcanic rocks. Analyses by electron microprobe (nd = not detected).

5. GEOCHEMISTRY

5.1 Characteristics

Forty-nine volcanic rocks from Batur volcano were analysed by XRF for nine major elements (plus H_2O- and LOI) and 13 trace elements. In addition, 11 of these rocks were further

analysed for 15 trace elements (including nine rare earth elements) by instrumental neutron activation analysis (INAA) at the Department of Geology, Australian National University (B.W.Chappell, analyst).

All XRF results, together with analytical methods and precision estimates, are given in Appendix 2. The analysed samples have been subdivided according to stratigraphy into precaldera, caldera and postcaldera groups. Representative analyses, including all of the INAA data from Batur, are listed in Table 1.7.

5.1.1 Major Elements

a) Characteristics

The Batur volcanic rocks show a wide range in major element compositions, with SiO_2 contents ranging between 49 and 68 wt % (all quoted and plotted values refer to analyses normalized to total 100 %, volatile-free, and with all Fe as FeO). However, each of the three groups shows relatively restricted SiO_2 ranges; the precaldera rocks lie between 49 and 60 wt %, the caldera rocks between 62 and 68 wt %, and the postcaldera lavas between 52 and 56 wt %.

On a plot of SiO_2 against total alkalis (Fig. 1.20) the postcaldera and caldera rocks define a colinear trend from basalts, through basaltic andesites, andesites and dacites to rhyolites, although there is a gap from 56 to 62 wt % SiO_2 between these two groups. SiO_2-rich members of the precaldera rocks partially fill this gap but, although its basaltic members are similar to those in the postcaldera group, the precaldera group lies at slightly higher total alkali contents than the caldera stage dacites.

Like most island arc volcanic rocks (Gill 1981) the Batur basalts possess K_2O contents that are generally higher than those of mid-ocean ridge basalts, with K_2O/Na_2O values ranging from 0.2 to 0.4 in the basaltic (< 53 wt % SiO_2) members of the pre- and postcaldera groups. On a plot of K_2O against SiO_2 (Fig. 1.21) most of the Batur volcanics fall in

	PRECALDERA			CALDERA		
sample	67341	67328	67299	67275	67273	67277
major elements (wt %)						
SiO_2	48.74	52.28	55.32	61.75	64.59	66.70
TiO_2	0.91	1.01	1.12	0.88	0.77	0.54
Al_2O_3	19.41	18.33	16.24	16.81	16.18	15.38
Fe_2O_3	10.66	10.54	9.37	7.21	5.83	5.25
MnO	0.19	0.20	0.21	0.22	0.22	0.21
MgO	5.94	3.74	2.49	1.64	1.16	0.54
CaO	11.04	9.19	5.93	4.59	3.25	2.35
Na_2O	3.04	3.49	4.27	4.95	5.50	5.88
K_2O	0.57	1.08	1.95	1.63	1.60	2.94
P_2O_5	0.16	0.22	0.77	0.39	0.28	0.13
LOI	-0.33	-0.42	0.86	-0.06	0.03	0.01
H_2O-	0.17	0.17	0.83	0.13	0.07	0.01
rest	0.13	0.15	0.18	0.13	0.13	0.14
total	100.63	99.98	99.54	100.27	99.61	100.08
trace elements (p.p.m.)						
Ba	142	258	467	400	437	525
Rb	11	23	69	39	49	59
Sr	366	393	369	322	280	194
Zr	43	87	239	137	156	195
Nb	2	4	14	9	10	12
Y	18	22	57	32	33	37
La	5.6(7)	10.8(12)	28 (34)	17.0(17)	18.0(18)	19.9(22)
Ce	13.5(9)	24 (24)	64 (72)	37 (37)	40 (34)	41 (45)
Nd	8.7(13)	14.7(18)	38 (44)	21 (23)	22 (22)	23 (26)
Sm	2.3	3.6	9.0	5.2	5.2	5.2
Eu	0.91	1.17	2.2	1.62	1.60	1.48
Gd	2.9	4.1	9.3	5.7	5.6	5.7
Ho	0.6	0.8	1.7	1.2	1.2	1.3
Yb	1.6	2.2	4.7	3.2	3.4	3.8
Lu	0.24	0.34	0.71	0.50	0.53	0.59
Cs	<0.2	<0.2	1.8	1.3	1.6	1.7
Hf	0.3	1.5	5.3	3.0	3.6	4.3
Th	0.7	2.4	7.9	3.9	6.0	6.8
U	<1	<1	1.6	<1	1.2	1.1
Sc	26 (30)	28 (30)	20 (26)	17 (18)	15 (16)	14 (16)
V	288	292	95	54	18	1
Ni	23	12	3	2	2	1
Cr	27 (33)	13 (16)	<1 (3)	<1 (4)	<1 (4)	<1 (5)

Table 1.7

continued over ..

	POSTCALDERA				
sample	67244	67257	67238	67240	67259
major elements (wt %)					
SiO_2	51.78	52.63	52.94	53.54	54.12
TiO_2	0.98	1.00	1.02	1.03	1.00
Al_2O_3	18.00	18.06	18.16	18.96	18.84
Fe_2O_3	10.80	10.66	10.20	9.65	9.33
MnO	0.21	0.21	0.21	0.19	0.19
MgO	4.73	4.47	3.62	3.06	2.85
CaO	8.97	8.93	8.78	9.06	8.78
Na_2O	3.97	3.49	3.63	3.85	4.23
K_2O	0.95	0.75	1.29	0.99	0.93
P_2O_5	0.22	0.23	0.23	0.24	0.27
LOI	-0.65	-0.56	-0.57	-0.54	-0.46
H_2O-	0.09	0.09	0.42	0.09	0.10
rest	0.15	0.14	0.14	0.15	0.14
total	100.20	100.10	100.07	100.27	100.32
trace elements (p.p.m.)					
Ba	216	231	232	239	254
Rb	18	18	22	21	21
Sr	429	426	428	428	442
Zr	66	71	78	81	79
Nb	4	4	5	5	5
Y	19	22	22	20	24
La	9.2(10)	9.7(13)	10.3(16)	10.4(12)	10.5(12)
Ce	21 (16)	23 (16)	23 (24)	24 (23)	24 (24)
Nd	12.7(14)	14.5(15)	13.9(15)	14.3(17)	14.6(17)
Sm	3.1	3.4	3.4	3.5	3.5
Eu	1.08	1.17	1.16	1.19	1.21
Gd	3.6	3.9	4.1	4.0	4.2
Ho	0.8	1.0	0.9	1.0	0.8
Yb	1.8	2.0	2.0	2.0	2.1
Lu	0.30	0.32	0.33	0.33	0.34
Cs	0.5	0.6	0.7	0.6	0.6
Hf	0.7	0.8	1.1	1.2	1.2
Th	1.4	1.6	1.8	1.9	2.3
U	<1	<1	<1	<1	<1
Sc	27 (28)	28 (27)	26 (27)	27 (28)	25 (26)
V	284	269	265	274	233
Ni	39	16	9	7	7
Cr	15 (13)	11 (10)	7 (9)	4 (5)	3 (10)
year of eruption	1926	1888	1974	1963	1849

Table 1.7 Compositions of representative Batur volcanic rocks. La, Ce, Nd, Sm, Eu, Gd, Ho, Yb, Lu, Cs, Hf, Th, U, Sc and Cr by INAA (B.W. Chappell, analyst). All other elements and values in brackets by XRF.

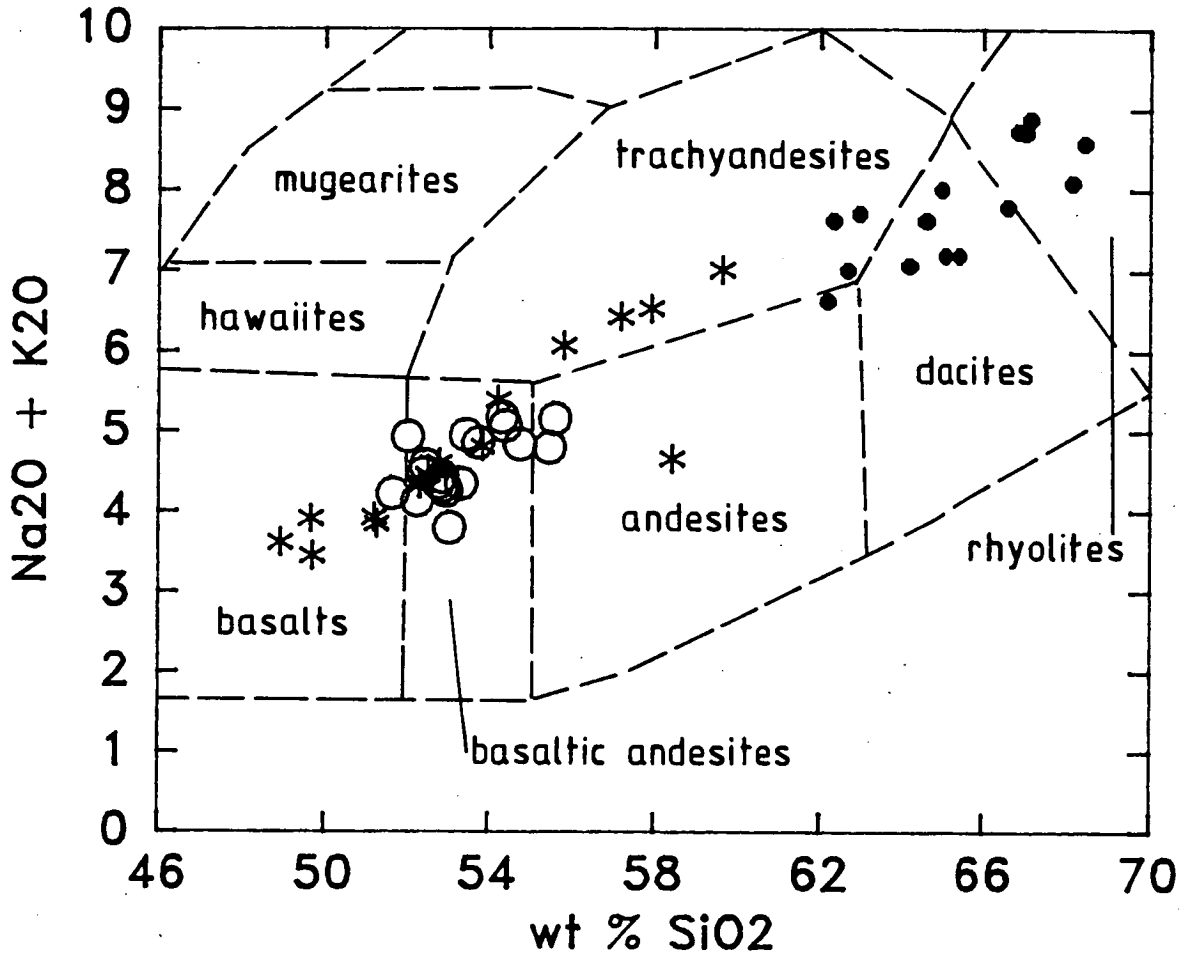

Figure 1.20 SiO_2 against total alkalis in Batur volcanic rocks (open circles = postcaldera stage; dots = caldera stage; asterisks = precaldera stage). Comparison fields from Cox et al. (1979).

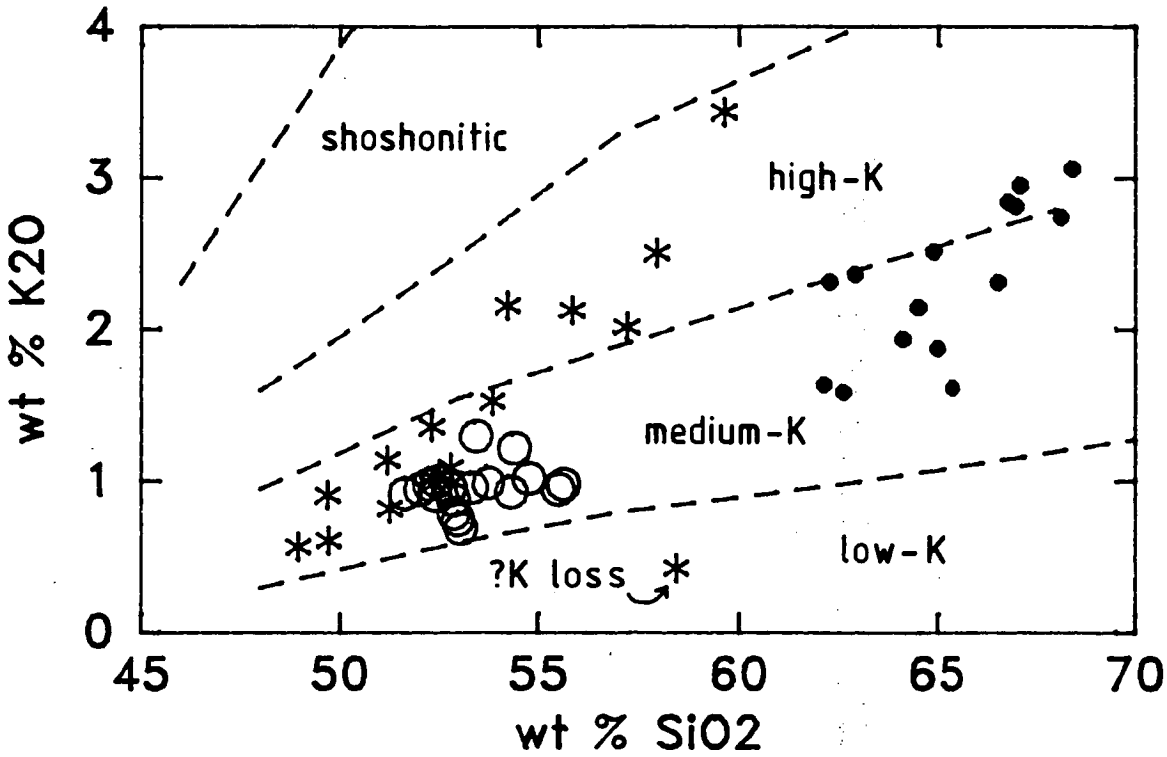

Figure 1.21 SiO_2 against K_2O in Batur volcanic rocks (symbols as for Fig. 1.20). Classification scheme after Peccerillo and Taylor (1976) and Part 2.

the field for medium-K suites. The precaldera stage basaltic andesites and andesites fall in the high-K field, with one pumiceous clast (67295) apparently having lost K_2O.

The ranges of values of the other major elements are shown by Harker diagrams in Figure 1.22. Within each group, the variation of each oxide forms a curvilinear trend with increasing SiO_2 contents, with abundances of Al_2O_3, FeO, MgO and CaO generally decreasing and that of Na_2O increasing. TiO_2 and P_2O_5 contents increase in the pre- and postcaldera rocks but decrease in the caldera dacites. Also, the TiO_2, FeO and P_2O_5 contents of the intermediate-SiO_2 precaldera rocks are distinctly higher than those of the postcaldera rocks. Those precaldera rocks also contain relatively less Al_2O_3.

Previous analyses of Batur basalts, obtained by wet chemical methods (quoted by Neumann van Padang 1951), show particularly high Al_2O_3 contents of about 20 wt %. Using these data, Hutchison (1982) suggested that the Batur postcaldera lavas were unlike other calcalkaline suites in Indonesia. However, wet chemical Al_2O_3 results are typically high compared to XRF values, and are less accurate than those obtained by XRF. These new data show that, compared to mid-ocean ridge basalts, the Batur postcaldera basalts generally contain high amounts of Al_2O_3 (about 18 %) and low amounts of TiO_2 (about 1.0 %), and are generally very similar in major element composition to medium-K basalts from other volcanoes in the Sunda-Banda arc (Part 2) and from other orogenic regions (Gill 1981; Ewart 1982). However, the precaldera lavas are more variable in composition, with some possessing particularly high Al_2O_3 contents of 20-21 wt %.

b) Fe-Enrichment

On an AFM diagram (Fig. 1.23) the Batur volcanic rocks show a clear trend of Fe-enrichment which is intermediate in degree between those of the anorogenic, tholeiitic Thingmuli volcanic rocks and the orogenic, calcalkaline Cascade suite. The Batur rocks also show a substantial degree of Fe-enrichment on a plot of FeO/MgO against SiO_2 (Fig. 1.24) and fall within the

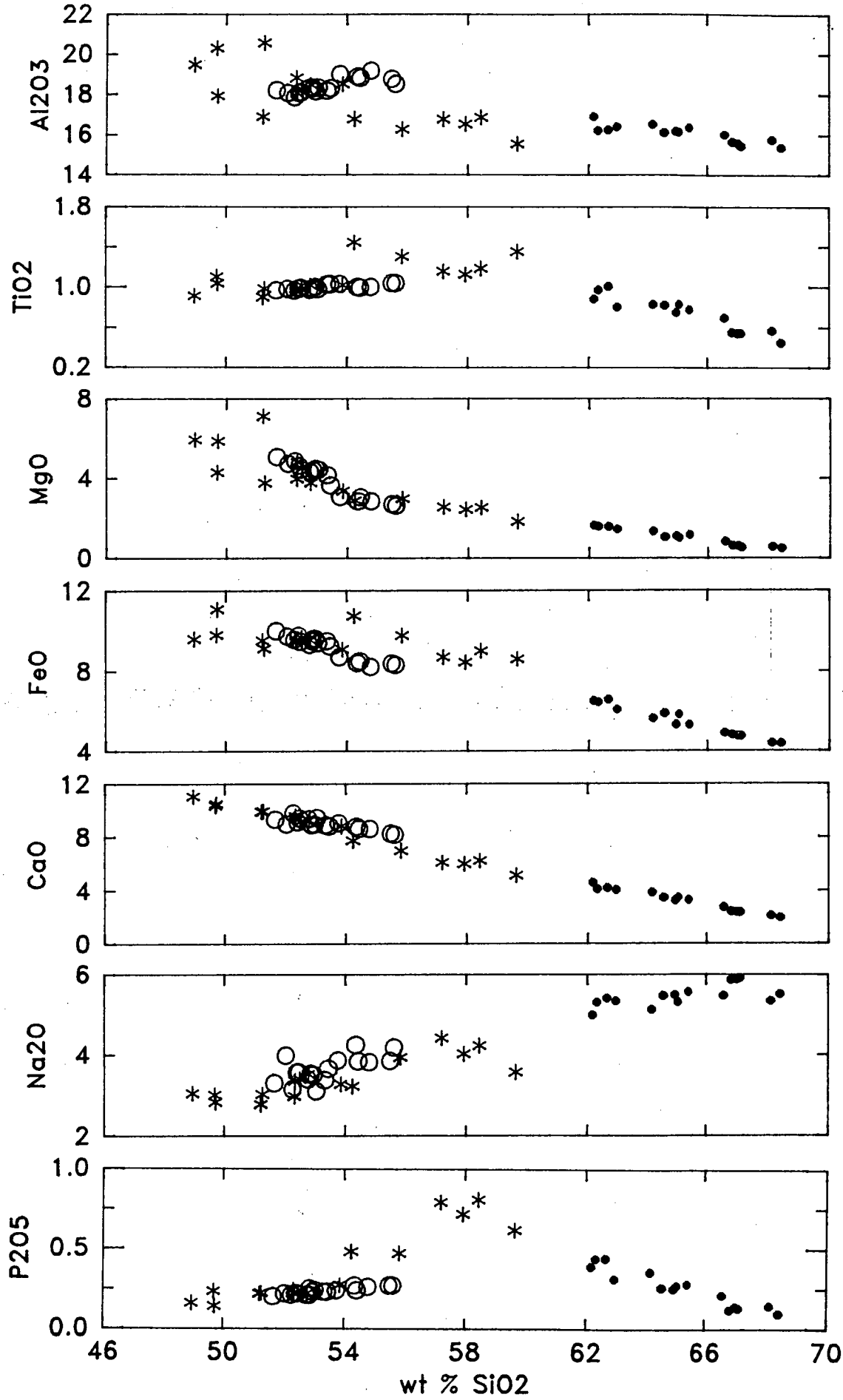

Figure 1.22 Major element Harker diagrams of Batur volcanic rocks (open circles = postcaldera; dots = caldera; asterisks = precaldera).

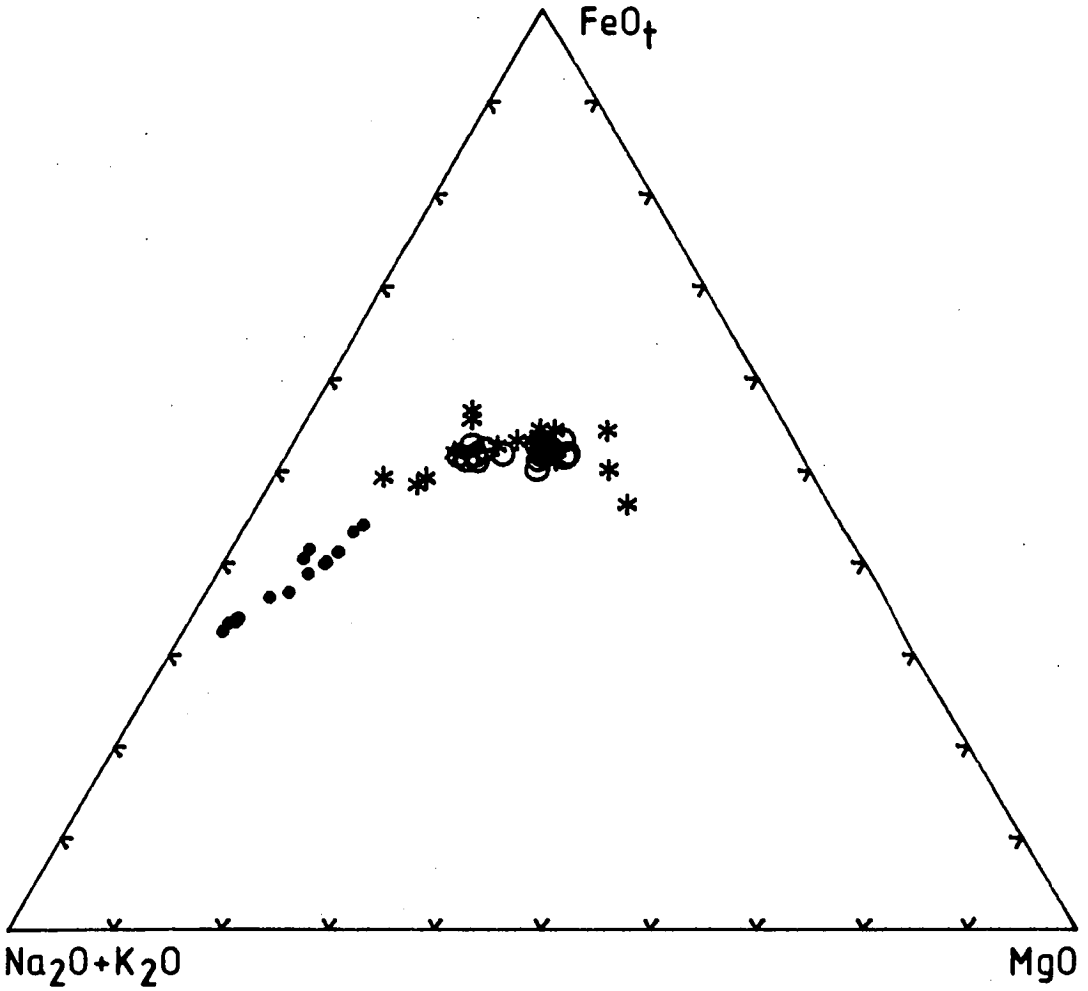

Figure 1.23 AFM diagram for Batur volcanic rocks (symbols as for Fig. 1.22).

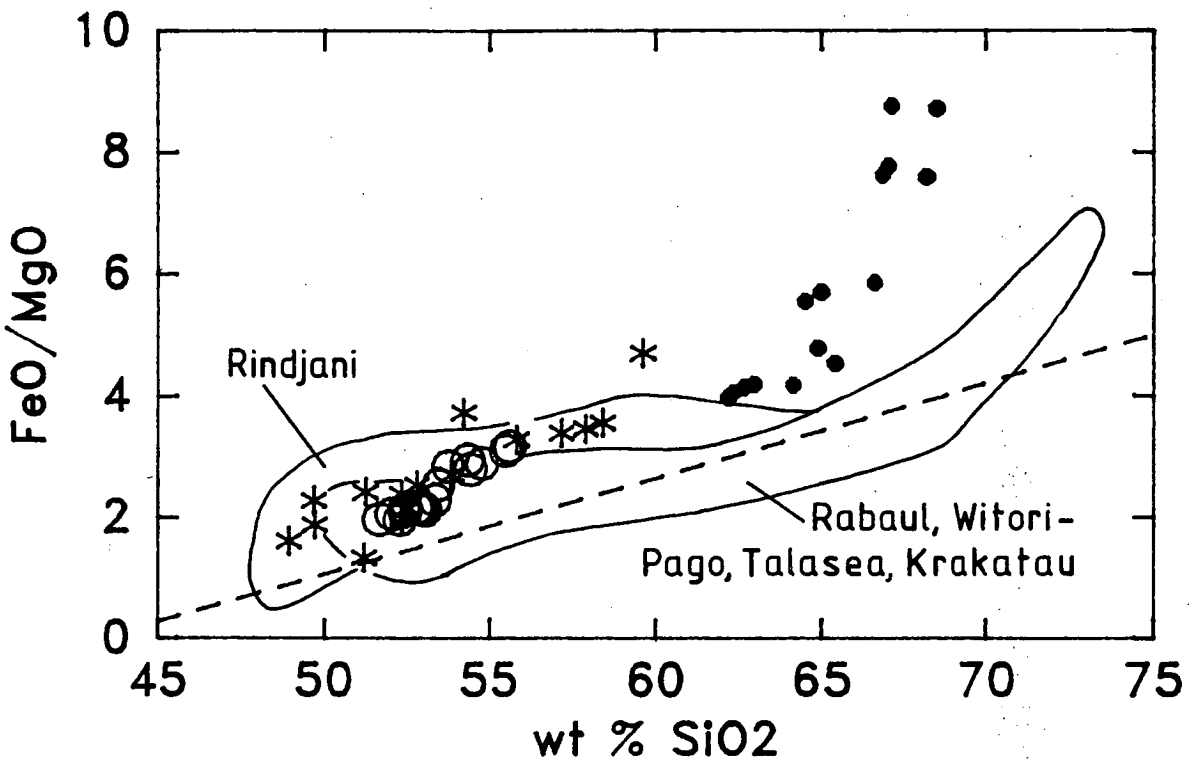

Figure 1.24 FeO/MgO against SiO_2 in Batur volcanics compared to some other orogenic basalt-andesite-dacite volcanic suites (symbols as for Fig. 1.22). Other data from Lowder and Carmichael (1970), Heming (1974), Blake and Ewart (1974), Whitford (1975a) and Foden (1979).

tholeiitic field of Miyashiro (1974). The Batur trend also shows a marked increase in the rate of Fe-enrichment at SiO_2 contents higher than 65 wt %. Trends formed by suites from some other young, island arc, stratovolcano calderas also appear to show increases in Fe-enrichment rate at high SiO_2 contents but these suites show markedly lower degrees of Fe-enrichment at intermediate SiO_2 contents than does Batur.

c) CIPW norm compositions

The Batur basalts are hy-normative (Fig. 1.25), with one olivine-rich basalt containing normative nepheline (all Fe as FeO). The more SiO_2-rich rocks from these groups and all of the caldera dacites are Q-normative.

d) Colour Bands in Dacite Bombs

Samples of the light- and dark-coloured bands in two Batur glassy dacite bombs were also analysed for major and trace elements. The results are listed in Table 1.8. For each rock, the compositions of the bands are identical within analytical error.

5.1.2 Trace Elements

The concentration ranges of trace elements analysed by XRF in the Batur volcanics are shown by Harker diagrams in Figure 1.26. Like the major elements, each group forms a curvilinear trend with increasing SiO_2 contents, with incompatible elements Ba, Rb, Zr, Nb, La, Ce, Nd and Y increasing in concentration, and compatible elements Sc, V, Ni and Cr decreasing. Sr shows a slight rise in abundance at intermediate SiO_2 contents but progressively decreases in abundance at higher SiO_2 values.

It is particularly notable that, for each trace element, the caldera dacites lie on extensions of the postcaldera trends, although the two groups are separated by a 6 % SiO_2 gap. In contrast, the precaldera rocks show clear trends towards markedly higher abundances of each of the incompatible elements compared to the postcaldera-caldera trends.

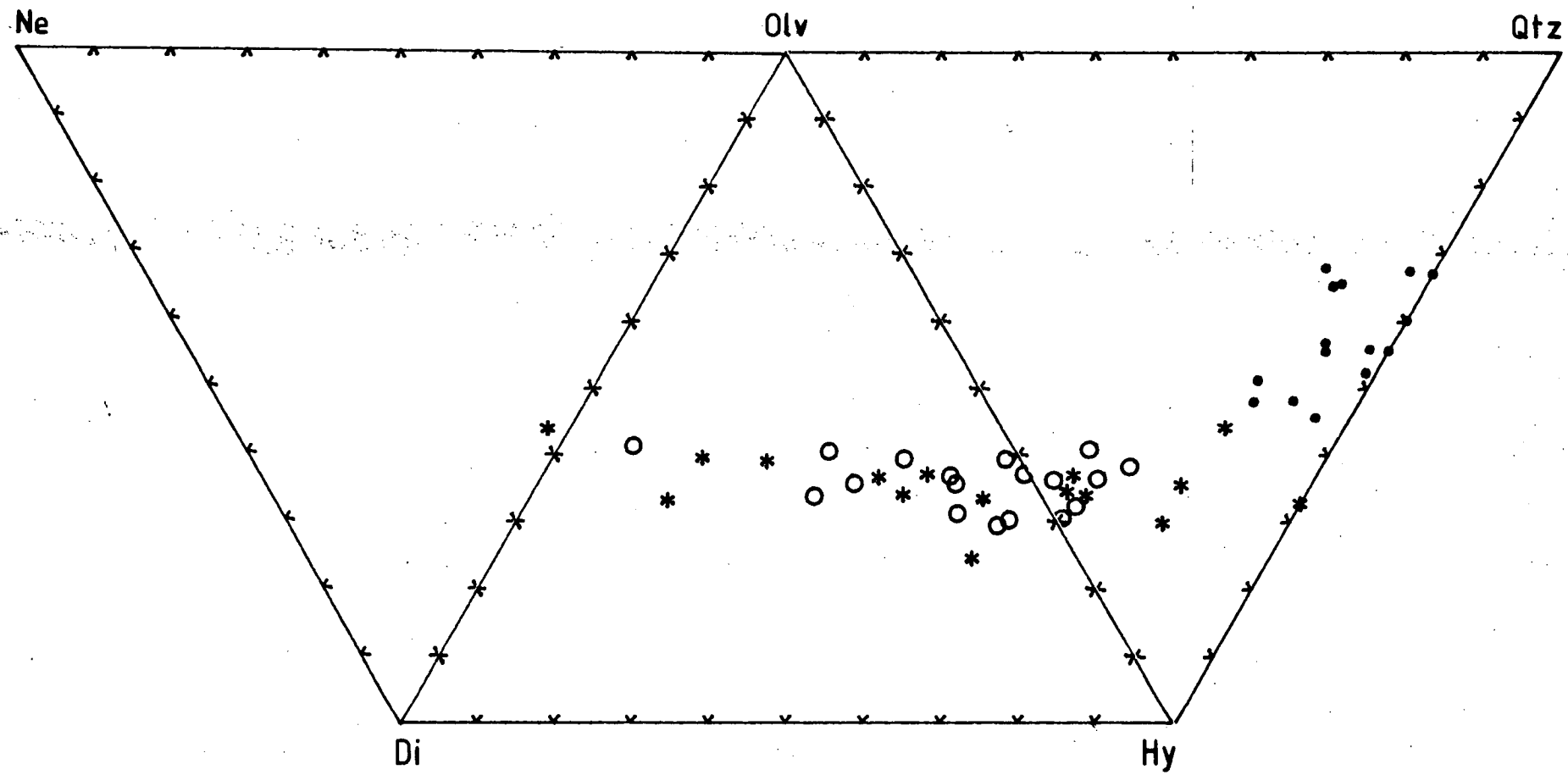

Figure 1.25 CIPW normative compositions of Batur volcanic rocks (all Fe as FeO; symbols as for Fig. 1.22).

	67281		67282	
	light	dark	light	dark
major elements (wt %)				
SiO_2	66.68	66.41	66.18	66.47
TiO_2	0.53	0.55	0.53	0.54
Al_2O_3	15.46	15.60	15.54	15.50
Fe_2O_3	5.14	5.33	5.22	5.26
MnO	0.19	0.19	0.20	0.20
MgO	0.55	0.63	0.58	0.61
CaO	2.25	2.43	2.38	2.37
Na_2O	5.90	5.84	5.97	5.84
K_2O	2.86	2.83	2.79	2.80
P_2O_5	0.12	0.12	0.15	0.14
LOI	-0.01	0.06	0.02	0.18
H_2O-	0.02	0.13	0.02	0.00
total	99.69	100.12	99.58	99.91
trace elements (p.p.m.)				
Ba	522	527	515	524
Rb	60	59	60	60
Sr	192	200	200	202
Zr	192	189	188	190
Nb	11	10	10	10
Y	41	41	41	42
La	23	20	22	22
Ce	48	44	50	47
Nd	25	27	25	26
Sc	17	18	17	17
V	5	9	7	8
Ni	1	2	1	1
Cr	3	1	7	3

Table 1.8 Compositions of light- and dark-coloured bands in two Batur glassy dacite bombs.

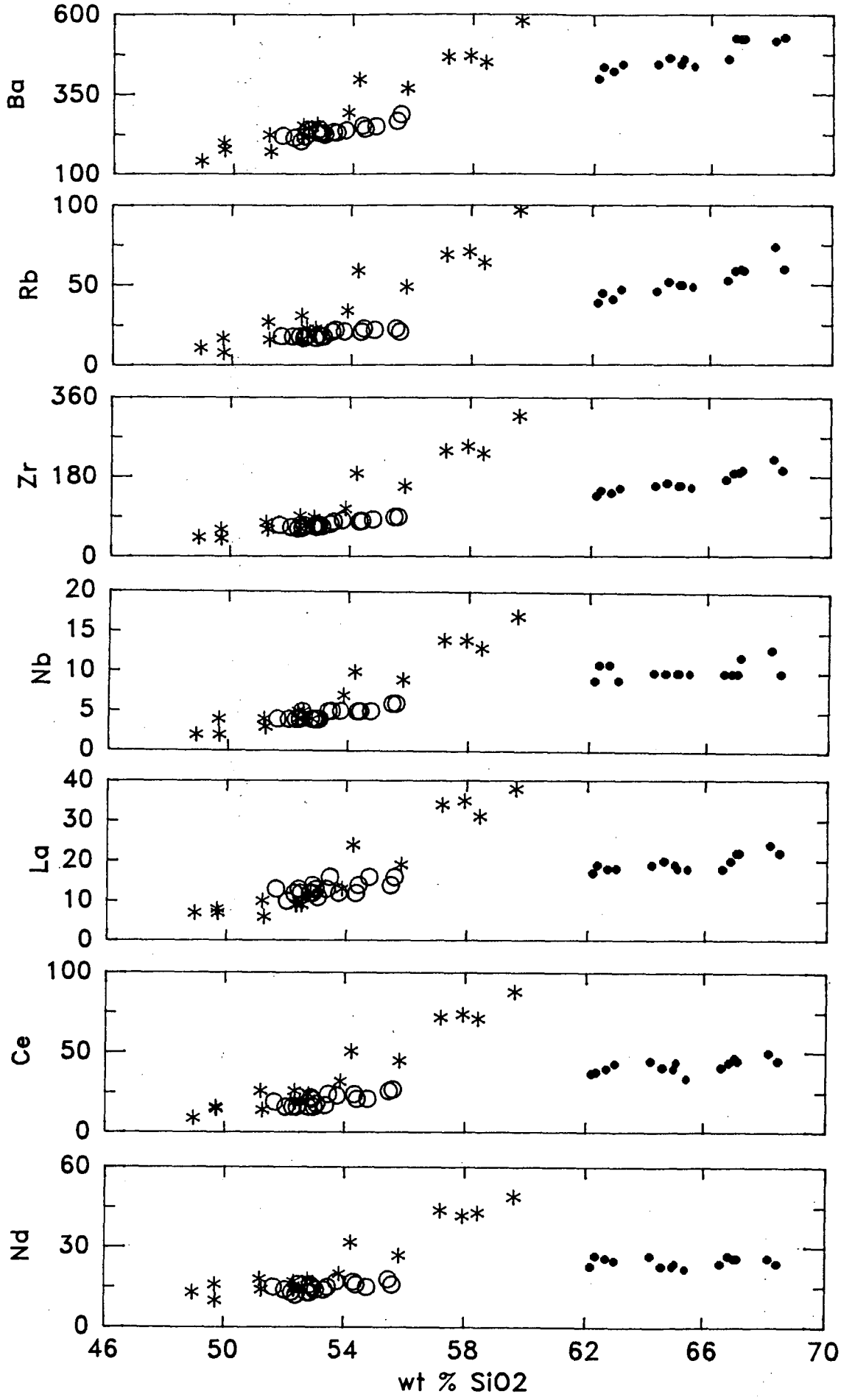

Fig. 1.26

continued over ..

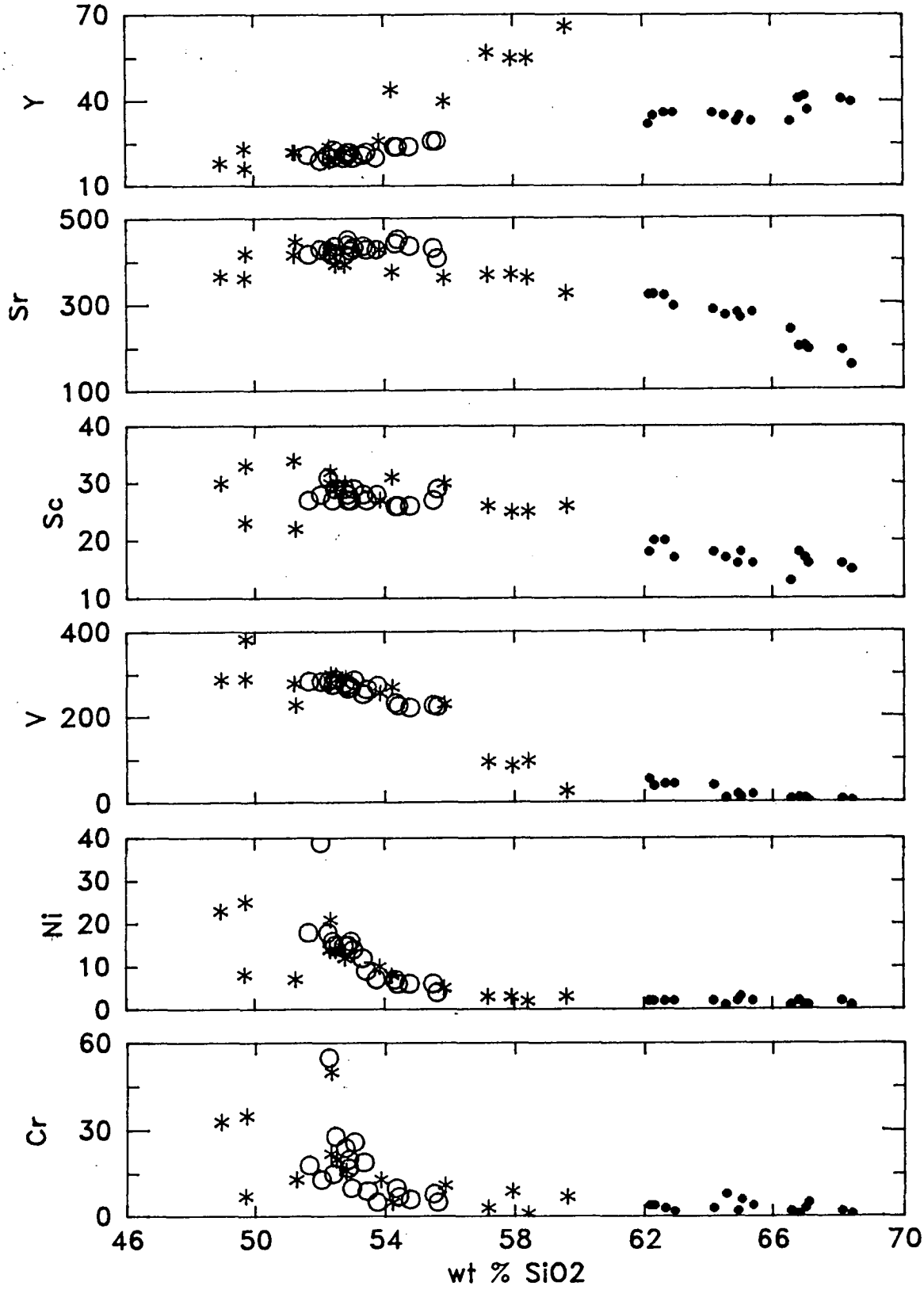

Figure 1.26 Trace element Harker diagrams of Batur volcanic rocks (symbols as for Fig. 1.22).

This relationship is also shown by a chondrite-normalized plot ('spidergram') of the representative Batur volcanic rocks listed in Table 1.7. On this diagram (Fig. 1.27) the Batur rocks generally show the characteristics usually associated with subduction- related igneous rocks, such as enrichments of K-group elements (Ba, Rb, K and Sr), light rare earth elements (La, Ce, Nd) and depletions of Nb relative to K and La. Each of the postcaldera and caldera rocks show restricted compositional ranges, with the caldera group lying above and generally parallel to the postcaldera group. The precaldera group, however, shows a wide range which exceeds that shown by the other two groups combined. In particular, the most enriched prcaldera rock, a pumiceous andesite clast, is clearly more enriched in incompatible elements than any of the dacites, even though it contains less SiO_2 (57.2 %) and MgO (2.6 %) and has a higher 100Mg/(Mg+Fe) value (34.5) than the most enriched of the dacites (67.1, 0.5, 16.9 respectively).

5.1.3 Rare Earth Elements

Chondrite-normalized REE patterns of the Batur postcaldera basaltic lavas show only small variation in their range of enrichment (Fig. 1.28), with La_N varying from 29 to 33 (Table 1.9). The patterns are characterized generally by slight to moderate LREE-enrichment (La_N/Yb_N = 3.2 to 3.4) and small, negative Eu anomalies (Eu/Eu^*-1 = 0.00 to -0.04). Also, in contrast to arc lavas from the Mariana-Izu arc and from Grenada in the Antilles arc (Dixon & Batiza 1979; Hole et al. 1984; White & Patchett 1984; Thirlwell & Graham 1984) the Batur basalts, like all basalts in the Sunda-Banda arc so far analysed for REE (Part 2), do not show negative Ce anomalies (Ce/Ce^*-1 = 0.01 to 0.04).

Although their SiO_2 and Zr contents and Mg/(Mg+Fe) values vary widely, the caldera dacites also show only a restricted range of REE enrichment, with La_N ranging between 54 and 63. These rocks are characterized by slightly higher LREE enrichment than the postcaldera lavas (La_N/Yb_N = 3.5 to 3.9) and their REE patterns are distinctly more concave upwards (La_N/Sm_N = 2.0 to 2.3) than those of the post-caldera lavas (La_N/Sm_N = 1.7 to 1.8). The dacites also show

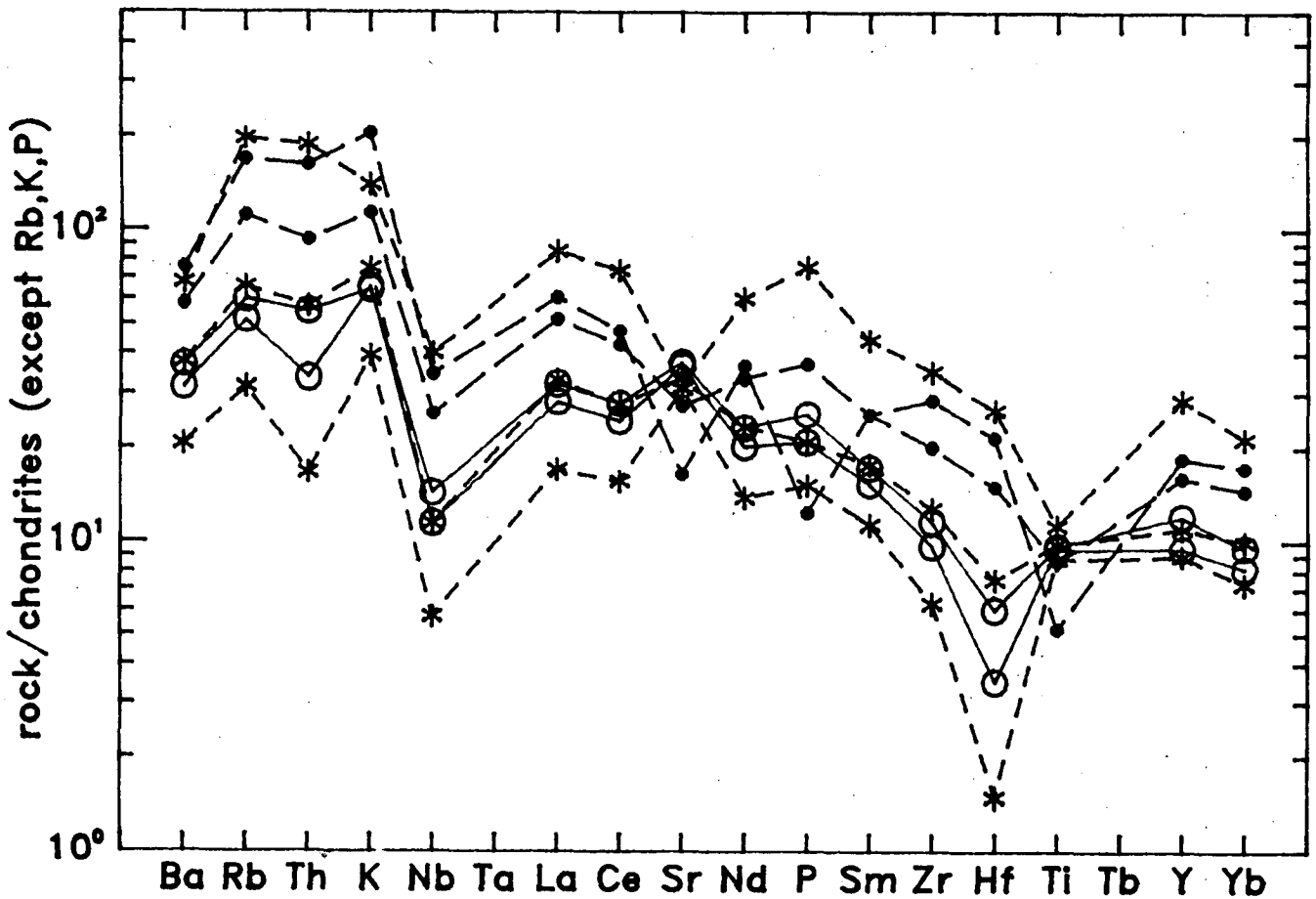

Figure 1.27 Spidergram of representative Batur volcanic rocks (Table 6). Normalizing values and element order after Thompson (1982) (symbols as for Fig. 1.22).

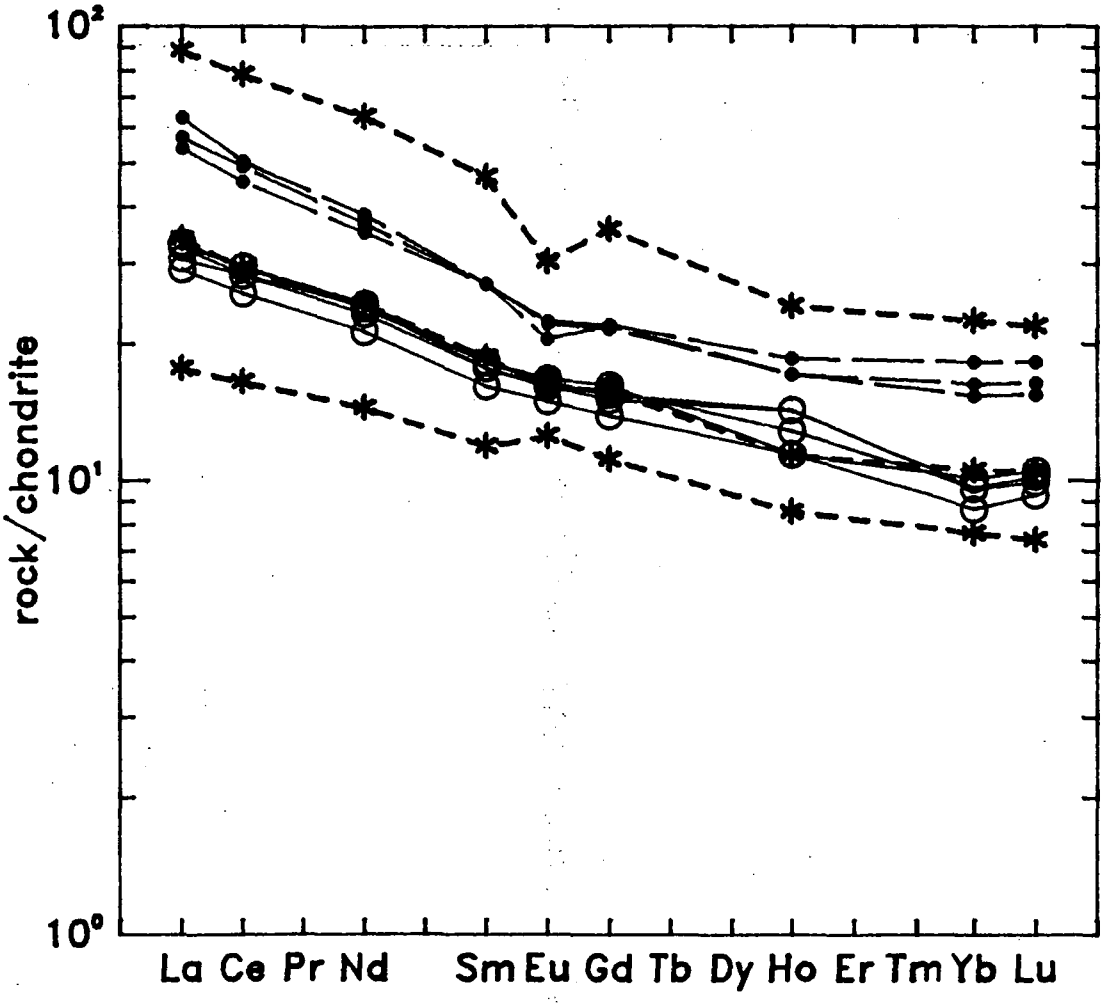

Figure 1.28 Chondrite-normalized rare earth element patterns of selected Batur volcanic rocks (symbols as for Fig. 1.22). Chondrite values (Leedey/1.2) based on Masuda et al. (1973).

rock	SiO_2	Mg/(Mg+Fe)	Zr	La_N	La_N/Yb_N	La_N/Sm_N	Eu/Eu^*-1	Ce/Ce^*-1
precaldera								
67341	48.94	52.3	43	17.8	2.31	1.48	0.09	0.03
67328	52.80	41.3	87	34.3	3.24	1.83	-0.06	0.00
67299	57.19	34.5	239	88.9	3.93	1.90	-0.26	0.03
caldera								
67275	62.16	31.1	137	54.0	3.51	1.99	-0.09	0.02
67273	65.38	28.3	156	57.1	3.50	2.11	-0.09	0.05
67277	67.11	16.9	195	63.2	3.46	2.33	-0.16	-0.01
postcaldera								
67244	52.03	46.4	66	29.2	3.37	1.81	0.00	0.02
67257	52.97	45.4	71	30.8	3.20	1.74	-0.01	0.03
67238	53.44	41.3	78	32.7	3.40	1.85	-0.04	0.01
67240	53.75	38.6	81	33.0	3.43	1.81	-0.02	0.04
67259	54.33	37.7	79	33.3	3.30	1.83	-0.03	0.02

$Eu^* = 0.0722(Gd_N+(Sm_N-Gd_N)/2 \qquad Ce^* = 0.813(Nd_N+(La_N-Nd_N)/2)$

Table 1.9 Rare earth element characteristics of selected Batur volcanics. Chondrite values (Leedey/1.2) based on Masuda et al. (1973).

negative Eu anomalies (Eu/Eu^*-1 = -0.09 to -0.16) with the most REE enriched rock (67277) showing the largest magnitude anomaly.

The precaldera rocks show by far the widest range of REE enrichment, including a basalt (67341) possessing the least enriched pattern of any Batur volcanic rock (La_N = 18) and an andesitic pumice clast (67299) with the most enriched (La_N = 89). Within the precaldera group, LREE enrichment increases progressively (La_N/Yb_N = 2.3 to 3.9), spanning the range covered by the postcaldera and caldera rocks. The degree of concavity of the patterns also increases progressively (La_N/Sm_N = 1.5 to 1.9) but not to the same extent as the caldera dacites. The two precaldera basaltic rocks (67341 and 67328) show small, negative Eu anomalies (Eu/Eu^*-1 = -0.06 to -.09), like the postcaldera basalts, but the andesitic pumice clast shows the largest magnitude anomaly of any Batur volcanic rocks (Eu/Eu^*-1 = -0.26).

Like the spidergram pattern, a significant feature of the REE patterns of the Batur volcanics is that although the precaldera andesitic pumice clast (67299) is less SiO_2-rich and shows a higher 100Mg/(Mg+Fe) value than any of the caldera dacites (Table 1.7) it is substantially more REE enriched than the dacitic rocks. This relationship is consistent with the respective abundances of other incompatible trace elements in the two groups and indicates that the more SiO_2-rich members of the precaldera group cannot be related directly by fractional crystallization to the caldera dacites.

5.2 Geochemical Evolution of Batur volcanism

In general, during the growth of Batur volcano, the chemical composition of its products has varied progressively from basaltic through andesitic to dacitic. Eruption of the dacitic rocks culminated in formation of Batur caldera and was followed by the production of rocks of basaltic and basaltic andesite compositions. This general pattern has occurred at many island arc stratovolcano calderas, such as Krakatau, but it is clear that, at Batur volcano, there are marked geochemical and petrographic differences between the caldera stage dacites and the andesites and basaltic andesites that preceded them.

This distinction is clearly shown by plots of major elements against Zr, which shows the widest concentration range of the incompatible trace elements. As will be shown later, Zr contents also form the best differentiation index of any geochemical parameter of the Batur rocks. Figure 1.29 shows the variation of some of the major elements against Zr. In each case, the postcaldera lavas and the caldera dacitic lavas and pyroclastics form colinear trends which clearly diverge from those of the precaldera basalts, basaltic andesites and andesites. Yet, it is important to note that, although their geochemical characteristics indicate that they are genetically related in some way, the postcaldera basaltic rocks were erupted after the caldera dacites. This unusual and very significant characteristic of Batur volcanism will be recalled in later discussion of the processes by which the products of Batur were formed.

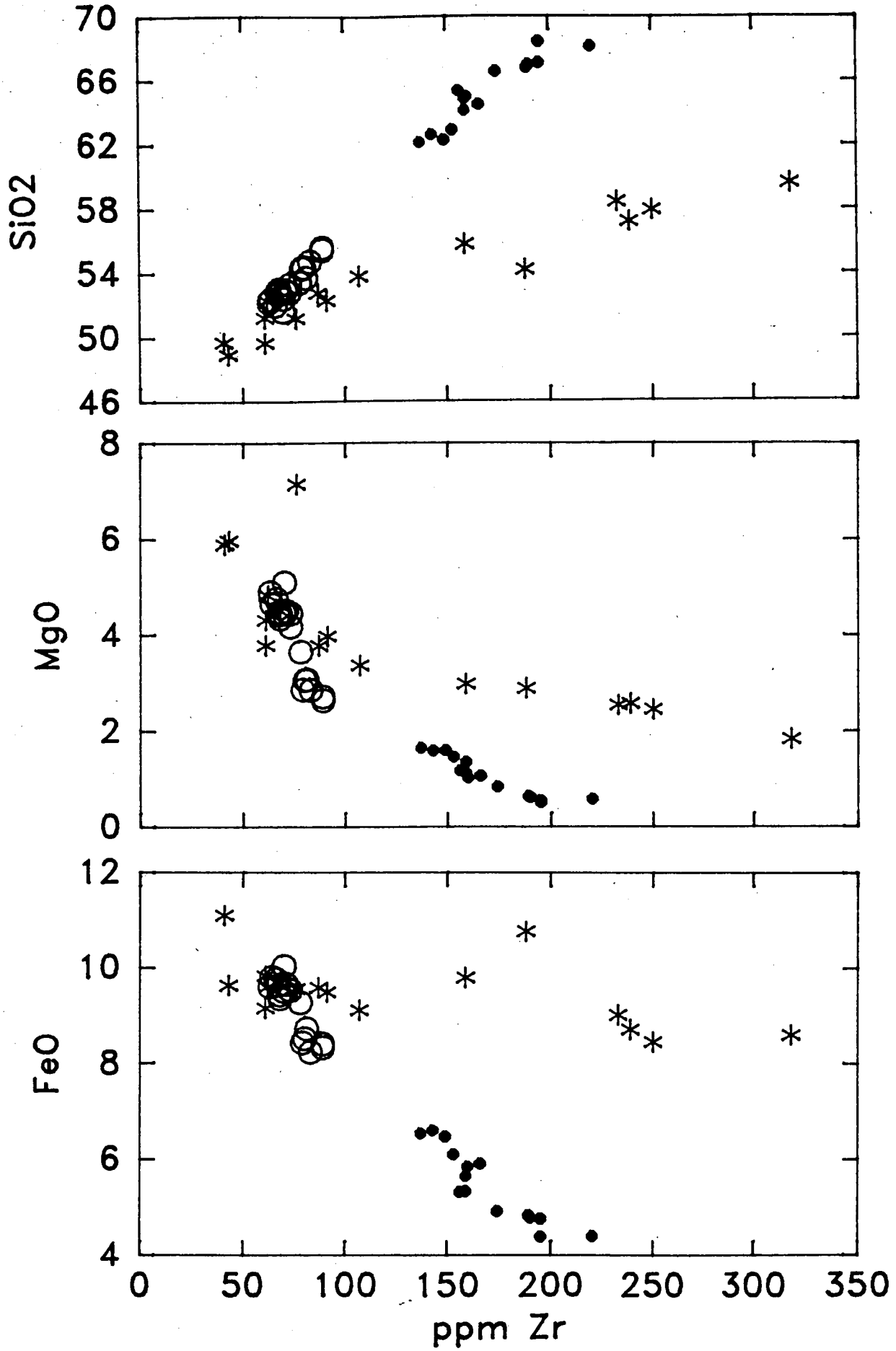

Fig. 1.29

continued over ..

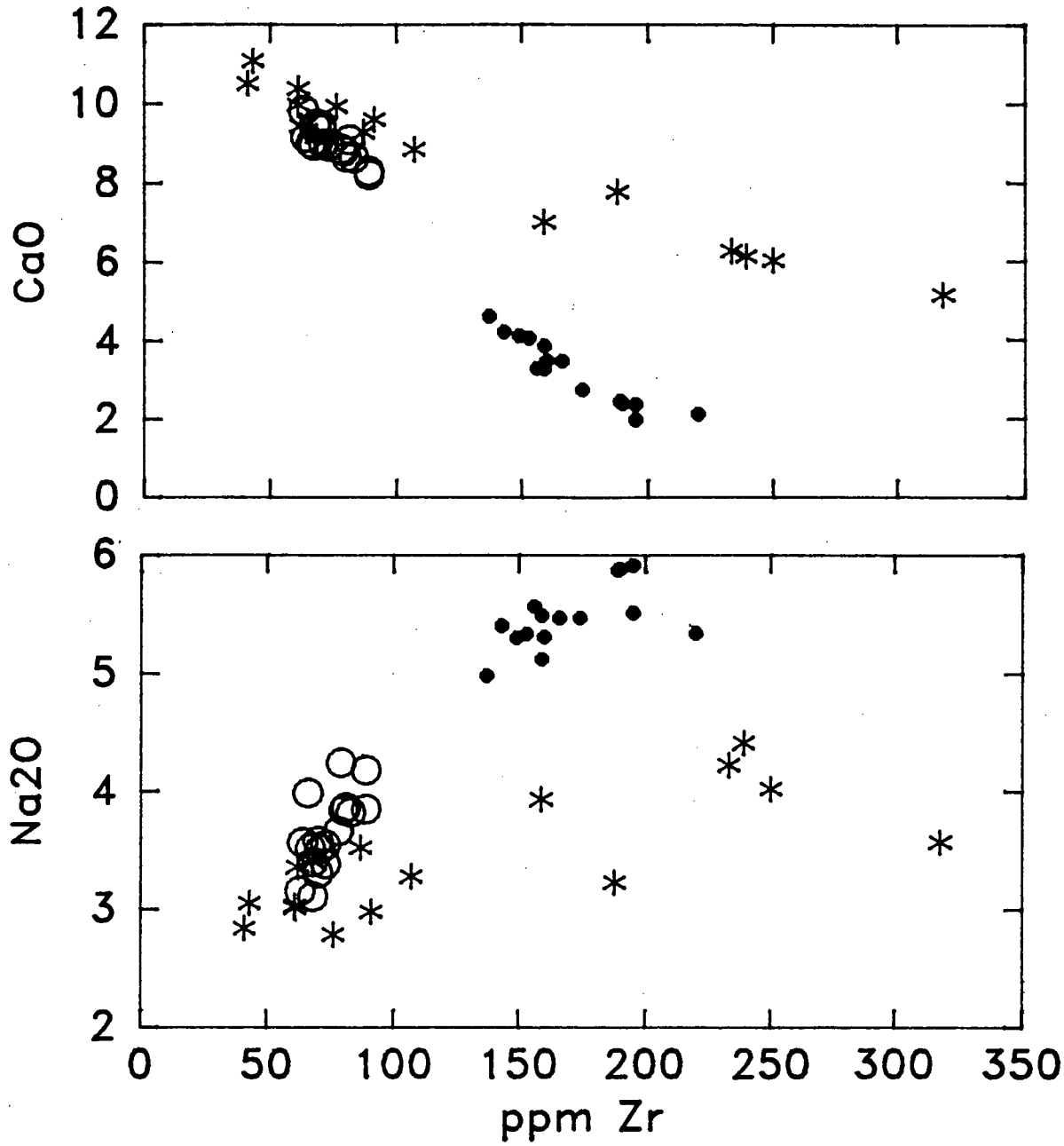

Figure 1.29 Selected major elements against Zr in Batur volcanic rocks (symbols as for Fig. 1.22).

5.3 Compositional Variation With Time of Postcaldera Lavas

Seven of the nine historical lavas from Batur volcano have been sampled (the 1921 lava was completely covered by that erupted in 1963, and the 1968 lava has not yet been sampled) and the relative ages of four prehistoric postcaldera lava flows from near Songan are known from superposition.

The variations with time of several compositional and phenocryst modal parameters are shown in Figure 1.30. Marked variation is present within both the Songan and historical lavas, indicating that their source chamber is either compositionally heterogeneous or is subject to dynamic behaviour of some kind, such as periodic influxes of new magma.

5.4 Geochemical Comparisons With Other Balinese Volcanoes

Seventy-seven new wholerock major and trace element analyses of lava samples from Agung, Seraja, Bratan, Tapak, Lesong and Batukau volcanoes, and from the Ulakan Formation, provide a regional geochemical context for Batur volcanism. All analyses are listed in Appendix 2.

The oldest and most distinctive, petrographically and chemically, of these rocks are the pillow basalts from the Ulakan Formation. These typically contain abundant large, normally-zoned, euhedral phenocrysts of olivine and clinopyroxene, as well as smaller phenocrysts of plagioclase and Ti-magnetite in some rocks. Cr-spinel occurs as small euhedral inclusions in olivine. In two samples from which microprobe mineral analyses are available (67415 and 67418) the 100Mg/(Mg+Fe) values of olivine phenocryst cores vary from 89 to 81, and those of clinopyroxene from 97 to 80. Cr-spinel shows a range in 100Mg/(Mg+Fe) values from 66 to 35, in $100Fe^{3+}/(\text{total Fe})$ values from 61 to 42, and in $100Cr/(Cr+Fe^{3+}+Al)$ values from 61 to 18 (see Fig. 1.19).

The Ulakan rocks possess high MgO contents, 7-13 wt % excepting sample 67424 with 17.5 wt %, and 100Mg/(Mg+Fe) values (75-56) and low Al_2O_3 (9-16 wt %) and TiO_2 (0.5-0.8 wt %)

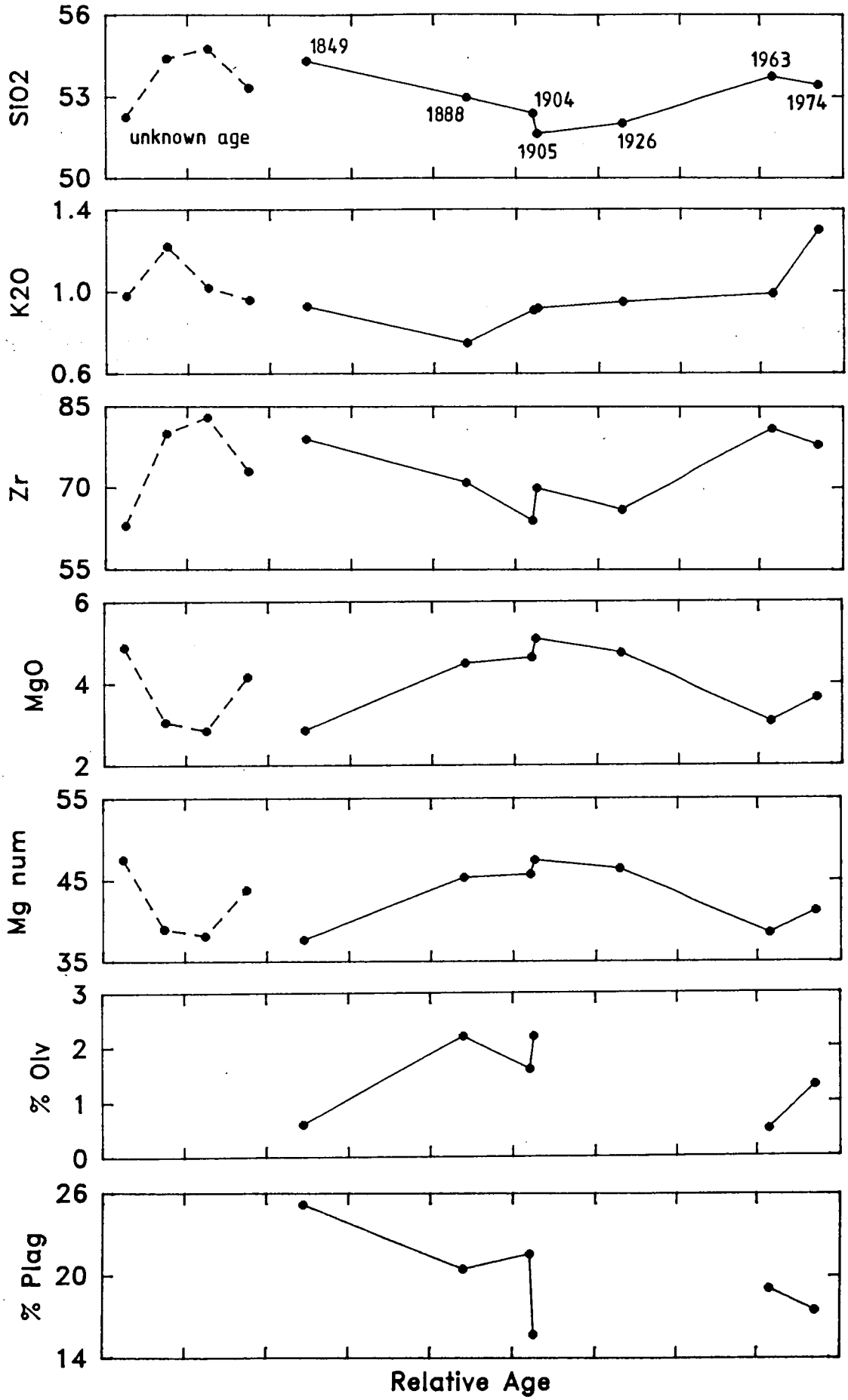

Figure 1.30 Variation with time of selected geochemical and modal parameters in Batur postcaldera lavas.

contents, as well as the orogenic characteristic of low Nb abundances. They are similar to primitive rocks found in some other orogenic regions which Ramsay et al. (1984) referred to as 'arc picrites'. However, similar olivine- and clinopyroxene-rich lavas associated with Rindjani volcano on Lombok and Grenada were termed 'ankaramites' by Foden (1979,1983) and Arculus (1978) respectively. The latter terminology is applied here to the Ulakan rocks because it correctly implies that they contain substantial proportions of clinopyroxene, as well as olivine, phenocrysts.

Most of the Ulakan rocks show evidence of alteration, including the presence of vesicle-filling zeolites and groundmass chlorite and clays. Whitford (1975a) analysed six samples and found that they contain high K_2O contents which correlate negatively with MgO contents and positively with light rare earth abundances. Due to these correlations Whitford (1975a) suggested that the high K_2O contents were a primary characteristic rather than a product of alteration. The new data show similar correlations, supporting Whitford's (1975a) interpretation.

All of the other eastern Bali volcanics possess typical orogenic basaltic to andesitic compositions and petrographic characteristics. Basalts from Agung volcano are generally similar to the basaltic lavas from Batur, containing abundant plagioclase and less abundant clinopyroxene, olivine and Ti-magnetite phenocrysts. However, unlike Batur, Agung has also erupted crystal-rich andesites which contain plagioclase, clino- pyroxene, orthopyroxene and Ti-magnetite phenocrysts. Some of these, including the andesitic 1963 lava flow, also possess small, disseminated crystals of olivine. Samples of lavas from Seraja volcano show a similar petrographic range.

Most of the samples collected from Tapak and Lesong volcanoes, in the central group of volcanoes, contain plagioclase, clinopyroxene, orthopyroxene and Ti-magnetite phenocrysts, with many also containing disseminated, small olivine phenocrysts. Those from Batukau volcano include orthopyroxene-free rocks, which contain moderately abundant olivine phenocrysts, as well as 2-pyroxene lavas.

In contrast to those from the other volcanoes, the lavas from Bratan volcano are typically phenocryst-poor, although plagioclase is still the dominant mineral phase. Two samples contain only plagioclase and olivine, while most others also possess clinopyroxene and Ti-magnetite phenocrysts. One rock (67409), from a lava flow lying midway up the northern Bratan caldera wall, contains plagioclase (100Ca/(Ca+Na) typically 50-65), clinopyroxene (100Mg/(Mg+Fe) = 65-63), orthopyroxene (100Mg/(Mg+Fe) = 60-58), olivine (100Mg/(Mg+Fe) = 48) and Ti-magnetite (Ulv_{57}) phenocrysts. These crystals show no evidence of substantial disequilibrium with the groundmass and their evolved compositions are similar to those of phenocrysts in the Batur caldera stage dacites.

The range of compositions shown by the eastern Balinese volcanics, compared to the postcaldera and caldera Batur rocks, is indicated by a K_2O-SiO_2 plot (Figure 1.31). The ankaramitic Ulakan volcanics (excluding Whitford's data), which fall mostly in the shoshonitic field in this diagram, are clearly the most K-rich and Si-poor of these rocks.

Rocks from Bratan, Tapak and Lesong fall mostly within the high-K field while those from Seraja lie on both sides of the boundary between the high- and medium-K fields. The Batur, Agung and Batukau rocks all possess medium-K compositions. It is notable that only the two caldera-volcanoes Batur and Bratan appear to have erupted rocks containing more than 60 wt % SiO_2. Except for the Ulakan rocks, all suites lie close to the Batur trend on AFM diagrams (Fig. 1.32).

In addition to variable K_2O contents, other compositional differences, involving trace and minor elements, occur among these suites. For example, on a plot of K_2O against Ba (Fig. 1.33) the Ulakan rocks are clearly distinguished from the others by their markedly higher Ba/K_2O values. They also possess the highest La/Zr (Fig. 1.34) and Ba/La (Fig. 1.35) values.

The Bratan rocks are distinguished from all of the other eastern Bali volcanics on a plot of TiO_2 against K_2O (Fig. 1.36). They possess unusually high TiO_2 contents for island

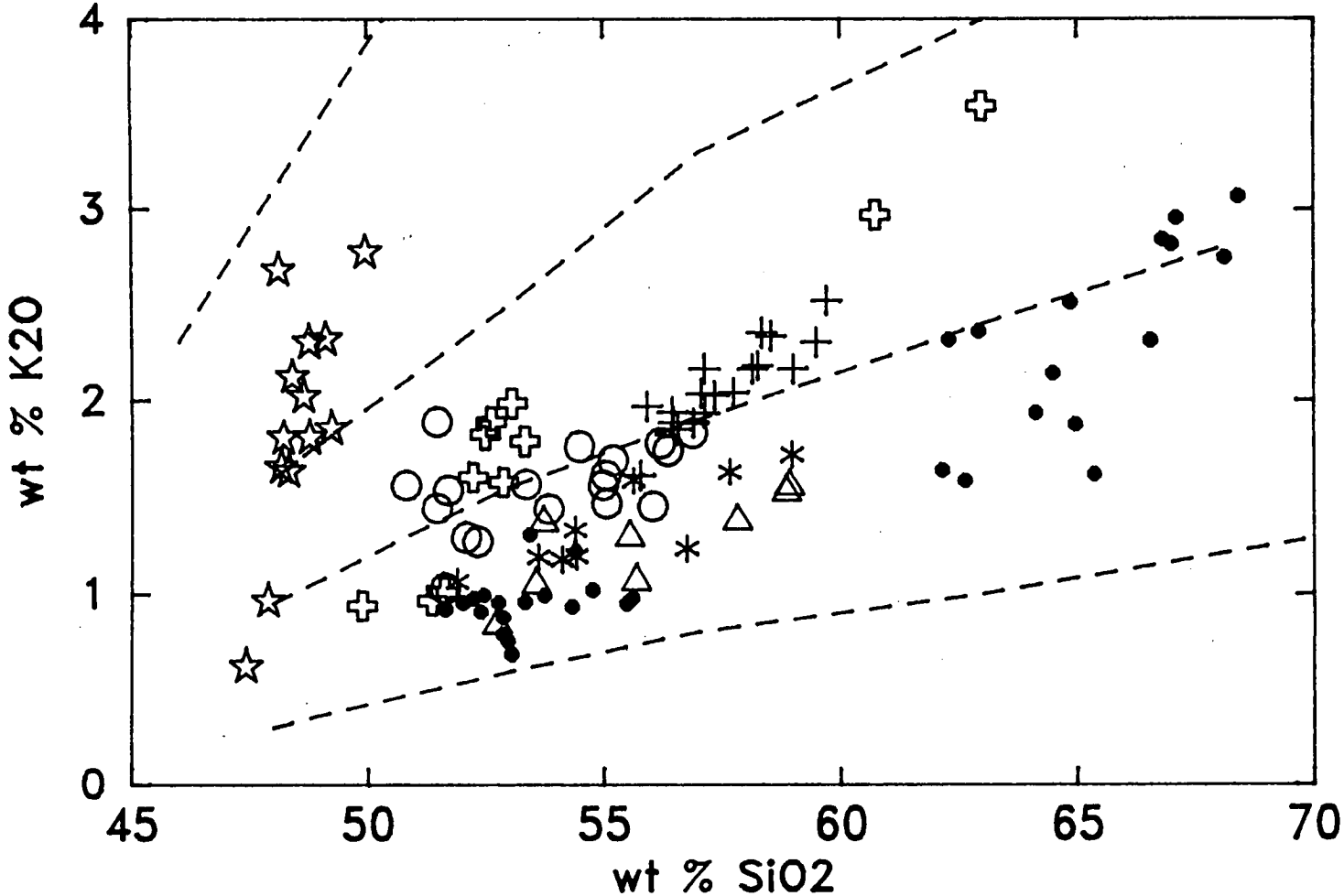

Figure 1.31 K_2O against SiO_2 in volcanics from central and eastern Bali (dots = Batur postcaldera and caldera; open stars = Ulakan; open circles = Seraja; asterisks = Agung; Swiss crosses = Bratan; open triangle = Batukau; crosses = Tapak and Lesong).

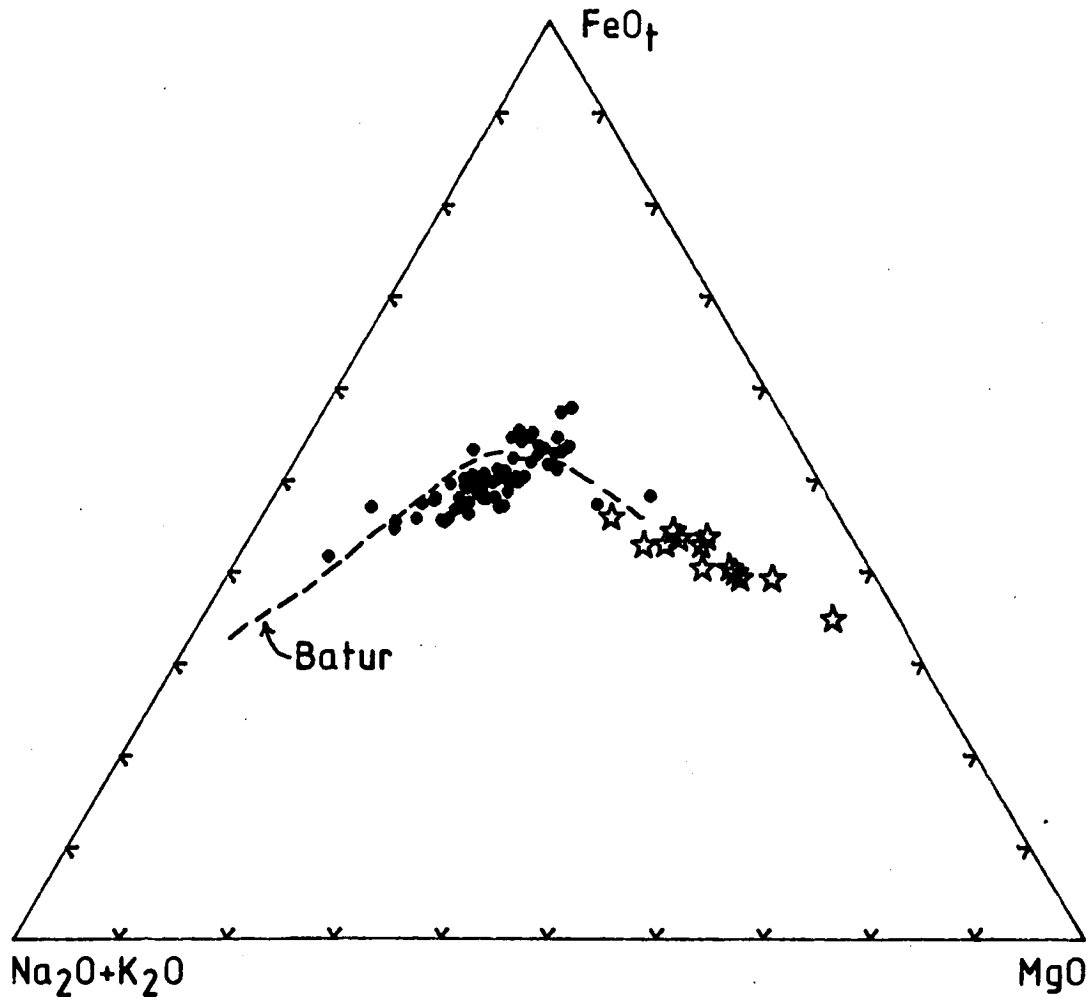

Figure 1.32 AFM diagram for volcanic rocks from central and eastern group Bali volcanoes (dots), and from the Ulakan Formation (open stars), compared to Batur.

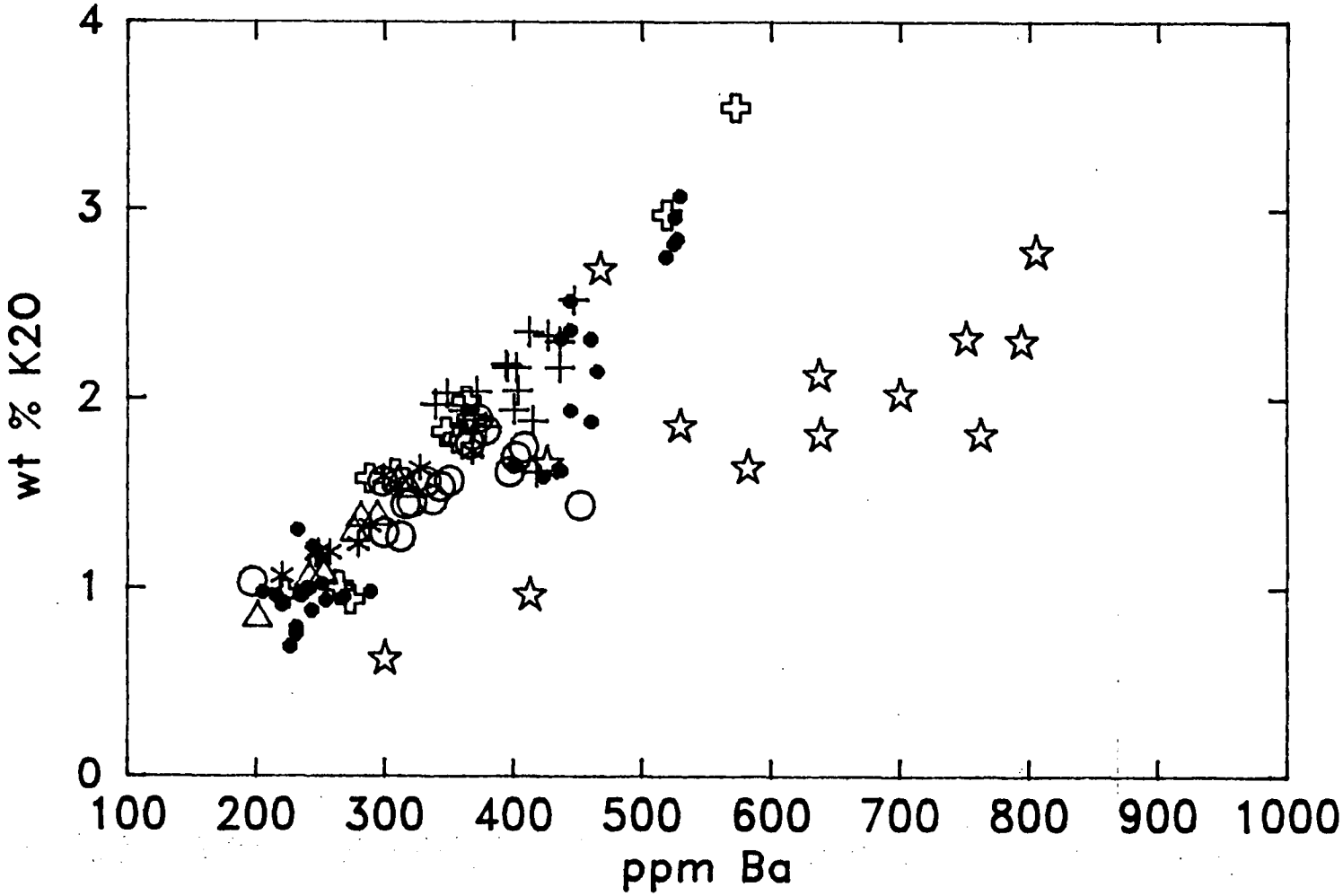

Figure 1.33 K_2O against Ba in volcanics from central and eastern Bali (symbols as for Fig. 1.31).

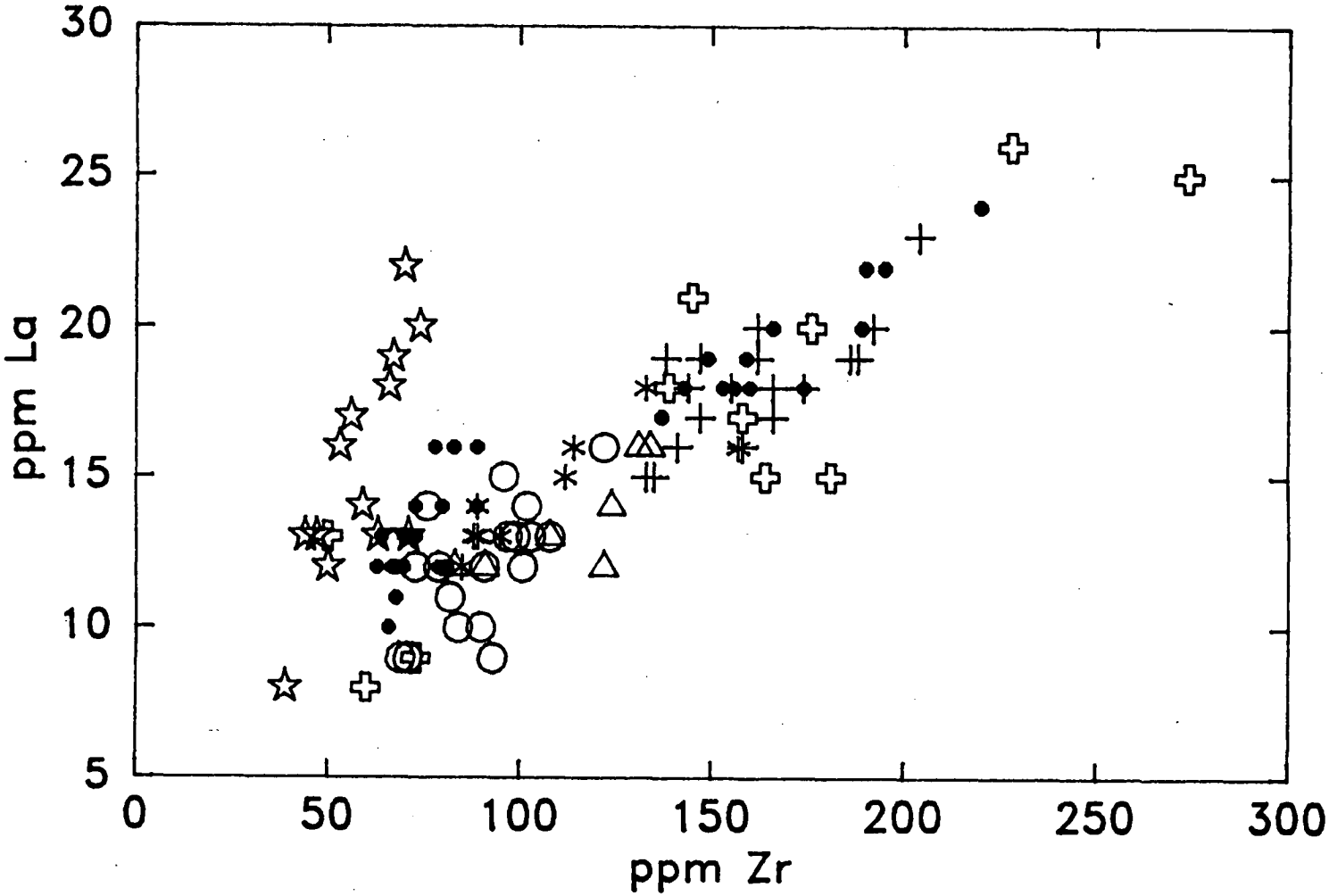

Figure 1.34 La against Zr in volcanics from central and eastern Bali (symbols as for Fig. 1.31).

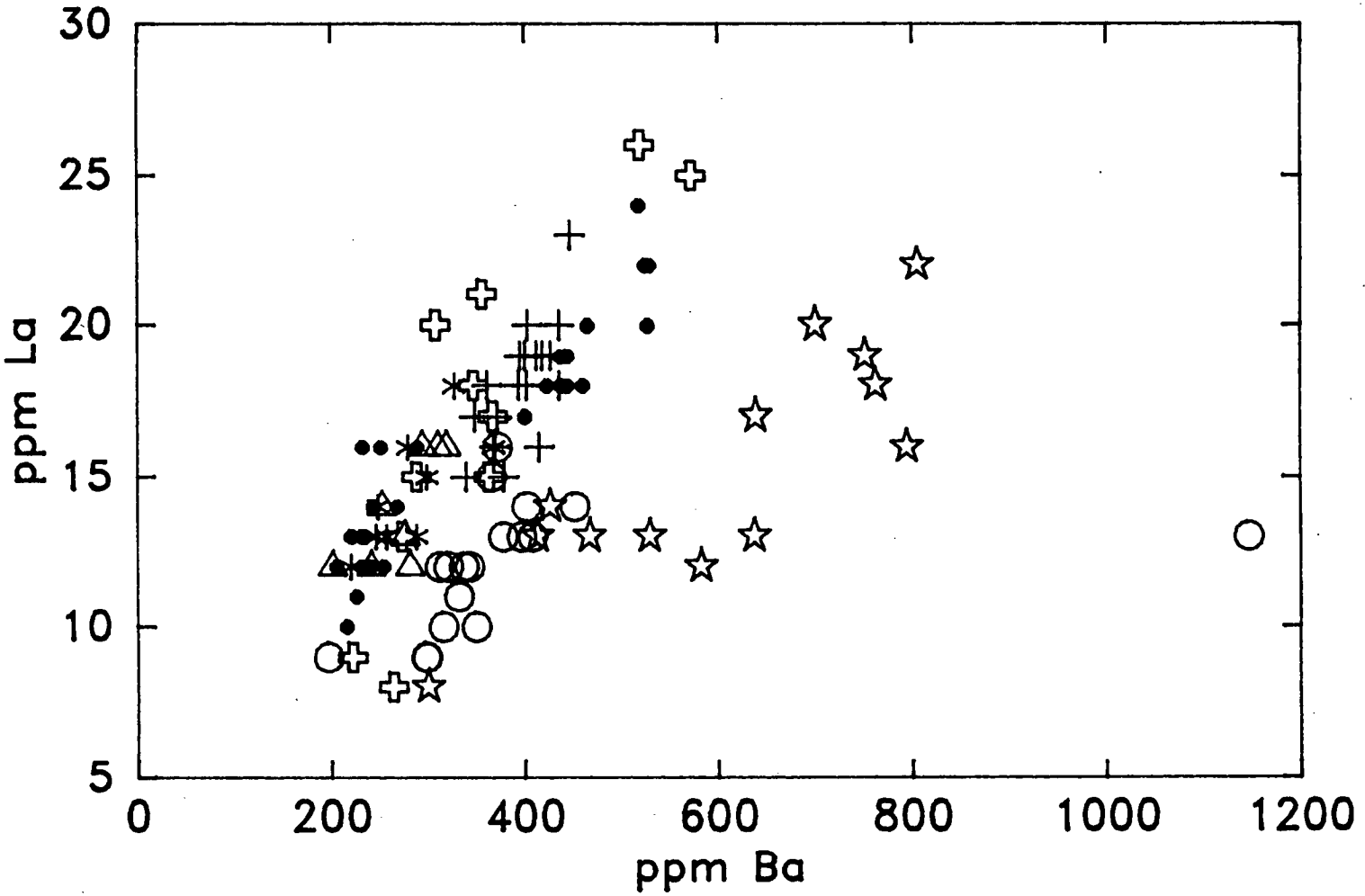

Figure 1.35 La against Ba in volcanics from central and eastern Bali (symbols as for Fig. 1.31).

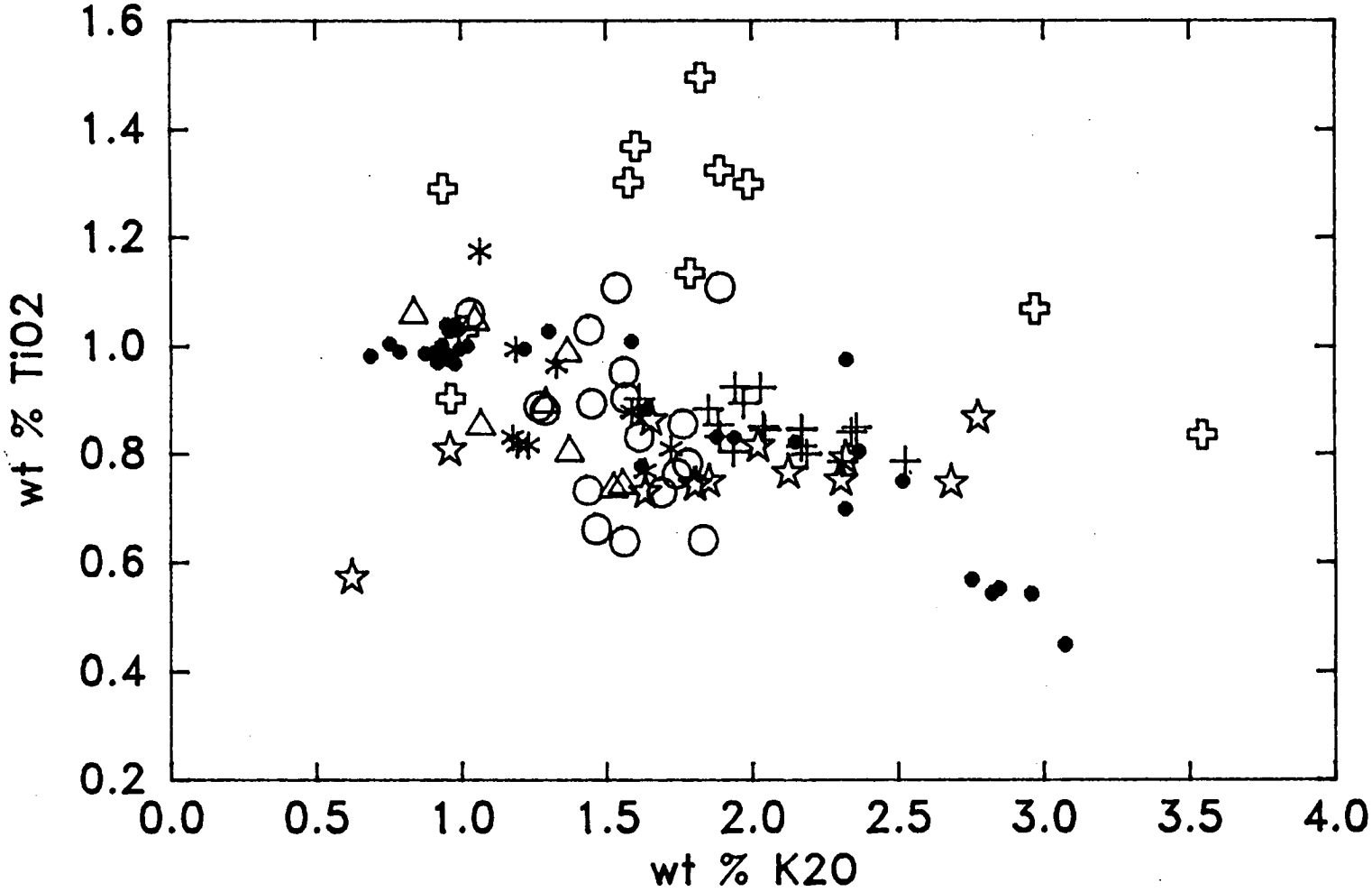

Figure 1.36 TiO_2 against K_2O in volcanics from central and eastern Bali (symbols as for Fig. 1.31).

arc volcanics and, in this respect, are similar to rocks from Slamet volcano in central Java. It is notable that lavas from the Tapak, Lesong and Batukau volcanoes are chemically different from the Bratan volcanics, even though they formed close to and within Bratan caldera. The Tapak and Lesong suites are also different from the Batukau and other suites by possessing high Zr/Y values (Fig. 1.37). Interestingly, although the Ulakan rocks contain relatively high K_2O and La (and Ce and Nd) contents, their Zr/Y values are similar to those of the other volcanics.

In summary, several geochemically distinct groups of volcanic suites are present in eastern Bali. Rocks from Batukau and the active Batur and Agung volcanoes possess generally similar compositions, with the lowest K_2O contents, while those of the Bratan, Tapak and Lesong, Seraja and Ulakan suites each show distinctive geochemical characteristics. It is notable that in central and eastern Bali there appears to be a general trend of increasing K_2O and light rare earth element concentrations with increasing age.

6. CAUSES OF COMPOSITIONAL VARIATION

6.1 Gravitative versus Liquid Fractional Crystallization

Since the pioneering work of Bowen (1928) the process of fractional crystallization of parental magmas has become widely favoured as the primary cause of the compositional variation observed within suites of volcanic rocks. Briefly, during cooling of a body of magma, the crystallization and removal of crystal assemblages having different bulk chemical compositions from those of the initial magmatic liquid leads to the production of residual liquids with progressively varying chemical compositions. These liquids may be tapped at any stage and erupted at the surface to form a co-genetic sequence of volcanic rocks.

With the development of precise methods of isotopic and chemical analysis of rocks and phenocrysts, additional processes such as magma mixing, periodic magma chamber replenishment and wallrock assimilation have been recognized

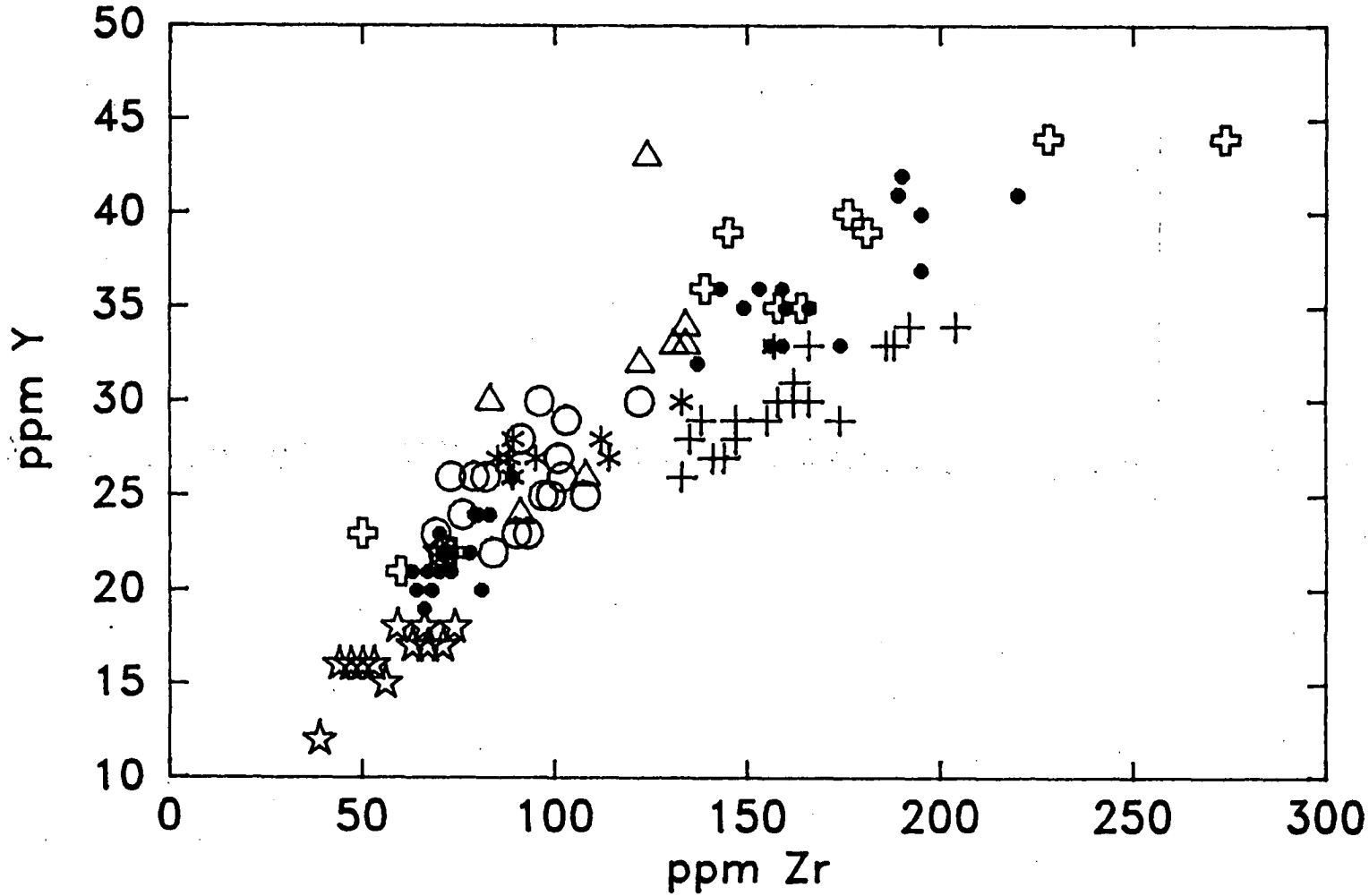

Figure 1.37 Y against Zr in volcanics from central and eastern Bali (symbols as for Fig. 1.31).

to be potentially important in causing compositional variation in volcanic rocks. In recent years, evidence has also been presented suggesting that thermogravitational diffusion may have been important during production of some very high SiO_2 magmas (e.g. Hildreth 1979).

Two contrasting mechanisms of crystal-liquid separation have been applied to crystallizing basaltic parental magmas. It is important to recognize which of these is most likely to have occurred because of their different implications for the evolution of large volcanoes, as will be shown later. During pure 'gravitative fractionation', the mechanism of fractional crystallization in basaltic magmas promoted by Bowen (1928) and established largely by subsequent studies of large layered basaltic intrusions such as Skaergaard (Wager & Brown 1968), crystals are thought to fall towards the base of a tranquil magma chamber with a terminal settling velocity (Stokes' Law) that is related to the crystal radius, crystal-liquid density contrast and the liquid viscosity.

However, for typical values of heat flux out of basaltic magma chambers, particularly in the early stages of intrusion when heat flux is likely to be high, and chamber size (a few kilometres high), convective circulation of intrusive basaltic magma typically must occur given the thermal characteristics and viscosities of molten magma (Bartlett 1969). Because this process retards gravitational settling by transporting crystals upwards in suspension, a complication recognized by Bowen (1928) and Wager and Brown (1968), the 'traditional' concept of fractionation by crystal settling under gravity therefore involves a balance between two opposing effects.

However, in recent years, experimental observations of the crystallization behaviour of hot, saturated aqueous solutions indicate that crystallization at the margins of a magma chamber, termed 'liquid fractionation' by McBirney et al. (1985) ('convective fractionation' by Sparks et al. 1984) may be the dominant mechanism of crystal-liquid fractionation (Sparks et al. 1984). This process was recognized by Bowen (1928 p. 22) but dismissed because '.. the great majority of large-scale examples do not suggest this origin.'. Bowen (1928

p. 23), however, appears not to have completely discounted the process, saying that '.. since the evidence of the rocks usually points merely to the fact of fractional crystallization rather than to the method whereby it is accomplished, it is essential to have in mind all processes of fractionation by crystallization.'.

Liquid fractionation occurs in addition to the formation of double-diffusive, horizontal convection cells when, in the simplest case, a horizontal thermal gradient is imposed on the solutions by cooling at vertical sidewalls (Chen & Turner 1980; McBirney 1980; Turner & Gustafson 1981). This process leads generally to the production of residual liquids which, depending on their densities relative to that of the unmodified solution, may either rise or sink along thin boundary layers between the crystal crust and the convection cells.

Although in magmatic systems the boundary layer liquids are colder than the initially homogeneous magma forming the bulk of the chamber, the positive buoyancy effects of the density contrast, particularly in calcalkaline systems in which the heavy oxides such as FeO are concentrated in the crystallizing components, is thought typically to outweigh the negative effect of the thermal contrast leading to ponding of chemically evolved liquids at the top of the chamber. In tholeiitic systems, however, substantial enrichment of Fe in the residual liquids during the intermediate stage of differentiation may increase their density, causing the boundary layer to flow downwards towards the floor (McBirney 1985;1980; McBirney et al. 1985; Lowell 1985),

In contrast to gravitative fractionation, therefore, a magma chamber may form that is essentially bimodal in chemical composition, possessing a cap of differentiated liquids overlying a main body of relatively unmodified magma. Nilson et al. (1985) calculate that a basaltic intrusion 1 km in diameter should possess a compositional boundary layer a few centimetres thick at its vertical margins flowing at about 1 cm s^{-1}. This would lead to accumulation of several cubic kilometres of differentiated magma in the roof zone each year. It is important to note, therefore, that liquid fractionation may

generate large amounts of SiO_2-rich magma early in the development of a basaltic magma chamber (Sparks et al. 1984).

The following discussion firstly examines the hypothesis that the Batur volcnic rocks were produced by fractional crystallization of a single, parental basaltic magma. Determination of the events that caused crystallization and whether it occurred by either gravitative or liquid fractionation mechanisms requires additional information, which is provided by integration of the geochemical, mineralogical, isotopic and stratigraphic data in a later section.

6.2 Trace Element Modelling

6.2.1 Trace Element Differentiation Models

Because of their typically low concentrations, the activities of trace elements in magmas may be treated as proportional to their concentrations (Henry's Law), so that the distribution of a particular trace element between a particular solid phase and the host liquid can be described simply by a Nernst distribution coefficient:

$$K_D = C^s/C^l$$

C^s = the concentration of the trace element in the solid phase
C^l = the concentration of the trace element in the liquid.

Typically, however, trace elements are also distributed to varying extents between two or more crystallizing mineral phases, which in a crystallizing magma, form a bulk fractionating assemblage. In that case, the Nernst coefficients are replaced by the bulk distribution coefficient, D, for each trace element:

$$D = \sum x_i K_D^i$$

x_i = weight fraction of mineral phase i in the bulk fractionating assemblage
K_D^i = Nernst distribution coefficient for the particular trace element in mineral phase i.

During closed system fractional crystallization of a cooling magma body, it may usually be assumed that only the outermost surfaces of growing crystals are in equilibrium with the host liquid, because of the low elemental diffusion rates within crystals compared to the rates of crystal growth and the common occurrence of zoned crystals. As a result, the concentration of a particular trace element in the residual liquid, C^l, is described by the Rayleigh fractionation law (derived in Wood & Fraser 1977, Chapter 6):

$$C^l = C^o.F^{D-1}$$

C^o = the concentration of the trace element in the parental magma
F = weight fraction of residual liquid
D = bulk distribution coefficient.

Pioneering studies by Schilling and Winchester (1967) and Gast (1968) and subsequent work by other authors have established the applicability of petrogenetic models based on this equation, as well as the equivalent equation for processes, such as partial melting, in which elemental diffusion within crystals is less important.

The Rayleigh equation was expanded by O'Hara (1977), and later by O'Hara and Mathews (1981) in a detailed discussion that encompassed a range of dynamic magmatic processes, to describe trace element concentrations in a model open system magma chamber that is periodically replenished by new magma and tapped during eruptions. De Paolo (1981) expanded the Rayleigh equation to model the effects of combined fractional crystallization and wallrock assimilation processes. De Paolo's equation may also incorporate the effects of periodic magma chamber replenishment. Similarly, Cann (1982) derived an equation based on the Rayleigh equation which applies in cases where liquid is lost continuously from the magma chamber.

In practice, the Nernst distribution coefficients for most trace elements have proven difficult to measure because of the uncertainty in many cases that phenocryst assemblages in

volcanic rocks have crystallized in equilibrium with the groundmass (=residual liquid) in which they occur, and because of the difficulty in some cases of obtaining sufficiently pure mineral separates prior to analysis. Also, Nernst distribution coefficients typically show dependence on liquid composition, temperature and pressure (reviewed by Wood & Fraser 1977), causing uncertainty in the application of coefficients measured from one suite of rocks to others.

To overcome these difficulties, Allegre et al. (1977) developed an inverse approach in which the bulk distribution coefficient, D, of each trace element in a cogenetic suite of volcanic rocks is calculated from the variation shown by the wholerock geochemical characteristics. This approach assumes that volcanic rocks forming a particular suite are related genetically by closed-system fractional crystallization, that is, without magma replenishment or a wallrock involvement, and requires that at least one trace element was perfectly incompatible (D=0) during crystallization.

This approach provides a test which determines whether a consanguineous suites of volcanic rocks are related by closed-system fractional crystallization or whether another process, possibly an open-system kind like those suggested by O'Hara and Mathews (1981), De Paolo (1981) and Cann (1982), was responsible. In particular, closed-system fractional crystallization, involving mixing of the major element compositions of rocks and phenocrysts, may also be modelled using 'least squares' calculations. Closed-system fractional crystallization is the most likely process to have occurred if these independent trace and major element approaches yield similar results for a particular suite of volcanic rocks. Inconsistent results suggest that a more complex process may have occurred.

The trace element approach of Allegre et al. (1977) may also reveal changes of distribution coefficients during fractionation. These may be caused by particular phenocryst minerals either ceasing or beginning to crystallize. Phase changes may be important indicators of substantial variations in the physical environment of the crystallizing magma chamber.

6.2.2 Calculation of Bulk Partition Coefficients

Allegre and Minster (1978) suggested that Ta, Th, La and Ce may be considered as being perfectly incompatible during crystallization of basaltic magmas. However, as will be shown, in the Batur volcanics La and Ce show different patterns of behaviour in the dacites compared to the basaltic rocks, indicating that these two elements were not perfectly incompatible throughout the differentiation process.

Abundances of Ta and Th have been measured in a range of Batur volcanics by INAA (Table 1.7). However, the absolute abundances of Th are substantially greater than those of Ta in these rocks and Th is therefore used here as the normalizing element.

Log-log plots of 12 trace elements against Th are shown in Figure 1.38. In almost all plots the postcaldera lavas are colinear with the precaldera group, while the dacites lie on divergent trends. In most cases, the lines drawn through the pre- and postcaldera samples are least squares best fits to the data. However, for Sr, P_2O_5, Ni and V the data points show some scatter (mostly due to the least Th-rich sample) and the lines shown have been fitted by eye.

For Rb, Ba, Zr, Ce (and La), Nd, Y, P_2O_5 and TiO_2 these basalt trends possess positive slopes, indicating incompatible-element behaviour, whereas those for Sr, Ni (and Cr), Sc and V possess negative trends, indicating compatible-element behaviour. These patterns are consistent with those shown earlier by Harker diagrams and are qualitatively consistent with the pre- and postcaldera volcanics having undergone fractionation of olivine, clinopyroxene and plagioclase, for which the bulk distribution coefficients for Sr, Ni, Cr, Sc and V are expected to be substantially greater than one [Gill (1981 p. 200-201) gives a convenient compilation of crystal/liquid coefficients].

Regression lines drawn through the three dacites for all elements, except Rb, Zr and Ba, show distinctly lower slopes than those drawn through the basaltic rocks, indicating

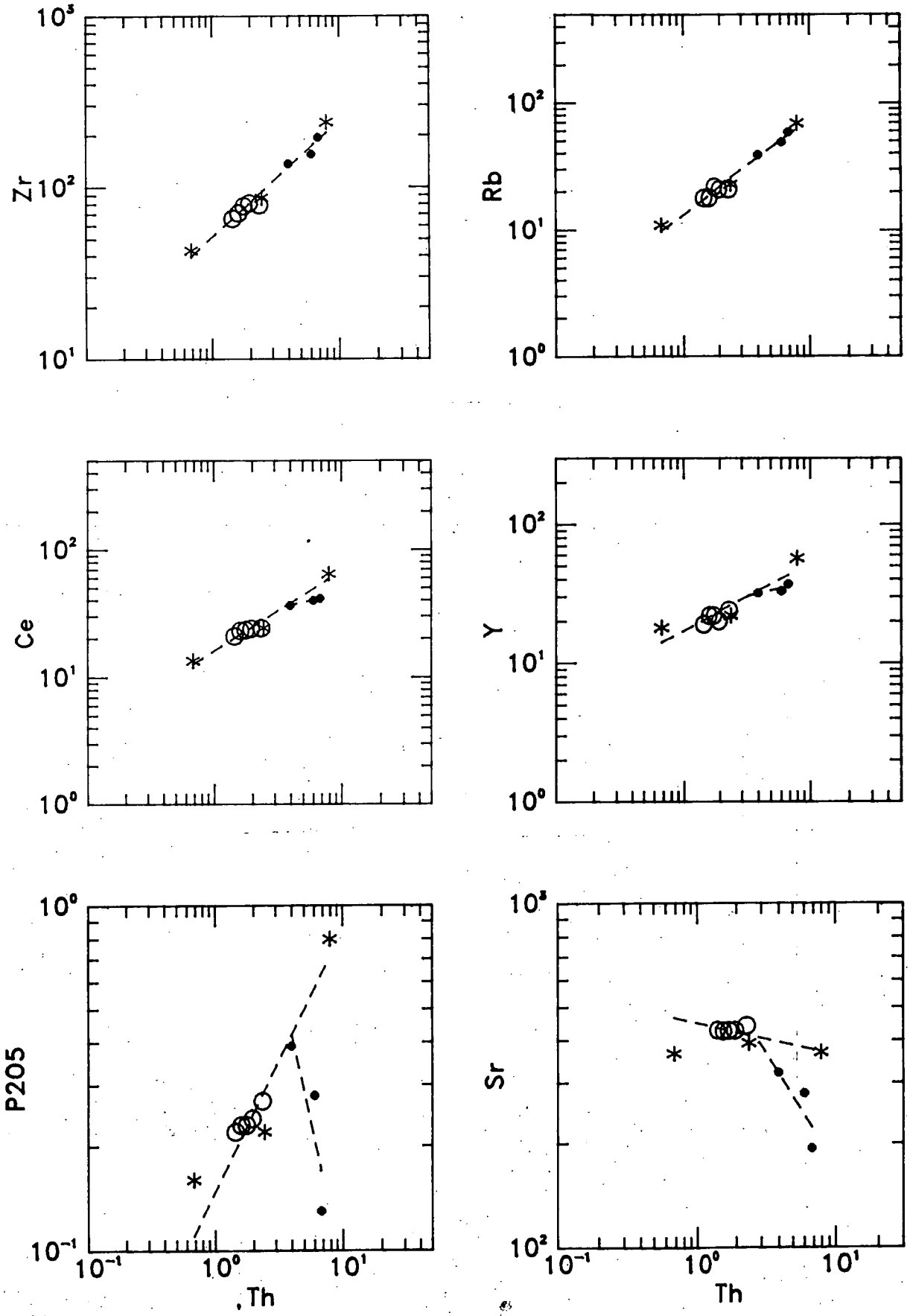

Fig. 1.38

continued over ..

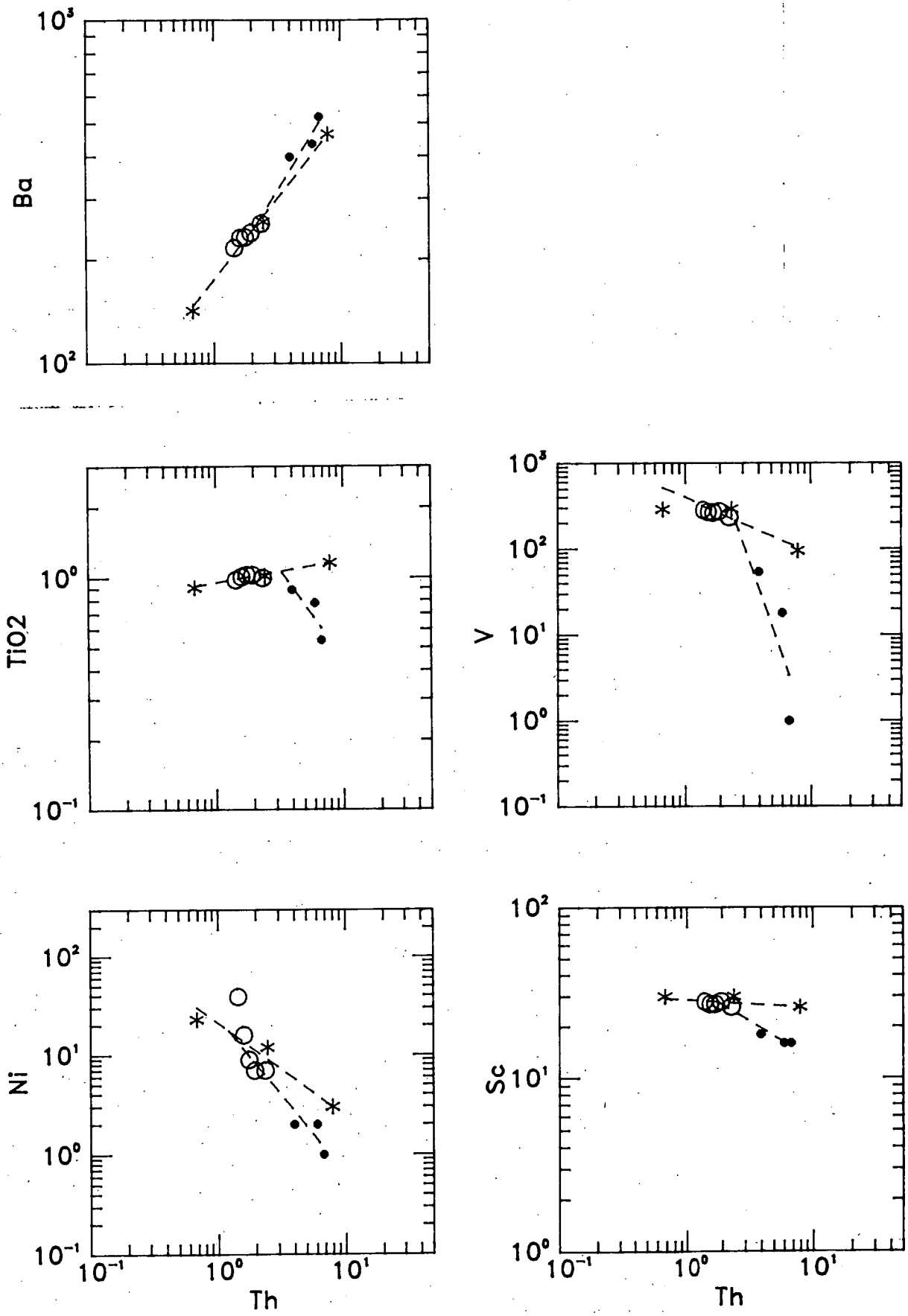

Figure 1.38 Log-log plots of Th against selected trace and minor elements selected Batur volcanic rocks (dots = caldera dacites; open circles = postcaldera basalts; asterisks = precaldera basalts and basaltic andesite).

substantial increases in the bulk distribution coefficients of these elements during differentiation. The intersection points of the dacite trends with those of the basalts for Ce (and La), Nd, Y, TiO_2 and P_2O_5 occur at higher Th contents than possessed by any of the postcaldera rocks (that is, within the 6 wt % SiO_2 gap), and coincide with the appearance in the dacites of apatite and Ti-magnetite phenocrysts, for which the crystal/liquid distribution coefficients of these elements are generally high. These minerals are either absent or have low abundance in the pre- and postcaldera rocks.

However, the intersection points for Ba, Sr, Ni, Sc and V occur within the postcaldera lavas. This relationship suggests that the process that was responsible for these inflexions began to occur earlier during differentiation than that which caused the inflexions in the first group of elements. It is notable that Ba, Sr, Sc, V and Ni generally partition into the major phenocryst minerals plagioclase, pyroxenes and olivine. The differences in slopes between the basalt and dacite trends suggest qualitatively that the dacite fractionating phenocryst assemblage contained more pyroxene and olivine and less plagioclase than that of the basalts.

All of the Batur volcanics lie on the same trend for Rb and Zr. Given that different phenocryst assemblages are present in the dacitic and basaltic rocks, this indicates that neither of these elements partitions substantially into any mineral present in the Batur volcanics. These two elements, together with Th (by assumption), are therefore potentially useful as direct differentiation indices.

Following Allegre et al. (1977), the bulk distribution coefficient of each trace and minor element has been calculated from the slopes of the lines in Figure 1.38, using the relation: slope = 1-D. These are listed in Table 1.10. Stage 1 refers to the trends formed by the pre- and postcaldera basaltic rocks, while stage 2 refers to the dacite trends. The D values for all elements, except for Ba, Zr, Rb and Th, are higher in stage 2 compared to stage 1, indicating relatively more compatible behaviour, while the D of Ba is lower.

	Th	Zr	Rb	Ba	La	Ce	Nd	Y	Sr	P_2O_5	TiO_2	Ni	Sc	V
Stage 1														
D	0	0.32	0.25	0.53	0.36	0.38	0.42	0.52	1.09	0.24	0.91	1.94	1.05	1.66
C_i	0.68	40.0	9.9	146	6.0	14.1	8.8	14.1	466	0.11	0.92	30.4	29.2	518
Stage 2														
D	-	-	-	0.40	0.75	0.77	0.92	0.78	1.67	2.71	1.80	2.58	1.46	5.3
C_i	-	-	-	252	18.9	40.0	23.3	30.5	410	0.42	1.06	17.7	27.8	215

Table 1.10 Bulk distribution coefficients (D) of selected trace and minor elements in Batur volcanic rocks calculated using the algorithm of Allegre et al. (1977), assuming D of Th = 0. Initial liquid concentrations (C_i) for each fractionation stage are also given, in wt % for TiO_2 and P_2O_5 and ppm for all other elements.

Table 1.10 also lists the initial concentrations (C^i) of each element for both stage 1 and stage 2. For stage 1, these are given by the pre- and postcaldera trends in Fig. 1.38 at the lowest Th content (0.7 ppm) shown by the Batur basalts. This value is from one of the least differentiated Batur olivine basalts (67341), as indicated by its low SiO_2 (48.7 wt %) and high MgO (5.9 wt %) contents and high 100Mg/(Mg+Fe) value (52.5). The C_i values for stage 1 therefore form a model parental magma for all of the Batur volcanics for minor and trace elements although, because 67341 is unlikely to represent a magma that was in equilibrium with mantle peridotite, it does not represent a primary magma composition.

Values of C_i for stage 2 are given by the intersections of the dacite and basalt trends in Fig. 1.38. These values are concentrations reached by particular elements during stage 1 differentiation at which substantial changes of D values occurred and are not intended to represent a single magma composition.

6.2.3 Application of the Trace Element Model

The general applicability of the calculated bulk distribution coefficients to modelling of the compositional variation shown by the Batur volcanic rocks is illustrated by curves derived by solving the Rayleigh fractionation equation for progressively varying degrees of crystallization. In this model, the simplifying assumption is first made that all of the Batur volcanic rocks were produced by fractional crystallization of a single, parental basaltic magma represented by the values of C_i for stage 1 in Table 1.10. This assumption is consistent with the close compositional and petrographic similarities of the pre- and postcaldera basalts despite the divergence of the caldera-postcaldera and precaldera geochemical trends.

The Rayleigh fractional crystallization curves calculated for each of the elements plotted in Figure 1.38 are shown in Figure 1.39, using Zr as the differentiation index. The weight fraction of the model parental magma crystallized is marked in increments of 10 % by crosses on the curves, starting at 0 %.

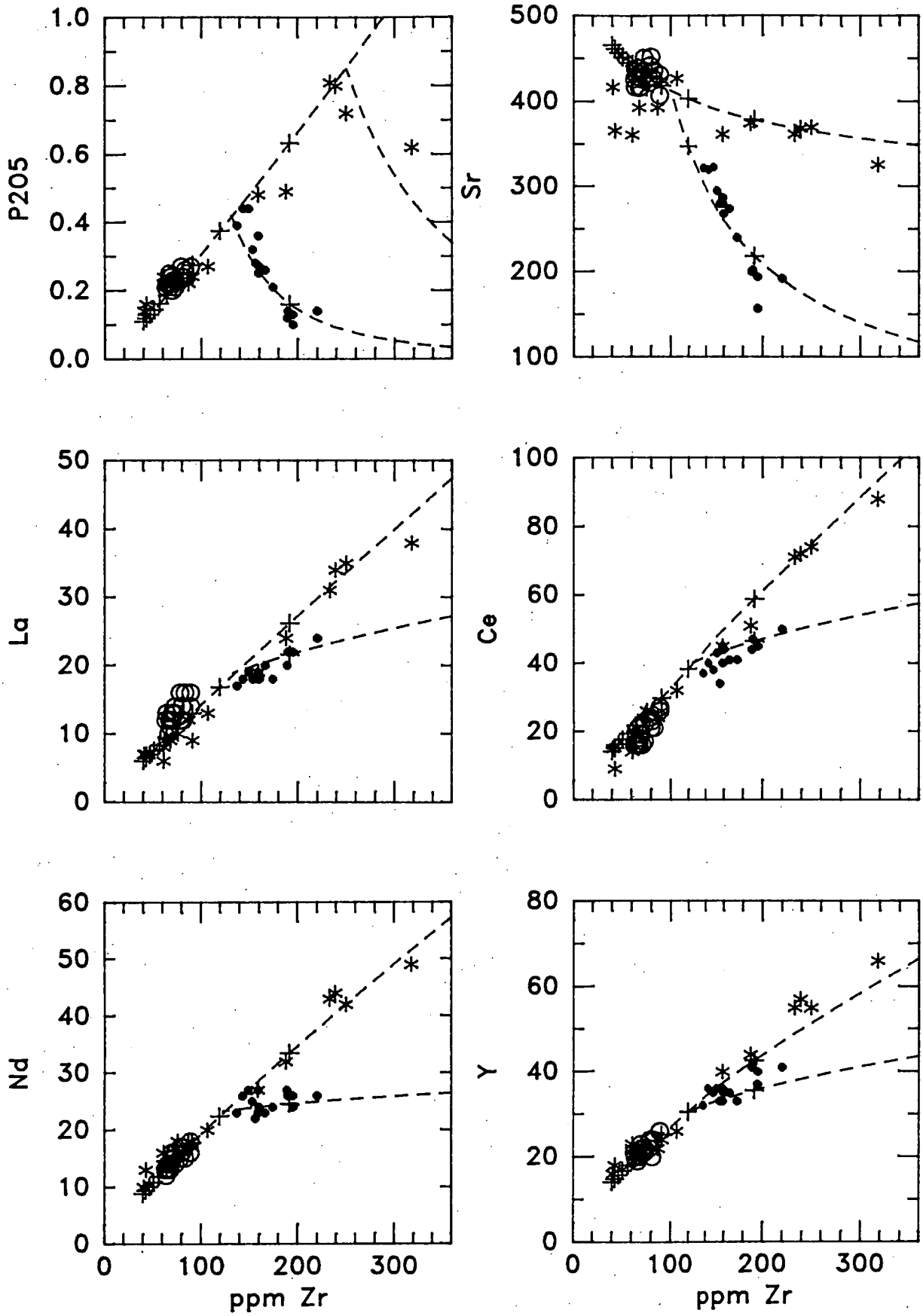

Fig. 1.39

continued over ..

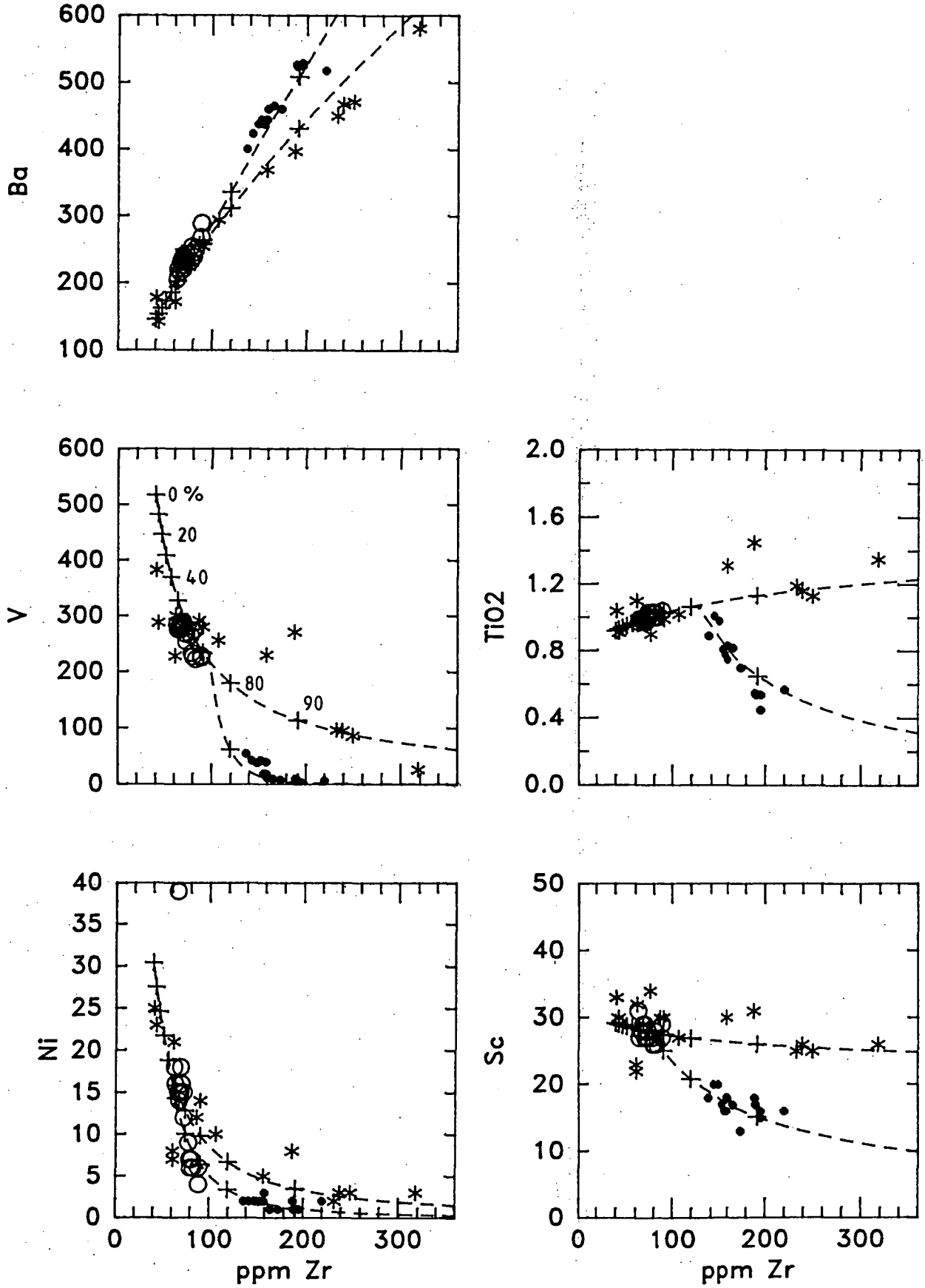

Figure 1.39 Selected minor and trace elements against Zr in Batur volcanic rocks compared to model fractional crystallization trends (symbols as for Fig. 1.22).

Some scatter of data away from the curves is to be expected because many of the rocks, particularly the basalts and basaltic andesites, contain abundant phenocrysts and their bulk compositions are therefore unlikely to represent liquid compositions. However, for virtually all elements, the Batur volcanics closely follow the model fractional crystallization curves,

The pre- and postcaldera rocks generally lie along the model stage 1 curves, while the caldera dacites lie along the model stage 2 curves. However, it is notable that for Ni the Zr-rich (basaltic andesite) members of the postcaldera rocks lie along the stage 2 curve rather than along the stage 1 curve. An additional curve is drawn for P_2O_5 to reflect the relative decrease of P_2O_5 contents in the most Zr-rich members of the precaldera group.

It is also notable that, based on Zr contents, the caldera dacites and the precaldera andesites appear to have been produced by similar amounts of crystallization of the model parental magma, with the precaldera rocks falling between 4 and 93 % crystallization, the caldera dacites between 84 and 92 %, and the postcaldera rocks between 49 and 69 %.

However, as a group, the dacites possess markedly higher SiO_2 contents (> 62.2 % compared to < 59.6 %), lower MgO contents (< 1.6 % compared to > 1.8 %) and lower 100Mg/(Mg+Fe) values (17-31 compared to 28-57) than the precaldera rocks. These parameters would normally be interpreted as indicating that the dacites were produced by substantially higher degrees of crystal-liquid fractionation than the precaldera rocks.

The clear adherence of the Batur volcanic rocks to the modelled trace and minor element model trends is consistent, at this stage, with the hypothesis that fractional crystallization of a single parental, basaltic magma could have yielded magmas with the observed compositional variations, except that different fractionating phenocryst assemblages are required to produce the diverging precaldera and postcaldera-caldera geochemical trends.

This conclusion is qualitatively supported by the appearance of apatite and Ti-magnetite, in particular, in the dacitic rocks. Fractionation of these minerals could account for the variation in behaviour of P, Ti and rare earth elements. Variations shown by Ba, Sc, V, Ni and Cr could be explained by differences in the relative proportions of olivine, pyroxenes and plagioclase. These possibilities are assessed later in conjunction with the results of the major element modelling.

6.3 Major Element 'Least Squares' Calculations

Major element variations within consanguineous volcanic suites are commonly modelled by estimating the weight proportions of phenocrysts with known compositions that need to be added to a specified residual liquid composition to obtain a specified parental liquid composition. When there are fewer potentially fractionating mineral phases involved than there are major element oxide components and a unique solution therefore cannot be obtained, a 'least squares' technique is used, in which the sum of the squares of the residuals between the estimated and specified parental liquid compositions are minimized (Bryan et al. 1969; Wright & Doherty 1970). Close agreements between the estimated and specified target parental liquid composition lead to low values of the sum of the residuals squared.

This method essentially models an 'equilibrium' crystal fractionation process, which more closely approximates true fractional crystallization the smaller the fractionation steps that are modelled. The results of these calculations include estimates of the degrees of crystallization required to produce successive residual liquids, of the phenocryst mineral proportions involved and of the bulk major element composition of the fractionating phenocryst assemblage. The calculations for the Batur volcanics were done using the Fortran program GENMIX (Le Maitre 1979).

Because together they form colinear trends on plots of major elements against Zr (Fig. 1.29) which diverge markedly

from those formed by the precaldera rocks, the postcaldera- and caldera-stage rocks are assumed here to be geochemically related. Although most trace and minor elements show markedly different behaviour in the caldera dacites compared to either the post- or precaldera rocks, this assumption is also supported by the tendency of some trace elements in the postcaldera lavas, particularly Ni and possibly Sc, Sr and Ba (Fig. 1.39), to show variations in concentration against Zr that are colinear with those in the caldera dacites. This assumption can be tested by major element modelling in three steps: 1) from high-SiO_2 dacite (67277) to low-SiO_2 dacite (67275), 2) from low-SiO_2 dacite across the SiO_2 gap to basaltic andesite (67272), and 3) from basaltic andesite to basalt (67244).

The major element geochemical trends formed by the precaldera rocks are also modelled in three steps: 1) from andesite (67318) to basaltic andesite (67336), 2) from basaltic andesite to basalt (67328), and 3) from basalt to olivine basalt (67341). The compositions of the phenocryst phases used for both trends are either averages of phenocrysts present in the two endmember rocks or are taken from rocks of intermediate compositions. Details of the input data and the results obtained are given in Table 1.11 for the postcaldera-caldera trend and Table 1.12 for the precaldera trend.

The types of phenocrysts used in each step were chosen by minimizing the sums of the residuals squared. In most cases the lowest values were obtained using phenocrysts present in both of the endmember rocks. However, step 1 of the postcaldera-caldera trend does not require use of Fe-rich olivine, although it is present in small amounts in most of the dacitic rocks. This may be because its composition is generally similar to that of orthopyroxene, which is required in the calculations. Also, step 2 of the postcaldera-caldera trend bridges the geochemical gap between the dacites and the postcaldera basaltic andesites, which have different phenocryst assemblages. In this case, the best fit was obtained using the phenocryst assemblage in the basaltic andesites.

Satisfactorily low sums of the residuals squared were

STEP 1	target 67275		reactants					
	meas.	calc.	67277	CPX	MAG	PLG	OPX	APT
SiO2	62.16	61.94	67.11	51.27		58.24	51.67	1.37
TiO2	0.89	0.73	0.54	0.40	18.64		0.18	
Al2O3	16.92	16.76	15.47	1.83	2.53	26.55	0.74	0.22
Fe2O3	0.73	1.12	0.53	1.75	30.89		2.15	
FeO	5.88	5.23	4.27	10.38	44.56	0.23	21.60	0.52
MnO	0.22	0.25	0.21	0.59	0.97		1.30	
MgO	1.65	1.98	0.54	13.91	2.27		20.71	0.17
CaO	4.62	4.39	2.36	19.72		8.71	1.65	55.41
Na2O	4.98	5.30	5.92			5.94		
K2O	1.64	1.97	2.96			0.31		
P2O5	0.39	0.30	0.13					42.31
calculated % proportions:			64.05	1.38	1.98	25.34	6.74	0.51
% fractionating assemblage:				3.8	5.5	70.5	18.7	1.4

sum of residuals squared: 1.00

STEP 2	target 67272		reactants				
	meas.	calc.	67275	OLV	CPX	MAG	PLG
SiO2	55.06	55.09	62.16	35.46	51.44		53.35
TiO2	1.03	1.19	0.89		0.46	14.71	
Al2O3	18.35	18.42	16.92		1.96	3.33	29.50
Fe2O3	1.83	2.22	0.73		1.42	37.56	
FeO	7.42	6.97	5.88	33.09	9.80	42.11	0.46
MnO	0.19	0.20	0.22	0.86	0.43	0.52	
MgO	2.61	3.03	1.65	30.49	15.00	1.73	
CaO	8.13	7.86	4.62	0.10	19.42		12.62
Na2O	4.14	3.89	4.98				3.90
K2O	0.97	0.95	1.64				0.19
P2O5	0.27	0.21	0.39				
calculated % proportions:			54.69	2.80	7.95	4.54	30.01
% fractionating assemblage:				6.2	17.5	10.0	66.2

sum of residuals squared: 0.69

STEP 3	target 67244		reactants				
	meas.	calc.	67272	OLV	CPX	MAG	PLG
SiO2	51.41	51.64	55.06	36.28	51.38		50.79
TiO2	0.97	1.09	1.03		0.46	13.13	
Al2O3	17.87	18.00	18.35		2.42	3.53	30.85
Fe2O3	2.14	2.41	1.83		1.70	40.65	
FeO	8.68	8.66	7.42	28.35	8.35	39.39	0.70
MnO	0.21	0.18	0.19	0.50	0.08	0.39	
MgO	4.70	4.84	2.61	34.74	15.18	2.69	
CaO	8.91	8.82	8.13	0.12	20.38		14.62
Na2O	3.94	3.41	4.14				2.86
K2O	0.94	0.72	0.97				0.13
P2O5	0.22	0.19	0.27				
calculated % proportions:			72.20	6.66	3.79	2.53	14.81
% fractionating assemblage:				24.0	13.6	9.1	53.3

sum of residuals squared: 0.52

Table 1.11 Input data and results for 'least squares' modelling of the Batur postcaldera-caldera geochemical trend.

STEP 1	target 67336		reactants				
	meas.	calc.	67318	OLV	CPX	MAG	PLG
SiO2	55.83	55.83	57.92	35.60	48.65		51.62
TiO2	1.31	1.30	1.13		1.16	17.39	
Al2O3	16.28	16.30	16.55		3.14	2.87	30.54
Fe2O3	1.09	1.47	0.94		3.25	33.05	
FeO	8.82	8.44	7.61	33.13	12.74	44.36	0.48
MnO	0.25	0.23	0.22	0.66	0.51	0.46	
MgO	2.98	3.27	2.45	30.44	13.50	1.87	
CaO	7.00	6.75	6.02	0.16	16.90		13.96
Na2O	3.94	3.66	4.02				3.11
K2O	2.13	2.19	2.51				0.29
P2O5	0.48	0.62	0.72				
calculated % proportions:			86.41	1.81	4.23	1.58	5.97
% fractionating assemblage:				13.3	31.1	11.6	43.9

sum of residuals squared: 0.53

STEP 2	target 67328		reactants				
	meas.	calc.	67336	OLV	CPX	MAG	PLG
SiO2	52.80	52.75	55.83	35.60	48.65		51.62
TiO2	1.02	1.03	1.31		1.16	17.39	
Al2O3	18.51	18.49	16.28		3.14	2.87	30.54
Fe2O3	1.06	1.25	1.09		3.25	33.05	
FeO	8.62	8.28	8.82	33.13	12.74	44.36	0.48
MnO	0.20	0.22	0.25	0.66	0.51	0.46	
MgO	3.78	3.97	2.98	30.44	13.58	1.87	
CaO	9.28	9.07	7.00	0.16	16.98		13.96
Na2O	3.52	3.27	3.94				3.11
K2O	1.09	1.39	2.13				0.29
P2O5	0.22	0.30	0.48				
calculated % proportions:			61.81	4.35	5.78	1.18	26.88
% fractionating assemblage:				11.4	15.1	3.1	70.4

sum of residuals squared: 0.40

STEP 3	target 67341		reactants			
	meas.	calc.	67328	OLV	MAG	PLG
SiO2	48.94	49.17	52.80	36.56		47.48
TiO2	0.91	0.81	1.02		13.64	
Al2O3	19.49	20.12	18.51		2.97	33.15
Fe2O3	1.07	1.15	1.06		40.06	
FeO	8.67	8.99	8.62	28.28	41.23	0.59
MnO	0.19	0.18	0.20	0.48	0.43	
MgO	5.96	5.94	3.78	34.56	1.67	
CaO	11.09	10.24	9.28	0.11		17.23
Na2O	3.05	2.50	3.52			1.05
K2O	0.57	0.69	1.09			
P2O5	0.16	0.14	0.22			
calculated % proportions:			63.40	10.21	1.19	25.20
% fractionating assemblage:				27.9	3.3	68.9

sum of residuals squared: 1.63

Table 1.12 Input data and results for 'least squares' modelling of the Batur precaldera geochemical trend.

obtained for each step in both trends and there are no systematic, substantial discrepancies between the measured and calculated target compositions for any particular major element. However, by recasting the calculated phenocryst mixing proportions into fractionating assemblage proportions it becomes apparent that there are systematic differences between the andesite to basalt stages of the two trends. From step 2 to step 3 of the postcaldera-caldera trend the proportion of olivine increases while that of plagioclase decreases. Clinopyroxene and magnetite contents change little.

In contrast, from step 1 to step 2 of the precaldera trend the olivine content decreases, and there is a marked increase in plagioclase content. In addition, there are substantial decreases in the proportions of clinopyroxene and magnetite. Overall, with increasing differentiation towards more SiO_2-rich compositions, the postcaldera-caldera trend fractionating assemblage becomes more felsic, which is the expected trend, while that of the precaldera trend becomes more mafic. A possible reason for this unusual result, which appears to be consistent with the presence of quench olivine in the precaldera andesite lava (67342), will be discussed later.

6.4 Integration of Trace and Major Element Modelling

The degree of mutual consistency between the trace and major element models developed in the previous sections for the Batur volcanics is most easily shown graphically, using plots of major elements against trace elements. Plots of selected major elements against Zr shown in Figure 1.40 represent an attempt to reproduce the geochemical trends shown by the Batur volcanics in Figure 1.29, using the representative rocks involved in the major element 'least squares' calculations. These rocks are indicated in Figure 1.40 by open symbols. The model compositions are indicated by dots at the ends of tielines with their starting rocks.

The model major element concentrations are given by the calculated target rock compositions from the 'least squares' calculations (Tables 1.11 and 1.12), while the corresponding model trace element abundances (C^o) are calculated from the

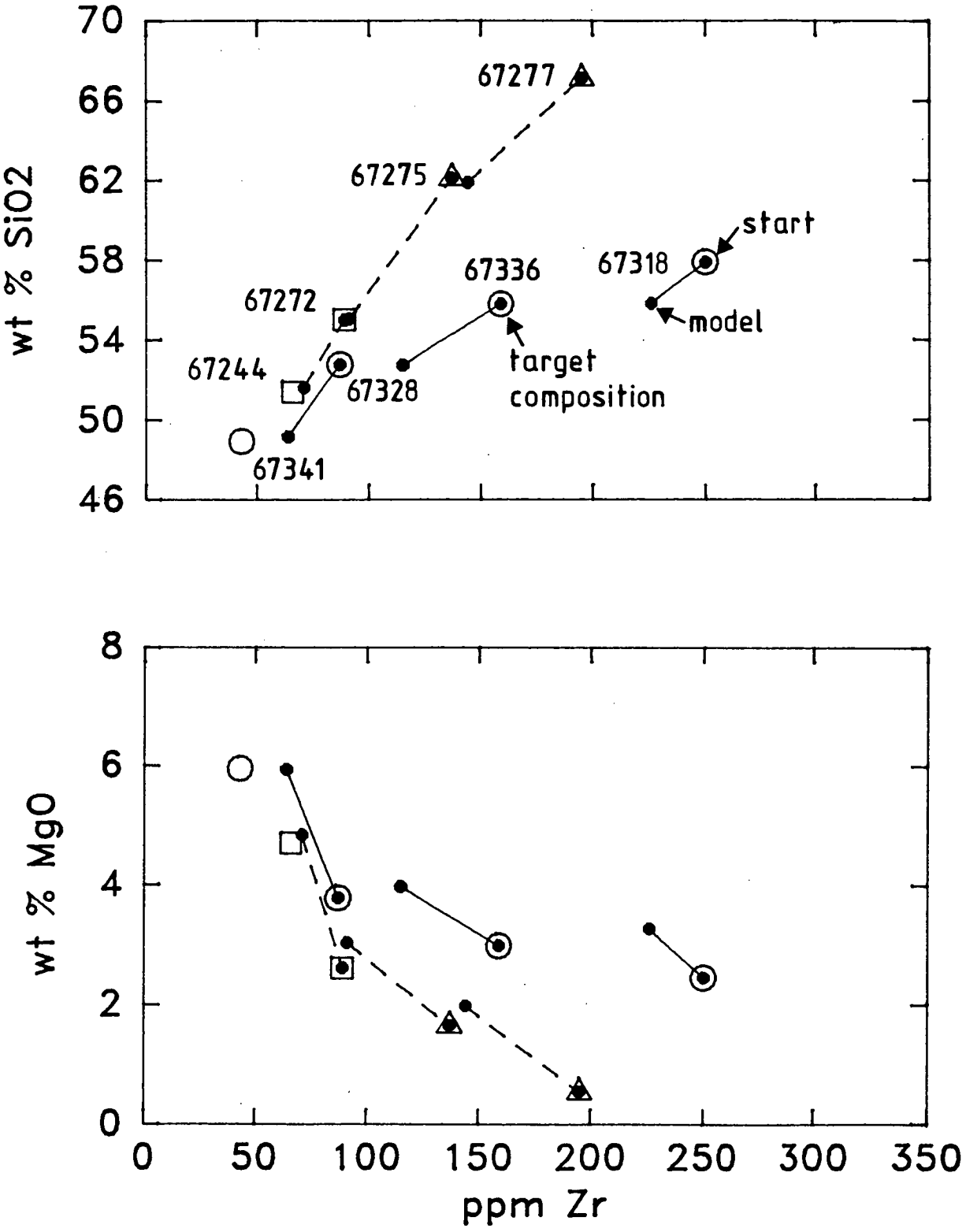

Fig. 1.40

continued over ..

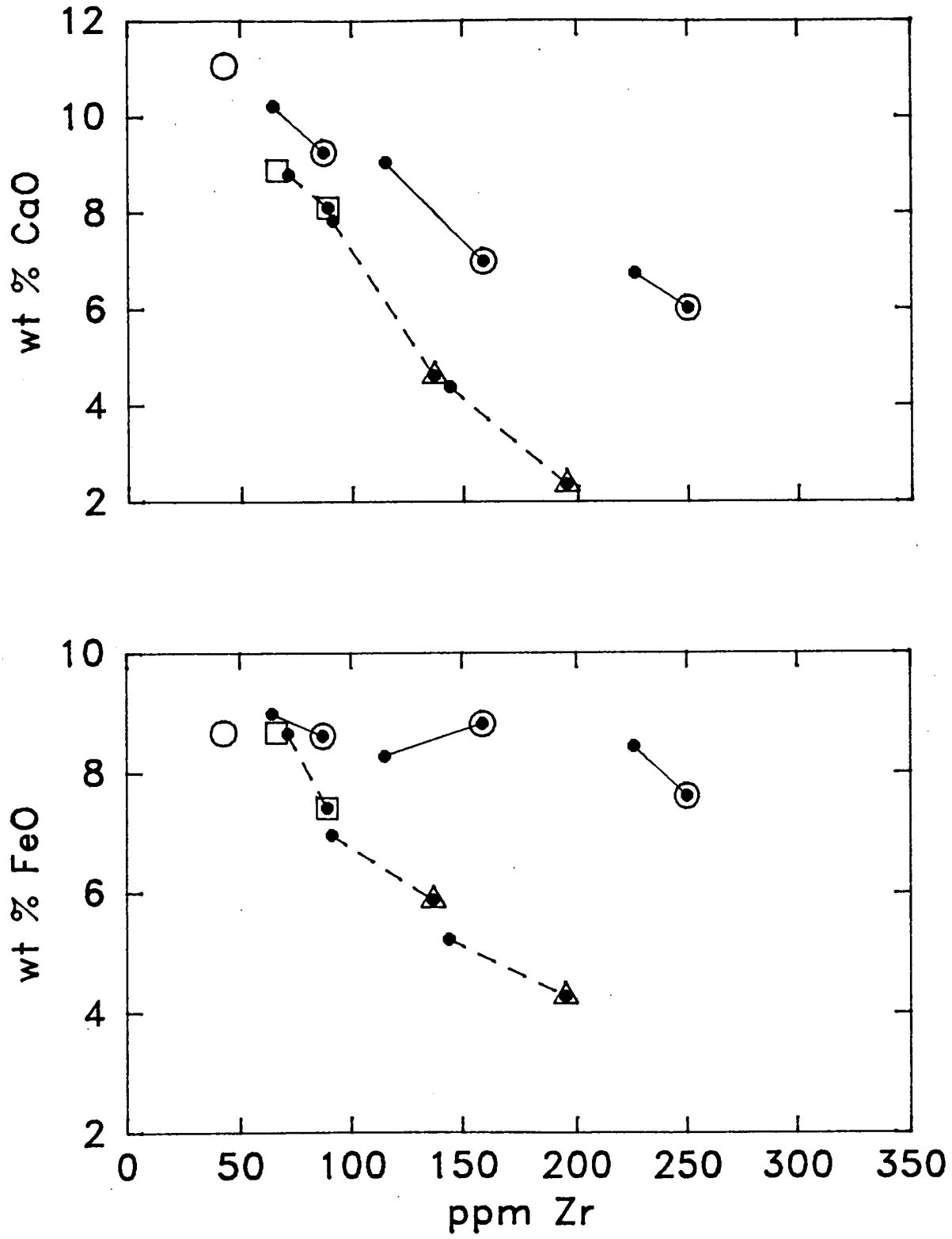

Figure 1.40 Attempt to reproduce trends formed by selected major elements against Zr by integrating major and trace element closed-system fractionational crystallization modelling (open squares = postcaldera; open triangles = caldera; open circles = precaldera). See text for explanation.

Rayleigh equation using the calculated bulk distribution coefficients (D) listed in Table 1.10, the trace element concentrations in the respective starting rocks (C^l), and the calculated weight fractions of the starting rocks (F) obtained from the 'least squares' calculations.

For the postcaldera-caldera trend, the close fit between the measured and model target compositions at each step indicates that the major and trace element models for this trend are mutually consistent. Similar close fits are shown when Rb replaces Zr (Fig. 1.41). This high degree of mutual consistency is excellent support for the hypothesis that closed system fractional crystallization of basaltic magma was the process by which the Batur dacitic rocks formed. It also supports the hypothesis that the dacitic rocks are genetically related to the postcaldera lavas.

However, for the precaldera rocks, the model target compositions clearly do not match the measured compositions for any fractionation step, although the differences decrease from step 1 to step 3. This discrepant relationship is mainly due to the different trace element concentrations in the calculated and measured target rocks. However, for these values to match in a closed system, based on the 'least squares' results, the bulk distribution coefficients for Zr and Rb would have to be negative, which obviously is not possible.

Table 1.13 lists the bulk distribution coefficients for the trace and minor elements that are required in each fractionation step for mutual consistency to occur between the precaldera major and trace element fractionation models. Most of these 'required' distribution coefficients decrease substantially in value from step 3 to step 1 (that is, with increasing differentiation from SiO_2-poor to SiO_2-rich rock compositions) for those elements which possess apparent distribution coefficients of less than 1 (Zr, Rb, Ba, La, Ce, Nd, Y, P_2O_5), indicating that these elements progressively become more incompatible with increasing differentiation.

Conversely, the required coefficients of those elements which possess apparent distribution coefficients close to or

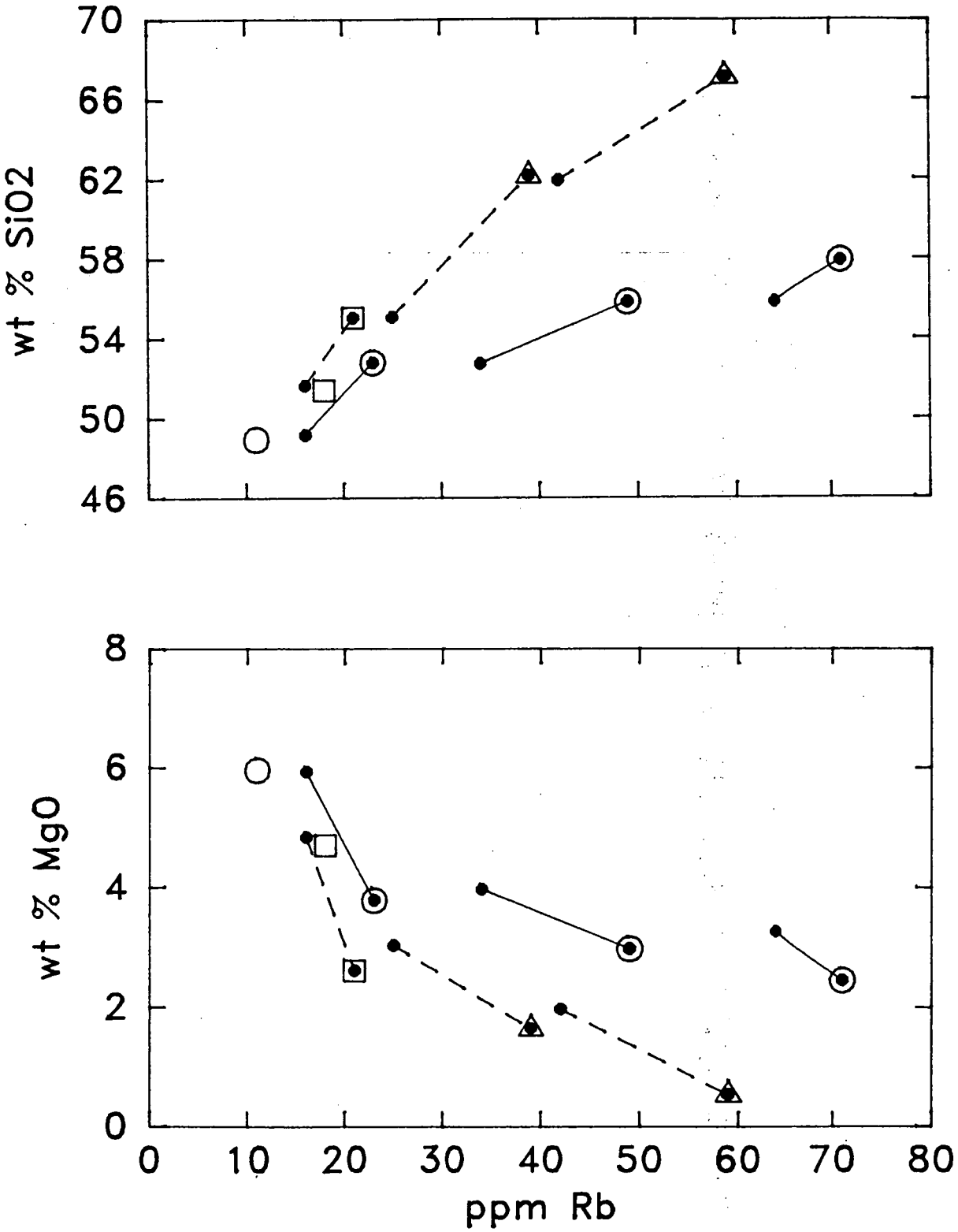

Fig. 1.41

continued over..

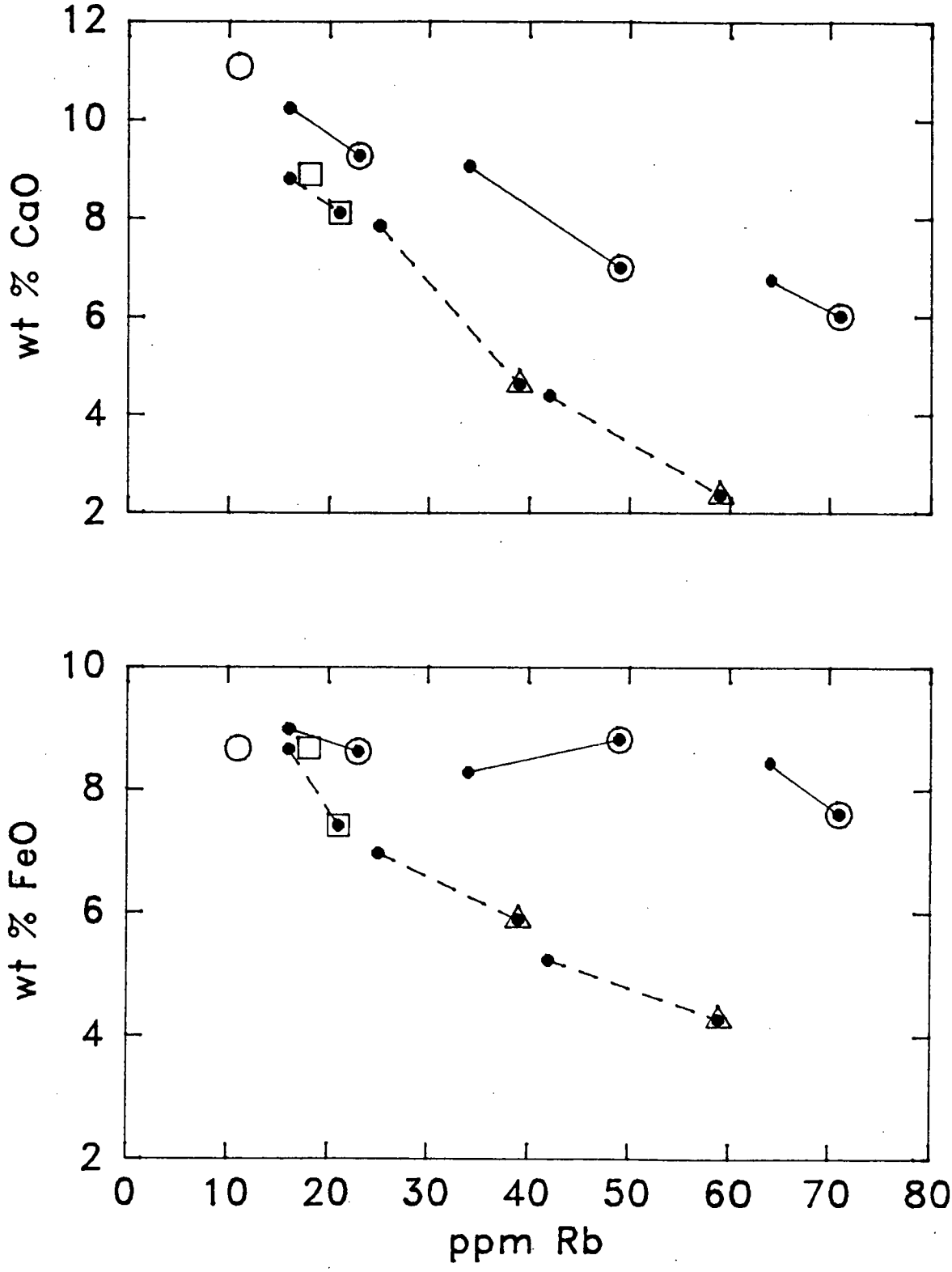

Figure 1.41 Attempt to reproduce trends formed by selected major elements against Rb by integrating major end trace element closed-system fractional crystallization modelling (symbols as for Fig. 1.40). See text for explanation.

	apparent bulk distribution coefficient	required bulk distribution coefficient step 3	step 2	step 1
incompatible elements				
Zr	0.32	-0.24	-0.15	-1.48
Rb	0.25	-0.30	-0.44	-1.03
Ba	0.53	-0.05	0.32	-0.34
La	0.36	0.05	0.13	-2.34
Ce	0.38	-0.72	-0.20	-1.72
Nd	0.42	0.43	0.23	-1.42
Y	0.52	0.65	-0.14	-0.74
compatible elements				
P2O5	0.24	0.44	-0.48	-1.22
Sr	1.09	0.87	1.16	0.88
TiO2	0.91	0.80	0.52	1.81
Ni	1.94	2.14	2.66	3.80
Sc	1.05	1.00	1.00	2.00
V	1.66	0.98	1.45	6.38

Table 1.13 Comparison between apparent bulk distribution coefficients (from Table 1.10) of minor and trace elements in the precaldera differentiation trend and those required in each fractionation step (Table 1.12) for mutual consistency between trace and major element fractionation models.

greater than 1 (TiO_2, Ni, Sc, V, ?Sr) generally increase in value from step 3 to step 1, indicating that these elements become more compatible with differentiation. This pattern is qualitatively consistent with the increasing mafic character of the fractionating phenocryst assemblage in the precaldera differentiation trend identified from the 'least squares' calculations.

Recently, Dupuy et al. (1985) also found discrepancies between the trace element compositions of andesites and dacites erupted from Mt Pelee on Martinique in the Antilles arc and those predicted by major and trace element modelling of closed-system fractional crystallization. However, the discrepancies noted by Dupuy et al. (1985) between model and measured compositions are opposite in sign to those observed in the Batur precaldera lavas, in that the Pelean volcanics are more depleted in incompatible elements than would be expected for closed-system fractional crystallization.

These characteristics of the Batur precaldera geochemical trend indicate clearly that, unlike the products of the caldera and postcaldera stages, the precaldera basaltic andesites and andesites could not have been produced by a plausible closed-system process. This conclusion suggests the possibility that an open-system process of the kind envisaged by O'Hara and Mathews (1981), De Paolo (1981) and Cann (1982) may have been involved in the production of the precaldera basaltic andesites and andesites. Possible mechanisms that may explain the contrasting Batur geochemical trends are discussed in a later section.

7. COMPARISON WITH EXPERIMENTAL STUDIES

7.1 Low Pressure Liquidus Relationships

Grove and Baker (1984) have recently used experimentally-determined low pressure liquidus phenocryst relationships to discuss the causes of tholeiitic and calcalkaline differentiation trends in basaltic to dacitic magmas, and have produced a pseudoternary plagioclase-saturated olivine-augite-quartz phase diagram phase diagram useful for illustrating the liquid-line-of-descent of the Batur volcanic rocks. The Batur basaltic lavas are similar to those used by Grove and Baker (1984) to determine the phase boundaries. In particular, they include olivine-normative basalts and possess an anhydrous phenocryst assemblage of plagioclase, olivine, clinopyroxene and magnetite.

On this diagram (Fig. 1.42) both the pre- and postcaldera rocks lie between the inferred parental basalt field and the 1 atm augite+olivine+plagioclase cotectic on the high temperature side of the reaction Point A where, under equilibrium conditions, olivine reacts with liquid to form pigeonite+ augite+plagioclase. The Batur dacites and andesites lie generally along the 1 atm tholeiitic pigeonite+augite+ plagioclase cotectic trend, consistent with the results obtained previously by major and trace element modelling which indicate that the dacitic rocks formed by closed-system fractional crystallization at low pressures of basaltic magma.

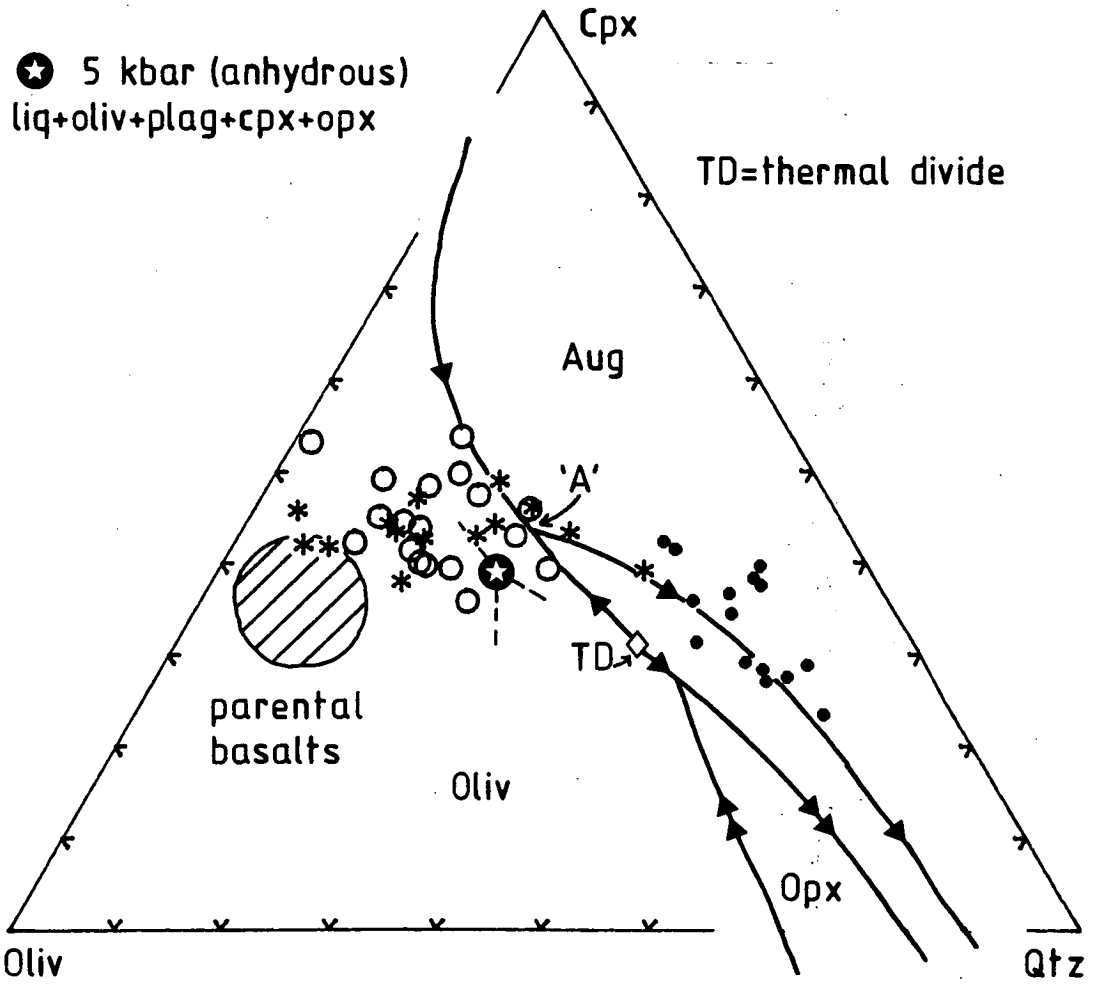

Figure 1.42 Batur volcanic rocks projected onto the plagioclase-saturated olivine-augite-quartz pseudoternary phase diagram of Grove and Baker (1984) (symbols as for Fig. 1.22). Four-phase saturated liquid at 5 kbar (anhydrous) from Takahashi and Kushiro (1983).

The field formed by the Batur basaltic rocks is unlike those formed by the calcalkaline Witu and Medicine Lake volcanics (see figs 8 and 10 of Grove and Baker 1984) and its position suggests that the Batur rocks have been affected generallly by low-pressure fractional crystallization of olivine+plagioclase. Some of the rocks also lie close to the 1 atm olivine+augite+plagioclase cotectic, indicating that low-pressure fractionation of clinopyroxene may have also occurred. In addition, using published experimental results, Grove and Baker (1984) showed that increasing pressure leads to a marked expansion of the orthopyroxene and clinopyroxene stability fields and contraction of the olivine field. These results, in conjunction with the absence of orthopyroxene in the Batur basalts, indicate that the Batur basaltic rocks could have crystallized at pressures of up to approximately 5 kbar (Fig. 1.42).

7.2 Dacite P-T Environment

The Batur dacitic rocks are generally similar in bulk composition to those erupted from Mt St Helens from 1980 to 1982 which have been studied experimentally by Merzbacher and Eggler (1984) and by Rutherford et al. (1985), although the Batur dacites contain a phenocryst assemblage unlike that of the Mt St Helens dacites. Like most dacitic rocks erupted in orogenic settings (Ewart 1979), those produced from Mt St Helens contain amphibole, together with plagioclase, orthopyroxene and Fe-Ti oxide phenocrysts, whereas the Batur dacite phenocryst assemblage consists mainly of Fe-rich olivine, clinopyroxene, orthopyroxene, plagioclase and Ti-magnetite.

It is notable that in none of these experiments was olivine reported as a liquidus phase, possibly because Merzbacher and Eggler's (1984) experiments mainly involved oxygen fugacities along the NNO buffer, rather than QFM, and those of Rutherford et al. (1985) involved substantial H_2O contents which led to amphibole crystallization.

Combining their experimental results, which involved

a ranges of temperatures, H_2O contents and confining pressures, with others from the literature, Merzbacher and Eggler (1984) developed a graphical 'geohygrometer' based on plagioclase-pyroxene liquidus relationships from which the volatile content of dacitic magmas formed at up to 5 kbar can be estimated. Application of this 'geohygrometer' (Fig. 1.43) suggests that unlike the Mt St Helens magma, which seems to have contained 4-5 wt % H_2O at 900-975 ^oC, the Batur dacitic magmas contained between < 1 to 2 wt % H_2O, assuming that their dissolved CO_2 contents were negligible.

In addition, the pressure-dependent temperature-H_2O content liquidus diagrams of Merzbacher and Eggler (1984) indicate that the Batur dacites crystallized at less than 0.5 kbar, equivalent to about 1.5 km depth, given the unusual Batur dacite phenocryst assemblage and the relatively high liquidus temperatures of 1070 to 930 ^oC obtained from the pyroxene and Fe-Ti oxide compositions.

Similar experiments by Rutherford et al. (1985) on a Mt St Helens dacite with a composition which is also similar to the Batur low-SiO_2 dacites, yield similar results. Although substantial extrapolation is required from the relatively high pressures of these experiments (about 1-3 kbar), and assuming that the activity of CO_2 in the Batur dacite magma was negligible, the P_{fluid}-T phase diagram of Rutherford et al. (1985) suggests that the Batur low-SiO_2 dacites crystallized at approximately 0.25 kbar, equivalent to approximately 0.8 km depth.

7.3 Apatite Saturation

Green and Watson (1982) have determined experimentally the levels of P_2O_5 in hydrous magmas at which apatite crystallizes, as a function of SiO_2 contents, temperature and pressure. The variation of P_2O_5 contents with SiO_2 in the Batur volcanic rocks is shown in Figure 1.44, together with the apatite saturation curves determined by Green and Watson (1982). The postcaldera-caldera and precaldera differentiation trends both show initially positive correlations between P_2O_5 and SiO_2 contents, but these reach maxima at about

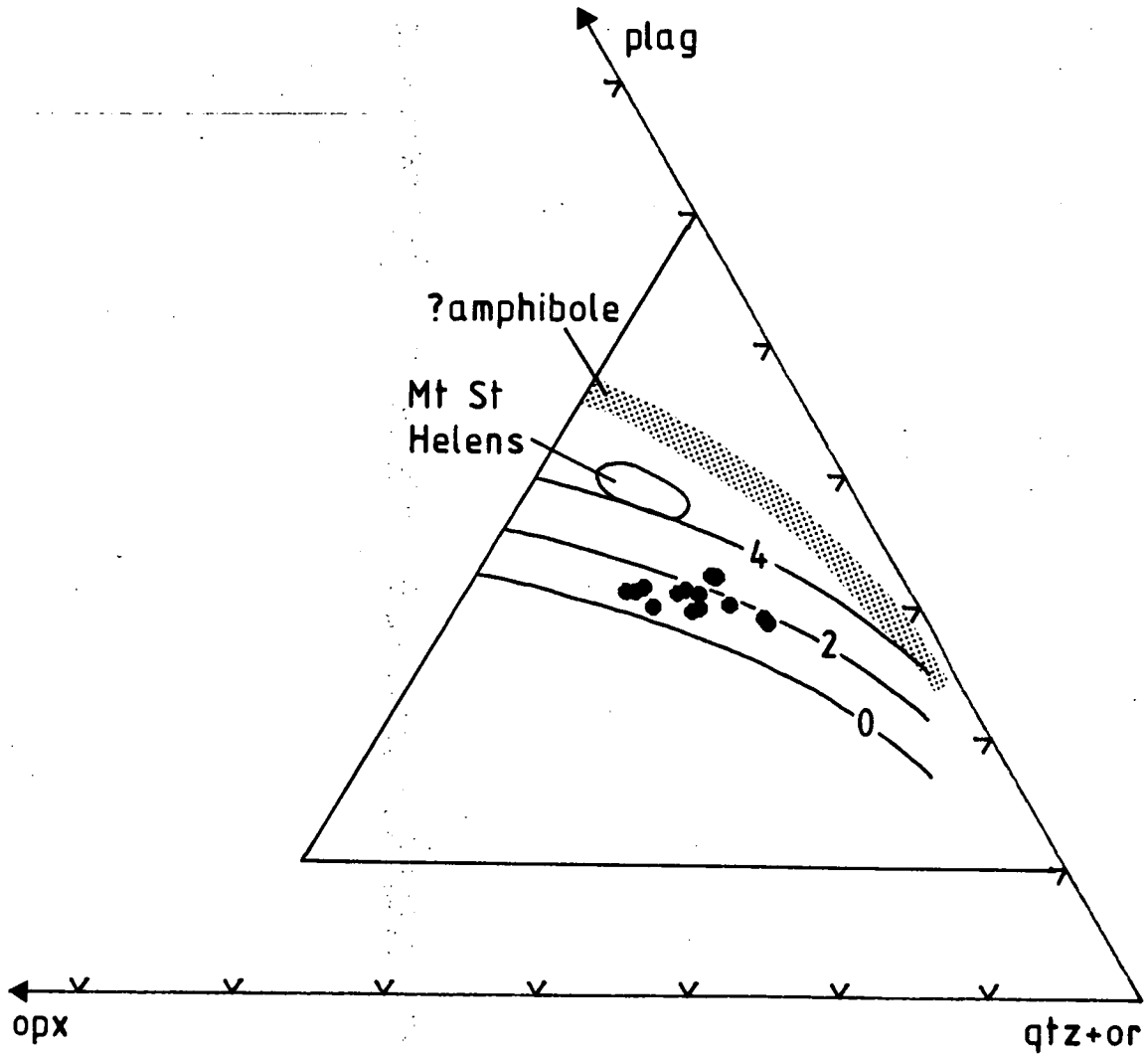

Figure 1.43 Batur caldera stage dacites projected onto the 'geohygrometer' of Merzbacher and Eggler (1984).

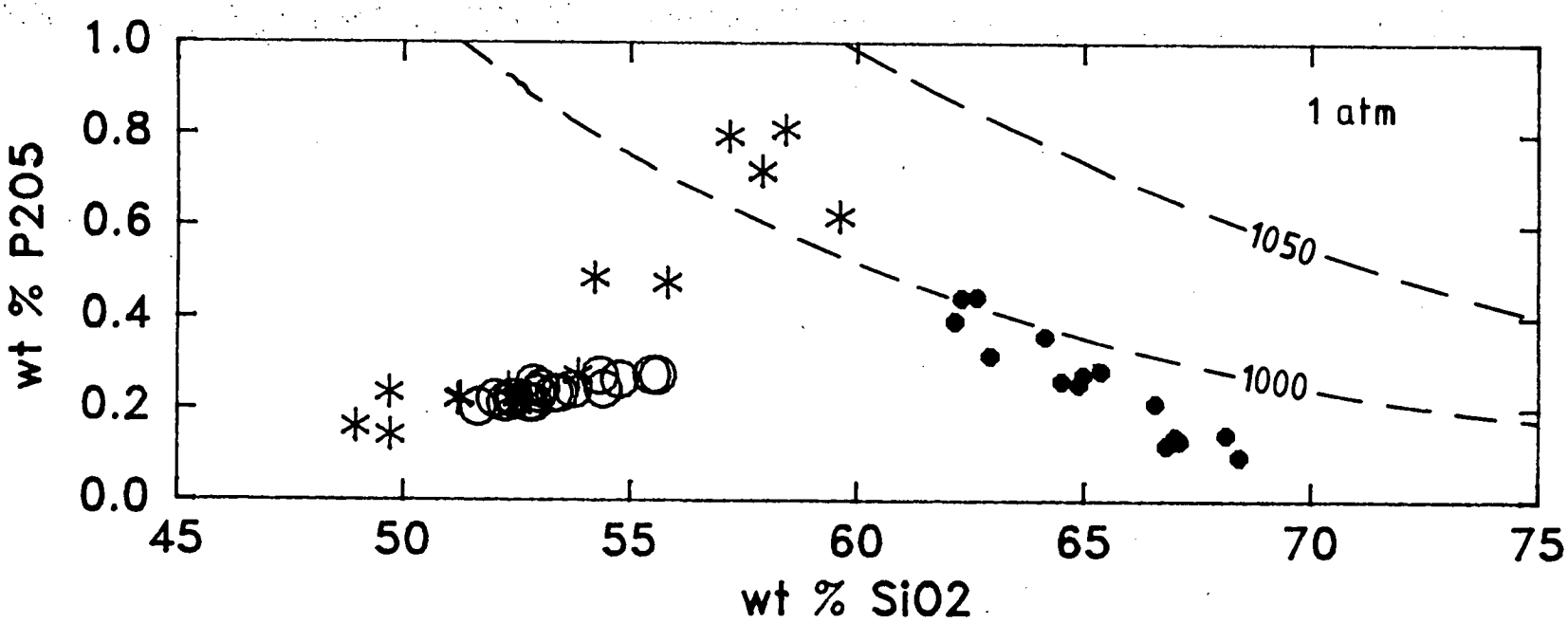

Figure 1.44 P_2O_5 against SiO_2 in Batur volcanics compared to experimentally determined apatite saturation curves of Green and Watson (1982).

62 and 58 % SiO_2 respectively. These inflections correspond with the first appearance of apatite phenocrysts in the SiO_2-rich rocks. P_2O_5 contents then decrease with increasing SiO_2, implying fractionation of apatite.

The maximum in the postcaldera-caldera trend indicates that apatite precipitation from the Batur dacite magma occurred at approximately 1000 ^oC at 1 atm, which is about 50-70 ^oC less than the temperature estimates obtained for the low-SiO_2 Batur dacite magma from coexisting pyroxene pairs. In the precaldera trend, apatite saturation in andesitic magma occurred at temperatures at 1 atm of approximately 1000-1040 ^oC.

8. ISOTOPES

8.1 Oxygen

$^{18}O/^{16}O$ values of five basaltic lavas and four dacitic blocks from Batur volcano have been measured. Oxygen was extracted from 15-20 mg of sample powder by overnight reaction with BrF_5 at approximately 650 ^oC (Clayton & Mayeda 1963). The O_2 produced was reacted with resistance-heated graphite to form CO_2, the $^{18}O/^{16}O$ value of which was measured using a VG Micromass 602D mass spectrometer. Results were calibrated with the quartz standard NBS28 for which $\delta^{18}O$ was assumed to be +9.6 permil relative to Standard Mean Ocean Water (SMOW). Precision was monitored by replicate analyses of an internal high-Al basalt standard (BAT26) and is estimated to be 0.15 permil. None of the samples shows any evidence of secondary alteration. Results are listed in Table 1.14.

$\delta^{18}O$ values of Batur basaltic lavas fall between 5.8 and about 7 permil. The mean of these values is slightly higher than $\delta^{18}O$ values from most mid-ocean ridge tholeiites but is similar to those from continental tholeiites and from basalts produced at oceanic islands (Kyser et al. 1982). They are also similar to those measured in basaltic lavas from the Volcano-Mariana arc (Ito & Stern 1981; Douthitt & Dixon 1981). However, together with $\delta^{18}O$ values of other basaltic lavas from the eastern Sunda arc, including leucite-bearing types, these values are distinctly lower than those shown by mafic volcanics

sample	wt % SiO_2	ppm Zr	$\delta^{18}O$ (per mil)
basalts			
67250	52.4	64	5.8
67244	52.0	66	6.1
67257	53.0	68	6.4
67238	53.4	78	7.2
			6.7
67240	53.8	81	6.5
dacites			
67275	62.2	137	6.5
67273	65.4	156	6.6
67282D	67.0	190	6.4
67277	67.1	195	7.0

Table 1.14 Oxygen isotope compositions of selected Batur basaltic and dacitic rocks. Results reported relative to V-SMOW using the NBS28 quartz standard for which $\delta^{18}O$ is taken as 9.6 permil.

from the Banda arc which generally range from 6 to 9 permil. The implications of these differences are discussed in more detail in Part 2 of this thesis.

The Batur dacites show similar values to those of the basalts, ranging from 6.4 to 7.0 permil. From Figure 1.45, although there are few data, it seems apparent that the Batur volcanics do not show the marked increase of $\delta^{18}O$ values with fractionation that is observed in rocks erupted at the Galapagos Spreading Centre (Muehlenbachs & Byerly 1982) and from Japanese volcanoes (Matsuhisa et al. 1973). Those enrichments appear to have been caused by substantial fractionation of relatively ^{18}O-depleted minerals such as magnetite, pyroxenes and olivine (Matsuhisa et al. 1973; Muehlenbachs & Byerly 1982). The apparent lack of ^{18}O enrichment in the Batur rocks may imply that the Batur fractionating mineral assemblage contained a higher proportion of plagioclase, which has little effect (Kyser et al. 1981), than those in the Galapagos and Japanese rocks.

Irrespective of the possible differences in fractionating assemblages, the low $\delta^{18}O$ values shown by the Batur dacites

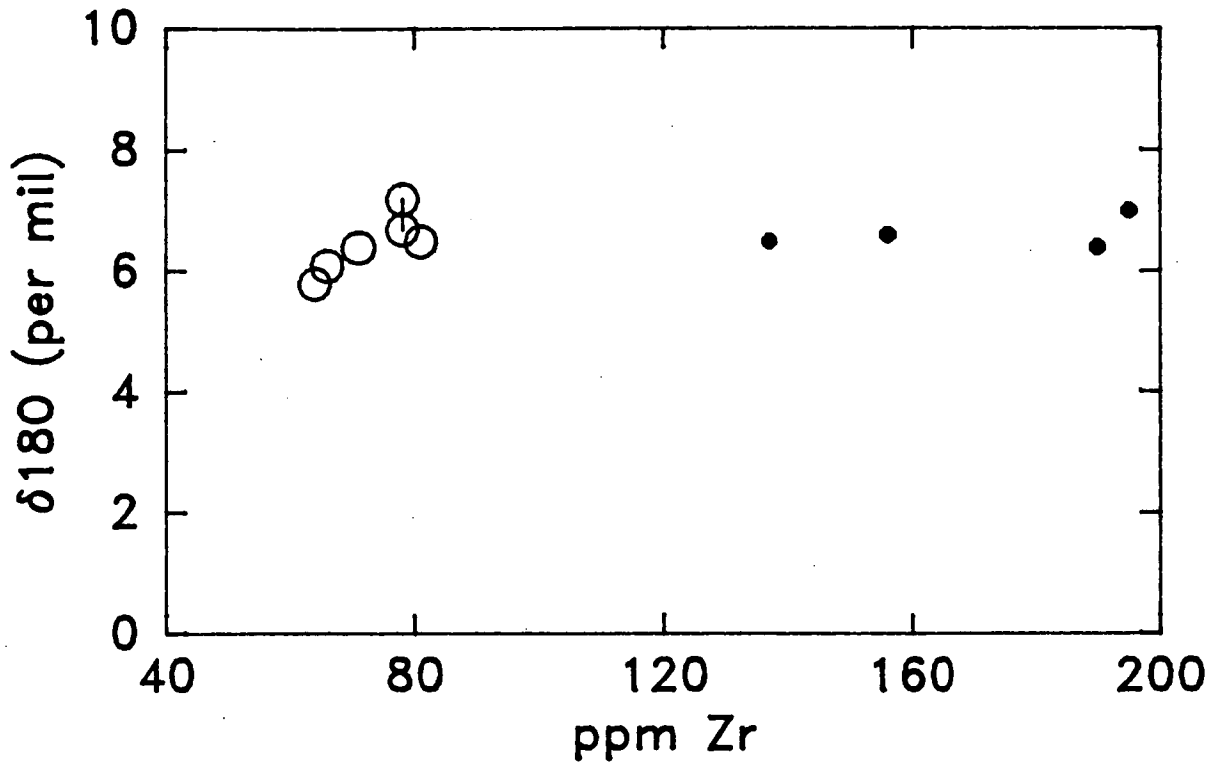

Figure 1.45 $\delta^{18}O$ against Zr in selected Batur volcanic rocks (dots = dacites; open circles = postcaldera basalts).

are consistent with the dacites having been produced by closed-system fractional crystallization of basaltic magma, rather than by a process involving anatexis or substantial assimilation of crustal material, which tends to be enriched in ^{18}O compared with mantle-derived rocks (James 1981).

8.2 U-Decay Series Radioisotopes

The activities of several U-decay series radioisotopes have been obtained from samples of six historical lavas and two basaltic blocks of unknown, but postcaldera-formation, age from Batur volcano (Tanzer 1985, Table 1.15). All of the rocks cluster close to the equiline in a ($^{230}Th/^{232}Th$) versus ($^{238}U/^{232}Th$) diagram (Fig. 1.46) and, within two standard deviations, Th and U are in radioactive equilibrium. Given that ^{230}Th has a halflife of 75,200 years, this suggests that no fractionation between Th and U has occurred within the last 300,000 years in either the source of the Batur postcaldera lavas or the magmas during their residence in the crust prior to eruption (Tanzer 1985).

Their low ($^{230}Th/^{232}Th$) values distinguish the Batur lavas from virtually all other basaltic rocks that have been analysed for U-decay series radioisotopes. These values, together with similar results from Galunggung volcano on Java (Williams et al. 1983) and Sangeang Api volcano near Sumbawa (Tanzer 1985), also clearly distinguish the Sunda arc from other island arcs, and help to highlight the distinctiveness of each island arc region (Fig. 1.46). Only lavas from the oceanic island of Samoa (Newman et al. 1984) have low ($^{230}Th/^{232}Th$) values which approach those from Batur and the other Sunda arc volcanoes. The significance of these results are discussed in more detail in Part 2 of this thesis.

It is interesting to note that, if one standard deviation errors are used, the Batur data points appear to define a linear trend which crosses the equiline at a high angle (Fig. 1.47). Although the data are not widely spread, this line (B-B', determined by simple linear regression) could be interpreted as the locus of points produced by radioactive decay of U and Th from points that initially had identical ($^{230}Th/^{232}Th$) values

Sample	Year of eruption	U (ppm)	Th (ppm)	^{230}Th(dpm/g)	Th/U	(^{234}U/^{238}U)	(^{230}Th/^{238}U)	(^{238}U/^{232}Th)	(^{230}Th/^{232}Th)	^{210}Pb(dpm/g)	(^{210}Pb/^{230}Th)
Batur											
67238	1974	0.55±0.02	2.19±0.02	0.40±0.01	4.02±0.14	0.97±0.04	0.97±0.05	0.76±0.03	0.74±0.02	0.79±0.02	1.98±0.04
67240	1963	0.53±0.02	2.22±0.02	0.41±0.01	4.18±0.14	0.99±0.04	1.02±0.04	0.74±0.03	0.75±0.02	0.70±0.02	1.71±0.04
67244	1926	0.43±0.02	1.99±0.02	0.33±0.01	4.69±0.17	0.97±0.04	1.05±0.05	0.66±0.03	0.69±0.02	0.62±0.02	1.88±0.04
67250	1904	0.44±0.01	1.77±0.01	0.31±0.01	4.00±0.13	0.96±0.04	0.92±0.04	0.77±0.03	0.71±0.02	0.62±0.02	2.00±0.04
67257	1888	0.44±0.02	2.27±0.02	0.37±0.02	5.15±0.21	1.00±0.05	1.14±0.06	0.60±0.03	0.68±0.03	0.69±0.02	1.86±0.04
67259	1849	0.53±0.02	2.55±0.02	0.42±0.02	4.83±0.17	1.01±0.04	1.07±0.05	0.64±0.03	0.68±0.02	0.59±0.02	1.40±0.04
67325		0.26±0.01	1.20±0.01	0.20±0.01	4.67±0.17	1.04±0.05	1.03±0.05	0.66±0.03	0.68±0.02	0.47±0.02	2.35±0.04
67328		0.60±0.02	2.49±0.02	0.45±0.02	4.14±0.15	1.05±0.04	1.01±0.05	0.74±0.03	0.75±0.02	0.48±0.02	1.07±0.04
Sangeang Api											
48073	1911	2.27±0.09	8.14±0.11	1.55±0.09	3.58±0.16	1.01±0.04	0.91±0.06	0.86±0.06	0.78±0.02	3.30±0.10	2.13±0.20

Table 1.15 Uranium, thorium and lead radioisotopic values in selected historical lava flows and bombs from Batur and Sangeang Api volcanoes. Data from Tanzer (1985). Errors quoted are one standard deviation resulting from counting statistics and tracer calibration uncertainties.

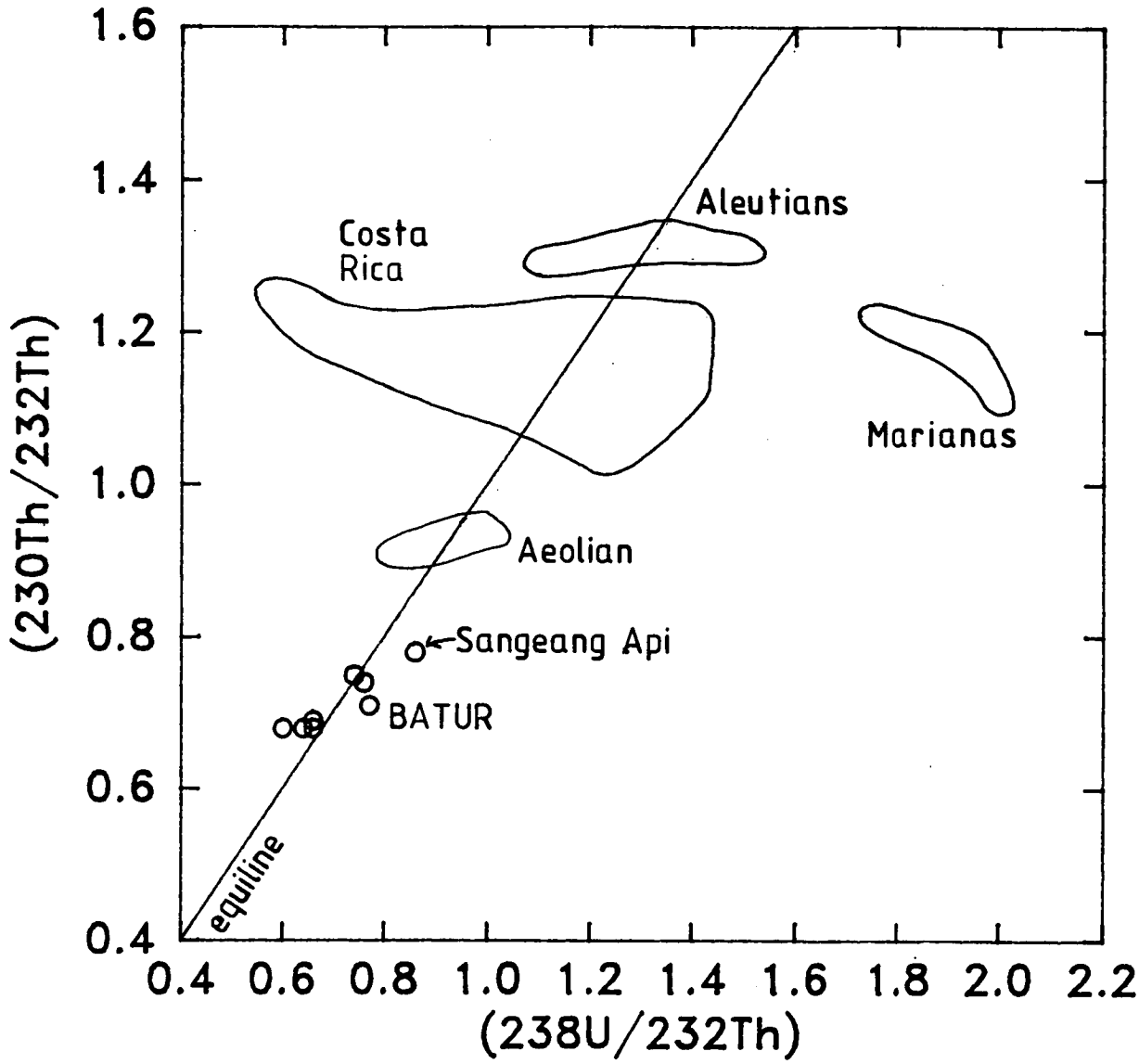

Figure 1.46 ($^{230}Th/^{232}Th$) against ($^{238}U/^{232}Th$) in selected Batur historical basaltic lavas compared to volcanic rocks from other subduction-related regions (Tanzer 1985). Other data from Allegre and Condomines (1976), Newman et al. (1984) and Capaldi et al. (1983).

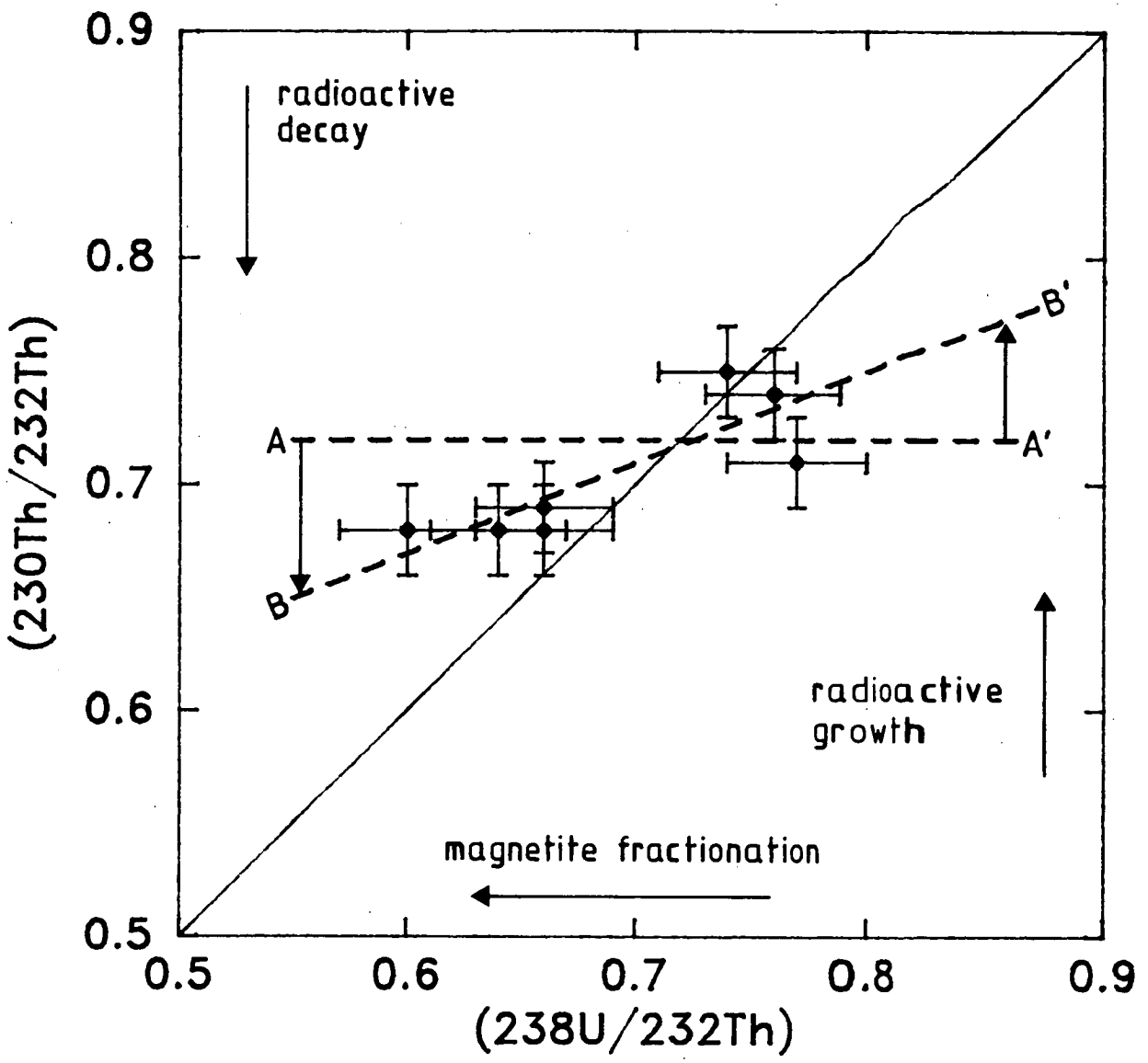

Figure 1.47 ($^{230}Th/^{232}Th$) against ($^{238}U/^{232}Th$) in selected Batur historical basaltic lavas showing possible isotopic evolution. See text for explanation.

but a range of ($^{238}U/^{232}Th$) values, that is, lay along the line A-A' at ($^{230}Th/^{232}Th$) = 0.72 (obtained from the intersection of B-B' with the equiline).

This could have occurred if the source of the Batur basalts was in isotopic equilibrium at the time the magmas were formed and that, either during partial melting or as a result of some other process, such as crystal fractionation, U and Th were fractionated from each other, leading with time to isotopic disequilibrium. Any point originally on A-A' in Figure 1.47 would have taken approximately 58,000 years to reach B-B', using the equation that describes the isotopic evolution of the U-Th system with time (Allegre & Condomines 1976) and taking the initial ($^{230}Th/^{232}Th$) value as 0.72.

However, the ($^{238}U/^{232}Th$) values shown by the Batur postcaldera lavas do not appear to correlate with any other geochemical or isotopic parameter and it is therefore difficult at this stage to assess the significance of the 'age' of 58,000 years. Clearly, more radioisotopic data are required, particularly from the dacitic blocks in the caldera wall and from the Bali ignimbrite, to clarify the possible temporal significance of the isotopic variations suggested in Figure 1.47.

The activities of ^{210}Pb in the Batur postcaldera lavas were also measured by Tanzer (1985). ^{210}Pb is produced, via several intermediate steps, by radioactive decay of ^{226}Ra which is, in turn, produced by decay of ^{230}Th. For samples older than about 100 years, ^{210}Pb will be in equilibrium with parental ^{226}Ra if there has been no loss of the intermediate product ^{222}Rn, a gas. Gill et al. (1985) have shown that all magmatic Rn was lost during eruptions of Kilauea and Arenal volcanoes, which would lead to isotopic disequilibrium between Pb and Ra, and between Pb and Th. However, even if all Rn is degassed from the lavas during eruption, isotopic equilibrium between Pb and Ra will be re-established within 2-3 weeks due to the short halflife of ^{222}Rn (3.82 days). Only continuous, post-eruption loss of Rn will affect isotopic activites involving ^{210}Pb (J.D. Macdougall, pers. comm.).

Most of the Batur historical lavas, and one of the blocks (67325), show ($^{210}Pb/^{230}Th$) values of around 2 (Table 1.15), and the activity of ^{226}Ra in the two youngest lavas (67238 and 67240) is approximately twice that of ^{230}Th (J.D. Macdougall, pers. comm.). The slightly lower ($^{210}Pb/^{230}Th$) value of the 1849 lava (67259) compared to those of the younger lavas may be explained if all the lavas were enriched in ^{210}Pb prior to eruption. Because of its 22.4 year halflife, any ^{210}Pb not supported by decay of ^{226}Ra would be expected to have decayed to negligible abundance in rocks older than about 100 years. The high ($^{210}Pb/^{230}Th$) values shown by the 1849 lava, and probably the 1888 lava also, therefore indicates that Ra has been enriched relative to Th in these samples (J.D. Macdougall pers. comm.).

These enrichments in the Batur postcaldera lavas of ^{226}Ra must have occurred within several thousand years of the present, because of the 1600 year halflife of ^{226}Ra. Similarly, if ^{210}Pb enrichment is confirmed by additional measurements of ^{226}Ra in the Batur lavas (in progress), then that enrichment must have occurred within about 100 years of the eruption dates.

Enrichments of Ra at other volcanoes have been attributed to crystal fractionation, vapour fractionation, or to a contribution from the upper crust (Bennett et al. 1982; Capaldi et al. 1976; Capaldi et al. 1983; Williams et al. 1983). Enrichment of Pb relative to Ra may also have occurred at Mt St Helens volcano. Although ($^{210}Pb/^{226}Ra$) values of pyroclastic rocks produced during the 1980-81 eruptions are generally close to 1, Bennett et al. (1982) inferred that enrichment of Pb relative to Ra had occurred but that much of the Pb had been volatilized from the rocks during the eruptions.

In contrast, Le Cloarec et al. (cited by Lambert et al. 1985) found that ^{210}Pb is in radioactive equilibrium with ^{226}Ra in recent lavas from Mt Etna volcano. Lambert et al. (1985) suggested therefore that outgassing of intermediate ^{222}Rn from the Etna magma chamber had been generally prevented for at least several halflives of ^{210}Pb.

8.3 Beryllium

The concentrations of ^{10}Be in three historical lavas from Batur have been measured by Tera et al. (1986). This radioactive isotope is produced from oxygen and nitrogen in the atmosphere by cosmic radiation and accumulates in the upper parts of sediments and soils at the Earth's surface. If the top layers of oceanic sediments are incorporated by subduction into the mantle sources of arc basaltic magmas then, because of its 1.5 Ma halflife, ^{10}Be is potentially observable in erupted lavas for up to 10 Ma after its production in the atmosphere (Brown et al. 1982).

Like other young lavas from Java and Flores that were also analyzed for ^{10}Be by Tera et al. (1986), the Batur lavas contain very low abundances of ^{10}Be ($< 1 \times 10^6$ atom/gm) that are indistinguishable from the concentrations observed in the non-arc 'control group' of Tera et al. (1986). There is no direct ^{10}Be evidence, therefore, for recent sediment involvement in the production of the Batur, or other Sunda arc, volcanic rocks. However, given that high ^{10}Be levels occur in basaltic lavas from the Aleutian arc, Japan and Central America, Tera et al. (1986) suggested that, for the Sunda arc, the upper, potentially ^{10}Be-rich layers of the oceanic sedimentary column may have been diluted with older, deeper sediments prior to their incorporation into the melting zones. These results are discussed in more detail in Part 2.

8.4 Strontium and Neodymium

Whitford (1975a,b) measured the $^{87}Sr/^{86}Sr$ values of a basalt (0.70399) and a dacite (0.70407) from Batur, and Macdougall and Tanzer (pers. comm. 1985) have measured $^{87}Sr/^{86}Sr$ and $^{143}Nd/^{144}Nd$ values from the 1974 Batur lava (0.70404 and 0.512907 respectively).

The Sr and Nd isotope data from the 1974 lava indicate that the postcaldera Batur lavas lie within the mantle array (Fig. 1.48), close to basaltic lavas from Rindjani volcano on neighbouring Lombok. Like the U-Th, O and ^{10}Be results, these data, although few, do not support the hypothesis that recent

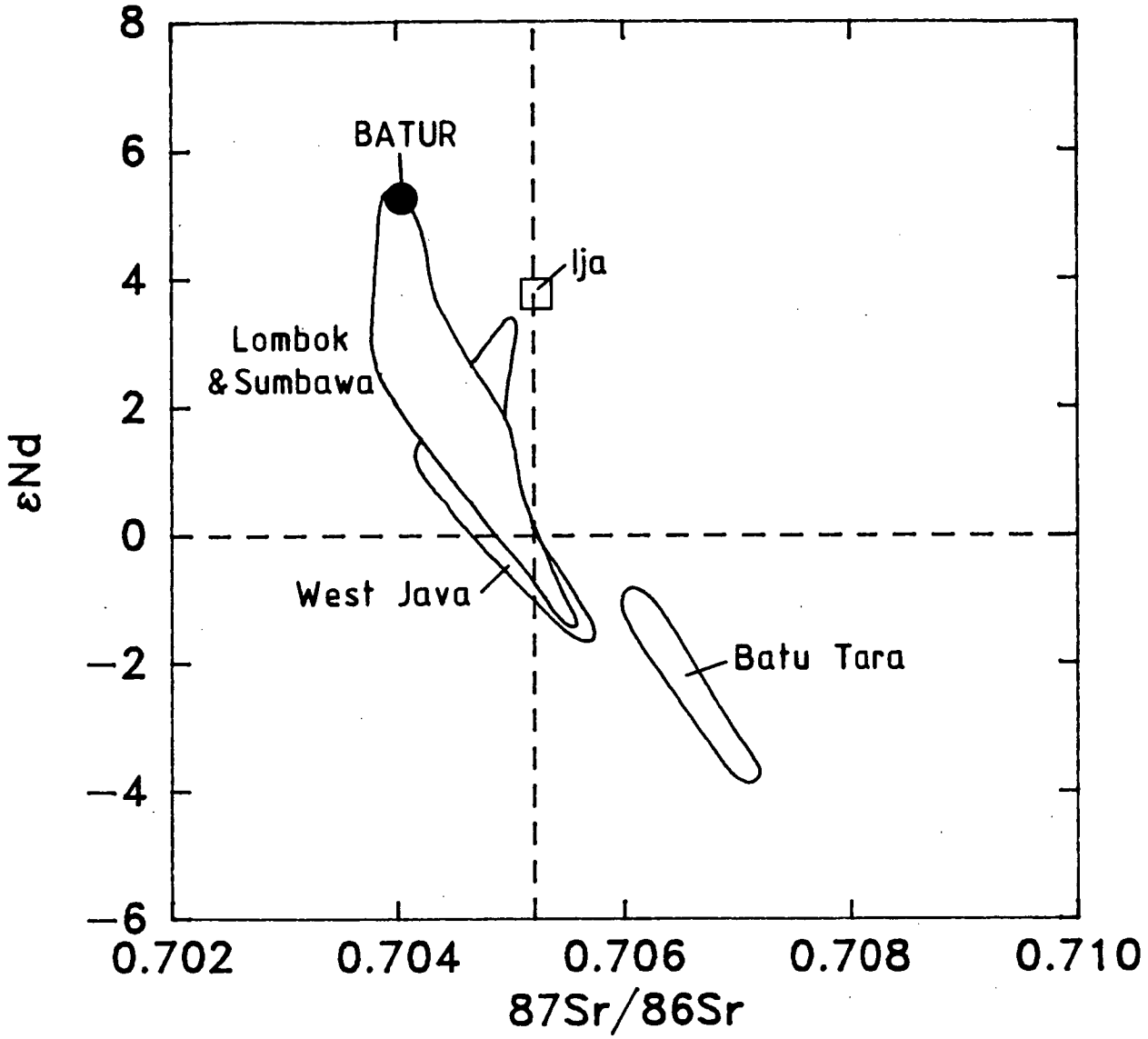

Figure 1.48 ε_{Nd} against $^{87}Sr/^{86}Sr$ in 1974 Batur lava (67238; Macdougall & Tanzer, unpublished data) compared to lavas from other parts of the Sunda arc, including Ija and Batu Tara volcanoes. Other data from Jenner et al. (in prep.), Whitford (1975) and Whitford et al. (1981).

incorporation of oceanic sediment or crust occurred in the melting zones of the Batur basaltic magmas, or that crustal contamination of the Batur magmas occurred.

The similar and low $^{87}Sr/^{86}Sr$ values shown by a dacite and the two basalt samples are consistent with the hypothesis that the Batur dacitic rocks were produced by fractional crystallization from basaltic magmas rather than by any process involving crustal materials.

9. POSSIBLE MECHANISMS OF MAGMATIC DIFFERENTIATION

9.1 Postcaldera-Caldera Trend

Integrated trace and major element modelling has shown that the Batur caldera stage dacites could have been formed by approximately 84 to 92 % closed-system, low-pressure fractional crystallization of an olivine basalt magma, by a two-stage fractionation process, each stage involving two different phenocryst assemblages. The modelling also indicates that the postcaldera lavas represent suitable intermediate members of this fractionation series.

The regular compositional variations and the lack of substantial reverse zoning shown by phenocryst minerals in the dacites provide no support for the possibility that mixing between different magmas was involved in the production of the dacitic magmas. There is also no evidence from O, Be, Nd, Sr and U-Th isotopes that much, if any, crustal material was involved in the genesis of either the basaltic or dacitic products of Batur volcanism.

At Batur, where the dacitic rocks were erupted before the postcaldera basaltic lavas, it is difficult to apply the traditional concept of a slowly cooling body of magma undergoing fractional crystallization to the genesis of the postcaldera and caldera stage volcanics. This concept, in particular, involves the production over time of a series of residual liquids of uniform composition throughout the chamber (Cox et al. 1979). Because each of these liquids is more differentiated than its predecessor, this process precludes the

possibility of basaltic magmas being erupted after geochemically related dacitic magmas, unless the chamber were to be replenished by new magma of similar composition to that from which the dacitic magmas were actually produced.

Accepting that the Batur postcaldera-caldera geochemical trend could have formed by closed-system fractional crystallization, the origins of the caldera dacites and the postcaldera basaltic lavas are better explained using the concept of liquid fractionation (McBirney et al. 1985) which, as outlined previously, involves early generation of dacitic magmas in thin boundary layers at the walls of a basaltic magma chamber,

It is envisaged that near-liquidus crystallization of a plagioclase, olivine, clinopyroxene and Ti-magnetite assemblage at the walls of a basaltic magma chamber led to production of relatively low-SiO_2 dacitic liquids which escaped upwards, carrying little, if any, crystalline material, to form a body of chemically evolved magma that remained isolated from the main bulk of basaltic magma. This fractionation process incorporates steps 3 and 2 of the major elements 'least squares' modelling of the postcaldera-caldera trend (Table 1.11) which span the 6 wt % SiO_2 gap between the postcaldera basaltic andesites and the low-SiO_2 dacites.

In addition to the experimental results discussed previously, Nilsen et al. (1985) and Lowell (1985) have shown from mathematical modelling that counterflow, involving upward moving residual liquids in a boundary layer and complementary downwards movement of adjacent parental magma in the interior of the chamber, will occur in a magma chamber if the positive buoyancy effect due to the relatively low compositional density of the residual liquids, compared to their parental basaltic magmas, exceeds the negative effect due to their relatively colder temperatures. Where these two opposing effects are approximately balanced then remixing of the residual liquids into the interior of the chamber will occur, whereas downwards movement of the residual liquids will occur if the thermal negative buoyancy effect dominates (Lowell 1985). Nilsen et al. (1985) suggested that the production of relatively high

viscosity liquid in the boundary layer also promotes counterflow by localizing high velocity gradients within the interior, low viscosity parental magma.

For the Batur volcanics, densities of the dacitic magmas, calculated from the compositions of the caldera stage dacites (Bottinga & Weill 1970), are markedly lower than those with the compositions of the post- and precaldera mafic rocks (Fig. 1.49), indicating that counterflow could have occurred.

However, this mechanism of crystal-liquid separation does not necessarily explain the origin of the SiO_2 gap observed between the Batur postcaldera and caldera stage volcanics. Possibly, the residual liquids had to evolve to a dacitic composition before the compositional buoyancy effect outweighed the thermal buoyancy effect.

As Lowell (1985) points out, the behaviour of the boundary layers of magma chambers is largely a function of bulk magma composition and phase relationships but there seems to be no way, using the geochemical and mineralogical characteristics of the volcanic rocks, to infer how the crystalline material deposited on the walls of the chamber might have evolved.

However, the SiO_2 gap may correspond with the compositional effect produced by the reaction relationship between olivine and liquid at Point A in Figure 1.42. At this point, during fractional crystallization, residual liquids become markedly enriched in Fe (Grove & Baker 1984). Because of the high density of Fe, the compositional buoyancy of these liquids may not be sufficient to permit counterflow. At Batur, therefore, the liquids which possessed compositions lying within the SiO_2-gap may have been remixed into the main body of magma or have flowed downwards to the floor of the chamber.

It is also interesting to note the possibility that the 'age' of 58,000 years suggested by the ^{238}U-^{230}Th data, using one standard deviation errors, may mark the production of the dacitic magmas according to the liquid fractionation model. An age of this order is consistent with the minimum age of 23,700 years b.p. indicated by ^{14}C dating of the Bali ignimbrite,

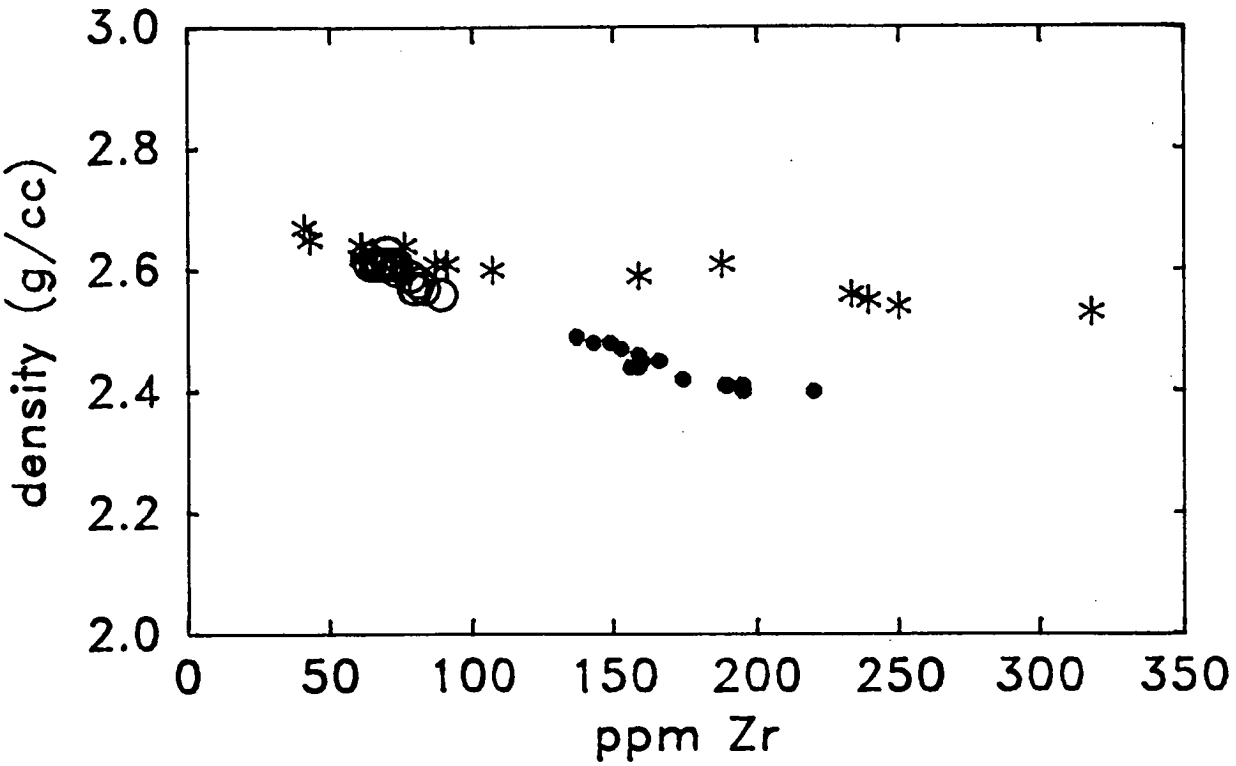

Figure 1.49 Densities of Batur magmas calculated from the rock compositions (Bottinga & Weill 1970) against Zr (symbols as for Fig. 1.22).

and the maximum age of less than 0.1 Ma ago given by K-Ar dating of basaltic lavas at the base of the Batur caldera wall. Moreover, if this hypothesis is correct then the ($^{230}Th/^{232}Th$) and ($^{238}U/^{232}Th$) values of the Batur dacitic rocks should lie along line B-B' in Figure 1.47, at low ($^{238}U/^{232}Th$) values given their origin by fractional crystallization involving Ti-magnetite, which typically fractionates U from Th when it precipitates (Allegre & Condomines 1976), leading to isotopic disequilibrium forming in the residual liquids.

Separation of the dacitic magma from its parental basaltic magma either into an overlying cap or into a separate, shallower chamber is also consistent with the reverse compositional zoning patterns shown by some plagioclase phenocrysts in the dacitic rocks, which can be interpreted as having been caused by a rapid decompression event. Comparison with published experimental determinations of the liquidus phase relatioships of Mt St Helens dacite, together with the low-pressure liquid-line-of-descent of basaltic magma, indicates that the dacite magma could have been situated at very shallow depths within the crust, possibly at much less than 1.5 km.

Although the compositional variation shown by the Batur dacitic rocks, from relatively low- to high-SiO_2 dacite, appears to have occurred by fractional crystallization, it is not yet clear how crystal-liquid separation may have occurred. The lack of any crystalline material in the dacites that could have precipitated from basaltic magma suggests that fractionation occurred within the dacite chamber or cap, isolated from the fractionating assemblage associated with the basaltic magma.

It is notable that the last products of the caldera stage, the Bali ignimbrite and the postcaldera plinian pumice from the Pajang vent, are also the most SiO_2-rich. In addition, involvement of apatite and Ti-magnetite, which possess relatively high densities, in the fractional crystallization process that produced the range of dacite compositions suggests that gravitative fractionation may have occurred. Alternatively, the high viscosity of the dacite magmas, about

$10^{6.5}$ poise at 950-1050 °C and 1-2 wt % H_2O (see Figure 4.6 of Carmichael et al. 1974), may have inhibited crystal settling. Resolution of by what mechanism crystal-liqyuid separation occurred requires information from a detailed study of the geochemical and temporal evolution of the Batur caldera stage dacite sequence.

After providing material for the highly explosive eruption of the thick Batur pyroclastic deposits over a period of, perhaps, a few tens of thousands of years, the shallow dacitic chamber or cap may have been largely exhausted by the major eruption about 23,670 years ago which produced the Bali ignimbrite. Collapse of the Batur volcanic edifice into the partly evacuated cap may explain the formation of Batur caldera.

The Batur postcaldera lavas lie within a relatively restricted compositional range. An important feature of the liquid fractionation concept is that, while cooling at the margins of a closed-system magma chamber leads to production of fractionated liquids in the sheath of magma near the walls, the composition of the main mass of magma in the core of the chamber is not significantly affected (Sparks et al. 1984). The occurrence of basaltic and basaltic andesite lava flows, the change to strombolian rather than plinian-type activity, and the growth of the new Batur stratovolcano during the 23,670 years since caldera formation may be explained, therefore, by eruption of this core material after the main mass of dacitic magma had been generated and erupted.

Additional evidence for the presence beneath Batur caldera of a modern basaltic magma chamber is provided by the gravity survey within the caldera by Yokoyama and Suparto (1970) who concluded that a body of excess mass (density > 2.5 g/cm^3) lies beneath the central part of the caldera at shallow depths. Experimental evidence noted previously also suggests that the basaltic lavas began to crystallize at depths of much less than 15 km.

Finally, at this stage, there appears to be no reason not to expect Batur volcano to continue to erupt basaltic and

basaltic andesite material during the geologically foreseeable future. It is envisaged that production of the dacitic magma led to formation of a thick crust of crystals at the walls of the basaltic magma chamber, which may effectively insulate the chamber from the colder wallrocks. In addition, the thermal gradient between the chamber and the wallrocks may have been gradually reduced over time by gradual conduction of heat away from the chamber. Given that production of dacitic magma at vertical sidewalls requires the presence of a substantial thermal gradient, it seems unlikely that highly differentiated magma will be produced again by the liquid fractionation mechanism during the existence of the modern Batur magma chamber, although it seems possible that, if the Batur magma chamber remains as a closed-system, more differentiated liquids may be produced as the chamber slowly cools and crystallizes.

9.1.1 Implications for Caldera-Formation

This model for the production of the Batur dacitic volcanics is the reverse of the traditional volcanic evolutionary cycle: the more SiO_2-rich liquids are erupted first and the basaltic magmas later.

In addition, at Batur, production of dacitic magmas, and subsequent onset of major explosive magmatic eruptions, appears to have been a geologically rapid process, occurring perhaps within a period of a few thousand years, and to have taken place independently of the previous history of the volcano. Therefore, studies of the recent products of volcanoes may not always provide satisfactory information on which to base predictions of possible future eruptions.

Although the Batur dacites possess an unusual phenocryst assemblage and display more marked Fe-enrichment with increasing SiO_2 contents than do some other arc dacite suites, the process suggested here for their genesis may not be uncommon. Most stratovolcano calderas occur, like Batur, in volcanic island arcs (Wood 1984), but virtually none of them has been the subject of integrated stratigraphic and petrogenetic studies. For example, seventeen young calderas that occur in Indonesia alone, from descriptions given in Neumann van Padang

(1951), are associated with basaltic to andesitic lavas and dacitic pyroclastics. Many of these, particularly Krakatau, are known to have produced basaltic to andesitic lavas after their calderas formed, suggesting that caldera collapse may have occurred following production of dacitic magma by a similar process to that postulated here for Batur.

In Papua New Guinea also, calderas are known with characteristics similar to those of Batur. The most notorious of these is Rabaul, located at the eastern tip of New Britain island, which was thought to be near eruption in 1983/84 (McKee et al. 1985). The geochemical characteristics of the Rabaul volcanic rocks are strikingly similar to those of Batur (Fig. 1.50) and the range of rocks erupted from Rabaul contains, like Batur, a pronounced gap between 55.5 and 60 wt % SiO_2 (Heming 1974). Caldera formation at this volcano occurred relatively recently, about 1,400 yrs b.p., and it has erupted postcaldera andesites (Heming 1974; McKee et al. 1985).

9.2 Precaldera Trend

The absence of consistency between the major and trace element modelling of the precaldera geochemical trend suggests that, unlike the postcaldera-caldera trend, it could not have been produced by any plausible closed-system fractionation process, implying that an open-system process may have occurred.

Specific characteristics of the precaldera differentiation trend, identified from the modelling calculations, which may be important to distinguishing the type of open-system process include a) the progressively increasing degrees of enrichments of incompatible elements during production of the more SiO_2-rich rocks that are substantially in excess of those predicted by closed-system fractional crystallization, b) analogous depletion of compatible elements, and c) increasingly mafic character of the fractionating phenocryst assemblage, which implies involvement in some way during fractional crystallization of a mafic liquid.

The simplest of the open-system magma chamber models, that

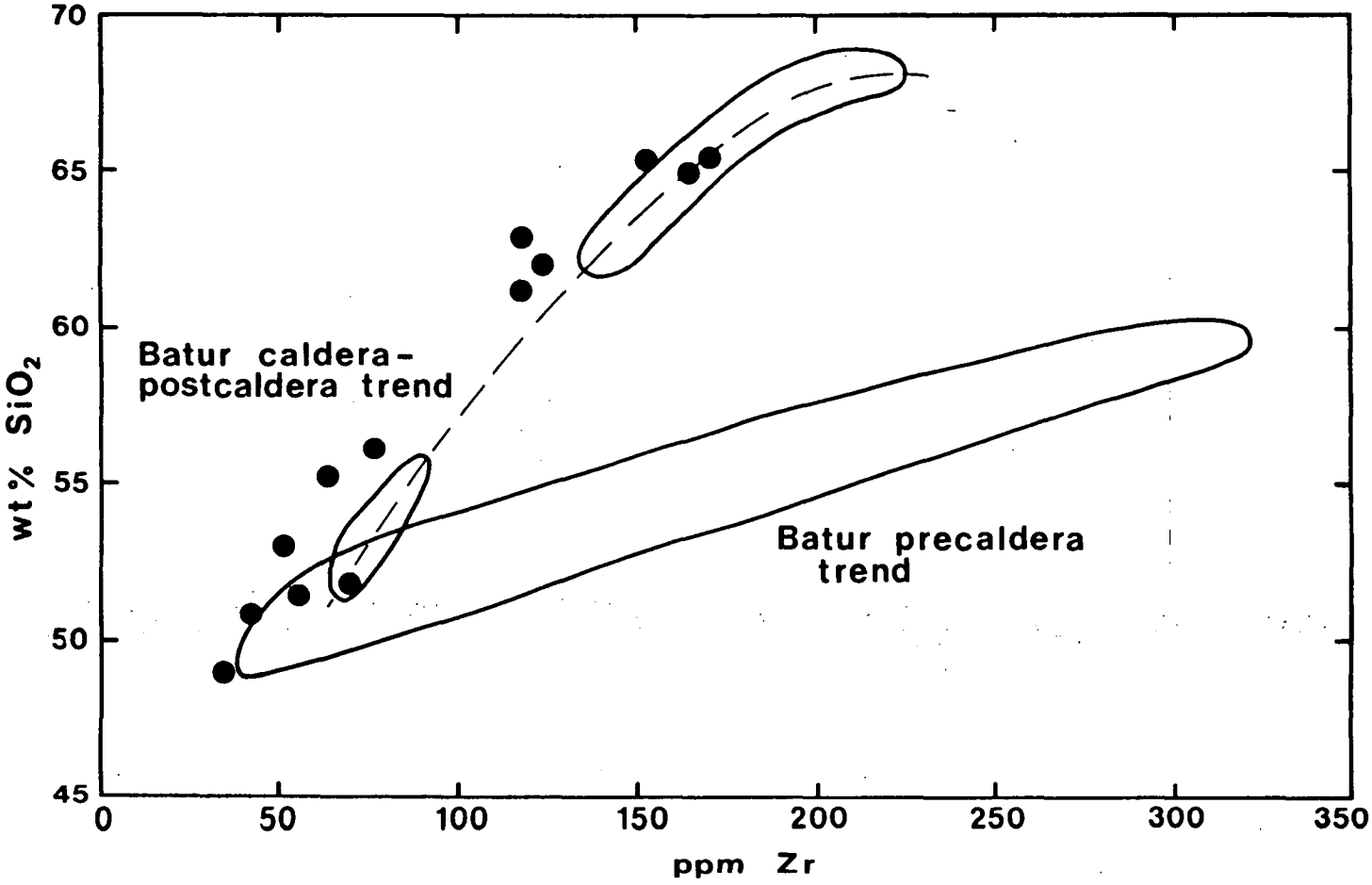

Figure 1.50 SiO_2 against Zr in Rabaul volcanic rocks compared to Batur. Rabaul data from Heming (1974).

of Cann (1982), involves a body of magma undergoing fractional crystallization from which liquid is continuously removed either by eruption or by its intrusion elsewhere. Cann's (1982) calculations indicate that, compared to the closed-system case, the effective bulk distribution coefficients of incompatible elements increase, and those of compatible elements decrease, as the weight ratio of liquid leaked to solid precipitated increases. These results suggest that, compared to those produced by closed-system fractional crystallization, liquids produced by this process will be less enriched in incompatible elements and less depleted in compatible elements. This geochemical effect is the opposite to that observed in the Batur precaldera volcanics

The combined fractional crystallization and assimilation model of De Paolo (1981) treats the case in which the composition of a body of magma undergoing fractional crystallization is also modified either by wallrock assimilation or by periodic replenishment of the chamber with new magma. De Paolo's (1981) calculations indicate that as the ratio of assimilation rate to fractional crystallization rate increases incompatible elements become substantially more enriched in evolved magmas compared to their abundances in magmas of similar major element compositions produced by the closed-system process.

However, the abundances of compatible elements rapidly approach steady state values as the degree of crystallization increases, rather than becoming progressively more depleted (see De Paolo's (1981) Fig. 2). Therefore, although the behaviour of incompatible elements predicted by De Paolo's (1981) model appears to be consistent with their observed behaviour in the Batur precaldera volcanics, it is less certain that the pattern of variation of compatible element abundances is also consistent. In addition, there is no evidence from the Batur precaldera rocks, such as abundance of xenolithic or xenocrystic material, suggesting that substantial wallrock assimilation has occurred.

O'Hara and Mathews (1981) examined the geochemical variation that may result from the additional processes of

periodic magma chamber replenishment, of mixing between this magma and that already in the chamber, and of periodic eruption of the residual liquids from the chamber.

In particular, if the mass fraction of magma crystallized in each cycle of these processes is very much greater than the fraction of magma erupted, then the abundances of incompatible elements in the residual liquids will be substantially more enriched, relative to the parental magma, than would be expected had closed-system fractional crystallization occurred. Also, if a steady state is maintained, that is, if the mass fractions of new and erupted material and the degree of crystallization remain constant, the material erupted from the chamber would approach a constant composition.

As O'Hara and Mathews (1981) point out, it is not possible to use their treatment of a model, general open-system chamber to identify uniquely the processes that may have occurred by inverting geochemical data from a given volcanic suite. However, additional data, such as stratigraphic relationships, may be used to eliminate some of the model alternatives.

At Batur, the range of compositions shown by the precaldera rocks, with the pumiceous basaltic andesites clasts and andesite lava apparently having been erupted near the end of the precaldera stage, together with the indications from the modelling that the rate of enrichment of incompatible elements and the rate of depletion of compatible elements progressively increase from basalt to andesite, suggests that any precaldera open-system magma chamber had not reached a steady state.

These relationships may be explained if the model Batur precaldera magma chamber was waning, rather than evolving towards a steady state. O'Hara and Mathews (1981) model a waning, or dying, magma chamber as one in which the amounts of magma added to the chamber by replenishment, and removed from it by eruption, both gradually decrease, and the degree of fractional crystallization of the remaining magma in the chamber gradually increases, until the chamber is completely solidified. In particular, they show that the final products of

such a chamber can possess extreme enrichments in incompatible elements, and depletions of compatible elements, compared to their parental magmas, and to the majority of the material erupted during the life of the chamber (see their Fig. 23).

Finally, it is notable that the volatile-rich nature of the precaldera basaltic andesites and andesites, as indicated by their largely pumiceous nature and eruption by pyroclastic mechanisms, is consistent with their high concentrations of incompatible elements, given that volatile components largely behave incompatibly when no (OH,F,Cl)-bearing phenocryst phases are present. Periodic replenishment by relatively undegassed and chemically primitive magmas in an open-system chamber could therefore also lead to markedly higher degrees of enrichment of volatiles in derivative magmas than would be expected for closed-system fractional crystallization. The explosive mode by which these mafic rocks were erupted, as well as their unusual compositions, may also be explained by their possible origin in an open-system magma chamber. The postcaldera lavas of similar major element composition, in contrast, were erupted as lava flows accompanied by less explosive strombolian pyroclastic activity.

10. SUMMARY AND CONCLUSIONS

The active Batur volcano on the island of Bali in the eastern Sunda arc, Indonesia, has produced during the last 0.5 Ma a wide variety of volcanic rock types, including olivine basalts, andesites and high-SiO_2 dacites. It now possesses a large, well-formed, elliptical caldera, 13 km by 10 km, with an inner circular collapse zone 7.5 km in diameter, in which a new basaltic stratovolcano is being formed.

The evolution of Batur can be subdivided into precaldera, caldera and postcaldera stages from the volcanic stratigraphy. The precaldera stage was characterized by production of basaltic to andesitic lava flows and pyroclastics, including distal deposits apparently formed by pyroclastic flow which contain dense pumiceous clasts of basaltic andesite composition. These deposits are overlain by thick sequences of dacitic lava flows and pyroclastics, including widely

distributed plinian pumice deposits and both welded and non-welded ignimbrites, formed during the subsequent caldera stage. These rocks are well exposed in the Batur caldera walls and are markedly unlike those of the precaldera stage in lithology, mineralogy and composition.

Explosive eruption of the caldera dacitic pyroclastics culminated about 23,670 years ago (^{14}C) with the generation and deposition of the Bali ignimbrite and formation of Batur caldera. The Bali ignimbrite is more than 16 m thick in places, shows marked pumice-enrichment towards its top and distal margins and is distributed over at least 450 km^2 of southern Bali.

Batur is now in an active postcaldera stage, with the summit of the new stratovolcano having reached 700 m above the caldera floor. Many intracaldera basaltic and basaltic andesite lava flows, including nine flows erupted between 1849 and 1974, have been erupted from this cone, mainly from vents lying on its western and northeastern sides.

The pre- and postcaldera basaltic rocks (49-56 % SiO_2) are similar and range from slightly ne- to Q-normative (all Fe as FeO). Their phenocrysts comprise abundant plagioclase (cores Ca# 59-94) together with clinopyroxene (Mg# 67-77), olivine (Mg# 66-71) and Ti-magnetite. The rocks contain low TiO_2 (0.9-1.4 %) and high Al_2O_3 (16.3-20.6 %) abundances, and low to moderate amounts of K_2O, Rb and Ba, with similarly moderate LREE enrichment.

There is no evidence from O, U-Th, Sr, Nd and Be isotopes of any substantial involvement of pelagic sediments or altered oceanic crust from the subducted slab, or material from the arc crust, in the production of any of the Batur rocks.

The precaldera andesites (56-60 % SiO_2) and caldera stage dacites (62-68 % SiO_2) contain markedly different phenocryst assemblages and show diverging chemical differentiation trends away from the basaltic rocks. Although separated by a 6 wt % SiO_2 gap, the caldera dacitic rocks are more closely related geochemically to the postcaldera basaltic and basaltic andesite

lava flows, including those erupted in historical time, than to the precaldera basaltic andesite and andesitic pyroclastics and lavas.

Combined major and trace element modelling indicates that the dacites and postcaldera lavas could be genetically related by closed-system fractional crystallization involving the observed phenocryst assemblages. This temporal and geochemical relationship, which is consistent with O and Sr isotopic evidence, suggests an evolutionary model involving fractional crystallization at the walls of a newly established basaltic magma chamber, which led to production and buoyant transfer upwards in thin boundary layers of dacitic residual liquid. This liquid appears to have accumulated in either a separate, shallow-level magma chamber or formed a cap overlying the basaltic magma, and to have been erupted explosively to form the Batur caldera stage dacitic volcanics. The postcaldera lavas are interpreted to be derived from the relatively unmodified basaltic magma that still forms the core of the chamber. The existence of such a basaltic chamber accounts for the occurrence of a positive gravity anomaly within Batur caldera.

Comparison of the unusual Batur dacite phenocryst assemblage of Fe-rich olivine (Mg# 32-56), clinopyroxene (Mg# 55-78) and orthopyroxene (Mg# 59-67), together with plagioclase (Ca# 31-60), Ti-magnetite and apatite, with published experimental results indicates that the dacitic magma contained from < 1 to 2 wt % H_2O, and last crystallized at < 1.5 km depth, at 1070-930 ^{o}C and at oxygen fugacities close to those of the FMQ buffer.

In marked contrast to the dacites and postcaldera basalts and basaltic andesites, some of the precaldera mafic volcanics show unusual enrichments of incompatible elements that are substantially in excess of those expected from closed-system fractional crystallization. Comparison of these characteristics with those of published theoretical differentiation models suggests that these rocks could have been produced by open-system magmatic processes involving fractional crystallization of a waning basaltic magma chamber undergoing periodic, but

decreasing, magma replenishment and extraction.

The marked enrichment of magmatic volatile contents that would result from such open-system processes may also explain the occurrence of many precaldera basaltic andesites and andesites as pumiceous clasts in deposits apparently formed by pyroclastic flow, whereas postcaldera rocks of similar major element composition occur as lava flows.

The formation of calderas at basalt-andesite-dacite stratovolcanoes may therefore result from an evolutionary process which is the reverse of that traditionally associated with evolving basaltic magma chambers, leading to the early eruption of derivative siliceous magmas followed by the eruption of parental basaltic magmas. The Batur model implies that sudden and marked changes in eruption styles and products may be expected during volcano evolution and that dynamic magma chamber processes could have a substantial effect on the mechanisms by which mafic material is erupted.

PART 2

A REVIEW OF THE GEOLOGICAL, GEOCHEMICAL AND ISOTOPIC CHARACTERISTICS OF QUATERNARY VOLCANISM IN THE SUNDA-BANDA ARC: THE ROLE OF SUBCONTINENTAL MANTLE ENRICHMENT IN ARC BASALT GENESIS

1. INTRODUCTION

The Sunda and Banda island arcs form a continuous geological structure that extends for approximately 4700 km from the northern tip of Sumatra in the west to the small island of Nila in the east, after which it curves tightly northwards for a further 600 km, towards Ambon (Fig. 2.1). The oceanic Sunda Trench lies south of and parallel to the Sunda arc and delineates the site of subduction of the northward-moving Indian-Australian plate beneath the southeastern extension of the Eurasian plate. South of Sumbawa the Sunda Trench passes eastwards into the Timor Trough. Volcanism appears to have occurred continuously since the Triassic in parts of the western Sunda arc (Sumatra and western Java), but in the eastern Sunda arc (Bali to Wetar) and the Banda arc (eastwards from Romang) volcanism appears to have initiated in the Middle-Late Tertiary (Hamilton 1979).

This part of the thesis reviews and extends the data obtained from Quaternary volcanoes in the Sunda-Banda arc in order to test contemporary models of mafic magma genesis in volcanic island arcs. Modern petrogenetic models have largely developed from studies of volcanic rocks in many active continental and oceanic volcanic arcs, including those in Indonesia, but none has been able to take advantage of the range of compositions present among the Sunda-Banda arc volcanic rocks. This range is the widest known from any active orogenic region. The Sunda-Banda arc also possesses the Earth's only active example of collision between ancient continent and a young intra-oceanic volcanic island arc.

The most recent comprehensive review of Indonesian volcanism is that of Hutchison (1982). His review, however,

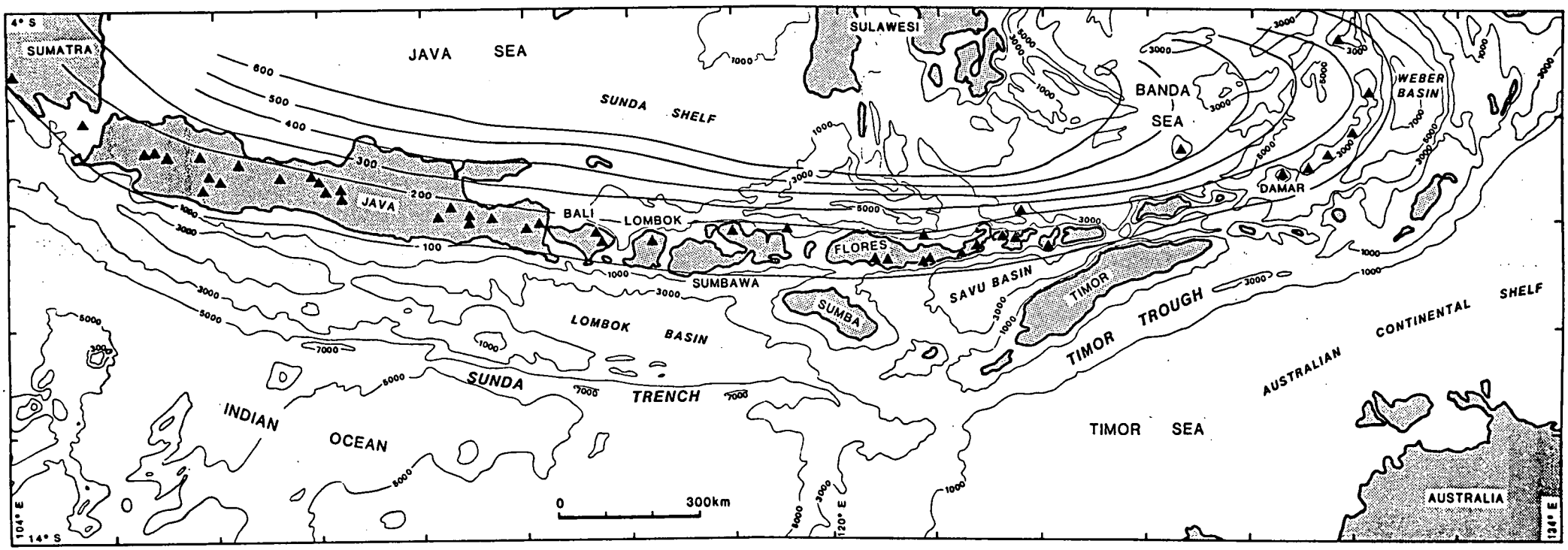

Figure 2.1 Map of the Sunda-Banda arc region showing locations of volcanoes known to have erupted within the last 10,000 years (solid triangles; Simkin et al. 1981). Contours indicate depth to the Benioff zone (Hamilton 1979).

incorporates chemical analyses of volcanic rocks obtained by wet chemical methods, cited by Neumann van Padang (1951), which are not directly comparable to chemical analyses produced by modern X-ray methods. Results obtained for some oxides by wet chemical methods, particularly SiO_2, Al_2O_3 and alkalis, are notoriously imprecise and possibly inaccurate. For example, Hutchison (1982) remarked that the chemical analyses of Stehn (1928) show the recently erupted basaltic lava flows from Batur volcano on Bali to be unusually rich in Al_2O_3. New XRF analyses, however, show that these rocks contain similar Al_2O_3 contents to most other island arc basalts (Part 1). Therefore, only modern data are used in this chapter.

Except for some analyses by Brouwer (1940), few chemical analyses of samples from volcanoes in the arc sector from Flores to Pantar were available for Hutchison to include in his review. This discussion incorporates 315 new, unpublished analyses of lava samples from most of these volcanoes, which were obtained during a reconnaisance geochemical survey of eastern Sunda arc volcanism by R. Varne (University of Tasmania), J.D. Foden (University of Adelaide) and M.J. Abbott (Flinders University of South Australia) and myself. Together with data obtained from Quaternary volcanoes on Java by Whitford (1975a), on Lombok and Sumbawa by Foden (1979), and from the Banda arc by Jezek and Hutchison (1978) and Whitford and Jezek (1979), the data set totals 679 X-ray analyses of young volcanic rocks from 56 volcanoes lying between Krakatau in the west and the Banda Islands in the east. Some initial results of this work have already been reported (Wheller et al. 1983;1986).

2. TECTONIC SETTING

2.1 Geology and Tectonic Evolution

The geology and tectonic setting of the Indonesian region has been summarized by van Bemmelen (1949) and by Hamilton (1979). The following outline of the geology of the Sunda-Banda arc is largely based on Hamilton's compilation.

The oldest rocks in the Sunda-Banda arc are widespread

sequences along the Barisan Mountains in Sumatra of isoclinally-folded limestones, shales, sandstones and radiolarian cherts of Late Carboniferous-Permian and Triassic ages. In eastern Sumatra, the sequence also contains intercalated siliceous volcanic rocks, mainly tuffs. These rocks are generally interpreted to have been deposited at a continental margin, varying from a shallow-water, probably platform, environment in western Sumatra to an abyssal environment in eastern Sumatra.

Limestones, siliceous marl, shale, radiolarian chert, andesite and basalt of Cretaceous age also occur in southern Sumatra. These and the older rocks are intruded by tourmaline-bearing ("tin") granites, like those of the Thai-Malay peninsula, which are mainly of Triassic and Cretaceous ages. Similar volcanic and sedimentary sequences to those in Sumatra are the oldest-known rocks in Java, forming a highly deformed and sheared melange of greywackes, greenschists, eclogites, serpentinites, gabbro, pillow basalt, radiolarian chert and pelagic limestone containing Cretaceous fossils which crops out in the central and southwestern parts of the island.

Early Tertiary continental clastics, including coarse conglomerates and lacustrine shales lie northeast of the Barisan Mountains in Sumatra, and are overlain by thick deposits of marine, quartz-rich shales and sandstones of Late Oligocene to Early Miocene ages. This sequence includes limestone reefs and carbonate banks and appears to have been deposited in a regional basin that progressively deepened towards the northeast (Hamilton 1979). Subsequent regression of the marine basin is indicated by the presence of overlying shallow-marine to terrestrial sediments. Both the transgressive and regressive sequences contain major petroleum reservoirs.

Intercalated terrestrial clastics and shallow-marine carbonate sediments, including limestone reefs, of Middle Eocene to Late Oligocene age overly the Cretaceous melange sequences in western and central Java and Hamilton (1979) suggests a stable, continental margin was present in this region during much of the Early Tertiary. However, voluminous calcalkaline volcanic rocks, the "Old Andesites" of van

Bemmelen (1949), and intercalated Oligocene to Pliocene limestones occur along the southern parts of Java. Intermediate and siliceous volcanic rocks younger than Oligocene or Early Miocene in age also form most of the Barisan Mountains in southwestern Sumatra, becoming less voluminous northwestwards. Basaltic to andesitic lavas and intrusives from the Tertiary volcanic sequence in the West Progo Mountains and Djiwo Hills region in south-central Java show the low TiO_2 and MgO, high Al_2O_3 and moderate K_2O characteristics of calcalkaline magmas (Whitford 1975a) but abundant alkaline rocks, some containing leucite, occur in addition to Miocene and younger calcalkaline rocks in the South Arm of Sulawesi (Iddings & Morley 1915; Hamilton 1979).

Openly folded shales, sandstones, marls and limestones in northern Java are also of Oligocene to Pliocene age and indicate sedimentation was occurring in deep basins behind the volcanic arc (Hamilton 1979). This sequence now contains major oil fields.

Middle Miocene to Pliocene limestones and calcareous marls crop out sporadically along the eastern Sunda-Banda arc. The oldest of these rocks crop out in Lombok, Sumbawa and western Flores (van Bemmelen 1949). Basal sediments younger than Late Miocene occur in Bali (Kadar 1972), eastern Flores, Lembata, Alor and Wetar (van Bemmelen 1949). Mafic lavas and tuffs are intercalated with these sediments in many places and, in Wetar and central Flores, granodioritic plutons intrude the sequence. K-Ar dating of basal ankaramitic pillow basalts on Bali gives Late Pliocene ages of 2.5 and 2.8 Ma (Part 1) and mafic lavas and intrusives on Flores and Wetar show a spread of K-Ar ages from 12 Ma to < 0.5 Ma (Abbott & Chamalaun 1978).

The evolution of the Sunda-Banda arc since the Mesozoic has apparently involved the progressive, eastward migration of a series of subduction zones, beginning with a Cretaceous to Early Tertiary arc that extended through Sumatra, Java and southeastern Kalimantan and which was followed by a Middle-Late Tertiary arc through eastern Java, Sumbawa, Flores, Wetar and southern Sulawesi (Katili 1975; Hamilton 1979). The reason for the apparent Late Tertiary reorientation of subduction in

eastern Indonesia from a system trending northwards through Sulawesi to one trending eastwards along the Banda arc is not yet clear. As indicated in the next section, the crustal structure of the Banda Sea region is complex and interpretations of its origins are still being debated.

2.2 Structure and Seismicity

2.2.1 Crustal Thickness

The Indonesian region is characterized by complex tectonic relationships between continental and oceanic terranes. Exposed continental crust in Sumatra, Java and southeastern Kalimantan comprises Late Palaeozoic continental margin sediments and Triassic to Cretaceous melange and granitic rocks. These rocks also form the floor basement of the Java Sea (Hamilton 1979), which is an extensive but shallow (< 80 m deep) shelf region between Java and Kalimantan, termed the Sunda Shelf, whose eastern boundary lies generally north of Bali where water depths rapidly increase eastwards.

Seismic refraction studies in the forearc region seaward of Sumatra (Kieckhefer et al. 1980), in the eastern Sunda arc (Curray et al. 1977) and in the Java Sea (Ben-Avraham & Emery 1973) indicate crustal thicknesses of 20-30 km beneath Sumatra and Java, and about 18 km near Bali. These values were considered as being transitional between typical continental and oceanic thicknesses by Curray et al. (1977).

Hamilton (1979) suggestd that the crust forming western Java and the Sunda Shelf formed by accretion of Late Cretaceous - Early Tertiary subduction melange against the Late Palaeozoic - Mesozoic continental margin as the trench progressively migrated seawards during the Early Tertiary towards its present position. However, Curray et al. (1977) suggested the Java-Bali forearc crust is more likely to be oceanic crust of Jurassic or older age that was trapped seawards of a Late Cretaceous - Early Tertiary subduction zone by relocation of the subduction process to its present position during the Middle Tertiary. The thickness of the crust in the forearc region, according to the latter model, may be due to old age combined with reverse or

thrust faulting caused by horizontal compression.

The origin of the Banda sea crust in the east is at present controversial. Deep (4-5 km), narrow basins in the southern parts of the Flores and Banda seas have underlying crustal thicknesses of 8-10 km (Curray et al. 1977). Purdy and Detrick (1978) obtained similar results of 9-10 km for crustal thickness in the eastern Banda Sea and suggested the southern parts of the Banda Sea were floored by typical oceanic crust. Heat flow in the Banda Sea is low, averaging about 4.6 mW/m^2 (Jacobson et al. 1977; Bowin et al. 1980). Hamilton (1979) suggested the crust of the southern Banda Sea formed in the Middle Tertiary by back-arc spreading, leading to migration of the Banda volcanic arc to its present position but Bowin et al. (1980) infer from water depth, low heat flow and the possible presence of linear magnetic anomalies that it is trapped, oceanic crust of Mesozoic age.

Pigram and Panggabean (1983) reached a similar conclusion to that of Bowin et al. (1980). They suggested that an early Jurassic unconformity, present on each of the continental fragments that lie around the northern and western margins of the Banda Sea, was formed during the early stages of the break-up of Gondwanaland. Because they found no evidence of either transcurrent faulting or subduction along the margins of these fragments, Pigram and Panggabean (1983) inferred that the adjacent crust forming the floor of the Banda Sea must be oceanic crust of Late Jurassic to Cretaceous age.

However, Silver et al. (1985) have recently dredged slates, phyllites, conglomerates and other continent-derived rocks from prominent ridges in the Banda Sea, and have suggested that the ridges represent fault slices derived by lateral shearing from the continental margin of Irian Jaya. The ridges are separated by narrow rift basins and K-Ar ages of some basaltic volcanic rocks dredged from these basins suggest that faulting, and therefore formation of the Banda Sea floor, occurred during the Late Miocene.

2.2.2 Convergence and Collision

The Sunda Trench lies parallel to the volcanic arc and extends from northern Sumatra to south of eastern Sumbawa. The trench reaches depths ranging from about 4.5 km off Sumatra to 6-7 km south of Java. An outer arc ridge lies between the trench and the volcanic arc seawards of the western Sunda volcanic arc, rising above sea-level off Sumatra where it is composed of imbricated melange (Hamilton 1977; Moore & Karig 1980).

The Indian-Australian plate south of the Sunda trench is oceanic and converging with the Sunda arc at approximately 7.0 to 7.5 cm/yr south of Java (Moore et al. 1980). Due to the curvature of the volcanic arc, convergence is oriented obliquely near Sumatra, but is near-normal between Java and Sumbawa. In the Argo Abyssal Plain, between the trench and the continental margin of northwestern Australia, linear magnetic anomalies of Middle Jurassic and younger age lie parallel to the Australian coastline (Larsen 1975; Powell & Luyendyk 1982; Veevers et al. 1985) and the oldest-known sediments in DSDP holes 211, 212, 260 and 261 south of the Sunda trench are Cretaceous in age (von der Borch et al. 1974a,b; Heirtzler et al. 1974a,b).

The Timor Trough lies south of Sumba and Timor and the Banda arc and is bathymetrically continuous with the Sunda trench, although it is much shallower. Proterozoic Australian continental crust lies south and east of the Banda and easternmost Sunda arcs, extending beneath the Timor trough (Bowin et al. 1980), possibly to near the northern coast of Timor (Chamalaun et al. 1976). The trough is thought to have formed by down-warping of the continental crust during collision (Bowin et el. 1980). The prominent kink in the trend of the Timor Trough south of Flores was thought by Bowin et al. (1980) to have been produced by northward displacement of the trough axis during collision combined with high rates of 'forearc' growth due to the transport of thick continental margin sediments into the subduction zone.

Collision of the Australian continent with the Banda arc was thought by Bowin et al. (1980) to have begun at about 3 Ma ago, based on the northward displacement of the Timor Trough during the collision and the convergence rate of the Australian continent. However, recent K/Ar and $^{40}Ar/^{39}Ar$ age dating of metamorphic events associated with amphibolites from the Aileu Formation in the northern part of East Timor by Berry and McDougall (1985) suggest that the collision began at 8 +- 1 Ma, in the Late Miocene. The presence of two, south-dipping thrusts in the back arc regions of the Lombok-Sumbawa-western Flores and Alor-Wetar-Romang arc sectors may indicate that the process of arc polarity reversal has begun (Hamilton 1979; Silver et al. 1983).

2.2.3 Earthquakes

Earthquake foci form a seismic zone about 500 km wide that extends along the length of the Sunda-Banda arc. The deepest earthquakes beneath Sumatra have occurred at about 200 km depth but earthquakes are recorded from depths of up to 650-680 km from Java to the Banda arc (Fitch 1970; Cardwell & Isacks 1978). Shallow earthquake foci (< 70 km deep) are mostly confined to the forearc region of the arc and deeper foci define a north-dipping plane that is consistent with northward subduction of oceanic crust beneath the volcanic arc. Below 100 km depth, the seismic plane dips at 20-30^{o} beneath Sumatra and 65-75^{o} from Java to the Banda arc (Hamilton 1979).

Few earthquakes have been recorded from between 300 and 500 km depth beneath Java and Bali (Fitch & Molnar 1970; Cardwell & Isacks 1978). Similarly, few intermediate-depth (71-300 km) earthquakes have been recorded in a zone 700 km long north of Timor. Isacks and Molnar (1969) interpreted the presence of similar deep vertical seismic gaps beneath some volcanic arcs to generally indicate detachment of the lower parts of the descending slabs. Chamalaun & Grady (1976) use the presence of the seismic gap north of Timor to help infer detachment of the oceanic slab from the leading edge of the Australian continent as part of the process of collision.

3. LATE TERTIARY - QUATERNARY VOLCANISM

3.1 Distribution

Active Quaternary volcanoes occur along the entire length of the Sunda-Banda arc, except for three sectors in which volcanism appears to have become extinct. The best-known of these coincides with the location of the along-arc gap in intermediate-depth earthquakes north of Timor. Volcanic activity on the two islands in this sector, Alor and Wetar, seems to have ceased about 3 Ma ago (Abbott & Chamalaun 1978) although basaltic rocks only 0.4 Ma old have been recently dredged from the back-arc region of this sector (Silver et al. 1985).

A less obvious extinct arc sector occurs in the western half of Flores. This sector is about 180 km long and bounded by the active volcanoes of Sangeang Api to the west and Inerie to the east. The only recorded volcanic process still occurring between these two volcanoes is weak hot springs activity at Wai Sano and Pocok Leok calderas, which may be interpreted as indicating waning volcanism at those places. Other Quaternary stratovolcanoes in this sector are deeply eroded. Intermediate-depth earthquakes are also absent from this sector (see Fig. 2 in Cardwell & Isacks 1978).

Further evidence of an extinct arc sector in western Flores comes from a comparison between the Wetar and Flores back arc thrusts. Silver et al. (1983) found that the Wetar thrust is best developed behind the volcanically extinct Alor-Wetar sector and is not present where volcanism is still active, either side of this sector. They also found that the Flores thrust is best developed in a zone extending from behind western Flores to eastern Sumbawa. North of the active volcanism on Bali and Lombok, the thrust zone appears to be weakly developed, with only folding of sediments apparent in seismic profiles. Extinction of volcanism in the western Flores arc sector may explain the presence of back-arc thrusts in that region, consistent with the suggestion of Silver et al. (1983) that the thermal effects of active volcanism may inhibit the development of brittle crustal deformation.

Another extinct sector, approximately 200 km long, occurs in central Java, between Merapi volcano in the west and Kelud volcano in the east. Only two significant volcanic peaks lie within this sector (Neumann van Padang 1951). One of these, Lawu, is deeply eroded and the other shows only weak solfataric activity (Neumann van Padang 1951).

Contrary to suggestions by Audley-Charles (1975) and Hamilton (1979), there is no offset of the volcanic row between the Bali-Lombok sector of the Sunda arc and the Flores-Pantar sector. Instead, the line of volcanoes lying along the northern parts of Bali, Lombok and Sumbawa continues along the northern side of Flores as far east as Lembata (formerly named Lomblen) and comprises the historically active volcanoes Paluweh, Boleng, Lewotolo and Batu Tara together with several extinct Quaternary volcanoes. The active volcanoes lying along the southern sides of Flores, Lembata and Pantar form an additional, forward volcanic row. A similar, forward volcanic row occurs in western Java (Fig. 1).

3.2 Geochemistry

The following discussion is based on the data set of 679 wholerock analyses of samples, mainly of lavas, from Quaternary volcanoes in the Sunda-Banda arc. This data set specifically excludes volcanic rocks from the extinct Wetar arc sector and from northern Sumatra. Although young and probably related in some way to the present subduction process, these rocks are mainly dacitic and rhyolitic in composition and are petrographically, geochemically and isotopically unlike the mainly basaltic and andesitic volcanics from the remainder of the Sunda-Banda arc. Their genesis may involve either substantial assimilation or anatexis of upper crustal material (Magaritz et al. 1978; Rock et al. 1982; McCulloch et al. 1983; Beddoe-Stephens et al. 1983; Aldiss et al. 1984). Their inclusion, therefore, would hamper recognition of compositional variations caused by processes occurring in the subarc mantle.

3.2.1 Major elements

Like most other island arc volcanics (Gill 1981; Ewart 1982), those from the Sunda-Banda arc are characterized generally by a wide variation in SiO_2 contents, high amounts of Al_2O_3 (mostly 16-22 wt %, except for many leucite-bearing rocks which contain only 10-16 wt %), low TiO_2 contents (mostly < 1.3 wt %), and low Na_2O and MgO contents compared to most basalts from mid-ocean ridge and ocean island settings. Except for Na_2O and K_2O, all of the major elements decrease in abundance with increasing SiO_2 contents (Fig. 2.2). It is also notable that, compared to hy-normative rocks, the ne-normative rocks show trends of increasing Al_2O_3 with increasing SiO_2, together with slightly more rapid depletion of CaO and enrichment of Na_2O with increasing SiO_2. These trends may be explained generally by low pressure crystal fractionation processes involving olivine, pyroxenes, plagioclase, hornblende and Fe-Ti oxides, and, in addition, leucite, sanidine and phlogopite in SiO_2-undersaturated suites (Nicholls & Whitford 1976,1983; Foden 1983; Wheller & Varne 1986; Foden 1986; Part 1 of this thesis).

3.2.2 Classification

The low-SiO_2, high-MgO members of the various volcanic suites from the Sunda-Banda arc vary mostly in their abundances of K_2O, P_2O_5 and related trace elements. Because these rocks are the least likely to have had their compositions affected by substantial degrees of crystal fractionation, and in the absence of evidence for the widespread occurrence of crustal assimilation, these differences are probably inherited from their parental magmas. The following discussion identifies regular patterns of geochemical and isotopic variation among these rocks.

Because there is little variation within most other major elements at similar SiO_2 contents, suites of lavas from individual volcanoes in the Sunda-Banda arc are best characterized chemically by their K_2O-SiO_2 relationships. This observation has been long recognized for volcanic arc rocks generally. The K_2O and SiO_2 contents of the Sunda-

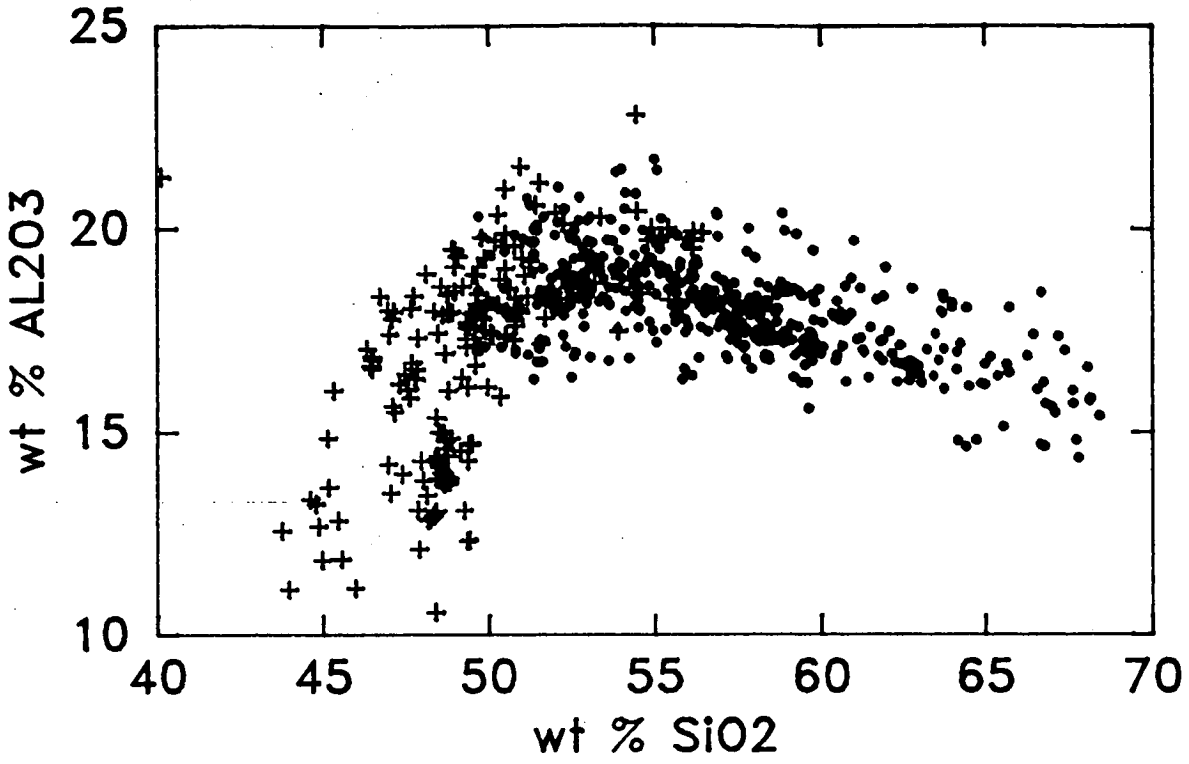

Figure 2.2a

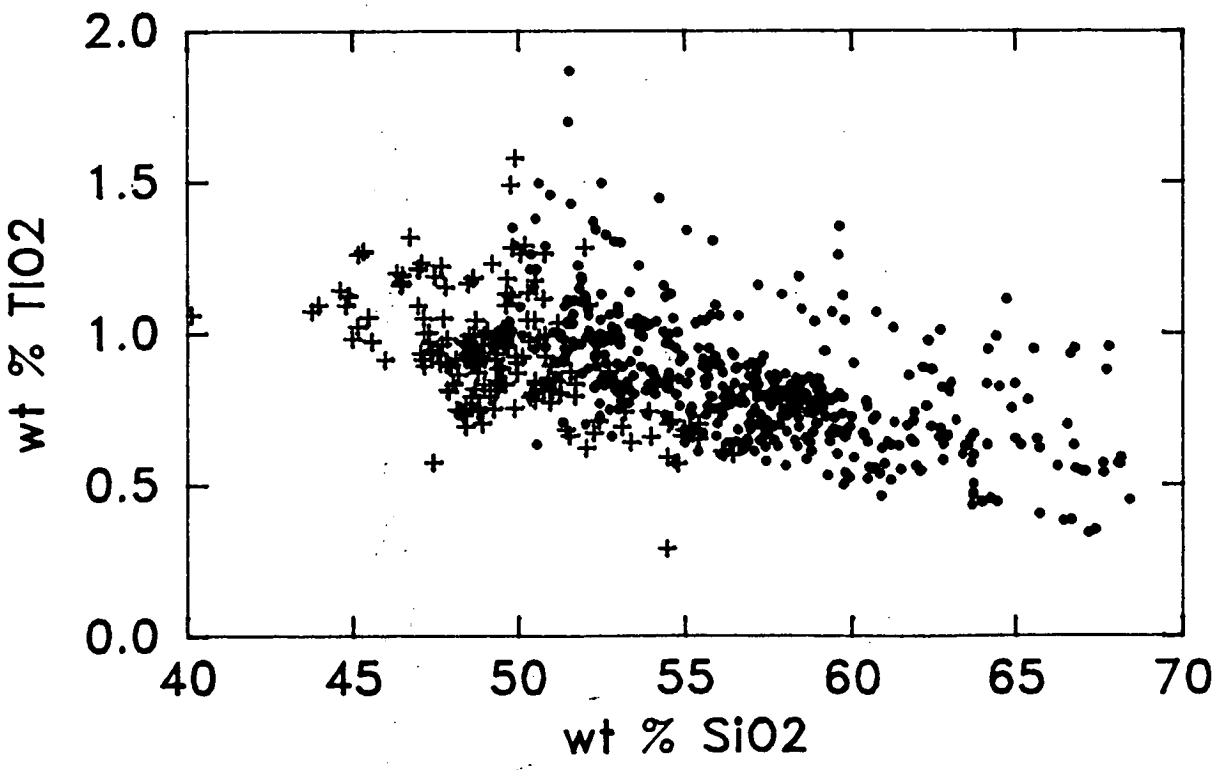

Figure 2.2b

continued over ..

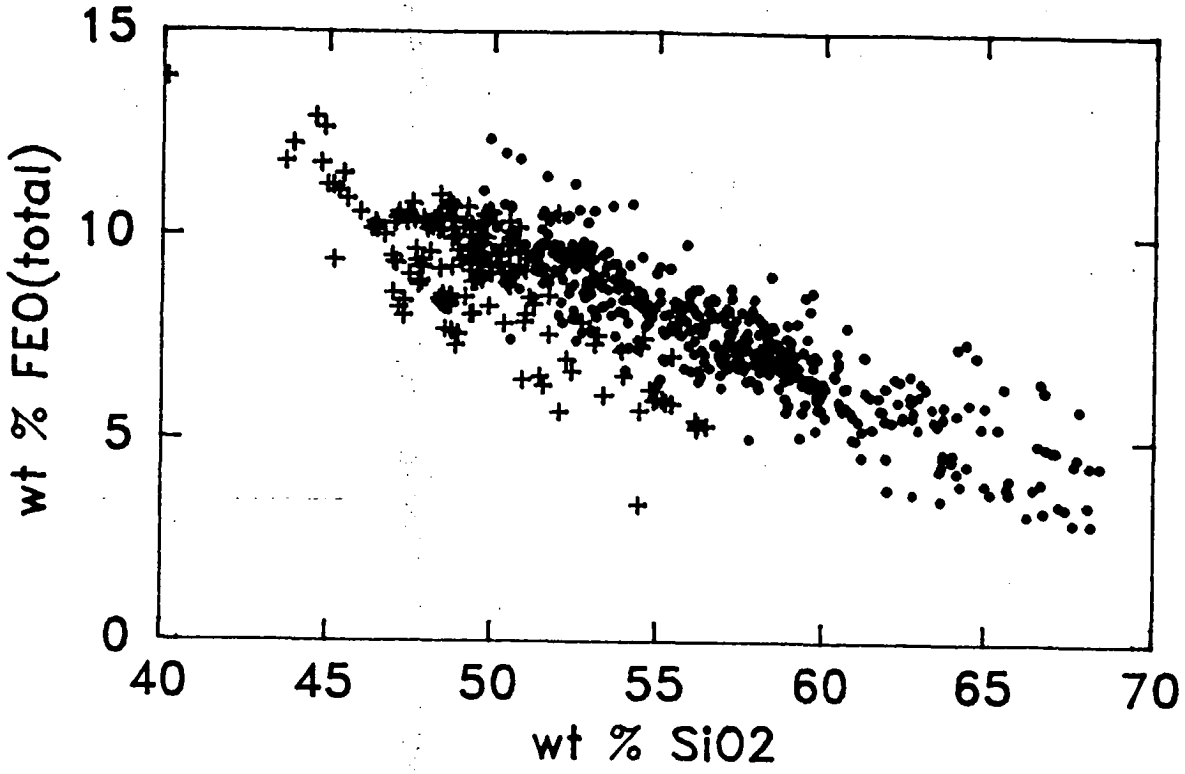

Figure 2.2c

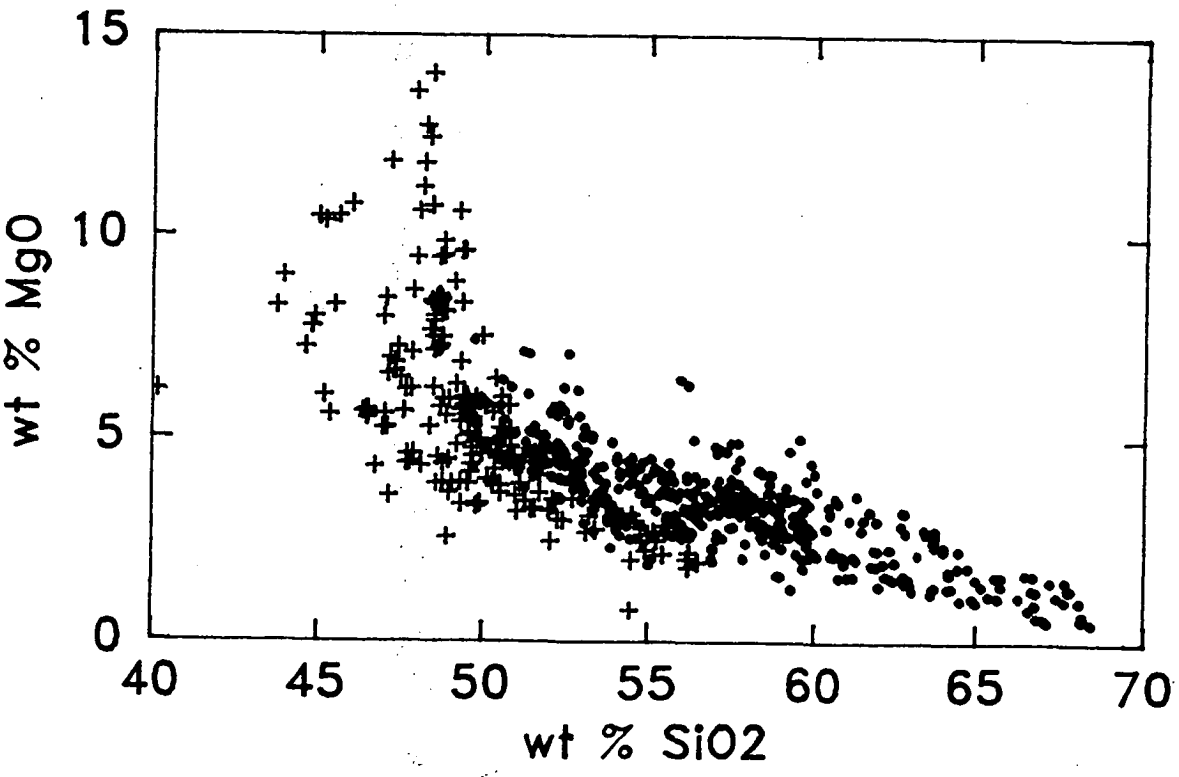

Figure 2.2d

continued over ..

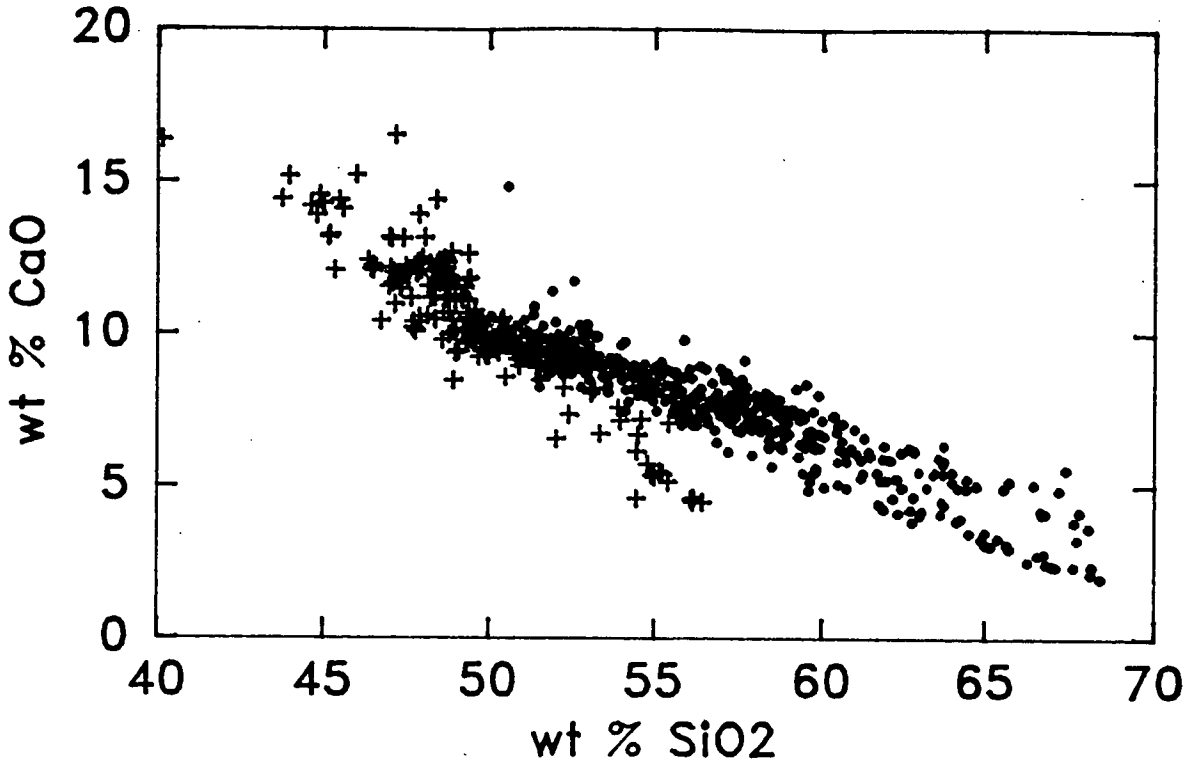

Figure 2.2e

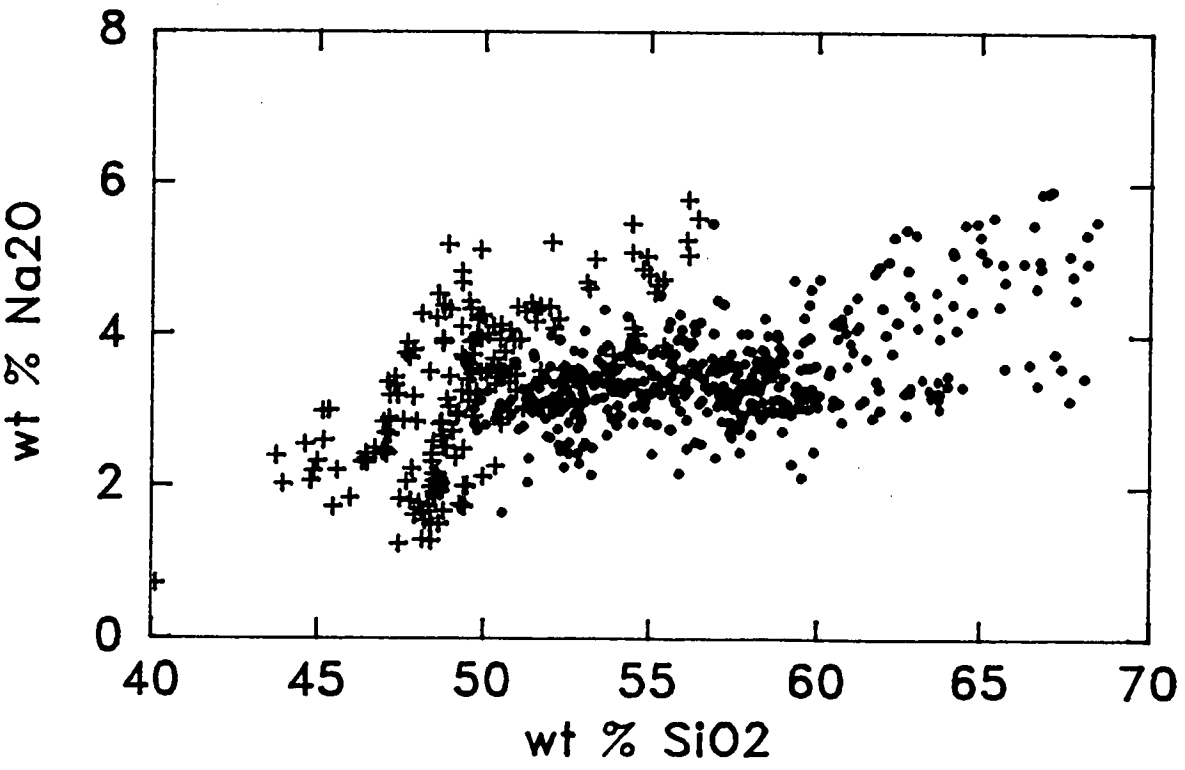

Figure 2.2f

continued over ..

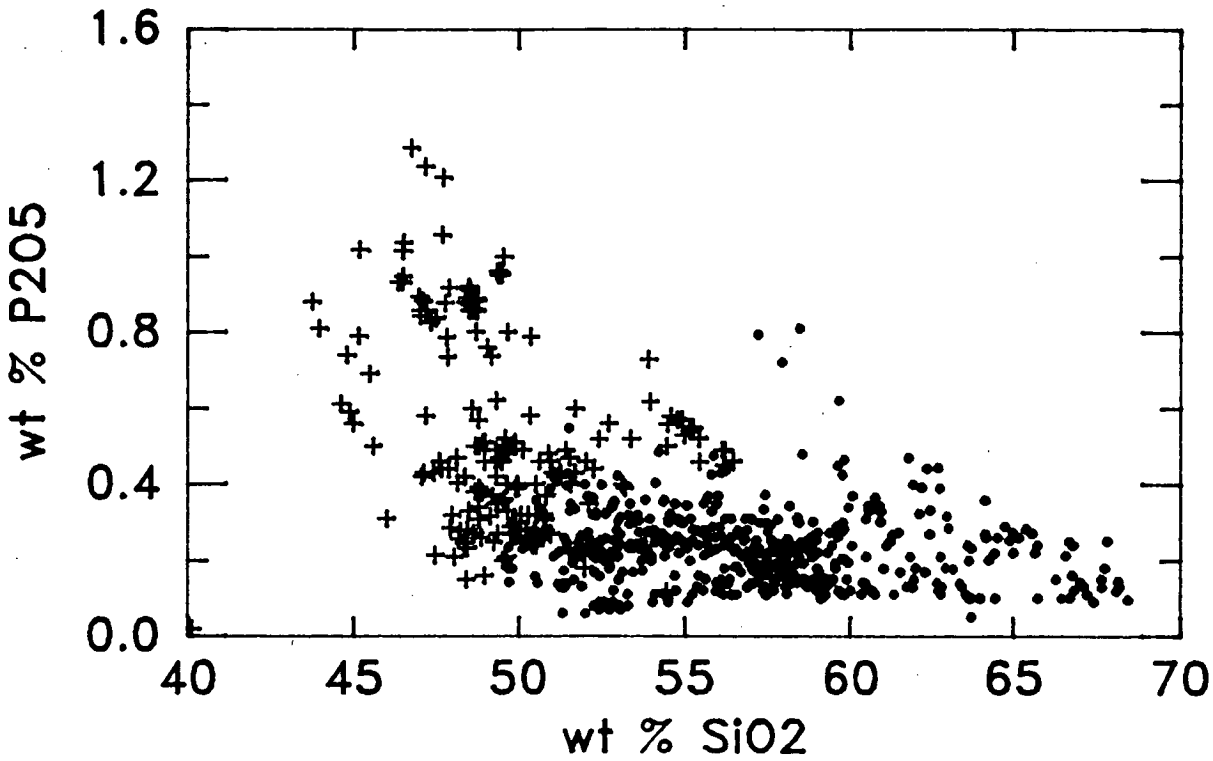

Figure 2.2g

Figure 2.2 Harker diagrams showing variation of major element abundances of 679 Quaternary-Recent volcanic rocks from the Sunda-Banda arc (dots = hy-normative; crosses = ne-normative). Data sources given in text.

Banda arc volcanic rocks are shown in Figure 2.3, together with the classification fields of Peccerillo and Taylor (1976). A new line which separates suites which contain phenocrystic leucite (leucititic series) from those which also contain phenocrystic sanidine and groundmass alkali feldspar (shoshonitic series) is also drawn.

This simple, chemical scheme is an adaption of those used by Whitford (1975a) and Hutchison (1982) to classify Indonesian volcanic rocks although use of the term 'shoshonite' was specifically avoided by Whitford (1975a) because of apparently confusing definitions. The high-K alkaline association of Whitford and Nicholls (1976) includes the leucititic and shoshonitic series of this scheme, which are also synonymous with the highly-undersaturated alkaline and ne-trachybasalt-trachyandesite suites respectively of Foden and Varne (1980).

The particularly wide range in K_2O contents in the Sunda-Banda mafic arc rocks is the widest known from any subduction-related tectonic setting. The full range of magma compositions may, in fact, be observed on just two neigbouring islands in the eastern Sunda arc, Sumbawa and Flores. The Aeolian volcanic island arc in the eastern Mediterranean Sea shows a similarly wide range of K_2O-SiO_2 contents but lacks low-K types (Keller 1982).

3.2.3 Trace Elements

The concentrations of many trace elements vary widely in volcanic rocks from the Sunda-Banda arc and therefore are more potentially useful than the major elements for identifying mantle geochemical processes (cf. Gast 1968). To minimize the effects usually attributed to intra-suite fractional crystallization the following discussion involves only mafic rocks.

Few rocks which could represent primary, mantle-derived magmas (having high MgO, Ni and Cr contents and high 100Mg/(Mg+Fe) values) are known from the Sunda-Banda arc. As a reasonable compromise which still provides a wide spread of data, mafic rocks are arbitrarily defined here as those which

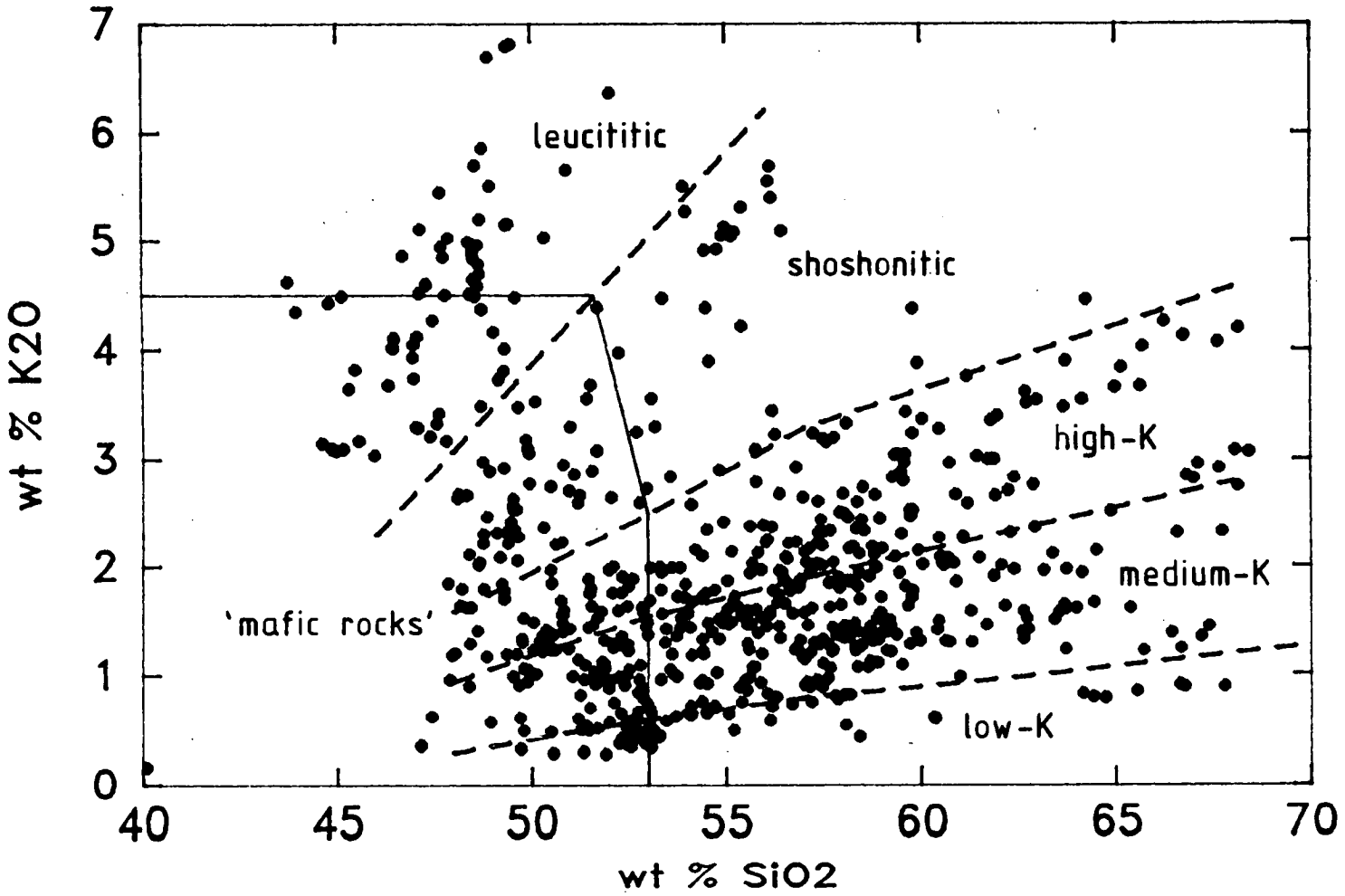

Figure 2.3 K_2O-SiO_2 diagram for 679 Quaternary volcanic rocks from the Sunda-Banda arc, showing K-series classification fields after Peccerillo and Taylor (1976). The equation of the line separating the leucititic and shoshonitic series is $K_2O = 0.4SiO_2 - 15.6$ for $46 < SiO_2 < 56$. The field at bottom left is explained in the text.

fall within a field at the low SiO_2 (< 53 %) and low K_2O (< 4.5 %) region of Figure 2.3. The abundances of these two oxides typically increase with fractional crystallization in arc volcanic rocks. In addition, rocks which fall within this field but which possess values of $100Mg/(Mg+Fe_t) < 40$ have also been excluded from the mafic rocks, leaving a total of 223 samples. No high-MgO andesites (or 'boninites') are known from the Sunda-Banda arc so the problem of incorporating high-SiO_2 mafic primary magmas in the discussion is not raised.

Unfortunately, few basalts have so far been sampled from the Banda arc volcanoes and few trace elements have been analysed from them. New data are being obtained at present from samples collected by the 1984/85 Indonesian-Dutch Snellius II expedition (van Bergen et al. 1985). In addition, the rocks have been analysed at different times and in different laboratories so there is wide variation in the availability and, possibly, comparability of trace element data.

The trace and minor elements are considered as groups according to similarites in their geochemical behaviour (Gill 1981).

(a) K-group elements (K,Ba,Rb,Sr)

These elements are characterized by their relatively large ionic radii and low charge and are generally excluded from most minerals that crystallize in basaltic magmas, although Sr and, to a lesser extent, Ba are camouflaged by Ca in plagioclase feldspars and pyroxenes. In the Sunda-Banda arc basaltic rocks they generally correlate positively with each other, progressively increasing in abundance from low-K to leucititic suites although relative abundances may change.

For example, in Figure 2.4, K and Rb concentrations increase regularly between low-K and leucititic suites, showing clear chemical continuity between K-rich and K-poor compositions. Note that there is little variation away from the general trend by individual suites, except for those from Flores which possess relatively high Rb contents. Rb and Sr show a similar pattern of covariation, although with more

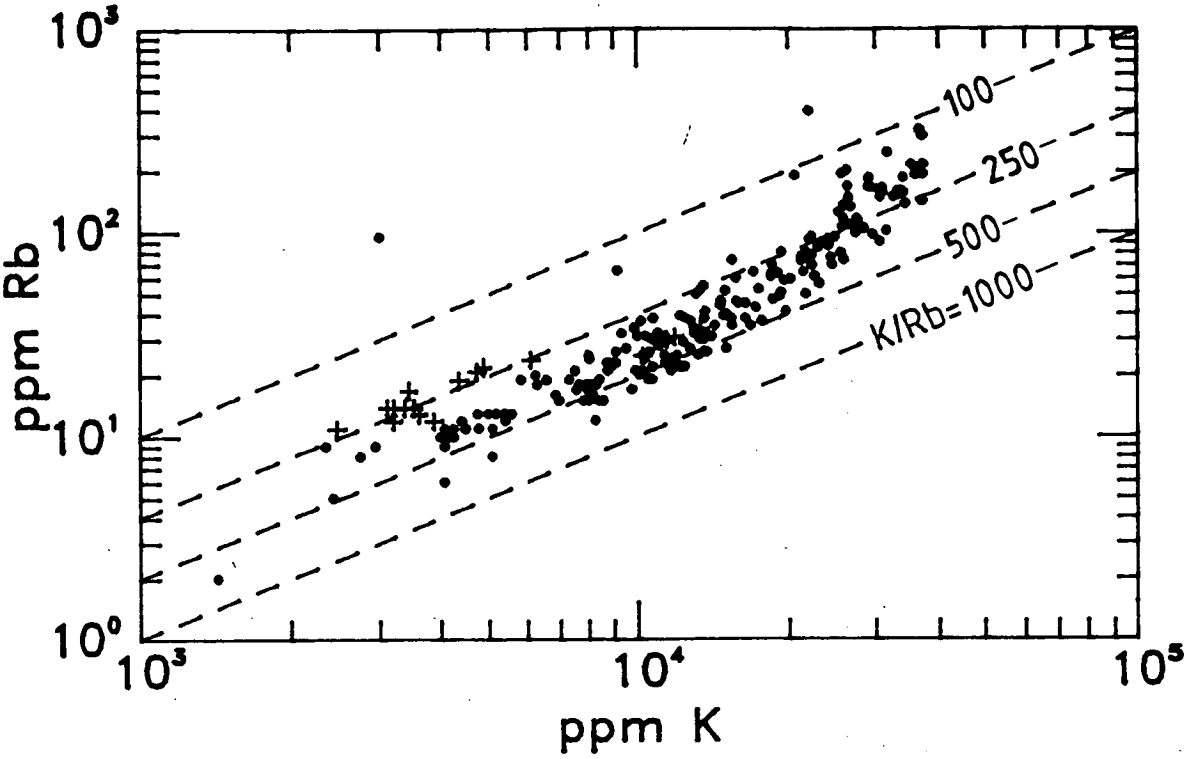

Figure 2.4 Rb against K in Sunda-Banda mafic volcanics (N = 223). Low- and medium-K rocks from Flores shown by crosses.

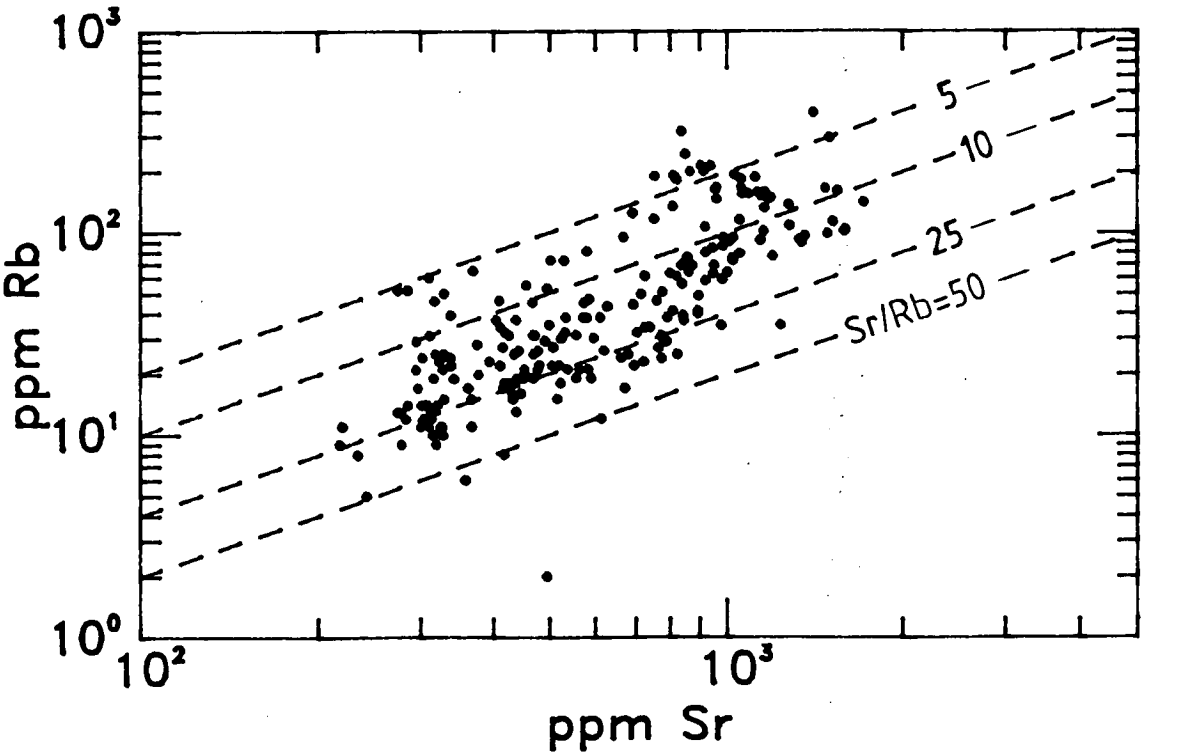

Figure 2.5 Rb against Sr in Sunda-Banda mafic volcanics (N = 223).

scatter (Fig. 2.5), possibly due to the presence of abundant plagioclase phenocrysts in most of these rocks.

In contrast to the generally continuous trends observed between K, Rb and Sr, and the slight regional variations they show, the variation of Ba with K shows an apparent displacement towards slightly higher Ba/K values in shoshonitic and leucititic suites compared to the low-, medium- and high-K suites (Fig. 2.6).

(b) Rare earth elements

Like K-group elements, the rare earth elements (REE) partition strongly into residual liquids during crystallization of basaltic magmas and also correlate positively with K concentrations (for example, Fig. 2.7).

Chondrite-normalized REE patterns in Sunda-Banda arc basaltic volcanic rocks, using data from Java (Whitford 1975a), Bali (Part 1; B.W. Chappell analyst), Lombok and Sumbawa (Varne & Foden, submitted for publication) and Flores and Batu Tara (Varne et al., unpublished data), show generally increasing LREE enrichment from low-K to leucititic suites (Fig. 2.8). REE patterns of leucititic rocks from Muriah volcano are distinctive compared to all others because they show depletion of heavy REE. They also show more marked LREE enrichment than other leucite-bearing rocks from the eastern Sunda arc. Ankaramitic pillow lavas from the Ulakan Formation on Bali show less LREE enrichment than other suites with similar K_2O contents.

The low-K basalts show slightly more LREE-enrichment than most rocks of similar composition from other island arcs. Whitford et al. (1979) found that low-K rocks from western Java contained slightly higher abundances of light REE and other incompatible elements than was proposed by Jakes and Gill (1970) for members of the island arc tholeiitic series, although the rocks show phenocryst characteristics, such as a reaction relationship between olivine phenocrysts and host liquid, and the presence of orthopyroxene, that are typical of tholeiitic mafic volcanic rocks. The low-K lavas from Ija and

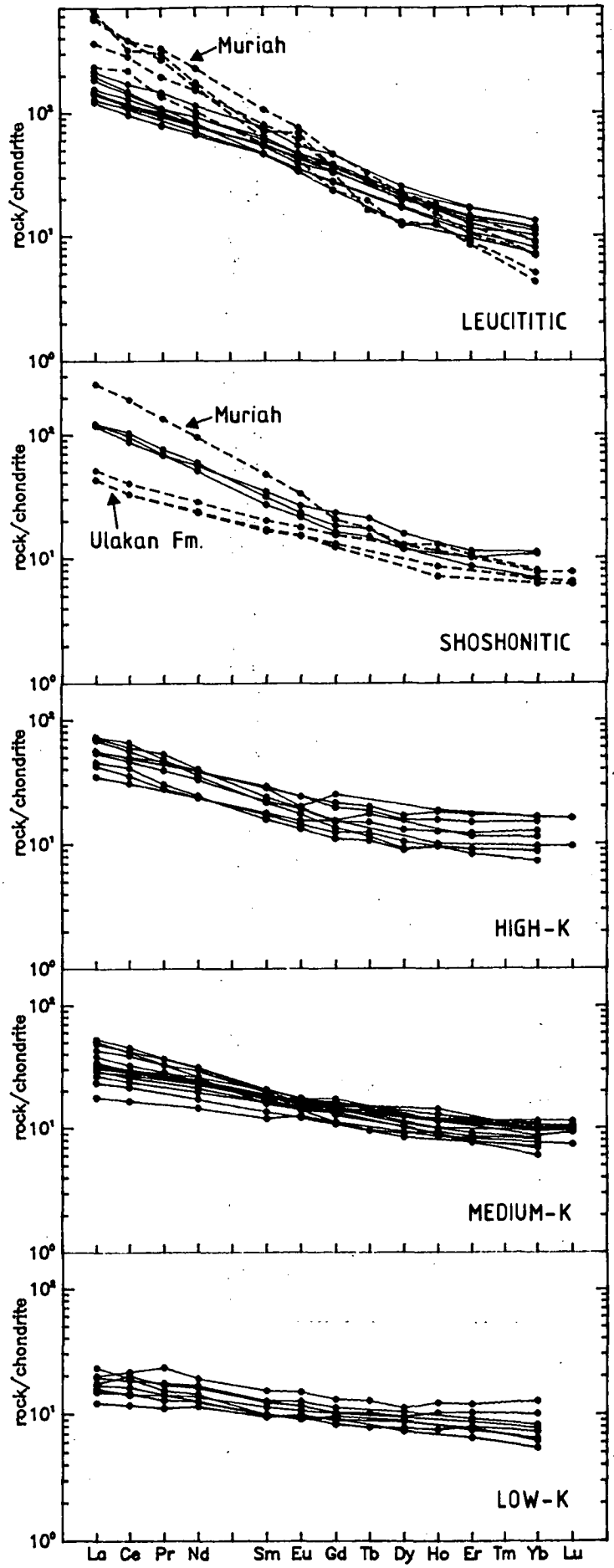

Figure 2.8 Chondrite-normalized rare earth element plots of Sunda-Banda mafic volcanics. Data sources given in text. Chondrite values from Masuda et al. (1973).

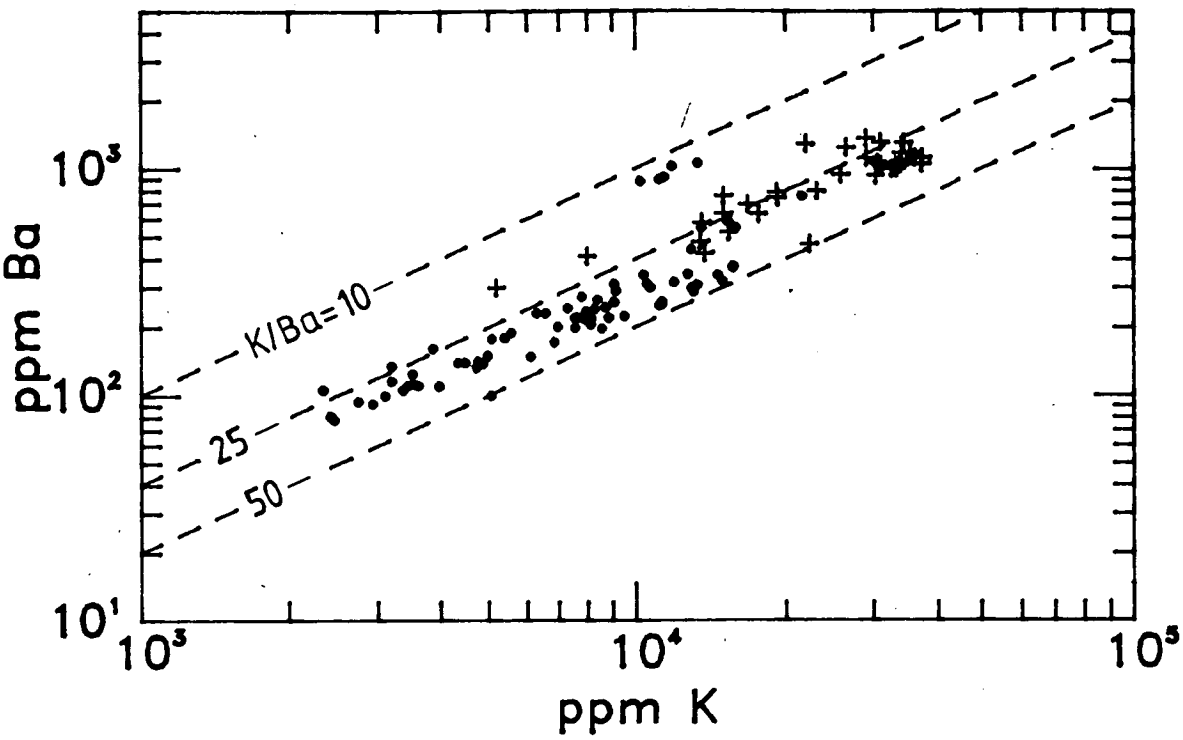

Figure 2.6 Ba against K in Sunda-Banda mafic volcanics (N = 108). Shoshonitic and leucititic volcanoes (Batu Tara and Javanese vocanoes) shown by crosses.

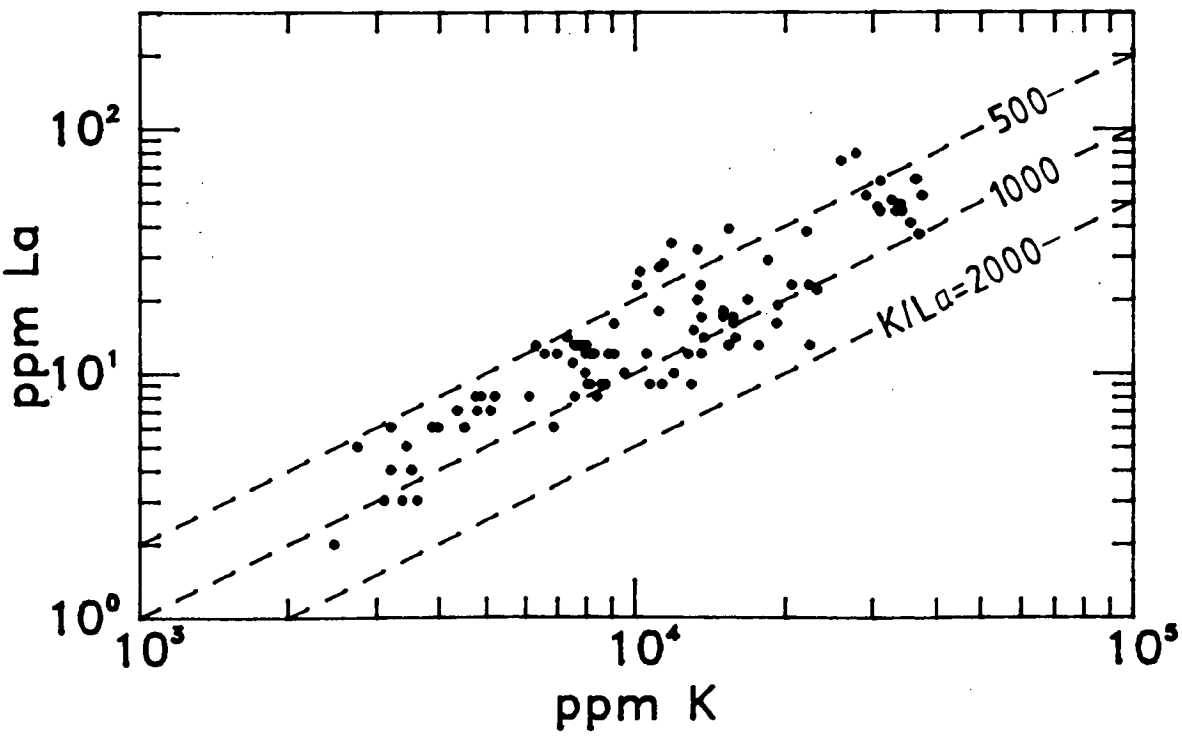

Figure 2.7 La against K in Sunda-Banda mafic volcanics (N = 95).

Inerie volcanoes in southern Flores show similar REE and petrographic characteristics to those from western Java. It is notable that these two groups of low-K volcanoes each form distinct, forward volcanic rows (Fig. 1).

In contrast to basalts from other tectonic settings, few, if any, of the Sunda-Banda arc basalts show Eu anomalies, indicating either that plagioclase was not an important fractionating phase during production of the basaltic rocks or that Eu was present in the magmas as Eu^{3+} rather than as Eu^{2+}.

Also, as pointed out by White and Patchett (1984), none of the Sunda-Banda rocks show negative Ce anomalies. These anomalies, in volcanic rocks from some other arcs, have been interpreted as indicating the involvement of the subducted slab in magmagenesis, either by providing Ce-depleted oceanic sediments or altered basaltic crust, or by producing Ce^{4+} during dehydration (Dixon & Batiza 1979; Hole et al. 1984; White & Patchett 1984; Thirlwell & Graham 1984).

(c) Ti-group elements (Ti,Zr,Nb,P,Y)

The Ti-group elements are characterized by their small ionic radii and high charge, and contrast sharply in their geochemical behaviour with the K-group elements. Island arc mafic volcanics are generally thought to be characterized by low abundances of these elements compared to volcanic rocks from other tectonic settings (Pearce & Cann 1973; Pearce & Norry 1979; Wood et al. 1979).

However, in Sunda-Banda arc basalts, these elements show varying patterns of correlation with K. For example, P and K show the most regular, positive correlations (Fig. 2.9), with K/P values generally increasing from low-K to leucititic suites, although low- and medium-K suites from Flores show relatively high K/P values. K and Nb also correlate positively and K/Nb values generally increase slightly from low-K to leucititic suites (Fig. 2.10). Ankaramitic pillow lavas from the Pliocene Ulakan Formation in southeastern Bali show low Nb contents which approach XRF detection limits. Nb and Zr

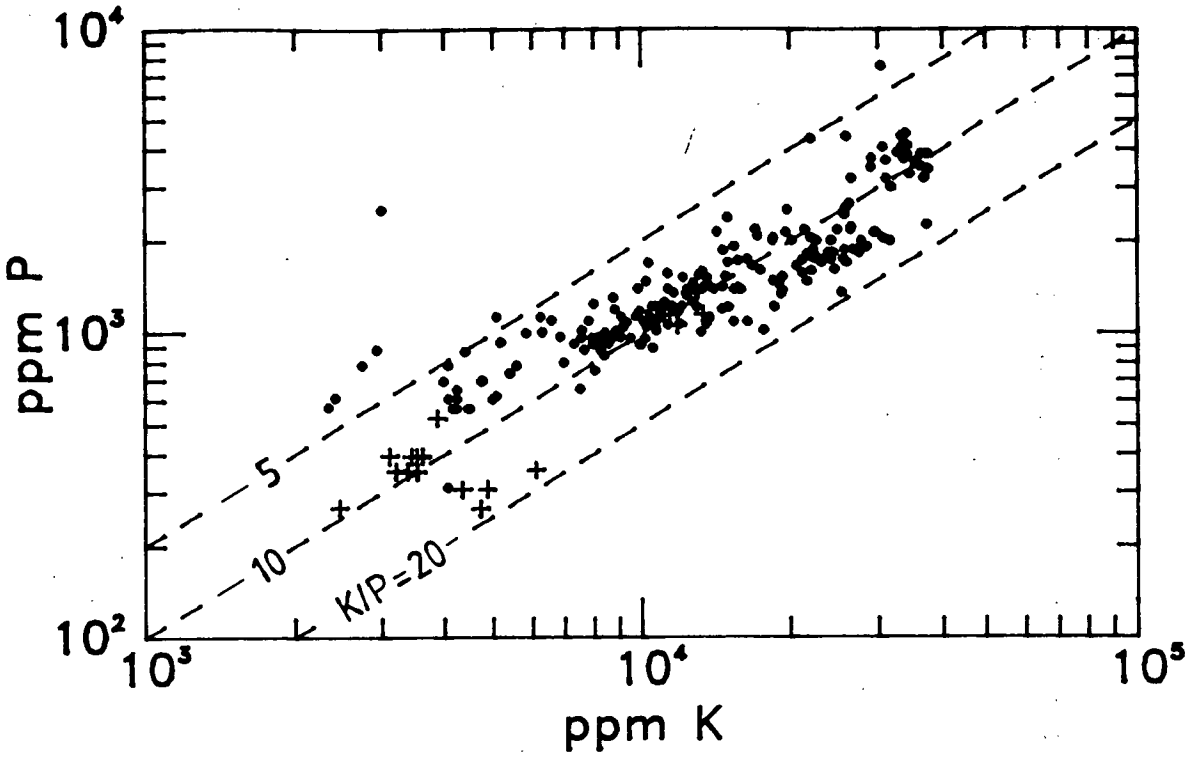

Figure 2.9 P against K in Sunda-Banda mafic volcanics (N = 223). Low- and medium-K rocks from Flores given by crosses.

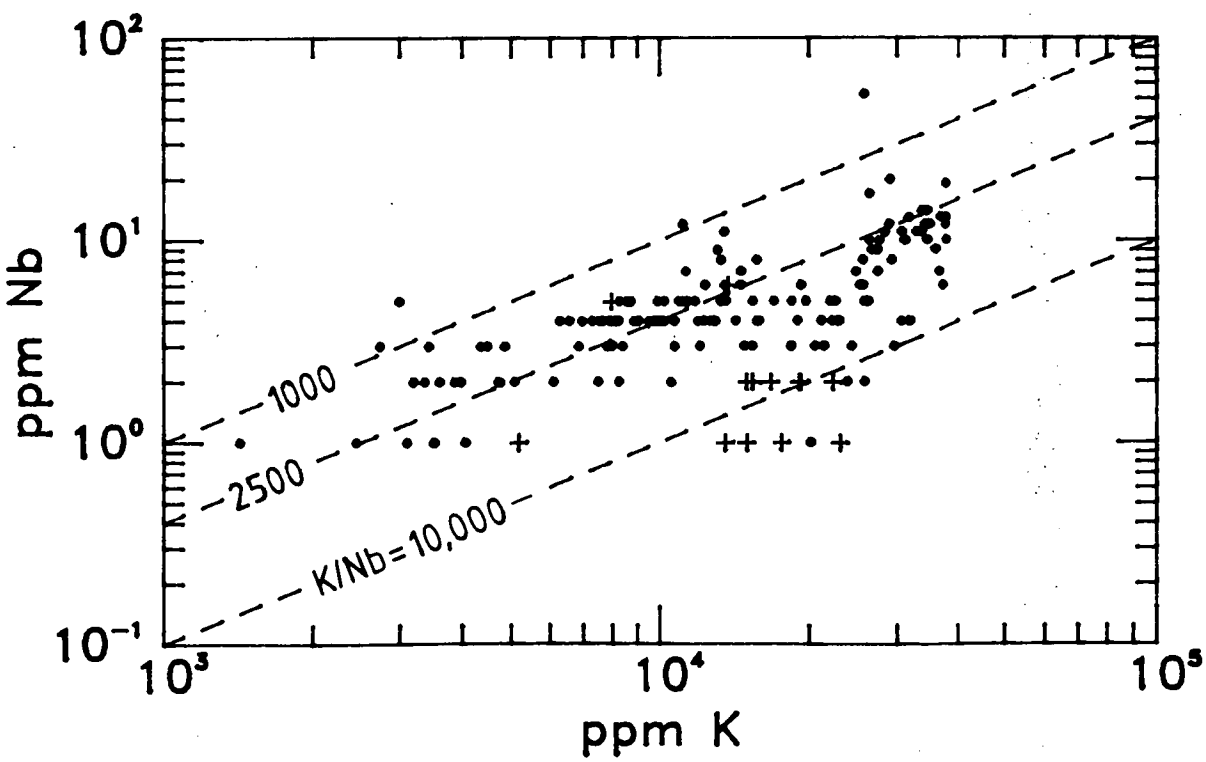

Figure 2.10 Nb against K in Sunda-Banda mafic volcanics (N = 160). Ulakan Formation rocks (Bali) shown by crosses.

concentrations also correlate positively (Fig. 2.11). Although they also generally correlate positively, Rb and Zr show substantial scatter among suites (Fig. 2.12) and Rb/Zr values increase markedly with increasing abundances of both elements.

However, in marked contrast to P, Nb and Zr, the abundances of Ti (Fig. 2.13) and Y (Fig. 2.14) increase only very slightly from low-K to leucititic lavas. Sc, a transition element, shows similar behaviour (Fig. 2.15).

3.3 Isotopes

3.3.1 Strontium and Neodymium

Samples of mafic rocks from most parts of the Sunda-Banda arc have been analysed for $^{87}Sr/^{86}Sr$ and values range generally from 0.704 to 0.710 (Whitford 1975a,b; Whitford et al. 1978; Whitford & Jezek 1979; Jenner et al. unpublished data; Foden et al. unpublished data). Nd isotope data are at present less abundant; ε_{Nd} values show a wide range from +5.2 to -4.2 (Whitford et al. 1981; Jenner et al. unpublished data).

Whitford (1975b) observed an eastwards decrease of $^{87}Sr/^{86}Sr$ values in the arc volcanics along the arc between Krakatau volcano, located between Sumatra and Java, and Bali which he attributed to varying combinations of disequilibrium melting, involvement of subducted, altered oceanic crust in the magma sources and crustal contamination.

Farther east, on Lombok and Sumbawa, Sr isotope values of lavas show substantial variation between and within volcanoes (Whitford et al. 1978). They also show a general, positive correlation with Rb/Sr from which an 'age' of approximately 100 Ma may be calculated. Whitford et al. (1978) suggested this pseudoisochron may reflect enrichment of the subarc mantle in that sector during an older subduction event. In the Banda arc, high $^{87}Sr/^{86}Sr$ and low ε_{Nd} values in mafic lavas are thought to have resulted from subduction of sialic detritus derived possibly from the Australian continent to the south (Magaritz et al. 1978; Whitford & Jezek 1979; Whitford et al. 1981).

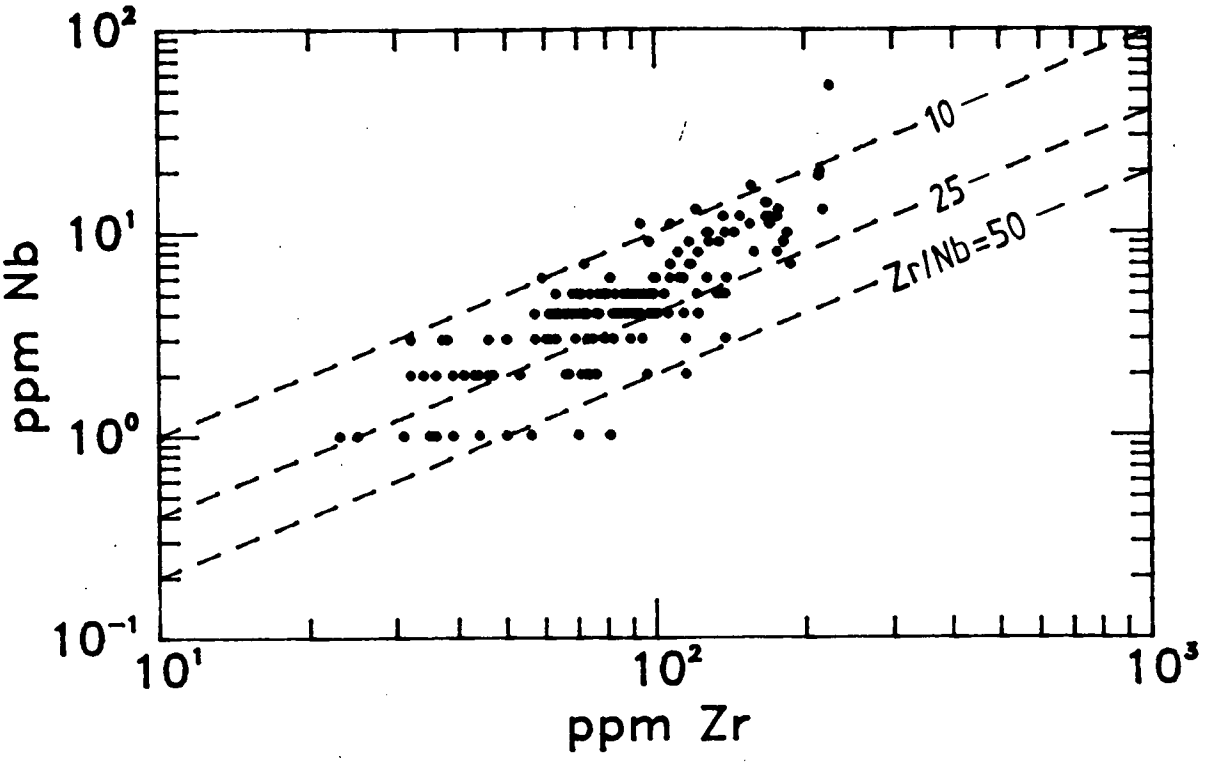

Figure 2.11 Nb against Zr in Sunda-Banda mafic volcanics (N = 160).

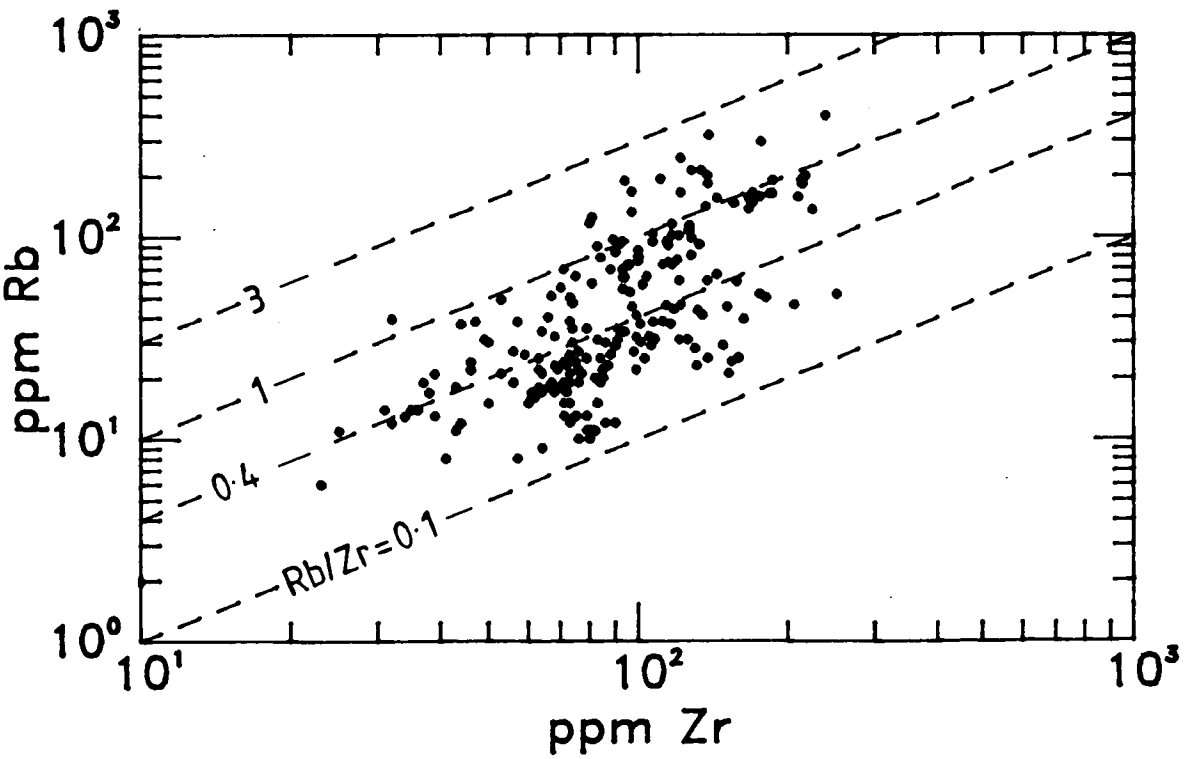

Figure 2.12 Rb against Zr in Sunda-Banda mafic volcanics (N = 220).

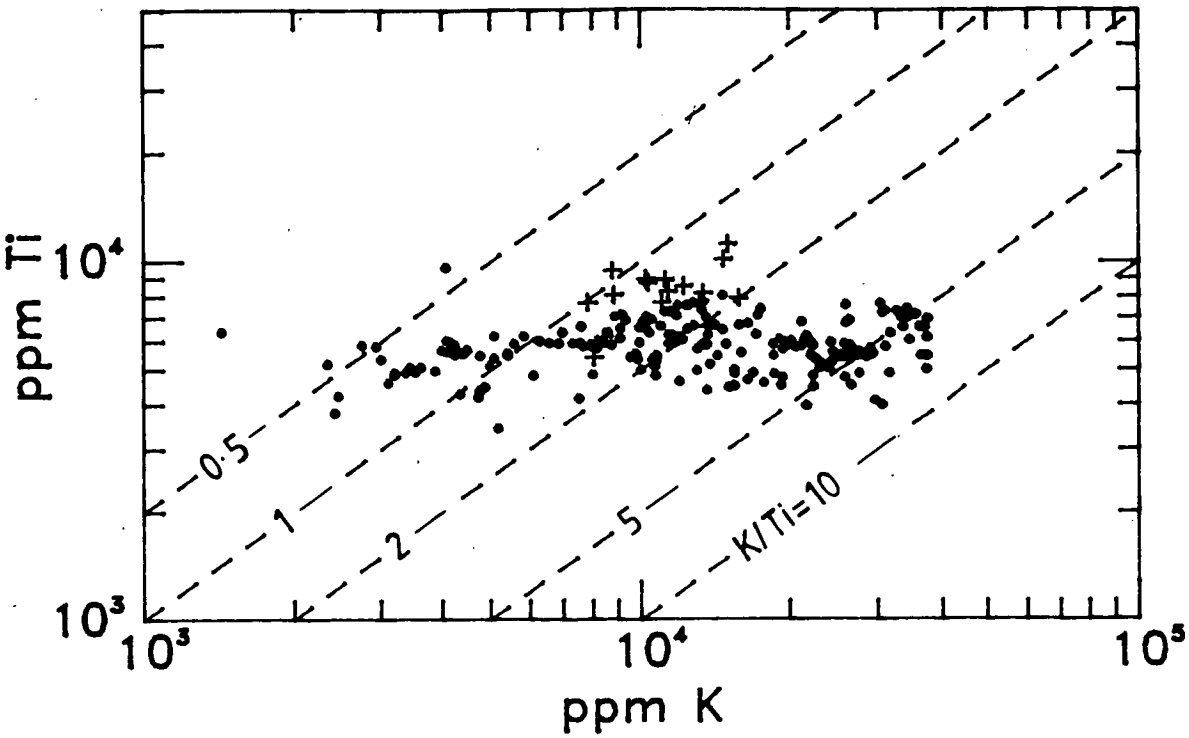

Figure 2.13 Ti against K in Sunda-Banda mafic volcanics (N = 223). Slamet (Java) and Bratan (Bali) volcanoes shown by crosses.

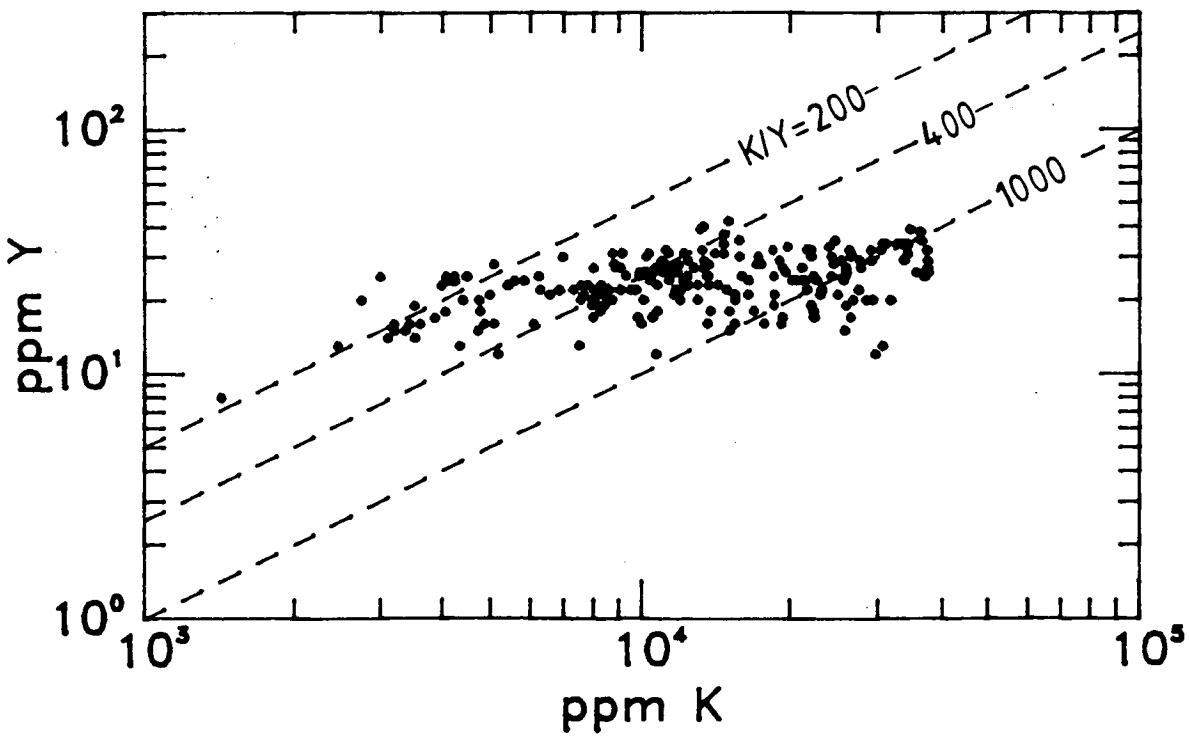

Figure 2.14 Y against K in Sunda-Banda mafic volcanics (N = 219).

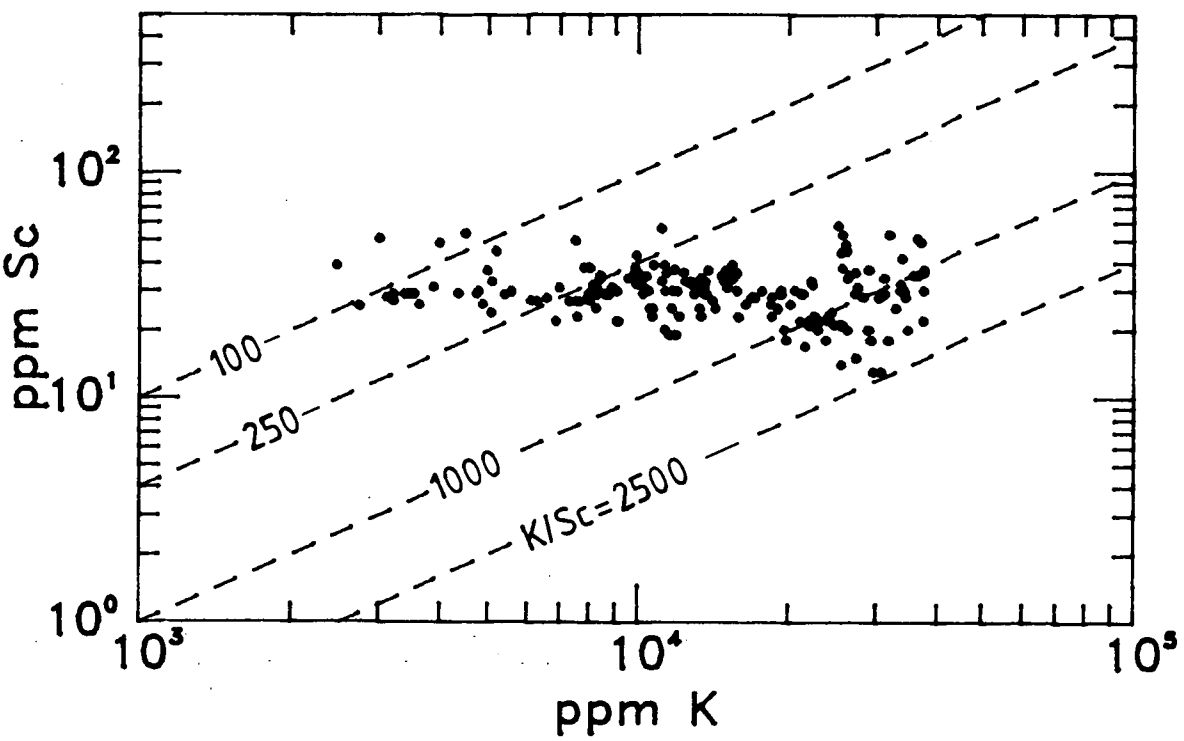

Figure 2.15 Sc against K in Sunda-Banda mafic volcanics (N = 188).

In an ε_{Nd}-$^{87}Sr/^{86}Sr$ plot (Fig. 2.16a), except for the sample from Merapi volcano, rocks from Java, Bali, Lombok and Sumbawa form a wide field within the 'mantle array' defined by MORB and OIB (De Paolo & Wasserburg 1976; O'Nions et al. 1977; Allegre et al. 1979; Zindler et al. 1982). Samples from Ija and Batu Tara volcanoes are displaced to slightly higher $^{87}Sr/^{86}Sr$ values and the mainly andesitic rocks from the Banda arc form a separate trend at markedly higher $^{87}Sr/^{86}Sr$ and lower ε_{Nd} values.

The combination of high, positive ε_{Nd} values and LREE enrichment of Javanese rocks was interpreted by Whitford et al. (1981) as indicating that enrichment of the mantle wedge by material derived from the subducted slab must have occurred relatively recently and that the unmodified, Sunda subarc mantle showed lower $^{143}Nd/^{144}Nd$ values than those of MORB sources.

Compared to some intra-oceanic volcanic island arcs (Fig. 16a), in which the possibility of crustal contamination is minmized, there is a wide spread of Nd and Sr isotope values in the Sunda-Banda arc rocks. However, they have higher ε_{Nd} values than rocks from the Andean continental volcanic arc that are thought to be substantially contaminated by continental crust material (Hawkesworth et al. 1979; James 1982). Their Sr and Nd isotopic compositions are most similar, and display a comparable range of values, to Indian Ocean MORB, ocean island basaltic rocks from the Kerguelen Islands in the southern Indian Ocean, and Tertiary continental intraplate basalts, including leucitites, from southeast Australia (Fig. 2.16b).

3.3.2 Uranium-Decay Series Radioisotopes

Studies of the shortlived nuclides in the U-Th-Pb decay series from island arc volcanic rocks are still uncommon. Young basaltic lavas from Batur and Sangeang Api (Tanzer 1985) and Galunggung (Williams et al. 1983) volcanoes in the Sunda arc show secular isotopic equilibrium between ^{230}Th and parental ^{238}U that indicates that no fractionation between Th and U has occurred within the last 300,000 years (approximately four halflives of ^{230}Th) (Fig. 17). Mafic lavas from the Aleutian

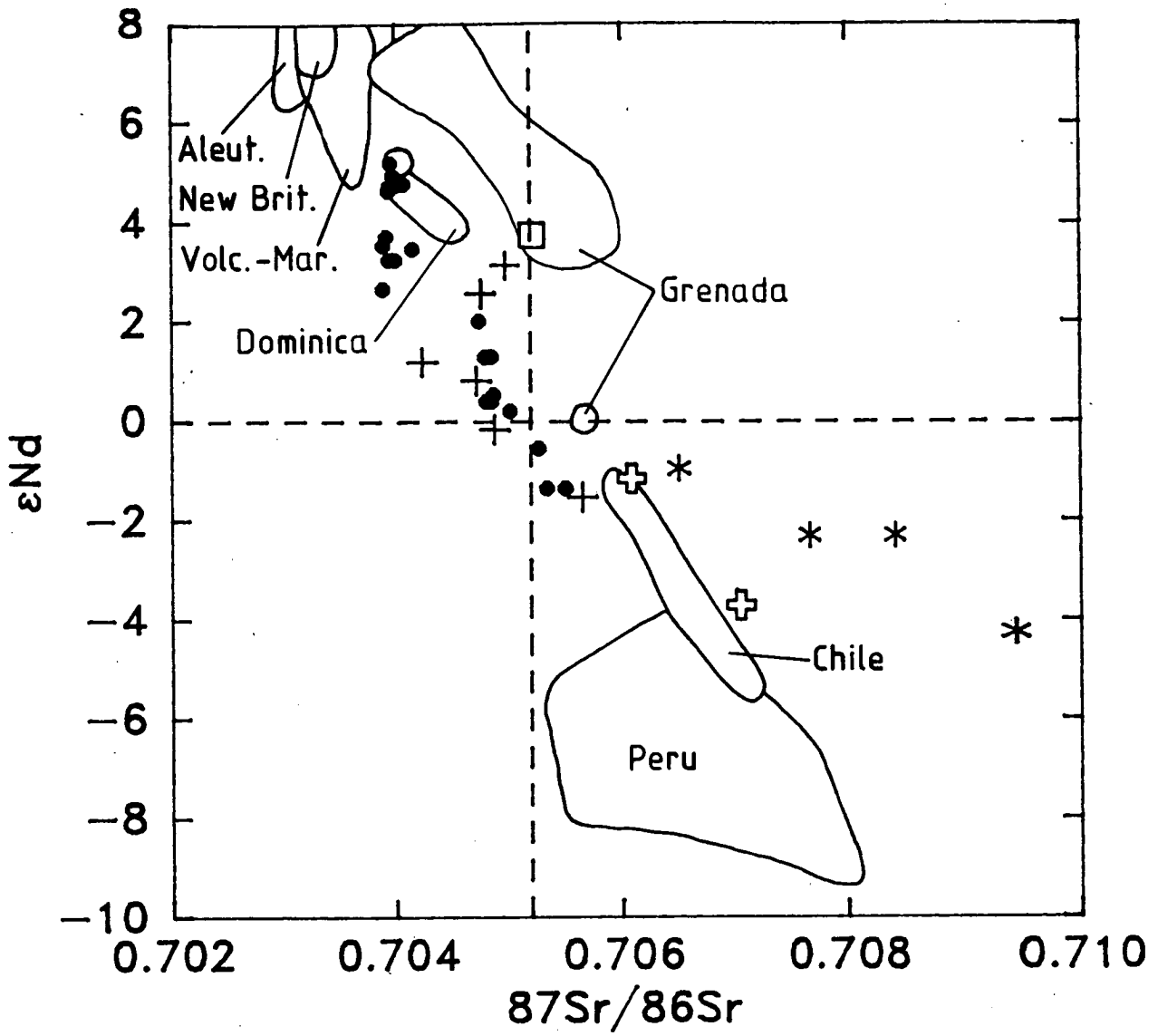

Figure 2.16a ε_{Nd} against $^{87}Sr/^{86}Sr$ in Sunda-Banda volcanics compared to those from other orogenic regions (crosses = Java volcanoes; dots = Lombok and Sumbawa volcanoes; open circle = Batur volcano (Bali); open square = Ija volcano (Flores); Swiss crosses = Batu Tara volcano; asterisks = Banda arc volcanics). Sources of these data given in text. Other data from White & Patchett (1984), DePaolo & Wasserburg (1977), Stern & Bibee (1980), Stern (1981) [MARIANA-VOLCANO], DePaolo & Wasserburg (1977), DePaolo & Johnson (1979) [NEW BRITAIN], White & Patchett (1984), McCulloch & Perfit (1981), Morris & Hart (1983) [ALEUTIANS], Hawkesworth et al. (1979), Hawkesworth & Powell (1980) [ANTILLES], Hawkesworth et al. (1979), Francis et al. (1977) [CHILE] and James (1982) [PERU]. 'Bulk Earth' value from Zindler et al. (1982).

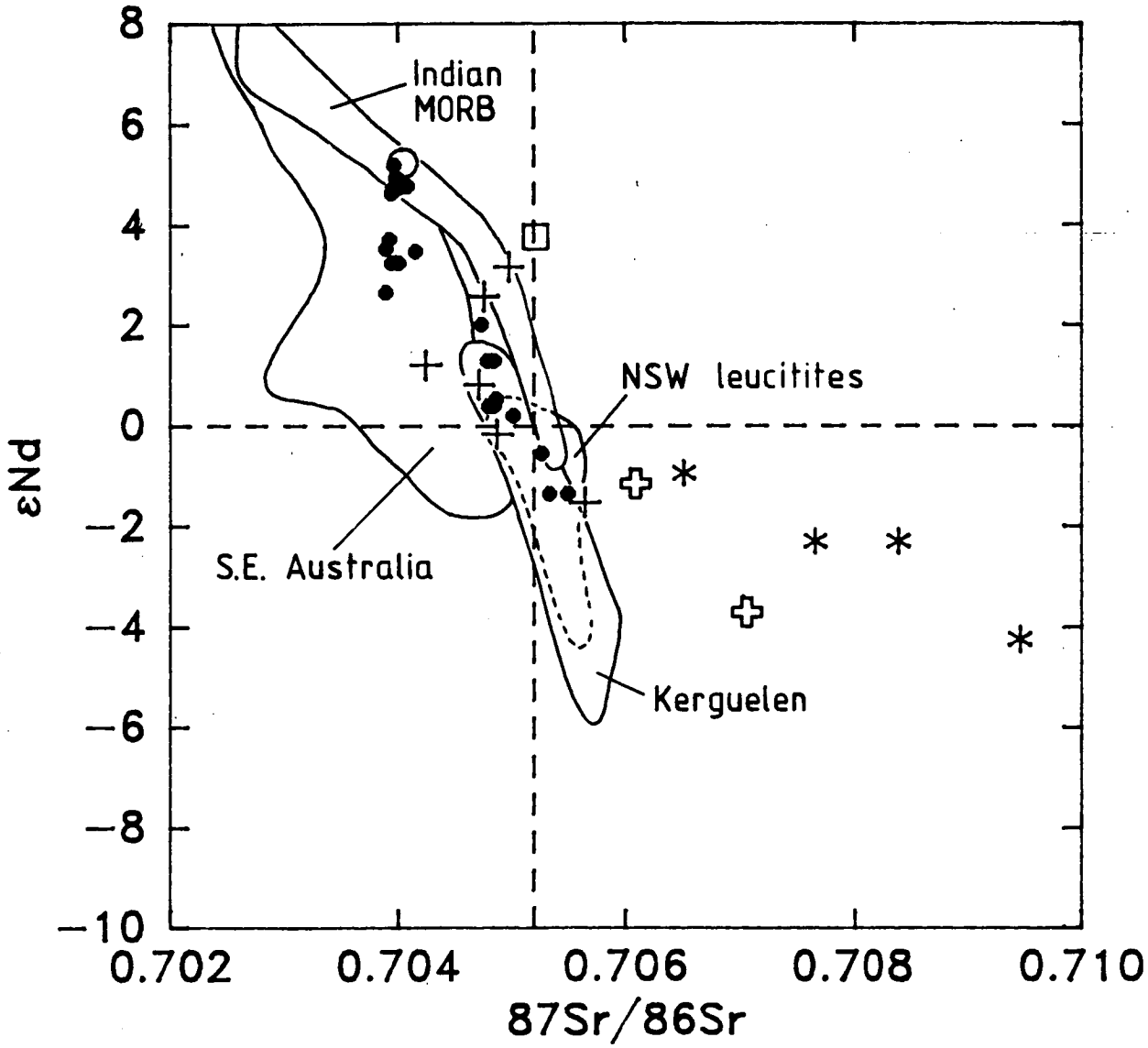

Figure 2.16b ε_{Nd} against $^{87}Sr/^{86}Sr$ in Sunda-Banda volcanics compared to Indian MORB (Hamelin & Allegre 1985; Hamelin et al. 1986) and intra-plate basaltic volcanics from the Kerguelen Islands (Dosso et al. 1979; Dosso & Murthy 1980) southeast Australia (Menzies & Wass 1983; McDonough et al. 1985) and olivine leucitites from New South Wales, southeast Australia (Nelson et al. 1986) (symbols as for Fig. 2.16a).

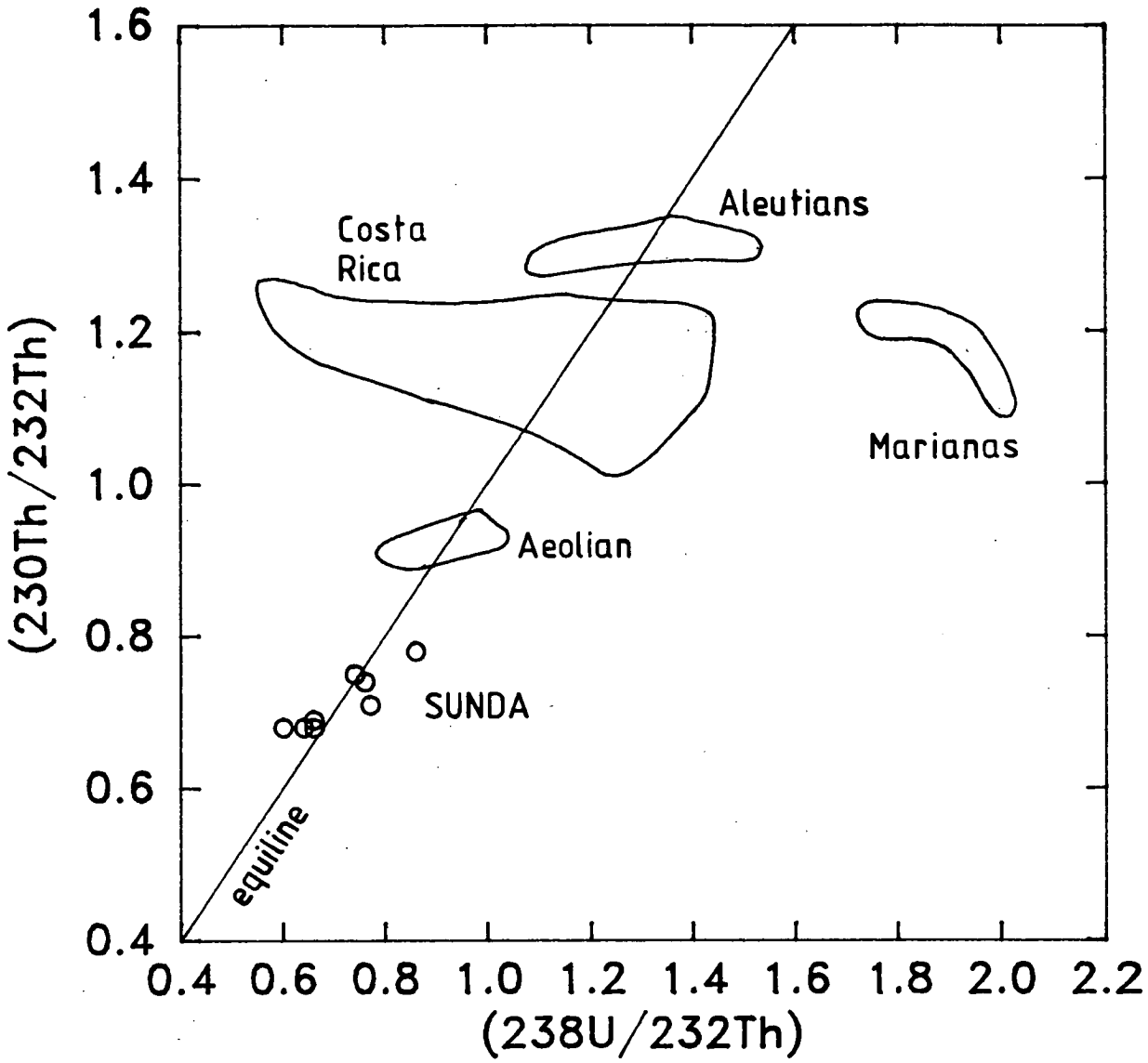

Figure 2.17 $^{230}Th/^{232}Th$ against $^{238}U/^{232}Th$ in young volcanics from the Sunda arc and other orogenic regions. Data from Tanzer (1985) [SUNDA], Newman et al. (1984) [MARIANAS & ALEUTIANS], Allegre & Condomines (1976) [COSTA RICA] and Capaldi et al. (1983) [AEOLIAN].

and Aeolian arcs also show secular equilibrium between ^{230}Th and ^{238}U.

These results contrast with those from orogenic basaltic lavas from Costa Rica and the Marianas arc in which substantial disequilibrium between ^{230}Th and ^{238}U has been observed (Fig. 2.17). In contrast to disequilibrium patterns observed in basalts from ocean ridge and intra-plate tectonic settings (Allegre & Condomines 1982), the Mariana arc basalts show ($^{230}Th/^{238}U$) (activity ratio) < 1, indicating enrichment of U relative to Th in these rocks or in their sources within the last 300,000 years.

Interestingly, although the rock samples from the Aeolian and Sunda arcs range widely in chemical composition from K-poor to K-rich, each arc is clearly characterized by distinct ($^{230}Th/^{232}Th$) values. This observation shows that the sources of basaltic magmas within each arc, even if separated laterally by several hundred kilometres and possessing substantially different chemical compositions, are chemically and isotopically related and that subarc mantle source compositions are distinctive for each arc.

This compositional variation among arcs also occurs over a range of Th/U values that exceeds that found in other oceanic basaltic volcanic rocks (Allegre & Condomines 1982). The Sunda arc lavas, and by inference their mantle source regions, show the highest Th/U values (approximately 4.3) so far obtained from basaltic samples in any tectonic setting. Only basaltic lavas from the oceanic islands of Samoa (Newman et al. 1984) and Tristan da Cunha (Oversby & Gast 1968) show high Th/U values inferred from U-Th isotopic data that approach those of the Sunda arc samples. It is notable that high $^{208}Pb/^{204}Pb$ values of many intraplate basalts which Hart (1984) used to characterize a globe-encircling ('DUPAL') isotopic anomaly imply long-term, high source Th/U values.

The production of ^{210}Pb from decay of its immediate parent ^{222}Rn, and ultimately via ^{226}Ra and ^{230}Th from ^{238}U, allows fractionations less than 100 years old (approximately 4.5 half-lives of ^{210}Pb) to be detected. In the historical

lavas from Batur volcano, including those erupted in 1849 and 1888, and in a single historical lava from Sangeang Api volcano, $(^{210}Pb/^{230}Th) > 1$, indicating that both Ra and Pb were recently enriched relative to U and Th in the erupted rocks (Part 1).

3.3.3 Lead

On plots of $^{208}Pb/^{204}Pb$ and $^{207}Pb/^{204}Pb$ versus $^{206}Pb/^{204}Pb$ volcanic rocks from Java (Whitford 1975a) and Lombok, Sumbawa, and Ija volcano on Flores (Jenner et al. unpublished data) all plot close to several Indian oceanic island volcanics, particularly those from the central and northern parts of the Indian Ocean, and Victorian basanites and New South Wales leucitites (Fig. 2.18a,b). The average $^{208}Pb/^{204}Pb$ value of the Tertiary oceanic alkaline basalts of Christmas Island (Hart 1984), which lies only 400 km southwest of western Java, is also very close to the Lombok-Flores field.

However, the Java and Lombok-Flores rocks show contrasting trends. In Figure 2.18a, rocks from Java form a trend that is subparallel to that formed by the Lombok-Sumbawa-Flores samples but which lies at higher $^{208}Pb/^{204}Pb$ values. The distinction between the Javanese volcanoes and those from farther east in the Sunda arc is even more pronounced in Figure 2.18b. In this plot, the slope of the Javanese trend is much higher (0.61) than that of the trend produced by the Lombok and Sumbawa data (0.09). Data from the Banda arc appear to form a trend similar to that of the Lombok-Sumbawa rocks (Morris et al. 1980) but at higher $^{207}Pb/^{206}Pb$ values. Sun (1980) found that most oceanic islands are characterized by slopes of about 0.1 and that higher values appear to indicate involvement of upper crustal material.

3.3.4 Oxygen

Preliminary analyses of $^{18}O/^{16}O$ values in selected samples encompassing the range of K_2O compositions in eastern Sunda lavas have been obtained. Oxygen was extracted from 15-20 mg of sample powder by overnight reaction with BrF_5 at approximately 650 ^{o}C (Clayton & Mayeda 1963). The O_2 produced was reacted

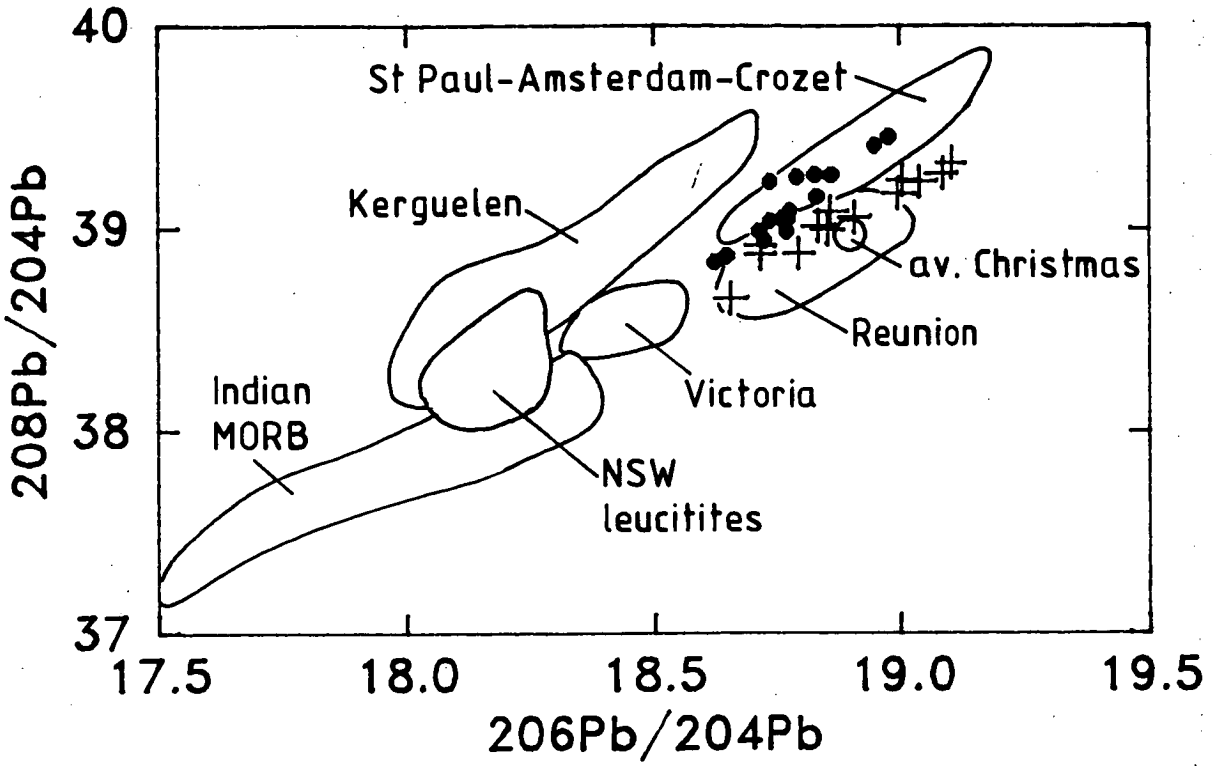

Figure 2.18a $^{208}Pb/^{204}Pb$ against $^{206}Pb/^{204}Pb$ in Sunda-Banda volcanics (crosses = Lombok and Sumbawa; dots = west Java). Sources of these data given in text. Comparative data from Cooper and Green (1969), Oversby (1972), Dosso et al. (1979), Sun (1980), Dupre and Allegre (1983), Hart (1984), Hamelin and Allegre (1985), Hamelin et al. (1986) and Nelson et al. (1986),

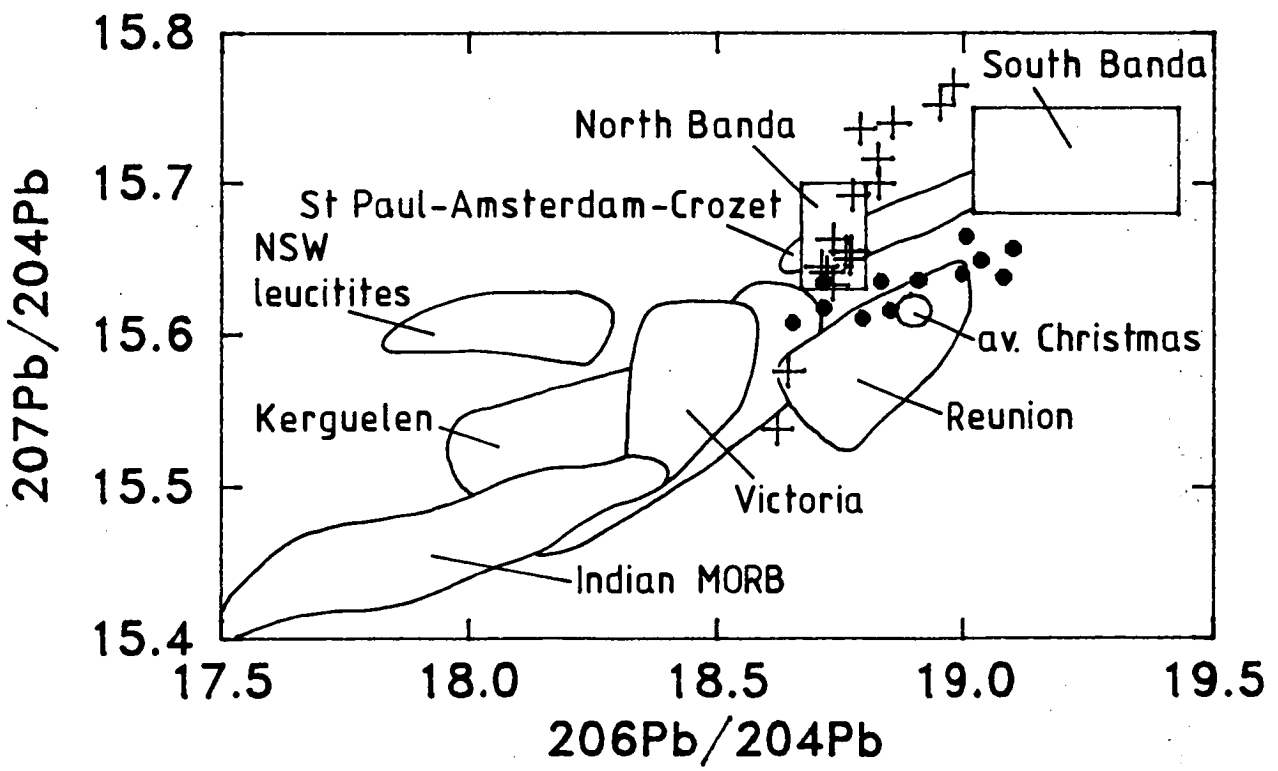

Figure 2.18b $^{207}Pb/^{204}Pb$ against $^{208}Pb/^{204}Pb$ in Sunda-Banda volcanic rocks. Symbols and data sources as for Fig 2.18a.

with resistance-heated graphite to form CO_2, the $^{18}O/^{16}O$ value of which was measured using a VG Micromass 602D mass spectrometer. Results were calibrated with the quartz-standard NBS28, for which $\delta^{18}O$ was assumed to be 9.6 permil relative to Standard Mean Ocean Water (SMOW). Precision was monitored by replicate analyses of an internal high-Al basalt standard (BAT26) and is estimated to be +-0.15 permil. None of the samples show any evidence of secondary alteration. The results are listed in Table 2.1, together with SiO_2, K_2O and, where available, $^{87}Sr/^{86}Sr$ values.

The samples range in composition from low-K to leucititic and their oxygen isotope values range between 3.8 and 7.0 permil. These values show negative correlations with K content and $^{87}Sr/^{86}Sr$ values (Figs 2.19 & 2.20) which contrast with those of samples from the Banda arc analysed by Magaritz et al. (1978). Magaritz et al. (1978) suggested the positive correlation between Sr and O isotope values in the Banda arc

VOLCANO	SAMPLE	SiO_2	K_2O	$^{87}Sr/^{86}Sr$	$\delta^{18}O$
BATUR	67238	53.44	1.30	0.7040	7.2
					6.7
	67250	52.40	0.91	-	5.8
	67240	53.75	0.99	-	6.5
	67244	52.03	0.95	-	6.1
	67257	52.97	0.75	-	6.4
BATUR	average	52.92	0.98	0.7040	6.4
RINDJANI	41632	49.08	1.26	0.70395	5.9
SANGENGES	48115	44.08	4.26	0.70550	3.9
					3.8
					3.8
SANGEANG API	48067	47.77	1.85	0.70502	5.1
SOROMUNDI	48136	47.53	3.40	0.70480	4.8
TAMBORA	48048	51.49	2.89	0.70400	6.4
BATU TARA	67130	48.71	3.49	(0.70609)	4.9
IJA	61268	51.33	0.39	(0.70522)	5.4
EBULOBO	61338	56.41	1.36	-	7.0

Table 2.1 Oxygen isotope results from Quaternary lavas in the eastern Sunda arc. Strontium isotope results from Batu Tara and Ija volcanoes obtained using different samples (J.D. Foden et al., unpubl. data). Other Sr data from Macdougall et al. (unpubl.) (Batur) and Whitford et al. (1978).

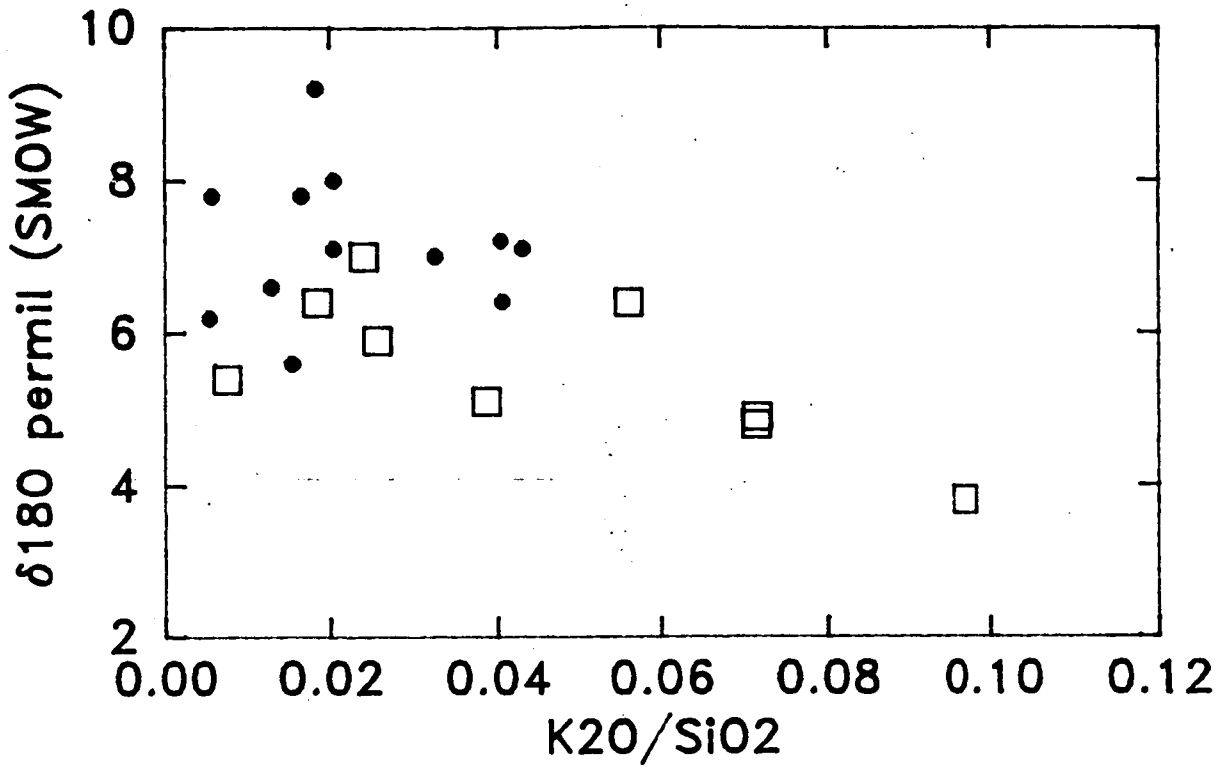

Figure 2.19 $\delta^{18}O$ against K_2O/SiO_2 values in Sunda-Banda volcanics (open squares = eastern Sunda arc; dots = Banda arc). Banda arc data from Magaritz et al. (1978).

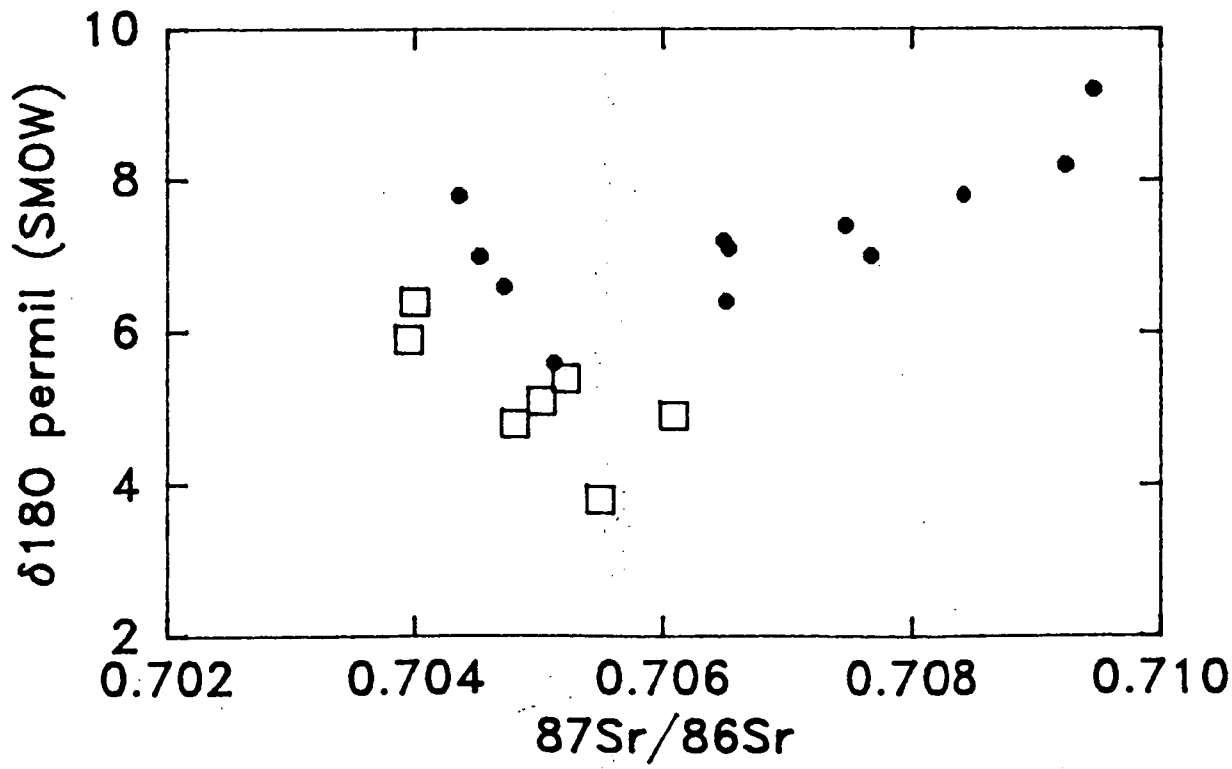

Figure 2.20 $\delta^{18}O$ against $^{87}Sr/^{86}Sr$ values in Sunda-Banda volcanics. Symbols and data sources as for Figure 2.19.

samples was caused by involvement of subducted sialic material derived from Australian continental crust.

For comparison, mafic rocks from the Mariana island arc show no variation of oxygen isotope values with either K or $^{87}Sr/^{86}Sr$ (Ito & Stern 1981). Tholeiitic, alkaline and calcalkaline volcanic rocks from the Japanese arc also show 'normal' $\delta^{18}O > 5.5$ permil (Matsuhisa 1979). Some Italian K-rich volcanic rocks, including leucite-bearing types, possess higher $\delta^{18}O$ values that are thought to indicate contamination by continental crust (Turi & Taylor 1976; Taylor & Turi 1976; Taylor et al. 1979; Taylor et al. 1984; Ferrara et al. 1985). Other leucite-bearing volcanic rocks, from New South Wales, Bufumbira and Gaussberg, possess inferred primary $\delta^{18}O$ values of between 5.8 and 7.9 permil which are thought to reflect uncontaminated mantle values (Taylor et al. 1984).

Icelandic alkaline and tholeiitic basalts have low $\delta^{18}O$ values, ranging between 1.8 and 5.7 , which Muehlenbachs et al. (1974) suggested could be due to exchange with low-^{18}O meteoric fluids in the crust, assimilation of low-^{18}O hydrothermally altered crustal rocks, or derivation from an 'anomalous' mantle source. Skaergaard gabbros and basalts, some continental and oceanic basalts and eucritic meteorites also show low $\delta^{18}O$ values (Fig. 7.1.12 of Basaltic Volcanism Study Project 1981).

3.3.5 Beryllium

Like the U-decay series, analyses of ^{10}Be in island arc basalts are still uncommon, with most work being done at present by one group centred on the Carnegie Institution of Washington. This isotope is produced from oxygen and nitrogen in the atmosphere by cosmic radiation and accumulates in sediments and soils after transport to the Earth's surface by rain and snow. If sediments are incorporated into the source regions of island arc magmas by the subduction process, ^{10}Be is potentially observable in erupted lavas for up to 10 Ma (approximately 6.5 half-lives of ^{10}Be) after its production in the atmosphere (Tera et al. 1982).

High abundances of ^{10}Be (up to 24 x 10^6 atom g^{-1}) in volcanic rocks from the Aleutian arc, Japan and Central America appear to correlate positively with Pliocene - Pleistocene sedimentation rates seaward of the respective trenches, suggesting that recent subduction of sediment has occurred in those arcs (Tera et al. 1986). Their high ^{10}Be concentrations suggest that a sediment component formed up to 10 % of their source materials.

Three historical lava flows from Batur volcano on Bali, and one from Ebulobo volcano on Flores, together with samples of unknown but morphologically young age from active Javanese volcanoes, have been analysed for ^{10}Be (Tera et al. 1985). All of these rocks contain low ^{10}Be concentrations (< 1 x 10^6 atom g^{-1}) which are indistinguishable from those of the 'control group' comprising MORB and intra-plate basalts. Tera et al. (1985) suggested that in the Sunda, Halmahera and Mariana arcs, whose lavas all show similarly low ^{10}Be contents, the upper, ^{10}Be-rich sediment layers of the oceanic crust may have been diluted by mixing with lower, ^{10}Be-poor sediments during the subduction process prior to their incorporation into the melting zones.

3.4 Regional Geochemical Trends

3.4.1 Across-arc variations

Following publication of the Catalogue of Active Volcanoes in the Indonesian region (Neumann van Padang 1951), which included a compilation of chemical analyses of lavas and ashes from Indonesian volcanoes, Rittman (1953) showed that those rocks became more alkaline with distance away from the 'foredeep' or trench. With the development of plate tectonic concepts, Hatherton and Dickinson (1969) calculated by linear regression the K_2O contents of the magmas at 55 and 60 wt % SiO_2 (K_{55} and K_{60}), and showed that these 'K values' correlated positively with increasing depth to the seismic plane ('h') beneath the arc. Similar across-arc compositional variations are observed in many, but not all, island arcs (Arculus & Johnson 1978; Gill 1981).

Whitford and Nicholls (1976), using new chemical analyses, confirmed statistically this relationship among the Quaternary volcanoes of Java and Bali. Their preferred result, however, excluded data from volcanoes in which there were insufficient analyses to obtain a significant intra-suite correlation between K_2O and SiO_2 and volcanoes whose lavas showed relatively high $^{87}Sr/^{86}Sr$ values, which they considered may be due to secondary contamination by upper crust during magma ascent. Whitford and Nicholls (1976) found that although the shoshonitic suite from Muriah volcano (their 'wet series') plotted near the trend defined by the other volcanoes, which they thought suggested a genetic relationship, the leucititic suite from Muriah ('dry series') did not. Using all of Whitford's (1975a) data, Hutchison (1976) extended the apparent relationship between K_2O contents of the lavas and depth to seismic plane to include the K-group trace elements, Rb and Sr.

Foden and Varne (1980,1981) showed, however, that the seismic plane occurs at approximately the same depth beneath Quaternary volcanoes on Sumbawa and Lombok that have erupted a very wide range of lava compositions and that, therefore, the postulated general trend of increasing K-group element enrichment with increasing depth to the seismic plane does not exist in that sector of the arc.

3.4.2 Along-arc

In some arcs, variations in the compositions of volcanic products occur along the strike of the arcs. Gill (1981) decribes four types of variations: random, regular, and those apparently related to crustal thickness and to 'edge' effects. Along-arc variations have been observed in the $^{87}Sr/^{86}Sr$ values of lavas in Java and Bali (Whitford 1975b), in the chemistry and isotope compositions of lavas in the Banda arc (Whitford & Jezek 1979), and in the bulk compositions of the volcanic products, from rhyolitic and dacitic in Sumatra to mafic rocks in the eastern part of the Sunda-Banda arc (Hamilton 1977).

To investigate further the regional geochemical and isotopic trends in the Sunda-Banda arc, a new approach is used

here to characterize numerically the composition of the source of each volcanic suite. On a K_2O-SiO_2 diagram, consanguineous suites typically form positive, linear trends. The slopes of these trends progressively increase from low-K to leucititic suites, and fan about an origin at approximately 40 wt % SiO_2 and 0 wt % K_2O (see Fig. 2.3). A numerical parameter, K_{Si}, which represents these slopes, may be calculated by averaging the values of $100.K_2O/(SiO_2-40)$ from the chemical analysis of each sample (normalized to total 100 %, volatile-free, all Fe as FeO) in a suite.

This parameter is an improvement over K_{55} and K_{60} values because even a single analysis, if that is all that is available, can be used to characterize a suite, and its calculation does not require that suites show a spread of SiO_2 contents. Also, values obtained for K_{55} and K_{60} cannot be calculated for some shoshonitic and leucititic suites because because even their most siliceous members do not approach 55 wt % SiO_2 (Fig. 2.3).

The disadvantages of using K_{Si} result from intra-suite fractionation processes in which K-rich phenocrysts are important components, causing depletion of K_2O with increasing SiO_2. Also, Foden and Varne (1980) observed chemical scatter within the leucititic suites from Soromundi and Sangenges volcanoes which they suggested was due to the presence in those suites of several primary magmas. Those features of a few suites may lead to relatively large standard deviations from their K_{Si} values.

It should be noted that K_{Si} values (and K_{55} and K_{60} values) reflect source compositions only if the slopes formed by consanguinous volcanic suites are proportional to the K_2O contents of their sources. It seems possible that this relationship may be affected by the conditions and degree of partial melting and, later, by the bulk compositions of low-pressure phenocryst assemblages. However, the usefulness of the K_{Si} value as a quantitative measure of the degree of enrichment of incompatible elements in arc volcanic rocks is supported by the positive correlation between K_{Si} values and averaged chondrite-normalized La/Yb values among Sunda-Banda

volcanics rocks (Fig. 2.21). The K_{Si} values of each of the volcanic suites identified from the Sunda-Banda arc, together with their average $^{87}Sr/^{86}Sr$ values, are given in Table 2.2.

In many volcanoes in the Sunda-Banda arc there are two or more distinct magma series present (Whitford 1975a; Foden 1979). Identification of these separate suites in this thesis has involved more rigorous application of the K_2O-SiO_2 classification fields than was done by Whitford (1975a) but, in all cases, differences were confirmed by variations in the concentrations of elements other than K_2O, particularly Zr and P_2O_5, which are unlikely to be due to crystal fractionation processes.

It is notable that in volcanoes where different suites are present, those suites plot in adjacent fields in Figure 2.3. Some volcanoes have, for example, both medium-K and high-K suites but none has only low-K and high-K suites. These differences within individual volcanoes may represent small but significant changes in the compositions of inferred parental or primitive magmas and suggest that the process that is mainly responsible for chemical variation among the Sunda-Banda arc volcanoes is gradational in character.

Because the Sunda-Banda volcanic arc lies generally east-west, the longitude of each volcano is a convenient measure of its position along the arc. From a plot of K_{Si} versus longitude (Fig. 2.22), the Sunda-Banda arc can be divided into four sectors. Three of these sectors, named here the West Java, Bali and Flores sectors, show trends of progressively increasing K_{Si} values of volcanic suites from west to east, which reach maxima at the leucite-bearing volcanoes Muriah, Soromundi and Sangenges, and Batu Tara respectively.

It is important to note that these eastward increases along the arc of K_{Si} values, which incorporate the across-arc variations where they are present, terminate at the leucitite volcanoes. East of these volcanoes, there are abrupt changes to low- and medium-K suites. In addition, it is notable that these sectors are also characterized by the presence in

Volcano	longitude	N	series	seismic height	average K_{Si}	average $^{87}Sr/^{86}Sr$
West Java						
Krakatau	105.423	3	MK	145	7.0	0.70449
Danau	106.3	1	MK	170	5.9	0.70465
"	"	1	HK	"	12.2	0.70513
Salak	106.73	2	MK	165	9.1	0.70472
Tjikurai	107.30	8	LK	135	4.5	0.70411
Guntur	107.33	9	LK	155	4.5	0.70434
"	"	6	MK	"	6.9	0.70492
Tangkuban	107.60	5	MK	180	8.7	0.70506
"	"	10	HK	"	13.8	0.70504
Papandajan	107.73	9	MK	135	7.7	0.70572
"	"	1	HK	"	10.6	0.70579
Galunggung	108.05	8	LK	155	4.3	0.70437
"	"	6	MK	"	5.6	0.70435
Tjerimai	108.40	11	MK	185	9.8	0.70494
Slamet	109.208	5	MK	175	10.8	-
"	"	6	HK	"	13.9	0.70533
Dieng	109.92	5	HK	190	14.3	0.70522
Sundoro	109.992	8	MK	185	9.9	0.70483
"	"	6	HK	"	11.7	0.70519
Sumbing	110.058	6	MK	180	9.9	0.70499
"	"	5	HK	"	11.7	0.70467
Ungaran	110.33	4	HK	190	17.2	0.70495
"	"	6	SH	"	22.8	0.70497
Merbabu	110.43	7	MK	175	10.2	0.70522
"	"	4	HK	"	19.3	0.70576
Merapi	110.442	10	HK	160	14.0	0.70556
Muriah	110.86	5	SH	385	30.3	0.70479
"	"	19	LC	"	61.2	0.70451
East Java to Sumbawa						
Kelud	112.308	4	MK	155	5.1	0.70452
Semeru	112.92	2	MK	150	7.5	0.70469
Bromo	112.95	2	HK	165	16.4	0.70442
Batukau	115.09	8	MK	145	7.9	-
Lesong	115.11	10	HK	155	11.8	-
Tapak	115.13	8	HK	155	11.8	-
Bratan	115.13	3	MK	155	8.9	-
"	"	8	HK	"	14.2	-
Batur	115.375	49	MK	165	8.8	0.70403
Agung	115.508	9	MK	150	8.8	0.70399
Ulakan	115.51	13	SH	130	21.9	0.70369
Seraja	115.65	14	MK	155	10.5	0.70391
"	"	4	HK	"	14.1	-
Rindjani	116.47	22	MK	160	9.4	0.70395
"	"	48	HK	"	14.3	0.70395
Sangenges	117.12	1	MK	145	5.0	-
"	"	5	HK	"	12.9	-
"	"	5	SH	"	23.5	0.70412
"	"	7	LC	"	82.7	0.70529

continued over ..

Volcano	longitude	N	series	seismic height	average K_{SI}	average $^{87}Sr/^{86}Sr$
Satonda	117.75	5	SH	195	24.0	-
Tambora	118.00	24	SH	185	31.5	0.70392
Soromundi	118.61	12	LC	165	49.7	0.70508
Sangeang Api	119.08	15	SH	190	27.2	0.70483
Flores to Lembata						
Wai Sano	120.025	11	MK	145	5.8	-
Inerie	120.95	14	LK	140	4.8	0.7058
"	"	3	MK	"	7.1	0.7046
Ebulobo	121.18	8	MK	130	7.2	0.7047
Ija	121.63	19	LK	120	3.5	0.7053
Rockatenda	121.708	16	MK	195	9.4	-
Egon	122.45	15	MK	135	6.3	-
Lewotobi Lakilaki	122.775	6	MK	140	6.6	-
Lewotobi Perampuan	122.78	15	MK	140	7.5	-
Mandiri	123.00	7	HK	170	14.0	-
Boleng	123.258	10	HK	155	12.7	0.70646
Lewotolo	123.505	11	HK	160	17.9	0.70577
Batu Tara	123.579	37	LC	235	55.7	0.70658
Kedang	123.77	15	HK	165	16.3	-
Banda arc						
Api	126.65	1	HK	425	18.0	-
Romang	126.70	2	HK	145	10.6	-
Damar	128.675	5	HK	160	13.5	0.70654
Teun	129.125	4	MK	155	10.4	0.70756
Nila	129.50	5	HK	155	12.7	0.70771
Serua	130.00	6	MK	150	6.3	0.70871
Manuk	130.292	5	MK	165	5.3	0.70518
Banda I.	129.87	8	LK	155	3.2	0.70471
Ambon		2	LK		2.8	0.70429

Table 2.2 Geographical and compositional characteristics of Sunda-Banda volcanic suites.

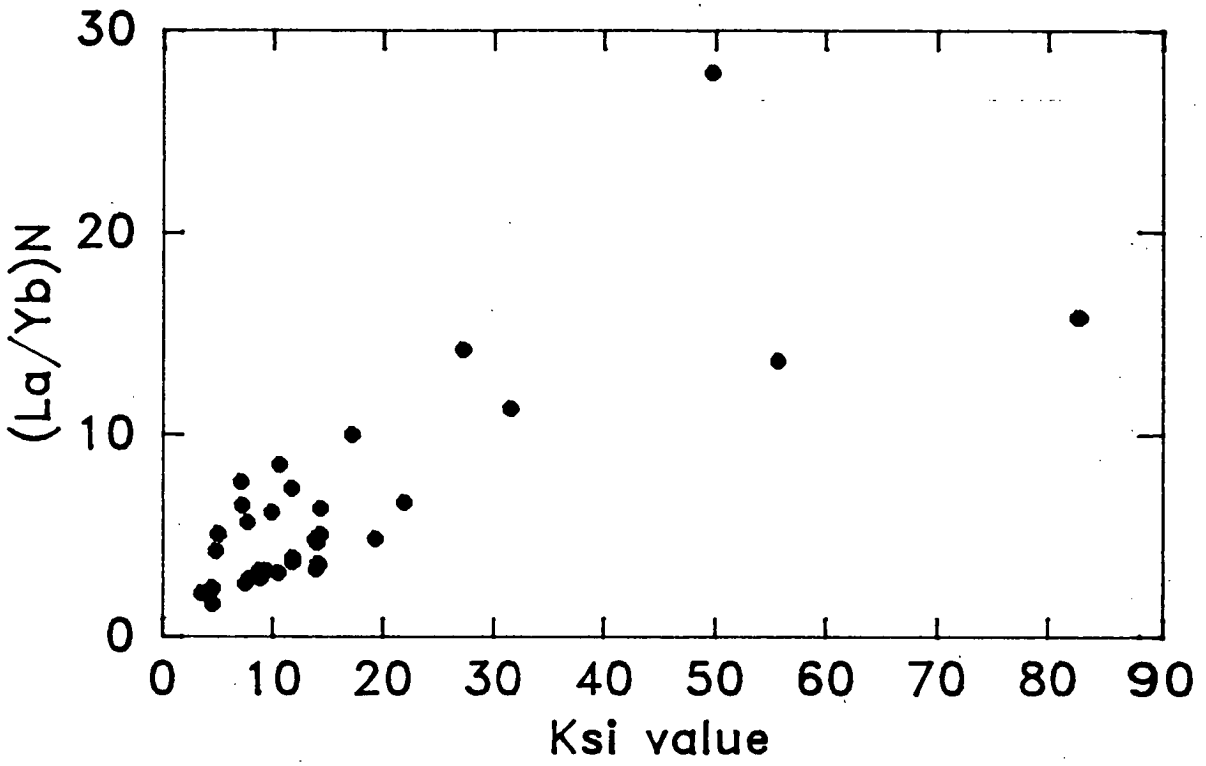

Figure 2.21. Chondrite-normalized La/Yb against K_{Si} values in Sunda volcanics.

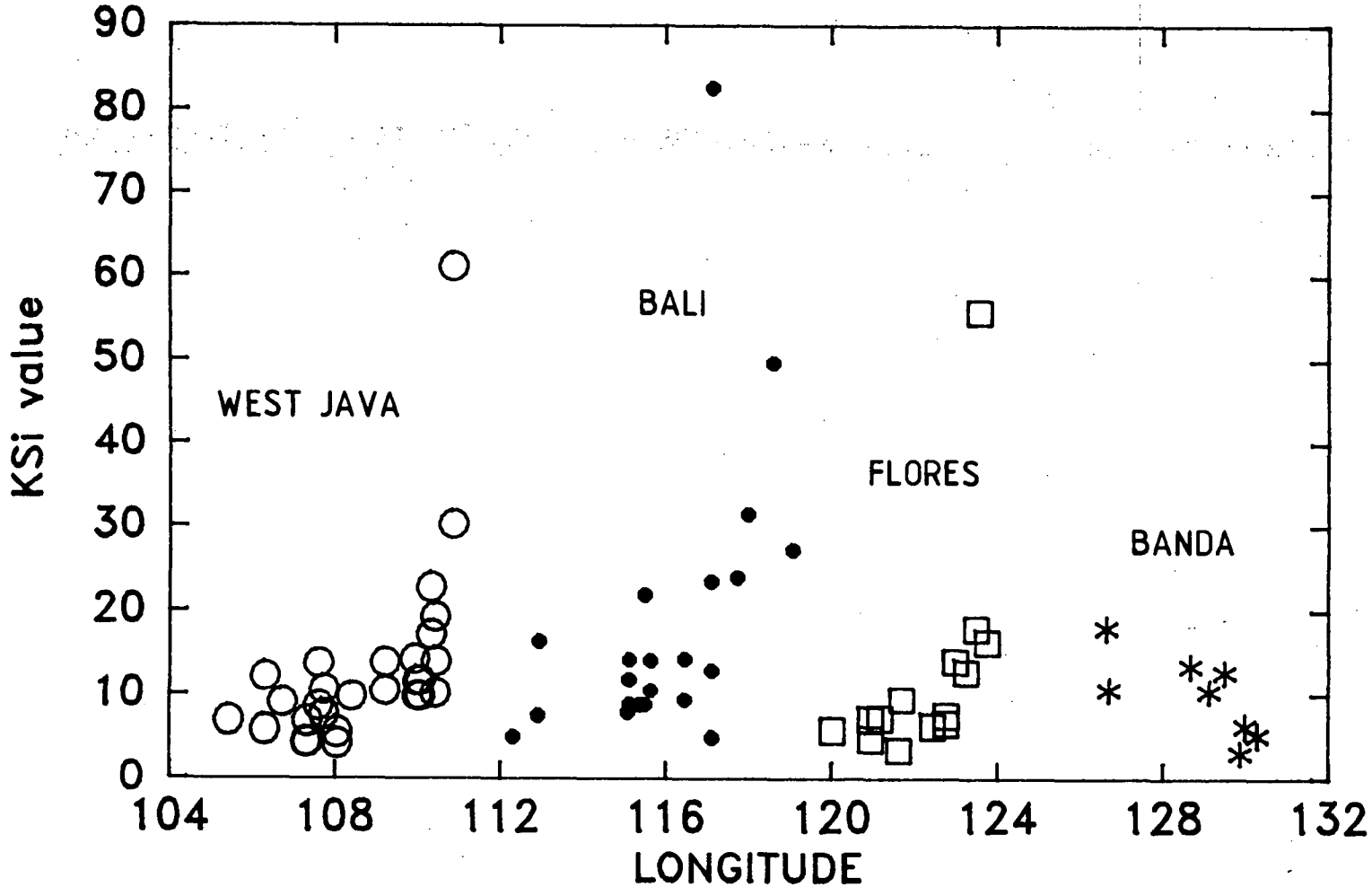

Figure 2.22 K_{Si} values against longitude for Sunda-Banda arc volcanic suites. See text for explanation.

their western parts of arc sectors of low volcanic intensity. The fourth sector, Banda, comprises only low- to high-K suites and K_{Si} values in this sector tend to decrease around the arc northeastwards from Wetar, as observed by Whitford and Jezek (1979).

The relative positions of these four arc sectors correlate broadly with successive stages in the tectonic evolution of the Sunda-Banda arc. The West Java sector lies along the line of the Cretaceous to Early Tertiary volcanic arc that extended into southeastern Kalimantan. The Bali sector lies along the line of the Middle Tertiary volcanic arc that is thought to have continued to southern Sulawesi. The Flores sector correlates with the Middle to Late Tertiary eastern extension of the Sunda volcanic arc, and the Banda sector represents the most recent stage in the growth of the Sunda-Banda arc.

None of the leucite-bearing volcanoes is known to lie on or near major across-arc fractures. The existence of the Sumba Fracture, proposed by Audley-Charles (1975) and suggested by Foden and Varne (1980) to be a possible conduit for transport of K-rich material from depth in the mantle to the source regions of the Sumbawan potassic volcanoes, is not supported by subsequent studies of the tectonics of the eastern Sunda arc region (Cardwell & Isacks 1978; Hamilton 1979; Silver et al. 1983). There is no evidence, therefore, that these regular, along-arc compositional variations are related to surface 'edge' effects, nor are there any apparent correlations within each sector with crustal thickness.

4. GENESIS OF SUNDA-BANDA ARC BASALTIC LAVAS

4.1 Island Arc Basalt Genesis

Models of the origins of mafic volcanic rocks in island arc tectonic settings have grown in complexity with evolution of plate tectonic concepts, experimental investigations of mantle melting processes, and improved resolution of trace element and isotopic analysis in volcanic rocks. The observation that volcanic rocks associated with subduction zones showed distinctive compositions compared to those from other

tectonic environments led to petrogenetic models which related their generation genetically and specifically to the subduction process.

Early experiments aimed to test whether these 'calcalkaline andesites', then thought to be the volumetrically most significant magmatic product of island arc volcanism, were produced directly by fusion of either the subducted oceanic plate (Green & Ringwood 1968; Green 1972; Stern & Wyllie 1978) or water-saturated peridotitic mantle that is thought to form a wedge overlying the subducted plate (Green 1973; Kushiro 1974; Mysen & Boettcher 1975). The liquids produced by these experiments are generally accepted now as being dissimilar chemically to most, if not all, island arc mafic volcanic rocks (e.g. Gill 1981).

Continued studies in island arc regions, particularly in arcs flanked on both sides by oceanic crust (Baker 1978), showed that basaltic lavas are at least as important volumetrically as andesites and that low-pressure fractional crystallization processes can lead to derivation of andesites from parental basaltic magmas (e.g. Osborn 1969). These basalts are thought to be the products of melting of peridotitic mantle triggered by subduction of oceanic crust (Ringwood 1977).

However, island arc basalts (IAB) often show distinctive chemical compositions compared to mid-ocean ridge basalts (MORB), in particular by containing, at similar SiO_2 contents, more Al_2O_3 and K_2O and less TiO_2 and MgO. Their differentiation trends are also different, which may be illustrated by the covariation of CaO and Al_2O_3 (Fig. 2.23), which mainly reflects the characteristic late appearance of plagioclase in IAB (Perfit et al. 1980; Marcelot et al. 1983). These observations have been largely explained by experimental studies which have shown the effects of volatiles (particularly H_2O), pressure and oxygen fugacity on determining the liquidus phenocryst assemblages of crystallizing island arc basaltic magmas (e.g. Nicholls & Ringwood 1973; Grove & Baker 1984).

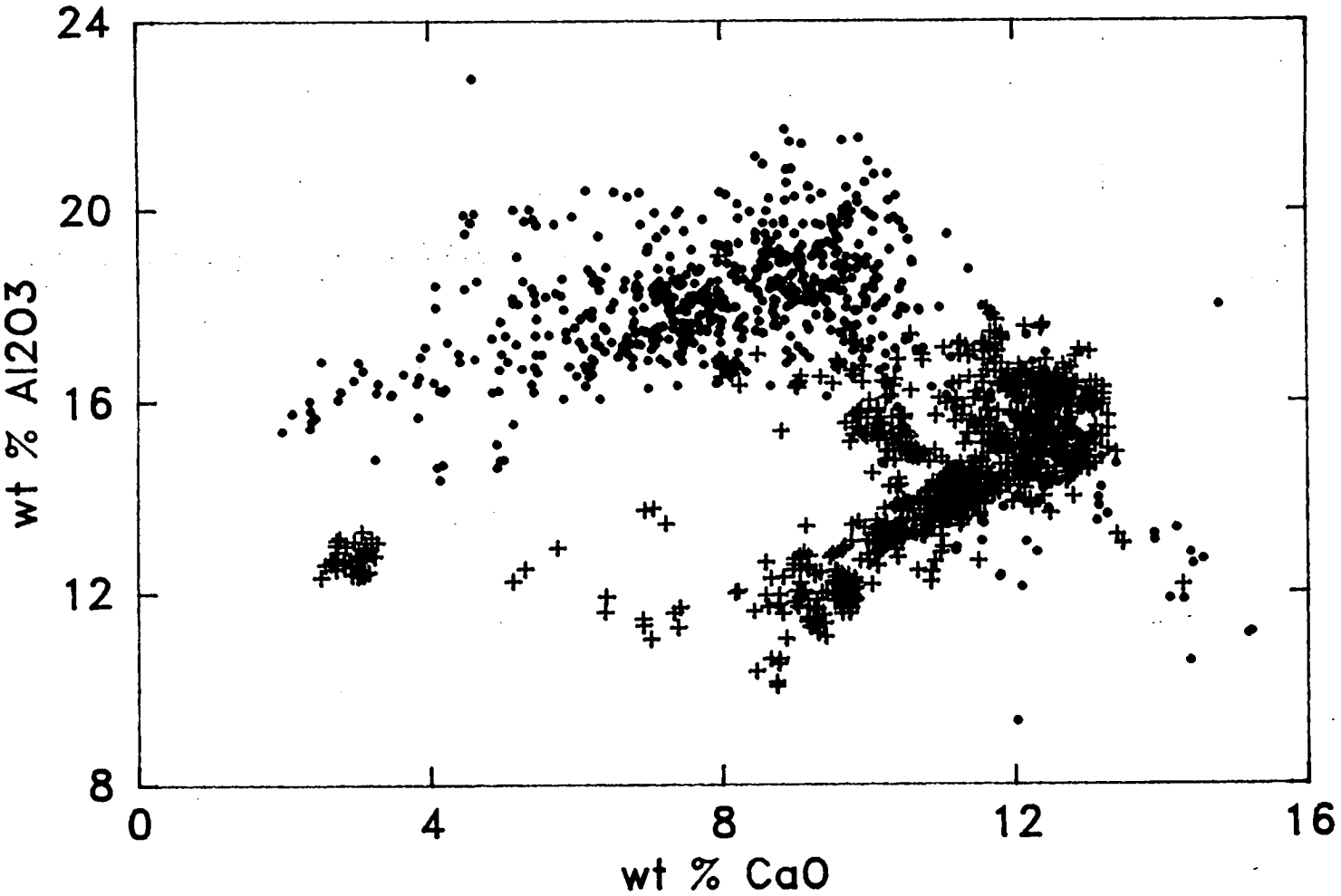

Figure 2.23 Al_2O_3 against CaO in 679 Sunda-Banda arc volcanics (dots) and Pacific mid-ocean ridge rocks and glasses (crosses). Pacific data from an unpublished compilation by T. Falloon and D.H. Green based on the catalogue of MORB glasses by Melson et al. (1977).

Contemporary debate largely concerns the origins of incompatible-element and isotopic differences in IAB compared to MORB, particularly the degree to which the subducted slab contributes chemically to the source regions of IAB. Gill' (1981) review favoured models based on that proposed by Nicholls and Ringwood (1972) that derived H_2O, K, and other incompatible elements which are enriched in arc magmas, from the slab, by production of either hydrous fluids or siliceous melts, or both, which moved into the overlying mantle wedge. Gill (1981) acknowledged, however, that in some places there is no positive isotopic or other evidence for the involvement of either pelagic sediments or altered oceanic crust from the slab in the magma sources. Several recent studies have made this observation explicitly (Stern & Ito 1983; Johnson et al. 1985) or have indicated that a mantle-derived 'enriched' component may also be involved (Saunders et al. 1980; Thirlwell 1982; Gill 1984; Varne 1985).

Basaltic magmas in the Java-Bali sector of the Sunda-Banda arc were thought by Whitford et al. (1979) to have been primarily derived from subarc mantle that was geochemically zoned by addition of small fractions of an 'enriched' component produced by melting of the subducted oceanic crust. A similar, but isotopically more extreme, slab-derived component is thought to have been added to the source regions of the Banda arc magmas (Whitford & Jezek 1979; Magaritz et al. 1978). However, Foden and Varne (1980, 1981) implied that the K-rich component in lavas from the Lombok-Sumbawa sector was derived from within the mantle rather than from the subducted slab or other crustal sources. Varne (1985) suggested it may have been derived from ancient subcontinental mantle involved in the active collision or beneath Mesozoic 'Gondwanaland' continental fragments lying close to the arc.

Recently, some geochemists have used relative abundances of incompatible elements and Sr, Nd and Pb isotopic data to suggest that a close geochemical relationship exists between IAB and ocean island basalts (OIB). Using this relationship, Stern and Ito (1982) and Gill (1984) inferred that IAB from the Volcano-Mariana island arc and Fiji respectively had sampled OIB-source mantle. However, Chase (1981), White and Hofmann

(1982), Morris and Hart (1983) and White and Patchett (1984) interpreted the correlation in the opposite sense, suggesting that ancient, subducted oceanic crust may form the sources of some, if not all, OIB. Ringwood (1982), White and Hofmann (1982) and Morris and Hart (1983) suggest mechanisms for this process, arguing that enrichment of the sources of OIB, as well as the subcontinental lithosphere, occurs as a result of long-term storage of subducted oceanic crust deep in the Earth's mantle.

4.2 Compositional Variation in the Sunda-Banda Subarc Mantle

A plot of K_{Si} against average $^{87}Sr/^{86}Sr$ values in volcanic suites for which data are available (Table 2) shows that each of the four arc sectors possess distinct and characteristic variations in these parameters (Fig. 2.24). At one extreme, the Banda sector is characterized by low K_{Si} and high $^{87}Sr/^{86}Sr$ values while, at the other, the Bali sector shows high K_{Si} and low $^{87}Sr/^{86}Sr$ values. The West Java and Flores sectors fall between the Bali and Banda sectors on this diagram. This pattern of variation among the arc sectors implies that at least three isotopically distinct components were involved on a regional scale in the sources of the arc rocks. The points A, B and C on Figure 2.24 indicate qualitatively the compositions of these components.

Only one component (component A) is common to each of the sectors, and its low K_{Si} and Sr isotope values are those generally expected of MORB-source peridotite. It is assumed therefore that this component is also the source of the major oxides, compatible trace elements, and radiogenic Nd in the Sunda-Banda arc mafic rocks.

A second component (component B), which also possesses a low K_{Si} value, shows high $^{87}Sr/^{86}Sr$ values that are characteristic of crustal material, including either pelagic sediments or hydrothermally altered oceanic slab. If this is a crustal component, then it would generally be expected also to possess heavy O, radiogenic Pb and non-radiogenic Nd. However, because of its low K_{Si} value, this component could not have been responsible for the wide geochemical variation shown by

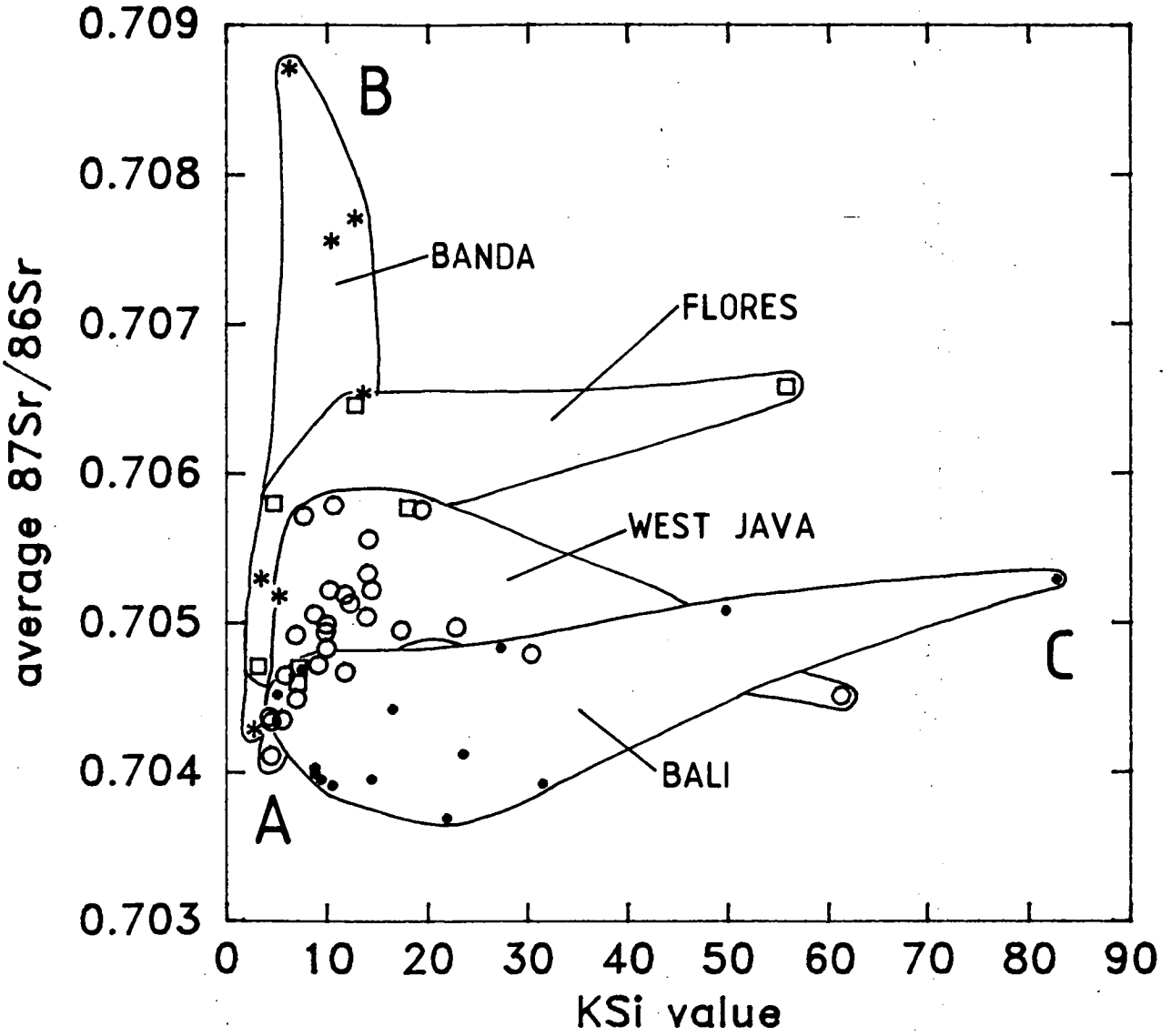

Figure 2.24 Average $^{87}Sr/^{86}Sr$ against K_{Si} values in volcanic suites from the Sunda-Banda arc. See text for explanation.

the Sunda-Banda arc mafic rocks.

The third component (component C) is difficult to identify because its characteristics of high K_{Si} and relatively low $^{87}Sr/^{86}Sr$ values do not fit those of any generally recognized mantle or crustal reservoir. However, from their other isotopic characteristics, the basaltic rocks in the Bali sector seem to have had the least amount, if any, of crustal materials involved in their genesis compared to those in the other arc sectors. In particular, rocks from that sector show little or no disequilibrium between U and Th isotopes (Tanzer 1985; Fig. 2.17), low ^{10}Be contents that are indistinguishable from those of non-arc lavas (Tera et al. 1986), low $\delta^{18}O$ values (Figs 2.19 & 2.20), lie within the 'mantle array' for Sr and Nd isotopes (Fig. 2.16) and possess Pb isotope compositions similar to those of some Indian Ocean and southeast Australian intraplate basalts (Fig. 2.18).

Moreover, the regular positive correlations shown by rocks from the Bali sector between K_2O and $^{87}Sr/^{86}Sr$ (Fig. 2.25) and K_2O and $^{206}Pb/^{204}Pb$ (Fig. 2.26), together with the negative correlations between ε_{Nd} and chondrite-normalized La/Yb values (Fig. 27), and between $\delta^{18}O$ and $^{87}Sr/^{86}Sr$ and K_2O (Fig. 2.19 & 2.20), indicate that the K-rich component C is also responsible for the isotopic variation shown by these rocks. In addition, it is seems likely that, because U and Th are typically strongly incompatible elements, the K-rich component is also responsible for the distinctive U-Th isotopic compositions of the Batur, Sangeang Api and Galunggung sources.

Basaltic rocks in the other arc sectors show more evidence of crustal involvement. The steep trend formed by the West Java rocks on the plot of $^{207}Pb/^{204}Pb$ against $^{206}Pb/^{204}Pb$ diagram and the relatively radiogenic Pb isotope compositions of the Banda sector lavas (Fig. 2.18) suggest contamination by continental crust material, either in the mantle source regions or during ascent to the surface. Rocks from the Flores and Banda sectors show generally high $^{87}Sr/^{86}Sr$ values compared to those from the Bali sector and plot slightly to the right of the mantle array on an ε_{Nd} versus $^{87}Sr/^{86}Sr$ diagram (Fig. 2.16).

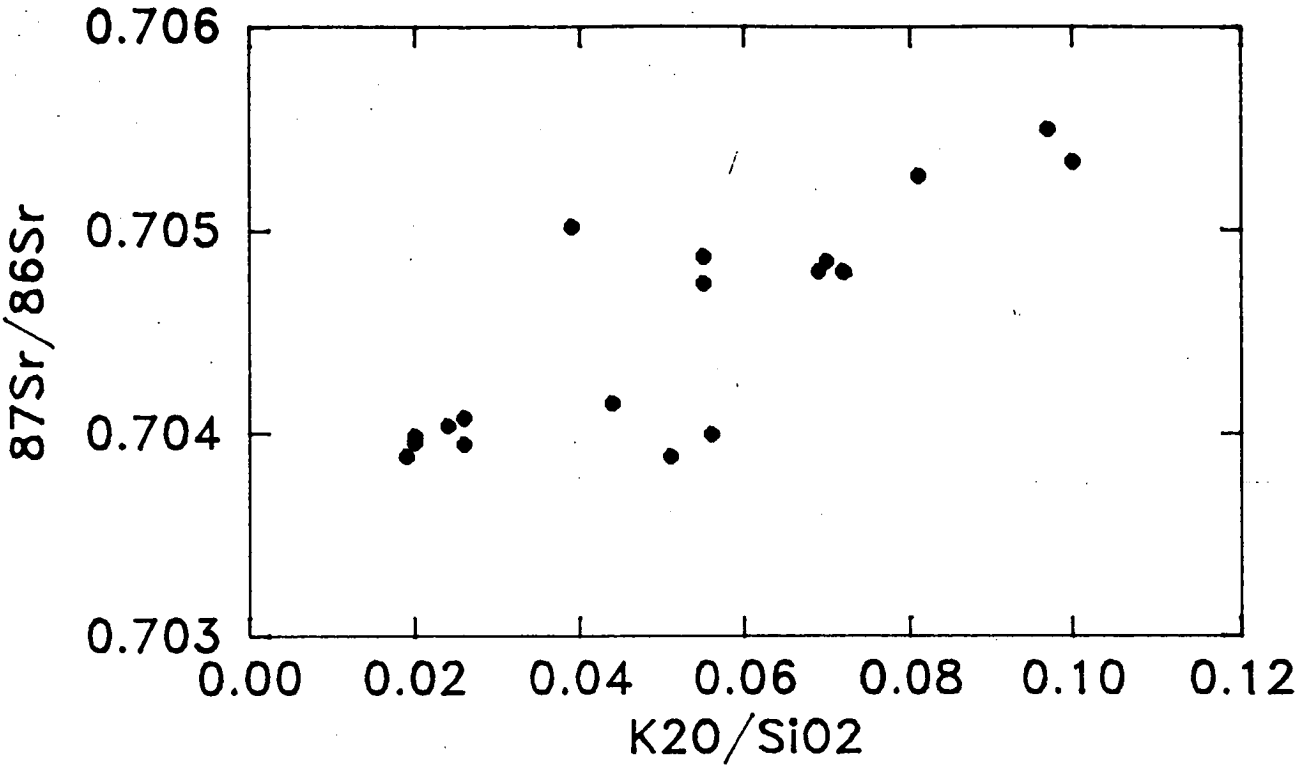

Figure 2.25 $^{87}Sr/^{86}$ against K_2O/SiO_2 values in volcanic rocks from the Bali arc sector.

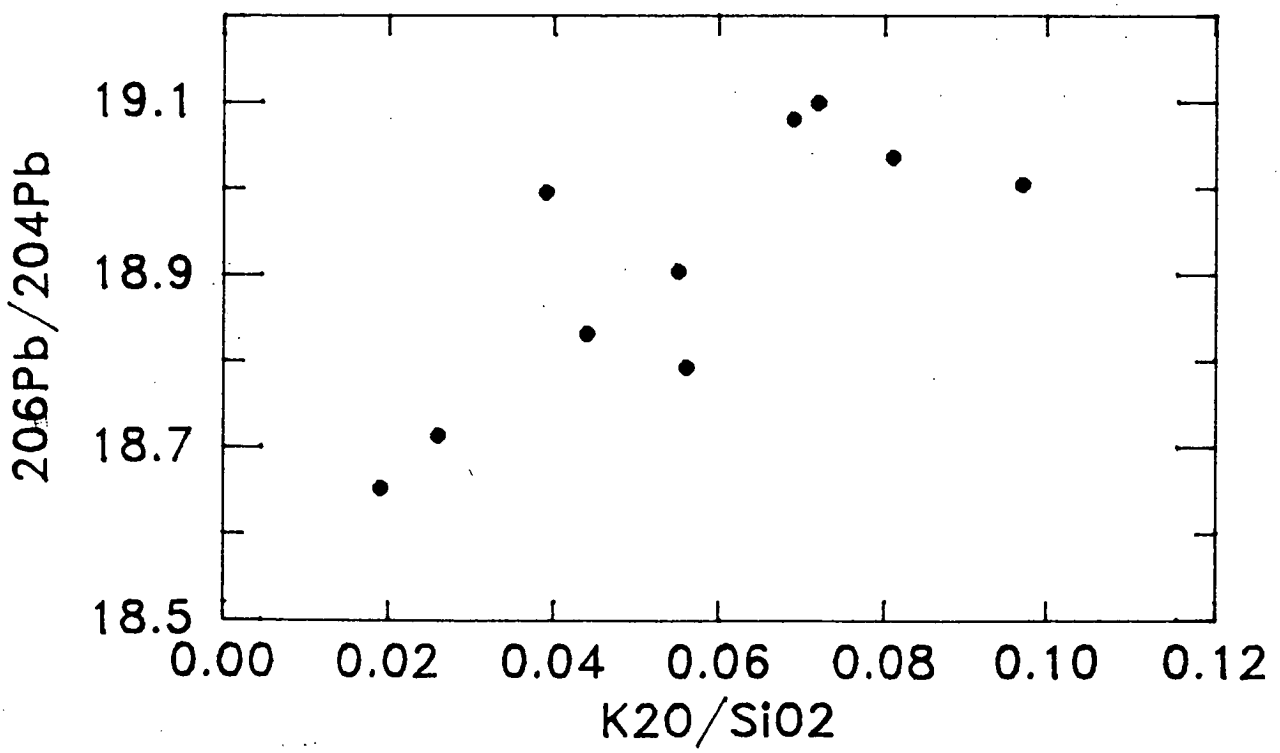

Figure 2.26 $^{206}Pb/^{204}Pb$ against K_2O/SiO_2 values in volcanic rocks from the Bali arc sector.

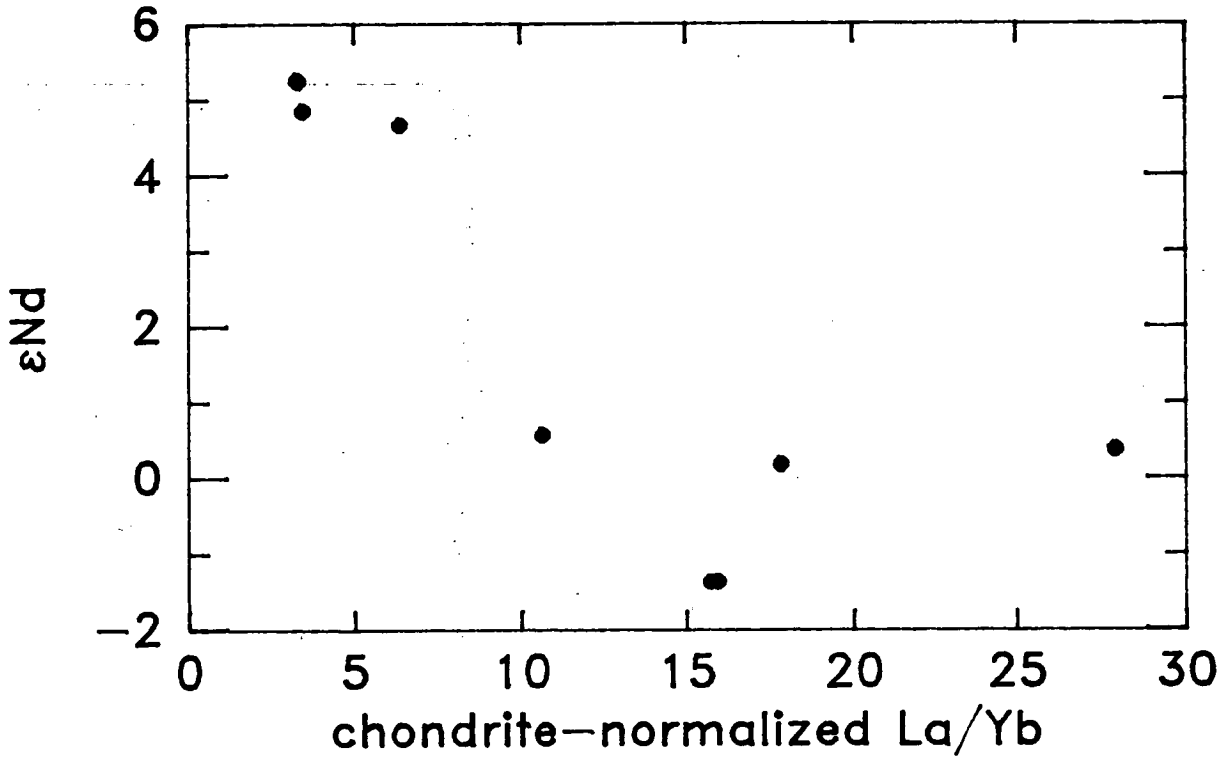

Figure 2.27 ε_{Nd} against chondrite normalized La/Yb values in volcanic rocks from the Bali arc sector.

This suggests contamination by altered oceanic crust but, from the negative ε_{Nd} values and high $\delta^{18}O$ values of the Banda rocks, it seems likely that a sedimentary component, derived from mature continental crust, is also involved.

The isotopic characteristics of volcanic rocks in the Bali arc sector are inconsistent with substantial, recent involvement of crustal material as the enriched component, yet the volcanic rocks in this sector include some of the most chemically enriched rocks found in volcanic island arcs. The high K_{Si} value shown by component C, combined with the positive correlations between K and other incompatible trace and minor elements (including Nb but not Ti), indicates that it is involvement of varying amounts of this component which is primarily responsible for the geochemically continuous variation from low-K to leucititic rock series in the Sunda-Banda arc. Assimilation of crustal material, either by involvement of material from the subducted slab or during magma ascent through the arc crust, appears to have had only an overprinting effect on volcanic rock compositions.

To help identify the origins of component C, the island arc rocks from the Sunda-Banda arc are compared geochemically to K-rich rocks that have been produced in continental settings. These tectonic settings contrast markedly with island arcs yet, as will be shown in the next section, there exist close geochemical similarities between the two rock groups which suggest common factors in their genesis.

4.3 Island Arc Basalts and Ultrapotassic Rocks

Although some authors have compared the chemical and isotopic characteristics of IAB with those of OIB, as previously mentioned, a more appropriate igneous rock type to compare with IAB is the ultrapotassic group, which shares with IAB the general characteristic of strong K-enrichment, which IAB and OIB do not.

Foley et al. (1986) have recently reviewed the geochemical, isotopic, mineralogical and tectonic characteristics of ultrapotassic rocks and have classified them on a

'resemblance' basis relative to three end-member types: continental, rift and orogenic. Compared to the orogenic types, which include some of the leucititic rocks from the Sunda arc, the continental types (lamproites) contain low CaO and Al_2O_3 contents and high abundances of incompatible elements, and were erupted in stable continental regions usually spatially and temporally distant from convergent tectonic settings. Foley et al. (1986) suggest that these rocks were produced under H_2O- and F-rich, CO_2-poor, conditions from harzburgitic mantle that had been metasomatized by a incompatible element enriched component. The rift-related types (kamafugites) contain low SiO_2 and high CaO and Sr contents, together with high incompatible element abundances. They may also have been produced from metasomatized mantle but melting seems to have occurred in CO_2-rich, H_2O-poor environments.

In the following discussion, the geochemical characteristics of Sunda-Banda IAB are compared with those of continental lamproites (CL), rather than with rift types, because IAB and CL seem to share the additional characteristic of H_2O-rich melting environments.

In the past, geochemical comparisons between IAB and OIB have been based on only a few geochemical ratios. IAB and CL are compared here using a variety of geochemical ratios which have been chosen to compare compositional variation between and within the K-group, rare earth and Ti-group elements. Ratios are also calculated from representative MORB and OIB (Sun 1980) for comparison.

Varne (1985) has previously noted that high 'arc-like' Ba/La and Ba/Nb values also occur in continental lamproites from the West Kimberley region of northwestern Australia.

4.3.1 Selection of Data

(a) Island arc basalts

The mean and standard deviations of the selected geochemical ratios in the medium- and high-K Sunda-Banda mafic rocks (as defined previously) are given in Table 2.3. Because

	SUNDA-BANDA			KIMBERLY & GAUSSBERG			MORB	OIB		
	mean	std dev	N	mean	std dev	N	Sun '80	Sun '80	M&H '83	Gill '84
K/Rb	412.4	98.6	99	224	108	24	1060	436	479	400
K/Nb	2430	886	61	716	383	24	342	181	-	-
Sr/Rb	20.11	8.78	99	4.09	1.74	24	124	36.4	29.2	-
K/Ce	410	122	44	221	81.6	24	118	133	-	-
Ti/Zr	76.5	20.6	99	25.3	4.58	24	109	90.9	-	-
K/Ba	33.6	9.13	55	11.7	6.39	24	88.3	25.3	30.0	-
Zr/Rb	3.66	1.28	99	2.84	1.02	24	85.0	10.0	-	10
P/Ce	46.3	14.5	44	15.3	4.69	24	66.7	38.3	-	-
Sr/La	36.0	11.9	46	6.28	2.40	24	41.3	22.9	18.7	-
Ba/La	24.8	7.02	44	34.6	17.2	24	4.00	10.9	10.2	12
K/P	8.95	1.20	99	14.6	4.10	24	1.77	3.48	-	-
Ce/Nd	1.50	0.42	44	0.00	0.00	1	1.17	2.06	-	-
K/Sc	355	159	85	3017	1449	7	37.9	320	-	-
Zr/Sc	2.94	1.18	85	56.4	37.4	7	3.04	7.33	-	-
Zr/Y	3.66	0.85	99	65.2	28.2	24	2.93	7.33	-	6.7

Table 2.3 Values of selected geochemical ratios in IAB (Sunda-Banda), CL (Kimberly & Gaussberg), OIB and MORB.

these rocks possess relatively undifferentiated major element compositions, values of ratios involving incompatible elements in these rocks are unlikely to have been substantially changed from those of their parental magmas by crystal-liquid fractionation processes. These values will closely approximate those of the mantle sources of the arc magmas if the residual mineralogy after melting comprised only olivine and pyroxenes.

In order to show that the geochemical comparison has application to volcanic arc basalts in general, ratio values have also been calculated from the average compositions of basalts (< 52 wt % SiO_2) from northwest and southwest Pacific island arcs determined by Ewart (1982). These values are closely similar to those from the Sunda-Banda volcanics (Fig. 2.28).

(b) Continental lamproites

The continental lamproites rocks used here, also with SiO_2 < 53 wt % and $100Mg/(Mg+Fe_t)$ > 40, are from Miocene lamproites, some diamond-bearing, from the West Kimberley region of northwestern Australia (Jaques et al. 1984) and leucitites from the extinct Late Pleistocene Gaussberg volcano, located at the eastern edge of Antarctica (Sheraton & Cundari 1980). These two suites are regarded by Foley et al. (1986) as the standard members of the continental lamproite type. Foley et al. (1986) and Nelson et al. (1986) have already noted that some lamproites possess geochemical characteristics which are transitional towards those of orogenic ultrapotassic rocks.

The Gaussberg and West Kimberly rocks both occur close to continental margins formed by Mesozoic rifting (Powell & Luyendyk 1982) and neither locality is known to have been associated with Phanerozoic subduction zones. Assimilation of continental crust during magma ascent is considered not to have contributed significantly to the chemical and isotopic compositions of these rocks (McCulloch et al. 1983; Collerson & McCulloch 1983). Average ratio values from these rocks are listed in Table 3.

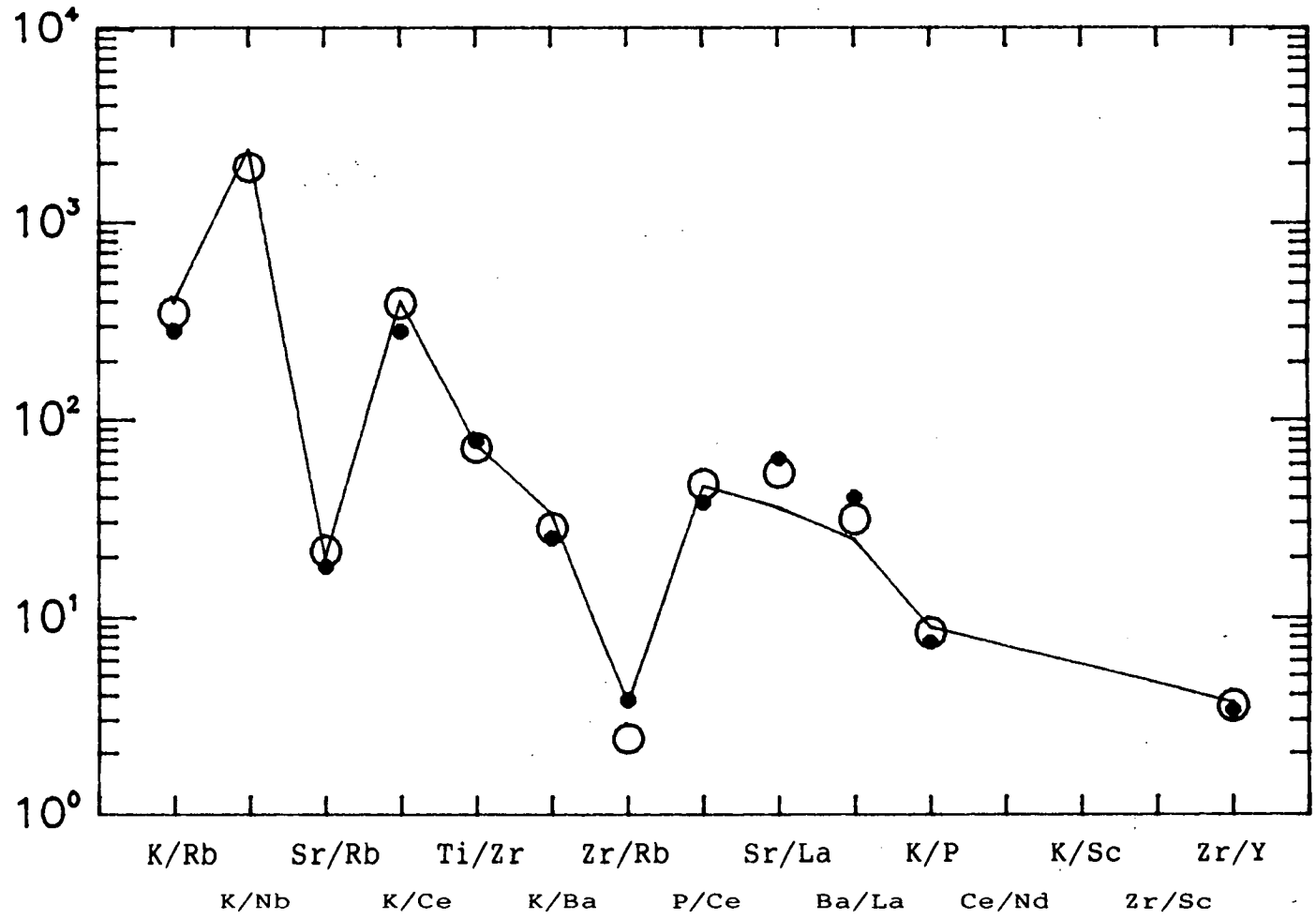

Figure 2.28 Geochemical ratio plot of volcanic rocks from Pacific island arc basalts (< 52 % SiO_2; data from Ewart (1982); open circles = southwest Pacific; dots = northwest Pacific), compared to the average of the medium- and high-K series from the Sunda-Banda arc (line).

(c) Oceanic basalts

Geochemical ratios were calculated for 'N-type' mid-ocean ridge (MORB) and oceanic island basalts (OIB) using the representative analyses of these rock types given by Sun (1980). Results are given in Table 2.3. The estimates by Morris and Hart (1983) and Gill (1984) of some of these ratios in OIB are also given for comparison with those calculated from Sun's OIB data. There are no pronounced differences between these sets of data.

4.3.2 Geochemical Comparison Between IAB and CL

The broad geochemical similarity between CL and Sunda-Banda IAB is seen in Figure 2.29, in which the Gaussberg leucitites are compared to medium-K and leucititic mafic rocks from Batur (postcaldera) and Batu Tara volcanoes respectively. Note that the 'arc signature' of Nb depletion relative to K and La is present in the Gaussberg pattern as well as in those from the Sunda arc rocks.

In more detail, OIB, IAB and CL all show patterns in Figure 2.30 that are broadly similar to each other. Neither CL nor OIB resemble MORB, and IAB resembles MORB only in a few ratios, mainly those involving Ti-group elements.

For all ratios plotted to the left of and including Sr/La, IAB shows higher values than CL, but the two magma types show mutually parallel patterns. The OIB pattern, however, diverges markedly from both CL and IAB in that part of the diagram, showing lower values for some ratios and higher values for others.

For ratios lying to the right of and including Ba/La, IAB shows lower values than CL, although again the two patterns are near-parallel. The OIB pattern is distinguished from those of both IAB and CL by showing much lower Ba/La and K/P values. Note that CL shows substantially higher values for K/Sc, Zr/Sc and Zr/Y than either IAB or OIB.

The close similarities between the patterns shown by mean

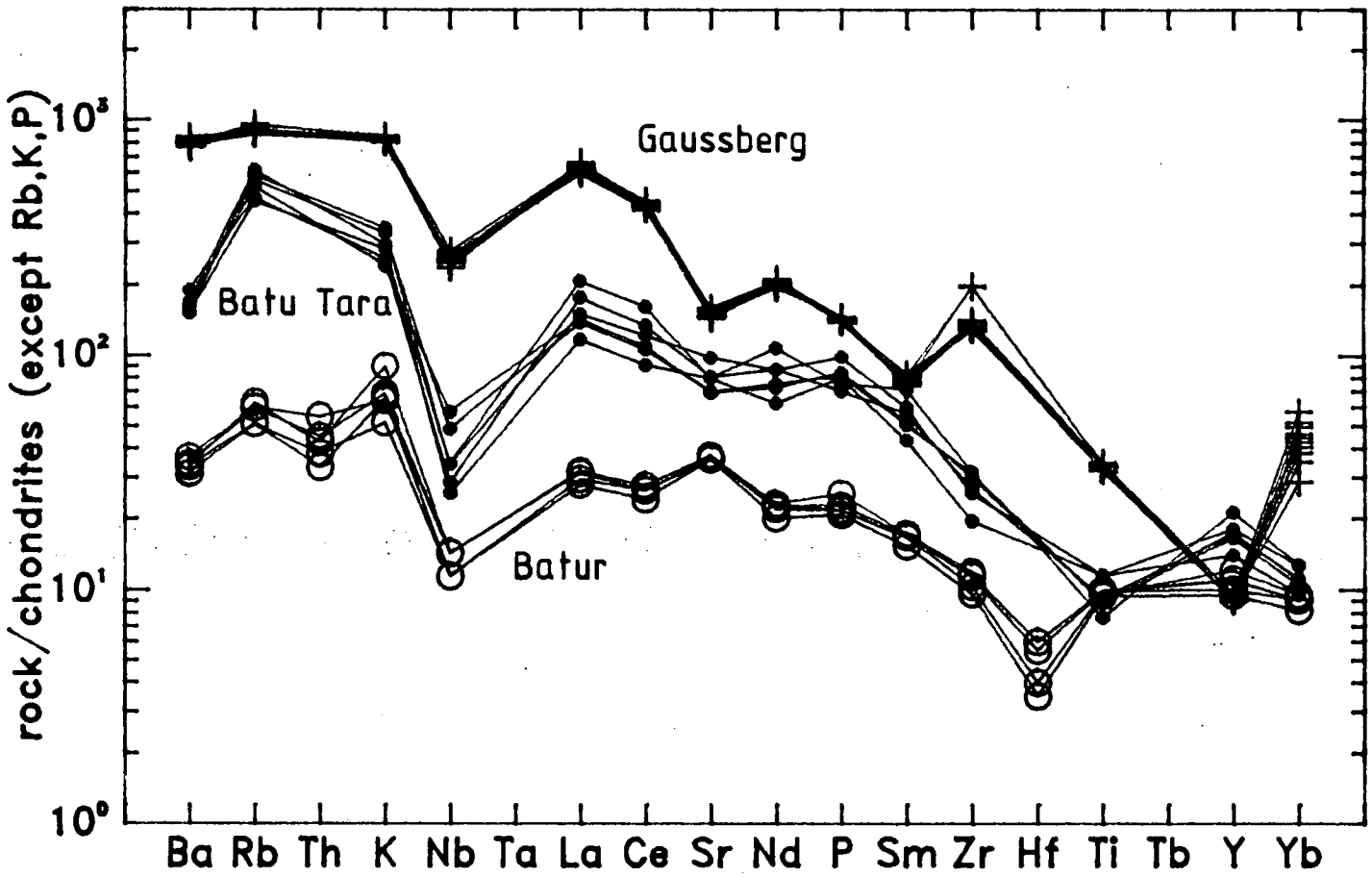

Figure 2.29 Spiderplot of basaltic volcanic rocks from Batur and Batu Tara volcanoes in the Sunda-Banda arc, and from Gaussberg volcano in Antarctica. Data sources given in text. Normalizing values from Thompson (1982).

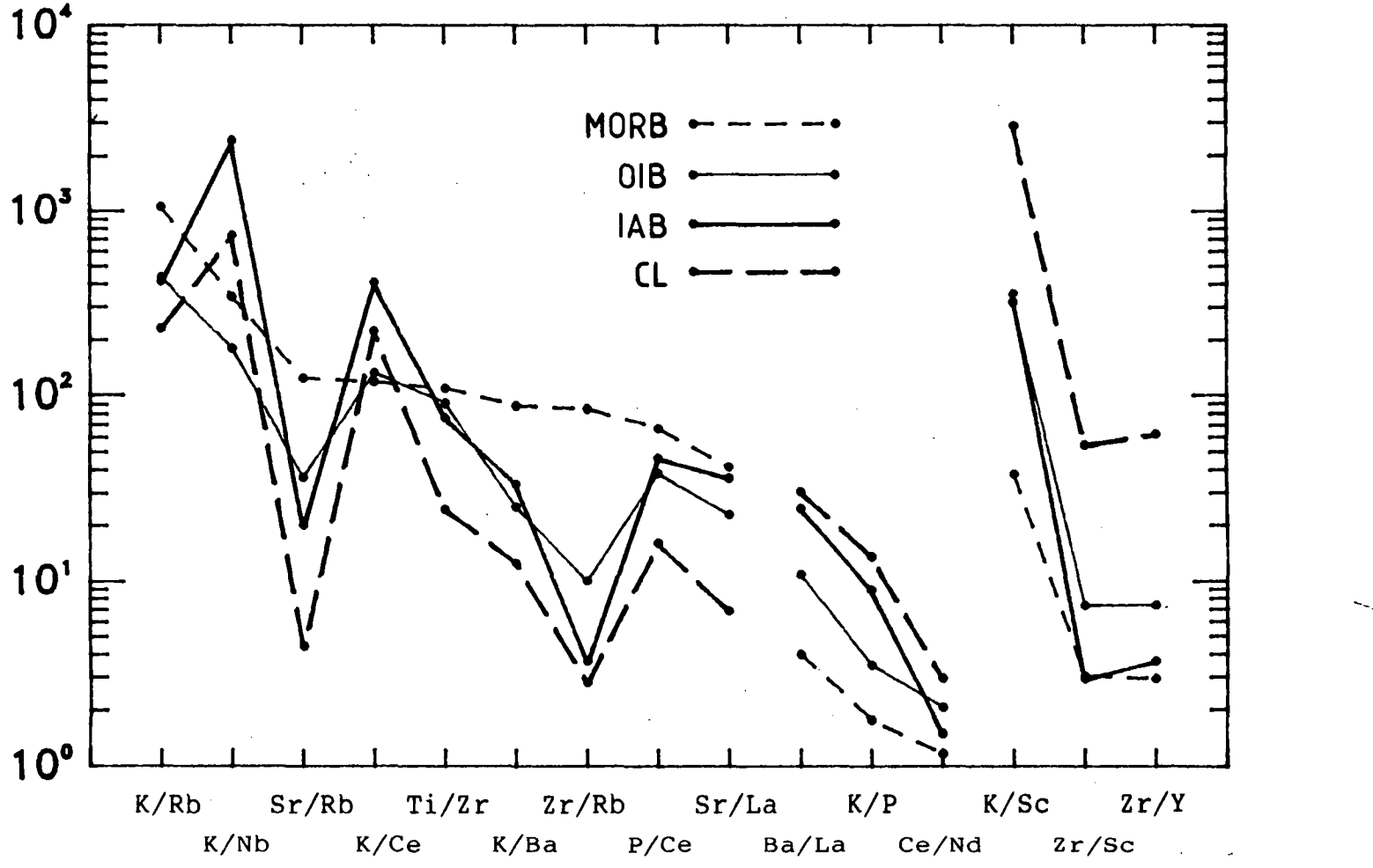

Figure 2.30 Geochemical ratio plot of representative groups of IAB, CL, MORB and OIB. Explanation given in text.

values of incompatible element ratios in IAB and CL indicate that CL and IAB, although apparently from contrasting tectonic settings, are more closely related chemically than are IAB and OIB. Therefore, the geochemistry of the arc basalts seems more consistent with derivation of those rocks from mantle sources with subcontinental, rather than OIB-source, affinities.

The cause of the vertical separation of the IAB and CL patterns in Figure 30 may be related to the possibly refractory nature of the peridotite component in the CL mantle sources (Foley et al. 1986) and to the higher absolute abundances of the incompatible elements in CL compared to the arc rocks. In particular, the high values for Zr/Sc, Zr/Y and K/Sc in CL compared with those of IAB, implies that the sources of CL yield relatively low amounts of Sc and Y. Mantle nodules in the West Kimberley lamproites are typically harzburgitic and dunitic rather than lherzolitic (Jaques et al. 1984), suggesting that their sources possess low abundances of these elements. Alternatively, the presence of residual garnet, or perovskite (Varne, in prep.), in the sources of CL may lead to depletion of Y and Sc in CL magmas.

4.4 Mechanisms of Compositional Variation in the Subarc Mantle

4.4.1 Mixing or Undepleted Mantle?

The close chemical association between the sources of island arc basalts, particularly those from the Sunda-Banda arc, and those of continental ultrapotassic rocks, as suggested by the geochemical comparison in the previous section, leads to the question of how apparently similar mantle compositions could develop beneath areas of crust possessing contrasting tectonic regimes. Hypotheses that attempt to explain compositional variation in the mantle, other than effects due to residual minerals during melting, appeal mainly to three scenarios: 1) a 2-layer mantle, in which plumes of material from an undepleted 'chondritic' (or 'primordial') lower mantle mix with chemically depleted upper mantle, 2) mantle metasomatism, involving a chemically enriched fluid-melt component which infiltrates peridotitic mantle material, and 3) injection into the mantle, by subduction, of crustal material.

Given that K-variation in the Sunda-Banda arc basalts is unlikely to have been primarily due to recent subduction of crustal material, only involvment of either undepleted mantle or a metasomatic component seem to be possible explanations.

The existence of undepleted mantle reservoirs beneath the Sunda-Banda arc is supported firstly by the Sr and Nd isotopic compositions of K-rich lavas in the Bali arc sector, which lie close to those expected of a 'bulk earth' chondritic reservoir (Fig. 2.16a), and secondly by the progressive eastwards K-enrichment of the arc lavas towards the leucititic volcanoes in three arc sectors (Fig. 2.23). Although substantially more pronounced, this pattern is similar to regional geochemical gradients associated with some 'hot spot' volcanic provinces (e.g. Schilling 1973).

Alternatively, the Sunda-Banda arc K gradients, including the lack of gradients east of the leucitite volcanoes, may be better explained by the existence of a mobile metasomatic component, as envisaged by Foden and Varne (1980,1981). The progressive K-enrichment of the arc volcanics towards the leucititic volcanoes in the West Java, Bali and Flores arc sectors suggests that the sources of those volcanoes represent, or overlie, point sources of the metasomatic agent which subsequently moved westwards, with progressively decreasing effect, along each of these arc sectors.

The westerly direction taken by the metasomatic agent from each point source may be due to regional compressive shear stress produced by north-northeast plate convergence. In addition, the well-known K-h relationship shown by the arc volcanics in the West Java sector, in particular, indicates that the effect of the K-rich component also decreases upwards, indicating that its source lies at deep levels in the mantle.

The compositional characteristics of basalts generally, particularly ultrapotassic rocks, are widely thought to be largely due to mixing in their mantle source regions of 'depleted' and 'enriched' components. Evidence for mixing generally includes the occurrence of veined peridotite

nodules (e.g. Lloyd & Bailey 1975), as well as the differences between the observed abundances of some trace elements in basalts and their expected concentrations calculated using inferred degrees of melting and assumed source compositions (e.g. Frey et al. 1978). The apparently contradictory relationship between measured positive ε_{Nd} values, indicating long-lived source LREE depletion, and measured LREE enrichment in many basalts that are thought to be produced by relatively high degrees of melting is also important evidence for mixing (DePaolo & Wasserburg 1976).

Most of the Sunda-Banda basalts show positive ε_{Nd} values (Fig. 2.16a) and all show some degree of LREE enrichment (Fig. 2.8), indicating that if most of the Sunda-Banda arc basalts were produced by moderate to high degrees of melting (5-25 %) then their sources must have comprised a mixture of at least two geochemically and isotopically distinct components. This conclusion is consistent with the positive correlations shown previously between geochemical and isotopic parameters in rocks from the Bali arc sector (Figs 2.19, 2.20, 2.25, 2.26, 2.27).

It is interesting to note that some authors have recently raised the question of whether many, or even all, mantle-derived magmas are produced by very small degrees of melting. For example, Thompson et al. (1984) have shown how all mantle-derived magmas could be produced by repeated episodes of very small degrees of melting of an initially chemically homogeneous mantle. Their melting model is consistent with the suggestion of Allegre and Condomines (1982) that small degrees of melting are required to explain the U-Th isotopic disequilibrium they observed in oceanic basalts.

Low degrees of melting would explain the enigmatic relationship between measured positive ε_{Nd} values and LREE enrichment by preferential partitioning of HREE into residual minerals. This explanation would remove a strong argument for source metasomatism. In that case, K-variation in the Sunda-Banda arc volcanics would probably be interpreted as indicating the existence of long-lived subarc mantle sources that have been variably depleted from an initially approximately 'chondritic' composition.

4.4.2 Mixing Model

The concept of mixing between distinct mantle materials is commonly invoked by geochemists to help explain mantle compositional variations (e.g. Kay 1980; Stern & Ito 1983; McCulloch et al. 1983). Previous discussion has shown that the geochemical and isotopic variation displayed by basaltic Sunda-Banda arc rocks implies that peridotite mantle, continental sialic crust and a mantle-derived K-rich component could all have been involved in magmagenesis. The process by which these components may have mixed together to form the range of magma sources observed in the Sunda-Banda arc can be illustrated using a simple 3-component mathematical mixing model following the adoption of plausible Nd and Sr isotopic compositions and concentrations for each of the three components. In addition to conveniently illustrating how the source compositional variation may have occurred this technique also provides an estimate of the relative proportions of the components in the magma sources.

Ideally, the isotopic and chemical compositions of the endmembers should be obtained by direct measurement. In particular, the composition of the mantle peridotite component could be obtained from ultramafic xenoliths, the crustal component from oceanic sediments lying south of the Sunda trench, and the K-rich component, perhaps, from material forming amphibole- or phlogopite-rich veins in ultramafic xenoliths. However, at present, no suitable xenoliths are known from the Sunda-Banda arc volcanics and only reconnaisance analyses of oceanic sediments have been made. Suitable estimates must therefore be obtained indirectly. Values adopted for the mixing calculations are listed in Table 2.4 and their derivation is discussed below.

The composition of the LILE-depleted (high $^{143}Nd/^{144}Nd$ and low $^{87}Sr/^{86}Sr$), MORB-source, periditotite component could be estimated using data obtained from least-fractionated oceanic spreading ridge basalts lying close to the arc instead of ultramafic xenoliths. However, in the northern part of the Indian Ocean, there are wide areas where LILE-enriched alkaline and ferrotholeiites occur, possibly due to hotspot volcanism

Component		Nd	ppm Nd	$^{87}Sr/^{86}Sr$	ppm Sr
MORB-mantle	(A)	+7.4	0.83	0.703	15.2
crust	(B)	-15	26	0.72	350
K-rich	(C)	-4	6	0.7058	55

Table 2.4 Sr and Nd concentrations and isotopic compositions of the postulated three components used in mixing model calculations.

associated with the Ninetyeast Ridge and nearby oceanic island volcanoes (Frey et al., 1977). These sample are unsuitable because of their LILE-rich character. LILE-depleted spreading ridge basalts have only been sampled from close to the Sunda-Banda arc in DSDP drillholes 213 and 261 but, although their Sr and Nd concentrations have been measured, these basalts are substantially fractionated and there are only two Sr isotope analyses available (Frey et al. 1977; Whitford 1975a).

To overcome this problem, the composition of the peridotite mantle component was estimated using the most LILE-depleted and relatively primitive oceanic ridge basalt yet sampled from the Indian Ocean, sample A56-27 dredged from the Southwest Indian Ridge by Le Roex et al. (1983). To obtain the an estimate of the Sr and Nd concentrations of the mantle source of this rock a simple melting model was assumed in which A56-27 was produced by 20 % modal batch partial melting of peridotite in which the crystal-liquid partition coefficients of Sr and Nd were essentially zero. The Sr and Nd isotopic compositions adopted are values which lie within the range of the most isotopically 'depleted' MORB from the East and Southwest Indian Ridges (Hamelin & Allegre 1985; Hamelin et al. 1986).

The chemical and isotopic characteristics of the 'K-rich' component are to a large extent speculative and model-dependent. A component of this type is thought to cause geochemical enrichment in the sources of many K-rich continental magmas such as lamproites, in particular, and is usually envisaged as a silicate melt or volatile-rich 'fluid' phase (e.g. Lloyd & Bailey 1975; Bailey 1982; Roden & Murthy 1985). Varne and Graham (1971) and Frey et al. (1978) have suggested that a kimberlite-, olivine melilitite- or basanite-type partial melt (the 'trickle' OIB-type magmatism of Thompson et al. 1984), derived by low degrees of melting in the low velocity zone, may be responsible for widespread enrichment of the upper mantle.

However, it is difficult to constrain the isotopic and chemical composition of the K-rich component that may be involved in the Sunda-Banda subarc mantle. One approach may involve using the extreme Sr and Nd characteristics of the northwestern Australian subcontinental mantle, which is thought to have been produced by mixing between peridotitic mantle and an 'enriched mantle', or LILE-rich, component more than 1,000 Ma ago (McCulloch et al. 1983). This approach was used by Varne (1985) to help explain the cause of compositional variation in the sources of eastern Sunda arc K-rich basalts. Varne (1985) noted the general increase in K contents of the arc volcanics towards the collision zone and postulated that there the northwestern Australian subcontinental mantle may have mixed with the subarc mantle and subducted oceanic slab to form the arc magma sources.

Alternatively, the composition of the K-rich component can be modelled hypothetically using Sr and Nd isotope compositions more similar to those of the most 'enriched' volcanics from the Bali sector of the arc. Suitable isotopic compositions exist in the Indian Ocean in the sources of the Tertiary oceanic island basalts of Iles Kerguelen (Dosso and Murthy 1980). For modelling purposes, the Sr and Nd isotopic compositions of the K-rich component are taken to lie within the range shown by the most 'enriched' Kerguelen basalts and which lead to a mixing model which encompasses all of the

variation shown by the arc volcanics. Pb isotopic compositions of the Kerguelen basalts differ from those of the arc basalts (Fig. 2.18) and therefore involvement of a Kerguelen-type K-rich component in the subarc mantle cannot be invoked directly.

As a substitute for the lack of geochemical information about the K-rich mantle metasomatic component, the composition of an highly alkaline primitive basanite is taken as a guide. The particular composition chosen is that of a basanite from Mt Shadwell in western Victoria (Frey et al. 1978). This rock is comprehensively analysed, particularly for Sr and Nd concentrations, and its high Mg-number (71.4) and Ni (342 ppm) and Cr (310 ppm) concentrations indicate that it is a primary mantle-derived magma.

Estimating the composition of the crustal component is also difficult. DSDP reports indicate the existence of a wide range of lithologies and probable ages of sediments south of the Sunda trench, and the meagre geochemical data shows that the sediments also vary widely in their compositions. Sediments of highly variable lithology in DSDP Holes 260, 261 and 262 in the eastern Indian Ocean were analysed for major and some trace elements by Cook (1974). Sr concentrations in those materials vary widely in from < 100 to > 1500 ppm. There are no isotopic data available.

To overcome this absence of data from northern Indian Ocean seafloor sediments, Nd and Sr isotopic compositions of the sedimentary component are taken from those of a Triassic shale from the Timor Trough and analysed by McCulloch et al. (1983). These authors considered that this material possessed the isotopic characteristics which when mixed with subarc peridotite explained the wide variation in isotopic compositions observed in some Banda arc volcanics. These extreme $^{87}Sr/^{86}Sr$ and $^{143}Nd/^{144}Nd$ values, which are probably due to the provenance of the sediment from ancient Australian continental crust to the south, are substantially outside the range shown by the arc basalts and are likely also to represent an end-member composition among northern Indian Ocean sediments generally.

The average Sr and Nd concentrations of any sedimentary material carried down by the slab into the magma source regions is approximated using the composition of average upper continental crust determined by Taylor and McClennan (1985). This yields Sr and Nd abundances of 350 and 26 ppm respectively.

Fig. 2.31 shows a grid based on the $_{Nd}$-$^{87}Sr/^{86}Sr$ diagram obtained from mixing the three components, MORB-type peridotite, an hypothetical K-rich component, and a crustal component, that are thought to have been involved in producing the source regions of the arc magmas. The grid completely encloses the range of isotopic compositions observed in the Sunda-Banda arc, indicating that the variation may be explained by a process involving mixing of these three components in the subarc mantle. Any variations in the compositions of the end-member components, which is likely given the length and variable geological and structural nature of the Sunda-Banda arc, will of course ead to changes in the proportions of the components. The possible extent of these changes is not thought likely to significantly alter the general conclusions derived from this mixing model.

The grid shows that the Sr and Nd isotopic variation shown by the low-K to leucitic basaltic rocks from the Bali sector of the Sunda-Banda arc may be explained by addition of up to 20-30 % of the K-rich component to peridotitic mantle. In these rocks the amount of crustal material could be much less than 1 % and therefore negligible. Rocks from the West Java sector show similar characteristics except for two low-K samples which appear to have been contaminated by slightly higher amounts of crustal material.

The three analysed samples from the Flores sector, from low-K Ija volcano and leucititic Batu Tara volcano, also appear to have been affected by addition of 0.5 to 1.5 % crustal material to their source regions. The compositions of the two Batu Tara samples also imply a marked degree of source heterogeneity beneath this volcano. These two samples could require about 15-20 % and 40-50 % respectively of the K-rich

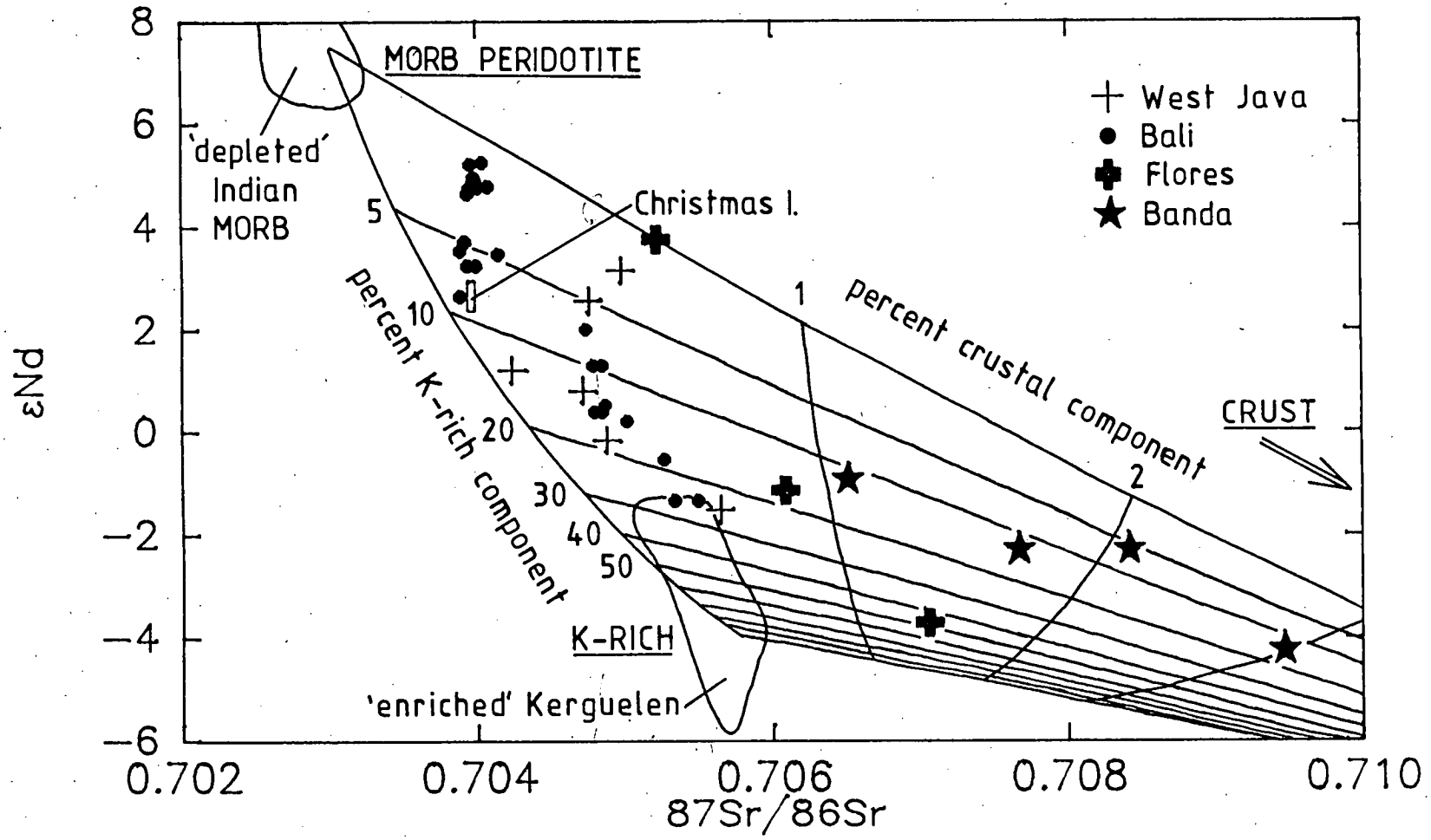

Figure 2.31 Three-component source mixing grid for Sunda-Banda arc basaltic volcanics based on Nd and Sr isotopic compositions. End-member compositions given in Table 2.4.

component in their respective sources.

The samples from the Banda sector of the arc show the highest proportions of crustal material in their mantle sources, ranging between about 1 and 3 %. However, consistent with their medium- to high-K character, only about 5-15 % of the K-rich component appears to have been involved in their sources.

Also, it is interesting to note that the isotopic composition of Tertiary oceanic island basalts from Christmas Island, about 600 km south of Java and south of the Sunda Trench, can also be explained by mixing of 8-10 % of the K-rich component with 'depleted' Indian peridotitic mantle, and with no involvement of crustal material. The Pb isotopic compositions of the Christmas Island basalts also lie very close to the range shown by the Bali sector arc basalts (Fig. 2.18).

It is notable that the results of these mixing calculations are consistent with the qualitative relationships between samples from each of the arc sectors shown in Fig. 2.24, in which Sr isotopic compositions are related to K contents, and in previous discussion of the isotopic characteristics generally of the Sunda-Banda arc volcanics. In particular, the basaltic rocks from the Bali sector of the arc appear to have been least affected by contamination by crustal material, while those from the Banda sector may have had up to 3 % crustal material added to their sources. Rocks from the West Java and Flores sectors show intermediate character, with at least some rocks showing small degrees of involvement of material derived from the upper crust.

In summary, the mixing calculations show that the entire Sr and Nd isotopic variation of the Sunda-Banda arc basalts, and by inference the geochemical variation, can be satisfactorily explained primarily by mixing between 'depleted' MORB-type peridotitic mantle and an hypothetical 'enriched' K-rich component. Mixing of a third component, upper crustal material, also occurs to varying extents along the arc but only in small amounts. The nature of the K-rich component is at this stage

speculative except for its Sr and Nd isotopic compositions which are similar to those of the most isotopically 'enriched' Kerguelen basalts.

4.5 Arc Evolution and K-Variation in Arc Volcanics

Varne (1985) has argued that involvement of crustal material is unlikely to have been a significant influence on the geochemistry of K-rich magmas in the eastern Sunda arc, and has proposed a model involving mechanical mixing of ancient, K-rich subcontinental mantle, derived from beneath either the Proterozoic northwestern Australian continental crust or the 'Gondwanaland' continental fragments lying close to the arc, with subarc oceanic mantle to account for the chemical and isotopic characteristics of the arc volcanic rocks. The demonstration here of strong geochemical similarities between continental lamproites and Sunda-Banda island arc basalts supports Varne's interpretation.

However, this particular mechanism for involving subcontinental mantle does not readily explain the K_{Si}-longitude relationships observed along the Sunda-Banda arc, and cannot easily be applied to the genesis of island arc volcanic rocks that are erupted in regions which are not spatially associated with ancient subcontinental lithosphere. An alternative mechanism involves progressive metasomatic enrichment of the Sunda-Banda subarc mantle as part of the process of regional development of Southeast Asian continental crust and lithosphere by volcanism and by accretion of island arc and microcontinental terranes.

Although there is much regional variability, regional heat flows of island arcs appear to correlate negatively with ages of the backarc crusts (e.g. Figure 3.1 of Gill 1981), which suggests that a similar correlation may exist between regional heat flow and arc maturity. If mantle metasomatism is a continuous process (Bailey 1982) then the degrees of enrichment of subarc mantles may, therefore, be expected to generally increase as regional heat flows decrease and arc crusts thicken by accretion and volcanism. In that case, Lloyd and Bailey's (1975) suggestion that low regional geothermal gradients

promote the formation of K-rich mantle sources by permitting crystallization of phlogopite at high pressure could be applied to the enrichment of subarc mantles.

Melting of those mantle source regions, triggered perhaps either by the influx of the metasomatic agent itself or by volatile dehydration of the subducted slab, would lead to progressively more K-rich magmas with arc evolution. In this way, young arcs (for example, South Sandwich (Baker 1978) and Banda) would be characterized by the presence of K-poor arc volcanics (particularly arc tholeiites) whereas relatively old arcs, such as Sunda, would produce more K-rich volcanic rocks. The apparent westwards decrease in volcanic intensity in three of the Sunda-Banda arc sectors, together with the decreases in K-enrichment of the arc lavas, suggests that the abundance of the metasomatic agent in the arc magma sources is a major factor in melting potential.

The amount of subarc mantle enrichment may also be expected to be high in regions of tectonic complexity, particularly those in which subduction has occurred previously. The geological evolution of the Sunda arc, for example, appears to have involved several periods of subduction which, notably, were apparently aligned obliquely to the present subduction system. This previous history may have led to substantial, across-arc structural heterogeneties in the Sunda subarc mantle, possibly associated with the old subducted slabs, which may have provided pathways by which metasomatic material moved into the basalt sources (cf Foden & Varne 1980,1981). Given that the subduction-related processes which produced them are no longer active, it is unlikely that these heterogeneities would be reflected by major surface fractures.

5. SUMMARY AND CONCLUSIONS

Volcanic rocks produced during Quaternary subduction along the Sunda-Banda island arc range continuously in composition from low-K to leucititic types, the widest compositional span of mafic volcanism known from an active arc setting.

Including new analyses of volcanic rocks from twelve

Quaternary volcanoes from the previously little-known Flores-Lembata arc sector and from seven Quaternary Balinese volcanoes, these rocks are characterized by low TiO_2 (< 1.5 %) and high Al_2O_3 (generally 16-22 %) contents. The variation from tholeiite to leucitite is accompanied by marked increases in K_2O and 'incompatible' element abundances, but little variation in Na_2O contents.

All show the depletion of Nb relative to K and La that is typical of arc volcanics and a geochemical continuum exists between the low-K tholeiitic and high-K leucititic rocks. The abundances of P, Ba, Rb, Sr, La, Ce, Nd, Zr and Nb in mafic rocks increase sympathetically with increasing K_2O contents, but those of Na, Ti, Y and Sc vary little, if at all.

Excluding Sumatra and Wetar, which possess mainly dacitic and ryholitic volcanics, the Sunda-Banda arc is divisible into four geochemical arc sectors, based on the inferred K contents of the primary magmas at each volcano, characterized numerically by K_{Si} values. Each of these sectors named here the West Java, Bali, Flores and Banda sectors, possess boundaries that correlate broadly with major changes in regional tectonic setting and geological history.

From west to east, the West Java, Bali and Flores sectors are characterized by the presence at their western ends of short arc segments of low volcanic intensity, which pass eastwards into progressively more K-rich volcanism that culminates at the leucite-bearing volcanoes Muriah (West Java), Sangenges and Soromundi (Bali) and Batu Tara (Flores). The Banda sector is separated from the eastern part of the Flores sector by the volcanically extinct Wetar segment which lies at the core of the collision zone between the Australian continent and the Sunda-Banda island arc. The volcanic rocks of the Banda sector are, in general, less K-rich than those of the other arc sectors but they also show a progressive longitudinal variation, with K contents decreasing eastwards.

Correlations between geochemistry and $^{87}Sr/^{86}Sr$ values show separate trends for each of the four sectors, and which are inferred to reflect variations in mantle source

compositions. These correlations indicate that the cause of compositional variation among the arc volcanics could be due to mixing of three components.

The dominant component, common to all sectors, has $^{87}Sr/^{86}Sr < 0.7038$ and $\varepsilon_{Nd} > +6$, and is isotopically similar to the sources of Indian Ocean MORB. A second component appears to be crustal material, with generally high $^{87}Sr/^{86}Sr$ and ^{207}Pb, and negative ε_{Nd} values, low K_2O and 'incompatible' element abundances, and high $\delta^{18}O$ values.

The crustal component is most apparent in the Banda sector volcanics, where its relative abundance is probably due in some way to the collision with the Australian continent. It is also present in volcanic rocks from the West Java sector, possibly because of the thickness of the West Java continental crust, and in rocks from the Flores sector, which lies close to the collision zone. The Bali sector is the sector least associated with continental crust and its volcanic rocks show no evidence of involvement with a crustal component.

However, the geochemical variation shown by the arc volcanics appears to be primarily due to involvement of variable amounts of the the third component, which is rich in K and other incompatible elements but which possesses Sr and Nd isotopic compositions approximately those of 'bulk earth'. These and other isotopic characteristics of this component, including Pb isotope compositions like those oceanic islands and low ^{18}O values, indicate that, in contrast to the generally held view, it is unlikely to be recently subducted pelagic sediments and oceanic crust or arc crust. This conclusion is supported by the very low ^{10}Be contents of some Sunda volcanics. In particular, Sr, Nd and Pb isotopic data, together with the high and regionally persistent Th/U value (about 4.3) of the Sunda subarc mantle, inferred from ^{238}U-^{230}Th isotopic data, suggests a close association exists between the K-rich component and the sources of intraplate basalts produced at some Indian oceanic islands and in southeastern Australia.

Because of a general geochemical similarity between

island arc volcanic rocks and ultrapotassic rocks from stable continental regions it is suggested that enrichment of the sources of island arc magmas occurs primarily as part of the general and continuous process of subcontinental lithosphere enrichment by metasomatic fluids or melts, and not by involvement of subducted materials, which have only an over-printing effect. In island arcs generally, the degree of geochemical and isotopic enrichment of arc volcanism is envisaged to increase with arc maturity as the subarc mantle gradually loses its ability to dilute and dissipate by convection (as measured by regional heat flow and the presence of back-arc spreading) enriching material derived from lower parts of the mantle.

In the Sunda-Banda island arc, it is speculated that the pattern of geochemically and isotopically distinctive arc sectors, and the abundance of extremely K-rich volcanic rocks, is due to the presence of deep, inactive structural hetero-geneities in the subarc mantle that have resulted from successive subduction zones from the Cretaceous to the Late Tertiary, and from the collision of the Australian continent with the modern arc. These may have permitted access of metasomatic material from deep parts of the subarc mantle into shallower regions where it was distributed westwards along the arc sectors by the regional shear stress.

REFERENCES

ABBOTT,M.J. & CHAMALAUN,F.H., 1978, New K/Ar age data for Banda arc volcanics. **Institute for Australasian Geodynamics, Flinders, University of South Australia, Publ.** 78/5.

ALDISS,D.T. & GHAZALI,S.A., 1984, The regional geology and evolution of the Toba volcano-tectonic depression, Indonesia. **J. Geol. Soc. Lond.**, 141, 487-500.

ALLEGRE,C.J. & CONDOMINES,M., 1976, Fine chronology of volcanic processes using ^{238}U-^{230}Th systematics. **Earth Planet. Sci. Lett.**, 28, 395-406.

ALLEGRE,C.J. & CONDOMINES,M., 1982, Basalt genesis and mantle structure studied through Th-isotope geochemistry. **Nature**, 299, 21-24.

ALLEGRE,C.J. & MINSTER,J.F., 1978, Quantitative models of trace elements behaviour in magmatic processes. **Earth Planet. Sci. Lett.**, 38, 1-25.

ALLEGRE,C.J., OTHMAN,D.B., POLVE,M. & RICHARD,P., 1979, The Nd-Sr isotopic correlation in mantle minerals and geodynamic consequences. **Phys. Earth Planet. Inter.**, 19, 293-306.

ALLEGRE,C.J., TREUIL,M., MINSTER,J.F., MINSTER,B. & ALBAREDE,F., 1977, Systematic use of trace element in igneous processes. Part I: fractional crystallization processes in volcanic suites. **Contrib. Mineral. Petrol.**, 60, 57-75.

ANDERSON,A.T., 1974, Evidence for a picritic, volatile-rich magma beneath Mt. Shasta, California. **J. Petrol.**, 15, 243-267.

ARCULUS,R.J., 1978, Mineralogy and petrology of Grenada, Lesser Antilles island arc. **Contrib. Mineral. Petrol.**, 65, 413-424.

ARCULUS,R.J. & JOHNSON,R.W., 1978, Criticism of generalised models for the magmatic evolution of arc-trench systems. **Earth Planet. Sci. Lett.**, 39, 118-126.

AUDLEY-CHARLES,M.G., 1975, The Sumba Fracture: a major discontinuity between eastern and western Indonesia. **Tectonophysics**, 26, 213-228.

BAILEY,D.K., 1982, Mantle metasomatism - continuing chemical change within the Earth. **Nature**, 296, 525-530.

BAKER,P.E., 1978, The South Sandwich Islands: III Petrology of the volcanic rocks. **Brit. Ant. Surv. Sci. Rep.**, 93.

BARTLETT,R.W., 1969, Magma convection, temperature distribution, and differentiation. **Amer. J. Sci.**, 267, 1067-1082.

BASALTIC VOLCANISM STUDY PROJECT, 1981, **Basaltic Volcanism on the Terrestrial Planets**, Pergamon Press, 1286 pp.

BEDDOE-STEPHENS,B., ASPDEN,J.A. & SHEPHERD,T.J., 1983, Glass inclusions and melt compositions of the Toba Tuffs, northern Sumatra. **Contrib. Mineral. Petrol.**, 83, 278-287.

BEN-AVRAHAM,Z. & EMERY,K.O., 1973, Structural framework of Sunda Shelf. **Amer. Assoc. Petrol. Geol. Bull.**, 57, 2323-2366.

BENNETT,J.T, KRISHNASWAMI,S., TUREKIAN,K.K., MELSON,W.G. & HOPSON,C.A., 1982, The uranium and thorium decay series nuclides in Mt St. Helens effusives. **Earth Planet. Sci. Lett.**, 60, 61-69.

BERRY,R.F. & McDOUGALL,I.A., 1985, Regional metamorphism in East Timor: $^{40}Ar/^{39}Ar$ and K/Ar evidence from the Aileu Formation. submitted to **Isotope Geoscience.**

BLAKE,D.H. & EWART,A., 1974, Petrology and geochemistry of the Cape Hoskins volcanoes, New Britain, Papua New Guinea. **J. Geol. Soc. Aust.**, 21, 319-331.

BOTTINGA,Y. & WEILL,D.F., 1970, Densities of liquid silicate systems calculated from partial molar volumes of oxide components. **Amer. J. Sci.**, 269, 169-182.

BOWEN,N.L., 1928, **The Evolution of the Igneous Rocks**, Princeton University Press. 332pp.

BOWIN,C., PURDY,G.M., JOHNSTON,C., SHOR,G., LAWVER,L., HARTONO, H.M.S. & JEZEK,P., 1980, Arc-continent collision in Banda Sea region. **Amer. Assoc. Petrol. Geol. Bull.**, 64, 868-915.

BROUWER,H.A., 1940, Geological and petrological investigations on alkali and calcalkali rocks of the islands Adonara, Lomblen and Batoe Tara. **Geological Expedition to the Lesser Sunda Islands**, Vol. II, Amsterdam.

BROWN,L., KLEIN,J., MIDDLETON,R., SACKS,I.S. & TERA,F., 1982, ^{10}Be in island-arc volcanoes and implications for subduction, **Nature**, 299, 718-720.

BRYAN,W.B., FINGER,L.W. & CHAYES,F., 1969, Estimating proportions in petrographic mixing equations by least squares approximation. **Science**, 163, 926-927.

CANN,J.R., 1982, Rayleigh fractionation with continuous removal of liquid. **Earth Planet. Sci. Lett.**, 60, 114-116.

CANTAGREL,J.M., ROBIN,C. & VINCENT,P., 1981, Les grandes etapes

d'evolution d'un volcan andesitique composite: example du Nevado de Toluca (Mexique). **Bull. Volcanol.**, 44, 177-188.

CAPALDI,G., CORTINI,M. & PECE,R., 1983, U and Th decay-series disequilibrium in historical lavas from the Eolian islands, Tyrrhenian Sea, **Isotop. Geosc.**, 1, 39-55.

CAPALDI,G., DEL POZZO,E., PECE,R. & SCARPA,R., 1976, Correlation of deep earthquakes, eruptive activity at Stromboli volcano and age of the radium fractionation. **J. Volcanol. Geotherm. Res.**, 1, 381-385.

CARDWELL,R.K. & ISACKS,B.L., 1978, Geometry of the subducted lithosphere beneath the Banda Sea in eastern Indonesia from seismicity and fault plane solutions. **J. Geophys. Res.**, 83, 2825-2838.

CARMICHAEL,I.S.E., 1967, The mineralogy of Thingmuli, a Tertiary volcano in eastern Iceland. **Amer. Mineral.**, 52, 1815-1841.

CARMICHAEL,I.S.E, TURNER,F.J. & VERHOOGEN,J., 1974, **Igneous Petrology**, McGraw-Hill, 739 pp.

CASTLEMAN Jr,A.W. & KEESEE,R.G., 1981, Nucleation and growth of stratospheric aerosols. **Amer. J. Sci.**, 9, 227-249.

CHAMALAUN,F.H. & GRADY,A.E., 1978, The tectonic development of Timor: a new model and its implications for petroleum exploration. **APEA Jour.**, 18, 102-108.

CHAMALAUN,F.H., LOCKWOOD,K. & WHITE,A., 1976, The Bouguer gravity field and crustal structure of eastern Timor. **Tectonophysics**, 30, 241-259.

CHASE,C.G., 1981, Oceanic island Pb: two-stage histories and mantle evolution. **Earth Planet. Sci. Lett.**, 52, 277-284.

CHEN,C.F. & TURNER,J.S., 1980, Crystallization in a double-diffusive system. **J. Geophys. Res.**, 85, 2573-2593.

CHESNER,C.A. & ROSE,W.I., 1984, Geochemistry and evolution of the Fuego volcanic complex, Guatemala. **J. Volcanol. Geotherm. Res.**, 21, 25-44.

CLAYTON,R.N. & MAYEDA,T.K., 1963, The use of bromine pentafluoride in the extraction of oxygen from oxides and silicates for isotopic analysis. **Geochim. Cosmochim. Acta**, 27, 43-52.

COLLERSON,K.D. & McCULLOCH,M.T., 1983, Nd and Sr isotope geochemistry of leucite-bearing lavas from Gaussberg, eastern Antarctica. In: Oliver,R.L., James,P.R. & Jago,J.B. (editors), **Antarctic Earth Science**, Australian Academy

of Science, 676-680.

COOK,P.J., 1974, Major and trace element geochemistry of sediments from Deep Sea Drilling Project, Leg 27, Sites 259-263, eastern Indian Ocean. In Veevers,J.J., Heirtzler, J.R. et al., **Initial Reports of the Deep Sea Drilling Project**, Vol. 27, Washington (U.S. Government Printing Office), 481-497.

COOPER,J.A. & GREEN,D.H., 1969, Lead isotope measurements on lherzolite inclusions and host basanites from western Victoria, Australia. **Earth Planet. Sci. Lett.**, 6, 69-76.

COX,K.G., BELL,J.D. & PANKHURST,R.J., 1979, **The Interpretation of Igneous Rocks**, Allen & Unwin, 450pp.

CURRAY,J.R., SHOR Jr,G.G., RAITT,R.W. & HENRY,M., 1977, Seismic refraction and reflection studies of crustal structure of the eastern Sunda and western Banda arcs. **J. Geophys. Res.**, 82, 2479-2489.

De PAOLO,D.J., 1981, Trace element and isotopic effects of combined wallrock assimilation and fractional crystallization. **Earth Planet. Sci. Lett.**, 53, 189-202.

De PAOLO,D.J. & JOHNSON,R.W., 1979, Magma genesis in the New Britain island-arc: constraints from nd and Sr isotopes and trace element patterns. **Contrib. Mineral. Petrol.**, 70, 367-379.

De PAOLO,D.J. & WASSERBURG,G.J., 1976, Inferences about magma sources and mantle structure from variations of $^{143}Nd/^{144}Nd$. **Geophys. Res. Lett.**, 3, 743-746.

De PAOLO,D.J. & WASSERBURG,G.J., 1977, The sources of island arcs as indicated by Nd and Sr isotopic studies. **Geophys. Res. Lett.**, 4, 465-468.

DICK,H.J.B. & BULLEN,T., 1984, Chromium spinel as a petrogenetic indicator in abyssal and alpine-type peridotites and spatially associated lavas. **Contrib. Mineral. Petrol.**, 86, 54-76.

DIXON,T.H. & BATIZA,R., 1979, Petrology and chemistry of recent lavas in the northern Marianas: implications for the origin of island arc basalts. **Contrib. Mineral. Petrol.**, 70, 167-181.

DOSSO,L. & MURTHY,V.R., 1980, A Nd isotopic study of the Kerguelen Islands: inferences on enriched oceanic mantle sources. **Earth Planet. Sci. Lett.**, 48, 268-276.

DOSSO,L., VIDAL,P., CANTAGREL,J.M., LAMEYRE,J., MAROT,A. &

ZIMINE,S., 1979, "Kerguelen: continental fragment or oceanic island?": petrology and isotopic geochemistry evidence. **Earth Planet. Sci. Lett.**, 43, 46-60.

DOUTHITT,C. & DIXON,T., 1981, Oxygen and strontium isotopic ratio of volcanic rocks from the Mariana island arc (abstract). **Eos**, 62, 1091.

DUPRE,B. & ALLEGRE,C.J., 1983, Pb-Sr isotope variation in Indian Ocean basalts and mixing phenomena. **Nature**, 303, 142-146.

DUPUY,C., DOSTAL,J. & TRAINEAU,H., 1985, Geochemistry of volcanic rocks from Mt Pelee, Martinique. **J. Volcanol. Geotherm. Res.**, 26, 147-165.

EICHELBERGER,J.C., 1975, Origin of andesite and dacite: evidence of mixing at Glass Mountain and at other circum-Pacific volcanoes. **Geol. Soc. Amer. Bull.**, 86, 1381-1391.

EWART,A., 1979, A review of the mineralogy and chemistry of Tertiary-Recent dacitic, latitic, rhyolitic, and related salic volcanic rocks. In: Barker,F. (editor), **Trondhjemites, Dacites and Related Rocks**, Elsevier, 13-121.

EWART,A., 1982, The mineralogy and petrology of Tertiary-Recent orogenic volcanic rocks: with special reference to the andesite-basaltic compositional range. In: Thorpe,R.S. (editor), **Andesites: Orogenic Andesites and Related Rocks**, Wiley, 25-95.

FERRARA,G., LAURENZI,M.A., TAYLOR,H.P.Jr, TONARINI,S. & TURI,B., 1985, Oxygen and strontium isotope studies of K-rich volcanic rocks from the Alban Hills, Italy. **Earth Planet. Sci. Lett.**, 75, 13-28.

FITCH,T.J., 1970, Earthquake mechanisms and island arc tectonics in the Indonesian-Philippine region. **Bull. Seismol. Soc. Amer.**, 60, 565-591.

FITCH,T.J. & MOLNAR,P., 1970, Focal mechanisms along inclined earthquake zones in the Indonesian-Philippine region. **J. Geophys. Res.**, 75, 1431-1444.

FODEN,J.D., 1979, The petrology of some young volcanic rocks from Lombok and Sumbawa, Lesser Sunda Islands. unpubl. Ph.D. thesis, University of Tasmania.

FODEN,J.D., 1983, The petrology of the calcalkaline lavas of Rindjani volcano, east Sunda arc: a model for island arc petrogenesis. **J. Petrol.**, 24, 98-130.

FODEN,J.D., 1986, The petrology of Tambora volcano, Indonesia: a model for the 1815 eruption. **J. Volcanol. Geotherm. Res.**, 27, 1-41.

FODEN,J.D. & VARNE,R., 1980, The petrology and tectonic setting of Quaternary-Recent volcanic centres of Lombok and Sumbawa, Sunda arc. **Chem. Geol.**, 30, 201-226.

FODEN,J.D. & VARNE,R., 1981, Petrogenetic and tectonic implications of near coeval calcalkaline to highly alkaline volcanism on Lombok and Sumbawa islands in the eastern Sunda arc. In: The Geology and Tectonics of Eastern Indonesia, **Geol. Res. Develop. Centre Spec. Publ.**, 2, 135-152.

FOLEY,S.F., VENTURELLI,G., GREEN,D.H. & TOSCANI,L., 1986, The ultrapotassic rocks: characteristics, classification, and constraints for petrogenetic models. submitted to **Earth Science Reviews.**

FRANCIS,P.W., MOORBATH,S. & THORPE,R.S., 1977, Strontium isotope data for recent andesites in Ecuador and North Chile. **Earth Planet. Sci. Lett.**, 37, 197-202.

FREY,F.A., GREEN,D.H. & ROY,S.D., 1978, Integrated models of basalt petrogenesis: a study of quartz tholeiites to olivine melilitites from south eastern Australia utilizing geochemical and experimental petrological data. **J. Petrol.**, 19, 463-513.

GAST,P.W., 1968, Trace element fractionation and the origin of tholeiitic and alkaline magma types. **Geochim. Cosmochim. Acta**, 32, 1057-1086.

GILL,J.B., 1981, **Orogenic Andesites and Plate Tectonics**, Springer-Verlag, 390 pp.

GILL,J.B., 1984, Sr-Pb-Nd isotopic evidence that both MORB and OIB sources contribute to oceanic island arc magmas in Fiji. **Earth Planet. Sci. Lett.**, 68, 443-458.

GILL,J., WILLIAMS,R. & BRULAND,K., 1985, Eruption of basalt and andesite lava degasses ^{222}Rn and ^{210}Po. **Geophys. Res. Lett.**, 12, 17-20.

GREEN,D.H., 1973, Experimental melting studies on a model upper mantle composition at high pressures under water-saturated and water-undersaturated conditions. **Earth Planet. Sci. Lett.**, 19, 37-53.

GREEN,D.H. & RINGWOOD,A.E., 1967, The genesis of basaltic magmas. **Contrib. Mineral. Petrol.**, 15, 103-190.

GREEN,T.H., 1972, Crystallization of calcalkaline andesite under controlled high-pressure hydrous conditions. **Contrib. Mineral. Petrol.**, 34, 150-166.

GREEN,T.H. & RINGWOOD,A.E., 1968, Genesis of the calc-alkaline igneous rock suite. **Contrib. Mineral. Petrol.**, 65, 59-67.

GREEN,T.H. & WATSON,E.B., 1982, Crystallization of apatite in natural magmas under high pressure, hydrous conditions, with particular reference to 'orogenic' rock series. **Contrib. Mineral. Petrol.**, 79, 96-105.

GRIFFIN,B.J., 1979, Energy dispersive analysis system calibration and operation with TAS-SUEDS, and advanced interactive data-reduction package. **University of Tasmania, Department of Geology Publication.**

GROVE,T.L. & BAKER, M.B., 1984, Phase equilibrium controls on the tholeiitic versus calc-alkaline differentiation trends. **J. Geophys. Res.**, 89, 3253-3274.

HAMELIN,B. & ALLEGRE,C.J., 1985, Large-scale regional units in the depleted upper mantle revealed by an isotope study of the South-West Indian Ridge. **Nature**, 315, 196-199.

HAMELIN,B., DUPRE,B. & ALLEGRE,C.J., 1986, Pb-Sr-Nd isotopic data of Indian Ocean ridges: new evidence of larfe-scale mapping of mantle heterogeneities. **Earth Planet. Sci. Lett.**, 76, 288-298.

HAMILTON,W., 1977, Subduction in the Indonesian region. In: Talwani,M. & Pitman III,W.C. (editors), **Island Arcs, Deep Sea Trenches and Back-Arc Basins**, American Geophysical Union, 15-31.

HAMILTON,W., 1979, Tectonics of the Indonesian region. **United States Geol. Surv. Prof. Pap.**, 1078, 345 p.

HART,S.R., 1984, A large-scale isotope anomaly in the southern hemisphere mantle. **Nature**, 309, 753-757.

HATHERTON,T. & DICKINSON,W.R., 1969, The relationship between andesite volcanism and seismicity in Indonesia, the Lesser Antilles, and other island arcs. **J. Geophys. Res.**, 74, 5301-5310.

HAWKESWORTH,C.J., NORRY,M.J., RODDICK,J.C., BAKER,P.E., FRANCIS,P.W. & THORPE,R.S., 1979, $^{143}Nd/^{144}Nd$, $^{87}Sr/^{86}Sr$, and incompatible element variations in calc-alkaline andesites and plateau lavas from South America. **Earth Planet. Sci. Lett.**, 42, 45-57.

HAWKESWORTH,C.J., O'NIONS,R.K. & ARCULUS,R.J., 1979, Nd and Sr

isotope geochemistry of island arc volcanics, Grenada, Lesser Antilles. **Earth Planet. Sci. Lett.**, 45, 237-248.

HAWKESWORTH,C.J. & POWELL,M., 1980, Magma genesis in the Lesser Antilles island arc. **Earth Planet. Sci. Lett.**, 51, 297-308.

HEIRTZLER,J.R. & SHIPBOARD SCIENTIFIC PARTY, 1974a, Site 260, In: Veevers,J.J., Heirtzler,J.R., et al., **Initial Reports of the Deep Sea Drilling Project**, Volume 27, Washington (U.S. Government Printing Office), 89-127.

HEIRTZLER,J.R. & SHIPBOARD SCIENTIFIC PARTY, 1974b, Site 261, In: Veevers,J.J., Heirtzler,J.R., et al., **Initial Reports of the Deep Sea Drilling Project**, Volume 27, Washington (U.S. Government Printing Office), 129-192.

HEMING,R.F., 1974, Geology and petrology of Rabaul caldera, Papua New Guinea. **Geol. Soc. Amer. Bull.**, 85, 1253-1264.

HEMING,R.F. & CARMICHAEL,I.S.E., 1973, High-temperature pumice flows from the Rabaul caldera, New Guinea. **Contrib. Mineral. Petrol.**, 38, 1-20.

HILDRETH,W., 1979, The Bishop Tuff: evidence for the origin of compositional zonation in silicic magma chambers. **Geol. Soc. Amer. Spec. Pap.**, 180, 45-73.

HOLE,M.J., SAUNDERS,A.D., MARRINER,G.F. & TARNEY,J., 1984, Subduction of pelagic sediments: implications for the origin of Ce-anomalous basalts from the Mariana Islands. **J. Geol. Soc. Lond.**, 141, 453-472.

HUTCHISON,C.S., 1976, Indonesian active volcanic arc: K, Sr and Rb variation with depth to the Benioff zone. **Geology**, 4, 407-408.

HUTCHISON,C.S., 1982, Indonesia. In: Thorpe,R.S. (editor), **Andesites: Orogenic Andesites and related Rocks**, Wiley, 207-224.

IDDINGS,J.P. & MORLEY,E.W., 1915, Contributions to the petrography of Java and Celebes. **J. Geol.**, 23, 231-245.

ISACKS,B. & MOLNAR,P., 1969, Mantle earthquake mechanisms and the sinking of the lithosphere. **Nature**, 223, 1121-1124.

ITO,E. & STERN,R.J., 1981, Oxygen and strontium isotopic investigations on the origin of volcanism in the Izu-Volcano-Mariana island arc. **Carnegie Institution of Washington Yearbook**, 80, 449-455.

JACOBSON,R.S., LAWVER,L.A., BECKER,K. & SHOR Jr,G.G., 1977, Anomalously uniform heat flow in the Banda Sea (abstract), **Eos**, 58, 515.

JAKES,P. & GILL,J., 1970, Rare earth elements and the island arc tholeiitic series. **Earth Planet. Sci. Lett.**, 9, 17-28.

JAMES,D.E., 1981, The combined use of oxygen and radiogenic isotopes as indicators of crustal contamination. **Ann. Rev. Earth Sci.**, 9, 311-344.

JAMES,D.E., 1982, A combined O, Sr, Nd, and Pb isotopic and trace element study of crustal contamination in central Andean lavas, I. Local geochemical variations. **Earth Planet. Sci. Lett.**, 57, 47-62.

JAQUES,A.L., LEWIS,J.D., SMITH,C.B., GREGORY,G.P., FERGUSON,J., CHAPPELL, B.W. & McCULLOCH,M.T., 1984, The diamond bearing ultrapotassic (lamproitic) rocks of the West Kimberly region, Western Australia. In: Kornprost,J. (editor), **Kimberlites I: Kimberlites and Related Rocks**, Elsevier, 225-254.

JEZEK,P.A. & HUTCHISON,C.S., 1978, Banda arc of eastern Indonesia: petrography and geochemistry of the volcanic rocks. **Bull. Volcanol.**, 41, 586-608.

JOHNSON,R.W., DAVIES,R.A. & WHITE,A.J.R., 1972, Ulawan volcano, New Britain. **Aust. Bur. Min. Resour. Geol. Geophys. Bull.**, 142, 1-42.

JOHNSON,R.W., JAQUES,A.L., HICKEY,R.L., McKEE,C.O. & CHAPPELL, B.W., 1985, Manam Island, Papua New Guinea: petrology and geochemistry of a low TiO_2 basaltic island-arc volcano. **J. Petrol.**, 26, 283-323.

JUDD,J.W., 1888, On the volcanic phenomena of the eruption, and on the nature and distribution of the ejected materials. In: **The Eruption of Krakatoa and Subsequent Phenomena.** Report of the Krakatoa Committee of the Royal Society, 1-56.

KADAR,D., 1972, Upper Miocene planktonic foraminifera from Bali. **Jahrbuch der Geologischen Bundesanstalt**, Sonderband 19, 58-70.

KADAR,D., 1977, Upper Pliocene planktonic foraminiferal zonation of Ambengan drill hole, southern part of Bali island. **Geol. Res. Devel. Centre (Indonesia), Spec. Publ.**, 1, 137-158.

KATILI,J.A., 1975, Volcanism and plate tectonics in the Indonesian island arcs. **Tectonophysics**, 26, 165-188.

KELLER,J., 1982, Mediterranean island arcs. In: Thorpe,R.S. (editor), **Andesites: Orogenic Andesites and Related Rocks**, Wiley, 307-325.

KEMMERLING,G.L.L., 1918, De aarbeving van Bali van 21 Januari 1917. **Natuurk. Tijdschr. Nederl. Ind.**, 77, 172-179.

KIECKHEFER,R.M., SHOR Jr,G.G. & CURRAY,J.R., 1980, Seismic refraction studies of the Sunda trench and forearc basin. **J. Geophys. Res.**, 85, 863-889.

KLUSMAN,R.W., 1972, Calcium fractionation in zoned plagioclase from the Tobacco Root batholith, southwestern Monatana. **Chem. Geol.**, 9, 45-56.

KRETZ,R., 1982, Transfer and exchange equilibria in a portion of the pyroxene quadrilateral as deduced from natural and experimental data. **Geochim. Cosmochim. Acta.**, 46, 411-422.

KUNO,H., 1969, Pigeonite-bearing andesite and associated dacite from Asio, Japan. **Amer. J. Sci.**, 267-A, 257-268.

KUSHIRO,I., 1974, Melting of hydrous upper mantle and possible generation of andesitic magma: an approach from synthetic systems. **Earth Planet. Sci. Lett.**, 22, 294-299.

KUSUMADINATA,K., 1963, The eruption of the Batur volcano in Bali in 1963. unpublished manuscript. **Direkt. Geol. (Indonesia).**

KUSUMADINATA,K., 1964, Nota umum mengenai aktivita efusiva tahun 1963 di dalam kaldera Batur (Bali), bagian 1 dan 2. unpublished manuscript, **Direkt. Geol. (Indonesia)**

KUSUMADINATA,K. (editor), 1979, **Data Dasar Gunungapi Indonesia**, Volcanological Survey of Indonesia, 820 pp.

KYSER,T.K., O'NEIL,J.R. & CARMICHAEL,I.S.E., 1981, Oxygen isotope thermometry of basic lavas and mantle nodules. **Contrib. Mineral. Petrol.**, 77, 11-23.

KYSER,T.K., O'NEIL,J.R. & CARMICHAEL,I.S.E., 1982, Genetic relations among basic lavas and ultramafic nodules: evidence from oxygen isotope compositions. **Contrib. Mineral. Petrol.**, 81, 88-102.

LAMBERT,G., LE CLOAREC,M.E., ARDOUIN,B. & LE ROULLEY,J.C., 1985, Volcanic emission of radionuclides and magma dynamics. **Earth Planet. Sci. Lett.**, 76, 185-192.

LARSEN,R.L., 1975, Late Jurassic sea-floor spreading in the eastern Indian Ocean. **Geology**, 3, 69-71.

LE GUEN DE KERNEIZON,M., CARRON,J-P., MAURY,R.C., BELLON,H., DUPUY,C., 1982, Les rhyolites a fayalite et ferroaugite de Sainte-Lucie (arc insulaire des Petites Antilles). **Bull. Mineral.**, 105, 203-211.

LE MAITRE,R.W., 1979, A new generalised petrological mixing model. **Contrib. Mineral. Petrol.**, 71, 133-137.

LE ROEX,A.P., DICK,H.J.B., ERLANK,A.J., REID,A.M., FREY,F.A. & HART,S.R., 1983, Geochemistry, mineralogy and petrogenesis of lavas erupted along the Southwest Indian Ridge between the Bouvet Triple Junction and 11 degrees East. **J. Petrol.**, 24, 267-318.

LINDSLEY,D.H. & ANDERSON,D.J., 1983, A two-pyroxene thermometer. **J. Geophys. Res.**, 88, A887-A906.

LLOYD,F.E. & BAILEY,D.K., 1975, Light element metasomatism of the continental mantle: the evidence and the consequences. **Phys. Chem. Earth**, 9, 389-416.

LOFGREN,G., 1972, Temperature induced zoning in synthetic plagioclase feldspar. In: Mackenzie,W.S. (editor), **The Feldspars**, University of Manchester Press, 362-377.

LOFGREN,G.E., 1980, Experimental studies on the dynamic crystallization of silicate melts. In: Hargraves,R.B. (editor), **Physics of Magmatic Processes**, Princeton University Press, 487-551.

LOOMIS,T.P., 1982, Numerical simulations of crystallization processes of plagioclase in complex melts: the origin of major and oscillatory zoning in plagioclase. **Contrib. Mineral. Petrol.**, 81, 219-229.

LOWDER,G.G. & CARMICHAEL,I.S.E., 1970, The volcanoes and caldera of Talasea, New Britain: geology and petrology. **Geol. Soc. Amer. Bull.**, 81, 17-38.

LOWELL,R.P., 1985, Double-diffusive convection in partially molten silicate systems: its role during magma production and in magma chambers. **J. Volcanol. Geotherm. Res.**, 26, 1-24.

MACDONALD,G.A., 1972, **Volcanoes**, Prentice-Hall, 510pp.

MAGARITZ,M., WHITFORD,D.J. & JAMES,D.E., 1978, Oxygen isotopes and the origin of high-$^{87}Sr/^{86}Sr$ andesites. **Earth Planet. Sci. Lett.**, 40, 220-230.

MARCELOT,G., MAURY,R.C., & LEFEVRE,C., 1983, Mineralogy of Erromango lavas (New Hebrides): evidence of an early stage of fractionation in island arc basalts. **Lithos**, 16, 135-151.

MARINELLI,G. & TAZIEFF,H., 1968, L'Ignimbrite et la Caldera de Batur (Bali, Indonesie). **Bull. Volcanol.**, 32, 89-120.

MASUDA,A., NAKAMURA,N. & TANAKA,T., 1973, Fine structures of mutually normalised rare-earth patterns of chondrites.

Geochim. Cosmochim. Acta, 37, 239-248.

MATSUHISA,Y., 1979, Oxygen isotopic compositions of volcanic rocks from the East Japan island arcs and their bearing on petrogenesis. **J. Volcanol. Geotherm. Res.**, 5, 271-296.

MATSUHISA,Y., MATSUBAYA,O. & SAKAI,H., 1973, Oxygen isotope variations in magmatic differentiation processes of the volcanic rocks in Japan. **Contrib. Mineral. Petrol.**, 39, 277-288.

McBIRNEY,A.R., 1980, Mixing and unmixing of magmas. **J. Volcanol. Geotherm. Res.**, 7, 357-371.

McBIRNEY,A.R., 1985, Further considerations of double-diffusive stratification and layering in the Skaergaard Intrusion. **J. Petrol.**, 26, 993-1001.

McBIRNEY,A.R., BAKER,B. & NILSON,R.H., 1985, Liquid fractionation. Part I: basic principles and experimental simulations. **J. Volcanol. Geotherm. Res.**, 24, 1-24.

McCULLOCH,M.T., COMPSTON,W., ABBOTT,M. & CHIVAS,A., 1983, Neodymium, strontium, lead and oxygen isotopic and trace element constraints on magma genesis in the Banda island-arc, Wetar. **Geological Society of Australia Abstracts Series (Sixth Australian Geological Convention)**, 9, 152-153.

McCULLOCH,M.T., JAQUES,A.L., NELSON,D.R. & LEWIS,J.D., 1983, Nd and Sr isotopes in kimberlites and lamproites from Western Australia: an enriched mantle origin. **Nature**, 302, 400-403.

McCULLOCH,M.T. & PERFIT,M.R., 1981, $^{143}Nd/^{144}Nd$, $^{87}Sr/^{86}Sr$ and trace element constraints on the petrogenesis of Aleutian island arc magmas. **Earth Planet. Sci. Lett.**, 56, 167-179.

McDONOUGH,W.F., McCULLOCH,M.T. & SUN,S.S., 1985, Isotopic and geochemical systematics in Tertiary-Recent basalts from southeastern Australia and implications for the evolution of the sub-continental lithosphere. **Geochim. Cosmochim. Acta**, 49, 2051-2067.

McDOUGALL,I., POLACH,H.A. & STIPP,J.J., 1969, Excess radiogenic argon in young subaerial basalts from the Auckland volcanic field, New Zealand. **Geochim. Cosmochim. Acta.**, 33, 1485-1520.

McKEE,C.O., JOHNSON,R.W., LOWENSTEIN,P.L., RILEY,S.J., BLONG, R.J., DE SAINT OURS,P. & TALAI,B., 1985, Rabaul caldera,

Papua New Guinea: volcanic hazards, surveillance, and eruption contingency planning. **J. Volcanol. Geotherm. Res.**, 23, 195-237.

MEINEL,A.B. & MEINEL,M.P., 1964, Height of the glow stratum from the eruption of Agung on Bali. **Nature**, 201, 657-658.

MELSON,W.G., BYERLY,G.R., NELEN,J.A., O'HEARN,T., WRIGHT,T.L. & VALLIER,T., 1977, A catalog of the major element chemistry of abyssal volcanic glasses. **Smithsonian Contrib. Earth Sci.**, 19, 31-60.

MENZIES,M.A. & WASS,S.Y., 1983, CO_2- and LREE-rich mantle below eastern Australia: a REE and isotopic study of alkaline magmas and apatite-rich mantle xenoliths from the Southern Highlands Province. **Earth Planet. Sci. Lett.**, 65, 287-302.

MERZBACHER,C. & EGGLER,D.H., 1984, A magmatic geohygrometer: application to Mount St. Helens and other dacitic magmas. **Geology**, 12, 587-590.

MIYASHIRO,A., 1974, Volcanic rock series in island arcs and active continental margins. **Am. J. Sci.**, 274, 321-355.

MOORE,G.F. & KARIG,D.E., 1980, Structural geology of Nias Island, Indonesia, implications for subduction zone tectonics. **Amer. J. Sci.**, 280, 193-223.

MOORE,G.F., CURRAY,J.R., MOORE,D.G. & KARIG,D.E., 1980, Variations in geologic structure along the Sunda forearc, northeastern Indian Ocean. In: Hayes,D.E. (editor), **The Tectonic and Geologic Evolution of Southeast Asian Seas and Islands.** Amer. Geopys. Union Mongr., 23, 145-160.

MORRICE,M.G., JEZEK,P.A., GILL,J.B., WHITFORD,D.J. & MONOARFA,M., 1983, An introduction to the Sangihe arc: volcanism accompanying arc-arc collision in the Molucca Sea, Indonesia. **J. Volcanol. Geotherm. Res.**, 19, 135-165.

MORRIS,J.D. & HART,S.R., 1980, Lead isotope geochemistry of the Banda arc (abstract). **Eos**, 61, 1157.

MORRIS,J.D. & HART,S.R., 1983, Isotopic and incompatible element constraints on the genesis of island arc volcanics from Cold Bay and Amak Island, Aleutians, and implications for mantle structure. **Geochim. Cosmochim. Acta**, 47, 2015-2030.

MORRIS,J.D., JEZEK,P., HART,S.R. & GILL,J.B., 1983, The Halmahera island arc, Molucca Sea collision zone, Indonesia: a geochemical survey. In: **The Tectonic and**

Geologic Evolution of Southeast Asian Seas and Islands, Part 2, D.E. Hayes (editor), Amer. Geophys. Union Monogr., 27, 373-387.

MUEHLENBACHS,K., ANDERSON,A.T.,Jr, SIGVALDASON,G.E., 1974, Low-^{18}O basalts from Iceland. **Geochim. Cosmochim. Acta**, 38, 577-588.

MUEHLENBACHS,K. & BYERLY,G., 1982, ^{18}O-enrichment of silicic magmas caused by crystal fractionation at the Galapagos Spreading Center, **Contrib. Mineral. Petrol.**, 79, 76-79.

MYSEN,B.O. & BOETTCHER,A.L., 1975, Melting of a hydrous mantle: II. Geochemistry of crystals and liquids formed by anatexis of mantle peridotite at high pressures and high temperature as a function of controlled activities of water, hydrogen and carbon dioxide. **J. Petrol.**, 16, 549-593.

NELSON,D.R., McCULLOCH,M.T. & SUN,S-S., 1986, The origins of ultrapotassic rocks as inferred from Sr, Nd and Pb isotopes. **Geochim. Cosmochim. Acta**, 50, 231-245.

NEUMANN VAN PADANG,M., 1951, **Catalogue of the Active Volcanoes of the World Including Solfatara Fields, Part 1.** International Volcanological Association, Napoli, 271 p.

NEWMAN,S., FINKEL,R.C. & MACDOUGALL,J.D., 1984, Comparison of ^{230}Th-^{238}U disequilibrium systematics in lavas from three hot spot regions: Hawaii, Prince Edward and Samoa. **Geochim. Cosmochim. Acta**, 48, 315-324.

NEWMAN,S., MACDOUGALL,J.D. & FINKEL,R.C., 1984, ^{230}Th-^{238}U disequilibrium in island arcs: evidence from the Aleutians and the Marianas. **Nature**, 308, 268-270.

NICHOLLS,I.A., 1974, Liquids in equilibrium with peridotitic mineral assemblages at high water pressures. **Contrib. Mineral. Petrol.**, 45, 289-316.

NICHOLLS,I.A. & RINGWOOD,A.E., 1972, Production of silica-saturated tholeiitic magmas in island arcs. **Earth Planet. Sci. Lett.**, 17, 243-246.

NICHOLLS,I.A. & RINGWOOD,A.E., 1973, Effect of water on olivine stability in tholeiites and the production of silica-saturated magmas in the island arc environment. **J. Geol. Soc. Lond.**, 81, 285-300.

NICHOLLS,I.A. & WHITFORD,D.J., 1976, Primary magmas associated with Quaternary volcanism in the western Sunda arc, Indonesia. In: **Volcanism in Australasia**, R.W. Johnson

(editor), Elsevier, 77-90.

NICHOLLS,I.A. & WHITFORD,D.J., 1983, Potassium-rich volcanic rocks of the Muriah complex, Java, Indonesia: products of multiple magma sources? **J. Volcanol. Geotherm. Res.**, 18, 337-359.

NILSON,R.H., McBIRNEY,A.R. & BAKER,B.H., 1985, Liquid fractionation. Part II: fluid dynamics and quantitative implications for magmatic systems. **J. Volcanol. Geotherm. Res.**, 24, 25-54.

NORRISH,K. & CHAPPELL,B.W., 1967, X-ray fluorescent spectrography. In: Zussman,J. (editor), **Physical Methods in Determinative Mineralogy**, Academic Press, 161-214.

NORRISH,K. & HUTTON,J.T., 1969, An accurate X-ray spectrographic method for the analysis of a wide range of geological samples. **Geochim. Cosmochim. Acta**, 33, 431-455.

O'HARA,M.J., 1977, Geochemical evolution during fractional crystallization of a periodically refilled magma chamber. **Nature**, 266, 503-507.

O'HARA,M.J. & MATHEWS,R.E., 1981, Geochemical evolution in an advancing, periodically replenished, periodically tapped, continuously fractionated magma chamber. **J. Geol. Soc. Lond.**, 138, 237-277.

O'NIONS,R.K., HAMILTON,P.J. & EVENSEN,N.M., 1977, Variations in $^{143}Nd/^{144}Nd$ and $^{87}Sr/^{86}Sr$ ratios in oceanic basalts. **Earth Planet. Sci. Lett.**, 34, 13-22.

OSBORN,E.F., 1969, Experimental aspects of calc-alkaline differentiation. In: **Proceedings of the Andesite Conference**, A.R. McBirney (editor), **Dept. Geol. Min. Res. Oreg. Bull.**, 65, 33-42.

OVERSBY,V., 1972, Genetic relations among the volcanic rocks of Reunion: chemical and lead isotopic evidence. **Geochim. Cosmochim. Acta**, 36, 1167-1179.

OVERSBY,V.M. & GAST,P.W., 1968, Lead isotope evidence and uranium decay series disequilibrium in recent volcanic rocks. **Earth Planet. Sci. Lett.**, 5, 199-206.

PEARCE,J.A. & CANN,J.R., 1973, Tectonic setting of basic volcanic rocks determined using trace element analyses. **Earth Planet. Sci. Lett.**, 19, 290-300.

PEARCE,J.A. & NORRY,M.J., 1979, Petrogenetic implications of Ti, Zr, Y, and Nb variations in volcanic rocks. **Contrib. Mineral. Petrol.**, 69, 33-47.

PECCERILLO,A. & TAYLOR,S.R., 1976, Geochemistry of Eocene calc-alkaline volcanic rocks from the Kastamonu area, northern Turkey. **Contrib. Mineral. Petrol.**, 58, 63-81.

PERFIT,M.R., GUST,D.A., BENCE,A.E., ARCULUS,R.J. & TAYLOR,S.R., 1980, Chemical characteristics of island arc basalts: implications for mantle sources. **Chem. Geol.**, 30, 227-256.

PIGRAM,C.J. & PANGGABEAN,H., 1983, Age of the Banda Sea, eastern Indonesia. **Nature**, 301, 231-234.

POWELL,T.S. & LUYENDYK,B.P., 1982, The sea-floor spreading history of the eastern Indian Ocean. **Mar. Geophys. Res.**, 5, 225-247.

PURBO-HADIWIDJOJO,M.M., 1971, Geological Map of Bali 1:250000. **Geol. Surv. Indon. Publ.**.

PURDY,G.M. & DETRICK,R.S., 1978, A seismic refraction experiment in the central Banda Sea. **J. Geophys. Res.**, 83, 2247-2257.

RAMPINO,M.R. & SELF,S., 1982, Historic eruptions of Tambora (1815), Krakatau (1883) and Agung (1963), their stratospheric aerosols and climatic impact. **Quat. Res.**, 18, 127-143.

RAMSAY,W.R.H., CRAWFORD,A.J. & FODEN,J.D., 1984, Field setting, mineralogy, chemistry, and genesis of arc picrites, New Georgia, Solomon Islands. **Contrib. Mineral. Petrol.**, 88, 386-402.

RINGWOOD,A.E., 1977, Petrogenesis in island arc systems. In: Talwani,M. & Pitman III,W.C. (editors), **Island Arcs, Deep Sea Trenches and Back-Arc Basins.** Amer. Geophys. Union, 311-324.

RINGWOOD,A.E., 1982, Phase transformations and differentiation in subducted lithosphere: implications for mantle dynamics, basalt petrogenesis, and crustal evolution. **J. Geol.**, 90, 611-643.

RITTMAN,A., 1953, Magmatic character and tectonic position of the Indonesian volcanoes. **Bull. Volcanol.**, 14, 45-58.

ROBIN,C. 1984, Le volcan Popocateptl (Mexique): structure, evolution petrologique et risques. **Bull. Volcanol.**, 47, 1-23.

ROBIN,C. & CANTAGREL,J.M., 1982, Le Pico de Orizaba (Mexique): structure et evolution d'un grand volcano andesitique complexe. **Bull. Volcanol.**, 45, 299-315.

ROBINSON,P.T. & WHITFORD,D.J., 1974, Basalts from the eastern

Indian Ocean, DSDP Leg 27. In: Veevers,J.J., Heirtzler,J.R. et al., **Initial Reports of the Deep Sea Drilling Project**, Vol. 27, Washington (U.S. Government Printing Office), 551-559.

ROCK,N.M.S., SYAH,H.H., DAVIS,A.E., HUTCHISON,D., STYLES,M.T. & RAHAYU LENA, 1982, Permian to Recent volcanism in northern Sumatra, Indonesia: a preliminary study of its distribution, chemistry and peculiarities. **Bull. Volcanol.**, 45, 127-152.

RODEN,M.F. & MURTHY,V.R., 1985, Mantle metasomatism. **Ann. Rev. Earth Planet. Sci.**, 13, 269-296.

ROEDER,P.L. & EMSLIE,R.F., 1970, Olivine-liquid equilibrium. **Contrib. Mineral. Petrol.**, 29, 275-289.

ROOBOL,M.J. & SMITH,A.L., 1976, Mount Pelee, Martinique: a pattern of alternating eruptive styles. **Geology**, 4, 521-524.

RUTHERFORD,M.J., SIGURDSSON,H., CAREY,S. & DAVIS,A., 1985, The May 18, 1980, eruption of Mount St. Helens I. melt composition and experimental phase equilibria. **J. Geophys. Res.**, 90, 2929-2947.

SAKUYAMA.M., 1981, Petrological study of the Myoko and Kurohime volcanoes, Japan: crystallization sequence and evidence for magma mixing. **J. Petrol.**, 22, 553-583.

SAUNDERS,A.D., TARNEY,J. & WEAVER,S.D., 1980, Transverse geochemical variations across the Antartic Peninsula: implications for the genesis of calc-alkaline magmas. **Earth Planet. Sci. Lett.**, 46, 344-360.

SCHILLING,J.-G., 1973, Iceland mantle plume: geochemical study of Reykjanes ridge. **Nature**, 242, 565-571.

SCHILLING,J.G. & WINCHESTER,J.W., 1967, Rare earth fractionation and magmatic processes. In: Runcorn,S.K. (editor), **Mantles of the Earth and Terrestrial Planets**, Interscience, 267-283.

SELF,S. & RAMPINO,M.R. & BARBERA,J.J., 1981, The possible effects of large 19th and 20th century volcanic eruptions on zonal and hemispheric surface temperatures. **J. Volcanol. Geotherm. Res.**, 11, 41-60.

SHERIDAN,M.F., 1979, Emplacement of pyroclastic flows: a review. In: Chapin,C.E. & Elston,W.E. (editors), **Ash-Flow Tuffs**, Geol. Soc. Amer. Spec. Pap., 180, 125-136.

SHERATON,J.W. & CUNDARI,A., 1980, Leucitites from Gaussberg,

Antarctica. **Contrib. Mineral. Petrol.**, 71, 417-427.

SILVER,E.A., GILL,J.B., SCHWARTZ,D., PRASETYO,H. & DUNCAN,R.A., 1985, Evidence for a submerged and displaced continental borderland, north Banda sea, Indonesia. **Geology**, 13, 687-691.

SILVER,E.A., REED,D., McCAFFREY,R. & JOYODIWIRYO,Y., 1983, Back arc thrusting in the eastern Sunda arc, Indonesia: a consequence of arc-continent collision. **J. Geophys. Res.**, 88, 7429-7448.

SIMKIN,T., SIEBERT,L., McCLELLAND,L., BRIDGE,D., NEWHALL,C. & LATTER,J.H., 1981, **Volcanoes of the World.** Smithsonian Institution, 232 p.

SMITH,R.K. & LOFGREN,G.E., 1983, An analytical and experimental study of zoning in plagioclase. **Lithos**, 16, 153-168.

SPARKS,R.S.J., 1976, Grain size variations in ignumbrites and implications for the transport of pyroclastic flows. **Sedimentology**, 23, 147-188.

SPARKS,R.S.J., HUPPERT,H.E. & TURNER,J.S., 1984, The fluid dynamics of evolving magma chambers. **Phil. Trans. R. Soc. Lond.**, A310, 511-534.

SPARKS,R.S.J., SELF,S. & WALKER,G.P.L., 1973, Products of ignimbrite eruptions. **Geology**, 1, 115-118.

SPARKS,R.S.J. & WILSON,L., 1976, A model for the formation of ignimbrite by gravitational column collapse. **J. Geol. Soc. Lond.**, 132, 441-451.

SPARKS,R.S.J., WILSON,L. & HULME,G., 1978, Theoretical modeling of the generation, movement and emplacement of pyroclastic flows by column collapse. **J. Geophys. Res.**, 83, 1727-1739.

SPARKS,R.S.J. & WRIGHT,J.V., 1979, Welded air-fall tuffs. In: Chapin,C.E. & Elston,W.E. (editors), **Ash-Flow Tuffs**, Geol. Soc. Amer. Spec. Pap., 180, 15-166.

SPENCER,K.J. & LINDSLEY,D.H., 1981, A solution model for co-existing iron-titanium oxides. **Amer. Mineral.**, 66, 1189-1201.

STEHN,CH.E., 1928, De Batoer op Bali en zijn erupties in 1926. **Vulk. Seism. Meded.**, 9, 1-67.

STEIGER,R.H. & JAGER,E., 1977, Subcommission on geochronology: convention on the use of decay constants in geo- and cosmochronology. **Earth Planet. Sci. Lett.**, 36, 359-362.

STERN,C.R. & WYLLIE,P.J., 1978, Phase compositions through crystallization intervals in basalt-andesite-H_2O at 30

kb with implications for subduction zone magmas. **Amer. Mineral.**, 63, 641-663.

STERN,R.J., 1981, A common mantle source for western Pacific island arc and "hot-spot" magmas - implications for layering in the upper mantle. **Carnegie Institution of Washington Yearbook**, 80, 455-462.

STERN,R.J. & BIBEE,L.D., 1980, Esmeralda Bank: geochemistry of an active submarine volcano in the Mariana island arc and its implications for magmagenesis in island arcs. **Carnegie Institution of Washington Yearbook**, 79, 465-472.

STERN,R.J. & ITO,E., 1983, Trace-element and isotopic constraints on the source of magmas in the active Volcano and Mariana island arcs, western Pacific. **J. Volcanol. Geotherm. Res.**, 18, 461-482.

STORMER,J.C., 1983, The effects of recalculation on estimates of temperature and oxygen fugacity from analyses of multi-component iron-titanium oxides. **Amer. Mineral.**, 68, 586-594.

SUN,S.-S., 1980, Lead isotopic study of young volcanic rocks from mid-ocean ridges, ocean islands and island arcs. **Phil. Trans. R. Soc. Lond.**, A297, 409-445.

SURJO,I., 1965, Casualties of the latest activity of the Agung volcano. **Geol. Surv. Indon. Bull.**, 2, 22-26.

SUSSMAN,D., 1985, Apoyo caldera, Nicaragua: a major Quaternary silicic eruptive center. **J. Volcanol. Geotherm. Res.**, 24, 249-282.

SUTHREN,R.J. & FURNES,H. 1980, Origin of some bedded welded tuffs. **Bull. Volcanol.**, 43, 61-71.

TAKAHASHI,E. & KUSHIRO,I. 1983, Melting of a dry peridotite at high pressures and implications for petrogenesis. **Amer. Mineral.**, 68, 859-879.

TANGUY,J.C., 1978, Tholeiitic basalt magmatism of Mt Etna and its relations with the alkaline series. **Contrib. Mineral. Petrol.**, 66, 51-67.

TANZER,M.O., 1985, Mantle sources and magmatic processes studied through Uranium series disequilibrium in young volcanic rocks. M.Sc. thesis, University of California (San Diego).

TAYLOR,H.P., GIANNETTI,B. & TURI,B., 1979, Oxygen isotope geochemistry of the potassic igneous rocks from Roccamonfina volcano, Roman Comagmatic Region. **Earth Planet. Sci. Lett.**,

46, 81-106.

TAYLOR,H.P. & TURI,B., 1976, High-^{18}O igneous rocks from the Tuscan Magmatic Province, Italy. **Contrib. Mineral. Petrol.**, 55, 33-54.

TAYLOR,H.P., TURI,B. & CUNDARI,A., 1984, $^{18}O/^{16}O$ and chemical relationships in K-rich volcanic rocks from Australia, East Africa, Antartica, and San Vernanzo-Cupaello, Italy. **Earth Planet. Sci. Lett.**, 69, 263-276.

TERA,F., BROWN,L., MORRIS,J., SACKS,I.S., KLEIN,J. & MIDDLETON,R., 1986, Sediment incorporation in island-arc magmas: inferences from ^{10}Be.
Geochimica et Cosmochimica Acta., in press

THIRWELL,M.F., 1982, Systematic variation in chemistry and Nd-Sr isotopes across a Caledonian calc-alkaline volcanic arc: implications for source materials. **Earth Planet. Sci. Lett.**, 58, 27-50.

THIRLWELL,M.F. & GRAHAM,A.M., 1984, Evolution of high-Ca, high-Sr C-series basalts from Grenada, Lesser Antilles: the effects of intra-crustal contamination. **J. Geol. Soc. Lond.**, 141, 427-445.

THOMPSON,R.N., 1982, Magmatism of the British Tertiary Volcanic Province. **Scott. J. Geol.**, 18, 49-107.

THOMPSON,R.N., MORRISON,M.A., HENDRY,G.L. & PARRY,S.J., 1984, An assessment of the relative roles of crust and mantle in magma genesis: an elemental approach. **Phil. Trans. R. Soc. Lond.**, A310, 549-590.

TURI,B. & TAYLOR,H.P., 1976, Oxygen isotope studies of potassic volcanic rocks of the Roman Province, central Italy. **Contrib. Mineral. Petrol.**, 55, 4-31.

TURNER,J.S. & GUSTAFSON,L.B., 1981, Fluid motions and compositional gradients produced by crystallization or melting at vertical boundaries. **J. Volcanol. Geotherm. Res.**, 11, 93-125.

VAN BEMMELEN,R.W., 1949, **The geology of Indonesia, Vol 1A.** Government Printing Office, The Hague, 732 p.

VAN BERGEN,M.J., ERFAN,R., DE JONG,A., POORTER,R.P.E., SRIWANA, T., SUHARYONO,K., VAREKAMP,J.C., VROON,P.Z. & WIRAKUSUMAH, A.D., 1985, Potassic volcanism in the eastern Sunda arc (Indonesia) (abstract). **IAVCEI 1985 Scientific Assembly,** Giardini-Naxos (Italy).

VARNE,R., 1985, Ancient subcontinental mantle: a source for

K-rich orogenic volcanics. **Geology**, 13, 405-408.

VARNE,R. & GRAHAM,A.L., 1971, Rare earth abundances in hornblende and clinopyroxene of a hornblende lherzolite xenolith: implications for upper mantle fractionation processes. **Earth Planet. Sci. Lett.**, 13, 11-18.

VEEVERS,J.J., TAYTON,J.W. & JOHNSON,B.D., 1985, Prominent magnetic anomaly along the continent-ocean boundary between the northwestern margin of Australia (Exmouth and Scott Plateaus) and the Argo Abyssal Plain. **Earth Planet. Sci. Lett.**, 72, 415-426.

VON DER BORCH,C.C. & SHIPBOARD SCIENTIFIC PARTY, 1974a, Site 211. In: von der Borch,C.C., Sclater,J.G., et al., **Initial Reports of the Deep Sea Drilling Project**, Volume 22, Washington (U.S. Government Printing Office), 13-36.

VON DER DORCH,C.C. & SHIPBOARD SCIENTIFIC PARTY, 1974b, Site 212. In: von der Borch,C.C., Sclater,J.G., et al., **Initial Reports of the Deep Sea Drilling Project**, Volume 22, Washington, (U.S. Government Printing Office), 37-83.

WAGER,L.R. & BROWN,G.M., 1968, **Layered Igneous Rocks**, Oliver & Boyd, 588pp.

WALKER,G.P.L., SELF,S., & WILSON,L., 1984, Tarawera 1886, New Zealand - a basaltic plinian fissure eruption. **J. Volcanol. Geotherm. res.**, 21, 61-78.

WEDEPOHL,K.H., CORRENS,C.W., SHAW,D., TUREKIAN,K.K. & ZEMANN,J. (editors), 1970, **Handbook of Geochemistry**, Volume II-2.

WELLS,P.R.A., 1977, Pyroxene thermometry in simple and complex systems. **Contrib. Mineral. Petrol.**, 62, 129-139.

WHELLER,G.E. & VARNE,R., 1984, Evolution and petrogenesis of the Batur volcano, Bali (abstract). Seventh Australian Geological Convention (Sydney), **Geol. Soc. Aust. Abstr. Ser.**, 12, 544-545.

WHELLER,G.E. & VARNE,R., 1985, Genesis of dacitic magmatism at Batur volcano, Bali, Indonesia: implications for the origins of stratovolcano calderas (abstract). **1985 IAVCEI Assembly**, (Giardini-Naxos).

WHELLER,G.E. & VARNE,R., 1986a, Petrogenesis of basalt-andesite-dacite-basalt volcanism at the active Batur volcano, Bali, eastern Sunda arc, and the origins of stratovolcano calderas (abstract). **1986 International Volcanological Congress** (Auckland-Hamilton-Rotorua, New Zealand), abstracts volume, 359.

WHELLER,G.E. & VARNE,R., 1986b, Genesis of dacitic magmatism at Batur volcano, Bali, Indonesia: implications for the origins of stratovolcano calderas. **J. Volcanol. Geotherm. Res.**, in press.

WHELLER,G.E., VARNE,R., FODEN,J.D. & ABBOTT,M., 1983, Volcanism from the continent-arc collision zone of Flores, Sunda arc (abstract). Sixth Australian Geological Convention (Canberra). **Geol. Soc. Aust. Abstr. Ser.**, 9, 151-152.

WHELLER,G.E., VARNE,R., FODEN,J.D. & ABBOTT,M.J., 1986, Geochemistry of Quaternary volcanism in the Sunda-Banda arc, Indonesia, and three-component genesis of island arc basaltic magmas. **J. Volcanol. Geotherm. Res.**, accepted for publication. (special issue: 1986 International Volcanological Congress, New Zealand).

WHITE,W.M. & HOFMANN,A.W., 1982, Sr and Nd isotope geochemistry of oceanic basalts and mantle evolution. **Nature**, 296, 821-825.

WHITE,W.M. & PATCHETT,J., 1984, Hf-Nd-Sr isotopes and incompatible element abundances in island arcs: implications for magma origins and crust-mantle evolution. **Earth Planet. Sci. Lett.**, 67, 167-185.

WHITFORD,D.J., 1975a, Geochemistry and petrology of volcanic rocks from the Sunda arc, Indonesia. unpubl. Ph.D. thesis, Australian National University.

WHITFORD,D.J., 1975b, Strontium isotopic studies of the volcanic rocks of the Sunda arc, Indonesia, and their petrogenetic implications. **Geochim. Cosmochim. Acta**, 39, 1287-1302.

WHITFORD,D.J., FODEN,J.D. & VARNE,R., 1978, Sr isotope geochemistry of calcalkaline and alkaline lavas lavas from the Sunda arc in Lombok and Sumbawa, Indonesia. **Carnegie Institution of Washington Yearbook**, 77, 613-620.

WHITFORD,D.J. & JEZEK,P.A., 1979, Origin of Late Cenozoic lavas from the Banda Sea, Indonesia: trace element and Sr isotope evidence. **Contrib. Mineral. Petrol.**, 68, 141-150.

WHITFORD,D.J. & JEZEK,P.A., 1982, Isotopic constraints on the role of subducted sialic material in Indonesian island-arc magmatism. **Geol. Soc. Amer. Bull.**, 93, 504-513.

WHITFORD,D.J. & NICHOLLS,I.A., 1976, Potassium variation in lavas across the Sunda arc in Java and Bali. In: **Volcanism in Australasia**, R.W. Johnson (editor), Elsevier, 63-75.

WHITFORD,D.J., NICHOLLS,I.A. & TAYLOR,S.R., 1979, Spatial variations in the geochemistry of Quaternary lavas across the Sunda arc in Java and Bali. **Contrib. Mineral. Petrol.**, 70, 341-356.

WHITFORD,D.J., WHITE,W.M. & JEZEK,P.A., 1981, Neodymium isotopic studies of Quaternary island arc lavas from Indonesia. **Geochim. Cosmochim. Acta**, 45, 989-995.

WILLIAMS,H. & McBIRNEY,A.R., 1979, **Volcanology**, Freeman-Cooper, 397pp.

WILLIAMS,R.W., GILL,J.B. & BRULAND,K.W., 1983, Th and U decay series nuclides in historic arc lavas from Java, Japan and Mt St Helens (abstract) **Eos**, 64, 906.

WOOD,B.A. & BANNO,S., 1973, Garnet-orthopyroxene and orthopyroxene-clinopyroxene relationships in simple and complex systems. **Contrib. Mineral. Petrol.**, 42, 109-124.

WOOD,B.J. & FRASER,D.G., 1977, **Elementary Thermodynamics for Geologists**, Oxford University Press, 298pp.

WOOD,C.A., 1984, Calderas, a planetary perspective. **J. Geophys. Res.**, 89, 8391-8406.

WOOD,D.A., JORON,J.-L., & TREUIL,M., 1979, A re-appraisal of the use of trace elements to classify and discriminate between magma series erupted in different tectonic settings. **Earth Planet. Sci. Lett.**, 45, 326-336.

WRIGHT,J.V., 1980, Stratigraphy and geology of the welded air-fall tuffs of Pantelleria, Italy. **Geol. Rundsch.**, 69, 263-291.

WRIGHT,T.L. & DOHERTY,P.C., 1970, A linear programming and least squares computer method for solving petrologic mixing problems. **Geol. Soc. Amer. Bull.**, 81, 1995-??.

YOKOYAMA,I. & SUPARTO,S., 1970, A gravity survey on and around Batur caldera, Bali. **Bull. Earthq. Res. Inst.**, 48, 317-329.

ZEN,M.T. & HADIKUSUMO,D., 1964, Preliminary report of the 1963 eruption of Mt Agung in Bali (Indonesia). **Bull. Volcanol.**, 24, 269-299.

ZINDLER,A., JAGOUTZ,E. & GOLDSTEIN,S., 1982, Nd, Sr and Pb isotopic systematics in a three-component mantle: a new perspective. **Nature**, 298, 519-523.

SUPPLEMENTARY REFERENCES

CAMUS,G. & VINCENT,P.M., 1983, Discussion of a new hypothesis for the Krakatau volcanic eruption in 1883. **J. Volcanol. Geotherm. Res.**, 19, 167-173.

De NEVE,G.A., 1981, The Krakatau's eruption of 1883, it's earlier activities in historic time and in the Quaternary. **Proceedings of the Fourth Regional Conference on the Geology of Southeast Asia**, Geological Society of the Philippines, 155-178.

FRANCIS,P.W. & SELF,S., 1983, The eruption of Krakatau. **Sci. Amer.**, 249, 172-187.

FREY,F.A., DICKEY,J.S., THOMPSON,G. & BRYAN,W.B., 1977, Eastern Indian Ocean DSDP sites: correlations between petrography, geochemistry and tectonic setting. In: J.R. Heirtzler et al. (editors), **Indian Ocean Geology and Biostratigraphy**, Amer. Geophys. Union, Washington, 189-256.

SIMKIN,T. & FISKE,R., 1983, Krakatau 1883. Smithsonian Institute Press, Washington, 464pp.

VARNE,R. & FODEN,J.D., 1986, Geochemical and isotopic systematics of eastern Sunda arc volcanics: implications for mantle sources and mantle mixing processes. In: F.-C. Wezel (editor), **The Origin of Arcs**, Elsevier, Amsterdam, 159-189.

VERBEEK,R.D., 1884, The Krakatoa eruption. Nature, 30,10-15.

WILLEMS,H.W.V., 1940, On the magmatic provinces in the Netherlands East Indies. **Verh. Geol. Mijnb. Gen. Geol.**, Ser. 12, 289-477.

APPENDIX 1

Catalogue of Volcanic Rocks From Bali, Indonesia

Samples collected by G.E. Wheller, November-December 1982 and April-May 1984

Explanation of Table

UT# - University of Tasmania, Department Of Geology, Collection Number

SUITE - Volcano or Formation sample is derived from or associated with (for samples from Batur volcano PO, CA and PR refer to postcaldera, caldera and pre-caldera stages respectively)

DESCRIPTION - sample type and minor stratigraphic details

PHENOCRYSTS - list of phenocryst minerals

O - Y if sample from outcrop

SHEET - sample locality, JAVA 1:50000 mapsheet (U.S. Army Series T725, Edition 1-AMS(29ETB))

G.REF - sample locality, grid reference

T - Y if thin section available

P - Y if microprobe mineral analyses available

X - Y if XRF major and trace element analysis available

OTHER -list of other data available (samples collected specifically for Be-10 analysis and not yet analysed are marked as ?Be-10)

UT#	SUITE	DESCRIPTION	PHENOCRYSTS	O	SHEET	G.REF	T	P	X	OTHER
67238	BATUR/PO	1974 lava	plg,olv,cpx	Y	KINTAMANI	188890	Y	Y	Y	REE
67239	BATUR/PO	1974 lava		Y	KINTAMANI	188890	.	.	.	?Be-10
67240	BATUR/PO	1963 lava	plg,cpx,olv	Y	KINTAMANI	192906	Y	.	Y	REE
67241	BATUR/PO	1963 lava		Y	KINTAMANI	193902	.	.	.	-------
67242	BATUR/PO	1963 lava		Y	KINTAMANI	193906	.	.	.	?Be-10
67243	BATUR/PO	1963 lava		Y	KINTAMANI	196858	.	.	.	?Be-10
67244	BATUR/PO	1926 lava	plg,olv,cpx	Y	KINTAMANI	193855	Y	Y	Y	REE
67245	BATUR/PO	1926 lava		Y	KINTAMANI	200858	.	.	.	?Be-10
67246	BATUR/PO	1905 lava	plg,olv,cpx	Y	KINTAMANI	------	Y	.	.	-------
67247	BATUR/PO	1905 lava	plg,olv,cpx	Y	KINTAMANI	219875	Y	.	Y	-------
67248	BATUR/PO	1905 lava with xen.		Y	KINTAMANI	217873	.	.	.	-------
67249	BATUR/PO	1905 lava		Y	KINTAMANI	------	.	.	.	?Be-10
67250	BATUR/PO	1904 lava	plg,olv,cpx	Y	KINTAMANI	186890	Y	.	Y	-------
67251	BATUR/PO	1904 lava		Y	KINTAMANI	------	.	.	.	?Be-10
67252	BATUR/PO	1888 lava section (top)		Y	KINTAMANI	231875	.	.	Y	-------
67253	BATUR/PO	1888 lava section		Y	KINTAMANI	231875	.	.	Y	-------
67254	BATUR/PO	1888 lava section		Y	KINTAMANI	231875	.	.	Y	-------
67255	BATUR/PO	1888 lava section		Y	KINTAMANI	231875	.	.	Y	-------
67256	BATUR/PO	1888 lava section		Y	KINTAMANI	231875	.	.	Y	-------
67257	BATUR/PO	1888 lava	plg,olv,cpx	Y	KINTAMANI	231875	Y	.	Y	REE
67258	BATUR/PO	1888 lava		Y	KINTAMANI	------	.	.	.	?Be-10
67259	BATUR/PO	1849 lava	plg,olv,cpx	Y	KINTAMANI	213852	Y	Y	Y	REE

UT#	SUITE	DESCRIPTION	PHENOCRYSTS	O	SHEET	G.REF	T	P	X	OTHER
67260	BATUR/PO	1849 lava		Y	KINTAMANI	220856	.	.	.	?Be-10
67261	BATUR/PO	lava	plg,cpx,olv	.	KINTAMANI	201894	Y	.	Y	-------
67262	BATUR/PO	lava	plg,olv,cpx,mag	.	KINTAMANI	201894	Y	.	Y	-------
67263	BATUR/CA	postcaldera bomb	plg,opx,cpx,mag	.	KINTAMANI	201894	Y	.	Y	-------
67264	BATUR/PO	lava	plg,olv,cpx,mag	.	KINTAMANI	201894	Y	.	Y	-------
67265	BATUR/PO	lava	plg,olv,mag,cpx	.	KINTAMANI	201894	Y	.	Y	-------
67266	BATUR/PO	lava	plg,olv,cpx	.	KINTAMANI	219871	Y	.	Y	-------
67267	BATUR/PO	lava	plg,cpx,olv,mag	.	KINTAMANI	244894	Y	.	Y	-------
67268	BATUR/PO	lava	plg,cpx,olv,opx,mag	.	KINTAMANI	232906	Y	.	Y	-------
67269	BATUR/PO	lava	plg,olv,cpx,mag	.	KINTAMANI	229911	Y	.	Y	-------
67270	BATUR/PO	lava	plg,olv,cpx,mag	.	KINTAMANI	229913	Y	.	Y	-------
67271	BATUR/PO	lava	plg,cpx,mag,olv	.	KINTAMANI	240880	Y	.	Y	-------
67272	BATUR/PO	lava	plg,olv,cpx,mag	.	KINTAMANI	205909	Y	Y	Y	-------
67273	BATUR/CA	banded dacite clast	plg,opx,cpx,olv,mag	.	KINTAMANI	188906	Y	Y	Y	REE
67274	BATUR/CA	dacite clast	plg,cpx,olv,opx,apt	.	KINTAMANI	184907	Y	.	Y	-------
67275	BATUR/CA	dacite clast	plg,cpx,opx,olv,mag	.	KINTAMANI	188906	Y	Y	Y	REE
67276	BATUR/CA	dacite lava clast	plg,cpx,olv,mag,opx	.	KINTAMANI	180895	Y	.	Y	-------
67277	BATUR/CA	banded dacite clast	plg,cpx,opx,olv,mag,apt	.	KINTAMANI	170928	Y	Y	Y	REE
67278	BATUR/CA	dacite clast	plg,cpx,opx,olv,mag	.	KINTAMANI	774925	Y	Y	Y	-------
67279	BATUR/CA	banded dacite clast		.	--------	------	.	.	.	-------
67280	BATUR/CA	dacite/pumice bomb		.	--------	------	.	.	.	-------
67281	BATUR/CA	banded dacite clast		.	KINTAMANI	184907	.	.	Y	-------

UT#	SUITE	DESCRIPTION	PHENOCRYSTS	O	SHEET	G.REF	T	P	X	OTHER
67282	BATUR/CA	banded dacite clast	plg,olv,mag,cpx	.	KINTAMANI	184907	Y	.	Y	-------
67283	BATUR/CA	dacite clast		.	KINTAMANI	184907	.	.	.	-------
67284	BATUR/CA	dacite clast		.	KINTAMANI	184907	.	.	.	-------
67285	BATUR/CA	dacite bomb		.	KINTAMANI	213837	.	.	.	-------
67286	BATUR/CA	banded dacite clast		.	KINTAMANI	213837	.	.	.	-------
67287	BATUR/CA	dacite clast with xens.		.	KINTAMANI	213837	.	.	.	-------
67288	BATUR/CA	banded black pumice		.	KINTAMANI	178908	.	.	.	-------
67289	BATUR/CA	black pumice		.	KINTAMANI	213837	.	.	.	-------
67290	BATUR/CA	black pumice		.	KINTAMANI	213837	.	.	.	-------
67291	BATUR/CA	black pumice	plg,cpx,mag,?olv	.	KINTAMANI	210854	Y	.	.	-------
67292	BATUR/CA	black pumice		.	DENPASAR	105643	.	.	.	-------
67293	BATUR/CA	banded pumice		.	DENPASAR	112576	.	.	.	-------
67294	BATUR/CA	black pumice (Bali ig.)	plg,opx,cpx,olv,mag	.	BANGLI	105643	Y	.	Y	-------
67295	BATUR/PR	black pumice	plg	.	DENPASAR	203530	Y	.	Y	-------
67296	BATUR/CA	black pumice (Bali ig.)		.	DENPASAR	203530	.	.	.	-------
67297	BATUR/CA	black pumice (Bali ig.)		.	DENPASAR	203530	.	.	.	-------
67298	BATUR/CA	black pumice (Bali ig.)		.	DENPASAR	203530	.	.	.	-------
67299	BATUR/PR	black pumice u Bali ig.	plg	.	TABANAN	899479	Y	.	Y	REE
67300	BATUR/CA	lowest welded breccia		Y	KINTAMANI	187909	Y	.	.	-------
67301	BATUR/CA	mid. welded breccia		Y	KINTAMANI	187909	.	.	.	-------
67302	BATUR/CA	welded breccia		.	KINTAMANI	------	Y	.	.	-------
67303	BATUR/CA	welded breccia(KWT top)	plg,opx,olv,cpx,mag	.	KINTAMANI	184901	Y	.	.	-------

UT#	SUITE	DESCRIPTION	PHENOCRYSTS	O	SHEET	G.REF	T	P	X	OTHER
67304	BATUR/CA	welded breccia(KWT base)		.	KINTAMANI	180895	.	.	.	-------
67305	BATUR/CA	welded breccia (KWT)		.	KINTAMANI	------	Y	.	.	-------
67306	BATUR/CA	welded breccia (KWT)		.	KINTAMANI	------	Y	.	.	-------
67307	BATUR/CA	welded breccia (KWT)		.	KINTAMANI	------	Y	.	.	-------
67308	BATUR/CA	welded black ?breccia		.	KINTAMANI	------	Y	.	.	-------
67309	BATUR/CA	welded grey ?breccia		.	KINTAMANI	------	Y	.	.	-------
67310	BATUR/CA	welded grey breccia		.	KINTAMANI	------	Y	.	.	-------
67311	BATUR/CA	welded breccia		.	KINTAMANI	------	Y	.	.	-------
67312	BATUR/CA	banded pumice	plg,cpx,mag,olv	.	KINTAMANI	------	Y	.	.	-------
67313	BATUR/CA	banded pumice		.	KINTAMANI	------	.	.	.	-------
67314	BATUR/CA	Bali ignimbrite		Y	DENPASAR	077547	.	.	.	-------
67315	BATUR/CA	Bali ignimbrite	plg,cpx,olv,mag,opx	.	TABANAN	105643	Y	.	.	-------
67316	BATUR/CA	pumice-rich Bali ignim.		.	DENPASAR	105643	.	.	.	-------
67317	BATUR/CA	black pumice		Y	SINGARADJA	978055	.	.	.	-------
67318	BATUR/CA	black pumice	no phens	Y	SINGARADJA	978055	Y	.	Y	-------
67319	BATUR/CA	banded pumice		Y	SINGARADJA	969065	.	.	.	-------
67320	BATUR/CA	welded breccia (charc)		.	DENPASAR	198550	.	.	.	-------
67321	BATUR/CA	white tuff		Y	DENPASAR	167557	.	.	.	-------
67322	BATUR/CA	white pumice		Y	DENPASAR	167557	.	.	.	-------
67323	BATUR/CA	white tuff (fossilfish)		.	DENPASAR	167557	.	.	.	-------
67324	BATUR/CA	pumice breccia		Y	DENPASAR	200583	.	.	.	-------
67325	BATUR/PR	lava	plg,olv,cpx,mag	.	KINTAMANI	187905	Y	.	Y	-------

UT#	SUITE	DESCRIPTION	PHENOCRYSTS	O	SHEET	G.REF	T	P	X	OTHER
67326	BATUR/PR	lava	plg,olv,mag,cpx	.	KINTAMANI	186915	Y	Y	Y	-------
67327	BATUR/PR	lava	plg,cpx,olv,mag	.	KINTAMANI	187905	.	.	Y	-------
67328	BATUR/PR	lava	plg,olv	.	KINTAMANI	190916	Y	Y	Y	REE
67329	BATUR/CA	dacite ?breccia		.	KINTAMANI	240924	Y	.	Y	-------
67330	BATUR/CA	dacite lava	plg,olv,mag,cpx	.	KINTAMANI	242922	Y	.	Y	-------
67331	BATUR/CA	dacite ?lava	plg,cpx,opx,mag,olv	.	KINTAMANI	230913	Y	Y	Y	-------
67332	BATUR/CA	dacite ?lava	plg,olv,cpx,mag	.	KINTAMANI	188906	Y	.	Y	-------
67333	BATUR/PR	lava		.	KINTAMANI	214838	.	.	Y	KAr
67334	BATUR/PR	lava		.	KINTAMANI	214838	.	.	Y	KAr
67335	BATUR/PR	lava	plg,cpx,olv,mag	.	KINTAMANI	214838	Y	.	Y	-------
67336	BATUR/PR	lava	plg,cpx,olv,mag	.	TEDJAKULA	153998	Y	.	Y	-------
67337	BATUR/PR	lava	plg,olv,mag,cpx	.	TEDJAKULA	153998	Y	.	Y	-------
67338		NO ROCK								
67339	BATUR/PR	lava	plg,olv,mag	.	TEDJAKULA	153998	Y	Y	Y	-------
67340	BATUR/PR	lava		.	TEDJAKULA	153998	.	.	Y	KAr
67341	BATUR/PR	lava		.	TEDJAKULA	153998	.	.	Y	KAr
67342	BATUR/PR	lava	plg,olv	Y	TEDJAKULA	110038	Y	Y	Y	-------
67343	BATUR/PR	lava	plg,cpx,olv,mag	Y	TEDJAKULA	102045	Y	.	.	-------
67344	AGUNG	lava	plg,cpx,opx,mag	Y	KUBU	472822	Y	.	Y	-------
67345	AGUNG	lava	plg,olv,mag,cpx	Y	KUBU	468830	Y	.	Y	REE
67346	AGUNG	lava	plg,cpx,opx,mag,olv	.	--------	summit	Y	.	Y	-------
67347	AGUNG	lava	plg,olv,cpx,mag	.	--------	summit	Y	.	Y	-------

UT#	SUITE	DESCRIPTION	PHENOCRYSTS	O	SHEET	G.REF	T	P	X	OTHER
67348	AGUNG	lava	plg,cpx,mag	.	--------	summit	Y	.	Y	-------
67349	AGUNG	lava	plg,olv,cpx,mag	.	--------	summit	Y	.	Y	-------
67350	AGUNG	lava	plg,opx,cpx,mag	Y	KUBU	479802	Y	.	Y	-------
67351	AGUNG	lava	plg,opx,mag,cpx,olv	.	KARANGASEM	455721	Y	.	Y	-------
67352	AGUNG	1963 bomb		.	--------	summit	.	.	.	-------
67353	AGUNG	1963 lava (2 samples)	plg,cpx,opx,mag,olv	.	KUBU	364843	Y	.	Y	REE,?Be-10
67354	AGUNG	?1963 pumice		.	--------	summit	.	.	.	-------
67355	TAPAK	lava	plg,opx,cpx,mag,olv	.	PLAGA	927874	Y	.	Y	-------
67356	TAPAK	lava		.	PLAGA	927874	.	.	Y	-------
67357	TAPAK	lava	plg,opx,cpx,mag,olv	.	PLAGA	927874	Y	.	Y	-------
67358	TAPAK	lava	plg,opx,cpx,mag,olv	.	PLAGA	927874	Y	.	.	-------
67359	TAPAK	lava	plg,opx,cpx,mag	.	PLAGA	927874	Y	.	Y	-------
67360	TAPAK	lava	plg,opx,cpx,mag	.	PLAGA	927874	Y	.	Y	-------
67361	TAPAK	lava	plg,opx,cpx,mag	.	PLAGA	927874	Y	.	Y	-------
67362	TAPAK	lava	plg,opx,cpx,mag,olv	.	PLAGA	927874	Y	.	Y	-------
67363	TAPAK	lava	plg,opx,cpx,mag,olv	.	PLAGA	932875	Y	.	Y	REE
67364	LESONG	lava	plg,opx,cpx,mag,olv	.	PLAGA	904841	Y	.	Y	-------
67365	LESONG	lava	plg,opx,cpx,mag	.	PLAGA	907837	Y	.	Y	-------
67366	LESONG	lava	plg,opx,cpx,mag,olv	.	PLAGA	909838	Y	.	Y	-------
67367	LESONG	lava	plg,opx,cpx,mag	.	PLAGA	914833	Y	.	Y	-------
67368	LESONG	lava	plg,opx,cpx,mag	.	PLAGA	914833	Y	.	Y	-------
67369	LESONG	lava	plg,opx,cpx,mag,olv	.	PLAGA	916857	Y	.	Y	-------

UT#	SUITE	DESCRIPTION	PHENOCRYSTS	O	SHEET	G.REF	T	P	X	OTHER
67370	LESONG	lava	plg,opx,cpx,mag,olv	.	PLAGA	915859	Y	.	Y	-------
67371	LESONG	lava	plg,opx,cpx,mag,olv	.	PLAGA	904860	Y	.	Y	REE
67372	LESONG	lava	plg,opx,cpx,mag,olv	.	PLAGA	904860	Y	.	Y	-------
67373	LESONG	lava	plg,opx,cpx,mag,olv	.	PLAGA	900860	Y	.	Y	REE
67374	BATUKAU	lava	plg,olv,cpx,mag	.	PAJANGAN	939750	Y	.	Y	-------
67375	BATUKAU	lava	plg,mag,opx,cpx	.	PAJANGAN	933748	Y	.	Y	-------
67376	BATUKAU	lava	plg,mag,cpx	.	PAJANGAN	933748	Y	.	Y	REE
67377	BATUKAU	lava	plg,cpx,mag,opx	.	PAJANGAN	930748	Y	.	Y	-------
67378	BATUKAU	lava	plg,cpx,olv,mag	.	PAJANGAN	930728	Y	.	Y	REE
67379	BATUKAU	lava	plg,cpx,mag,opx	.	--------	------	Y	.	Y	-------
67380	BATUKAU	lava	plg,olv,mag,cpx	.	PAJANGAN	916714	Y	.	Y	-------
67381	BATUKAU	lava	plg,cpx,mag,opx	.	--------	------	Y	.	Y	-------
67382	SERAJA	lava	plg,olv,mag,cpx	.	KARANGASEM	484715	Y	.	Y	KAr
67383	SERAJA	lava	plg,cpx,mag	.	KARANGASEM	485714	Y	.	Y	KAr
67384	SERAJA	lava	plg,cpx,mag	.	KARANGASEM	485714	Y	.	Y	-------
67385	SERAJA	lava	plg,olv,cpx,mag	.	KARANGASEM	485714	Y	.	Y	-------
67386	SERAJA	lava	plg,opx,cpx,mag,?olv	.	KARANGASEM	485714	Y	.	Y	KAr
67387	SERAJA	lava	plg,olv,mag,cpx	.	KARANGASEM	511654	Y	.	Y	-------
67388	SERAJA	lava	plg,cpx,mag,olv	.	KARANGASEM	518659	Y	.	Y	-------
67389	SERAJA	lava	plg,olv,cpx,mag	.	KARANGASEM	523681	Y	.	Y	-------
67390	SERAJA	lava	plg,olv,cpx,mag	.	KARANGASEM	523681	Y	.	Y	-------
67391	SERAJA	lava		.	KARANGASEM	521679	.	.	Y	-------

UT#	SUITE	DESCRIPTION	PHENOCRYSTS	O	SHEET	G.REF	T	P	X	OTHER
67392	SERAJA	lava	olv,plg,cpx,mag	.	KARANGASEM	482780	Y	.	Y	REE
67393	SERAJA	lava	no phens	.	KARANGASEM	482780	Y	.	Y	-------
67394	SERAJA	lava	plg,olv,cpx,mag	.	KARANGASEM	482780	Y	.	Y	REE
67395	SERAJA	lava	plg,cpx,olv,mag	.	KARANGASEM	482780	Y	.	Y	-------
67396	SERAJA	lava		Y	KARANGASEM	517784	.	.	Y	KAr
67397	SERAJA	lava	plg,cpx,olv,mag,opx	.	KARANGASEM	527780	Y	.	Y	REE
67398	SERAJA	lava	plg,olv,mag,cpx	Y	KARANGASEM	519784	Y	.	Y	-------
67399	SERAJA	lava	plg,cpx,mag,?opx	.	KARANGASEM	470748	Y	.	Y	-------
67400	BRATAN	lava	plg,cpx,mag,olv	.	PLAGA	859875	Y	.	.	-------
67401	BRATAN	lava	plg,olv,cpx	.	PLAGA	859875	Y	.	Y	REE
67402	BRATAN	lava	plg,mag	.	PLAGA	843877	Y	.	Y	-------
67403	BRATAN	lava	plg,olv,cpx,mag	.	PLAGA	843877	Y	.	Y	-------
67404	BRATAN	lava	plg,olv,mag,cpx	.	PLAGA	843877	Y	.	Y	-------
67405	BRATAN	lava	plg,cpx,olv	.	PLAGA	843877	Y	.	Y	KAr
67406	BRATAN	lava	plg,olv,mag,cpx	.	PLAGA	827893	Y	.	Y	-------
67407	BRATAN	lava	plg,olv,cpx,mag	.	PLAGA	827893	Y	.	Y	-------
67408	BRATAN	lava	plg,olv	.	PLAGA	827893	Y	.	Y	REE
67409	BRATAN	lava	plg,mag,cpx,opx,olv	.	PLAGA	958882	Y	.	Y	REE
67410	BRATAN	lava	plg,olv	.	PLAGA	983839	Y	.	Y	REE,KAr
67411	?BRATAN	lava		.	TABANAN	938505	Y	.	Y	-------
67412	ULAKAN	pillow lava	olv,cpx,plg,mag	Y	PADANG	346586	Y	.	Y	KAr
67413	ULAKAN	pillow lava	olv,cpx,mag,plg	.	PADANG	295586	Y	.	Y	-------

UT#	SUITE	DESCRIPTION	PHENOCRYSTS	O	SHEET	G.REF	T	P	X	OTHER
67414	ULAKAN	pillow lava	olv,cpx	.	PADANG	295586	Y	.	Y	-------
67415	ULAKAN	pillow lava		.	PADANG	438584	Y	Y	Y	-------
67416	ULAKAN	pillow lava	olv,cpx	.	PADANG	465597	Y	.	.	-------
67417	ULAKAN	pillow lava		.	PADANG	465597	.	.	Y	-------
67418	ULAKAN	pillow lava	olv,cpx	Y	PADANG	461596	Y	.	Y	REE
67419	ULAKAN	pillow lava	olv,cpx	.	PADANG	336581	Y	.	Y	REE
67420	ULAKAN	pillow lava		.	PADANG	336581	.	.	Y	-------
67421	ULAKAN	pillow lava		.	PADANG	336581	.	.	Y	REE,KAr
67422	ULAKAN	pillow lava	olv,cpx	.	PADANG	336581	Y	.	Y	-------
67423	ULAKAN	crystal tuff		.	PADANG	336581	.	.	.	-------
67424	ULAKAN	pillow lava	olv,cpx	.	PADANG	336581	Y	.	Y	-------
67425	ULAKAN	pillow lava		.	PADANG	330599	.	.	Y	-------
67426	ULAKAN	pillow lava	olv,cpx,mag	.	PADANG	330599	Y	.	Y	-------
67427	ULAKAN	sinter		Y	PADANG	461596	.	.	.	-------
67428	S.Bali	limestone		.	--------	------	.	.	.	-------
67429	KRAKATAU	1972 lava Anak Krakatau	plg,cpx,olv,opx,mag	.	--------	------	Y	.	Y	-------
67430	--------	welded tuff (cobbles)		.	FLORES	------	.	.	.	-------

APPENDIX 2

Major and Trace Element Analyses of Volcanic Rocks from Central and Eastern Bali, Indonesia

This appendix lists chemical analyses of volcanic rocks from the following volcanoes:

1. Agung
2. Batukau
3. Batur - postcaldera stage
   - caldera stage
   - precaldera stage
4. Bratan
5. Lesong
6. Seraja
7. Tapak
8. Ulakan Formation

Rock samples were prepared for analysis by firstly removing weathered surfaces by hammer and splitter, followed by coarse crushing in a steel jaw crusher. A 50-80 g aliquot of this material was then ground in a tungsten-carbide swing mill.

Except for H_2O all major and trace element analyses were obtained using an automated Philips PW1410 X-ray fluorescence spectrometer. Major elements were measured from glass discs prepared with 1.50 g lithium borate flux, 0.02 g lithium nitrate and 0.28 g sample powder (Norrish & Chappell 1967; Norrish & Hutton 1969). Trace elements were measured from pressed powder pills backed by boric acid. Mass absorption coefficients were calculated from the major element composition. Volatile components were determined by heating 1 g of sample powder to 110 ^{o}C (H_2O^-) and 1000 ^{o}C (Loss On Ignition) for 12 hours. In the tables of analyses, 'rest' is the sum of trace elements expressed as oxides.

A range of international standards was used for

calibration and precision was monitored by replicate analyses of internal secondary standards. Typical precisions (99 % confidence level) for the elements measured are:

major elements (wt %; standard = TASBAS)

SiO_2	44.56 +- 0.25
TiO_2	2.31 +- 0.02
Al_2O_3	14.14 +- 0.12
Fe_2O_3	12.65 +- 0.06
MnO	0.17 +- 0.004
MgO	8.16 +- 0.15
CaO	7.81 +- 5.43
Na_2O	5.43 +- 0.21
K_2O	1.86 +- 0.04
P_2O_5	0.97 +- 0.02

trace elements (p.p.m.)

Ba	500 +- 5,	1200 +- 5	
Rb	10 +- 1,	70 +- 1,	170 +- 2
Sr	10 +- 1,	200 +- 2,	500 +- 5
Zr	100 +- 2,	250 +- 4,	500 +-10
Nb	10 +- 0.5,	20 +- 1	
Y	10 +- 2,	20 +- 1,	100 +- 2
La	20 +- 1,	40 +- 2,	100 +- 2
Ce	30 +- 2,	80 +- 3,	150 +- 1
Nd	15 +- 1,	30 +- 2,	50 +- 2
Sc	10 +- 1,	30 +- 1	
V	30 +- 2,	100 +- 1	
Ni	3 +- 0.5,	20 +- 0.5,	200 +- 2
Cr	10 +- 2,	400 +- 4	

number	67345	67344	67351	67350	67348	67349	67346	67353	67347
(major elements: wt %)									
SiO2	51.20	52.78	53.34	53.85	54.10	55.02	56.27	56.88	58.24
TiO2	1.16	0.98	0.82	0.81	0.96	0.87	0.81	0.76	0.80
Al2O3	17.90	18.28	20.57	20.63	18.26	17.78	17.85	17.35	17.16
Fe2O3	11.53	10.19	7.95	7.91	9.57	9.14	8.83	8.30	7.95
FeO									
MnO	0.23	0.21	0.17	0.17	0.23	0.19	0.19	0.17	0.19
MgO	4.82	4.26	2.58	2.51	3.84	3.66	3.54	3.50	2.98
CaO	8.61	8.19	8.84	8.81	8.62	7.92	7.81	7.41	6.62
Na2O	3.08	3.12	3.66	3.60	3.30	3.41	3.24	3.25	3.61
K2O	1.05	1.17	1.16	1.18	1.32	1.57	1.22	1.61	1.70
P2O5	0.23	0.27	0.26	0.26	0.21	0.24	0.25	0.24	0.27
LOI	-0.30	-0.10	-0.10	0.07	-0.41	-0.16	-0.32	-0.18	-0.12
H2O-	0.19	0.19	0.20	0.29	0.02	0.08	0.06	0.08	0.04
rest	0.16	0.15	0.14	0.14	0.15	0.16	0.15	0.15	0.15
total	99.86	99.69	99.59	100.23	100.17	99.88	99.90	99.52	99.59
(trace elements: ppm)									
Ba	220	257	246	248	288	299	279	327	368
Rb	22	23	24	25	26	33	31	40	46
Sr	411	452	518	509	418	439	439	435	369
Zr	85	95	88	89	89	112	114	133	157
Nb	4	4	3	3	3	4	6	4	7
Y	27	27	27	26	28	28	27	30	33
La	12	13	13	14	13	15	16	18	16
Ce	25	25	23	22	27	26	29	35	40
Nd	18	19	18	18	16	19	19	21	22
Sc	31	25	21	21	22	25	21	22	19
V	363	261	146	154	254	229	193	168	152
Ni	19	15	5	6	6	13	10	11	9
Cr	8	8	7	6	2	14	7	16	12
Mg#	45.30	45.30	39.13	38.60	44.28	44.23	44.26	45.51	42.61

Agung Volcano

number	67380	67378	67374	67381	67377	67379	67375	67376
(major elements: wt %)								
SiO2	51.73	52.68	52.76	54.71	54.88	56.93	57.60	57.98
TiO2	1.04	1.03	0.97	0.88	0.84	0.79	0.72	0.73
Al2O3	18.28	19.39	18.68	18.26	19.53	19.68	19.93	19.62
Fe2O3	10.74	9.15	10.17	9.16	8.30	7.08	6.19	6.41
FeO								
MnO	0.21	0.17	0.21	0.20	0.18	0.15	0.14	0.15
MgO	4.15	3.40	3.47	3.56	2.59	2.04	1.63	1.62
CaO	8.96	8.44	8.81	7.84	8.12	7.31	6.74	6.98
Na2O	3.05	3.73	2.63	3.30	3.66	3.57	3.76	3.75
K2O	0.82	1.03	1.34	1.27	1.05	1.35	1.49	1.53
P2O5	0.18	0.24	0.17	0.21	0.22	0.24	0.26	0.25
LOI	0.14	0.03	0.07	-0.23	0.05	0.15	0.62	0.26
H2O-	0.29	0.30	0.32	0.19	0.21	0.24	0.30	0.26
rest	0.14	0.13	0.15	0.14	0.12	0.13	0.13	0.13
total	99.73	99.72	99.75	99.49	99.75	99.66	99.51	99.67
(trace elements: ppm)								
Ba	201	241	281	276	252	294	319	310
Rb	15	18	34	30	23	34	37	37
Sr	329	312	397	342	314	358	355	364
Zr	83	122	91	108	124	131	134	134
Nb	4	5	6	6	5	7	8	6
Y	30	32	24	26	43	33	33	34
La	12	12	12	13	14	16	16	16
Ce	15	21	27	29	20	28	32	32
Nd	15	18	16	19	19	18	21	22
Sc	31	26	30	24	20	18	14	17
V	303	224	287	224	151	137	86	91
Ni	11	8	4	8	4	5	3	3
Cr	18	12	6	12	4	9	4	6
Mg#	43.35	42.40	40.33	43.50	38.20	36.34	34.28	33.36

Batukau Volcano

number	67247	67244	67270	67250	67264	67271	67261	67262	67265	67257
(major elements: wt %)										
SiO2	51.08	51.78	51.79	51.95	52.11	52.28	52.34	52.39	52.44	52.63
TiO2	0.96	0.98	0.96	0.98	0.99	0.98	0.97	0.97	0.98	1.00
Al2O3	18.03	18.00	17.72	17.95	18.01	18.12	18.12	18.24	18.21	18.06
Fe2O3	11.03	10.80	10.58	10.80	10.49	10.58	10.33	10.31	10.50	10.66
FeO										
MnO	0.22	0.21	0.21	0.21	0.21	0.22	0.20	0.21	0.21	0.21
MgO	5.04	4.73	4.85	4.60	4.42	4.38	4.39	4.31	4.41	4.47
CaO	9.26	8.97	9.75	9.08	9.38	8.86	9.36	9.33	8.88	8.93
Na2O	3.27	3.97	3.13	3.54	3.56	3.48	3.07	3.38	3.52	3.49
K2O	0.91	0.95	0.97	0.90	0.99	0.78	0.68	0.95	0.87	0.75
P2O5	0.20	0.22	0.21	0.22	0.22	0.25	0.24	0.21	0.21	0.23
LOI	-0.62	-0.65	-0.44	-0.63	-0.59	-0.34	-0.37	-0.49	-0.53	-0.56
H2O-	0.09	0.09	0.08	0.07	0.06	0.17	0.18	0.13	0.12	0.09
rest	0.14	0.15	0.15	0.14	0.15	0.15	0.15	0.14	0.15	0.14
total	99.61	100.20	99.96	99.81	100.00	99.91	99.66	100.08	99.97	100.10
(trace elements: ppm)										
Ba	221	216	205	220	241	231	226	235	243	231
Rb	18	18	18	17	18	19	18	17	19	18
Sr	417	429	426	417	435	439	432	416	451	426
Zr	70	66	63	64	70	67	68	68	73	71
Nb	4	4	4	4	5	4	4	4	4	4
Y	21	19	21	20	23	21	20	20	22	22
La	13	10	12	13	12	12	11	12	14	13
Ce	19	16	16	16	22	21	18	16	22	16
Nd	15	14	13	12	16	13	14	13	16	15
Sc	27	28	31	27	29	28	29	29	27	27
V	284	284	285	276	289	275	287	279	267	269
Ni	18	39	18	16	15	15	14	15	15	16
Cr	18	13	55	15	28	20	26	24	17	10
Mg#	47.51	46.45	47.59	45.76	45.49	45.06	45.70	45.30	45.41	45.37

Batur Volcano - postcaldera stage

number	67267	67238	67240	67269	67259	67268	67266	67272
(major elements: wt %)								
SiO2	52.78	52.94	53.54	54.06	54.12	54.13	54.86	55.04
TiO2	1.02	1.02	1.03	0.99	1.00	0.99	1.03	1.03
Al2O3	18.02	18.16	18.96	18.73	18.84	18.97	18.57	18.34
Fe2O3	10.48	10.20	9.65	9.40	9.33	9.04	9.23	9.16
FeO								
MnO	0.21	0.21	0.19	0.20	0.19	0.19	0.20	0.19
MgO	4.13	3.62	3.06	3.04	2.85	2.82	2.68	2.61
CaO	8.84	8.78	9.06	8.60	8.78	8.54	8.20	8.13
Na2O	3.35	3.63	3.85	3.82	4.23	3.78	3.81	4.14
K2O	0.95	1.29	0.99	1.21	0.93	1.01	0.94	0.97
P2O5	0.23	0.23	0.24	0.24	0.27	0.26	0.27	0.27
LOI	-0.53	-0.57	-0.54	-0.40	-0.46	-0.45	-0.41	-0.53
H2O-	0.16	0.42	0.09	0.12	0.10	0.15	0.08	0.03
rest	0.14	0.14	0.15	0.14	0.14	0.14	0.15	0.14
total	99.78	100.07	100.27	100.15	100.32	99.57	99.61	99.52
(trace elements: ppm)								
Ba	234	232	239	244	254	251	268	289
Rb	21	22	21	23	21	22	23	21
Sr	436	428	428	452	442	436	431	407
Zr	73	78	81	80	79	83	89	89
Nb	5	5	5	5	5	5	6	6
Y	21	22	20	24	24	24	26	26
La	13	16	12	14	12	16	14	16
Ce	17	24	23	21	24	21	26	27
Nd	14	15	17	16	17	15	18	16
Sc	28	27	28	26	26	26	27	29
V	254	265	274	227	233	222	228	225
Ni	12	9	7	6	7	6	6	4
Cr	19	9	5	7	10	6	8	5
Mg#	43.84	41.28	38.58	39.05	37.70	38.19	36.51	36.08

Batur Volcano - postcaldera stage

number	67331	67275	67329	67330	67263	PUM1	67274	67332	67278	67273
(major elements: wt %)										
SiO2	61.69	61.75	61.92	61.99	62.50	63.91	63.93	64.00	64.27	64.59
TiO2	0.79	0.88	0.97	1.00	0.81	0.42	0.74	0.82	0.82	0.77
Al2O3	16.09	16.81	16.13	16.10	16.11	14.38	15.95	15.92	16.07	16.18
Fe2O3	6.64	7.21	7.14	7.25	6.11	4.55	5.83	6.39	6.53	5.83
FeO										
MnO	0.21	0.22	0.23	0.23	0.21	0.17	0.21	0.21	0.22	0.22
MgO	1.43	1.64	1.59	1.58	1.32	0.47	1.10	1.01	1.06	1.16
CaO	3.98	4.59	4.10	4.18	3.76	1.85	3.22	3.43	3.46	3.25
Na2O	5.23	4.95	5.27	5.35	4.99	5.15	5.41	5.23	5.45	5.50
K2O	2.32	1.63	2.31	1.57	1.89	2.87	2.48	1.85	2.14	1.60
P2O5	0.31	0.39	0.44	0.44	0.35	0.09	0.25	0.27	0.26	0.28
LOI	0.55	-0.06	-0.21	-0.30	0.68	2.55	0.10	0.13	-0.19	0.03
H2O-	0.35	0.13	0.09	0.12	0.56	2.41	0.07	0.37	0.07	0.07
rest	0.14	0.13	0.14	0.13	0.14	0.13	0.13	0.13	0.13	0.13
total	99.73	100.27	100.12	99.64	99.43	98.95	99.42	99.76	100.29	99.61
(trace elements: ppm)										
Ba	444	400	437	423	444	529	444	460	465	437
Rb	47	39	45	41	46	60	50	50	52	49
Sr	295	322	323	320	287	157	280	268	274	280
Zr	153	137	149	143	159	195	159	160	166	156
Nb	9	9	11	11	10	10	10	10	10	10
Y	36	32	35	36	36	40	33	35	35	33
La	18	17	19	18	19	22	19	18	20	18
Ce	43	37	38	40	45	45	40	44	41	34
Nd	25	23	27	26	27	24	23	24	23	22
Sc	17	18	20	20	18	15	16	18	17	16
V	42	54	37	42	39	3	18	11	9	18
Ni	2	2	2	2	2	1	2	3	1	2
Cr	2	4	4	3	3	1	2	6	8	4
Mg#	29.90	31.06	30.61	30.15	29.97	16.99	27.21	23.84	24.33	28.27

Batur Volcano - caldera stage

number	67276	67294	67281D	67282D	67277
(major elements: wt %)					
SiO2	65.72	65.83	66.41	66.47	66.70
TiO2	0.69	0.55	0.55	0.54	0.54
Al2O3	15.84	15.25	15.60	15.50	15.38
Fe2O3	5.39	4.72	5.33	5.26	5.25
FeO					
MnO	0.19	0.18	0.19	0.20	0.21
MgO	0.83	0.56	0.63	0.61	0.54
CaO	2.71	2.05	2.43	2.37	2.35
Na2O	5.40	5.16	5.84	5.84	5.88
K2O	2.29	2.66	2.83	2.80	2.94
P2O5	0.21	0.14	0.12	0.14	0.13
LOI	0.09	1.65	0.06	0.18	0.01
H2O-	0.05	0.54	0.13		0.01
rest	0.13	0.14	0.14	0.14	0.14
total	99.54	99.43	100.26	100.05	100.08
(trace elements: ppm)					
Ba	460	518	527	524	525
Rb	53	74	59	60	59
Sr	240	192	200	202	194
Zr	174	220	189	190	195
Nb	10	13	10	10	12
Y	33	41	41	42	37
La	18	24	20	22	22
Ce	41	50	44	47	45
Nd	24	26	27	26	26
Sc	13	16	18	17	16
V	7	6	9	8	1
Ni	1	2	2	1	1
Cr	2	2	1	3	5
Mg#	23.37	19.03	18.97	18.68	16.93

Batur Volcano - caldera stage

number	67337	67341	67325	67340	67333	67334	67327	67326	67328	67335
(major elements: wt %)										
SiO2	48.62	48.74	48.83	50.42	51.09	51.44	51.85	52.08	52.28	53.21
TiO2	1.08	0.91	1.02	0.97	0.90	0.97	0.95	0.97	1.01	1.01
Al2O3	19.88	19.41	17.62	20.25	16.87	18.53	17.91	18.11	18.33	18.32
Fe2O3	10.69	10.66	12.12	10.00	10.60	10.36	10.56	10.68	10.54	10.00
FeO										
MnO	0.20	0.19	0.22	0.19	0.20	0.19	0.21	0.21	0.20	0.18
MgO	4.22	5.94	5.78	3.72	7.13	3.91	4.78	4.47	3.74	3.33
CaO	10.17	11.04	10.33	9.81	9.91	9.44	9.35	9.10	9.19	8.74
Na2O	2.95	3.04	2.79	2.98	2.78	2.93	3.33	3.38	3.49	3.24
K2O	0.89	0.57	0.60	0.81	1.14	1.34	0.97	1.04	1.08	1.51
P2O5	0.23	0.16	0.14	0.22	0.22	0.24	0.22	0.22	0.22	0.27
LOI	0.48	-0.33	-0.39	-0.03	-0.57	-0.06	-0.56	-0.62	-0.42	-0.39
H2O-	0.66	0.17	0.34	0.43	0.10	0.24	0.04	0.06	0.17	0.11
rest	0.13	0.13	0.15	0.13	0.18	0.15	0.15	0.15	0.15	0.16
total	100.20	100.63	99.55	99.90	100.55	99.68	99.76	99.85	99.98	99.69
(trace elements: ppm)										
Ba	199	142	178	172	224	254	218	245	258	294
Rb	17	11	8	16	27	31	16	23	23	34
Sr	361	366	417	446	415	425	432	393	393	427
Zr	61	43	41	61	76	91	62	68	87	107
Nb	4	2	2	3	4	5	4	5	4	7
Y	23	18	16	22	22	24	19	20	22	26
La	8	7	7	6	10	9	9	9	12	13
Ce	16	9	15	14	26	26	19	19	24	32
Nd	16	13	10	14	18	17	14	14	18	20
Sc	23	30	33	22	34	30	32	29	30	27
V	289	288	383	228	279	280	301	298	292	256
Ni	8	23	25	7	124	14	21	14	12	10
Cr	7	33	35	13	197	22	50	20	16	13
Mg#	43.88	52.47	48.58	42.42	57.12	42.78	47.27	45.33	41.27	39.74

Batur Volcano - precaldera stage

number	67339	67336	67299	67295	67318	67342
(major elements: wt %)						
SiO2	53.58	55.18	55.32	56.12	57.01	58.58
TiO2	1.43	1.29	1.12	1.14	1.11	1.33
Al2O3	16.60	16.09	16.24	16.21	16.29	15.29
Fe2O3	11.83	10.76	9.37	9.63	9.25	9.40
FeO						
MnO	0.22	0.25	0.21	0.21	0.22	0.23
MgO	2.86	2.95	2.49	2.44	2.41	1.80
CaO	7.67	6.92	5.93	6.02	5.93	5.06
Na2O	3.19	3.89	4.27	4.06	3.96	3.51
K2O	2.13	2.11	1.95	0.41	2.47	3.38
P2O5	0.48	0.47	0.77	0.78	0.71	0.61
LOI	-0.26	-0.28	0.86	0.40	0.04	0.01
H2O-	0.28	0.21	0.83	0.51	0.26	0.50
rest	0.19	0.17	0.18	0.18	0.18	0.20
total	100.20	100.01	99.54	98.11	99.84	99.90
(trace elements: ppm)						
Ba	397	369	467	450	471	581
Rb	59	49	69	64	71	97
Sr	375	362	369	362	370	326
Zr	188	159	239	233	250	318
Nb	10	9	14	13	14	17
Y	44	40	57	55	55	66
La	24	19	34	31	35	38
Ce	51	45	72	71	74	88
Nd	32	27	44	43	42	49
Sc	31	30	26	25	25	26
V	271	230	95	96	86	26
Ni	8	5	3	2	3	3
Cr	5	11	3	1	9	7
Mg#	32.38	35.19	34.49	33.42	34.04	27.50

Batur Volcano - precaldera stage

number	67410	67405	67401	67411	67404	67408	67403	67407	67402	67406	67409
(major elements: wt %)											
SiO2	49.49	50.59	50.66	51.20	51.53	52.00	52.07	52.19	52.31	59.68	61.82
TiO2	1.28	0.89	1.01	1.46	1.35	1.28	1.31	1.11	1.28	1.05	0.82
Al2O3	16.98	16.05	16.42	15.94	17.15	17.30	16.77	18.77	16.59	15.94	15.91
Fe2O3	13.64	10.66	12.48	12.22	11.42	11.29	11.69	9.75	11.62	8.48	6.99
FeO											
MnO	0.25	0.20	0.24	0.26	0.20	0.22	0.21	0.16	0.20	0.15	0.13
MgO	4.90	7.00	4.38	3.86	4.39	3.88	3.94	2.67	3.65	1.58	1.27
CaO	9.75	10.72	10.05	8.46	8.83	8.62	8.87	8.88	8.76	4.86	4.11
Na2O	3.10	2.33	2.96	3.20	2.98	2.98	3.07	3.26	3.06	4.07	4.03
K2O	0.93	0.95	0.99	1.78	1.58	1.55	1.87	1.75	1.96	2.92	3.48
P2O5	0.25	0.17	0.19	0.39	0.36	0.35	0.32	0.29	0.31	0.36	0.28
LOI	-0.66	-0.23	-0.03	0.55	-0.26	0.07	-0.27	0.10	-0.25	0.22	0.27
H2O-	0.18	0.21	0.41	0.78	0.28	0.52	0.33	0.35	0.31	0.62	0.51
rest	0.18	0.17	0.16	0.17	0.16	0.17	0.18	0.17	0.18	0.17	0.17
total	100.27	99.71	99.92	100.27	99.97	100.23	100.36	99.45	99.98	100.10	99.79
(trace elements: ppm)											
Ba	273	222	264	347	308	288	367	356	363	519	572
Rb	15	24	15	39	52	50	60	57	64	87	90
Sr	432	302	366	334	284	329	310	363	308	288	244
Zr	50	73	60	139	176	181	158	145	164	228	274
Nb	3	4	3	8	8	9	8	8	8	10	11
Y	23	22	21	36	40	39	35	39	35	44	44
La	13	9	8	18	20	15	17	21	15	26	25
Ce	24	13	14	35	37	36	42	30	38	45	58
Nd	17	14	12	24	26	25	24	26	24	31	33
Sc	38	38	34	31	32	31	36	27	35	22	17
V	445	323	422	338	276	279	328	252	328	90	44
Ni	19	67	19	17	15	19	14	13	14	2	3
Cr	26	223	16	13	21	24	22	21	22	5	5
Mg#	41.57	56.53	41.01	38.49	43.23	40.50	40.03	35.17	38.35	26.96	26.46

Bratan Volcano

number	67372	67366	67373	67367	67369	67370	67365	67368	67371	67364
(major elements: wt %)										
SiO2	54.33	55.53	55.66	55.88	56.07	57.37	57.65	57.77	58.42	58.49
TiO2	0.88	0.91	0.87	0.84	0.83	0.84	0.84	0.83	0.77	0.84
Al2O3	18.68	17.74	17.92	17.26	16.55	17.42	17.01	17.01	17.00	17.09
Fe2O3	8.94	9.21	8.92	8.82	8.88	8.79	8.22	8.10	7.67	8.16
FeO										
MnO	0.19	0.20	0.18	0.19	0.19	0.19	0.18	0.17	0.17	0.17
MgO	3.06	2.99	3.19	3.43	3.69	3.09	2.84	2.79	2.57	2.78
CaO	7.40	7.16	7.45	7.34	7.33	7.05	6.82	6.67	6.14	6.66
Na2O	3.03	3.41	3.09	3.27	3.17	3.24	3.54	3.63	3.17	3.41
K2O	1.57	1.91	1.82	1.85	2.13	2.03	2.33	2.31	2.47	2.15
P2O5	0.22	0.22	0.18	0.19	0.18	0.19	0.19	0.19	0.20	0.17
LOI	0.90	0.01	0.04	0.20	0.20	-0.20	-0.16	0.06	0.58	-0.26
H2O-	0.55	0.31	0.21	0.31	0.32	0.13	0.09	0.26	0.38	0.06
rest	0.17	0.16	0.16	0.16	0.16	0.16	0.16	0.16	0.17	0.16
total	99.92	99.76	99.69	99.74	99.70	100.30	99.71	99.95	99.71	99.88
(trace elements: ppm)										
Ba	418	400	378	415	402	403	412	427	447	436
Rb	50	54	54	59	60	62	73	72	82	74
Sr	436	350	416	338	325	348	318	326	310	317
Zr	138	147	135	158	155	162	188	186	204	192
Nb	7	7	7	7	7	8	8	8	9	10
Y	29	29	28	30	29	31	33	33	34	34
La	19	19	15	16	18	20	19	19	23	20
Ce	41	38	38	33	35	37	40	41	45	38
Nd	23	23	21	23	19	22	22	22	23	20
Sc	22	21	22	22	22	20	19	18	17	19
V	192	199	195	187	193	185	173	162	147	167
Ni	6	6	6	9	13	8	5	10	5	4
Cr	10	5	5	14	37	10	8	10	10	11
Mg#	40.40	39.14	41.46	43.51	45.15	41.05	40.63	40.56	39.89	40.29

Lesong Volcano

number	67392	67390	67395	67393	67394	67398	67388	67385	67387	67389
(major elements: wt %)										
SiO2	50.14	50.40	50.60	50.88	51.12	51.20	51.35	52.48	52.89	53.48
TiO2	0.94	1.01	1.09	1.09	1.05	0.87	0.87	0.89	0.72	0.84
Al2O3	16.79	17.76	16.44	16.97	18.85	18.63	18.62	18.63	21.01	18.69
Fe2O3	10.63	11.05	11.46	11.33	10.77	10.22	10.45	9.91	7.87	9.16
FeO										
MnO	0.19	0.22	0.22	0.20	0.22	0.20	0.21	0.20	0.17	0.20
MgO	6.19	4.11	5.06	4.63	4.48	3.95	4.02	3.47	2.28	3.01
CaO	10.11	9.78	9.41	9.68	9.30	9.05	9.48	8.91	8.95	8.45
Na2O	2.89	3.04	2.92	2.92	3.05	3.30	3.13	3.08	3.51	3.27
K2O	1.54	1.41	1.86	1.51	1.02	1.24	1.27	1.54	1.41	1.73
P2O5	0.31	0.24	0.39	0.33	0.21	0.20	0.23	0.24	0.21	0.23
LOI	-0.33	0.30	-0.04	-0.04	-0.48	0.01	-0.19	-0.06	0.44	-0.04
H2O-	0.21	0.58	0.28	0.30	0.14	0.62	0.12	0.23	0.37	0.30
rest	0.21	0.17	0.19	0.19	0.15	0.16	0.16	0.17	0.17	0.17
total	99.82	100.07	99.88	99.99	99.88	99.65	99.72	99.69	100.00	99.49
(trace elements: ppm)										
Ba	298	316	372	343	197	312	299	350	452	366
Rb	34	25	46	37	15	26	22	33	26	38
Sr	411	434	409	438	433	478	506	449	551	501
Zr	93	84	122	101	71	73	69	90	76	96
Nb	4	4	4	4	5	2	3	3	4	4
Y	23	22	30	27	22	26	23	23	24	30
La	9	10	16	12	9	12	9	10	14	15
Ce	28	19	24	24	19	18	24	14	19	21
Nd	18	15	21	18	16	15	14	14	16	17
Sc	31	30	30	33	29	25	25	26	20	23
V	332	370	336	363	322	284	302	302	179	256
Ni	85	16	38	33	14	11	13	9	6	7
Cr	305	12	74	47	18	6	6	6	9	4
Mg#	53.56	42.42	46.65	44.73	45.17	43.36	43.25	40.95	36.46	39.43

Seraja Volcano

number	67382	67383	67386	67399	67391	67396	67397	67384
(major elements: wt %)								
SiO2	54.13	54.25	54.26	54.51	54.53	55.28	55.33	55.91
TiO2	0.65	0.63	0.82	0.87	0.72	0.77	0.75	0.63
Al2O3	21.07	21.41	18.12	18.25	20.00	18.02	17.77	19.98
Fe2O3	7.07	6.96	9.44	8.90	7.60	8.81	8.58	6.86
FeO								
MnO	0.17	0.17	0.20	0.30	0.17	0.20	0.20	0.15
MgO	2.02	1.89	3.40	2.71	2.63	3.09	3.18	1.97
CaO	8.80	8.76	8.27	7.12	8.55	7.63	7.80	7.93
Na2O	3.41	3.50	3.18	3.82	3.42	3.43	3.47	3.52
K2O	1.44	1.54	1.59	1.41	1.67	1.75	1.71	1.80
P2O5	0.24	0.24	0.23	0.26	0.25	0.25	0.23	0.22
LOI	0.25	0.40		0.74	0.09	0.54	0.27	0.31
H2O-	0.30	0.34	0.24	1.08	0.32	0.38	0.29	0.39
rest	0.15	0.15	0.17	0.15	0.17	0.26	0.16	0.15
total	99.70	100.24	99.92	100.12	100.12	100.41	99.74	99.82
(trace elements: ppm)								
Ba	337	332	397	321	402	1147	408	378
Rb	29	30	38	30	41	39	39	42
Sr	553	545	494	512	569	531	469	501
Zr	79	82	97	91	102	103	108	99
Nb	3	3	4	3	4	4	4	4
Y	26	26	25	28	26	29	25	25
La	12	11	13	12	14	13	13	13
Ce	22	27	28	24	21	26	27	27
Nd	14	18	17	17	17	18	15	16
Sc	19	18	20	16	19	18	18	17
V	139	133	232	150	180	217	198	132
Ni	5	5	9	3	12	9	8	5
Cr	6	5	9	6	22	6	7	8
Mg#	36.14	34.98	41.64	37.62	40.67	40.99	42.33	36.26

Seraja Volcano

number	67363	67361	67356	67360	67362	67357	67355	67359
(major elements: wt %)								
SiO2	55.02	55.61	56.08	56.27	56.51	57.10	57.53	58.99
TiO2	0.88	0.82	0.79	0.84	0.91	0.80	0.79	0.78
Al2O3	17.48	17.76	17.55	17.44	17.33	17.19	17.29	17.12
Fe2O3	9.35	9.15	8.93	9.03	8.70	8.60	8.43	8.25
FeO								
MnO	0.19	0.19	0.19	0.19	0.18	0.18	0.18	0.18
MgO	3.64	3.29	3.22	3.11	3.28	2.90	2.98	2.70
CaO	7.73	7.47	7.39	7.27	7.10	7.00	6.83	6.44
Na2O	2.95	3.05	2.81	3.17	3.20	2.96	3.22	3.02
K2O	1.94	1.86	1.90	2.01	2.00	2.13	2.16	2.29
P2O5	0.14	0.18	0.17	0.17	0.18	0.18	0.16	0.19
LOI	0.03	-0.06	0.20		0.14	0.11	0.14	-0.09
H2O-	0.31	0.22	0.28	0.23	0.20	0.24	0.24	0.10
rest	0.16	0.16	0.15	0.16	0.16	0.16	0.16	0.16
total	99.82	99.70	99.66	99.89	99.89	99.55	100.11	100.13
(trace elements: ppm)								
Ba	339	369	361	371	348	395	394	436
Rb	54	52	58	61	62	66	67	68
Sr	369	360	353	357	317	342	344	323
Zr	133	141	144	147	166	162	166	174
Nb	7	6	7	7	7	7	8	8
Y	26	27	27	28	33	30	30	29
La	15	16	18	17	17	19	18	18
Ce	37	33	31	33	40	42	35	38
Nd	20	20	18	19	22	21	20	22
Sc	22	22	22	21	22	22	20	18
V	229	203	199	202	200	187	172	150
Ni	11	9	9	7	7	7	7	5
Cr	10	9	8	8	11	10	9	9
Mg#	43.54	41.60	41.66	40.55	42.75	40.05	41.18	39.33

Tapak Volcano

number	67413	67424	67420	67425	67418	67422	67412	67417	67415	67426
(major elements: wt %)										
SiO2	45.56	46.44	46.45	46.55	46.76	46.86	46.90	47.08	47.19	47.28
TiO2	0.72	0.56	0.72	0.75	0.72	0.79	0.84	0.71	0.79	0.72
Al2O3	12.27	9.12	12.97	13.78	12.46	11.84	12.48	12.60	14.16	13.35
Fe2O3	11.51	11.45	11.04	10.74	11.22	11.34	11.07	11.38	11.57	11.24
FeO										
MnO	0.20	0.20	0.19	0.19	0.19	0.19	0.20	0.20	0.21	0.19
MgO	10.14	17.48	10.83	8.41	12.37	13.30	11.51	12.14	9.21	9.24
CaO	11.45	11.78	11.18	10.67	10.86	11.84	11.99	10.92	10.82	11.49
Na2O	1.21	1.22	1.26	2.26	1.51	1.59	1.63	1.70	1.88	2.44
K2O	2.00	0.61	2.59	2.20	1.75	0.94	1.61	1.59	1.96	1.75
P2O5	0.22	0.21	0.39	0.30	0.27	0.28	0.25	0.24	0.37	0.38
LOI	3.41	0.41	1.81	3.05	1.49	0.42	0.72	1.29	1.11	1.51
H2O-	1.23	0.37	0.40	0.97	0.31	0.40	0.28	0.31	0.47	0.37
rest	0.31	0.33	0.31	0.30	0.33	0.31	0.29	0.30	0.34	0.32
total	100.23	100.18	100.14	100.17	100.24	100.10	99.77	100.46	100.08	100.28
(trace elements: ppm)										
Ba	637	300	467	751	638	413	426	582	700	762
Rb	37	13	69	51	27	25	26	30	35	40
Sr	844	438	835	776	763	680	621	595	976	893
Zr	44	39	71	67	56	63	59	50	74	66
Nb	1	1	2	2	1	5	6	1	2	2
Y	16	12	17	17	15	17	18	16	18	18
La	13	8	13	19	17	13	14	12	20	18
Ce	33	10	30	34	33	28	27	24	40	28
Nd	17	12	17	18	17	17	16	15	20	18
Sc	30	45	32	29	31	38	37	33	28	32
V	313	252	307	284	311	275	299	308	335	300
Ni	145	392	187	102	201	246	195	199	139	117
Cr	398	1055	482	269	554	618	546	527	355	351
Mg#	63.57	75.15	66.02	60.80	68.59	69.91	67.31	67.88	61.19	61.95

Ulakan Formation

number	67414	67421	67419
(major elements: wt %)			
SiO2	47.34	47.38	48.41
TiO2	0.72	0.73	0.84
Al2O3	12.56	13.47	15.61
Fe2O3	11.44	11.59	11.38
FeO			
MnO	0.18	0.20	0.19
MgO	10.23	9.62	7.31
CaO	11.10	11.16	9.15
Na2O	1.70	1.63	2.07
K2O	1.78	2.24	2.69
P2O5	0.24	0.30	0.38
LOI	1.43	1.09	1.28
H2O-	0.57	0.28	0.43
rest	0.27	0.34	0.31
total	99.56	100.03	100.05
(trace elements: ppm)			
Ba	529	794	805
Rb	38	49	56
Sr	533	895	840
Zr	47	53	70
Nb	2	2	1
Y	16	16	22
La	13	16	22
Ce	28	29	34
Nd	17	18	21
Sc	34	29	22
V	335	324	348
Ni	147	143	96
Cr	396	375	182
Mg#	63.92	62.18	55.99

APPENDIX 3

Microprobe Mineral Analyses from Batur Volcanic Rocks

Analyses are listed by mineral, with oxide and cation compositions given on alternating pages:

mineral	rocks analysed						page
plagioclase	67238	67244	67259	67272	67273	67275	A3.2
	67277	67278	67326	67328	67331	67339	
	67342						
olivine	67238	67244	67259	67272	67273	67275	A3.26
	67277	67278	67326	67328	67332	67339	
	67342						
clinopyroxene	67238	67244	67259	67272	67273	67275	A3.34
	67277	67278	67326	67328	67331	67342	
orthopyroxene	67273	67275	67331				A3.40
pigeonite	67278	67331					A3.42
Ti-magnetite	67238	67244	67259	67272	67273	67275	A3.43
	67277	67278	67326	67328	67331	67342	
ilmenite	67277						A3.47
Cr-spinel	67339						A3.47

Notes

a. All oxide compositions are quoted normalised to sum to 100 %, with the prenormalised total given under (SUM).

b. Cations normalised to 8, 4, 6, 4, 3 and 4 oxygens for plagioclase, olivine, pyroxenes, Ti-magnetite, ilmenite and Cr-spinel respectively.

c. Fe^{3+} has been calculated for pyroxenes, Ti-magnetite, ilmenite and Cr-spinel by normalising cation totals to sum to 4, 3, 2 and 3 respectively.

d. NUM is an identifying number for each analysis.

e. L indicates the analysis type: C=core, R=rim, I=crystal occurs as an inclusion, X=crystal occurs as a xenocryst.

f. For plagioclase, sequential analyses shown by Z.. under NOTE represent a series of equidistant analyses across a phenocryst.

g. $Mg\#=100Mg/(Mg+Fe^{2+})$; $Ca\#=100Ca/(Ca+Na)$

h. For Ti-magnetite and ilmenite, % ULV and ILM molecules have been calculated using Stormer's (1983) algorithm.

Batur Volcano:- PLAGIOCLASE (OXIDES)

ROCK	NUM	L	SiO2	Al2O3	FeO	MgO	CaO	Na2O	K2O	(SUM)	NOTE
67238	45	C	48.94	32.15	0.67		16.03	2.08	0.13	95.12	
67238	46	C	48.90	31.97	0.79		16.08	2.14	0.12	96.57	
67238	47	R	49.60	31.70	0.65		15.85	2.21		98.78	RIM TO #46
67238	48	C	51.13	30.54	0.70	0.25	14.29	2.96	0.13	100.64	
67238	49	R	48.45	32.02	1.04		16.64	1.84		100.88	RIM TO #48
67238	51	G	54.32	28.38	0.95		11.83	4.21	0.30	99.74	
67238	53	G	54.08	28.56	0.90		12.11	4.04	0.31	101.07	
67238	55	G	53.94	28.73	0.76		12.28	4.06	0.23	100.62	
67238	56	G	54.31	28.24	0.96	0.18	11.66	4.35	0.31	100.80	
67238	59	C	47.69	33.18	0.48		17.30	1.35		99.85	
67238	60	R	53.39	29.20	0.86		12.51	3.83	0.21	100.41	RIM TO #59
67238	61	C	48.84	32.29	0.75		15.91	2.10	0.11	100.06	
67238	62	R	58.25	25.73	0.87		8.88	5.79	0.49	100.38	RIM TO #61
67238	63	C	51.10	30.54	0.86		14.45	2.87	0.18	99.44	
67238	73	G	53.60	29.05	0.81		12.44	3.89	0.21	100.47	
67238	78	C	46.55	33.87	0.51		18.00	1.07		99.43	
67238	79	R	46.79	33.78	0.63		17.68	1.12		98.56	RIM TO #78
67238	80	C	48.39	32.56	0.56		16.40	1.99	0.10	98.86	
67238	81	C	51.71	30.26	0.80		13.82	3.25	0.16	99.64	
67238	84	R	51.77	30.08	0.72		13.80	3.48	0.15	99.41	RIM TO CPX
67238	88	C	50.04	31.31	0.76		15.08	2.69	0.12	100.45	
67238	89	C	49.25	31.75	0.72		15.91	2.22	0.15	100.80	
67238	90	R	54.33	28.25	1.05		11.74	4.35	0.29	100.78	RIM TO #89
67244	2	C	48.80	32.43	0.54	0.18	15.99	2.05		102.99	
67244	3	C	48.96	32.31	0.55	0.18	15.98	2.02		102.72	RPT #2
67244	4	R	49.87	31.38	0.74	0.26	15.05	2.70		103.23	RIM TO #2
67244	5	C	50.18	30.78	0.84	0.34	14.56	3.09	0.21	101.35	
67244	5	R	51.19	30.58	0.76	0.21	14.01	3.06	0.19	100.04	Z1 RIM TO #13
67244	6		50.86	30.90	0.73	0.21	14.16	2.99	0.15	99.73	Z2
67244	6	R	53.88	28.40	0.93	0.21	11.92	4.35	0.31	100.41	RIM TO #5
67244	7	C	52.83	29.20	0.87	0.27	12.76	3.84	0.23	100.36	

Batur Volcano:- PLAGIOCLASE (CATIONS)

ROCK	NUM	L	Si	Al	Fe	Mg	Ca	Na	K	SUM	Ca#
67238	45	C	2.2429	1.7367	0.0258		0.7873	0.1850	0.0074	4.9851	81.0
67238	46	C	2.2436	1.7288	0.0302		0.7906	0.1907	0.0073	4.9912	80.6
67238	47	R	2.2686	1.7089	0.0248		0.7770	0.1957		4.9750	79.9
67238	48	C	2.3311	1.6413	0.0265	0.0169	0.6979	0.2617	0.0075	4.9829	72.7
67238	49	R	2.2277	1.7351	0.0400		0.8199	0.1644		4.9871	83.3
67238	51	G	2.4612	1.5158	0.0361		0.5743	0.3699	0.0174	4.9747	60.8
67238	53	G	2.4513	1.5260	0.0341		0.5881	0.3548	0.0177	4.9720	62.4
67238	55	G	2.4441	1.5345	0.0286		0.5964	0.3571	0.0132	4.9739	62.5
67238	56	G	2.4613	1.5088	0.0365	0.0121	0.5660	0.3818	0.0178	4.9843	59.7
67238	59	C	2.1891	1.7951	0.0185		0.8506	0.1203		4.9736	87.6
67238	60	R	2.4217	1.5611	0.0325		0.6079	0.3372	0.0121	4.9725	64.3
67238	61	C	2.2385	1.7444	0.0287		0.7813	0.1865	0.0064	4.9858	80.7
67238	62	R	2.6158	1.3620	0.0325		0.4271	0.5040	0.0280	4.9694	45.9
67238	63	C	2.3320	1.6429	0.0330		0.7066	0.2536	0.0105	4.9786	73.6
67238	73	G	2.4298	1.5524	0.0306		0.6043	0.3421	0.0121	4.9713	63.9
67238	78	C	2.1434	1.8385	0.0198		0.8882	0.0952		4.9851	90.3
67238	79	R	2.1532	1.8319	0.0242		0.8719	0.0996		4.9808	89.7
67238	80	C	2.2201	1.7607	0.0213		0.8060	0.1773	0.0059	4.9913	82.0
67238	81	C	2.3551	1.6244	0.0306		0.6744	0.2872	0.0093	4.9810	70.1
67238	84	R	2.3588	1.6154	0.0276		0.6738	0.3075	0.0088	4.9919	68.7
67238	88	C	2.2889	1.6878	0.0289		0.7391	0.2384	0.0070	4.9901	75.6
67238	89	C	2.2575	1.7152	0.0278		0.7815	0.1975	0.0087	4.9882	79.8
67238	90	R	2.4631	1.5096	0.0399		0.5702	0.3821	0.0166	4.9815	59.9
67244	2	C	2.2336	1.7495	0.0208	0.0126	0.7842	0.1818		4.9825	81.2
67244	3	C	2.2400	1.7424	0.0209	0.0126	0.7831	0.1796		4.9786	81.3
67244	4	R	2.2802	1.6909	0.0282	0.0178	0.7375	0.2396		4.9942	75.5
67244	5	C	2.2977	1.6614	0.0321	0.0229	0.7145	0.2742	0.0121	5.0149	72.3
67244	5	R	2.3336	1.6430	0.0290	0.0143	0.6845	0.2704	0.0110	4.9858	71.7
67244	6		2.3191	1.6610	0.0279	0.0143	0.6917	0.2642	0.0087	4.9869	72.4
67244	6	R	2.4456	1.5196	0.0352	0.0141	0.5798	0.3830	0.0179	4.9952	60.2
67244	7	C	2.4019	1.5650	0.0330	0.0182	0.6218	0.3382	0.0133	4.9914	64.8

Batur Volcano:- PLAGIOCLASE (OXIDES)

ROCK	NUM	L	SiO2	Al2O3	FeO	MgO	CaO	Na2O	K2O	(SUM)	NOTE
67244	7		49.17	32.11	0.55		15.97	2.08	0.13	99.70	Z3
67244	8		47.46	33.18	0.71	0.27	16.87	1.50		99.70	Z4
67244	8	R	51.62	30.09	0.81	0.20	13.91	3.23	0.14	99.44	RIM TO #7
67244	9		48.45	32.72	0.64		16.30	1.89		99.41	Z5
67244	10		48.34	32.42	0.70	0.19	16.30	1.96	0.10	100.01	Z6
67244	11		53.38	29.22	0.67	0.23	12.32	3.98	0.19	99.64	Z7
67244	12	C	53.28	29.16	0.70	0.25	12.53	3.85	0.23	96.87	
67244	12		50.96	30.50	0.82	0.30	14.05	3.15	0.22	100.26	Z8
67244	13	C	49.88	31.75	0.75		15.18	2.44		99.11	Z9
67244	14		53.74	28.85	0.67	0.34	12.23	3.96	0.20	99.38	Z10
67244	14	C	49.25	31.83	0.73	0.24	15.67	2.29		100.17	
67244	15		54.07	28.79	0.64	0.23	12.11	3.92	0.24	99.02	Z11
67244	15	R	52.55	29.64	0.72	0.19	13.30	3.43	0.17	100.21	CLEAR RIM TO #14
67244	16		53.37	29.41	0.65	0.19	12.50	3.73	0.15	98.95	Z12
67244	17		53.19	29.16	0.78	0.28	12.54	3.80	0.25	99.23	Z13
67244	18		54.61	28.58	0.70		11.84	3.98	0.29	98.51	Z14
67244	19		52.96	29.32	0.81	0.20	12.74	3.76	0.21	99.74	Z15
67244	20		52.26	29.85	0.80	0.31	13.09	3.47	0.22	100.30	Z20
67244	23	G	57.05	26.07	1.61	0.22	9.59	4.82	0.64	98.56	
67244	26	C	54.68	28.44	0.55	0.27	11.33	4.44	0.28	99.67	
67244	27	R	51.15	30.73	0.66	0.19	14.10	3.03	0.14	99.77	RIM TO #26
67244	41	C	53.41	29.24	0.68		12.68	3.76	0.23	99.20	
67244	42	R	50.96	30.49	0.83		14.34	3.20	0.18	99.82	RIM TO #41
67244	43	C	52.62	29.76	0.77		13.26	3.39	0.20	98.80	
67244	46	C	49.48	31.82	0.61		15.53	2.43	0.12	99.53	
67244	47	R	50.69	30.84	0.75		15.06	2.54	0.12	96.47	RIM TO #46
67244	61	I	55.75	27.06	1.16		10.73	4.86	0.44	99.44	INCL IN OLV
67244	62	C	51.14	29.48	1.98	0.36	14.07	2.72	0.26	98.32	
67244	63	R	53.82	28.55	0.94		12.28	4.16	0.24	99.49	RIM TO #62
67244	65	C	51.46	30.27	0.69		14.18	3.20	0.20	100.04	
67244	66	R	50.46	31.15	0.75		14.98	2.67		100.36	RIM TO #65

Batur Volcano:- PLAGIOCLASE (CATIONS)

ROCK	NUM	L	Si	Al	Fe	Mg	Ca	Na	K	SUM	Ca#
67244	7		2.2507	1.7323	0.0211		0.7832	0.1843	0.0076	4.9792	81.0
67244	8		2.1807	1.7968	0.0274	0.0185	0.8305	0.1340		4.9879	86.1
67244	8	R	2.3526	1.6163	0.0310	0.0137	0.6791	0.2853	0.0082	4.9862	70.4
67244	9		2.2201	1.7674	0.0247		0.8001	0.1680		4.9803	82.6
67244	10		2.2188	1.7539	0.0269	0.0130	0.8016	0.1744	0.0059	4.9945	82.1
67244	11		2.4195	1.5607	0.0255	0.0156	0.5985	0.3501	0.0110	4.9809	63.1
67244	12	C	2.4166	1.5591	0.0266	0.0168	0.6090	0.3386	0.0131	4.9798	64.3
67244	12		2.3266	1.6413	0.0312	0.0204	0.6875	0.2790	0.0128	4.9988	71.1
67244	13	C	2.2784	1.7094	0.0285		0.7426	0.2162		4.9751	77.5
67244	14		2.4341	1.5400	0.0255	0.0231	0.5933	0.3482	0.0116	4.9758	63.0
67244	14	C	2.2547	1.7174	0.0279	0.0164	0.7688	0.2029		4.9881	79.1
67244	15		2.4460	1.5352	0.0241	0.0157	0.5869	0.3437	0.0140	4.9656	63.1
67244	15	R	2.3877	1.5872	0.0273	0.0128	0.6476	0.3024	0.0098	4.9748	68.2
67244	16		2.4168	1.5696	0.0245	0.0130	0.6065	0.3274	0.0088	4.9666	64.9
67244	17		2.4138	1.5600	0.0294	0.0191	0.6096	0.3343	0.0146	4.9808	64.6
67244	18		2.4676	1.5218	0.0265		0.5730	0.3486	0.0170	4.9545	62.2
67244	19		2.4051	1.5692	0.0308	0.0136	0.6201	0.3311	0.0122	4.9821	65.2
67244	20		2.3762	1.5996	0.0303	0.0209	0.6377	0.3059	0.0127	4.9833	67.6
67244	23	G	2.5754	1.3868	0.0609	0.0150	0.4637	0.4218	0.0368	4.9604	52.4
67244	26	C	2.4695	1.5141	0.0208	0.0182	0.5481	0.3892	0.0162	4.9761	58.5
67244	27	R	2.3303	1.6502	0.0252	0.0129	0.6884	0.2674	0.0082	4.9826	72.0
67244	41	C	2.4213	1.5627	0.0256		0.6160	0.3305	0.0134	4.9695	65.1
67244	42	R	2.3283	1.6421	0.0318		0.7017	0.2831	0.0105	4.9975	71.3
67244	43	C	2.3903	1.5932	0.0292		0.6453	0.2986	0.0117	4.9683	68.4
67244	46	C	2.2646	1.7164	0.0235		0.7616	0.2157	0.0070	4.9888	77.9
67244	47	R	2.3146	1.6597	0.0285		0.7369	0.2248	0.0072	4.9717	76.6
67244	61	I	2.5227	1.4432	0.0438		0.5202	0.4261	0.0255	4.9815	55.0
67244	62	C	2.3452	1.5932	0.0761	0.0243	0.6911	0.2415	0.0155	4.9869	74.1
67244	63	R	2.4431	1.5271	0.0359		0.5973	0.3662	0.0140	4.9836	62.0
67244	65	C	2.3466	1.6268	0.0263		0.6930	0.2828	0.0116	4.9871	71.0
67244	66	R	2.3035	1.6760	0.0285		0.7325	0.2364		4.9769	75.6

Batur Volcano:- PLAGIOCLASE (OXIDES)

ROCK	NUM	L	SiO2	Al2O3	FeO	MgO	CaO	Na2O	K2O	(SUM)	NOTE
67244	67	C	51.29	30.64	0.73		14.29	2.93	0.12	98.07	
67244	68	R	51.93	30.08	0.77		13.97	3.13	0.12	99.33	RIM TO #67
67259	2	C	47.27	33.21	0.73		17.16	1.51	0.13	103.33	
67259	3	R	53.33	29.21	0.69		12.65	3.91	0.20	99.49	RIM TO #2
67259	5	C	49.72	31.77	0.64		15.21	2.58	0.10	103.57	
67259	6	R	50.38	31.24	0.65		14.97	2.76		102.94	RIM TO #5
67259	6	C	52.66	29.72	0.65		13.10	3.71	0.17	102.02	
67259	7	C	52.32	29.18	0.97	0.38	13.61	3.22	0.30	98.79	
67259	7	R	52.53	29.79	0.72		13.16	3.58	0.23	101.32	RIM TO #6
67259	8	R	49.03	32.07	0.70		15.82	2.26	0.13	102.37	RIM TO #7
67259	8	C	53.78	28.59	0.65		12.43	4.29	0.26	101.36	
67259	9	R	56.06	27.06	0.74		10.55	5.23	0.37	101.15	RIM TO #8
67259	10	C	51.07	30.79	0.55		14.73	2.73	0.13	100.68	
67259	11	R	60.04	24.61	0.83		7.06	6.66	0.81	100.58	RIM TO #10
67259	12	C	50.46	31.16	0.61		14.99	2.78		99.21	
67259	12	C	53.88	29.06	0.55		12.34	3.99	0.18	100.42	
67259	13	R	51.20	30.69	0.62		14.17	3.14	0.18	98.89	RIM TO #12
67259	14	C	50.18	31.56	0.62		15.13	2.52		98.89	
67259	15	C	53.17	28.29	1.51	0.23	12.47	3.82	0.51	99.34	
67259	15	R	49.41	31.76	0.67		15.76	2.29	0.11	99.82	CLEAR RIM TO #14
67259	16	G	52.12	30.02	0.70		13.58	3.40	0.18	99.10	
67259	16	R	57.12	26.73	0.72		9.60	5.41	0.42	99.67	RIM TO #15
67259	17	R	51.23	30.57	0.75		14.17	3.12	0.16	99.83	RIM TO #12
67259	17	G	56.82	26.77	0.86		9.72	5.44	0.39	99.29	
67259	18	G	48.89	31.99	0.85		16.00	2.16	0.12	102.93	
67259	19	R	50.66	30.80	0.79		14.72	2.87	0.17	102.71	Z1 RIM TO #25
67259	19	G	56.41	26.98	0.99		9.94	5.29	0.40	100.82	
67259	20		49.97	31.38	0.78		15.07	2.69	0.11	103.63	Z2
67259	21		50.19	31.29	0.66		15.27	2.46	0.14	96.88	Z3
67259	23		52.64	29.73	0.70		13.13	3.63	0.18	102.05	Z5
67259	24		53.45	29.22	0.55		12.64	3.98	0.16	101.71	Z6

Batur Volcano:- PLAGIOCLASE (CATIONS)

ROCK	NUM	L	Si	Al	Fe	Mg	Ca	Na	K	SUM	Ca#
67244	67	C	2.3369	1.6455	0.0280		0.6974	0.2585	0.0071	4.9734	73.0
67244	68	R	2.3636	1.6138	0.0291		0.6815	0.2763	0.0070	4.9713	71.2
67259	2	C	2.1758	1.8021	0.0279		0.8463	0.1347	0.0074	4.9942	86.3
67259	3	R	2.4193	1.5617	0.0263		0.6150	0.3439	0.0116	4.9778	64.1
67259	5	C	2.2730	1.7118	0.0244		0.7449	0.2285	0.0056	4.9882	76.5
67259	6	R	2.2998	1.6809	0.0248		0.7322	0.2442		4.9819	75.0
67259	6	C	2.3917	1.5910	0.0246		0.6373	0.3272	0.0097	4.9815	66.1
67259	7	C	2.3848	1.5677	0.0370	0.0261	0.6648	0.2845	0.0177	4.9826	70.0
67259	7	R	2.3872	1.5956	0.0274		0.6406	0.3157	0.0132	4.9797	67.0
67259	8	R	2.2470	1.7324	0.0270		0.7766	0.2005	0.0074	4.9909	79.5
67259	8	C	2.4405	1.5292	0.0247		0.6044	0.3776	0.0148	4.9912	61.5
67259	9	R	2.5311	1.4401	0.0280		0.5103	0.4579	0.0211	4.9885	52.7
67259	10	C	2.3275	1.6538	0.0208		0.7192	0.2413	0.0075	4.9701	74.9
67259	11	R	2.6863	1.2976	0.0309		0.3384	0.5778	0.0460	4.9770	36.9
67259	12	C	2.3032	1.6762	0.0235		0.7330	0.2462		4.9821	74.9
67259	12	C	2.4382	1.5497	0.0207		0.5982	0.3503	0.0103	4.9674	63.1
67259	13	R	2.3336	1.6488	0.0235		0.6919	0.2779	0.0106	4.9863	71.3
67259	14	C	2.2897	1.6974	0.0235		0.7396	0.2228		4.9730	76.8
67259	15	C	2.4259	1.5211	0.0576	0.0157	0.6097	0.3375	0.0299	4.9974	64.4
67259	15	R	2.2626	1.7140	0.0257		0.7732	0.2037	0.0064	4.9856	79.1
67259	16	G	2.3710	1.6096	0.0265		0.6620	0.2999	0.0105	4.9795	68.8
67259	16	R	2.5687	1.4167	0.0272		0.4626	0.4715	0.0242	4.9709	49.5
67259	17	R	2.3360	1.6431	0.0287		0.6925	0.2754	0.0093	4.9850	71.5
67259	17	G	2.5593	1.4211	0.0322		0.4690	0.4749	0.0226	4.9791	49.7
67259	18	G	2.2432	1.7302	0.0324		0.7866	0.1919	0.0068	4.9911	80.4
67259	19	R	2.3147	1.6585	0.0301		0.7207	0.2545	0.0096	4.9881	73.9
67259	19	G	2.5442	1.4342	0.0374		0.4803	0.4623	0.0228	4.9812	51.0
67259	20		2.2856	1.6919	0.0299		0.7387	0.2388	0.0062	4.9911	75.6
67259	21		2.2934	1.6851	0.0252		0.7475	0.2177	0.0084	4.9773	77.4
67259	23		2.3911	1.5917	0.0264		0.6391	0.3193	0.0102	4.9778	66.7
67259	24		2.4222	1.5609	0.0209		0.6140	0.3499	0.0091	4.9770	63.7

Batur Volcano:- PLAGIOCLASE (OXIDES)

ROCK	NUM	L	SiO2	Al2O3	FeO	MgO	CaO	Na2O	K2O	(SUM)	NOTE
67259	24		52.70	29.80	0.66		13.05	3.61	0.18	101.87	Z4
67259	25	C	53.55	29.20	0.60		12.34	4.06	0.25	101.63	Z7
67259	26		53.28	29.05	0.74		12.54	4.14	0.25	101.35	Z8
67259	27		53.70	29.26	0.45		12.55	3.88	0.16	100.28	Z9
67259	28	C	52.65	29.51	0.67		13.05	3.90	0.21	98.70	
67259	28		53.86	29.10	0.63		12.31	3.92	0.18	100.53	Z10
67259	29		51.51	30.44	0.61		14.11	3.19	0.14	101.02	Z11
67259	29	R	52.11	30.12	0.58		13.63	3.37	0.18	97.73	RIM TO #28
67259	30		50.93	30.87	0.64		14.50	2.91	0.15	101.51	Z12
67259	31		51.17	30.76	0.72		14.23	3.02	0.10	100.61	Z13
67259	31	G	52.76	29.77	0.61		13.08	3.62	0.16	97.50	
67259	32	C	46.84	33.66	0.54		17.87	1.09		98.21	
67259	33	R	55.41	27.69	0.72		11.11	4.79	0.29	97.33	RIM TO #32
67259	34	R	50.72	31.09	0.72		14.76	2.71		99.93	Z1
67259	35		49.79	31.79	0.63		15.41	2.39		99.04	Z2
67259	36		50.60	31.09	0.72		14.67	2.74	0.17	99.52	Z3
67259	36	G	51.27	30.32	0.94		13.87	3.38	0.23	101.02	
67259	37		50.47	31.37	0.48		15.20	2.49		98.76	Z4
67259	38		49.12	32.18	0.60		15.92	2.17		99.43	Z5
67259	39		49.57	31.77	0.68		15.72	2.27		100.21	Z6
67259	40	G	52.47	29.77	0.78		13.06	3.67	0.26	101.41	
67259	40		49.39	31.74	0.77		15.54	2.40	0.16	100.91	Z7
67259	41		49.41	32.00	0.55		15.63	2.42		100.41	Z8
67259	42	C	47.15	33.45	0.56		17.43	1.41		100.15	Z9 CORE TO #34
67259	43		45.72	34.35	0.53		18.54	0.86		100.81	Z10
67259	44		46.54	33.89	0.42		18.03	1.12		100.08	Z11
67259	45		47.34	33.43	0.56		17.28	1.39		100.36	Z12
67259	46		56.35	27.11	0.81		10.47	4.68	0.58	99.66	Z13
67259	47		49.59	31.89	0.70		15.50	2.33		100.03	Z14
67259	48		50.32	31.19	0.63		14.95	2.78	0.14	100.50	Z15
67259	49		49.27	32.11	0.65		15.74	2.23		100.97	Z16

Batur Volcano:- PLAGIOCLASE (CATIONS)

ROCK	NUM	L	Si	Al	Fe	Mg	Ca	Na	K	SUM	Ca#
67259	24		2.3924	1.5945	0.0250		0.6345	0.3179	0.0102	4.9745	66.6
67259	25	C	2.4265	1.5598	0.0227		0.5991	0.3570	0.0142	4.9793	62.7
67259	26		2.4199	1.5550	0.0281		0.6102	0.3649	0.0143	4.9924	62.6
67259	27		2.4297	1.5603	0.0170		0.6086	0.3403	0.0092	4.9651	64.1
67259	28	C	2.3942	1.5817	0.0254		0.6357	0.3439	0.0123	4.9932	64.9
67259	28		2.4373	1.5518	0.0237		0.5970	0.3438	0.0103	4.9639	63.5
67259	29		2.3463	1.6341	0.0234		0.6884	0.2815	0.0081	4.9818	71.0
67259	29	R	2.3694	1.6143	0.0222		0.6639	0.2968	0.0107	4.9773	69.1
67259	30		2.3226	1.6595	0.0244		0.7085	0.2570	0.0086	4.9806	73.4
67259	31		2.3316	1.6522	0.0273		0.6949	0.2670	0.0058	4.9788	72.2
67259	31	G	2.3942	1.5926	0.0230		0.6358	0.3186	0.0095	4.9737	66.6
67259	32	C	2.1555	1.8258	0.0208		0.8811	0.0972		4.9804	90.1
67259	33	R	2.5030	1.4743	0.0272		0.5376	0.4193	0.0166	4.9780	56.2
67259	34	R	2.3126	1.6710	0.0275		0.7211	0.2398		4.9720	75.0
67259	35		2.2745	1.7114	0.0239		0.7542	0.2120		4.9760	78.1
67259	36		2.3099	1.6726	0.0276		0.7175	0.2428	0.0099	4.9803	74.7
67259	36	G	2.3410	1.6318	0.0359		0.6785	0.2988	0.0133	4.9993	69.4
67259	37		2.3006	1.6855	0.0181		0.7424	0.2202		4.9668	77.1
67259	38		2.2480	1.7360	0.0231		0.7807	0.1928		4.9806	80.2
67259	39		2.2671	1.7129	0.0260		0.7702	0.2009		4.9771	79.3
67259	40	G	2.3860	1.5956	0.0296		0.6361	0.3234	0.0149	4.9856	66.3
67259	40		2.2628	1.7140	0.0296		0.7627	0.2130	0.0093	4.9914	78.2
67259	41		2.2595	1.7248	0.0209		0.7657	0.2146		4.9855	78.1
67259	42	C	2.1685	1.8132	0.0215		0.8591	0.1255		4.9878	87.3
67259	43		2.1104	1.8690	0.0203		0.9169	0.0772		4.9938	92.2
67259	44		2.1429	1.8393	0.0162		0.8892	0.0999		4.9875	89.9
67259	45		2.1752	1.8104	0.0214		0.8506	0.1243		4.9819	87.2
67259	46		2.5408	1.4408	0.0306		0.5056	0.4088	0.0335	4.9601	55.3
67259	47		2.2668	1.7183	0.0268		0.7590	0.2065		4.9774	78.6
67259	48		2.2989	1.6798	0.0240		0.7316	0.2459	0.0081	4.9883	74.8
67259	49		2.2540	1.7313	0.0250		0.7714	0.1977		4.9794	79.6

Batur Volcano:- PLAGIOCLASE (OXIDES)

ROCK	NUM	L	SiO2	Al2O3	FeO	MgO	CaO	Na2O	K2O	(SUM)	NOTE
67259	52	C	50.19	31.40	0.62		15.18	2.61		99.53	
67259	53	R	53.58	28.94	0.86		12.19	4.15	0.29	97.94	RIM TO #52
67259	54	C	51.05	30.87	0.63		14.44	2.89	0.12	99.34	
67259	55	R	52.61	29.71	0.61		13.25	3.66	0.16	99.20	RIM TO #54
67259	57	C	50.69	30.53	1.23		14.61	2.73	0.20	99.11	
67259	58	R	46.71	33.85	0.56		17.91	0.97		99.44	CLEAR RIM TO #57
67259	59	C	51.08	30.91	0.54		14.55	2.92		98.81	
67259	60	R	50.28	31.16	0.77		14.80	2.82	0.18	101.36	CLEAR RIM TO #59
67259	61	C	54.70	28.25	0.76		11.67	4.39	0.23	99.88	
67259	62	R	50.33	31.14	0.65		15.00	2.72	0.16	99.39	RIM TO #61
67259	63	C	48.62	32.29	0.67		16.43	2.00		98.62	
67259	64	R	49.97	31.57	0.68		15.08	2.70		100.88	
67259	67	G	55.39	27.66	0.93		11.04	4.67	0.31	100.66	
67259	68	C	48.69	32.42	0.48		16.17	2.13	0.10	100.30	
67259	68	C	48.79	32.33	0.69		16.24	1.96		99.18	
67259	69	R	48.70	32.35	0.66		16.45	1.72	0.12	99.58	RIM TO #68
67259	69	R	52.19	29.87	0.66		13.53	3.54	0.21	99.53	RIM TO #68
67259	70	C	49.71	31.43	0.70	0.18	15.19	2.64	0.15	100.73	
67259	71	R	49.14	31.90	0.65		15.83	2.39	0.11	100.58	RIM TO #70
67272	23	C	47.97	33.08	0.60		16.67	1.67		102.81	
67272	24	R	49.94	31.59	0.72		15.12	2.47	0.16	103.45	RIM TO #23
67272	25	C	52.69	29.90	0.64		13.26	3.40	0.11	103.13	
67272	26	R	57.15	26.35	0.92		9.37	5.76	0.45	102.35	RIM TO #25
67272	30	C	49.81	31.74	0.59		15.54	2.33		101.89	
67272	31	R	54.88	28.26	0.76		11.17	4.60	0.32	102.32	RIM TO #30
67272	32	C	51.37	30.53	0.66		14.19	3.15	0.10	102.35	
67272	33	R	51.16	30.76	0.73		14.16	3.01	0.18	102.66	RIM TO #32
67272	37	C	50.35	31.27	0.58		15.12	2.59	0.10	102.27	
67272	38	R	49.11	32.13	0.73		15.76	2.15	0.12	102.89	
67272	39	C	49.14	32.32	0.51		15.83	2.20		101.83	
67272	40	R	48.49	32.62	0.65		16.28	1.96		102.98	RIM TO #39

Batur Volcano:- PLAGIOCLASE (CATIONS)

ROCK	NUM	L	Si	Al	Fe	Mg	Ca	Na	K	SUM	Ca#
67259	52	C	2.2916	1.6898	0.0238		0.7427	0.2313		4.9792	76.3
67259	53	R	2.4314	1.5476	0.0325		0.5927	0.3647	0.0165	4.9854	61.9
67259	54	C	2.3263	1.6583	0.0242		0.7048	0.2553	0.0070	4.9759	73.4
67259	55	R	2.3901	1.5907	0.0234		0.6447	0.3223	0.0093	4.9805	66.7
67259	57	C	2.3197	1.6468	0.0471		0.7163	0.2426	0.0118	4.9843	74.7
67259	58	R	2.1494	1.8358	0.0217		0.8830	0.0861		4.9760	91.1
67259	59	C	2.3260	1.6590	0.0204		0.7101	0.2582		4.9737	73.3
67259	60	R	2.2986	1.6789	0.0294		0.7249	0.2501	0.0104	4.9923	74.3
67259	61	C	2.4738	1.5061	0.0288		0.5657	0.3845	0.0133	4.9722	59.5
67259	62	R	2.2999	1.6773	0.0250		0.7345	0.2407	0.0094	4.9868	75.3
67259	63	C	2.2301	1.7454	0.0257		0.8073	0.1776		4.9861	82.0
67259	64	R	2.2831	1.7002	0.0261		0.7381	0.2389		4.9864	75.5
67259	67	G	2.5035	1.4733	0.0353		0.5344	0.4091	0.0178	4.9734	56.6
67259	68	C	2.2315	1.7513	0.0183		0.7940	0.1896	0.0058	4.9905	80.7
67259	68	C	2.2355	1.7457	0.0263		0.7974	0.1738		4.9787	82.1
67259	69	R	2.2327	1.7477	0.0254		0.8079	0.1526	0.0070	4.9733	84.1
67259	69	R	2.3748	1.6022	0.0252		0.6599	0.3120	0.0122	4.9863	67.9
67259	70	C	2.2754	1.6958	0.0270	0.0122	0.7450	0.2344	0.0087	4.9985	76.1
67259	71	R	2.2521	1.7231	0.0248		0.7773	0.2121	0.0064	4.9958	78.6
67272	23	C	2.2004	1.7884	0.0231		0.8193	0.1488		4.9800	84.6
67272	24	R	2.2826	1.7019	0.0273		0.7404	0.2193	0.0096	4.9811	77.1
67272	25	C	2.3902	1.5989	0.0243		0.6442	0.2994	0.0062	4.9632	68.3
67272	26	R	2.5748	1.3993	0.0346		0.4523	0.5036	0.0258	4.9904	47.3
67272	30	C	2.2754	1.7090	0.0225		0.7604	0.2060		4.9733	78.7
67272	31	R	2.4804	1.5057	0.0288		0.5410	0.4034	0.0186	4.9779	57.3
67272	32	C	2.3406	1.6396	0.0253		0.6925	0.2779	0.0057	4.9816	71.4
67272	33	R	2.3318	1.6526	0.0278		0.6917	0.2660	0.0102	4.9801	72.2
67272	37	C	2.2986	1.6827	0.0220		0.7394	0.2294	0.0057	4.9778	76.3
67272	38	R	2.2491	1.7344	0.0279		0.7735	0.1907	0.0068	4.9824	80.2
67272	39	C	2.2472	1.7420	0.0195		0.7756	0.1950		4.9793	79.9
67272	40	R	2.2228	1.7621	0.0249		0.7993	0.1743		4.9834	82.1

Batur Volcano:- PLAGIOCLASE (OXIDES)

ROCK	NUM	L	SiO2	Al2O3	FeO	MgO	CaO	Na2O	K2O	(SUM)	NOTE
67272	41	C	51.74	30.24	0.63		13.80	3.30	0.28	102.72	
67272	42	R	48.96	32.25	0.64		16.15	2.00		102.25	RIM TO #41
67272	43	C	50.07	31.48	0.73		15.00	2.58	0.13	102.17	
67272	44	R	50.91	30.79	0.69		14.65	2.84	0.13	102.06	RIM TO #43
67272	48	C	48.97	32.12	0.56		16.10	2.14	0.11	101.83	
67272	49	R	48.87	32.43	0.63		15.88	2.09	0.10	102.12	RIM TO #48
67272	50	C	50.06	31.52	0.58		15.27	2.44	0.14	102.39	
67272	51	R	51.49	30.62	0.54		14.08	3.14	0.13	101.80	RIM TO #50
67272	55	C	50.02	31.60	0.60		15.16	2.52	0.11	102.16	
67272	56	R	48.79	32.35	0.78		15.90	2.02	0.17	102.55	RIM TO #55
67272	60	C	50.60	31.12	0.66		14.72	2.79	0.12	101.45	
67272	61	R	50.56	31.06	0.66		14.60	2.94	0.19	102.48	RIM TO #60
67273	5	C	58.21	26.68	0.30		8.63	5.90	0.29	101.07	
67273	9	C	58.73	26.41			8.50	6.02	0.33	97.61	
67273	17	C	58.74	26.12	0.23		8.47	6.10	0.35	98.52	
67273	20	C	58.55	26.51			8.75	5.89	0.30	98.62	
67273	21	C	56.42	27.67	0.26		10.19	5.18	0.27	98.76	
67273	22	C	58.95	26.03	0.29		8.24	6.14	0.35	101.07	
67273	23	R	57.17	27.22			9.79	5.55	0.27	100.83	RIM TO #22
67273	24	C	58.99	25.87	0.25		8.06	6.47	0.36	99.38	
67273	25	R	57.03	27.36	0.29		9.72	5.35	0.24	99.17	RIM TO #24
67273	26	C	58.30	26.44	0.26		8.72	5.97	0.31	99.25	
67273	27	C	57.40	27.08	0.43		9.28	5.58	0.23	98.50	
67273	27	C	57.46	26.78	0.38		9.09	5.94	0.35	98.53	
67273	28	C	58.50	26.37	0.35		8.58	5.91	0.30	99.90	
67273	30	C	58.26	26.81			8.78	5.85	0.28	98.38	
67273	32	C	58.42	26.38	0.32		8.38	6.20	0.30	100.31	
67273	38	C	59.93	25.66			7.51	6.55	0.34	99.28	
67273	43	C	57.63	26.94	0.23		9.16	5.75	0.29	99.89	
67273	44	C	57.40	27.09	0.35	0.20	9.07	5.56	0.34	98.44	
67275	24	R	57.01	26.95	0.55		9.58	5.52	0.40	96.99	RIM TO #25

Batur Volcano:- PLAGIOCLASE (CATIONS)

ROCK	NUM	L	Si	Al	Fe	Mg	Ca	Na	K	SUM	Ca#
67272	41	C	2.3568	1.6233	0.0241		0.6737	0.2914	0.0164	4.9857	69.8
67272	42	R	2.2418	1.7407	0.0243		0.7922	0.1780		4.9770	81.7
67272	43	C	2.2882	1.6953	0.0281		0.7346	0.2289	0.0074	4.9825	76.2
67272	44	R	2.3227	1.6554	0.0262		0.7160	0.2513	0.0074	4.9790	74.0
67272	48	C	2.2440	1.7348	0.0214		0.7902	0.1902	0.0063	4.9869	80.6
67272	49	R	2.2379	1.7504	0.0240		0.7792	0.1852	0.0057	4.9824	80.8
67272	50	C	2.2868	1.6968	0.0220		0.7471	0.2162	0.0080	4.9769	77.6
67272	51	R	2.3435	1.6425	0.0206		0.6864	0.2774	0.0074	4.9778	71.2
67272	55	C	2.2846	1.7010	0.0228		0.7420	0.2228	0.0063	4.9795	76.9
67272	56	R	2.2365	1.7477	0.0299		0.7812	0.1794	0.0097	4.9844	81.3
67272	60	C	2.3089	1.6738	0.0252		0.7195	0.2468	0.0069	4.9811	74.5
67272	61	R	2.3087	1.6718	0.0253		0.7143	0.2601	0.0108	4.9910	73.3
67273	5	C	2.6017	1.4058	0.0111		0.4132	0.5110	0.0164	4.9592	44.7
67273	9	C	2.6203	1.3888			0.4065	0.5211	0.0187	4.9554	43.8
67273	17	C	2.6245	1.3754	0.0087		0.4052	0.5285	0.0197	4.9620	43.4
67273	20	C	2.6132	1.3944			0.4185	0.5098	0.0173	4.9532	45.1
67273	21	C	2.5343	1.4651	0.0099		0.4902	0.4515	0.0157	4.9667	52.1
67273	22	C	2.6322	1.3700	0.0107		0.3943	0.5319	0.0197	4.9588	42.6
67273	23	R	2.5620	1.4381			0.4700	0.4826	0.0153	4.9680	49.3
67273	24	C	2.6354	1.3623	0.0094		0.3858	0.5605	0.0206	4.9740	40.8
67273	25	R	2.5570	1.4456	0.0110		0.4669	0.4655	0.0138	4.9598	50.1
67273	26	C	2.6072	1.3936	0.0098		0.4176	0.5181	0.0178	4.9641	44.6
67273	27	C	2.5722	1.4300	0.0160		0.4455	0.4851	0.0133	4.9621	47.9
67273	27	C	2.5782	1.4163	0.0141		0.4371	0.5165	0.0197	4.9819	45.8
67273	28	C	2.6143	1.3888	0.0131		0.4108	0.5117	0.0171	4.9558	44.5
67273	30	C	2.6011	1.4109			0.4201	0.5068	0.0162	4.9551	45.3
67273	32	C	2.6120	1.3901	0.0119		0.4016	0.5376	0.0171	4.9703	42.8
67273	38	C	2.6658	1.3455			0.3581	0.5646	0.0194	4.9534	38.8
67273	43	C	2.5808	1.4218	0.0086		0.4395	0.4989	0.0166	4.9662	46.8
67273	44	C	2.5709	1.4304	0.0129	0.0136	0.4354	0.4826	0.0192	4.9650	47.4
67275	24	R	2.5623	1.4278	0.0205		0.4613	0.4807	0.0231	4.9757	49.0

Batur Volcano:- PLAGIOCLASE (OXIDES)

ROCK	NUM	L	SiO2	Al2O3	FeO	MgO	CaO	Na2O	K2O	(SUM)	NOTE
67275	25	C	50.86	31.11	0.39		14.51	3.01	0.11	100.21	
67275	29	C	57.83	26.85			9.25	5.83	0.24	100.48	
67275	30	C	57.60	26.86	0.25		9.38	5.67	0.25	100.97	
67275	31	R	56.97	27.07	0.36		9.86	5.51	0.24	100.96	RIM TO #30
67275	34	C	55.71	28.10	0.35		10.70	4.89	0.25	97.91	
67275	37	C	57.88	26.70	0.43		8.97	5.70	0.32	99.37	
67275	43	C	56.67	27.49	0.39		9.92	5.26	0.26	99.05	
67275	44	R	58.93	25.72	0.85		7.92	5.98	0.60	97.21	
67275	45	C	56.47	27.48	0.34		10.22	5.21	0.27	99.38	
67275	47	C	56.59	27.57	0.30		10.16	5.14	0.24	99.10	
67275	48	R	56.89	27.24	0.37		9.73	5.44	0.32	99.05	RIM TO #47
67275	49	C	59.02	25.95	0.22		8.17	6.29	0.36	100.05	
67275	50	R	55.81	27.97	0.43		10.57	4.98	0.25	100.30	RIM TO #49
67275	51	C	55.92	27.79	0.38		10.47	5.05	0.39	100.44	
67275	52	R	59.74	25.14	0.41		7.29	6.79	0.63	100.15	RIM TO #51
67277	10	C	58.81	26.34			8.42	6.14	0.29	99.06	
67277	11	R	60.52	25.22			7.11	6.74	0.41	98.85	RIM TO #10
67277	13	C	60.89	24.74			6.72	7.19	0.45	98.93	
67277	14	R	60.92	24.93			7.01	6.72	0.43	98.20	RIM TO #13
67277	29	C	59.99	25.48			7.44	6.67	0.42	99.46	
67277	30	R	60.60	25.25			7.12	6.66	0.37	98.78	RIM TO #29
67277	43	C	61.15	24.78			6.47	7.15	0.45	100.50	
67277	44	R	59.89	25.81			7.48	6.39	0.43	99.53	RIM TO #43
67277	47	C	61.36	24.76			6.37	7.03	0.47	99.98	
67277	48	R	60.85	24.88			6.72	7.12	0.44	100.96	RIM TO #47
67277	50	C	61.96	24.44			5.92	7.22	0.45	99.82	
67277	51	R	61.36	24.50			6.42	7.26	0.46	100.52	RIM TO #50
67277	52	C	61.56	24.62			6.25	7.12	0.45	100.28	
67277	64	C	60.75	24.97			6.84	7.00	0.44	100.37	
67277	66	C	61.29	24.75			6.29	7.17	0.50	99.51	
67277	67	R	61.28	24.81			6.32	7.07	0.51	99.82	RIM TO #66

Batur Volcano:- PLAGIOCLASE (CATIONS)

ROCK	NUM	L	Si	Al	Fe	Mg	Ca	Na	K	SUM	Ca#
67275	25	C	2.3173	1.6708	0.0148		0.7083	0.2662	0.0064	4.9838	72.7
67275	29	C	2.5869	1.4156			0.4431	0.5058	0.0136	4.9650	46.7
67275	30	C	2.5802	1.4181	0.0093		0.4501	0.4920	0.0141	4.9638	47.8
67275	31	R	2.5584	1.4328	0.0134		0.4742	0.4795	0.0136	4.9719	49.7
67275	34	C	2.5074	1.4904	0.0131		0.5161	0.4269	0.0141	4.9680	54.7
67275	37	C	2.5919	1.4090	0.0162		0.4302	0.4945	0.0184	4.9602	46.5
67275	43	C	2.5445	1.4549	0.0148		0.4774	0.4579	0.0150	4.9645	51.0
67275	44	R	2.6382	1.3569	0.0320		0.3799	0.5188	0.0341	4.9599	42.3
67275	45	C	2.5382	1.4558	0.0129		0.4923	0.4542	0.0156	4.9690	52.0
67275	47	C	2.5406	1.4588	0.0114		0.4888	0.4471	0.0139	4.9606	52.2
67275	48	R	2.5546	1.4416	0.0140		0.4682	0.4738	0.0185	4.9707	49.7
67275	49	C	2.6353	1.3655	0.0082		0.3907	0.5443	0.0205	4.9645	41.8
67275	50	R	2.5123	1.4837	0.0161		0.5097	0.4342	0.0143	4.9703	54.0
67275	51	C	2.5184	1.4749	0.0142		0.5053	0.4407	0.0223	4.9758	53.4
67275	52	R	2.6690	1.3239	0.0153		0.3489	0.5881	0.0359	4.9811	37.2
67277	10	C	2.6235	1.3847			0.4024	0.5308	0.0167	4.9581	43.1
67277	11	R	2.6891	1.3209			0.3386	0.5805	0.0235	4.9526	36.8
67277	13	C	2.7065	1.2963			0.3201	0.6194	0.0258	4.9681	34.1
67277	14	R	2.7044	1.3044			0.3333	0.5785	0.0242	4.9448	36.6
67277	29	C	2.6704	1.3366			0.3548	0.5753	0.0240	4.9611	38.1
67277	30	R	2.6910	1.3215			0.3386	0.5735	0.0212	4.9458	37.1
67277	43	C	2.7140	1.2960			0.3075	0.6156	0.0253	4.9584	33.3
67277	44	R	2.6634	1.3529			0.3562	0.5510	0.0245	4.9480	39.3
67277	47	C	2.7204	1.2941			0.3026	0.6044	0.0266	4.9481	33.4
67277	48	R	2.7034	1.3030			0.3197	0.6135	0.0247	4.9643	34.3
67277	50	C	2.7421	1.2750			0.2807	0.6198	0.0254	4.9430	31.2
67277	51	R	2.7234	1.2818			0.3051	0.6249	0.0259	4.9611	32.8
67277	52	C	2.7279	1.2860			0.2969	0.6118	0.0254	4.9480	32.7
67277	64	C	2.6993	1.3077			0.3259	0.6034	0.0248	4.9611	35.1
67277	66	C	2.7188	1.2941			0.2990	0.6163	0.0284	4.9566	32.7
67277	67	R	2.7178	1.2971			0.3004	0.6082	0.0289	4.9524	33.1

Batur Volcano:- PLAGIOCLASE (OXIDES)

ROCK	NUM	L	SiO2	Al2O3	FeO	MgO	CaO	Na2O	K2O	(SUM)	NOTE
67277	80	C	60.50	25.27			7.17	6.66	0.39	99.55	
67277	82	C	61.61	24.51			6.20	7.17	0.51	100.08	
67277	83	R	60.33	25.13	0.23		7.10	6.81	0.39	99.96	RIM TO #82
67277	84	C	60.24	25.26			7.14	6.91	0.46	100.33	
67277	85	R	59.68	25.78			7.59	6.54	0.40	99.71	RIM TO #84
67278	20	C	57.34	27.27	0.23		9.43	5.48	0.26	101.77	
67278	21	R	57.42	27.30	0.24		9.38	5.40	0.26	100.34	Z1 RIM TO #28
67278	23		57.54	26.88	0.32		9.23	5.75	0.29	104.36	Z2
67278	24		57.56	26.82	0.26		9.17	5.88	0.31	102.88	Z3
67278	25		58.08	26.67	0.26		8.86	5.87	0.26	101.92	Z4
67278	26		57.42	26.88	0.35		9.32	5.74	0.29	102.58	Z5
67278	27		57.63	26.99	0.24		9.17	5.69	0.28	103.54	Z6
67278	28	C	58.15	26.82			8.89	5.84	0.29	102.42	Z7
67278	29		57.96	26.86		0.24	9.05	5.62	0.28	101.58	Z8
67278	30		58.09	26.71		0.20	8.83	5.83	0.35	101.24	Z9
67278	32		57.68	26.68	0.35		9.06	5.90	0.33	103.14	Z11
67278	33		57.81	27.07			9.28	5.52	0.32	101.07	Z10
67278	34		57.14	26.96	0.31		9.64	5.62	0.33	102.58	Z12
67278	94	C	54.87	28.54	0.31		11.33	4.74	0.20	102.49	
67278	95	R	57.09	27.10	0.28		9.65	5.56	0.32	102.85	RIM TO #94
67278	96	C	56.44	27.49	0.32		10.01	5.36	0.37	102.19	
67278	97	R	57.59	26.87	0.31		9.09	5.76	0.38	102.76	RIM TO #96
67326	50	C	52.83	29.35	0.74		13.09	3.43	0.57	100.68	
67326	51	C	52.44	30.08	0.67		13.14	3.48	0.18	100.89	
67326	52	R	51.38	30.48	0.81		14.08	3.07	0.18	100.92	RIM TO #51
67326	53	C	46.50	33.76	0.64		17.80	1.31		102.33	
67326	55	R	51.69	30.32	0.74		13.66	3.36	0.24	101.40	RIM TO #53
67328	71	C	48.21	32.63	0.65		16.72	1.79		100.28	
67328	72	R	47.13	33.10	1.22		17.28	1.27		99.77	RIM TO #71
67328	74	C	46.69	33.63	0.51		17.95	1.22		101.02	
67328	76	C	45.25	34.62	0.49		18.98	0.66		100.09	

Batur Volcano:- PLAGIOCLASE (CATIONS)

ROCK	NUM	L	Si	Al	Fe	Mg	Ca	Na	K	SUM	Ca#
67277	80	C	2.6879	1.3234			0.3414	0.5737	0.0222	4.9486	37.3
67277	82	C	2.7311	1.2806			0.2942	0.6166	0.0288	4.9513	32.3
67277	83	R	2.6852	1.3182	0.0086		0.3387	0.5879	0.0222	4.9608	36.6
67277	84	C	2.6808	1.3248			0.3403	0.5960	0.0260	4.9679	36.3
67277	85	R	2.6573	1.3531			0.3622	0.5645	0.0228	4.9599	39.1
67278	20	C	2.5675	1.4392	0.0085		0.4526	0.4760	0.0146	4.9584	48.7
67278	21	R	2.5700	1.4399	0.0090		0.4497	0.4687	0.0148	4.9521	49.0
67278	23		2.5788	1.4198	0.0119		0.4431	0.4996	0.0164	4.9696	47.0
67278	24		2.5802	1.4168	0.0098		0.4402	0.5111	0.0178	4.9759	46.3
67278	25		2.5977	1.4057	0.0095		0.4245	0.5088	0.0151	4.9613	45.5
67278	26		2.5751	1.4207	0.0132		0.4478	0.4993	0.0167	4.9728	47.3
67278	27		2.5800	1.4244	0.0090		0.4396	0.4938	0.0160	4.9628	47.1
67278	28	C	2.5976	1.4121			0.4257	0.5057	0.0167	4.9578	45.7
67278	29		2.5895	1.4141		0.0157	0.4330	0.4869	0.0157	4.9549	47.1
67278	30		2.5959	1.4068		0.0132	0.4228	0.5049	0.0197	4.9633	45.6
67278	32		2.5857	1.4098	0.0131		0.4349	0.5132	0.0189	4.9756	45.9
67278	33		2.5841	1.4262			0.4445	0.4785	0.0181	4.9514	48.2
67278	34		2.5652	1.4269	0.0117		0.4638	0.4888	0.0190	4.9754	48.7
67278	94	C	2.4756	1.5175	0.0118		0.5476	0.4148	0.0118	4.9791	56.9
67278	95	R	2.5623	1.4334	0.0106		0.4638	0.4839	0.0184	4.9724	48.9
67278	96	C	2.5380	1.4568	0.0121		0.4823	0.4675	0.0213	4.9780	50.8
67278	97	R	2.5810	1.4193	0.0117		0.4364	0.5006	0.0217	4.9707	46.6
67326	50	C	2.4031	1.5736	0.0280		0.6380	0.3022	0.0329	4.9778	67.9
67326	51	C	2.3811	1.6098	0.0256		0.6394	0.3063	0.0103	4.9725	67.6
67326	52	R	2.3420	1.6376	0.0310		0.6877	0.2715	0.0104	4.9802	71.7
67326	53	C	2.1433	1.8344	0.0245		0.8789	0.1170		4.9981	88.3
67326	55	R	2.3543	1.6276	0.0282		0.6666	0.2970	0.0138	4.9875	69.2
67328	71	C	2.2129	1.7651	0.0249		0.8224	0.1588		4.9841	83.8
67328	72	R	2.1726	1.7983	0.0471		0.8535	0.1138		4.9853	88.2
67328	74	C	2.1509	1.8257	0.0198		0.8857	0.1087		4.9908	89.1
67328	76	C	2.0914	1.8859	0.0189		0.9400	0.0591		4.9953	94.1

Batur Volcano:- PLAGIOCLASE (OXIDES)

ROCK	NUM	L	SiO2	Al2O3	FeO	MgO	CaO	Na2O	K2O	(SUM)	NOTE
67328	77	R	46.90	33.39	0.77		17.65	1.29		98.55	RIM TO #76
67328	78	C	46.69	33.50	0.62		17.84	1.22	0.12	99.39	
67328	79	R	52.36	29.77	0.78	0.19	13.22	3.45	0.24	100.11	RIM TO #78
67328	81	C	51.59	30.54	0.59		13.99	2.99	0.29	99.21	
67328	82	R	46.90	33.67	0.60		17.59	1.25		100.22	CLEAR RIM TO #81
67328	83	C	48.02	32.79	0.67		16.72	1.80		99.37	
67328	84	R	55.23	27.75	1.03		10.90	4.78	0.32	98.28	RIM TO #83
67328	87	C	46.96	33.45	0.64		17.66	1.29		98.59	
67328	88	R	57.81	25.09	1.72	0.52	9.07	5.19	0.60	96.37	RIM TO #87
67328	89	C	46.39	34.04	0.57		18.00	1.00		98.81	
67328	90	R	46.51	33.74	0.71		17.80	1.25		98.62	RIM TO #89
67328	91	R	55.18	27.95	0.90		10.84	4.80	0.34	97.79	RPT #88
67331	7	C	57.41	26.89	0.35		9.36	5.70	0.29	102.15	
67331	9	C	57.48	26.85	0.42		8.99	5.89	0.36	98.76	
67331	10	R	56.72	27.60	0.25		9.77	5.31	0.34	99.24	RIM TO #9
67331	10	I	57.76	26.62	0.55		8.91	5.83	0.33	97.14	INCL IN OLV
67331	11	C	57.88	26.66	0.27		9.03	5.87	0.29	98.59	
67331	12	R	57.89	26.77	0.36		8.97	5.65	0.35	97.16	RIM TO #11
67331	12	C	57.33	27.22			9.63	5.54	0.27	98.85	
67331	13	R	57.33	27.00	0.27		9.42	5.70	0.28	98.94	RIM TO #12
67331	14	C	57.20	27.05	0.29		9.49	5.69	0.28	99.34	
67331	15	R	56.90	27.09	0.32		9.54	5.82	0.33	100.06	RIM TO #14
67331	16	C	56.19	27.89	0.30		10.33	5.07	0.22	99.48	
67331	16	I	57.71	26.64	0.42		9.02	5.91	0.31	100.23	INCL IN OLV
67331	17	R	55.52	28.14	0.29		10.88	4.88	0.28	99.49	RIM TO #16
67331	17	C	56.78	27.26	0.29		9.83	5.58	0.27	100.20	
67331	18	G	58.13	26.64	0.31		8.61	5.90	0.40	98.57	
67331	19	R	55.87	27.91	0.35		10.52	5.05	0.30	99.85	Z1 RIM TO #25
67331	19	G	58.80	25.78	0.47		8.04	6.51	0.41	100.36	
67331	20		58.73	26.13	0.26		8.37	6.18	0.34	100.36	Z2
67331	21		57.59	26.90	0.24		9.13	5.80	0.34	100.18	Z3

Batur Volcano:- PLAGIOCLASE (CATIONS)

ROCK	NUM	L	Si	Al	Fe	Mg	Ca	Na	K	SUM	Ca#
67328	77	R	2.1608	1.8134	0.0297		0.8711	0.1151		4.9901	88.3
67328	78	C	2.1529	1.8207	0.0241		0.8812	0.1088	0.0071	4.9948	89.0
67328	79	R	2.3810	1.5953	0.0296	0.0129	0.6438	0.3038	0.0139	4.9803	67.9
67328	81	C	2.3483	1.6386	0.0226		0.6823	0.2642	0.0170	4.9730	72.1
67328	82	R	2.1578	1.8258	0.0230		0.8672	0.1113		4.9851	88.6
67328	83	C	2.2051	1.7744	0.0259		0.8223	0.1604		4.9881	83.7
67328	84	R	2.4979	1.4791	0.0389		0.5281	0.4194	0.0182	4.9816	55.7
67328	87	C	2.1621	1.8152	0.0246		0.8711	0.1150		4.9880	88.3
67328	88	R	2.6081	1.3342	0.0650	0.0349	0.4384	0.4539	0.0346	4.9691	49.1
67328	89	C	2.1368	1.8477	0.0218		0.8885	0.0895		4.9843	90.8
67328	90	R	2.1442	1.8331	0.0274		0.8790	0.1115		4.9952	88.7
67328	91	R	2.4940	1.4888	0.0340		0.5249	0.4203	0.0195	4.9815	55.5
67331	7	C	2.5745	1.4215	0.0132		0.4497	0.4954	0.0168	4.9711	47.6
67331	9	C	2.5782	1.4196	0.0156		0.4321	0.5125	0.0209	4.9789	45.7
67331	10	R	2.5452	1.4597	0.0095		0.4699	0.4620	0.0196	4.9659	50.4
67331	10	I	2.5894	1.4066	0.0205		0.4282	0.5064	0.0188	4.9699	45.8
67331	11	C	2.5916	1.4068	0.0103		0.4331	0.5099	0.0168	4.9685	45.9
67331	12	R	2.5913	1.4123	0.0135		0.4304	0.4904	0.0200	4.9579	46.7
67331	12	C	2.5672	1.4368			0.4621	0.4813	0.0156	4.9630	49.0
67331	13	R	2.5706	1.4268	0.0102		0.4526	0.4956	0.0162	4.9720	47.7
67331	14	C	2.5660	1.4302	0.0110		0.4563	0.4947	0.0161	4.9743	48.0
67331	15	R	2.5567	1.4350	0.0120		0.4595	0.5068	0.0189	4.9889	47.6
67331	16	C	2.5247	1.4767	0.0113		0.4974	0.4413	0.0127	4.9641	53.0
67331	16	I	2.5871	1.4076	0.0157		0.4332	0.5134	0.0177	4.9747	45.8
67331	17	R	2.5009	1.4941	0.0110		0.5248	0.4266	0.0162	4.9736	55.2
67331	17	C	2.5504	1.4430	0.0109		0.4731	0.4859	0.0154	4.9787	49.3
67331	18	G	2.6005	1.4047	0.0118		0.4128	0.5121	0.0226	4.9645	44.6
67331	19	R	2.5149	1.4808	0.0132		0.5071	0.4405	0.0173	4.9738	53.5
67331	19	G	2.6316	1.3598	0.0175		0.3856	0.5646	0.0233	4.9824	40.6
67331	20		2.6242	1.3760	0.0097		0.4007	0.5352	0.0193	4.9651	42.8
67331	21		2.5801	1.4206	0.0090		0.4384	0.5038	0.0194	4.9713	46.5

Batur Volcano:- PLAGIOCLASE (OXIDES)

ROCK	NUM	L	SiO2	Al2O3	FeO	MgO	CaO	Na2O	K2O	(SUM)	NOTE
67331	22		55.88	28.07	0.22		10.62	4.97	0.25	100.83	Z4
67331	23		55.93	28.19	0.27		10.60	4.78	0.22	96.97	Z5
67331	23	C	56.03	27.68	0.32		10.33	5.36	0.28	100.00	
67331	24		56.75	27.58			10.09	5.31	0.28	99.65	Z6
67331	24	R	56.88	27.19	0.42		9.43	5.68	0.39	99.58	RIM TO #23
67331	25	C	57.10	27.19	0.27		9.62	5.57	0.26	100.44	Z7
67331	25	C	56.06	27.83	0.27		10.43	5.22	0.18	99.41	
67331	26	R	57.05	27.10	0.30		9.56	5.71	0.28	99.00	RIM TO #25
67331	26		57.17	27.33	0.25		9.59	5.38	0.28	99.98	Z8
67331	27		57.03	27.20	0.29		9.59	5.60	0.29	100.61	Z9
67331	28		56.78	27.53			9.99	5.39	0.31	100.29	Z10
67331	29		55.51	28.09	0.31		10.86	4.94	0.29	100.74	Z11
67331	29	G	59.57	25.29	0.51		7.41	6.60	0.62	96.60	
67331	30		57.07	27.04	0.35		9.58	5.61	0.35	100.22	Z12
67331	31	G	59.88	25.29	0.37		7.14	6.68	0.64	98.72	
67331	31		55.85	27.93	0.37		10.41	5.15	0.29	100.30	Z13
67331	32	C	54.07	28.88	0.36		12.06	4.43	0.20	97.86	
67331	32	G	59.37	25.82	0.26		7.76	6.32	0.46	99.20	
67331	33	G	58.85	25.97	0.37		8.22	6.14	0.45	99.44	
67331	33	R	58.71	26.13	0.45		8.05	6.20	0.47	98.43	RIM TO #32
67331	34	G	59.27	25.51	0.41		7.66	6.58	0.57	100.18	
67331	35	G	58.38	26.40	0.27		8.74	5.85	0.36	100.31	
67331	40	C	56.36	27.48	0.33		10.09	5.49	0.26	100.99	
67331	41	R	58.79	25.89	0.42		8.18	6.26	0.46	100.61	RIM TO #40
67331	42	C	55.78	28.05	0.25		10.64	4.99	0.28	98.28	
67331	43	C	57.63	27.09			9.39	5.60	0.28	98.85	
67331	43	C	57.34	26.74	0.55		9.29	5.73	0.35	99.62	PART OF GLOMEROCRYST
67331	44	C	56.62	27.53	0.31		9.98	5.31	0.24	99.95	
67331	46	C	56.65	27.41	0.24		9.97	5.45	0.28	99.76	
67331	47	R	56.64	27.36	0.27		9.95	5.48	0.29	99.41	RIM TO #46
67331	49	R	56.87	27.07	0.46		9.72	5.54	0.34	96.86	Z1 RIM TO #57

Batur Volcano:- PLAGIOCLASE (CATIONS)

ROCK	NUM	L	Si	Al	Fe	Mg	Ca	Na	K	SUM	Ca#
67331	22		2.5126	1.4875	0.0082		0.5117	0.4332	0.0142	4.9674	54.2
67331	23		2.5129	1.4929	0.0101		0.5103	0.4168	0.0124	4.9554	55.0
67331	23	C	2.5224	1.4687	0.0120		0.4983	0.4678	0.0161	4.9853	51.6
67331	24		2.5451	1.4577			0.4846	0.4616	0.0161	4.9651	51.2
67331	24	R	2.5556	1.4401	0.0158		0.4539	0.4952	0.0224	4.9830	47.8
67331	25	C	2.5611	1.4375	0.0101		0.4622	0.4840	0.0148	4.9697	48.8
67331	25	C	2.5209	1.4752	0.0102		0.5026	0.4552	0.0104	4.9745	52.5
67331	26	R	2.5610	1.4339	0.0114		0.4596	0.4967	0.0162	4.9788	48.1
67331	26		2.5618	1.4432	0.0094		0.4605	0.4675	0.0160	4.9584	49.6
67331	27		2.5592	1.4388	0.0108		0.4611	0.4869	0.0165	4.9733	48.6
67331	28		2.5467	1.4555			0.4802	0.4691	0.0177	4.9692	50.6
67331	29		2.5011	1.4919	0.0116		0.5243	0.4319	0.0165	4.9773	54.8
67331	29	G	2.6621	1.3322	0.0190		0.3549	0.5723	0.0354	4.9759	38.3
67331	30		2.5627	1.4311	0.0131		0.4608	0.4882	0.0200	4.9759	48.6
67331	31	G	2.6714	1.3301	0.0140		0.3414	0.5774	0.0363	4.9706	37.2
67331	31		2.5142	1.4817	0.0139		0.5020	0.4499	0.0166	4.9783	52.7
67331	32	C	2.4460	1.5398	0.0135		0.5845	0.3890	0.0118	4.9846	60.0
67331	32	G	2.6485	1.3573	0.0098		0.3710	0.5466	0.0264	4.9596	40.4
67331	33	G	2.6307	1.3681	0.0139		0.3935	0.5325	0.0258	4.9645	42.5
67331	33	R	2.6252	1.3771	0.0167		0.3855	0.5373	0.0267	4.9685	41.8
67331	34	G	2.6500	1.3445	0.0153		0.3667	0.5702	0.0324	4.9791	39.1
67331	35	G	2.6103	1.3912	0.0101		0.4188	0.5073	0.0205	4.9582	45.2
67331	40	C	2.5350	1.4567	0.0123		0.4862	0.4784	0.0148	4.9834	50.4
67331	41	R	2.6300	1.3652	0.0156		0.3921	0.5431	0.0261	4.9721	41.9
67331	42	C	2.5100	1.4878	0.0096		0.5131	0.4350	0.0164	4.9719	54.1
67331	43	C	2.5782	1.4284			0.4500	0.4861	0.0162	4.9589	48.1
67331	43	C	2.5749	1.4154	0.0207		0.4468	0.4991	0.0201	4.9770	47.2
67331	44	C	2.5422	1.4571	0.0116		0.4803	0.4625	0.0138	4.9675	50.9
67331	46	C	2.5445	1.4510	0.0090		0.4800	0.4749	0.0161	4.9755	50.3
67331	47	R	2.5451	1.4490	0.0102		0.4789	0.4776	0.0167	4.9775	50.1
67331	49	R	2.5561	1.4342	0.0175		0.4679	0.4832	0.0195	4.9784	49.2

Batur Volcano:- PLAGIOCLASE (OXIDES)

ROCK	NUM	L	SiO2	Al2O3	FeO	MgO	CaO	Na2O	K2O	(SUM)	NOTE
67331	50		56.16	27.71	0.35		10.08	5.38	0.31	98.83	Z2
67331	51		54.72	28.51	0.49		11.44	4.62	0.21	99.25	Z3
67331	52		54.85	28.63	0.34		11.56	4.38	0.22	98.59	Z4
67331	53		54.61	28.76	0.33		11.69	4.42	0.18	98.64	Z5
67331	54		56.83	27.18	0.27		9.74	5.64	0.34	99.01	Z6
67331	55		56.80	27.22	0.34		9.91	5.50	0.23	98.80	Z7
67331	56		57.37	27.27			9.79	5.29	0.27	98.04	Z8
67331	57	C	56.71	27.38	0.25		9.88	5.48	0.31	98.22	Z9
67331	58		57.02	27.43			9.90	5.39	0.27	98.00	Z10
67331	59		56.70	27.31	0.27		9.89	5.62	0.21	97.76	Z11
67331	60		57.03	27.37			10.16	5.20	0.24	98.22	Z12
67331	61		56.58	27.54	0.34		10.21	5.07	0.27	98.11	Z13
67331	62		54.46	28.90	0.34		11.55	4.51	0.24	98.18	Z14
67331	63		54.59	28.71	0.27		11.47	4.73	0.22	99.27	Z15
67331	64	C	57.00	27.26	0.27		9.84	5.37	0.26	101.59	
67331	65	R	56.97	27.59			9.77	5.40	0.26	101.22	RIM TO #64
67331	72	C	57.27	27.06	0.36		9.26	5.70	0.34	102.11	
67331	73	R	59.34	25.45	0.27		7.81	6.60	0.54	101.44	RIM TO #72
67331	77	I	57.17	26.96	0.54		9.37	5.65	0.31	100.66	INCL IN OLV
67331	79	G	58.90	25.69	0.49		8.08	6.32	0.52	100.37	
67331	80	R	57.56	27.05			9.46	5.57	0.36	99.80	Z1 RIM TO #86
67331	81		57.81	26.91	0.25		9.24	5.49	0.30	98.79	Z2
67331	82		55.80	28.23			10.90	4.86	0.21	100.38	Z3
67331	83		56.91	27.64			9.84	5.34	0.26	100.38	Z4
67331	84		57.00	27.39	0.26		9.61	5.48	0.26	100.54	Z5
67331	85		58.35	26.61			8.84	5.89	0.30	99.77	Z6
67331	86	C	56.96	27.56			9.67	5.52	0.29	100.71	Z7
67331	87		56.85	27.53			10.00	5.41	0.21	100.60	Z8
67331	88		55.90	28.10	0.28		10.55	4.92	0.25	101.12	Z9
67331	89		55.96	28.06	0.30		10.59	4.85	0.24	101.48	Z10
67331	90		58.83	26.05	0.30		8.27	6.20	0.36	101.63	Z11

Batur Volcano:- PLAGIOCLASE (CATIONS)

ROCK	NUM	L	Si	Al	Fe	Mg	Ca	Na	K	SUM	Ca#
67331	50		2.5264	1.4696	0.0133		0.4858	0.4695	0.0180	4.9826	50.9
67331	51		2.4714	1.5178	0.0186		0.5534	0.4050	0.0122	4.9784	57.7
67331	52		2.4737	1.5220	0.0130		0.5587	0.3831	0.0128	4.9633	59.3
67331	53		2.4645	1.5298	0.0126		0.5652	0.3867	0.0105	4.9693	59.4
67331	54		2.5535	1.4393	0.0102		0.4687	0.4909	0.0197	4.9823	48.8
67331	55		2.5515	1.4409	0.0129		0.4769	0.4787	0.0133	4.9742	49.9
67331	56		2.5677	1.4387			0.4695	0.4593	0.0151	4.9503	50.5
67331	57	C	2.5471	1.4493	0.0096		0.4752	0.4770	0.0175	4.9757	49.9
67331	58		2.5551	1.4487			0.4752	0.4681	0.0152	4.9623	50.4
67331	59		2.5471	1.4461	0.0100		0.4761	0.4891	0.0123	4.9807	49.3
67331	60		2.5555	1.4455			0.4879	0.4520	0.0140	4.9549	51.9
67331	61		2.5407	1.4577	0.0126		0.4914	0.4411	0.0152	4.9587	52.7
67331	62		2.4588	1.5377	0.0127		0.5587	0.3950	0.0141	4.9770	58.6
67331	63		2.4647	1.5278	0.0103		0.5551	0.4145	0.0128	4.9852	57.3
67331	64	C	2.5571	1.4411	0.0100		0.4731	0.4675	0.0146	4.9634	50.3
67331	65	R	2.5520	1.4568			0.4689	0.4693	0.0147	4.9617	50.0
67331	72	C	2.5689	1.4305	0.0136		0.4452	0.4957	0.0196	4.9735	47.3
67331	73	R	2.6519	1.3408	0.0099		0.3739	0.5715	0.0309	4.9789	39.5
67331	77	I	2.5671	1.4269	0.0201		0.4507	0.4921	0.0176	4.9745	47.8
67331	79	G	2.6362	1.3554	0.0183		0.3875	0.5481	0.0296	4.9751	41.4
67331	80	R	2.5766	1.4275			0.4537	0.4836	0.0206	4.9620	48.4
67331	81		2.5864	1.4188	0.0095		0.4430	0.4759	0.0173	4.9509	48.2
67331	82		2.5073	1.4953			0.5247	0.4236	0.0120	4.9629	55.3
67331	83		2.5495	1.4596			0.4724	0.4638	0.0148	4.9601	50.5
67331	84		2.5559	1.4476	0.0097		0.4616	0.4764	0.0148	4.9660	49.2
67331	85		2.6061	1.4008			0.4230	0.5103	0.0171	4.9573	45.3
67331	86	C	2.5521	1.4557			0.4643	0.4796	0.0165	4.9682	49.2
67331	87		2.5483	1.4548			0.4803	0.4700	0.0119	4.9653	50.5
67331	88		2.5133	1.4887	0.0104		0.5083	0.4293	0.0142	4.9642	54.2
67331	89		2.5153	1.4868	0.0111		0.5101	0.4225	0.0136	4.9594	54.7
67331	90		2.6286	1.3716	0.0110		0.3957	0.5370	0.0208	4.9647	42.4

Batur Volcano:- PLAGIOCLASE (OXIDES)

ROCK	NUM	L	SiO2	Al2O3	FeO	MgO	CaO	Na2O	K2O	(SUM)	NOTE
67331	91		57.19	27.40			9.84	5.31	0.26	101.01	Z12
67339	34	X	45.54	34.58	0.54		18.66	0.68		100.90	
67339	35	X	45.39	34.72	0.42		18.81	0.67		101.13	
67339	42	X	46.29	34.15	0.56		18.07	0.93		103.05	
67339	46	X	45.67	34.64	0.47		18.41	0.81		101.51	
67339	48	X	46.18	34.30	0.55		18.10	0.86		99.93	RIM TO #46
67342	2	C	54.88	29.01			11.66	4.08	0.36	99.54	
67342	3	R	53.35	29.59	0.35		12.72	3.67	0.32	100.80	RIM TO #2
67342	10	C	55.20	28.46	0.33		11.19	4.41	0.42	100.49	
67342	11	R	54.56	28.69	0.51		11.51	4.31	0.43	100.94	RIM TO #10
67342	12	C	55.26	28.16	0.43		11.00	4.58	0.57	101.09	
67342	13	C	54.26	28.79	0.47		11.68	4.35	0.45	101.12	
67342	21	C	55.05	28.53	0.37		11.26	4.39	0.40	100.25	
67342	22	C	54.61	28.50	0.39		11.67	4.36	0.46	101.39	
67342	25	C	54.70	28.36	0.43		11.53	4.53	0.46	100.26	
67342	26	C	55.43	28.21	0.31		11.10	4.48	0.47	100.46	
67342	28	C	58.38	26.06	0.61		8.30	5.80	0.86	100.23	

Batur Volcano:- PLAGIOCLASE (CATIONS)

ROCK	NUM	L	Si	Al	Fe	Mg	Ca	Na	K	SUM	Ca#
67331	91		2.5606	1.4461			0.4721	0.4606	0.0147	4.9541	50.6
67339	34	X	2.1021	1.8812	0.0207		0.9229	0.0612		4.9881	93.8
67339	35	X	2.0952	1.8890	0.0160		0.9302	0.0602		4.9906	93.9
67339	42	X	2.1321	1.8539	0.0217		0.8917	0.0832		4.9826	91.5
67339	46	X	2.1061	1.8826	0.0182		0.9097	0.0722		4.9888	92.6
67339	48	X	2.1270	1.8622	0.0212		0.8933	0.0768		4.9805	92.1
67342	2	C	2.4703	1.5392			0.5625	0.3559	0.0208	4.9487	61.2
67342	3	R	2.4155	1.5792	0.0131		0.6169	0.3222	0.0183	4.9652	65.7
67342	10	C	2.4877	1.5118	0.0124		0.5401	0.3852	0.0240	4.9612	58.4
67342	11	R	2.4653	1.5280	0.0191		0.5573	0.3776	0.0246	4.9719	59.6
67342	12	C	2.4940	1.4982	0.0161		0.5319	0.4008	0.0330	4.9740	57.0
67342	13	C	2.4549	1.5350	0.0180		0.5661	0.3817	0.0257	4.9814	59.7
67342	21	C	2.4823	1.5161	0.0139		0.5441	0.3837	0.0229	4.9630	58.6
67342	22	C	2.4688	1.5187	0.0149		0.5651	0.3821	0.0267	4.9763	59.7
67342	25	C	2.4733	1.5113	0.0162		0.5586	0.3970	0.0265	4.9829	58.5
67342	26	C	2.4980	1.4983	0.0116		0.5359	0.3914	0.0269	4.9621	57.8
67342	28	C	2.6179	1.3774	0.0228		0.3988	0.5040	0.0491	4.9700	44.2

Batur Volcano:- OLIVINE (OXIDES)

ROCK	NUM	L	SiO2	FeO	MnO	MgO	CaO	(SUM)	NOTE
67238	31	C	36.37	28.93	0.52	34.02	0.16	103.16	
67238	32	R	35.56	32.53	0.66	31.06	0.19	99.91	RIM TO #31
67238	36	C	36.04	28.68	0.55	34.56	0.18	100.01	
67238	37	R	35.54	33.34	0.69	30.18	0.25	99.74	RIM TO #36
67238	39	C	36.42	28.69	0.50	34.39		98.57	
67238	44	R	35.31	35.59	0.69	28.20	0.21	96.99	
67238	58	C	36.17	27.79	0.45	35.60		103.00	
67238	66	C	36.37	28.05	0.47	35.11		103.39	
67238	69	C	35.93	30.29	0.58	33.05	0.15	103.38	
67238	77	C	36.44	28.27	0.47	34.67	0.16	102.03	
67238	86	C	36.40	28.14	0.52	34.75	0.20	102.42	
67238	96	I	36.40	28.24	0.42	34.76	0.18	101.41	INCL IN CPX
67238	99	C	36.51	27.92	0.50	34.90	0.17	103.56	
67244	10	R	36.18	30.38	0.66	32.49	0.29	101.80	RIM TO #11
67244	11	C	36.90	26.36	0.45	36.11	0.17	99.69	
67244	13	C	36.70	26.73	0.32	35.99	0.25	102.63	
67244	19	C	36.97	27.08	0.43	35.36	0.16	101.76	
67244	24	C	36.99	27.18		35.69	0.14	101.22	
67244	25	R	36.02	30.40	0.52	32.86	0.20	100.69	RIM TO #24
67244	30	G	33.99	43.25	0.87	21.61	0.28	100.27	
67244	35	R	36.28	29.00	0.47	34.12	0.14	101.77	RIM TO #36
67244	36	C	36.81	26.21	0.40	36.41	0.16	101.89	
67244	39	C	36.44	27.81	0.52	35.06	0.18	101.74	
67244	40	R	35.45	33.24	0.71	30.40	0.22	101.79	RIM TO #39
67244	54	C	36.72	26.93	0.46	35.73	0.16	100.35	
67244	55	R	35.93	30.53	0.63	32.70	0.22	100.34	RIM TO #54
67244	56	C	36.90	27.31	0.43	35.18	0.19	101.04	
67244	57	R	35.78	31.21	0.56	32.20	0.27	100.88	RIM TO #56
67244	58	C	36.76	27.45	0.60	35.01	0.18	101.88	
67244	59	R	36.16	29.68	0.38	33.53	0.24	101.51	RIM TO #58
67244	69	C	36.93	26.68	0.33	35.89	0.17	102.76	

Batur Volcano:- OLIVINE (CATIONS)

ROCK	NUM	L	Si	Fe	Mn	Mg	Ca	SUM	Mg#
67238	31	C	0.9813	0.6527	0.0120	1.3683	0.0045	3.0188	67.7
67238	32	R	0.9784	0.7485	0.0154	1.2737	0.0056	3.0216	63.0
67238	36	C	0.9725	0.6472	0.0126	1.3900	0.0052	3.0275	68.2
67238	37	R	0.9818	0.7701	0.0162	1.2426	0.0074	3.0181	61.7
67238	39	C	0.9809	0.6462	0.0113	1.3806		3.0190	68.1
67238	44	R	0.9862	0.8313	0.0163	1.1738	0.0062	3.0138	58.5
67238	58	C	0.9708	0.6238	0.0102	1.4245		3.0293	69.5
67238	66	C	0.9768	0.6300	0.0108	1.4056		3.0232	69.1
67238	69	C	0.9769	0.6887	0.0134	1.3396	0.0045	3.0231	66.0
67238	77	C	0.9799	0.6356	0.0107	1.3894	0.0045	3.0201	68.6
67238	86	C	0.9787	0.6327	0.0118	1.3926	0.0056	3.0214	68.8
67238	96	I	0.9786	0.6350	0.0097	1.3930	0.0051	3.0214	68.7
67238	99	C	0.9802	0.6268	0.0114	1.3964	0.0050	3.0198	69.0
67244	10	R	0.9841	0.6911	0.0152	1.3170	0.0086	3.0160	65.6
67244	11	C	0.9825	0.5869	0.0102	1.4330	0.0049	3.0175	70.9
67244	13	C	0.9791	0.5962	0.0073	1.4311	0.0072	3.0209	70.6
67244	19	C	0.9870	0.6047	0.0098	1.4070	0.0045	3.0130	69.9
67244	24	C	0.9860	0.6059		1.4182	0.0040	3.0141	70.1
67244	25	R	0.9795	0.6913	0.0119	1.3320	0.0058	3.0205	65.8
67244	30	G	0.9895	1.0531	0.0214	0.9378	0.0087	3.0105	47.1
67244	35	R	0.9791	0.6545	0.0108	1.3725	0.0040	3.0209	67.7
67244	36	C	0.9795	0.5833	0.0091	1.4441	0.0045	3.0205	71.2
67244	39	C	0.9781	0.6242	0.0118	1.4027	0.0051	3.0219	69.2
67244	40	R	0.9790	0.7677	0.0165	1.2513	0.0064	3.0209	62.0
67244	54	C	0.9807	0.6013	0.0104	1.4224	0.0046	3.0194	70.3
67244	55	R	0.9784	0.6952	0.0145	1.3272	0.0064	3.0217	65.6
67244	56	C	0.9863	0.6105	0.0096	1.4019	0.0054	3.0137	69.7
67244	57	R	0.9775	0.7131	0.0128	1.3112	0.0078	3.0224	64.8
67244	58	C	0.9844	0.6149	0.0136	1.3976	0.0051	3.0156	69.4
67244	59	R	0.9793	0.6722	0.0088	1.3535	0.0069	3.0207	66.8
67244	69	C	0.9840	0.5946	0.0075	1.4253	0.0047	3.0161	70.6

Batur Volcano:- OLIVINE (OXIDES)

ROCK	NUM	L	SiO2	FeO	MnO	MgO	CaO	(SUM)	NOTE
67259	11	C	36.28	28.26	0.53	34.81	0.13	102.56	
67259	22	C	36.60	28.07	0.49	34.70	0.14	101.96	
67259	27	C	36.14	28.51	0.55	34.64	0.16	101.57	
67259	30	C	36.38	28.37	0.48	34.78		100.86	
67259	35	G	34.79	35.96	0.60	28.46	0.19	103.62	
67259	39	C	36.06	29.06	0.49	34.25	0.14	105.58	
67259	41	G	34.80	38.33	0.67	26.00	0.20	102.24	
67259	45	C	36.20	28.43	0.47	34.73	0.18	102.71	
67259	46	R	35.75	31.70	0.53	31.88	0.14	103.01	
67259	56	C	36.42	28.24	0.51	34.66	0.16	103.14	
67259	56	C	36.69	26.87	0.42	36.02		101.84	
67259	57	R	33.54	45.35	0.90	19.91	0.29	101.79	RIM TO #56
67259	58	C	36.07	28.54	0.51	34.70	0.19	102.40	
67259	59	R	34.15	41.74	0.82	23.09	0.22	101.71	RIM TO #58
67259	65	C	36.05	28.86	0.54	34.32	0.22	103.04	PART OF GLOMEROCRYST
67259	65	C	36.30	28.53	0.50	34.67		102.86	
67259	66	R	34.15	40.93	0.93	23.82	0.18	101.53	RIM TO #65
67259	67	C	36.23	28.50	0.50	34.64	0.13	102.98	
67272	28	C	36.45	28.29	0.55	34.51	0.20	104.89	
67272	29	R	36.02	31.46	0.61	31.91		104.14	RIM TO #28
67272	47	C	36.69	27.91	0.57	34.68	0.14	104.90	
67272	57	G	36.00	33.14	0.74	29.78	0.34	104.21	MICROPHENOCRYST
67273	2	C	33.78	41.72	1.66	22.84		105.54	
67273	3	C	33.96	41.46	1.62	22.78	0.17	101.08	RPT #2
67273	4	R	34.09	40.65	1.50	23.76		100.84	RIM TO #2
67273	6	C	33.88	41.83	1.57	22.56	0.16	100.64	
67273	7	C	33.77	41.77	1.56	22.75	0.15	99.96	
67275	32	C	34.56	37.66	1.08	26.69		101.93	
67275	36	R	33.92	39.99	1.34	24.57	0.19	102.43	
67275	39	C	34.25	38.28	1.17	26.30		102.54	
67275	40	R	34.41	39.89	1.28	24.41		102.05	RIM TO #39

Batur Volcano:- OLIVINE (CATIONS)

ROCK	NUM	L	Si	Fe	Mn	Mg	Ca	SUM	Mg#
67259	11	C	0.9762	0.6358	0.0120	1.3960	0.0037	3.0237	68.7
67259	22	C	0.9829	0.6303	0.0112	1.3888	0.0040	3.0172	68.8
67259	27	C	0.9742	0.6428	0.0126	1.3916	0.0045	3.0257	68.4
67259	30	C	0.9784	0.6380	0.0108	1.3943		3.0215	68.6
67259	35	G	0.9746	0.8424	0.0142	1.1883	0.0058	3.0253	58.5
67259	39	C	0.9743	0.6566	0.0113	1.3794	0.0041	3.0257	67.8
67259	41	G	0.9859	0.9082	0.0162	1.0978	0.0059	3.0140	54.7
67259	45	C	0.9749	0.6403	0.0107	1.3941	0.0051	3.0251	68.5
67259	46	R	0.9787	0.7256	0.0124	1.3007	0.0040	3.0214	64.2
67259	56	C	0.9794	0.6352	0.0117	1.3895	0.0047	3.0205	68.6
67259	56	C	0.9792	0.5995	0.0095	1.4325		3.0207	70.5
67259	57	R	0.9882	1.1173	0.0226	0.8745	0.0093	3.0119	43.9
67259	58	C	0.9726	0.6434	0.0116	1.3944	0.0054	3.0274	68.4
67259	59	R	0.9860	1.0079	0.0200	0.9936	0.0067	3.0142	49.6
67259	65	C	0.9738	0.6520	0.0124	1.3815	0.0065	3.0262	67.9
67259	65	C	0.9774	0.6425	0.0113	1.3913		3.0225	68.4
67259	66	R	0.9827	0.9851	0.0226	1.0215	0.0055	3.0174	50.9
67259	67	C	0.9760	0.6421	0.0115	1.3908	0.0036	3.0240	68.4
67272	28	C	0.9806	0.6364	0.0126	1.3840	0.0058	3.0194	68.5
67272	29	R	0.9839	0.7187	0.0142	1.2992		3.0160	64.4
67272	47	C	0.9846	0.6264	0.0130	1.3872	0.0041	3.0153	68.9
67272	57	G	0.9926	0.7642	0.0173	1.2235	0.0099	3.0075	61.6
67273	2	C	0.9798	1.0120	0.0407	0.9877		3.0202	49.4
67273	3	C	0.9836	1.0042	0.0398	0.9835	0.0052	3.0163	49.5
67273	4	R	0.9821	0.9792	0.0365	1.0201		3.0179	51.0
67273	6	C	0.9830	1.0150	0.0386	0.9754	0.0049	3.0169	49.0
67273	7	C	0.9799	1.0134	0.0384	0.9838	0.0047	3.0202	49.3
67275	32	C	0.9782	0.8915	0.0259	1.1262		3.0218	55.8
67275	36	R	0.9744	0.9608	0.0325	1.0522	0.0057	3.0256	52.3
67275	39	C	0.9737	0.9100	0.0282	1.1145		3.0264	55.1
67275	40	R	0.9857	0.9555	0.0311	1.0420		3.0143	52.2

Batur Volcano:- OLIVINE (OXIDES)

ROCK	NUM	L	SiO2	FeO	MnO	MgO	CaO	(SUM)	NOTE
67275	41	C	34.24	38.29	1.19	26.15	0.13	101.90	
67277	18	C	32.12	49.93	2.32	15.40	0.23	100.28	
67277	20	C	32.32	49.82	2.16	15.49	0.21	99.10	RPT #18
67277	21	R	32.53	49.82	2.23	15.28	0.14	98.57	RIM TO #18
67277	27	C	32.43	49.86	2.30	15.24	0.16	98.66	
67277	28	R	32.48	49.86	2.19	15.27	0.20	100.86	RIM TO #27
67277	57	C	32.28	51.40	2.38	13.78	0.16	101.71	
67277	58	C	32.16	51.36	2.26	14.23		101.50	RPT #57
67278	17	C	33.65	42.34	1.42	22.59		104.34	
67278	18	R	33.41	43.16	1.39	21.88	0.15	104.24	RIM TO #17
67278	105	C	33.73	42.44	1.48	22.36		103.60	
67278	106	C	33.28	43.74	1.41	21.41	0.16	103.20	
67326	49	C	35.42	32.15	0.57	31.85		103.35	
67326	62	C	35.85	30.73	0.58	32.65	0.20	103.78	
67328	70	C	36.35	32.25	0.68	30.47	0.25	87.74	
67328	73	C	36.53	28.29	0.30	34.87		101.93	RPT #70
67328	75	C	36.92	26.08	0.41	36.45	0.14	102.51	
67328	85	C	36.65	26.00	0.52	36.67	0.15	102.06	
67328	86	C	36.07	29.82	0.53	33.44	0.13	101.43	
67328	93	C	36.83	27.27	0.43	35.47		100.15	
67331	8	C	34.25	39.19	1.34	25.22		102.38	
67331	11	R	33.46	42.97	1.73	21.69	0.15	101.10	RIM TO #9
67331	15	C	34.32	39.22	1.29	25.17		102.36	
67331	21	C	34.63	38.11	1.30	25.83	0.13	101.95	PART OF GLOMEROCRYST
67331	22	C	34.27	38.71	1.37	25.66		102.23	
67331	34	C	34.32	37.89	1.31	26.47		102.06	PART OF GLOMEROCRYST
67331	36	C	34.17	39.03	1.35	25.45		103.12	
67331	38	C	34.26	38.56	1.17	26.01		102.83	
67331	66	C	34.48	38.81	1.26	25.45		104.12	PART OF GLOMEROCRYST
67331	68	C	34.44	38.21	1.14	26.08	0.13	104.82	PART OF GLOMEROCRYST
67331	75	C	34.29	38.54	1.19	25.98		103.33	

Batur Volcano:- OLIVINE (CATIONS)

ROCK	NUM	L	Si	Fe	Mn	Mg	Ca	SUM	Mg#
67275	41	C	0.9739	0.9109	0.0286	1.1088	0.0039	3.0261	54.9
67277	18	C	0.9796	1.2735	0.0600	0.6999	0.0075	3.0205	35.5
67277	20	C	0.9835	1.2678	0.0557	0.7026	0.0069	3.0165	35.7
67277	21	R	0.9891	1.2671	0.0575	0.6925	0.0046	3.0108	35.3
67277	27	C	0.9873	1.2692	0.0593	0.6916	0.0053	3.0127	35.3
67277	28	R	0.9881	1.2685	0.0565	0.6923	0.0065	3.0119	35.3
67277	57	C	0.9911	1.3199	0.0619	0.6309	0.0052	3.0090	32.3
67277	58	C	0.9866	1.3177	0.0586	0.6505		3.0134	33.1
67278	17	C	0.9783	1.0295	0.0349	0.9789		3.0216	48.7
67278	18	R	0.9764	1.0548	0.0344	0.9531	0.0048	3.0235	47.5
67278	105	C	0.9810	1.0324	0.0364	0.9692		3.0190	48.4
67278	106	C	0.9759	1.0725	0.0349	0.9359	0.0049	3.0241	46.6
67326	49	C	0.9725	0.7382	0.0133	1.3035		3.0275	63.8
67326	62	C	0.9770	0.7004	0.0133	1.3263	0.0059	3.0229	65.4
67328	70	C	0.9963	0.7394	0.0159	1.2447	0.0074	3.0037	62.7
67328	73	C	0.9811	0.6354	0.0069	1.3955		3.0189	68.7
67328	75	C	0.9815	0.5796	0.0092	1.4443	0.0039	3.0185	71.4
67328	85	C	0.9754	0.5787	0.0117	1.4546	0.0042	3.0246	71.5
67328	86	C	0.9781	0.6763	0.0122	1.3515	0.0037	3.0218	66.6
67328	93	C	0.9842	0.6093	0.0097	1.4125		3.0157	69.9
67331	8	C	0.9787	0.9363	0.0324	1.0740		3.0214	53.4
67331	11	R	0.9783	1.0506	0.0429	0.9453	0.0046	3.0217	47.4
67331	15	C	0.9803	0.9369	0.0312	1.0714		3.0198	53.3
67331	21	C	0.9834	0.9049	0.0314	1.0930	0.0039	3.0166	54.7
67331	22	C	0.9769	0.9229	0.0331	1.0903		3.0232	54.2
67331	34	C	0.9744	0.8995	0.0316	1.1202		3.0257	55.5
67331	36	C	0.9760	0.9322	0.0326	1.0832		3.0240	53.7
67331	38	C	0.9752	0.9179	0.0281	1.1037		3.0249	54.6
67331	66	C	0.9822	0.9246	0.0304	1.0807		3.0179	53.9
67331	68	C	0.9783	0.9077	0.0273	1.1043	0.0041	3.0217	54.9
67331	75	C	0.9759	0.9172	0.0287	1.1023		3.0241	54.6

Batur Volcano:- OLIVINE (OXIDES)

ROCK	NUM	L	SiO2	FeO	MnO	MgO	CaO	(SUM)	NOTE
67331	76	R	34.32	38.42	1.32	25.78	0.16	102.26	RIM TO #75
67339	30	X	37.63	21.42	0.25	40.71		105.06	
67339	32	X	37.72	21.92		40.36		102.02	
67339	36	X	37.51	21.74	0.28	40.47		102.97	
67339	39	X	37.85	21.00	0.24	40.91		103.67	
67339	40	X	38.13	20.51	0.22	41.13		104.56	RIM TO #39
67342	5	G	33.34	45.19	1.18	20.01	0.28	103.25	MICROPHEN
67342	7	G	32.79	48.34	1.23	17.40	0.23	102.31	MICROPHEN
67342	14	C	33.10	45.85	1.14	19.64	0.26	103.11	SKELETAL HABIT
67342	16	G	32.20	53.00	1.38	12.40	1.02	100.49	MICROPHEN
67342	17	C	34.71	37.35	0.72	27.02	0.20	103.08	LARGE EUHEDRAL SKELETAL CRYSTAL
67342	18	R	33.31	45.15	1.17	20.06	0.30	102.28	LARGE EUHEDRAL SKELETAL CRYSTAL
67342	23	C	33.21	45.29	1.24	19.96	0.30	102.65	SKELETAL
67342	27	G	32.72	48.04	1.20	17.82	0.22	101.46	MICROPHEN

Batur Volcano:- OLIVINE (CATIONS)

ROCK	NUM	L	Si	Fe	Mn	Mg	Ca	SUM	Mg#
67331	76	R	0.9773	0.9149	0.0318	1.0939	0.0048	3.0227	54.5
67339	30	X	0.9770	0.4650	0.0054	1.5756		3.0230	77.2
67339	32	X	0.9801	0.4763		1.5634		3.0198	76.6
67339	36	X	0.9757	0.4731	0.0062	1.5692		3.0242	76.8
67339	39	X	0.9803	0.4548	0.0053	1.5792		3.0196	77.6
67339	40	X	0.9846	0.4430	0.0048	1.5831		3.0155	78.1
67342	5	G	0.9834	1.1149	0.0295	0.8798	0.0089	3.0165	44.1
67342	7	G	0.9845	1.2137	0.0313	0.7785	0.0075	3.0155	39.1
67342	14	C	0.9802	1.1356	0.0287	0.8669	0.0083	3.0197	43.3
67342	16	G	0.9949	1.3694	0.0362	0.5710	0.0336	3.0051	29.4
67342	17	C	0.9795	0.8814	0.0172	1.1364	0.0062	3.0207	56.3
67342	18	R	0.9826	1.1138	0.0293	0.8821	0.0096	3.0174	44.2
67342	23	C	0.9810	1.1188	0.0310	0.8788	0.0096	3.0192	44.0
67342	27	G	0.9810	1.2044	0.0305	0.7962	0.0070	3.0191	39.8

Batur Volcano:- CLINOPYROXENE (OXIDES)

ROCK	NUM	L	SiO2	TiO2	Al2O3	Fe2O3	FeO	MnO	MgO	CaO	Na2O	(SUM)	NOTE
67238	52	G	51.03	0.40	2.31	3.65	6.83		15.58	19.93	0.27	99.15	
67238	74	C	51.37	0.51	2.31	1.54	9.09		15.41	19.77		99.25	
67238	75	R	51.04	0.67	2.79	1.28	9.16		15.06	20.00		98.47	RIM TO #74
67238	76	C	51.21	0.48	2.50	1.75	8.46		15.16	20.44		99.01	
67238	83	C	51.40	0.53	2.40	1.54	8.32		15.45	20.36		99.29	
67238	85	C	50.82	0.56	2.81	2.08	8.25		15.09	20.39		96.74	
67238	91	C	51.53	0.37	1.63	2.28	9.29	0.35	16.06	18.49		101.15	
67238	95	C	51.62	0.41	2.37	1.46	8.11		15.61	20.42		100.60	
67238	98	R	51.17	0.59	2.51	1.34	9.86		15.18	19.36		99.62	RIM TO #95
67244	28	G	45.10	2.29	3.57	9.70	11.76	0.32	12.86	13.64	0.76	98.91	
67244	32	G	46.69	1.50	4.53	8.06	9.83	0.27	13.15	15.04	0.94	100.18	
67244	33	G	50.06	0.89	2.69	3.37	10.50	0.34	14.86	16.94	0.35	100.12	
67244	44	G	51.11	0.51	1.16	2.32	17.14	0.59	17.99	9.18		99.91	
67244	45	G	49.88	0.97	2.76	1.66	13.99	0.49	14.46	15.81		98.16	
67259	32	C	51.00	0.53	2.59	2.83	7.29	0.27	15.01	20.20	0.28	100.94	
67259	33	C	51.38	0.42	2.23	2.99	7.00		15.51	20.20	0.28	100.60	
67259	34	C	51.69	0.40	2.23	1.29	8.47		15.36	20.55		101.14	RPT #33
67259	37	C	51.56	0.43	2.55	1.13	8.58		15.27	20.48		100.53	
67259	50	C	51.74	0.46	2.09	1.19	8.77		15.42	20.32		99.91	
67259	51	C	51.09	0.52	2.61	1.83	8.01	0.23	15.09	20.62		99.82	
67259	52	C	51.50	0.46	2.44	1.17	8.79		15.06	20.58		99.27	
67259	61	C	51.41	0.38	2.46	1.71	8.21		15.39	20.43		98.70	
67259	62	C	51.59	0.45	2.38	1.00	9.14		15.07	20.38		98.54	PART OF GLOME
67259	64	C	50.82	0.50	2.64	1.91	9.20	0.25	14.66	20.01		99.06	PART OF GLOME
67272	34	C	51.77	0.45	1.64	1.57	10.87	0.53	16.78	16.39		102.58	
67272	35	R	51.38	0.50	2.65	1.18	8.69	0.24	15.27	20.09		101.90	RIM TO #34
67272	45	C	51.59	0.51	2.18	0.75	10.14	0.31	14.90	19.61		101.94	
67272	46	R	50.02	0.85	3.50	1.72	9.92	0.38	14.37	19.24		101.43	RIM TO #45
67272	52	C	51.12	0.60	2.79	1.37	8.19	0.29	15.00	20.65		101.55	
67272	53	R	50.75	0.64	3.27	1.34	8.60		14.62	20.77		100.96	RIM TO #52
67272	54	C	50.80	0.70	3.17	1.20	9.20		14.81	20.12		100.94	

Batur Volcano:- CLINOPYROXENE (CATIONS)

ROCK	NUM	L	Si	Ti	Al	Fe3+	Fe2+	Mn	Mg	Ca	Na	SUM	Mg#
67238	52	G	1.8968	0.0112	0.1013	0.1022	0.2123		0.8630	0.7936	0.0196	4.0000	80.3
67238	74	C	1.9133	0.0144	0.1016	0.0431	0.2831		0.8556	0.7889		4.0000	75.1
67238	75	R	1.9020	0.0188	0.1225	0.0360	0.2855		0.8366	0.7986		4.0000	74.6
67238	76	C	1.9071	0.0136	0.1098	0.0490	0.2634		0.8417	0.8155		4.0001	76.2
67238	83	C	1.9109	0.0149	0.1053	0.0431	0.2586		0.8560	0.8112		4.0000	76.8
67238	85	C	1.8936	0.0156	0.1232	0.0583	0.2570		0.8381	0.8141		3.9999	76.5
67238	91	C	1.9217	0.0105	0.0715	0.0641	0.2897	0.0109	0.8926	0.7390		4.0000	75.5
67238	95	C	1.9164	0.0114	0.1038	0.0406	0.2518		0.8639	0.8121		4.0000	77.4
67238	98	R	1.9095	0.0166	0.1102	0.0376	0.3078		0.8442	0.7740		3.9999	73.3
67244	28	G	1.7400	0.0665	0.1625	0.2815	0.3794	0.0105	0.7392	0.5636	0.0569	4.0001	66.1
67244	32	G	1.7751	0.0427	0.2032	0.2305	0.3126	0.0086	0.7452	0.6127	0.0693	3.9999	70.4
67244	33	G	1.8805	0.0250	0.1190	0.0953	0.3300	0.0108	0.8321	0.6819	0.0254	4.0000	71.6
67244	44	G	1.9269	0.0144	0.0515	0.0658	0.5406	0.0188	1.0112	0.3707		3.9999	65.2
67244	45	G	1.8875	0.0275	0.1229	0.0472	0.4427	0.0156	0.8158	0.6408		4.0000	64.8
67259	32	C	1.8986	0.0149	0.1136	0.0794	0.2269	0.0084	0.8326	0.8057	0.0200	4.0001	78.6
67259	33	C	1.9078	0.0116	0.0976	0.0836	0.2174		0.8584	0.8036	0.0200	4.0000	79.8
67259	34	C	1.9217	0.0113	0.0978	0.0361	0.2632		0.8514	0.8185		4.0000	76.4
67259	37	C	1.9163	0.0119	0.1119	0.0316	0.2667		0.8460	0.8155		3.9999	76.0
67259	50	C	1.9247	0.0129	0.0916	0.0334	0.2729		0.8546	0.8099		4.0000	75.8
67259	51	C	1.9025	0.0146	0.1146	0.0513	0.2496	0.0073	0.8376	0.8227		4.0002	77.0
67259	52	C	1.9170	0.0130	0.1073	0.0328	0.2735		0.8358	0.8207		4.0001	75.3
67259	61	C	1.9114	0.0107	0.1077	0.0479	0.2552		0.8531	0.8139		3.9999	77.0
67259	62	C	1.9212	0.0125	0.1046	0.0281	0.2845		0.8362	0.8130		4.0001	74.6
67259	64	C	1.9008	0.0142	0.1164	0.0538	0.2879	0.0080	0.8172	0.8019		4.0002	73.9
67272	34	C	1.9293	0.0125	0.0722	0.0441	0.3388	0.0166	0.9321	0.6544		4.0000	73.3
67272	35	R	1.9115	0.0140	0.1160	0.0331	0.2703	0.0074	0.8468	0.8009		4.0000	75.8
67272	45	C	1.9272	0.0143	0.0958	0.0212	0.3169	0.0099	0.8296	0.7851		4.0000	72.4
67272	46	R	1.8745	0.0239	0.1548	0.0485	0.3109	0.0122	0.8027	0.7726		4.0001	72.1
67272	52	C	1.9027	0.0168	0.1225	0.0384	0.2549	0.0090	0.8321	0.8236		4.0000	76.6
67272	53	R	1.8913	0.0180	0.1438	0.0375	0.2679		0.8120	0.8294		3.9999	75.2
67272	54	C	1.8939	0.0197	0.1391	0.0336	0.2870		0.8231	0.8035		3.9999	74.1

Batur Volcano:- CLINOPYROXENE (OXIDES)

ROCK	NUM	L	SiO2	TiO2	Al2O3	Fe2O3	FeO	MnO	MgO	CaO	Na2O	(SUM)	NOTE
67273	7	C	51.21	0.46	1.67	2.66	9.62	0.78	13.75	19.46	0.39	100.49	
67273	12	C	51.39	0.49	1.54	0.52	12.99	0.82	13.48	18.77		100.00	
67273	13	C	50.76	0.56	3.24	1.79	7.32		14.68	21.64		99.28	
67273	13	R	52.39	0.45	1.59		11.56	0.53	14.12	19.36		98.64	RIM TO #12
67273	14	C	51.15	0.38	1.42	3.49	8.79	0.67	13.87	19.82	0.41	100.93	
67273	15	C	51.85	0.28	1.27	0.71	12.27	0.76	14.23	18.62		99.73	
67273	19	C	51.88	0.22	1.32	1.03	11.10	0.52	14.22	19.71		99.27	
67273	20	R	51.68	0.33	1.66	0.83	10.98	0.70	14.09	19.74		97.56	RIM TO #15
67273	22	C	51.04	0.39	1.41	2.74	10.71	0.76	13.49	19.20	0.27	98.60	
67273	25	C	51.10	0.49	1.57	2.49	10.32	0.75	13.80	19.22	0.27	99.62	
67273	26	R	52.00	0.30	1.08	0.34	12.50	0.82	13.79	19.16		98.42	RIM TO #25
67273	29	C	50.95	0.42	3.56	1.36	7.49		14.80	21.42		99.00	
67273	30	R	49.55	0.75	4.41	2.06	8.38		13.77	21.08		99.59	RIM TO #29
67273	42	C	51.37	0.34	1.31	0.71	13.24	0.86	12.80	19.37		100.02	
67275	1	C	51.84	0.32	1.30	1.03	10.93	0.61	14.36	19.62		99.96	
67275	2	R	51.38	0.39	1.41	2.30	10.80	0.63	14.12	18.70	0.27	101.42	RIM TO #1
67275	3	C	51.48	0.36	1.53	1.97	9.65	0.58	15.01	19.43		101.08	
67275	35	C	51.37	0.38	1.55	1.85	9.91	0.55	14.49	19.89		98.64	
67277	23	C	51.04	0.32	1.02	0.69	15.26	1.01	11.48	19.19		95.43	
67277	24	R	51.08	0.27	1.06	0.58	15.35	0.96	11.32	19.38		96.22	RIM TO #23
67277	25	C	51.19	0.28	0.89	0.54	15.79	0.97	11.58	18.77		95.95	RPT #23
67277	33	C	51.39	0.22	0.83		16.73	1.03	11.31	18.48		99.92	
67277	39	C	50.84	0.19	1.12	1.21	14.94	0.99	11.35	19.36		99.99	
67277	40	R	50.29	0.31	1.34	3.11	14.03	1.02	11.34	18.15	0.41	100.63	RIM TO #33
67277	41	C	51.06	0.22	0.84	0.82	15.36	1.15	11.15	19.39		99.55	
67277	42	C	51.40	0.33	0.88		15.91	0.98	11.20	19.30		99.99	
67277	68	C	51.51	0.26	0.99		15.49	0.96	11.68	19.11		99.92	
67277	69	R	52.82	0.21	2.70		14.98	0.92	10.04	17.46	0.86	98.90	RIM TO #68
67277	79	G	51.45		0.66	1.83	14.28	1.05	11.54	18.88	0.31	100.08	
67278	92	C	51.30	0.51	1.88		13.73	0.66	12.92	19.01		101.71	
67278	100	C	50.55	0.46	1.68	0.99	15.08	0.84	11.93	18.47		102.20	

Batur Volcano:- CLINOPYROXENE (CATIONS)

ROCK	NUM	L	Si	Ti	Al	Fe3+	Fe2+	Mn	Mg	Ca	Na	SUM	Mg#
67273	7	C	1.9266	0.0129	0.0739	0.0753	0.3028	0.0250	0.7708	0.7845	0.0282	4.0000	71.8
67273	12	C	1.9444	0.0139	0.0686	0.0148	0.4109	0.0263	0.7603	0.7609		4.0001	64.9
67273	13	C	1.8882	0.0157	0.1419	0.0502	0.2278		0.8138	0.8623		3.9999	78.1
67273	13	R	1.9625	0.0126	0.0703		0.3620	0.0167	0.7885	0.7771		3.9897	68.5
67273	14	C	1.9237	0.0106	0.0630	0.0986	0.2765	0.0214	0.7776	0.7984	0.0302	4.0000	73.8
67273	15	C	1.9537	0.0079	0.0565	0.0202	0.3868	0.0243	0.7990	0.7515		3.9999	67.4
67273	19	C	1.9500	0.0063	0.0584	0.0291	0.3489	0.0167	0.7967	0.7940		4.0001	69.5
67273	20	R	1.9423	0.0093	0.0735	0.0234	0.3452	0.0222	0.7895	0.7947		4.0001	69.6
67273	22	C	1.9286	0.0112	0.0626	0.0778	0.3383	0.0243	0.7599	0.7772	0.0200	3.9999	69.2
67273	25	C	1.9258	0.0139	0.0698	0.0706	0.3252	0.0240	0.7751	0.7759	0.0198	4.0001	70.4
67273	26	R	1.9625	0.0086	0.0479	0.0098	0.3945	0.0263	0.7759	0.7746		4.0001	66.3
67273	29	C	1.8913	0.0118	0.1558	0.0379	0.2327		0.8188	0.8517		4.0000	77.9
67273	30	R	1.8527	0.0211	0.1943	0.0580	0.2620		0.7673	0.8446		4.0000	74.5
67273	42	C	1.9508	0.0097	0.0586	0.0204	0.4203	0.0276	0.7244	0.7882		4.0000	63.3
67275	1	C	1.9476	0.0090	0.0575	0.0291	0.3433	0.0194	0.8042	0.7897		3.9998	70.1
67275	2	R	1.9347	0.0111	0.0624	0.0653	0.3402	0.0201	0.7923	0.7545	0.0194	4.0000	70.0
67275	3	C	1.9285	0.0100	0.0676	0.0554	0.3022	0.0185	0.8380	0.7799		4.0001	73.5
67275	35	C	1.9287	0.0109	0.0685	0.0523	0.3111	0.0174	0.8109	0.8002		4.0000	72.3
67277	23	C	1.9578	0.0094	0.0459	0.0198	0.4894	0.0327	0.6562	0.7889		4.0001	57.3
67277	24	R	1.9599	0.0078	0.0479	0.0168	0.4924	0.0311	0.6474	0.7967		4.0000	56.8
67277	25	C	1.9641	0.0081	0.0400	0.0156	0.5066	0.0315	0.6625	0.7717		4.0001	56.7
67277	33	C	1.9752	0.0064	0.0376		0.5379	0.0336	0.6479	0.7612		3.9998	54.6
67277	39	C	1.9517	0.0055	0.0506	0.0351	0.4796	0.0322	0.6492	0.7962		4.0001	57.5
67277	40	R	1.9311	0.0089	0.0605	0.0899	0.4506	0.0332	0.6491	0.7466	0.0302	4.0001	59.0
67277	41	C	1.9627	0.0064	0.0382	0.0236	0.4939	0.0376	0.6389	0.7987		4.0000	56.4
67277	42	C	1.9722	0.0095	0.0398		0.5106	0.0319	0.6407	0.7936		3.9983	55.7
67277	68	C	1.9709	0.0075	0.0447		0.4957	0.0311	0.6661	0.7832		3.9992	57.3
67277	69	R	1.9989	0.0060	0.1204		0.4742	0.0295	0.5663	0.7080	0.0631	3.9664	54.4
67277	79	G	1.9702		0.0297	0.0529	0.4572	0.0340	0.6586	0.7746	0.0230	4.0002	59.0
67278	92	C	1.9439	0.0146	0.0839		0.4349	0.0211	0.7296	0.7716		3.9996	62.7
67278	100	C	1.9346	0.0132	0.0758	0.0286	0.4826	0.0273	0.6803	0.7576		4.0000	58.5

Batur Volcano:- CLINOPYROXENE (OXIDES)

ROCK	NUM	L	SiO2	TiO2	Al2O3	Fe2O3	FeO	MnO	MgO	CaO	Na2O	(SUM)	NOTE
67278	101	R	51.96	0.23	1.33	0.11	13.13	0.50	13.44	19.31		101.84	RIM TO #100
67326	54	C	51.11	0.53	2.47	1.69	9.37		15.16	19.67		100.37	
67326	63	C	51.32	0.56	2.04	1.21	11.48	0.27	15.32	17.81		99.96	
67326	64	C	51.12	0.45	2.48	2.02	8.80	0.28	15.59	19.26		101.49	
67328	94	G	51.00	0.47	2.18	1.23	12.63	0.31	14.46	17.72		97.46	
67328	95	I	51.65	0.33	1.20	1.70	13.83	0.45	16.50	14.34		98.53	INCL IN PLG
67331	3	C	50.70	0.59	2.47	1.55	10.44	0.58	13.93	19.75		101.66	
67331	3	R	51.70	0.27	1.46	1.23	10.70	0.61	14.25	19.79		103.67	RIM TO #4
67331	4	C	51.50	0.41	1.65	1.23	11.08	0.61	14.54	18.99		98.16	
67331	4	R	51.72	0.33	1.33	1.15	11.37	0.54	14.43	19.13		102.03	RIM TO #3
67331	18	C	51.42	0.40	1.38	2.08	10.85	0.74	13.81	19.07	0.26	100.30	
67331	41	C	51.25	0.50	1.89	2.65	8.64	0.52	14.61	19.65	0.29	99.82	
67331	42	R	50.84	0.51	1.64	2.71	12.49	0.85	14.26	16.38	0.32	98.47	RIM TO #41
67331	67	C	52.05	0.35	1.54	0.37	11.01	0.53	14.48	19.66		101.68	
67331	69	C	51.68	0.36	1.26	0.83	12.07	0.73	13.86	19.21		101.53	
67342	4	G	48.82	1.09	3.20	2.84	14.02	0.51	13.99	15.52		100.83	MICROPHEN
67342	6	C	49.77	0.99	2.79	1.73	13.81	0.42	14.17	16.32		99.73	
67342	15	G	49.84	0.71	1.52	1.39	24.02	1.02	15.23	6.27		100.38	MICROPHEN
67342	24	C	47.59	1.18	3.16	5.65	10.24	0.45	13.24	18.48		99.06	ANHEDRAL
67342	29	C	48.59	1.30	3.47	2.36	14.17	0.66	13.33	16.13		100.88	

Batur Volcano:- CLINOPYROXENE (CATIONS)

ROCK	NUM	L	Si	Ti	Al	Fe3+	Fe2+	Mn	Mg	Ca	Na	SUM	Mg#
67278	101	R	1.9625	0.0064	0.0590	0.0031	0.4146	0.0160	0.7567	0.7816		3.9999	64.6
67326	54	C	1.9073	0.0148	0.1085	0.0474	0.2925		0.8431	0.7865		4.0001	74.2
67326	63	C	1.9222	0.0158	0.0900	0.0341	0.3597	0.0086	0.8552	0.7146		4.0002	70.4
67326	64	C	1.9046	0.0127	0.1088	0.0567	0.2742	0.0087	0.8655	0.7689		4.0001	75.9
67328	94	G	1.9208	0.0134	0.0969	0.0348	0.3977	0.0098	0.8117	0.7150		4.0001	67.1
67328	95	I	1.9400	0.0094	0.0529	0.0481	0.4344	0.0142	0.9240	0.5769		3.9999	68.0
67331	3	C	1.9068	0.0167	0.1093	0.0439	0.3284	0.0185	0.7807	0.7959		4.0002	70.4
67331	3	R	1.9426	0.0076	0.0649	0.0347	0.3361	0.0193	0.7981	0.7967		4.0000	70.4
67331	4	C	1.9346	0.0115	0.0730	0.0347	0.3483	0.0194	0.8142	0.7643		4.0000	70.0
67331	4	R	1.9449	0.0094	0.0590	0.0325	0.3576	0.0171	0.8088	0.7707		4.0000	69.3
67331	18	C	1.9380	0.0113	0.0614	0.0589	0.3419	0.0235	0.7758	0.7702	0.0189	3.9999	69.4
67331	41	C	1.9175	0.0141	0.0833	0.0747	0.2705	0.0165	0.8147	0.7879	0.0210	4.0002	75.1
67331	42	R	1.9223	0.0144	0.0731	0.0772	0.3949	0.0272	0.8037	0.6634	0.0238	4.0000	67.1
67331	67	C	1.9507	0.0100	0.0682	0.0104	0.3453	0.0169	0.8090	0.7896		4.0001	70.1
67331	69	C	1.9498	0.0103	0.0560	0.0236	0.3810	0.0233	0.7793	0.7766		3.9999	67.2
67342	4	G	1.8565	0.0311	0.1436	0.0813	0.4458	0.0166	0.7931	0.6321		4.0001	64.0
67342	6	C	1.8848	0.0282	0.1247	0.0492	0.4374	0.0135	0.8001	0.6621		4.0000	64.7
67342	15	G	1.9247	0.0205	0.0693	0.0403	0.7757	0.0335	0.8767	0.2593		4.0000	53.1
67342	24	C	1.8139	0.0340	0.1421	0.1622	0.3264	0.0146	0.7522	0.7547		4.0001	69.7
67342	29	C	1.8512	0.0371	0.1559	0.0676	0.4514	0.0214	0.7570	0.6584		4.0000	62.6

Batur Volcano:- ORTHOPYROXENE (OXIDES)

ROCK	NUM	L	SiO2	TiO2	Al2O3	Fe2O3	FeO	MnO	MgO	CaO	Na2O	(SUM)	NOTE
67273	4	C	51.37	0.20	0.76	2.57	21.65	1.33	20.54	1.57		102.18	
67273	5	C	52.28		0.66	2.09	20.34	1.22	21.88	1.52		99.63	
67273	8	C	51.87	0.27	0.73	1.72	21.60	1.27	20.97	1.56		102.20	
67273	10	C	51.66	0.32	0.77	1.65	22.16	1.36	20.40	1.70		100.05	
67273	10	C	51.24	0.24	0.74	2.68	21.70	1.34	20.29	1.76		101.88	
67273	15	C	51.76	0.30	0.78	1.98	21.24	1.23	21.11	1.60		101.13	
67273	17	C	52.03		0.35	1.97	22.20	1.33	20.58	1.55		99.85	
67273	19	C	51.56	0.31	1.36	2.40	19.43	1.16	21.67	2.11		99.55	
67273	20	C	51.63		0.62	2.10	22.69	1.42	19.97	1.59		100.06	
67273	26	C	51.77	0.25	0.63	2.36	20.82	1.27	21.34	1.56		103.00	
67273	29	C	51.89	0.21	0.53	1.78	21.93	1.33	20.63	1.70		99.85	
67273	29	C	51.78	0.23	0.69	1.73	22.06	1.34	20.54	1.63		101.99	
67273	31	C	51.57	0.20	0.84	1.96	22.07	1.36	20.36	1.65		100.15	
67273	34	C	50.75	0.18	0.73	2.77	23.44	1.59	18.88	1.67		102.40	
67273	37	C	51.30	0.18	1.01	2.37	22.14	1.09	20.29	1.63		101.23	
67273	40	G	51.51	0.19	0.64	2.09	22.40	1.43	20.08	1.66		100.80	
67273	41	C	52.23		0.64	2.31	20.12	1.15	21.94	1.61		101.26	
67275	7	C	52.05		0.67	1.87	21.81	1.08	20.91	1.62		102.54	
67275	10	C	51.39	0.22	0.61	3.06	20.73	1.24	20.99	1.76		94.77	
67275	11	C	51.76	0.17	0.67	2.14	21.61	1.10	20.83	1.71		98.76	RPT #10
67275	21	C	51.52	0.20	0.70	2.85	20.87	1.00	21.22	1.63		99.26	
67275	26	C	52.21		0.60	2.43	20.15	0.96	21.96	1.69		101.40	
67275	53	C	51.30	0.27	0.78	3.03	20.77	1.05	21.09	1.70		101.73	
67275	54	R	51.71	0.28	1.04	2.32	20.17	1.08	21.63	1.77		101.44	RIM TO #53
67331	39	C	51.61	0.27	0.72	3.20	19.23	1.18	22.07	1.72		102.44	
67331	40	I	51.96	0.22	0.71	2.63	19.54	1.08	22.20	1.66		100.98	INCL IN CPX
67331	45	C	52.31		0.77	2.36	19.77	0.83	22.43	1.53		100.89	

Batur Volcano:- ORTHOPYROXENE (CATIONS)

ROCK	NUM	L	Si	Ti	Al	Fe3+	Fe2+	Mn	Mg	Ca	Na	SUM	Mg#
67273	4	C	1.9407	0.0058	0.0339	0.0730	0.6840	0.0425	1.1564	0.0636		3.9999	62.8
67273	5	C	1.9560		0.0291	0.0589	0.6364	0.0387	1.2198	0.0610		3.9999	65.7
67273	8	C	1.9516	0.0077	0.0325	0.0488	0.6797	0.0405	1.1762	0.0630		4.0000	63.4
67273	10	C	1.9505	0.0091	0.0342	0.0467	0.6997	0.0434	1.1478	0.0686		4.0000	62.1
67273	10	C	1.9384	0.0070	0.0332	0.0762	0.6866	0.0430	1.1443	0.0714		4.0001	62.5
67273	15	C	1.9463	0.0084	0.0346	0.0561	0.6679	0.0393	1.1831	0.0644		4.0001	63.9
67273	17	C	1.9643		0.0156	0.0559	0.7009	0.0425	1.1582	0.0627		4.0001	62.3
67273	19	C	1.9275	0.0087	0.0601	0.0674	0.6075	0.0368	1.2073	0.0847		4.0000	66.5
67273	20	C	1.9563		0.0276	0.0598	0.7189	0.0454	1.1276	0.0644		4.0000	61.1
67273	26	C	1.9455	0.0071	0.0279	0.0669	0.6543	0.0404	1.1952	0.0628		4.0001	64.6
67273	29	C	1.9570	0.0060	0.0236	0.0506	0.6918	0.0425	1.1600	0.0687		4.0002	62.6
67273	29	C	1.9536	0.0067	0.0305	0.0490	0.6959	0.0429	1.1554	0.0661		4.0001	62.4
67273	31	C	1.9479	0.0057	0.0373	0.0556	0.6971	0.0434	1.1462	0.0669		4.0001	62.2
67273	34	C	1.9387	0.0050	0.0329	0.0796	0.7490	0.0514	1.0753	0.0682		4.0001	58.9
67273	37	C	1.9388	0.0050	0.0448	0.0674	0.6998	0.0350	1.1432	0.0659		3.9999	62.0
67273	40	G	1.9505	0.0054	0.0287	0.0596	0.7095	0.0457	1.1332	0.0675		4.0001	61.5
67273	41	C	1.9534		0.0282	0.0650	0.6293	0.0365	1.2232	0.0644		4.0000	66.0
67275	7	C	1.9586		0.0298	0.0529	0.6863	0.0344	1.1728	0.0651		3.9999	63.1
67275	10	C	1.9368	0.0063	0.0271	0.0869	0.6535	0.0396	1.1789	0.0709		4.0000	64.3
67275	11	C	1.9500	0.0049	0.0296	0.0608	0.6809	0.0351	1.1698	0.0689		4.0000	63.2
67275	21	C	1.9384	0.0057	0.0312	0.0806	0.6568	0.0320	1.1897	0.0656		4.0000	64.4
67275	26	C	1.9526		0.0265	0.0683	0.6302	0.0305	1.2241	0.0678		4.0000	66.0
67275	53	C	1.9318	0.0078	0.0348	0.0860	0.6541	0.0334	1.1837	0.0684		4.0000	64.4
67275	54	R	1.9366	0.0078	0.0460	0.0652	0.6318	0.0343	1.2072	0.0710		3.9999	65.6
67331	39	C	1.9314	0.0077	0.0318	0.0902	0.6017	0.0373	1.2310	0.0691		4.0002	67.2
67331	40	I	1.9413	0.0061	0.0313	0.0739	0.6105	0.0341	1.2364	0.0664		4.0000	66.9
67331	45	C	1.9500		0.0339	0.0661	0.6164	0.0262	1.2461	0.0612		3.9999	66.9

Batur Volcano:- PIGEONITE (OXIDES)

ROCK	NUM	L	SiO2	TiO2	Al2O3	Fe2O3	FeO	MnO	MgO	CaO	Na2O	(SUM)	NOTE
67278	98	G	50.06	0.39	1.29	1.02	25.14	1.45	14.29	6.35		101.43	
67278	99	G	48.98	0.77	1.07	0.33	30.73	1.73	11.54	4.85		101.31	
67331	5	R	51.11	0.22	0.46	1.50	24.06	1.48	17.21	3.97		101.47	RIM TO CPX#3
67331	44	G	50.92	0.35	1.10	1.85	21.09	1.28	17.60	5.81		99.11	
67331	45	G	50.83	0.18	0.79	1.66	24.18	1.43	16.94	4.00		100.13	
67331	46	G	51.06		0.29	1.69	25.24	1.48	16.71	3.53		98.01	
67331	47	G	52.00		0.42	0.82	24.10	1.25	18.71	2.70		98.67	
67331	48	G	52.06		0.64	0.22	24.84	1.34	18.51	2.40		98.78	
67331	78	G	51.13	0.23	1.12		28.02	1.59	14.34	3.58		100.36	

Batur Volcano:- PIGEONITE (CATIONS)

ROCK	NUM	L	Si	Ti	Al	Fe3+	Fe2+	Mn	Mg	Ca	Na	SUM	Mg#
67278	98	G	1.9440	0.0115	0.0591	0.0299	0.8165	0.0476	0.8272	0.2643		4.0001	50.3
67278	99	G	1.9471	0.0230	0.0499	0.0099	1.0217	0.0581	0.6834	0.2068		3.9999	40.1
67331	5	R	1.9617	0.0062	0.0209	0.0433	0.7723	0.0480	0.9846	0.1631		4.0001	56.0
67331	44	G	1.9388	0.0101	0.0493	0.0529	0.6715	0.0412	0.9991	0.2371		4.0000	59.8
67331	45	G	1.9530	0.0052	0.0357	0.0479	0.7771	0.0464	0.9701	0.1646		4.0000	55.5
67331	46	G	1.9691		0.0130	0.0489	0.8140	0.0482	0.9607	0.1460		3.9999	54.1
67331	47	G	1.9789		0.0186	0.0236	0.7670	0.0401	1.0615	0.1102		3.9999	58.1
67331	48	G	1.9826		0.0286	0.0062	0.7909	0.0431	1.0507	0.0979		4.0000	57.1
67331	78	G	1.9848	0.0067	0.0511		0.9097	0.0524	0.8297	0.1488		3.9832	47.7

Batur Volcano:- Ti-MAGNETITE (OXIDES)

ROCK	NUM	L	SiO2	TiO2	Al2O3	Cr2O3	Fe2O3	FeO	MnO	MgO	(SUM)	NOTE
67238	33	I		12.07	4.00	0.35	42.28	37.75	0.51	3.05	93.66	INCL IN OLV
67238	67	C		13.00	3.69	0.42	40.83	38.45	0.42	3.19	95.36	
67238	68	C		13.15	3.30	0.23	41.11	38.87	0.33	3.01	95.26	
67238	70	C		12.48	3.68	0.30	41.85	38.46	0.28	2.95	94.30	
67238	87	I	0.23	11.88	4.03	0.39	42.10	37.80	0.38	3.19	93.13	INCL IN OLV
67238	92	I		10.57	4.30		45.56	35.52	0.27	3.78	95.46	INCL IN CPX
67238	93	C		13.06	3.23	0.30	40.91	39.94	0.27	2.30	95.64	
67238	94	I		9.46	4.59	0.31	47.07	34.44	0.31	3.83	95.36	INCL IN CPX
67238	100	I		10.68	5.85	0.34	43.27	35.67	0.26	3.94	95.70	INCL IN OLV
67244	37	C		10.84	3.95	1.78	43.52	35.89	0.46	3.56	94.04	
67244	38	C		10.98	4.07	1.73	43.12	36.36	0.26	3.48	93.91	
67244	64	C		10.67	4.16	1.71	43.57	36.21	0.31	3.38	93.47	
67259	18	C		13.88	3.16	0.23	39.63	40.24	0.29	2.57	95.16	
67259	20	C		14.18	3.18	0.27	38.92	40.55	0.44	2.46	94.40	
67259	21	C		11.60	4.37		43.21	37.30	0.29	3.24	93.56	
67259	43	I		10.64	4.08		45.16	37.00	0.33	2.80	93.70	INCL IN CPX
67259	44	C		12.98	3.41		41.32	39.19	0.46	2.63	95.54	
67259	63	I		9.86	4.29	0.28	46.69	34.67	0.40	3.82	93.51	INCL IN CPX#62
67259	66	C	0.23	13.01	3.55	0.37	40.15	39.65	0.49	2.54	97.00	
67272	27	C		11.64	4.42	0.25	42.30	39.08		2.31	95.41	
67272	58	C		13.71	3.87		38.65	42.20	0.30	1.27	95.20	
67272	59	C		11.15	4.30		43.51	38.69	0.28	2.07	94.75	
67273	1	I		18.66	2.35		31.34	44.76	0.80	2.10	93.55	INCL IN CPX
67273	2	C	0.53	18.39	2.87		30.03	45.01	1.00	2.17	97.19	
67273	2	I		18.57	2.48		31.37	44.59	0.86	2.13	95.56	INCL IN CPX
67273	3	G	0.23	18.56	2.67		30.60	44.97	0.87	2.09	96.93	
67273	8	I		19.25	2.39		30.09	45.43	0.85	1.99	93.68	INCL IN OLV
67273	9	C		18.69	2.63		31.03	44.38	1.04	2.24	94.32	
67273	10	C		18.42	2.47		31.82	43.94	0.95	2.40	95.20	
67273	11	C	0.21	18.75	2.51		30.58	44.77	0.90	2.28	97.20	
67273	11	R		18.08	2.46		32.41	43.82	0.98	2.25	95.72	

Batur Volcano:- Ti-MAGNETITE (CATIONS)

ROCK	NUM	L	Si	Ti	Al	Cr	Fe3+	Fe2+	Mn	Mg	SUM	ULV
67238	33	I		0.3302	0.1715	0.0100	1.1580	1.1492	0.0158	0.1653	3.0000	36.3
67238	67	C		0.3558	0.1583	0.0122	1.1179	1.1699	0.0130	0.1729	3.0000	38.8
67238	68	C		0.3609	0.1421	0.0067	1.1294	1.1869	0.0103	0.1638	3.0001	38.7
67238	70	C		0.3422	0.1581	0.0088	1.1486	1.1732	0.0088	0.1602	2.9999	37.4
67238	87	I	0.0082	0.3245	0.1726	0.0112	1.1508	1.1484	0.0117	0.1726	3.0000	36.0
67238	92	I		0.2877	0.1834		1.2412	1.0755	0.0083	0.2039	3.0000	30.8
67238	93	C		0.3605	0.1397	0.0087	1.1305	1.2264	0.0084	0.1257	2.9999	39.4
67238	94	I		0.2574	0.1955	0.0089	1.2809	1.0416	0.0095	0.2063	3.0001	27.9
67238	100	I		0.2879	0.2471	0.0096	1.1675	1.0695	0.0079	0.2105	3.0000	33.3
67244	37	C		0.2958	0.1688	0.0511	1.1885	1.0893	0.0141	0.1925	3.0001	33.1
67244	38	C		0.2997	0.1738	0.0497	1.1771	1.1031	0.0081	0.1884	2.9999	34.0
67244	64	C		0.2913	0.1782	0.0490	1.1901	1.0992	0.0094	0.1827	2.9999	33.2
67259	18	C		0.3822	0.1364	0.0067	1.0924	1.2327	0.0091	0.1405	3.0000	41.4
67259	20	C		0.3908	0.1372	0.0080	1.0732	1.2426	0.0136	0.1346	3.0000	42.5
67259	21	C		0.3165	0.1868		1.1802	1.1323	0.0088	0.1754	3.0000	34.8
67259	43	I		0.2920	0.1754		1.2406	1.1295	0.0101	0.1525	3.0001	32.0
67259	44	C		0.3574	0.1472		1.1381	1.1996	0.0143	0.1434	3.0000	38.5
67259	63	I		0.2684	0.1832	0.0079	1.2721	1.0499	0.0122	0.2063	3.0000	28.7
67259	66	C	0.0083	0.3577	0.1530	0.0106	1.1044	1.2121	0.0153	0.1385	2.9999	39.8
67272	27	C		0.3199	0.1902	0.0072	1.1628	1.1942		0.1257	3.0000	36.8
67272	58	C		0.3801	0.1680		1.0719	1.3007	0.0095	0.0699	3.0001	43.6
67272	59	C		0.3073	0.1857		1.1996	1.1856	0.0088	0.1130	3.0000	34.9
67273	1	I		0.5157	0.1018		0.8668	1.3757	0.0248	0.1151	2.9999	54.7
67273	2	C	0.0193	0.5056	0.1238		0.8262	1.3761	0.0309	0.1180	2.9999	55.9
67273	2	I		0.5128	0.1075		0.8669	1.3695	0.0268	0.1165	3.0000	54.6
67273	3	G	0.0084	0.5117	0.1154		0.8443	1.3789	0.0270	0.1142	2.9999	55.6
67273	8	I		0.5320	0.1036		0.8324	1.3967	0.0264	0.1089	3.0000	56.7
67273	9	C		0.5152	0.1136		0.8561	1.3606	0.0322	0.1224	3.0001	55.0
67273	10	C		0.5077	0.1068		0.8778	1.3472	0.0294	0.1311	3.0000	53.7
67273	11	C	0.0077	0.5166	0.1085		0.8430	1.3717	0.0279	0.1247	3.0001	55.5
67273	11	R		0.4992	0.1063		0.8952	1.3454	0.0305	0.1233	2.9999	52.8

Batur Volcano:- Ti-MAGNETITE (OXIDES)

ROCK	NUM	L	SiO2	TiO2	Al2O3	Cr2O3	Fe2O3	FeO	MnO	MgO	(SUM)	NOTE
67273	16	C	0.25	18.74	2.34		30.67	44.84	0.89	2.25	96.39	
67273	18	I		19.14	2.39		30.39	44.94	0.97	2.16	94.96	
67273	21	I		18.68	2.54		31.10	44.65	0.87	2.16	95.52	INCL IN OPX
67273	28	C		18.83	2.37		31.08	44.39	1.04	2.29	96.21	
67273	30	I	0.21	18.61	2.59		30.76	44.67	0.85	2.30	96.41	INCL IN OPX
67273	35	I		19.16	2.62		30.24	44.63	0.92	2.44	96.27	INCL IN OPX
67275	4	C		17.16	2.38		33.78	44.55	0.80	1.33	101.47	
67275	22	I		17.01	2.78		33.81	43.80	0.87	1.73	95.01	INCL IN OPX
67275	28	C		17.43	2.26		33.42	44.48	1.00	1.40	97.40	
67275	42	C		17.17	2.75		33.68	43.66	0.71	2.02	96.21	
67275	65	I	0.18	15.24	3.81		35.73	42.32	0.74	1.98	96.87	INCL IN OPX
67277	6	C		21.74	1.91		25.40	48.55	1.23	1.17	95.15	
67277	9	C		21.49	2.10		25.77	48.24	1.06	1.35	96.65	
67277	15	I	0.22	21.04	1.66		26.63	48.13	1.01	1.31	94.98	INCL IN PLG
67277	16	I		21.60	1.90		25.70	48.45	1.15	1.20	95.79	INCL IN PLG
67277	17	I	0.20	21.74	2.09		24.81	48.77	1.09	1.30	93.63	INCL IN PLG
67277	53	G		21.59	1.92		25.67	48.57	1.12	1.13	97.40	
67277	54	G		21.78	1.97		25.33	48.37	1.23	1.31	97.28	
67277	55	G		21.88	2.00		25.05	48.78	1.07	1.22	96.63	
67277	70	I		21.75	2.00		25.36	48.52	1.04	1.33	96.79	INCL IN CPX
67277	71	I		21.56	1.91		25.80	48.29	1.18	1.26	95.74	INCL IN CPX
67278	19	I		20.26	2.27		28.22	46.56	0.79	1.90	99.36	INCL IN OLV
67278	93	C		19.89	2.21		28.89	46.41	0.96	1.65	98.25	
67278	109	C		19.87	1.89		29.12	46.90	0.92	1.30	96.81	
67326	56	C		10.85	4.03		44.92	36.82	0.38	3.00	94.73	
67328	92	C		13.64	2.97		40.06	41.23	0.43	1.67	92.29	
67331	2	I		18.79	2.03		31.12	45.81	0.76	1.48	97.24	INCL IN CPX
67331	5	I		18.51	1.88		31.78	45.44	1.02	1.37	92.48	INCL IN CPX
67331	13	C		17.41	2.57		33.15	44.44	0.95	1.48	89.62	
67331	20	C		18.15	1.86		32.43	45.39	0.94	1.23	95.31	
67331	27	C		16.90	2.88		33.85	44.02	0.72	1.63	94.22	

Batur Volcano:- Ti-MAGNETITE (CATIONS)

ROCK	NUM	L	Si	Ti	Al	Cr	Fe3+	Fe2+	Mn	Mg	SUM	ULV
67273	16	C	0.0092	0.5169	0.1013		0.8465	1.3752	0.0278	0.1231	3.0000	55.2
67273	18	I		0.5285	0.1034		0.8395	1.3799	0.0302	0.1184	2.9999	56.1
67273	21	I		0.5157	0.1097		0.8590	1.3704	0.0271	0.1182	3.0001	55.0
67273	28	C		0.5197	0.1024		0.8583	1.3624	0.0322	0.1250	3.0000	54.9
67273	30	I	0.0077	0.5124	0.1119		0.8477	1.3680	0.0265	0.1257	2.9999	55.2
67273	35	I		0.5272	0.1130		0.8326	1.3658	0.0284	0.1330	3.0000	56.3
67275	4	C		0.4776	0.1039		0.9409	1.3790	0.0251	0.0735	3.0000	51.3
67275	22	I		0.4712	0.1205		0.9371	1.3490	0.0273	0.0949	3.0000	51.0
67275	28	C		0.4852	0.0987		0.9308	1.3766	0.0314	0.0772	2.9999	51.7
67275	42	C		0.4746	0.1192		0.9315	1.3419	0.0222	0.1106	3.0000	51.1
67275	65	I	0.0066	0.4193	0.1644		0.9838	1.2950	0.0228	0.1080	2.9999	47.5
67277	6	C		0.6049	0.0831		0.7071	1.5020	0.0385	0.0644	3.0000	64.2
67277	9	C		0.5965	0.0912		0.7157	1.4891	0.0331	0.0743	2.9999	63.7
67277	15	I	0.0080	0.5853	0.0724		0.7412	1.4891	0.0318	0.0723	3.0001	61.8
67277	16	I		0.6009	0.0829		0.7153	1.4987	0.0360	0.0662	3.0000	63.7
67277	17	I	0.0073	0.6029	0.0910		0.6885	1.5045	0.0342	0.0716	3.0000	64.9
67277	53	G		0.6007	0.0838		0.7148	1.5033	0.0351	0.0623	3.0000	63.8
67277	54	G		0.6050	0.0859		0.7041	1.4942	0.0386	0.0723	3.0001	64.2
67277	55	G		0.6081	0.0870		0.6967	1.5074	0.0335	0.0672	2.9999	64.8
67277	70	I		0.6040	0.0872		0.7048	1.4984	0.0324	0.0732	3.0000	64.3
67277	71	I		0.5995	0.0834		0.7177	1.4930	0.0370	0.0695	3.0001	63.5
67278	19	I		0.5604	0.0983		0.7809	1.4317	0.0247	0.1040	3.0000	59.7
67278	93	C		0.5513	0.0962		0.8013	1.4306	0.0299	0.0907	3.0000	58.7
67278	109	C		0.5531	0.0823		0.8114	1.4523	0.0289	0.0719	2.9999	58.4
67326	56	C		0.2973	0.1732		1.2321	1.1223	0.0118	0.1632	2.9999	32.3
67328	92	C		0.3786	0.1295		1.1133	1.2731	0.0133	0.0922	3.0000	41.2
67331	2	I		0.5226	0.0886		0.8661	1.4171	0.0237	0.0818	2.9999	55.3
67331	5	I		0.5158	0.0823		0.8862	1.4082	0.0319	0.0757	3.0001	54.2
67331	13	C		0.4835	0.1117		0.9212	1.3725	0.0297	0.0813	2.9999	52.1
67331	20	C		0.5066	0.0813		0.9056	1.4090	0.0297	0.0679	3.0001	53.3
67331	27	C		0.4682	0.1251		0.9386	1.3562	0.0224	0.0895	3.0000	51.1

Batur Volcano:- Ti-MAGNETITE (OXIDES)

ROCK	NUM	L	SiO2	TiO2	Al2O3	Cr2O3	Fe2O3	FeO	MnO	MgO	(SUM)	NOTE
67331	35	I		17.85	2.71		32.26	44.78	0.70	1.70	95.35	INCL IN OLV
67331	70	I	0.30	16.70	3.10		33.57	43.40	0.78	2.15	97.76	INCL IN CPX
67331	71	C		17.00	2.59		33.94	44.23	0.75	1.50	97.07	
67331	74	G		18.92	1.39		31.32	46.59	0.86	0.91	95.28	
67342	8	I		25.18	2.06		18.63	52.06	0.83	1.25	96.91	INCL IN OLV MICROPHEN
67342	19	I		24.62	3.48		18.35	51.10	0.63	1.82	97.36	INCL IN OLV PHEN
67342	20	C		21.14	2.77		26.04	47.49	0.48	2.08	96.94	

Batur Volcano:- ILMENITE (OXIDES)

ROCK	NUM	L	SiO2	TiO2	Al2O3	Cr2O3	Fe2O3	FeO	MnO	MgO	(SUM)	NOTE
67277	3	C	0.19	49.21	0.44		7.14	39.92	1.25	1.85	97.67	
67277	5	C		49.64	0.26		6.92	39.89	1.47	1.83	97.19	
67277	8	C		49.46	0.24		7.37	39.46	1.53	1.95	96.95	

Batur Volcano:- Cr-SPINEL (OXIDES)

ROCK	NUM	L	SiO2	TiO2	Al2O3	Cr2O3	Fe2O3	FeO	MnO	MgO	(SUM)	NOTE
67339	31	X		4.74	11.99	5.50	43.35	28.49		5.94	94.72	INCL IN OLV
67339	33	X		4.69	11.03	5.45	44.41	28.53	0.36	5.53	94.38	INCL IN OLV
67339	37	X		4.52	11.34	5.53	44.37	28.56		5.68	95.82	INCL IN OLV
67339	38	X		4.69	10.13	5.49	45.21	29.34		5.15	94.43	INCL IN OLV
67339	41	X		5.20	11.23	5.32	43.71	28.23		6.30	96.27	INCL IN OLV

Batur Volcano:- Ti-MAGNETITE (CATIONS)

ROCK	NUM	L	Si	Ti	Al	Cr	Fe3+	Fe2+	Mn	Mg	SUM	ULV
67331	35	I		0.4943	0.1176		0.8938	1.3789	0.0218	0.0936	3.0000	53.6
67331	70	I	0.0109	0.4597	0.1339		0.9250	1.3287	0.0242	0.1176	3.0000	50.7
67331	71	C		0.4721	0.1126		0.9432	1.3660	0.0233	0.0827	2.9999	51.0
67331	74	G		0.5302	0.0612		0.8783	1.4521	0.0273	0.0508	2.9999	55.1
67342	8	I		0.6974	0.0892		0.5161	1.6031	0.0259	0.0684	3.0001	75.0
67342	19	I		0.6740	0.1492		0.5027	1.5557	0.0193	0.0990	2.9999	76.4
67342	20	C		0.5817	0.1196		0.7170	1.4533	0.0149	0.1134	2.9999	63.5

Batur Volcano:- ILMENITE (CATIONS)

ROCK	NUM	L	Si	Ti	Al	Cr	Fe3+	Fe2+	Mn	Mg	SUM	ILM
67277	3	C	0.0048	0.9218	0.0128		0.1339	0.8316	0.0264	0.0687	2.0000	92.9
67277	5	C		0.9313	0.0075		0.1299	0.8322	0.0311	0.0680	2.0000	93.1
67277	8	C		0.9274	0.0069		0.1382	0.8229	0.0322	0.0723	1.9999	92.7

Batur Volcano:- Cr-SPINEL (CATIONS)

ROCK	NUM	L	Si	Ti	Al	Cr	Fe3+	Fe2+	Mn	Mg	SUM	ULV
67339	31	X		0.1223	0.4853	0.1495	1.1205	0.8183		0.3040	2.9999	
67339	33	X		0.1220	0.4498	0.1491	1.1570	0.8261	0.0107	0.2852	2.9999	
67339	37	X		0.1173	0.4615	0.1511	1.1528	0.8247		0.2926	3.0000	
67339	38	X		0.1230	0.4164	0.1514	1.1862	0.8555		0.2675	3.0000	
67339	41	X		0.1346	0.4553	0.1447	1.1309	0.8118		0.3227	3.0000	

APPENDIX 4

Major and Trace Element Analyses of Volcanic Rocks from Nusa Tenggara Timor, Indonesia

This appendix lists chemical analyses of samples of lava flows and dykes from the flanks of the following volcanoes:

1. Batu Tara
2. Ebulobo (Flores)
3. Ija (Flores)
4. Inerie (Flores)
5. Lewotolo (Lembata)
6. Mandiri (Flores - extinct)

Analytical methods are outlined in Appendix 2.

number	67125	67145	67146	67126	67143	67128	67129	67147	67148	67139
(major elements: wt %)										
SiO2	45.65	45.68	45.68	45.71	46.12	46.16	46.27	46.43	47.14	47.61
TiO2	1.18	1.17	1.29	1.15	1.19	1.19	1.21	1.16	0.93	0.91
Al2O3	16.80	16.49	17.95	16.58	17.69	17.10	17.49	16.07	13.76	14.15
Fe2O3	11.16	11.14	10.90	11.11	10.38	10.22	10.21	9.84	9.16	9.35
FeO										
MnO	0.20	0.20	0.20	0.20	0.19	0.18	0.18	0.17	0.17	0.18
MgO	5.59	5.51	4.22	5.43	5.18	5.51	5.19	6.35	7.68	7.39
CaO	12.26	11.90	10.20	12.06	11.37	11.97	11.49	11.97	12.05	11.83
Na2O	2.29	2.28	2.45	2.33	2.42	2.44	2.39	1.80	1.87	1.97
K2O	3.63	4.02	4.75	3.95	3.86	3.67	4.05	4.18	4.51	4.88
P2O5	0.92	1.02	1.26	1.00	0.88	0.83	0.87	0.82	0.85	0.90
LOI	-0.11	-0.17	0.19	-0.17	-0.03	-0.10	-0.21	0.38	0.24	-0.11
H2O-	0.08	0.13	0.26	0.07	0.19	0.10	0.09	0.39	0.19	0.14
rest	0.40	0.40	0.45	0.39	0.38	0.37	0.39	0.38	0.39	0.41
total	100.05	99.77	99.80	99.81	99.82	99.64	99.62	99.94	98.94	99.61
(trace elements: ppm)										
Ba	1070	1050	1513	1045	1005	1042	1179	1177	1072	1178
Rb	148	159	158	159	149	156	185	215	192	207
Sr	1168	1155	1248	1122	1183	1083	1053	937	847	924
Zr	170	176	208	170	155	144	138	134	212	215
Nb	11	12	16	11	11	10	10	9	18	14
Y	34	33	31	34	34	34	31	26	30	34
La	48	49	56	46	51	46	46	41	51	62
Ce	107	102	122	104	105	103	95	81	100	134
Nd	56	51	52	54	50	48	44	40	47	59
Sc	29	30	16	30	25	29	28	35	42	36
V	369	392	346	372	361	358	358	338	307	300
Ni	27	27	18	24	22	23	22	32	68	57
Cr	48	53	10	44	25	37	26	98	244	198
Mg#	49.80	49.49	43.40	49.19	49.71	51.64	50.17	56.11	62.42	61.02

Batu Tara Volcano

number	67136	67140	67130	67141	67133	67132	67131	67138	67134	67144
(major elements: wt %)										
SiO2	47.62	47.67	47.68	47.70	47.71	47.76	47.81	47.81	47.85	47.96
TiO2	0.89	0.90	0.90	0.95	0.89	0.90	0.92	0.89	0.91	0.98
Al2O3	13.72	13.64	13.58	14.13	13.60	13.48	13.64	14.15	14.07	14.84
Fe2O3	9.04	9.15	9.05	9.26	9.03	9.12	9.13	9.26	9.29	9.25
FeO										
MnO	0.17	0.17	0.17	0.17	0.17	0.17	0.17	0.17	0.17	0.17
MgO	8.33	8.22	8.28	7.56	8.24	8.38	8.19	7.36	7.94	7.11
CaO	11.80	12.00	12.08	12.00	11.92	12.24	12.12	11.62	11.52	11.76
Na2O	2.12	2.29	2.79	1.97	1.91	1.48	1.84	2.61	2.14	2.05
K2O	4.40	4.44	3.42	4.92	4.60	4.69	4.76	4.29	4.82	4.86
P2O5	0.87	0.88	0.84	0.87	0.87	0.87	0.90	0.87	0.91	0.85
LOI	0.19	0.28	0.76	-0.03	0.14	0.11	0.01	0.15	0.08	-0.10
H2O-	0.18	0.12	0.16	0.13	0.12	0.07	0.10	0.26	0.12	0.10
rest	0.39	0.40	0.40	0.41	0.39	0.40	0.40	0.40	0.41	0.41
total	99.72	100.16	100.11	100.04	99.59	99.67	99.99	99.84	100.23	100.24
(trace elements: ppm)										
Ba	1055	1181	1119	1189	1038	1128	1159	1126	1167	1275
Rb	192	193	184	194	196	196	196	201	199	198
Sr	810	823	818	888	809	819	856	912	900	883
Zr	213	214	214	216	212	206	210	217	216	217
Nb	19	18	20	19	18	17	20	13	20	20
Y	29	30	29	31	29	30	29	35	30	31
La	53	50	53	57	50	51	49	62	53	53
Ce	106	110	109	104	105	104	106	132	104	106
Nd	48	49	50	47	46	48	48	58	48	48
Sc	36	37	37	36	39	36	38	35	35	36
V	298	283	302	311	296	276	292	298	300	310
Ni	86	81	79	62	85	81	79	57	78	56
Cr	278	275	272	208	287	287	267	193	240	168
Mg#	64.60	64.02	64.44	61.79	64.38	64.54	63.99	61.16	62.87	60.36

Batu Tara Volcano

number	67142	67137	67135	67127
(major elements: wt %)				
SiO2	48.01	48.05	48.08	49.74
TiO2	0.98	0.94	0.90	0.78
Al2O3	14.79	15.98	13.83	15.68
Fe2O3	9.21	9.23	9.15	8.61
FeO				
MnO	0.17	0.17	0.17	0.17
MgO	7.14	6.19	8.28	6.40
CaO	11.63	10.86	11.94	10.28
Na2O	1.98	2.87	2.07	2.24
K2O	4.90	3.65	4.53	4.97
P2O5	0.85	0.72	0.85	0.78
LOI	-0.06	0.15	0.03	0.04
H2O-	0.10	0.20	0.15	0.10
rest	0.40	0.40	0.39	0.40
total	100.10	99.41	100.37	100.19
(trace elements: ppm)				
Ba	1221	1315	1049	1057
Rb	205	164	193	206
Sr	896	955	820	940
Zr	210	184	215	218
Nb	19	10	18	12
Y	30	34	31	39
La	52	61	52	76
Ce	109	126	106	148
Nd	48	53	50	65
Sc	34	34	38	32
V	304	300	287	278
Ni	55	38	89	51
Cr	171	91	282	194
Mg#	60.56	57.05	64.19	59.55

Batu Tara Volcano

number	61328	61330	61339	61340	61331	61333	61338	61335
(major elements: wt %)								
SiO2	53.64	55.22	55.53	56.35	56.73	56.95	57.09	57.78
TiO2	0.98	0.94	0.92	0.86	0.77	0.85	0.90	0.86
Al2O3	18.29	17.74	17.31	17.44	17.83	16.89	17.21	17.23
Fe2O3	9.41	9.16	8.60	8.22	8.03	7.94	8.56	7.94
FeO								
MnO	0.16	0.16	0.16	0.16	0.13	0.14	0.16	0.14
MgO	4.06	3.93	3.68	3.58	3.96	3.43	3.58	3.55
CaO	8.64	8.42	8.09	7.75	7.77	7.64	7.98	7.56
Na2O	3.01	3.14	3.50	3.62	3.01	3.97	3.55	3.77
K2O	0.91	1.06	1.32	1.18	1.09	1.42	1.30	1.33
P2O5	0.23	0.22	0.23	0.25	0.16	0.22	0.22	0.20
LOI	0.05	-0.14	-0.20	0.42		-0.18	-0.18	-0.17
H2O-	0.12	0.08	0.06	0.34	0.24	0.07	0.06	0.07
rest	0.16	0.16	0.17	0.17	0.13	0.16	0.17	0.16
total	99.66	100.09	99.37	100.34	99.85	99.50	100.60	100.42
(trace elements: ppm)								
Ba	280	244	313	308	236	329	318	316
Rb	31	37	48	39	48	47	48	46
Sr	567	574	610	640	403	581	611	561
Zr	79	73	85	85	76	90	90	89
Nb	2	1	4	3	3	3	3	3
Y	21	19	21	19	16	20	21	19
La	17	14	19	17	10	15	18	14
Ce	39	28	41	40	25	31	42	29
Nd	23	20	20	23	13	18	21	15
Sc	22	22	21	17	21	18	20	19
V	217	220	191	177	185	177	187	178
Ni	9	7	7	8	17	10	9	11
Cr	11	9	6	6	35	12	12	10
Mg#	46.08	45.94	45.88	46.31	49.41	46.11	45.31	46.97

Ebulobo Volcano

number	61290	61266	61273	61268	61291	61265	61270	61294	61287	61284
(major elements: wt %)										
SiO2	50.24	51.58	51.60	51.78	51.93	52.01	52.16	52.19	52.23	52.35
TiO2	0.69	0.81	0.81	0.82	0.76	0.84	0.82	0.82	0.80	0.84
Al2O3	18.56	18.61	18.78	18.51	18.32	19.07	18.69	17.69	18.55	19.36
Fe2O3	10.57	10.35	10.25	10.47	10.53	10.20	10.46	9.71	10.16	9.68
FeO										
MnO	0.16	0.17	0.16	0.16	0.16	0.16	0.16	0.15	0.16	0.15
MgO	5.97	5.67	5.49	5.76	6.20	5.31	5.41	6.12	5.48	4.77
CaO	10.38	9.54	9.72	9.56	9.50	9.43	9.48	9.75	9.63	9.99
Na2O	2.01	2.43	2.51	2.46	2.23	2.41	2.56	2.73	2.27	2.41
K2O	0.29	0.40	0.38	0.42	0.37	0.43	0.42	0.46	0.38	0.41
P2O5	0.06	0.08	0.08	0.08	0.09	0.09	0.09	0.12	0.08	0.09
LOI	0.06	-0.41	-0.44	-0.32	-0.33	0.15	-0.44	-0.43	-0.30	-0.31
H2O-	0.22	0.03	0.03	0.04	0.06	0.02	0.06	0.07	0.04	0.04
rest	0.10	0.10	0.11	0.11	0.10	0.11	0.11	0.14	0.11	0.11
total	99.31	99.36	99.48	99.85	99.92	100.23	99.98	99.52	99.59	99.89
(trace elements: ppm)										
Ba	78	106	116	113	100	111	125	162	135	111
Rb	11	14	12	14	14	13	14	12	14	17
Sr	219	308	303	300	284	312	305	313	320	296
Zr	25	36	32	36	31	34	35	44	36	38
Nb	1	2	2	1	1	2	1	2	2	3
Y	13	15	15	14	14	16	19	17	16	16
La	2	3	4	4	3	3	4	6	6	5
Ce	4	7	4	10	6	5	4	14	7	7
Nd	5	7	10	5	2	8	10	10	9	5
Sc	39	29	29	29	28	26	29	31	27	29
V	293	235	269	252	240	247	270	250	232	256
Ni	21	22	24	27	35	24	24	60	25	18
Cr	36	32	31	30	54	28	28	161	35	31
Mg#	52.80	52.04	51.48	52.15	53.84	50.77	50.60	55.52	51.65	49.39

Ija Volcano

number	61263	61269	61260	61264	61276	61289	61296	61292	61293
(major elements: wt %)									
SiO2	52.56	52.59	52.73	52.85	54.88	56.93	57.94	59.30	59.55
TiO2	0.82	0.77	0.83	0.81	0.75	0.66	0.92	0.65	0.66
Al2O3	18.85	18.98	19.09	18.80	18.96	17.98	15.99	17.52	17.68
Fe2O3	9.79	9.89	9.76	9.64	8.90	8.30	8.55	7.16	7.25
FeO									
MnO	0.16	0.16	0.15	0.15	0.15	0.18	0.14	0.16	0.16
MgO	5.01	5.22	4.95	5.04	4.24	3.40	3.41	2.75	2.78
CaO	9.91	9.51	9.79	9.82	9.02	7.79	7.24	7.18	7.20
Na2O	2.51	2.55	2.13	2.49	2.81	2.99	2.90	3.49	3.44
K2O	0.41	0.34	0.43	0.44	0.49	0.53	1.48	0.59	0.60
P2O5	0.08	0.07	0.11	0.08	0.11	0.11	0.15	0.14	0.11
LOI	-0.41	-0.33	-0.41	-0.20	-0.30	0.23	0.37		0.02
H2O-	0.01	0.01	0.02	0.05	0.08	0.15	0.19	0.11	0.12
rest	0.11	0.10	0.11	0.10	0.10	0.09	0.15	0.09	0.09
total	99.81	99.86	99.69	100.07	100.19	99.34	99.43	99.14	99.66
(trace elements: ppm)									
Ba	124	126	122	108	121	157	335	174	166
Rb	13	13	15	14	17	16	79	19	20
Sr	287	310	282	269	329	268	315	307	310
Zr	39	33	38	39	46	51	118	56	56
Nb	1	1	1	1	1	3	2	3	2
Y	16	15	14	16	18	22	26	19	20
La	4	5	5	3	5	4	11	6	6
Ce	7	5	7	7	6	10	32	12	10
Nd	4	10	9	7	10	9	16	11	12
Sc	30	24	31	32	23	21	24	17	17
V	247	216	242	267	171	125	214	123	132
Ni	18	21	19	17	12	5	10	6	7
Cr	28	30	34	29	17	4	15	6	4
Mg#	50.34	51.11	50.11	50.87	48.55	44.79	44.13	43.21	43.17

Ija Volcano

number	61304	61312	61311	61303	61308	61306	61317	61310	61301	61307
(major elements: wt %)										
SiO2	51.31	52.04	52.14	52.26	53.34	53.47	53.54	53.93	54.13	54.29
TiO2	0.69	0.79	0.71	0.74	0.82	0.81	0.82	0.83	0.81	0.79
Al2O3	19.58	19.84	19.74	20.58	20.19	18.87	18.35	18.86	18.80	18.96
Fe2O3	8.83	8.38	8.81	8.40	8.63	9.33	9.14	9.29	9.22	9.16
FeO										
MnO	0.13	0.13	0.13	0.12	0.15	0.15	0.16	0.15	0.15	0.15
MgO	5.56	3.78	5.66	4.08	3.12	4.50	4.37	4.46	4.51	4.23
CaO	10.23	10.11	10.04	10.19	9.58	8.95	8.82	8.80	8.84	8.64
Na2O	2.60	3.18	2.51	2.92	2.90	3.04	3.32	2.81	3.03	3.08
K2O	0.56	0.72	0.52	0.58	0.62	0.65	0.75	0.65	0.65	0.69
P2O5	0.06	0.08	0.07	0.07	0.11	0.09	0.11	0.10	0.09	0.12
LOI	-0.41	-0.23	-0.36	-0.24	-0.32	-0.32	-0.09	-0.17	-0.41	-0.37
H2O-	0.07	0.12	0.07	0.05	0.05	0.06	0.12	0.06		0.05
rest	0.12	0.12	0.12	0.12	0.11	0.11	0.11	0.11	0.11	0.11
total	99.33	99.06	100.16	99.87	99.30	99.71	99.52	99.88	99.93	99.90
(trace elements: ppm)										
Ba	133	149	140	139	128	159	143	139	159	169
Rb	21	24	19	22	24	24	25	26	22	25
Sr	327	337	315	338	340	310	300	310	298	301
Zr	39	46	37	46	44	51	50	52	51	55
Nb	2	2	3	3	1	3	2	3	3	2
Y	15	16	13	16	18	19	19	19	19	20
La	8	8	7	8	5	7	7	5	5	6
Ce	8	20	17	15	12	15	11	4	9	9
Nd	9	12	8	10	8	13	10	8	7	9
Sc	29	27	29	26	29	28	28	27	29	27
V	256	267	259	248	210	227	220	216	242	217
Ni	47	22	49	26	8	19	18	19	19	19
Cr	48	23	49	28	9	21	23	18	24	24
Mg#	55.50	47.19	56.00	49.03	41.73	48.86	48.64	48.74	49.21	47.77

Inerie Volcano

number	61315	61313	61321	61318	61322	61326	61325
(major elements: wt %)							
SiO2	54.60	54.75	54.98	56.00	56.62	57.34	58.58
TiO2	1.02	0.83	0.88	0.82	0.84	0.81	0.85
Al2O3	17.27	18.96	17.93	18.90	17.35	17.18	17.28
Fe2O3	10.09	9.28	9.09	8.99	8.22	7.95	7.95
FeO							
MnO	0.16	0.15	0.15	0.15	0.15	0.15	0.14
MgO	4.14	4.49	3.91	4.09	3.32	3.17	3.26
CaO	8.20	8.73	8.67	8.53	7.56	7.40	7.27
Na2O	3.17	2.42	3.34	2.50	3.54	3.39	3.61
K2O	0.88	0.64	0.85	0.58	1.26	1.25	1.31
P2O5	0.13	0.09	0.12	0.11	0.25	0.23	0.23
LOI	-0.49	-0.38	-0.34	-0.26	0.02	0.37	-0.04
H2O-	0.04	0.05	0.07	0.09	0.11	0.19	0.10
rest	0.13	0.11	0.12	0.11	0.16	0.16	0.17
total	99.34	100.12	99.77	100.61	99.40	99.59	100.71
(trace elements: ppm)							
Ba	222	161	178	148	321	312	340
Rb	32	22	31	28	42	44	44
Sr	303	307	306	304	581	577	593
Zr	65	48	64	54	85	96	92
Nb	2	3	2	2	4	4	3
Y	20	19	20	18	23	18	20
La	9	6	10	7	18	18	16
Ce	23	17	18	12	40	42	36
Nd	12	12	9	15	24	21	20
Sc	31	29	29	27	16	16	17
V	263	236	252	218	174	146	167
Ni	16	21	18	16	6	6	7
Cr	19	23	25	17	6	2	8
Mg#	44.83	48.94	46.00	47.40	44.44	44.13	44.82

Inerie Volcano

number	67163	67166	67164	67158	67165	67159	67157	67161	67160	67162	67167
(major elements: wt %)											
SiO2	54.93	55.37	55.42	55.63	56.24	56.65	56.76	58.33	58.76	60.52	62.29
TiO2	0.78	0.75	0.75	0.61	0.66	0.71	0.64	0.51	0.53	0.51	0.49
Al2O3	18.77	18.92	18.88	17.84	16.80	17.06	17.50	16.59	16.64	18.32	15.69
Fe2O3	7.40	7.17	7.05	7.74	7.46	7.25	7.55	6.23	6.30	5.04	6.04
FeO											
MnO	0.17	0.17	0.17	0.18	0.17	0.16	0.17	0.14	0.15	0.16	0.12
MgO	2.86	2.65	2.55	3.38	3.55	2.92	3.26	2.64	2.74	1.60	2.56
CaO	7.20	6.90	6.89	7.67	7.32	6.80	7.54	6.54	6.12	5.23	6.20
Na2O	3.69	3.58	3.80	3.23	2.97	3.20	3.05	3.02	3.15	4.04	2.96
K2O	3.04	3.18	3.40	2.18	3.12	3.25	3.21	3.78	4.30	3.72	1.93
P2O5	0.42	0.44	0.43	0.25	0.27	0.25	0.23	0.19	0.20	0.25	0.05
LOI	0.24	0.18	0.16	0.24	0.35	0.41	0.03	0.96	0.24	0.36	0.50
H2O-	0.29	0.21	0.27	0.38	0.43	0.34	0.19	0.32	0.19	0.14	0.44
rest	0.37	0.37	0.38	0.28	0.33	0.32	0.31	0.34	0.35	0.34	0.21
total	100.16	99.89	100.15	99.61	99.67	99.32	100.44	99.59	99.67	100.23	99.48
(trace elements: ppm)											
Ba	1462	1496	1563	1025	1261	1281	1230	1383	1432	1511	1049
Rb	87	91	91	76	103	99	88	117	123	112	63
Sr	930	943	942	718	726	710	773	770	772	736	278
Zr	160	167	169	140	156	163	133	182	186	178	68
Nb	8	10	10	9	8	8	7	9	9	9	2
Y	31	31	32	23	30	28	25	29	27	27	26
La	67	64	64	44	58	53	49	75	71	63	22
Ce	126	124	125	81	111	100	88	130	122	114	28
Nd	45	47	47	32	38	36	32	46	44	38	15
Sc	18	15	15	15	17	17	18	15	15	8	23
V	173	150	154	158	174	161	180	139	138	85	156
Ni	4	4	4	8	19	6	8	10	11	3	6
Cr	6	8	4	9	60	10	14	15	17	6	17
Mg#	43.36	42.27	41.74	46.38	48.52	44.38	46.10	45.63	46.28	38.61	45.64

Lewotolo Volcano

number	67151	67150	67155	67153	67154	67152	67149
(major elements: wt %)							
SiO2	48.86	49.53	49.57	49.71	49.72	52.65	62.97
TiO2	1.06	1.19	1.24	1.19	1.26	1.20	0.59
Al2O3	18.92	17.75	16.81	17.60	16.57	16.44	16.84
Fe2O3	10.51	11.78	13.16	11.70	12.92	11.71	5.09
FeO							
MnO	0.17	0.21	0.22	0.21	0.21	0.21	0.12
MgO	4.67	4.85	4.51	4.83	4.54	3.68	1.35
CaO	10.31	9.82	9.64	9.69	9.00	7.92	4.35
Na2O	2.74	2.84	2.92	2.97	3.07	3.30	3.92
K2O	1.20	1.32	1.40	1.35	1.57	1.95	3.85
P2O5	0.25	0.27	0.24	0.26	0.26	0.30	0.23
LOI	0.22	-0.39	-0.49	-0.42		-0.31	0.05
H2O-	1.04	0.27	0.26	0.24	1.01	0.26	0.29
rest	0.28	0.28	0.30	0.28	0.30	0.32	0.34
total	100.23	99.72	99.78	99.61	100.43	99.63	99.99
(trace elements: ppm)							
Ba	879	896	1027	920	1059	1267	1665
Rb	25	29	31	30	34	45	111
Sr	822	787	772	777	737	714	516
Zr	79	90	83	86	94	127	252
Nb	5	5	5	5	5	7	13
Y	26	28	28	27	29	32	37
La	26	27	34	28	32	38	61
Ce	49	60	61	56	63	77	108
Nd	26	28	29	27	28	34	40
Sc	29	33	37	36	34	31	11
V	300	327	379	331	369	306	64
Ni	12	10	8	10	7	5	4
Cr	20	14	16	18	10	8	8
Mg#	46.81	44.92	40.43	44.99	41.04	38.37	34.44

Mandiri Volcano